ABRASIVITY CHARACTERIZATION OF SELECTED ROCK FORMATIONS OF PAKISTAN

Submitted by:

YASIR MAJEED

(2011-Ph.D-MIN-01)

Supervisor:

Dr. Muhammad Zubair Abu Bakar

(Associate Professor)

Department of Mining Engineering
University of Engineering and Technology
Lahore, Pakistan
(2017)

ABRASIVITY CHARACTERIZATION OF SELECTED ROCK FORMATIONS OF PAKISTAN

This thesis is submitted to the Faculty of Earth Sciences and Engineering, University of Engineering and Technology, Lahore for the partial fulfillment of requirements for the Degree of

Doctor of Philosophy

in

Mining Engineering

by

Yasir Majeed (2011-PhD-MIN-01)

Approved on 05-04-2017

_____

External Examiner-I
Dr. Muhammad Akram
Professor (R) Mining Engineering
Department, UET, Lahore.

_____

External Examiner-II
Dr. F.A.K. Kirmani
Professor (R) Mining Engineering
Department, UET, Lahore.

_____

Supervisor (Internal Examiner)
Dr. Muhammad Zubair Abu Bakar
Associate Professor, Department of
Geological Engineering, UET, Lahore.

_____

Chairman
Dr. Zulfiqar Ali
Mining Engineering Department, UET,
Lahore.

_____

Prof. Dr. Nadeem Feroze
Dean, Faculty of Earth Sciences and
Engineering, UET, Lahore.

DEPARTMENT OF MINING ENGINEERING

UNIVERSITY OF ENGINEERING AND TECHNOLOGY LAHORE, PAKISTAN

NAME OF EXTERNAL EXAMINERS

From Abroad:

1. Dr. Richard L. Bullock
   Professor (Emeritus), Department of Mining & Nuclear Engineering,
   Missouri University of Science & Technology, Rolla Missouri, USA.
   6032 Bosque River Court,
   North Richland Hills, TX 76180, USA.
   Email: bullock@mst.edu

2. Dr. Jamal Rostami
   Alacer Gold / Hadden Endowed Chair,
   Associate Professor, Department of Mining Engineering, Colorado School of Mines (CSM), USA.
   Rm 217, Brown Building (CSM),
   1500 Illinois St. Golden, CO 80401, USA.
   Email: rostami@mines.edu

3. Dr. Robert John Fowell
   Associate Professor, Department of Mining Engineering, University of Leeds, UK.
   12 Otters Holt, Wakefield, West Yorkshire WF4 3QE, UK.
   Email: r.j.fowell@leeds.ac.uk

From within the Country:

1. Dr. Muhammad Akram
   Professor (R) Mining Engineering Department, University of Engineering & Technology, Lahore.
   House No. 253-E, Street No.5, Phase-6, DHA Lahore.
   Email: Akram@uet.edu.pk

2. Dr. F.A.K. Kirmani
   Professor (R) Mining Engineering Department, University of Engineering & Technology, Lahore.
   House No. 172-U, DHA Lahore.
   Email: f.a.k.kirmani@gmail.com

DECLARATION

I declare that the work contained in this thesis is my own, except where explicitly stated otherwise. In addition this work has not been submitted to obtain another degree or professional qualification.

Name: Yasir Majeed

Signed: _____

Dated: _____

ABSTRACT

This study characterized the abrasivity potential and evaluated different rock abrasivity measurement methods on 51 rock units selected from different regions of Pakistan. For abrasivity measurements CERCHAR, LCPC and NTNU/SINTEF abrasion tests were adopted. Laboratory tests also included a complete suite of engineering rock properties performed on all 51 rock units as well as petrographic analyses along with determination of Schimazek's F-value and Rock abrasivity Index (RAI).

The CERCHAR tests were conducted on sawn (CAI_s) and freshly broken (CAI_{fb}) rock surfaces employing top and side viewing measurement methods at the stylus tip. This study statistically confirms the previous work on the influence of wear flat measurement methods and rock surface conditions on the CERCHAR Abrasivity Index (CAI) values. It was found statistically that CAI_s and CAI_{fb} values measured from top view of test stylus were 17 and 19 % higher, respectively, in comparison to CAI_s and CAI_{fb} values measured from side view of test stylus. The correlations of CAI with rock properties are also discussed. Further 33 sedimentary rock samples out of total 51 rocks were subject to CAI measurements and rock properties tests in saturated condition. Overall 79% of CAI_{sat} values were less than CAI_{dry} values, meanwhile 52% of CAI_{sat} values showed significant reduction from CAI_{dry} values in the statistical analyses of CAI results with significance level of 15% ($\alpha = 0.15$) . The proposed correlation of CAI_{sat} with CAI_{dry} can be used to estimate CAI_{sat} from laboratory tests where reported CAI is often CAI_{dry}. This could lead into more accurate estimation of tool wear and related adjustments when CAI is used for estimation of tool wear when excavtion is done under wet rock condition. Moreover, a predictive model of CAI_{sat} with saturated rock properties was also developed.

This study also compared the results of LCPC dry and saturated tests for 20 selected rock types performed at 15, 30, 45 and 60 % water contents. Overall abrasivity decreased with the increase in water content with peak values attained at 15% and 30% water contents for low porosity and high porosity rocks respectively as compared to dry tests. Similarly, a gradual reduction in LCPC Breakability Index (BR %) was noted in the

case of low porosity rock samples with the corresponding rise in water content levels. However for high porosity rocks the breakability first reduced abruptly at 15% moisture content in contrast to the tests conducted at 0% moisture content followed by a rise at 30 % water content and finally at 45% and 60% water contents the breakability dropped down steadily in comparison to the dry test values. Moreover, possible correlations of LCPC test results for all 51 rocks with rock properties were discussed.

Finally a comparative study was performed on NTNU/SINTEF rock abrasivity device by varying the particle size of rock abrasion powder and test speed. The NTNU/SINTEF Abrasion Value Steel (AVS) test results showed a gradual decrease in abrasivity with the corresponding decrease in grain size of test fractions. Whereas, rise in the wear of test piece was observed at a test speed of 10 rpm as compared to the standard test speed of 20 rpm. Relevant correlations of CLI with CERCHAR and LCPC test results and rock properties were also included.

LIST OF PUBLICATIONS

- Majeed Y, Abu Bakar MZ (2015) Statistical evaluation of CERCHAR Abrasivity Index (CAI) measurement methods and dependence on petrographic and mechanical properties of selected rocks of Pakistan. Bulletin of Engineering Geology and the Environment 75(3):1341-1360, DOI: 10.1007/s10064-015-0799-5. [Springer (Impact Factor: 1.252)]

- Abu Bakar MZ, Majeed Y, Rostami J (2016) Effects of rock water content on CERCHAR abrasivity index. Wear 368-369: 132-145, DOI: 10.1016/j.wear.2016.09.007. [ELSEVIER (Impact Factor: 2.323)]

ACKNOWLEDGMENTS

Many thanks are due to the Departments of Mining Engineering, Geological Engineering and Industrial and Manufacturing Engineering of University of Engineering and Technology, Lahore for facilitating this research work.

Special acknowledgements are due to my parents for their continuous support and prayers. I am also grateful to my wife for her cooperation and encouragement. Without their support the completion of this research would have been very difficult.

Last, but not least, I would like to acknowledge the financial support provided by the University of Engineering and Technology (UET), Lahore for this PhD. research work.

Yasir Majeed

TABLE OF CONTENTS

LIST OF ILLUSTRATIONS

LIST OF TABLES

NOMENCLATURE

Symbol	Description
Qtz (%)	Quartz Content
Qtz-eq (%)	Equivalent Quartz Content
Ø-Qtz	Mean Diameter of Quartz Grains
Ø	Mean Diameter of Mineral Grains
EQC	Equivalent Quartz Content
F-value	Schimazek's F-value
RAI	Rock Abrasivity Index
Schimazek's F-value$_{(Sat)}$	Schimazek's F-value for Saturated Rock
RAI$_{(Sat)}$	Rock Abrasivity Index Value for Saturated Rock
CERCHAR	Centre d'Etudes et Recherches des Charbonages de France
CAI	CERCHAR Abrasivity Index
CAI$_{s(Top)}$	CAI Value for Sawn Rock Surface Measured Using Top Viewing Method at the Stylus Tip
CAI$_{s(Side)}$	CAI Value for Sawn Rock Surface Measured Using Side Viewing Method at the Stylus Tip
CAI$_{fb(Top)}$	CAI Value for Freshly Broken Rock Surface Measured Using Top Viewing Method at the Stylus Tip
CAI$_{fb(Side)}$	CAI Value for Freshly Broken Rock Surface Measured Using Side Viewing Method at the Stylus Tip
CAI$_{ss(Top)}$	CAI Value for Saturated Sawn Rock Surface Measured Using Top Viewing Method at the Stylus Tip
CAI$_{ss(Side)}$	CAI Value for Saturated Sawn Rock Surface Measured Using Side Viewing Method at the Stylus Tip
CAI$_{fbs(Top)}$	CAI Value for Saturated Freshly Broken Rock Surface Measured Using Top Viewing Method at the Stylus Tip
CAI$_{fbs(Side)}$	CAI Value for Saturated Freshly Broken Rock Surface Measured Using Side Viewing Method at the Stylus Tip
CAI$_{sat}$	CAI value for Saturated Freshly Broken Rock Surface

	Obtained Using the Side Viewing Wear Flat Measurement Technique
CAI_{dry}	CAI value for Freshly Broken Rock Surface Obtained Using the Side Viewing Wear Flat Measurement Technique
LCPC	Laboratoire Central des Ponts et Chaussees
A.F.T.E.S.	Association Francaise des Tunnels et de l'Espace Souterrain
ABR	LCPC Abrasivity Coefficient in (g/t)
$ABR_{(15\%)}$	LCPC Abrasivity Coefficient for 15% Water Content
$ABR_{(30\%)}$	LCPC Abrasivity Coefficient for 30% Water Content
$ABR_{(45\%)}$	LCPC Abrasivity Coefficient for 45% Water Content
$ABR_{(60\%)}$	LCPC Abrasivity Coefficient for 60% Water Content
BR	LCPC Breakability Index
$BR_{(15\%)}$	LCPC Breakability Index for 15% Water Content
$BR_{(30\%)}$	LCPC Breakability Index for 30% Water Content
$BR_{(45\%)}$	LCPC Breakability Index for 45% Water Content
$BR_{(60\%)}$	LCPC Breakability Index for 60% Water Content
NTNU	Norwegian University of Science and Technology, Trondheim, Norway
SINTEF	Stiftelsen for Industriell og Teknisk Forskning, Trondheim, Norway
SJ	Sievers' J-Value
AVS	Abrasion Value Steel
CLI	Cutter Life Index
UCS	Uniaxial Compressive Strength of Rock
$UCS_{(Sat)}$	Uniaxial Compressive Strength of Saturated Rock
BTS	Brazilian Disc Tensile Strength of Rock
$BTS_{(Sat)}$	Brazilian Disc Tensile Strength of Saturated Rock
σ	UCS of Rock
σ_t	BTS of Rock
ρ_d	Density of Dry Rock
ρ_{sat}	Density of Saturated Rock

V_v	Pore Space Volume
N	Porosity of Rock
V_p	Sonic Wave Velocity in Dry Rock
$V_{p\,(Sat)}$	Sonic Wave Velocity in Saturated Rock
α	Statistical Significance Level
ANOVA	Analysis of Variance
TBM	Tunnel Boring Machine
EPB	Earth Pressure Balance

1. INTRODUCTION

1.1. BACK GROUND

Natural resources play a vital role in the development and economic growth of a country. Nature has bestowed Pakistan with great mountain ranges containing variety of mineral deposits in considerable quantities. Minerals are excavated from rocks by developing underground and surface mines. Similarly, excavation of rock is also carried out for the construction of geotechnical projects comprising of hydropower projects, dams, communication tunnels, motorways, underground caverns for storage and other defense related purposes. At present numerous rock excavation projects for hydropower generation are being undertaken in the country including Nelum Jehlum, Patrind and Gulpur hydropower projects amongst others. Moreover, in developed and developing countries around the globe there is a growing need for tunnels and underground caverns (Kahraman and Kahraman, 2015). Similarly Ho et al. (2015) have highlighted the period of boom encountered in the construction activity of underground infrastructure in Hong Kong during the last ten years. Gotthard base tunnel is an example of recently completed (1st June, 2016) twin bore railway tunnel project passing through the Alps in Switzerland. At present it is the longest traffic tunnel of the world with a total tunneling length of 151.840 km. Moreover according to a conservative estimate each year in North America about 50 miles of hard rock tunnels are constructed by the mining industry. This is approximately the same as the total drivage of civil tunnels per annum (Abu Bakar, 2012).

Excavation of rock in mining, civil and geotechnical engineering applications is achieved either by utilizing conventional drilling and blasting method or by employing mechanized technologies including continuous miners, shearer or plow cutters, small scale cutting machines, tunnel boring machines (TBMs) and Roadheaders etc. (Hood and Roxborough, 1992). Mechanized excavation of rock in comparison to conventional techniques is rapid, more dependable and widely applicable due to its increased advance rates, flexibility, safety, and optimal functioning involved. Further the mechanical excavators decrease post excavation rock support expenditures due to minimizing rock

over break at the excavation walls and ground disturbance (Kahraman and Kahraman, 2015). However, the rock excavation machines being commonly capital intensive and generally site specific require a thorough consideration of the application conditions (mainly rock strength, abrasiveness and presence of water among others) for increased performance (Michalakopoulos et al., 2005).

Whatever is the cutting method employed, it involves interaction of cutting tools at the rock cutting face. The rock cutting tools mainly include disc cutters, picks and drill bits used in mining, civil and petroleum engineering sectors. Moreover, cutting teeth of different excavators like bucket wheel excavators, backhoes, front-end loaders, shovels, shearers and plows can also be included in this list. The mining and civil/geotechnical industries encounter excessive cutter wear caused by high abrasiveness of mined rock material resulting in high bit replacement frequency. As such a huge portion of excavation budget is expended in the repair and costly replacement of rock cutting tools (Fowell and Abu Bakar, 2007; Hamzaban et al., 2014b). It has also been noted that not only is tool wear a problem but other machine components coming in contact with the rock during excavation also experience wear, which results in expensive component replacements and downtime as well (Fowell and Abu Bakar, 2007). In some cases great financial losses have occurred for example in one case history reported by Verhoef (1997), it was sometimes necessary to replace the cutting picks mounted on the cutterhead after every 30 minutes of use, even though the excavator was cutting a moderately weak limestone rock (Calcarenite), but it contained substantial quantity of quartz grains up to 1cm size.

Abrasive wear is related to abrasive minerals (like quartz) present in the rock and is usually significant when the abrasive mineral is harder than the cutting tool material. The higher the quartz and hard mineral content in the rock, more is the abrasive wear of the tool. Uetz (1986) highlights abrasive wear as a function of relative hardness of the materials involved. Zum Gahr (1987) described the hardness ratio of abrasive and material as a function of abrasive wear and established that if the difference between the indentation hardness of two materials is larger than approximately 20% the abrasive wear will increase dramatically. When this difference is smaller the abrasive wear will be marginal. Abrasion at the tool-rock interface is the procedure causing continuous loss or

displacement of material (i.e. wear) from the surface of solid body due to the presence of hard particles in between or embedded in one or both of two solid surfaces in relative sliding motion, or due to the presence of hard protuberances on one or both of the two sliding surfaces. Therefore, rock abrasivity mainly depends upon the characteristics of cutting tool, the rock properties (particularly strength and abrasiveness) and the prevailing conditions of temperature and pressure (Verhoef, 1997).

Numerous studies have highlighted the impact of rock abrasivity on the excavation process and overall economy of the project. West (1989) mentioned abrasivity as one of the rock properties which is quantified for the suitability evaluation of rocks towards mechanized excavation. Deketh (1995) cautioned that failing to estimate rock abrasivity accurately generally results in unforeseen high tool wear rates accompanied by high financial losses. According to Rostami et al. (2005) the estimation accuracy of TBM disc cutter life depends on the parameters consisting of rock strength, hardness and abrasiveness. Cutter life affects machine downtime, utilization, rate of advance, project cost and ultimately economics. Perez et al. (2015) emphasized the importance of rock abrasivity in rock excavation process and linked it directly to the wear of rock cutting tool at the rock-tool interface. Further rock abrasivity effects tool life in rock cutting operations; conventional and mechanized excavation utilized in mining and geotechnical sectors, as well as drilling employed in oil and gas industry. Ho et al. (2015) explained that rock abrasivity is the main factor to evaluate tool wear rate, which in turn is crucial for the prediction of tool life span and hence construction costs. Excessive wear of the cutting tools on the excavation machinery increases the tool replacement rate, which also increases the cost of production not only due to the cost of the replaced tools but also the downtime in replacing these tools. Thus a proper measurement of the rock abrasion would be very useful in estimating the cutting tool's life and cost (Hamzaban et al., 2014a).

At present a variety of techniques are available for the measurement of rock abrasivity including quartz content, equivalent quartz content, Schimazek's F-value, RAI, modified taber abrasion test, core abrasion test, CERCHAR test, LCPC test, NTNU/SINTEF abrasion test amongst others. However, CERCHAR test, LCPC test, NTNU/SINTEF abrasion test and wear factors (Schimazek's F-value and RAI) from

petrographic studies are most commonly utilized for the determination of rock abrasivity. Although the abrasivity evaluations of different rock types and soils using rock properties have been studied by a number of investigators (Verhoef, 1997; Al-Ameen and Waller, 1994; Buchi et al., 1995; Plinninger et al., 2004; Rostami et al., 2005; Alber, 2008a,b; Fowell and Abu Bakar, 2007; Yarali et al., 2008; Plinninger, 2010; Kahraman et al., 2010; Drucker, 2011; Deliormanli, 2012; Dahl et al. 2012; Hamzaban et al., 2014a; Rostami et al., 2013; Hamzaban et al., 2014b; Gonzalez et al., 2014; Barzegari et al., 2015; Hashemnejad et al., 2015 among others), but at present absolutely no research work on the wear of rock cutting tools, evaluation of rock abrasiveness measurement methods and rock abrasivity characterization has been performed on the rocks in Pakistan.

1.2. OBJECTIVES OF RESEARCH

This research work contributes towards the body of knowledge on the abrasivity characterization as well as evaluation of rock abrasivity measurement methods including CERCHAR test, LCPC test and NTNU/SINTEF abrasion test by utilizing selected rocks of Pakistan. The main goals of this study were:

- To evaluate the abrasivity potential of rocks selected from different regions of Pakistan. The present study employs the selected rock abrasivity measurement methods to characterize the abrasivity potential of rocks from selected rock formations of Pakistan and also to evaluate the selected rock abrasivity measurement methods on different test parameters in order to validate or refute the past research findings.

- To assess the effect of water saturation of sedimentary rock samples on the resulting abrasivity values by utilizing CERCHAR abrasivity test.

- To evaluate the impact of water content on the LCPC test results on selected rock samples.

- To evaluate the effect of variation in particle size distribution of abrasion powder and the effect of change in test speed of NTNU/SINTEF rock abrasion test on the measured Abrasion Value Steel (AVS) on selected rock samples.

- To propose relationships between the rock abrasivity values measured on CERCHAR, LCPC and NTNU/SINTEF rock abrasivity measurement methods and also to develop correlations of abrasivity measurements with the rock properties including petrographical parameters, wear indices, mechanical and physical properties.

1.3. APPROACH

To accomplish the objectives of this research, three established rock abrasivity measurement methods; CERCHAR abrasivity test, LCPC abrasivity test and NTNU/SINTEF abrasivity test were included to determine the rock abrasivity indices including CERCHAR abrasivity index (CAI), LCPC abrasivity co-efficient (ABR, g/t) and Cutter Life Index (CLI) respectively. At present the CERCHAR abrasivity test is the only rock abrasivity measurement method which has been standardized by both ASTM D7625-10 and ISRM suggested method by (Alber et al., 2014). For conducting rock abrasivivty tests (CERCHAR, LCPC and NTNU/SINTEF) the laboratory scale setups were locally fabricated. Efforts were also made for the collection of selected rock samples from different regions of Pakistan. For the Petrological assessment of abrasivity, petrographic thin section study was conducted on selected rock samples to quantify the mineral contents, quartz equivalent content and mineral grain sizes. The prepared rock samples were tested to determine the complete suite of mechanical and physical rock properties. The petrographic parameters and mechanical properties of the rocks were further utilized for the computation of wear indices including Schimazek's F-value and Rock Abrasivity Index (RAI). In addition to the rock abrasivity tests (CERCHAR and LCPC), the physico-mechanical rock properties measurement tests were also performed in the saturated state on selected sedimentary rock samples to determine the impact of saturation on abrasive capacity of these rocks. The statistical analyses were performed on the test results including relevant abrasivity indices (CAI, ABR and CLI) and engineering properties to establish correlations applicable on rocks of Pakistan, as well as to validate past studies and to examine the impact of various parameters on the test results.

Finally a parametric study was also conducted to evaluate the NTNU/SINTEF Abrasion Value Steel (AVS) rock abrasivity test. This study was performed by varying

the grain size distribution of the rock abrasion powder and also by changing the rotational speed of the steel disc of test apparatus.

1.4. SCOPE OF RESEARCH

- The rock abrasivity values and complete suite of rock properties data base so developed would be valuable for machine manufacturers as well as contractors dealing with surface and underground rock excavation projects.
- The statistical regression models of rock abrasivity indices developed with petrographical, rock wear factors and physico-mechanical rock properties would be helpful for the bidders and consultants for the estimation of cost and budget plans for rock excavation projects.
- Evaluation of rock behavior towards abrasivity in laboratory saturated state would be directly applicable in actual filed conditions where rock excavators generally are exposed to both dry and wet rock strata. It would help to estimate the life time and in turn cost of rock cutting tools utilized for a particular excavation job.
- The data base developed in this research work for selected rock units of Pakistan would be useful to carry out further research work related to rock excavation area particularly in Pakistan. Moreover, the abrasivity data of rocks of Pakistan and its correlations with other rock engineering properties is not documented as yet.
- This research work will add to the body of knowledge associated with the abrasivity characterization and evaluation of selected rocks from different regions of Pakistan and will be particularly beneficial for the current and future rock excavation projects incorporating hydropower projects, dams, tunnels, motorways and other mega civil and geotechnical structures.

1.5. THESIS STRUCTURE

The dissertation is comprised of nine chapters, together with appendices containing the detailed results of CERCHAR, LCPC and NTNU/SINTEF rock abrasivity tests, the petrographical analyses, the mechanical rock properties tests, the computation of wear indices (Schimazek's F-value and RAI) as well as the published papers.

Chapter 1 contains back ground information addressing the research scope, objectives and approach to fulfill these goals.

Chapter 2 includes the theoretical deliberations in support of the research work, taken from relevant literature survey. More precisely, the chapter presents the terminology and definitions connected with the wear of rock cutting tools involved in rock excavation process, the rock abrasivity measurement methods along with reviewing the past investigations carried out by other researchers to evaluate abrasive wear in rock cutting procedure. Further the currently available soil abrasivity measurement setups are also discussed.

Chapter 3 provides information on the selected rock samples collected from different rock formations of Pakistan. It also discusses the research methodology adopted for laboratory research and analysis scheme. More specifically it lists the detailed research work conducted by adopting the relevant test standards like ASTM, ISRM suggested method, AFNOR, NTNU/SINTEF standards. Also describes the methodology of conducting petrographical thin section study.

Chapter 4 displays the results obtained from the laboratory work performed during this research study together with the computational procedures of different wear indices including Schimazek's F-Value, RAI and CLI.

Chapter 5 discusses the statistical evaluation of CERCHAR abrasivity index (CAI) measurement methods at the stylus tip, the effect of saw cut and freshly broken rock surfaces on CAI, as well as the relationships of CAI with quartz content, quartz equivalent content, mineral grain sizes, wear indices and rock mechanical and physical properties. Additionally an explanatory model is proposed explaining the dependence of CAI on petrographical paramteres and other rock properties.

Chapter 6 includes statistical evaluation of the effect of water saturation on the measured CAI values. A relationship between dry and saturated CAI values measured on fully saturated sedimentary rocks is also proposed. More over a multiple regression model is also developed based on saturated CAI values as well as wear indices including Schimazek's F-value and RAI computed from saturated rock strength properties and mechanical and physical properties of saturated sedimentary rocks.

Chapter 7 discusses the correlations of LCPC abrasivity co-efficient (ABR, g/t) with the CAI values, petrographical parameters and phyisico-mechanical rock properties. The dependence of LCPC breakability index (BR, %) on rock properties is also discussed. Additionally the effect of rock water content on the LCPC indices (ABR and BR) is also evaluated.

Chapter 8 discusses the parametric study carried out with NTNU/SINTEF rock abrasivity method comprising on Sievers'J-Value (SJ) and Abrasion Value Steel (AVS) tests on selected rock samples. The AVS test is explored by varying the grain size of rock abrasion powder as well as by changing the test speed. Moreover Cutter Life Index (CLI) is also computed using SJ and AVS values for the selected rock samples. Relevant relationships of CLI with CERCHAR abrasivity index (CAI), LCPC abrasivity coefficient (ABR) and rock properties are included.

Chapter 9 presents the main conclusions of this research study, and suggests recommendations for future work.

2. LITERATURE REVIEW

The review of literature presented in this chapter is divided into three major sections; the first section discusses rock abrasivity and wear of rock cutting tools, the second section describes various methods for the measurement of rock abrasivity; whereas different soil abrasivity measurement methods are detailed in the third section. To date numerous research studies have explored different laboratory scale test methods to measure wear of rock cutting tools and the influence of rock properties on them. The abrasivity of rocks can be assessed or evaluated either by performing laboratory tests or by using the empirical relationships already developed for similar rock formations. Normally, during planning or pre-feasibility stages of mega rock excavation projects, correlations are preferred due to time constraints and the ease of estimation of rock abrasivity they provide. Various researchers have proposed correlations based on rock properties to estimate wear indices (CERCHAR abrasivity index, LCPC abrasivity Coefficient, Cutter Life Index, Quartz content, Quartz-equivalent content, Schimazek's F-value, Rock Abrasivity Index amongst others) which in turn provide the abrasivity potential of specific rocks. These correlations provide theoretical support for the current research.

2.1. ROCK ABRASIVITY AND WEAR OF ROCK CUTTING TOOLS

2.1.1. Rock Abrasivity. Abrasion is the wearing or tearing away of particles from the working surface of a rock cutting tool (Yarali et al., 2008; Labas et al., 2012). Abrasion controls the wear life of cutting tools in any rock excavation process ranging from small holes drilled for blasting to large diameter tunnels bored by the tunnel boring machines (TBMs) (Rostami et al., 2013). Technical rock properties consist of hardness, drillability and rock abrasivity (Labas et al., 2012). According to Verhoef (1997) rock abrasivity depends upon the characteristics of cutting tool, the properties of rock and the prevailing conditions of temperature and pressure. Atkinson et al. (1986a) have mentioned numerous factors that affect the rock abrasiveness including its mineralogical composition, hardness of mineral constituents, shape and size of grains, type of matrix material and physical rock properties like strength, hardness and toughness. West (1981)

has also explained that the abrasiveness of a rock however, is not necessarily the same as the abrasiveness of its constituent minerals, other factors for instance cementing, grain size and angularity etc. all play a role in its abrasivity.

Numerous past studies define the term rock abrasivity in different ways; Verhoef (1997) refers abrasivity to characteristics of the interaction of two objects and as a concept has not been explicitly defined. Szlavin (1974) uniquely defines rock abrasivity as the mean rate of increase in specific energy required to drill consecutive holes. According to Suana and Peters (1982), the resistance of a tool to wear when in contact with a rock is the most common principle for measuring the abrasivity of a rock. Whereas, Labas et al. (2012) describes rock's abrasivity as its ability to wear off the working surface of cutting tool in process of mutual interaction between the tool and the rock in mechanical rock cutting.

2.1.2. Wear of Rock Cutting Tools. In mining and civil engineering projects rock excavation is achieved either through conventional drill and blast method or by employing mechanized excavators like TBMs, roadheaders, continuous miners, drum shearers, planers or plows, bucket wheel excavators, dozers, backhoe excavators and front end loaders etc. Even in the petroleum industry, extensive drilling is required to penetrate deep seated underground reservoirs. Rock cutting by aforementioned excavators and drilling is achieved by subjecting cutting tools to the rock. The rock cutting tools (bits, discs and picks among others) experience wear or blunting when they are exposed to the different rock surfaces. Not only the cutting tools suffer from wear but also other parts of the costly excavators coming in contact with the hard and abrasive ground suffer from excessive wear (Fowell and Abu Bakar, 2007). Therefore it is prudent to evaluate the replacement frequency of cutting tools earlier in the project planning phase because the cost of cutters as well as their replacement time will eventually decrease machine utilization and productivity (Hamzaban et al., 2014b).   In one case history (Port Hedland harbor dredging project) reported by Verhoef (1997) the wear on cutting teeth of the dredger was almost four times higher than what was anticipated, regardless of the fact that the rocks being dredged were low in strength. It was mainly due to the presence of large angular crystals of quartz in the dredged material.

Wear is defined as the progressive loss of material from the working surface of a solid body (cutting tool) due to its interaction with the counterbody (rock). Interaction means the contact and relative sliding motion of solid body against a solid, liquid or gaseous counterbody. In the discipline of friction, lubrication and wear called as tribology it is well known that wear is a system dependent process. For example the elements involved in a tribological system of a rock cutting tool consist of; the solid body (steel cutting tool) which is the wearing part of the system, the counter-body (rock) which is the body causing wear, the lubricant or interfacial medium (gouge or crushed rock) and the cutting environment of the system like air or water (Verhoef, 1997). According to Büchi et al. (1995) wear is the result of the material properties of the tool (steel quality), the rock properties (strength and mineralogical composition) and the type of interaction between them (impact, scraping, boring, grinding etc.). In effect wear and frictional characteristics of a material are not intrinsic properties but these are behavioral parameters related with the operational circumstances (Stolarski, 2000).

Zum Gahr (1987) describes five classes of wear based on the type of motion involved; sliding, rolling, oscillation, impacting and erosion. According to Deketh (1995) the wear of rock cutting tools (chisels, picks and bits) is mainly caused by impact and sliding motion at the tool rock interface. Impact directly causes wear by cracking or flaking and indirectly by weakening the tool material microstructure; whereas sliding wear or grooving wear is caused by the sliding motion of a rock cutting tool over a rock surface. There are two types of wear involved in mechanized excavation applications; (1) primary wear which is the likely wear of indenters mounted on a cutting tool from usual rock excavation process, allowing replacement at suitable time intervals, and (2) secondary wear, which is unexpected and usually takes place when the primary wear on the cutting indenters is excessive. It leads to the wear of the structures on which cutting tools are mounted (spokes of cutting head or cutter mounting saddles and wear on unexpected surfcaes) (Nilsen et al., 2007).

2.1.3. Wear Mechanisms. Johnson and Fowell (1986) citing Larson-Basse (1973) and Altinoulk (1981) report the four major wear mechanisms namely; (1) abrasion (2) impact encompassing micro-spalling and gross brittle failure (3) thermal fatigue causing deep cracks in the cutting tool and finally (4) damage due to vibration. In

roadheading applications the examination of worn out tools clearly demonstrated abrasion as the dominating wear mechanism. Zum Gahr (1987) also outlines four fundamental wear mechanisms including adhesive wear, abrasive wear, surface fatigue and tribochemical reaction. Figure 2.1 explains the four basic wear mechanisms.
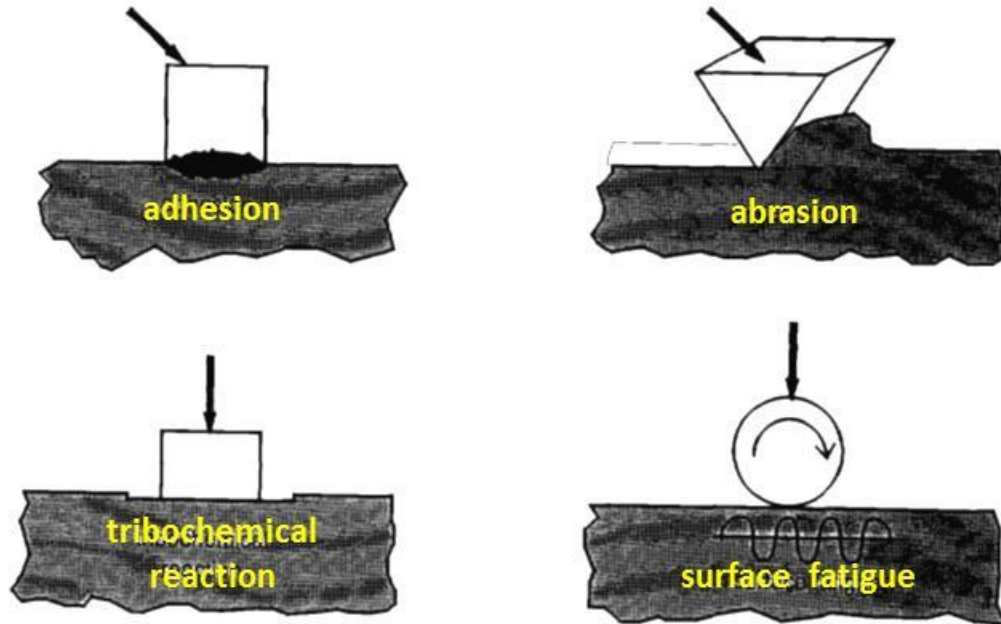
Figure 2.1. Four fundamental wear mechanisms (after Zum Gahr, 1987).

2.1.3.1. Abrasive wear. Abrasive wear is a process causing removal or displacement of material ("wear") at a solid surface due to the existence of hard particles in between or embedded in one or both of two solid surfaces in relative sliding motion or due to the presence of hard protuberances on one or both of the two moving surfaces (two-body abrasion). If the abrasive particles are allowed to roll, rolling abrasion or three-body abrasion occurs. The ratio of abrasive hardness to the material hardness (hardness contrast) of two solid surfaces is basic aspect in abrasive mechanisms. Wear does occur when a softer abrasive is rubbing against a harder material (low level wear) however, the amount of wear increases drastically when the contrast in hardness of two materials approaches about 0.7 to 1.0 (Verhoef, 1997). West (1989) emphasizes the quartz content of rocks to be one of the most important factors contributing towards the abrasive wear. The higher the quartz and hard mineral content in the rock, more is the abrasive wear of the tool.

According to Deketh (1995) in abrasive wear four types of material failure can exist: microploughing, microcutting, microfatigue and microcracking. In more ductile materials for example steel, microploughing, microcutting and microfatigue are the prevailing types of material failure. In an ideal case, microploughing due to single pass of an abrasive particle does not result in any detachment of material from a wearing surface. A prow is formed ahead of the abrading particle and material is continually displaced sideways to form ridges adjacent to the groove produced. However during microploughing material loss can occur due to many abrasive particles which are acting simultaneously or successively. Material may be ploughed aside repeatedly by passing particles and may break by fatigue. Microcracking is related to brittle materials like tungsten carbide. Figure 2.2 illustrates four types of material failure in abrasion.
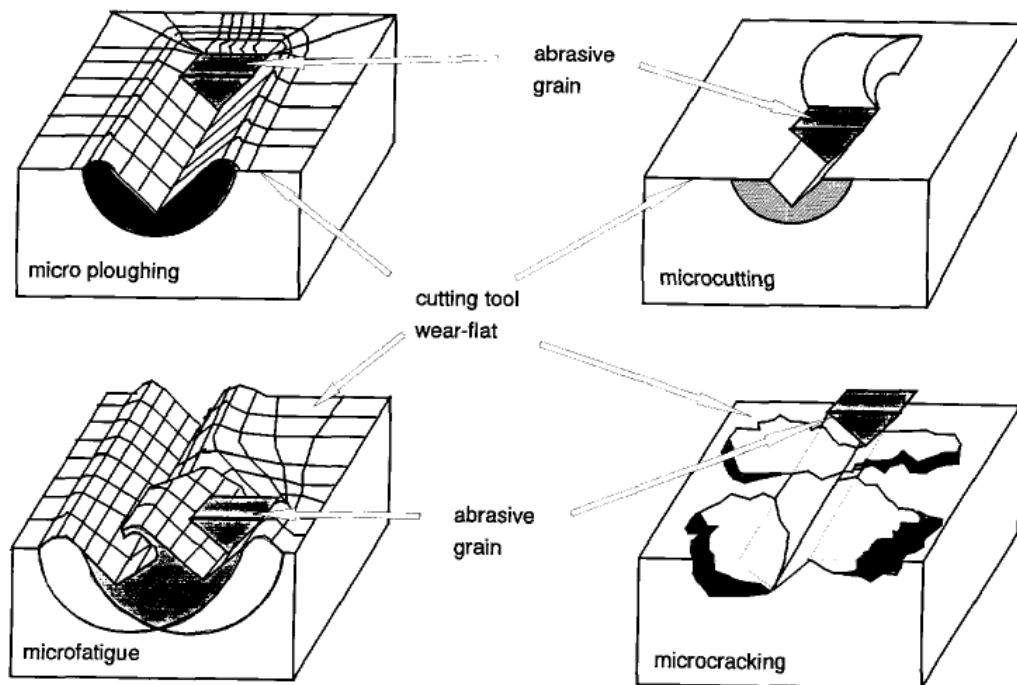
Figure 2.2. Types of material failure in abrasive wear (Zum Gahr, 1987).

2.1.3.2. Adhesive wear. Deketh (1995) describes that adhesive wear generally occurs due to local bonding between sliding solid surfaces resulting in material transfer through the development of localized cold welded junctions under a load and thereafter shearing of these junctions tangentially. Mechanism of adhesion is shown in Figure 2.1, during which material transfer can take place from one surface to the other. Adhesive

wear is less prevalent as compared to abrasive wear and is induced when similar materials slide past each other without lubrication. Adhesive wear is reported to be controlled by the cutting velocity, cutting tool geometry, conductivity and temperature sensitivity of the tool material, rock mechanics properties as well as texture and composition of rock fabric.

2.1.3.3. Surface fatigue. Wear due to surface fatigue is characterized by generation of cracks and subsequent material flaking caused by repetitive dynamic loading of the solid surface. Repeated sliding contact of asperities on the surface of solids in relative sliding motion may result in surface fatigue on a microscopic level (Deketh, 1995). The mechanism of surface fatigue is illustrated in Figure 2.1.

2.1.3.4. Tribochemical reaction. Wear due to tribochemical reaction is illustrated in Figure 2.1, and can be described as the corrosive or oxidation reaction caused during the rubbing contact of two surfaces with the environmental medium. Friction due to sliding motion of the surfaces results in temperature rise as well as removal of the protective oxide films. (Deketh, 1995).

2.1.4. Wear Mechanism of Cemented Carbide Tools. The main purpose of this part of literature review is to summarize in brief the past investigations carried out on the topic of tool wear during rock excavation. The earlier research shows that numerous wear mechanisms are operating when mechanized excavator is cutting rock with tungsten carbide equipped drag tools.

Doeg (1960) explained the sequence involved in the wear of tungsten carbide tools. In the first instance cobalt matrix wears away which leads towards the atmospheric exposure of tungsten carbide grains. Subsequently, the exposed tungsten carbide grains get fractured and finally their removal from the cobalt matrix occurs. He further suggested improving the wear resistance of tungsten carbide alloy by reduction in its cobalt content to a minimum.

Golden and Rowe (1960) proposed a rebuttal to the wear mechanism suggested by Doeg (1960). They proposed that with the cobalt-tungsten carbide alloy, soft cobalt matrix and the hard grains of tungsten carbide both wear together progressively during dry sliding.

Osburn (1969) studied the wear mechanisms of rock cutting tools and highlighted four wear mechanisms functional during rock cutting process as (1) abrasive and frictional wear (2) fatigue and micro cracking of surface layers (3) gross failure due to impact loading and (4) thermal shock and thermal fatigue.

Larsen-Basse (1973) explained that the severity and type of wear depends upon the abrasivity and strength of the rock as well as also on the properties of insert material. The author indicated abrasion, thermal fatigue, spalling due to surface impact and spalling due to surface impact-fatigue as major wear producing mechanisms.

Blombery et al. (1974) explained the probability that any of the five distinct micro-mechanisms of wear including micro machining, impact, adhesion, thermal stress and chemical reactions is responsible for the occurrence of all macroscopic wear phenomena.

Larsen-Basse et al. (1974) conducted rotary drilling tests and accomplished that the distribution of cobalt throughout the tungsten carbide skeleton is one of the most significant parameters in determining the physical properties of material and performance during drilling process. They concluded that the tools of all cobalt contents wear by a combination of cobalt erosion and micro-fracturing of cobalt framework.

Kenny and Wright (1974) performed scratch tests by sliding a quartz pin on a polished tungsten carbide surface and examined that on increasing the number on sliding passes, surface cobalt was appeared and formed coating over the carbide grains thereby destroying the structural details. However, as the number of sliding passes further increased, the surface cobalt was progressively removed and the grain structure was revealed once again.

Bailey and Perrot (1974) highlighted abrasion, thermal fatigue and surface impact spalling as three common mechanisms involved in the wear of tungsten carbide composites utilized in rotary cutting machines in the mining industry. The authors also described that in the case of abrasive rocks low cobalt contents ($\approx$ 6 wt. %) are appropriate, while for non-abrasive rocks higher cobalt contents ($\approx$ 12 wt. %) provide best performance. Similarly for stronger rocks where impact levels are high, small grains of tungsten carbide ($\approx$ 1 μm) should be used, and in the case of weaker rocks where thermal fatigue becomes important, large grains of tungsten carbide ($\approx$ 3 μm) are utilized.

Brainard and Buckley (1975) dynamically observed the wearing process at the microscopic level by employing a Scanning Electron Microscope (SEM). They concluded that the cobalt binder in tungsten carbide alloy mainly reduces both friction and wear. In other words the binding action of cobalt reduces separation of grains and builds a thick polished layer due to its low shear strength film-forming characteristics. These results were in agreement with the earlier findings of Osburn (1969) and Kenny and Wright (1974).

Stjernberg et al. (1975) performed rotary and percussion drilling in sandstone, magnetite and granitic rocks to study tool wear mechanisms. In the case of rotary drilling which is analogous to rock cutting, they found working temperature as the main factor influencing wear properties of rock drill inserts. At low temperatures wear occurs by fracturing and removal of individual grains. Alternatively at high working temperatures and stresses the cemented carbide may deform plastically due to deformation and sliding of the grains. In the case of percussive drilling the repeated hammer blows cause great temperature variations in the surface region of drill bits, leading to high tensile stresses.

Lagerquist (1975) studied the propagation of thermal fatigue cracks in tungsten carbide (WC-Co) substrate and observed that nucleation and propagation of surface cracks take place in cemented carbide tools when subject to repeated severe thermal shocks. Under low wear states these cracks are interconnected to develop a craze pattern in the surface, which is the preliminary stage in the formation of snake-skin surface. The cited author established that by increasing both the cobalt percentage and tungsten carbide grain size the number of thermal fatigue cracks increase.

Altinoluk (1981) described that multiple wear mechanisms may be active simultaneously although the prevailing mechanism generally masks the effects of other types. Also practically it is observed that controlling the occurrence of one wear type usually results in the appearance of another wear type, therefore a compromise is necessary for attaining optimum wear resistance. According to the cited author two parameters namely the cobalt content and carbide grain size play key role in wear resistance. For a given grain size the wear rises with increasing cobalt content and vice versa. Meaning wear increases with increasing cobalt percentage and carbide grain size in the range of 6% to 14% and 1.2 μm to 6.0 μm respectively. The highest resistance against

abrasion is achieved with the combination of low cobalt content and small grain size (6 wt. % Co and 1.2 μm powder grain size).

Rogers and Roberts (1991) worked on the wear mechanisms related with mechanical rock excavators equipped with point attack picks and concluded that the most probable reason of pick failure is initial blunting of the carbide insert either through abrasion or frictional mechanism. This blunting of the carbide insert will lead to pick failure in either of two ways; due to the considerable rise in cutting force magnitude results in serious increase in temperature and finally damage to the carbide insert or alternatively the insert fails catastrophically through a brittle failure mainly due to increase in cutting force.

Plinninger (2008) described four basic wear processes associated with button drill bits in hard rock drilling applications including abrasive wear, macroscopic brittle failure of material, thermal wear due to high tool temperature and Special wear processes (mainly cavitation and erosion among others). The cited author also developed a classification scheme of wear types for button bits which is presented below:

Table 2.1. Classification chart of Button bit wear type (after Plinninger et al., (2002)).

Type of wear	Wear code	Description
Abrasive wear	BB-A1	Normal wear- when tool body and button inserts are evenly worn out in abrasive rocks having high compressive strength.
	BB-A2	Predominant wear of tool body - Typical phenomenon observed in drilling abrasive and weak rocks due to deep penetration of bit into the rock mass accompanied by large flow of rock debris.
	BB-A3	Possible falling or breaking out of buttons as whole due to insufficient embedding. Drilling conditions are same as in BB-A2 wear scheme.
	BB-A4	Wear of diameter in which buttons and tool body are primarily worn down at the periphery walls. Typical phenomenon observed in hard and highly abrasive quartzites as well as under unstable and highly stressed abrasive rock conditions.
	BB-A5	Continual wear of diameter. Extreme reduction of the bits diameter with possible breaking out of the peripheral buttons.
Wear due to macroscopic tool material failure	BB-F1	Macroscopic button failure in which buttons are mainly broken. This failure occurs due to high rates of tool wear mostly related to the characteristics of rock mass, machinery and tools than to the rock abrasivity. The rock mass properties responsible for BB-F1 type failure are heterogeneous high strength rock types accompanied with open or soil filled joints or heterogeneous rocks with extremely hard components (>80 MPa) having diameter of around 5 cm such as conglomerates and breccias.
	BB-F2	Complete button removal out of the tool body mainly by virtue of lack or bad soldering of buttons into the steel body.
	BB-F3	Failure of bit shank due to mishandling or manufacturing faults.
Thermic wear	BB-T	Thermal wear of bit which depends on the efficiency of flushing system. For example under normal circumstances water acts as an effective flushing and cooling media for button bits. The safe temperature limit to avoid thermal wear is 40° C.

Type of wear	Wear code	Description
Special wear processes	BB-Sp1	Special type of wear in which bit is totally worn down below the buttons and usually occurs when the bit is not changed in timely manner. In BB-Sp1 wear type it may be difficult to identify the predominant wear process involved.
	BB-Sp2	Special type of wear in which flushing ports and flutes are widened and may even remove embedding of central buttons. Caused primarily due to utilization of aggressive flushing fluids or fluids containing abrasive particles in suspension.

2.2. ROCK ABRASIVITY MEASUREMENT METHODS

At present a number of rock abrasivity measurement methods are available that can be categorized into two broad categories, namely petrological methods and mechanical methods (West, 1981; Majeed and Abu Bakar, 2015). Petrological methods include Moh's scratch hardness, Rosiwal hardness, Vickers hardness, Knoop hardness, silica content, quartz content, quartz equivalent content, grain size, Schimazek's F-value, RAI amongst others. Mechanical methods comprise indentation hardness test, CERCHAR abrasiveness test, pin on disc test, modified taber abrasion test, core abrasion test, modified Schmidt hammer test, rock scrapping test, steel cube test, LCPC test and NTNU/SINTEF abrasion test. Amongst the test methods available for rock abrasivity measurement, the CERCHAR test, LCPC test, NTNU abrasion test and wear factors (Schimazek's F-value, RAI) from petrographic thin section analysis have gained popularity over the past several years.

2.2.1. Petrological Methods. These methods are based on the estimation of quantitative mineralogical composition of rocks either through petrographical thin section analyses or by using X-ray diffraction (XRD) technique if the rock sample contains fine grained minerals (i.e. grain size less than 0.1 mm). The mineral content is then combined in some way with the hardness values of the individual minerals (West, 1981). Many earlier investigations also defined abrasiveness of rocks in terms of wear factors including Schimazek's F-value and Rock Abrasivity Index (RAI) by combining petrographic parameters with the strength properties of rocks. The petrological rock parameters provide a suitable mean to determine the abrasiveness of broad variety of rocks (Atkinson et al., 1986a; Yarali et al., 2008) and have also been used in conjunction with the mechanical abrasivity measurement methods by a number of researchers.

According to Suana and Peters (1982) the mineral contents of rocks chiefly define the CERCHAR abrasivity index.

2.2.1.1. Mohs' scratch hardness. Rock abrasivity can be expressed in a convenient and simple way by using a relative scale of mineral hardness, known as Mohs' scale of hardness. This hardness scale was introduced by the Austrian mineralogist Friedrich Mohs in 1824 (West, 1989). It comprises of ten minerals organized in the order from softest to hardest. The scratch test corresponds to the likelihood of softer minerals getting wear or abrasion under the contact stresses with the harder minerals or objects (Ghasemi, 2010). West (1989) conducted CERCHAR abrasivity index (CAI) tests on six selected minerals of Mohs' scale including gypsum to quartz. The test results showed a high degree of correlation ($R^2 = 0.96$) between hardness values of Mohs' scale and the corresponding CAI values. Mohs' scratch hardness is further used for the calculation of a geotechnical parameter known as Abrasive Mineral Content (Plinninger, 2008).

2.2.1.1.1. <u>Abrasive mineral content (AMC)</u>. AMC also called the abrasiveness mean hardness of a rock using Mohs' hardness number can be determined by multiplying the fraction or percentage of each mineral by its Mohs' hardness number which are then summed up to give the mean hardness value for the entire rock (West, 1981; Plinninger, 2008). The major disadvantage of employing Mohs' hardness scale in the calculation of abrasiveness mean hardness of a rock is that Mohs' scale treats the hardness numbers as quantitative measure instead of the rank orders. Further, the parameter (AMC) does not take into account the grain size, grain angularity and its degree of cementation in the rock (West, 1981). Plinninger (2008) highlighted that since the rock strength is omitted in the calculation of AMC, therefore it is a drawback of using this parameter.

2.2.1.2. Rosiwal grinding hardness. Rosiwal (1896) developed a grinding test on a metallic or glass disc. He used an abrasive corundum powder (0.2 mm size) in very small quantities. During test the rock samples were hand-pressed against the rotating grinding disc until the abrasive powder had lost its effectiveness, generally after 5 to 8 minutes. Later a grinding time of 8 minutes was taken as standard and the quantity of corundum powder was specified at 100 mg (Rosiwal, 1916). The rock specimens used in

the test had a specified surface area of 400 mm^2. Verhoef (1997) regarded Rosiwal hardness scale as a measure of the resistance of rock or mineral against abrasive wear. He used the hardness data of Rosiwal (1896, 1916) and performed linear regression analysis over a data set of 50 pairs to establish the following correlation equation:

$$MH = 2.53 + 0.906 \text{ (ln RosH)} \qquad (R^2 = 0.88) \qquad\qquad (2.1)$$

Where; MH = Mohs' hardness number and RosH = Rosiwal hardness number.

2.2.1.3. Silica content. West (1981) described that the silica content of rocks can be used to measure rock abrasivity. Silica content is quantified by conducting a chemical analysis of a fine rock powder or alternatively by employing the X-ray fluorescence (XRF) technique (Er and Tugrul, 2016). The silica content of a rock specimen will show the quartz content as well as the content of other silicate minerals present such as feldspars, micas and clay minerals. The major drawback of using silica content as a measure of rock abrasiveness is that it does not consider the particle size, angularity and grain cementation into account. Recently some studies have used silica content to describe rock abrasivity and also to develop relationship for the prediction of rock cutting tools. Adebayo and Akande (2015) related the wear rate of button drill bit with the silica content of selected rocks at Navachab Gold mine location. They found a linearly positive correlation and developed the following prediction equation:

$$WR = 0.1734 \text{ (SiO}_2) - 12.343 \qquad\qquad (2.2)$$

Where; WR = Wear rate of button drill bit (mm/meter);

SiO_2 = Silica content expressed in volume %.

Er and Tugrul (2016) identified the chemical composition of selected granitic rocks from Turkey and found a reasonable correlation between the silica content (SiO_2) and the CERCHAR abrasivity index (CAI) values, which is reproduced below:

$$CAI = 3.41 + 0.03 \text{ (SiO}_2) \qquad\qquad (2.3)$$

2.2.1.4. Quartz content. Quartz content is also referred to as free silica content and is quantified either from running petroghraphical analysis or by using X-ray diffraction (XRD) technique. In case the rock specimen contains fine quartz particles (< 0.1mm) then XRD technique is preferred, as the petrographic analysis poses difficulty in identifying and counting fine grains therefore leading to under estimation of measured

quartz content. The best merit of using quartz content as a measure of rock abrasivity is its simplicity and rapid quantification instead of running the complete mineralogical analysis. The disadvantage is that, like AMC, EQC and silica content it also does not take into consideration the grain size, shape or angularity and binding strength of grains. West (1981) citing Mcfeat-Smith and Fowell (1977) has cautioned that quartz percentage only is not adequate to describe the rock abrasiveness; the cited authors established that during roadheading in Bunter and Keuper sandstone rocks, the tool wear rate was dependent on the grade of cementation rather than on the quartz content.

Some past investigators have used quartz content to estimate the wear rate of rock cutting tools. Schimazek et al. (1976) correlated the abrasive wear rate of point attack steel picks with the quartz content. Mcfeat-Smith and Fowell (1977) developed a multiple non-linear model based on laboratory tests of 71 sedimentary rock units for the estimation of cutting wear from rock properties including rebound hardness (Shore Scleroscope), cementation coefficient and quartz content. Similarly, Roxborough (1987) performed core abrasion tests on 112 different sedimentary rocks belonging to major formations occurring in different mining and tunnelling projects in Australia and UK. He developed a correlation chart between the quartz content and wear rate of medium grade tungsten carbide picks applied in sedimentary rocks. Farrokh et al. (2013) found quartz content as the most influential property for the prediction of TBM cutters life. They proposed a model based on quartz content and cutter life data from 135 TBM projects conducted in a variety of rock types. Adebayo and Akande (2015) observed an exponential relationship between the quartz content and wear rate of button bits and suggested the following correlation equation:

$$WR = 0.00000004e^{4.2669QZ} \tag{2.4}$$

Where; WR = Bit wear rate (mm/m);

QZ = Quartz content (%).

2.2.1.5. Equivalent quartz content (EQC). West (1981) utilized Rosiwal hardness scale for the determination of abrasiveness mean hardness in order to overcome the drawback of Mohs' hardness scale. He multiplied the mineral contents by their respective Rosiwal hardness numbers which were then summed up to give the abrasiveness mean hardness value for the entire rock. In Rosiwal scale the number

quantitatively expresses the hardness in relation to corundum. The author further mentioned that abrasiveness mean hardness values calculated using Rosiwal hardness scale do not consider the size, angularity and cementation strength of grains. Also it is not certain that how these parameters affect rock abrasiveness. Schimazek and Knatz (1970) defined equivalent quartz content (EQC) as the mineral content expressed in hardness of quartz using Rosiwal's hardness scale in volume percentage. Er and Tugrul (2016) citing Thuro (1997) report the following equation for the calculation of equivalent quartz content:

$$EQC = \sum_{i=1}^{n} A_i . R_i \qquad (2.5)$$

Where;

A = Mineral quantity (%);

R = Rosiwal hardness number;

n = number of minerals.

Very little work is available correlating EQC with the life time (m/bit) or wear rate of rock cutting tools. Plinninger (2008) citing Thuro and Plinninger (2003) report an estimation chart (Figure 2.3) for the calculation of lifetime of 43 to 45 mm button drill bits employed in hard rock drilling applications, by using equivalent quartz content (EQC) of different rocks.

Adebayo and Akande (2015) have proposed the following statistical model for the prediction of wear rate of button bits from equivalent quartz content and silica content of rocks:

$$WR = -10.354 - 0.64 \ (EQC) + 0.184 \ (SiO_2) \qquad (2.6)$$

Where;

WR = Wear rate in mm/m;

EQC = Equivalent quartz content (%);

SiO_2 = Silica content (%).
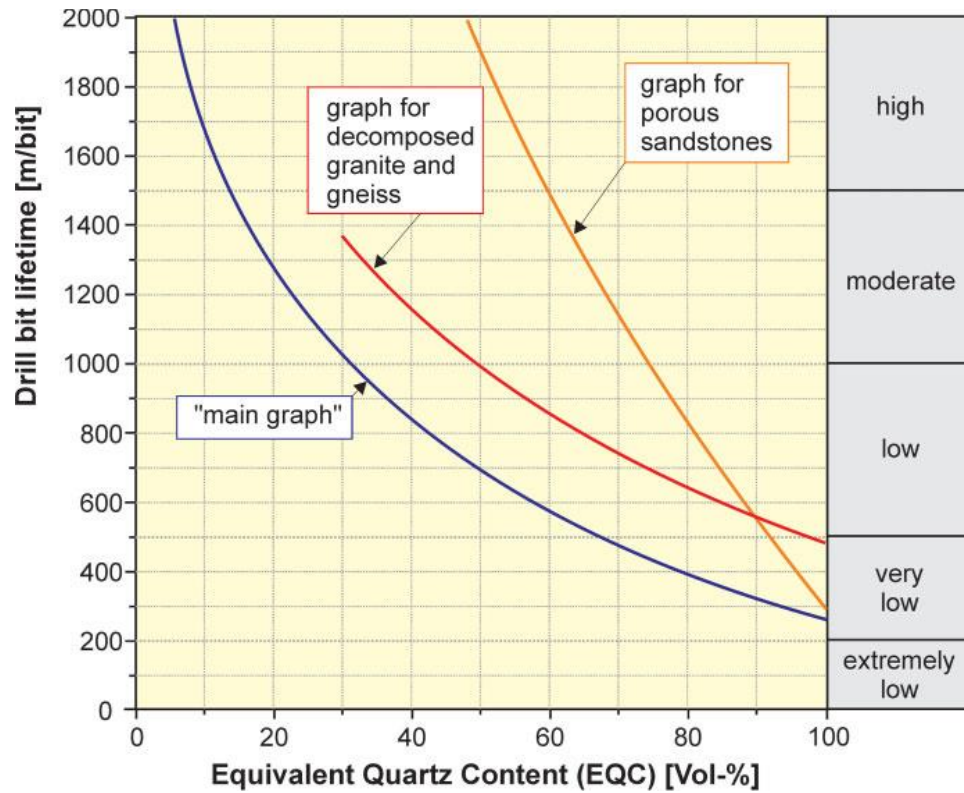
Figure 2.3. Graphs for the estimation of drill bit lifetime from equivalent quartz content (after Thuro and Plinninger, 2003).

2.2.1.6. Schimazek's F-value. The wear factor "F-value" was developed by Schimazek and Knatz (1970). They proposed the following equation based on Schimazek's pin-on-disc test cited in Verhoef (1997):

$$F = \frac{Qtz.eq \times \emptyset \times BTS}{100} \ (N/mm)$$

(2.7)

Where;

$Qtz.\,eq$ = Mineral content expressed in hardness of Quartz using Rosiwal's hardness scale (in volume %);

$\emptyset$ = Mean diameter of mineral grains (mm);

BTS = Brazilian tensile strength (MPa).

Verhoef (1997) gives a classification table (Table 2.2) for the abrasivity of rocks based on the Schimazek's F-value.

Table 2.2.Classification based on F-value of the abrasivity of rocks (after Verhoef, 1997).

Schimazek's F-value (N/mm)	Abrasiveness	Order of pick point consumption (m³/pp)
F < 0.05	Low abrasiveness	100
0.05 < F < 0.1	Abrasive	
0.1 < F < 0.5	Highly abrasive	
F > 0.5	Extremely abrasive	10

Schimazek's F-value has been used in past investigations to estimate the wear of rock cutting tools. While published literature also shows correlation developed between the results of wear obtained on experimental test pieces and Schimazek's F-value. Becker and Lemmes (1984) correlated CERCHAR abrasivity index (CAI) with the Schimazek's F-value and proposed a linear trend between the two rock abrasivity measurement methods. Kumaraswamy and Mozumdar (1987) studied the performance prediction of bucket wheel excavation machine applied for cutting lignite coal. They utilized Schimazek's F-value for the estimation of abrasivity of lignite as well as associated coal measures rocks and also determined the impacts of abrasive wear on the bucket teeth. Paschen (1980) conducted Schimazek's pin on disc tests on carboniferous rocks from Ruhr area. The statistical analysis of the test results with Schimazek's F-value showed good linearly positive correlation. Verhoef et al. (1990) performed modified pin on disc tests on glass concrete at the selected lathe rotational speeds of 145 rpm and 275 rpm. In both cases the Schimazek's F-value showed linearly increasing correlations with the measured mass loss on the pins. Deketh (1991) performed pin on disc tests on different rock specimens and found linearly positive relationship between F-value and wear rate of pin. Similarly Bisschop (1991) performed shaper abrasion tests on the same set of rocks earlier tested by Deketh (1991) using pin on disc test. He also found linearly increasing trend between the Schimazek's F-value and wear rate of shaper chisel.

According to Verhoef (1997) the Schimazek's F-value has become an established factor used to evaluate rock abrasivity. Its main value is contained in the combination of petrographical and rock mechanical information. The F-value has been used to compare the performance of roadheaders and other mining machines applied in rock cutting. The author has also provided graphs (Figure 2.4) developed by Voest-Alpine, manufacturers

of roadheaders (Alpine Miner) that predict pick point consumption based on the Schimazek's F-value.
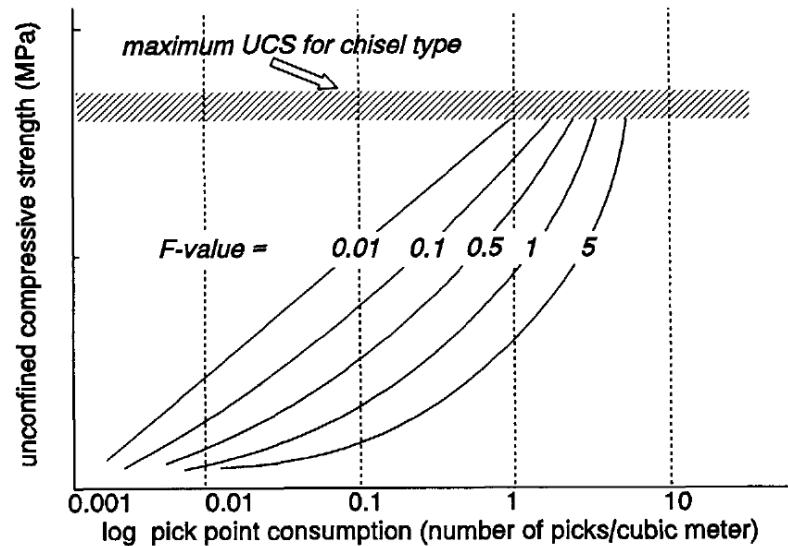
Figure 2.4. Graph being utilized by Voest-Alpine for the prediction of tool consumption (after Verhoef, 1997).

Schimazek and Knatz (1970) used the data from experiments of Krapivin et al. (1976) and proposed the following relationship of the F-value with the critical velocity, beyond which cutting tool experiences extreme rate of wear:

$$V_{critical} = k\, e^{-F} \text{ (m/sec)} \qquad (2.8)$$

Where; $V_{critical}$ = Critical velocity in (m/s);

K = Co-efficient of chisel geometry and critical temperature of the chisel material.

2.2.1.7. Rock abrasivity index (RAI). Plinninger (2010) reports that the Rock Abrasivity Index was introduced in year 2002 (Plinninger, 2002) and first time presented in proceedings of the 9th IAEG congress held in Durban, South Africa (Plinninger et al., 2002). The wear factor RAI suggests an amendment to the equivalent quartz content (EQC) and is mainly appropriate for wear estimations in hard rock applications; however it is also suitable to weak rock types. For relevant rock types the RAI is computed by multiplying EQC with the uniaxial compressive strength (UCS) value as given by the following equation:

$$RAI = \sum_{i=1}^{n} A_i . R_i \times UCS \qquad (2.9)$$

Where; A = Mineral quantity (%);

R = Rosiwal hardness number referred to quartz = 100;

n = Number of all minerals;

UCS = Uniaxial compressive strength (MPa).

According to Plinninger et al. (2002) RAI is suitable for the evaluation of both abrasive wear and wear due to breaking of tool parts, because it takes into account the abrasive minerals content and the rock strength respectively. Plinninger (2002) has also developed a classification table (Table 2.3) which is appropriate for the oral description of rock abrasiveness for using the wear factor RAI. To date limited work is present on correlations of RAI with other rock abrasivity indices. Plinninger et al. (2004) presents a fair logarithmic correlation between CERCHAR abrasivity index (CAI) and RAI based on a data set of 60 rock types, as shown in Figure 2.5.

Table 2.3.Classification based on RAI of the abrasivity of rocks (after Plinniger, 2002).

RAI	Classification
<10	Not abrasive
10-30	Slightly abrasive
30-60	Abrasive
60-120	Very abrasive
>120	Extremely abrasive
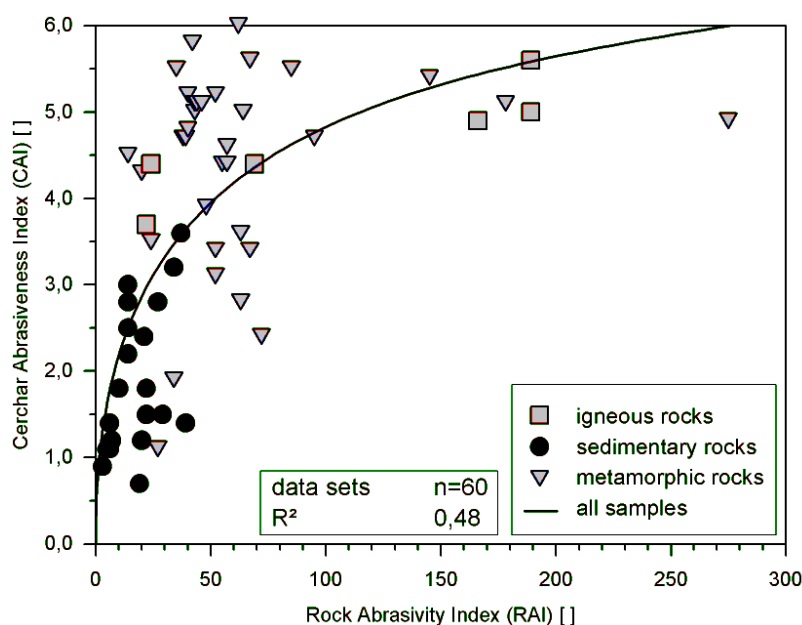
Figure 2.5. Relationship between CAI and RAI (after Plinninger et al., 2004).

Schumacher (2004) has developed the following function which is useful for practical purposes:

$$CAI = 0.9 \times \sqrt[3]{RAI} \qquad (2.10)$$

Where; CAI = CERCHAR abrasivity index;

RAI = Rock abrasivity index.

Plinninger (2002) has reported that RAI shows good prediction results for the evaluation of button bit wear. The author has developed a chart (Figure 2.6) for the estimation of lifetime of 38-56 mm button drill bits based on data from several drill and blast tunneling projects in Western Europe.
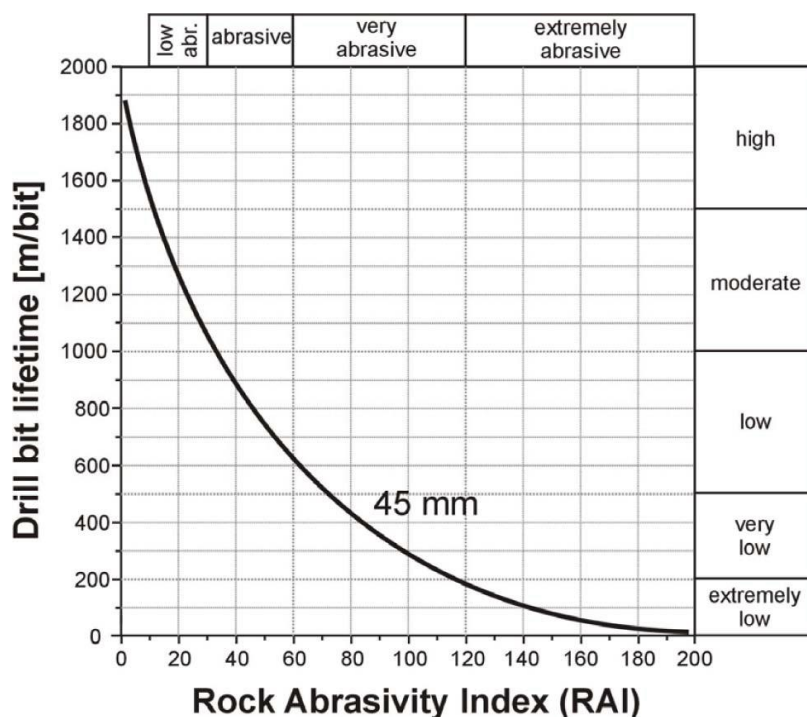
Figure 2.6. Chart for the estimation of button drill bit lifetime from RAI (after Plinninger, 2010).

2.2.2. Mechanical Methods. These test methods utilize either intact rock specimens or rock aggregate (West, 1981) to interact with experimental test pieces. Some of the mechanical tests consider the weight loss of the experimental test pieces before and after the test performance as a measure of rock abrasiveness, while others measure the wear flat developed at the tool-rock interface for the calculation of rock abrasivity index. Mechanical methods are intended for the evaluation of rock abrasivity for the purposes of

mechanical rock cutting by drill bits and roller discs (Labas et al., 2012). The commonly used tests are discussed in this section.

        2.2.2.1. The CERCHAR rock abrasivity test. The CERCHAR abrasivity test was introduced in 1970's by the Centre d'Etudes et Recherches des Charbonages de France (CERCHAR) for abrasivity measurements in French coal mining industry (Yarali et al. 2008; Kasling and Thuro, 2010). Later on this method was adopted by the British coal mining industry and progressively being used by the tunneling industry (West, 1989; Gharahbagh et al., 2011; Rostami et al. 2013). Rostami et al. (2005) classified CERCHAR test apparatus into three generations (Figure 2.7) where the original apparatus developed by CERCHAR (1986) is classed as the first generation machine; the test apparatus developed at Colorado School of Mines (CSM) as the second generation machine; and the CERCHAR test apparatus developed by West (1989) as the third generation machine. The machine design developed by West is commercially available from some manufacturers around the world. Initially CERCHAR test was regulated under the French standard NF P 94-430-1 (AFNOR, 2000), but at present it is the only abrasivity measurement method which has been standardized by the American Society for Testing and Materials (ASTM-D7625-10) and recently ISRM has also suggested method to perform this test (Alber et al., 2014).
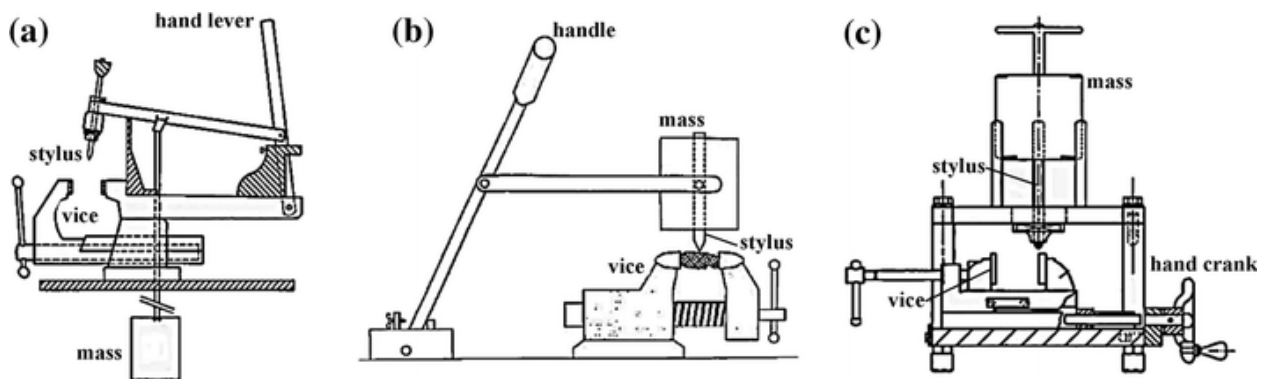
Figure 2.7. Schematic of CERCHAR test apparatus generations, (a) the first generation articulated hand lever type machine by CERCHAR (1986), (b) the second generation articulated hand lever type machine by CSM, (c) the third generation hand crank type machine by West (1989) (after Rostami et al., 2005; Hamzaban et al., 2014a).

The testing procedure of the CERCHAR test consists of applying a steel stylus or pin of 200 kg/mm^2 tensile strength, hardened to Rockwell hardness 54-56 HRC, sharpened to 90° cone angle over the rock surface under a constant load of 70N. The abrasiveness then corresponds to the wear diameter measured in 1/10th mm increments of the flat plane produced by scratching the stylus over a length of 10 mm on the surface of the rock sample, during about one second. The wear flat developed is then read under a microscope of minimum resolution of 30X, which is known as CERCHAR abrasivity index (CAI). The test is performed for at least five times on the same rock surface by using fresh re-sharpened stylus each time and then taking the arithmetic mean of the measured values (CERCHAR, 1986; ASTM-D7625-10; Alber et al., 2014). Table 2.4 presents the classification of CAI values.

Table 2.4. Classification of CAI values.

ASTM-D7625-10		ISRM Suggested Method (Alber et al., 2014)	
Average CAI (HRC=55)	Abrasivity classification	Mean CAI	Abrasivity classification
0.30-0.50	Very low abrasiveness	0.1-0.4	Extremely low
0.50-1.00	Low abrasiveness	0.5-0.9	Very low
1.00-2.00	Medium abrasiveness	1.0-1.9	Low
2.00-4.00	High abrasiveness	2.0-2.9	Medium
4.00-6.00	Extreme abrasiveness	3.0-3.9	High
6.0-7.0	Quartzitic	4.0-4.9	Very high
		≥ 5	Extremely high

The CERCHAR test has widely been used in the mining and tunneling industry due its simplicity and dependable results (Muftuoglu, 1983; Singh et al., 1983; Atkinson et al., 1986 a,b; Plinninger et al., 2004). The results of CERCHAR abrasivity test are utilized as an input parameter in the performance prediction models of TBMs and roadheaders (Rostami et al., 2005; Kasling and Thuro, 2010). Some key features including the simplicity of the testing principle, the ability to utilize small rock samples, relative cost effectiveness and the possibility of on-site testing have made this test globally popular in the field of rock engineering and tunnelling (Plinninger and Restner, 2008). In contrast major drawback of CAI is small scale testing of the rock surface. Another important shortcoming of the test is that the applied stress on the pin is not constant throughout the test due to geometry of the stylus (Rostami et al., 2013).

Although the CERCHAR test is commonly used but there were some reported discrepancies or variations in the test results primarily due to the variations in the testing procedures, test setup used, stylus hardness, rock surface condition and measurement of the wear flat from top or side of the stylus. A number of other parameters affecting the results of CERCHAR tests were also examined in detail by a number of researchers in the past and have been reported in the literature. These parameters include scratch length, force on stylus, speed of scratch, stylus metallurgy and rock properties amongst others (Al-Ameen and Waller, 1994; Plinninger et al., 2003; Fowell and Abu Bakar, 2007; Stanford and Hagan, 2009; Ghasemi, 2010; Hamzaban et al., 2014a; Rostami et al., 2013). Most of the issues mentioned leading to the inconsistent results of the CERCHAR test have been taken care of in the ISRM suggested method by Alber et al., (2014). Moreover limited work is present on the influence of rock saturation on CERCHAR abrasivity index (CAI). The effects of various testing parameters on CERCHAR abrasivity index (CAI) are discussed as under:

2.2.2.1.1. <u>Stylus hardness.</u> In general Higher CAI values are obtained with soft CERCHAR test styli and vice versa (Al-Ameen and Waller, 1994; Michalakopoulos et al., 2006; Fowell and Abu Bakar, 2007; Stanford and Hagan, 2009; Kasling and Thuro, 2010; Gharahbagh et al., 2011; Rostami et al., 2013).

The available standards including CERCHAR (1986), AFNOR NF P 94-430-1 (2000), ASTM D7625-10 and ISRM suggested methods (Alber et al., 2014) all recommend the use of testing pins made of steel with Rockwell hardness of HRC 54-56. However in some past investigations the steel qualities used in different testing sets have been varied in a wider range for different reasons (Plinninger et al., 2003).

West (1989) in a study program used tools made from an alternative EN24 steel heat treated to Rockwell Hardness of C40, as the steel suggested by CERCHAR (1986) specifications was unavailable in Britain. This value was chosen after heat treating EN24 steel tools to different hardnesses and testing them with a specimen of granite until a result about the same as reported for CERCHAR tools was obtained.

Al-Ameen and Waller (1994) in a study conducted on UK coal measures rocks used the standard EN24 test stylus (610 ± 10 Hv) and obtained significantly lower CAI values (less than 0.15). Therefore for weakly consolidated rocks a softer EN3 mild steel

stylus (225 Hv) was used for abrasivity testing relative to the majority of mining equipment. The authors conducted CERCHAR tests using both the hard EN24 and soft EN3 styli on sawn rock surfaces of a range of rocks and developed the following correlation:

CI (EN3) = 0.24 + 2.74 CI (En24) - 0.39 CI^2 (EN24);   (R = 0.87)   (2.11)

Where; CI = CERCHAR abrasivity index.

Rostami et al. (2005) evaluated the CERCHAR test results carried out by different laboratories on the same set of rock samples and concluded that the labs using softer pin can measure and report CAI values between 40-49% higher than those using standard CERCHAR stylus of hardness 56 HRC.

Michalakopoulos et al. (2006) performed CERCHAR tests on a total of 68 rock specimens from six different rock types with steel styli of both HRC 55 and 40. Their investigation came up with the general conclusion that CAI value of a rock sample is decreased with the corresponding increase in steel styli hardness and proposed the following linear relationship for the conversion of CAI_{40} to standard CAI_{55} values:

CAI_{55} = 0.110914 + 0.587356 CAI_{40};   (R^2 = 0.74)   (2.12)

Fowell and Abu Bakar (2007) tested 35 rock samples using soft (220 VPN) and hard (660 VPN) styli, on diamond sawn rock surfaces and proposed the following correlation:

CAI-soft = 1.29 + 1.46 x CAI-hard;   (R^2 = 0.74)   (2.13)

Stanford and Hagan (2009) performed tests on argillaceous quartz sandstone specimens using one steel type styli heat treated to obtain nine different hardness levels from HRC 15 to 60. They found that CAI decreases linearly with hardness and the proposed relationship (Equation 2.4) depicts that the CAI value varies inversely with steel hardness.

CAI = - 0.0766 HRC + 5.80;   (R^2 = 0.739)   (2.14)

Kasling and Thuro (2010) developed a linear correlation of CERCHAR test results carried out with both hard (HRC 54-56) and soft (HRC 40) steel styli. As

anticipated the CAI values obtained for soft pins were higher as compared to the values obtained for standard hard pins. They developed the following correlation:

$$CAI_{55} = 0.725 \text{ x } CAI_{40}; \qquad\qquad (R^2 = 0.94) \qquad\qquad (2.15)$$

Gharahbagh et al. (2011) and Rostami et al. (2013) performed a series of tests on selected suite of seven rock samples using standard styli of hardness (54-56 HRC) and softer styli of HRC (40-42). They conducted CERHAR tests on both saw cut and rough rock surfaces. As expected CAI values with pins HRC 41/43 are higher than CAI values with HRC 54/56 pins for both saw cut and rough rock surfaces.

      2.2.2.1.2. <u>Effect of wear flat measurement procedure.</u> The issue of measurement from top or side has recently been studied by a number of investigators (Rostami et al., 2005, Gharahbagh et al., 2011; Rostami et al., 2013). It is the view of these researchers that the top viewing of the wear flat is although a simple procedure but it poses its own difficulties due to highest operator sensitivity involved. This is more pronounced in fresh broken harder rock surfaces, resulting in non-uniform shape of the wear flat due to splinters or fragments of hard metal. In an earlier study by West (1989) formation of the burr or splinter on the downstream side of the test stylus has also been reported, who suggests disregarding the burr when measuring the wear flat. Rostami et al. (2013) found it difficult to disregard or remove the burr and recommended the use of a new technique developed at NTNU/SINTEF, Norway (Bruland, 2000), suggesting the side viewing of the wear flat of the stylus. The side measurement method developed at NTNU/SINTEF involves the measurement of the correct angle of the stylus tip to provide correct determination of the start and end points of the wear flat produced. This new approach (NTNU/SINTEF technique) of the wear flat measurement procedure from side view of the stylus tip is shown in Figure 2.8.

Recently the ISRM suggested method by Alber et al. (2014) has recommended the side view measurement technique developed at NTNU/SINTEF to determine the exact start and end points of the wear surface at the stylus tip as mentioned by Rostami et al. (2005).
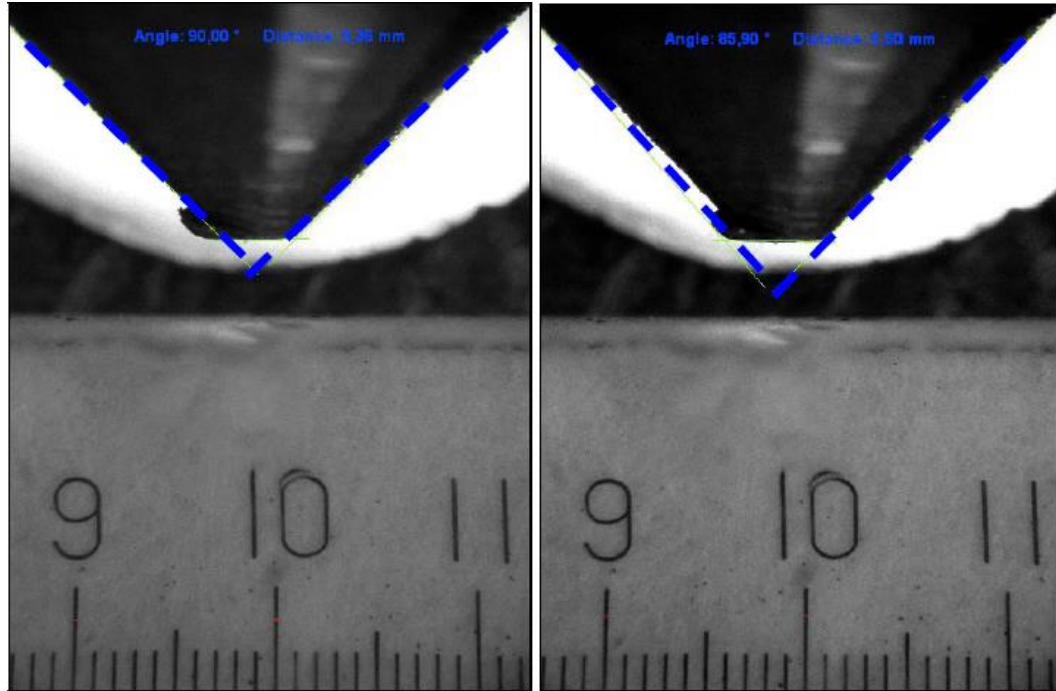
Figure 2.8. Picture of wear flat measurement method using side view of stylus tip by adopting the newly developed NTNU/SINTEF technique. (Left picture) gives the correct measurement with CAI value of 3.5, while (right picture) shows the incorrect measurement of wear flat with CAI value of 5.0 that could be measured from the top view (after Rostami et al., 2005).

2.2.2.1.3. Rock surface condition. The issue of conducting the CERCHAR test on freshly broken or sawn rock surfaces has also remained under investigation for past several years. These researchers (Al-Ameen and Waller, 1994; Plinninger et al. 2003, 2004; Rostami et al., 2005; Abu Bakar, 2006; Fowell and Abu Bakar, 2007; Kasling and Thuro; 2010; Gharahbagh et al., 2011; Rostami et al. 2013, among others) have shown that CERCHAR tests on rough rock surfaces give higher CAI values as compared to sawn surfaces and this difference is more pronounced when the rock is harder and more abrasive. Although the CERCHAR (1986) guidelines, ASTM D7625-10 standard and ISRM suggested methods (Alber et al., 2014) only recommend freshly broken rock surfaces for CERCHAR tests, which closely simulate the real field conditions, where cutting tools are always exposed to rough and broken rock surfaces, but in the case of heterogeneous rocks such as conglomerates, coarse grained granite or schistose rock, it is difficult to achieve suitable test surfaces, therefore, smooth surfaces produced by diamond saw are recommended. Most of the issues mentioned leading to the inconsistent

results of the CERCHAR test have been taken care of in the ISRM suggested method by Alber et al., (2014). Following is a summary of some past investigations correlating the CAI values obtained on freshly broken and saw cut rock surfaces:

Al-Ameen and Waller (1994) in a testing program (UK, coal measures rocks) measured CERCHAR index (CI) using soft EN3 styli (225 Hv) on both polished and natural rock surfaces and found very consistent results with very strong linear correlation ($R^2 = 0.93$) given below:

$$CI \text{ (EN3) natural surface} = -0.01 + CI \text{ (EN3) polished surface} \tag{2.16}$$

Plinninger et al. (2003) conducted CERCHAR tests using both sawn and rough natural rock surfaces, on a total of 77 rock samples. They proposed the following correlation which shows that the CAI values obtained on rough rock surfaces have a CAI of about 0.5 higher than the rock samples with saw cut surfaces:

$$CAI = 0.99 \text{ x } CAI_s + 0.48; \qquad (R^2 = 0.74) \tag{2.17}$$

Where;

CAI = CERCHAR abrasiveness index for standard rough surfaces;

CAI_s = CERCHAR abrasiveness index for saw cut surfaces.

The equation 2.17, proposed by Plinninger et al. (2003) has been adopted by ASTM D7625-10 standards for the normalization of CAI_s values to the standard CAI values for natural surface.

Plinninger et al. (2004) developed a good correlation between the standard rough and saw cut rock surfaces. They observed an increasing influence of surface roughness with increasing CAI values. In contrast with low CAI values, the tests conducted on both rough and saw cut surfaces lead to more or less equal results.

Rostami et al. (2005) in a comparative study program concluded that the CAI measurements conducted on rough rock surface is higher than those made on sawn rock surface. They also observed that although it is not a clear cut trend but it appears like the difference between rough and sawn measurements increases as rock gets harder and more abrasive. This observation matches with the earlier findings of Al-Amin and Waller (1994) and Plinninger et al. (2004). Finally the authors recommended that despite difficulties of obtaining reproducible results on fresh/rough rock surfaces, yet it seem to

be the best choice of test conditions since it represents a better simulation of rock cutting by a tool than a saw cut rock surface.

Fowell and Abu Bakar (2007) carried out CERCHAR tests on 35 rock samples comprising of all three generic rock types. The cited authors developed a correlation between CAI values for freshly broken and saw cut rock surfaces which is reproduced below:

$$CAI = 0.18 + 1.05 \text{ x } CAI_s; \qquad (R^2 = 0.89) \qquad (2.18)$$

Kasling and Thuro (2010) correlated the CAI results of 80 rock specimens, obtained on both rough and smooth rock surfaces and came up with the following relationship:

$$CAI \text{ (smooth surface)} = 0.878 \text{ x } CAI \text{ (rough surface)} \qquad (R^2 = 69\%) \qquad (2.19)$$

Recently the ISRM suggested methods (Alber et al., 2014) has also recommended correcting the CAI values measured on sawn rock surface to the rough rock surface by utilizing the correlation (equation 2.19) established by Kasling and Thuro (2010).

Gharahbagh et al. (2011) and Rostami et al. (2013) performed tests on a set of seven rock samples by utilizing 54/56 HRC and 40/42 HRC styli on both rough and sawn rock surfaces. They concluded that in lower CAI values (non-abrasive rocks) results of testing on sawn and rough surfaces are more or less similar. However in higher CAI values the results of testing on rough surface samples are higher than sawn.

2.2.2.1.4. Test length. According to the testing procedures outlined in CERCHAR (1986) document, AFNOR NF P 94-430-1 (2000), ASTM D7625-10 and ISRM suggested methods (Alber et al., 2014) the length of scratch on the rock specimen must be accurately 10.00 mm.

Al-Ameen and Waller (1994) measured the CERCHAR abrasivity index (CAI) using EN3 (mild steel, 225 Hv) styli at different sliding distances on a variety of rock types (granite, ironstone, sandstones, siltstone, mudstone and seatearth). They observed that the wear generated over approximately 3-10 mm sliding distance was very small relative to that generated by tip shear or abrasion over the first 3mm sliding distance. Finally they came up with the conclusion that 70% of CAI is related to the initial pin

slide of 1mm distance and 30% of the CAI can be attributed to the final 9mm of sliding distance.

Plinninger et al. (2003) performed a series of tests on identical rock samples with different testing lengths. They found that about 70% of the pin wear occurs during the first millimeter of the testing length, about 85% of the CAI is achieved after 2mm and only 15% of the change in CAI is achieved on the last 8mm of the testing length. According to them the testing length would have to be extended to some 5-10 cm to achieve noticeable greater wear flat on the testing pin. Contrary to that Hamzaban et al. (2014a) concluded that in the case of harder and extremely abrasive rocks (granites, quartzitic sandstone, quartzite, schist, anorthosite among others) it is expected that with continuation of the scratching, higher CAI values will be reached.

2.2.2.1.5. <u>Stylus metallurgy.</u> To date little work is available showing the effect of stylus metallurgy on CAI values. Stanford and Hagan (2009) carried out a study relating the CERCHAR test results of seven different steel types (Silver Steel, H13, M340, CALMAX, SVERKER 3, Rigor and S600), heat treated to a constant nominal hardness of HRC 52. They concluded that CAI does not appear to be significantly affected by changes in steel type of the stylus.

2.2.2.1.6. <u>Influence of static load.</u> The standardized testing procedure requires a static load of 70N to be applied on the stylus (CERCHAR, 1986; ASTM-D7625-10; Alber et al., 2014). However some past studies (Ghasemi, 2010; Rostami et al., 2013) have investigated the influence of applied load on CAI value. The cited researchers performed a set of tests on a saw cut quartzite using 40/42 HRC and 54/56 HRC steel styli and varying the applied loads. The test results showed a positively linear relationship between the applied load and CAI value for both the softer 40/42 HRC and standard 54/56 HRC styli. The correlations developed are reproduced below:

$$CAI_{40/42\ HRC} = 0.0144(\text{Applied Load}) + 2.1442 \qquad (R^2 = 0.99) \qquad (2.20)$$

$$CAI_{54/56\ HRC} = 0.0087(\text{Applied Load}) + 2.047 \qquad (R^2 = 0.99) \qquad (2.21)$$

2.2.2.1.7. <u>Influence of testing speed.</u> The standardized testing speed is 10mm/sec for articulated hand lever type machine and 1mm/sec for hand crank type machine (CERCHAR, 1986; ASTM-D7625-10; Alber et al., 2014).

Plinninger et al. (2004) observed that the CAI values derived from both types of testing setups (CERCHAR, 1986; West, 1989) despite the great difference in their testing velocities are generally estimated to be equal. The cited authors further explained that testing velocity may have a major influence on the testing results of the CERCHAR apparatus, when the testing surface is extremely rough or coarse grains force the stylus to bounce, the wear flat may be deformed and testing velocities should be reduced to some seconds/mm.

Rostami et al. (2005) in their comparative testing program highlighted that one of the participating laboratories using the hand crank type Ergotech machine, was consistently running the test on slower speed. The cited authors observed that slow testing speeds resulted in roughly 40% increase in CAI values measured on soft pins (HRC 43).

Ghasemi (2010) and Rostami et al. (2013) conducted a set of tests on limestone, sandstone and quartzite rock specimens to investigate the impact of variability of testing speed. Rock samples were tested for the pin sliding distance of 10 mm stroke in 5, 10, 30 and 60 seconds. They concluded that testing speed does not affect the CAI values significantly.

2.2.2.1.8. <u>Effect of rock properties.</u> Many investigators have proposed correlations of CERCHAR Abrasivity Index (CAI) with the petrographic, physical and mechanical properties of rocks. Table 2.5 summarizes the relationships between CAI and rock properties developed by some previous investigators.

Table 2.5. Correlations of CAI with Rock Properties.

Sr. No.	Parameters	Investigators	Correlation with CAI
1	Uniaxial Compressive Strength (MPa)	Jaeger (1988)	Positive linear correlation between CAI and UCS (Tests performed on hardened mortar-quartz mixture having constant mineralogical composition)
		Al-Ameen and Waller (1994)	1) CAI (EN3, 1mm) = $-$ 1.38 + 0.05 (UCS) $-$ 0.0001(UCS)^2 2) CAI (EN3, 10mm) = $-$ 0.5 + 0.03 {UCS x (1+ $\sum$ Abrasive mineral hardness)} 3) CAI (EN3, 10mm) = $-$ 0.2 + 0.0067 {UCS x (1+ $\sum$ Abrasive mineral hardness)} + 0.000002 {UCS x (1+ $\sum$ Abrasive mineral hardness)}^{2}
		Kahraman et al. (2010)	UCS = -366.0 $-$ 0.9 (VBP) + 155.8 (d) + 10.7 (Vp) + 16.7 (CAI)
		Gharahbagh et al. (2011)	Positive linear correlations of CAI $_{42\text{-HRC-Rough}}$ and CAI $_{54\text{-HRC-Rough}}$ with UCS
		Deliormanli (2012)	1) UCS = 54.457 (CAI) + 18.26 2) CAI = 0.0410 + 0.0224 (UCS) $-$ 0.0525 (DSS)
		Dipova (2012)	1) UCS = 30.07 (CAI) + 32.89 2) UCS = 30.39 + 23.25 (CAI) $-$ 10.88 $\times$ ln (YD)
		Er and Tugrul (2016)	1) CAI = 3.19 + 0.02 (UCS) 2) CAI = 5.66 + 0.01 (UCS) $-$ 0.43 (BTS) $-$ 0.09 (Δ_b)
		Ko T.Y. et al. (2016)	1) CAI = 0.0075 (UCS) + 1.7669 [data for igneous rocks] 2) CAI = 0.0113 (UCS) + 2.1393 [data for metamorphic rocks]
2	Brazilian Tensile Strength (MPa)	Dipova (2012)	1) BTS* = 2.99 (CAI) + 3.35 2) BTS = 2.96 + 2.26 (CAI) $-$ 1.02 $\times$ ln (YD)
		Er and Tugrul (2016)	CAI = 3.73 + 0.11 (BTS)
		Ko T.Y. et al. (2016)	1) CAI = $-$ 0.1037 (BTS) + 3.6905 [data for igneous rocks] 2) CAI = 0.1451 (BTS) + 1.778 [data for metamorphic rocks] 3) 1.607 + 0.00659 (UCS) + 0.10618 (BTS) [data for metamorphic rocks]
3	Direct Shear Strength (MPa)	Deliormanli (2012)	DSS = 7.72 (CAI) + 2.87
4	Confining Pressure (MPa)	Alber (2008a)	1) CAI = 1.16 + 0.115 (p) [data of one sandstone sample] 2) CAI$_p$ / CAI$_0$ = 1 + 0.0974 (p) [data of all sandstone samples] 3) CAI$_p$ / CAI$_0$ = 1 + 0.041 (p) [data of all greywacke samples] 4) CAI$_p$ / CAI$_0$ = 1 + 0.02 (p) [data of all granite samples] 5) CAI$_p$ / CAI$_0$ = 1 + 0.0272 (p) [data of all mica schist samples]
5	Young's Modulus (GPa)	Alber (2008a)	Increase in CAI per 1MPa confinement = 0.13 $-$ 0.0024 (E)*
6	Fracture toughness Mode I K_{1C} (MPa m$^{1/2}$)	Alber (2008a)	Scatter plot between CAI and fracture toughness Mode I K_{1C} showing no correlation between the two parameters.
7	Brittleness Index (B_1)	Ko T.Y. et al. (2016)	1) CAI = 0.0598 (B_1) + 1.7999 [data for igneous rocks] 2) CAI = 0.0171 (B_1) + 2.8257 [data for metamorphic rocks]

Sr. No.	Parameters	Investigators	Correlation with CAI
8	Brittleness Index (B_2)	Ko T.Y. et al. (2016)	1) CAI = 2.7205 (B_2) + 0.4843 [data for igneous rocks] 2) CAI = 0.656 (B_2) + 2.4852 [data for metamorphic rocks]
9	Brittleness Index (B_3)	Ko T.Y. et al. (2016)	1) CAI = 0.0208 (B_3) + 2.2527 [data for igneous rocks] 2) CAI = 0.0747 (B_3) + 1.7047 [data for metamorphic rocks] 3) CAI = 4.8668 + 0.05467 (UCS) − 0.1492 (B_1) − 0.2945 (B_3) [data for igneous rocks] 4) CAI = 2.6823 + 0.0192 (UCS) − 0.1042 (B_3) [data for igneous rocks] 5) CAI = 1.6096 + 0.0167 (UCS) + 0.191 (BTS) − 0.0855 (B_3) [data for metamorphic rocks]
10	Schmidt Hardness Number	Er and Tugrul (2016)	CAI = 2.73 + 0.04 (SHV)
11	Shore Hardness	Er and Tugrul (2016)	1) CAI = 1.87 + 0.04 (SH) 2) CAI = 4.61 + 0.01 (SH) − 1.53 (w_a) 3) CAI = 3.36 + 0.01 (SH) + 0.01 (*Wa*) − 0.84 (w_a)
12	CERCHAR Indentation Depth (mm)	Dipova (2012)	CAI = 0.1025 $(YD)^{-1.85}$
13	Bohme Abrasion Value	Deliormanli (2012)	BA = − 4.64 (CAI) + 25.06
		Er and Tugrul (2016)	CAI = 6.90 − 0.10 (Δ_b)
14	Wide Wheel Value (mm)	Deliormanli (2012)	1) WW = − 1.96 (CAI) + 23.09 2) CAI = 8.432 − 0.0587 (BA) − 0.291 (WW)
15	P-Wave Velocity (m/s)	Khandelwal and Ranjith (2010)	CAI = 0.0009 (Vp) + 1.9375
		Er and Tugrul (2016)	CAI = 2.55 + 0.58 (Vp)
16	Porosity (%)	Alber (2008a)	1) Scatter plot between CAI and porosity showing that CAI appears to be high when the porosity of the rocks is little and vice versa. 2) Increase in CAI per 1MPa confinement = 0.01310 + 0.0094 (n)[*]
		Er and Tugrul (2016)	CAI = 5.84 − 0.83 (n_t)
17	Water Absorption (%)	Er and Tugrul (2016)	CAI = 5.99 − 2.19 (w_a)
18	Dry Unit Weight (KN/m^3)	Er and Tugrul (2016)	CAI = − 26.71 + 1.20 (γ_d)
19	Surface Properties	Er and Tugrul (2016)	1) CAI = 3.67 + 0.52 (*Ra*) 2) CAI = 2.12 + 0.03 (*Wa*) 3) CAI = 4.19 + 0.08 (*Wshc*) 4) CAI = 2.65 − 0.16 (*Ra*) + 0.03 (*Wa*) + 0.04 (*Wshc*)
20	Quartz Content (%)	(West, 1986; West, 1989)	Positive linear correlation between CAI and quartz content (%)
		Yarali et al. (2008)	1) CAI = 0.0309 (Q) − 0.0795 [data for all rocks] 2) CAI = 0.0489 (Q) − 1.2909 [data excluding mudstones]

Sr. No.	Parameters	Investigators	Correlation with CAI
		Ko T.Y. et al. (2016)	1) CAI = − 0.0324 (Q) + 3.5717 [data for igneous rocks]
			2) CAI = − 0.0031 (Q) + 3.076 [data for metamorphic rocks]
			3) CAI = 5.6738 − 0.0257 (Q) + 0.0495 (UCS) − 0.1299 (B_1) − 0.285 (B_3) [data for igneous rocks]
			4) CAI = 1.636 − 0.0009 (Q) + 0.0169 (UCS) + 0.1958 (BTS) − 0.089 (B_3) [data for metamorphic rocks]
		Er and Tugrul (2016)	CAI = 4.74 + 0.02 (Q)
21	Quartz Equivalent Content (%)	Suana and Peters (1982)	Positive linear correlation between CAI and quartz equivalent content
		Plinninger et al. (2003)	1) Scatter plot between CAI and quartz equivalent content
			2) Positive linear correlation between CAI and (Young's Modulus x Q_{eq})
		Fowell and Abu Bakar (2007)	CAI_{-Sawn} = 0.127 (Q_{eq}) − 7.45 (Grain-size) + 2.008
		Yarali et al. (2008)	1) CAI = 0.0313 (Q_{eq}) − 0.1619 [data for all rocks]
			2) CAI = 0.052 (Q_{eq}) − 1.5769 [data excluding mudstones]
		Thuro and Kasling (2009)	CAI = 0.054 (Q_{eq})
		Gharahbagh et al. (2011)	1) Positive linear correlations of $CAI_{42-HRC-Rough}$ and $CAI_{54-HRC-Rough}$ with Q_{eq}
			2) $CAI_{42-HRC-Rough}$ = -0.127+ 0.0148 (UCS) + 0.0411 (Q_{eq})
			3) $CAI_{42-HRC-Rough}$ = 0.005917 $(UCS)^{1.14}$ $(Q_{eq})^{0.208}$
			4) $CAI_{54-HRC-Rough}$ = 0.127+ 0.0103 (UCS) + 0.0261 (Q_{eq})
			5) $CAI_{54-HRC-Rough}$ = 0.0151 $(UCS)^{0.788}$ $(Q_{eq})^{0.377}$
		Er and Tugrul (2016)	CAI = 3.79 + 0.03 (Q_{eq})
		Rostami et al. (2013)	$CAI_{55-HRC-Rough}$ = 0.056 $(UCS)^{0.431}$ $(Q_{eq})^{0.448}$
22	Quartz Grain Size (mm)	Yarali et al. (2008)	CAI = 2.7928 (d) + 0.6677
		Majeed and Abu Bakar (2015)	$CAI_{fb(Side)}$ = 0.811 + 0.289 (*F* value) + 1.285 (Ø-Qtz) + 0.007 (UCS)
		Er and Tugrul (2016)	1) CAI = 4.52 + 1.47 (Qs)
			2) CAI = 2.88 − 0.05 (Q) + 1.95 (Qs) + 0.06 (Q_{eq})
23	Degree of Cementation (%)	Yarali et al. (2008)	CAI = 0.0705 (CD) − 1.6126
24	Chemical Parameters	Er and Tugrul (2016)	1) CAI = 3.41 + 0.03 (SiO_2)
			2) CAI = 7.71 − 0.16 (Al_2O_3)
			3) CAI = 5.61 − 0.07 (Fe_2O_3)
			4) CAI = 4.61 + 0.03 (SiO_2) − 0.1 (Al_2O_3) + 0.04 (Fe_2O_3)

UCS- Uniaxial compressive strength; (EN3, 1mm)- Mild steel (VHN 225) stylus, 1mm sliding distance; (EN3, 10mm)- Mild steel (VHN 225) stylus, 10mm sliding distance; BTS- Brazilian tensile strength; VBP-Volumetric block proportion; d- Density; DSS-Direct shear strength; YD- Cerchar depth of indentation; n- Porosity; Q- Quartz content (%); Q_{eq}- Quartz equivalent content (%); CAI_p- CAI value at a given confining pressure; CAI_0- CAI value without confining pressure; d- Quartz grain size; CD- Cement degree; p- Confining pressure; E- Young's Modulus; Vp- P-Wave velocity; $CAI_{fb(Side)}$- CERCHAR abrasivity index measured on freshly broken rock surface using side viewing technique; *F* value- Schimazek's F-value; Ø-Qtz- Quartz grain size; Qs- Quartz size; SiO_2 - Silica Content; BA- Bohme abrasion value (cm^3 / $50cm^2$); Δ_b- Bohme abrasion (%); SHV- Schmidt hardness value; SH- Shore hardness; n_t- Total porosity; w_a- Water absorption; γ_d- Dry unit weight; *Ra*- Roughness average; *Wa*- Waveness average; *Wshc*- Peak number

2.2.2.1.9. <u>Influence of water saturation on CAI.</u> The mechanical excavation of saturated rocks has been studied by a number of past investigators in relation to the specific energy and tool wear rate using rock cutting tests. Some studies report reduction in specific energy with water saturation (Ford and Friedman, 1983; Verhoef, 1997; Tiryaki and Dikmen, 2006; Mammen et al., 2009), whereas O'Reilly et al. (1979) reported no change in the specific energy requirements to cut Chalk in both dry and wet conditions. Roxborough and Rispin (1973) found that the specific energy requirements of cutting wet chalk were 50% higher than the dry chalk drag pick cutting. Phillips and Roxborough (1981) reported decrease in wear of drag tools while performing cutting experiments on wet chalk and Bunter sandstone rocks. The cited authors also concluded that if a rock stays competent upon saturation, the pick forces required for cutting that rock can be greater as compared to the dry rock. Ford and Friedman (1983) established that water jet assisted wet rock cutting will reduce tool wear mainly by cooling and lubrication of the cutting tool. Verhoef (1997) explained that at cutting speeds higher than 3m/sec, the wear rate of a suction dredger cutting tool might increase due to temperature rise at the tool rock interface.

Few studies have also been conducted to investigate the effect of saturation on the wear of test pieces used in some laboratory rock abrasivity measurement tests. Iphar and Goktan (2003) performed Steel Cube Abrasiveness tests on sandstone, limestone and tuff rock fraction samples, saturated with liquids having 4.0, 7.5 and 10 PH degrees. All the three rock samples produced significantly high values of Steel Cube Abrasiveness Index (SCAI) which were saturated with the acidic liquid, while the lowest values of SCAI were obtained for all rock samples saturated in the alkaline media. Mammen et al. (2009) conducted CERCHAR abrasivity tests on an argillaceous quartz sandstone by varying the moisture content from dry (0.0%) to saturated (4.6%) in six increments and a reduction of up to 13% was registered for CAI values between the dry and saturated samples. Espallargas et al. (2014) investigated the abrasion-corrosion performance of cutter steel test pieces on exposure to hard rock and abrasive soil samples using four different liquid environments including water samples obtained from field, simple distilled water, saline distilled water, and water samples with conditioning additives. The abrasion rate of cutter

steel test piece was reduced when tests were performed in the presence of conditioning additives.

The influence of water saturation on the physical and mechanical properties of rocks has also been a subject of many earlier investigations. In general these studies have shown considerable decrease in the compressive and tensile strengths of saturated rocks in comparison to the air dried samples. Table 2.6 is a summary of the previous studies on reduction of UCS and BTS values with water saturation.

Table 2.6. Summary of previous studies on the effects of water saturation on rock strength (after Abu Bakar et al. 2016).

Reference	Effect of saturation on rock strength
Rehbinder and Lichtman (1957)	Postulated that the susceptibility of solids to deform and break increases due to adsorption from the surrounding medium mainly because of decrease in the surface energy of freshly formed edges in the solid under strain.
Colback and Wiid (1965)	Found a reduction of 50% in the compressive strength of Quartzitic Shale and Quartzitic Sandstone rock samples when tested under water saturation condition in comparison with dry tests. This reduction in strength was due to decrease in the surface free energy by submerging liquid.
Brace and Martin (1968)	Concluded rise in rock strength when tested under increased strain rate at some constant pore water pressure.
Vutukri (1974)	Noted a decrease in tensile strength of rock specimen primarily due to rise in surface tension and dielectric constant of saturating fluid.
Van Eeckhout (1976)	Ascribed the reduction in strength of the saturated rock due to decreases in rupture energy, capillary tension, internal friction and increase in pore pressure along with weakening effect due chemical action.
Broch (1979)	Conducted point load tests on igneous, metamorphic and sedimentary rocks in both dry as well as water saturated conditions and established 20% to 45% strength reduction.
Dyke and Dobereiner (1991)	Carried out unconfined compression tests on three sandstone varieties of UK, including Penrith, Bunter and Waterstone at five different moisture contents ranging from dry to fully saturated. They observed that the largest variations (reduction) in rock strength occur at moisture levels of less than 1.0%.
Hawkins and McConnell (1992)	Their study on 35 British sandstones showed that an increase in moisture content of as small as 1% from dry condition can have a considerable effect on both strength and deformability of sandstones. They reported a reduction of 78% and 8% in the uniaxial compressive strength (UCS) of saturated clay rich sandstone and siliceous sandstone respectively.
Vasarhelyi (2003)	Statistically analyzed the effect of water saturation on the UCS and Young's modulus utilizing the already published data by Hawkins and McConnell (1992). The cited author reported that saturated UCS is 75.6% of the UCS of dry rock specimens.
Erguler and Ulusay (2009)	They reported decreases of up to 90%, 93% and 90% in UCS, mean modulus of elasticity and tensile strength of clay bearing rocks with increasing water content.
Mammen et al. (2009)	Conducted UCS tests on a Argillaceous quartz sandstone rock sample at three levels of moisture content; oven dried state (0.0% moisture content), air dried state (0.2% moisture content) and fully saturated state (5.2% moisture content). Significant reductions of 63% and 68% in compressive strength were found at the moisture contents of 0.2% and 5.2% respectively compared to 0.0% moisture level.
Yilmaz (2010)	Found a significant decrease in the strength of rock gypsum with a little increase (1-2 %) in the water content.
Perera et al. (2011)	Performed UCS and Young's modulus tests on Latrobe valley brown coal samples under natural and water, carbon dioxide and nitrogen saturation conditions. Test results showed UCS reduction of about 17% and 10% in the case of water and carbon dioxide saturation respectively. Contrary to that nitrogen saturation caused an increase of 2% in UCS.

Reference	Effect of saturation on rock strength
Poulsen et al. (2014)	Quantified the strength reduction in coal and coal measures rocks (stoney coal, mudstone and sandstone) under unsaturated and saturated conditions by the aid of laboratory testing. The cited authors reported average reduction in UCS of 9.6%, 18.7%, 30.3% and 28.8% respectively.
Soni (2015)	Performed Brazilian tensile strength (BTS) tests on sandstone and limestone rock samples under wet and dry states and found tensile strength reductions of about 50% and around 20% under wet conditions respectively.

2.2.2.1.10. <u>Estimation of rock cutting tool wear using CAI.</u> The issue of estimating cutter life and cost is becoming increasingly sensitive issue when dealing with operation of mechanical excavation systems in mining, tunnelling and underground construction. Amongst the available tests for characterizing rock abrasivity as it pertains to cutter wear and bit life, CERCHAR abrasivity index has been widely accepted and have been used in bid documents in recent years (Rostami et al., 2005). During the last years work has been reported by a number of investigators correlating in-situ rock cutting tools wear rate with the laboratory wear rates which are discussed as under:

Nizamoglu (1978) developed a linear correlation between tool consumption (TC) and CAI values as follows:

$$TC = 0.2228 \, (CAI) + 0.0258 \tag{2.22}$$

Johnson and Fowell (1986) established a correlation (Figure 2.9) between the abrasivity coefficient (AB; proportional averaging of CAI value for each rock type within a mixed face) and tool consumption (TC) given by the following equation:

$$TC = 0.25 \, AB - 0.07 \tag{2.23}$$
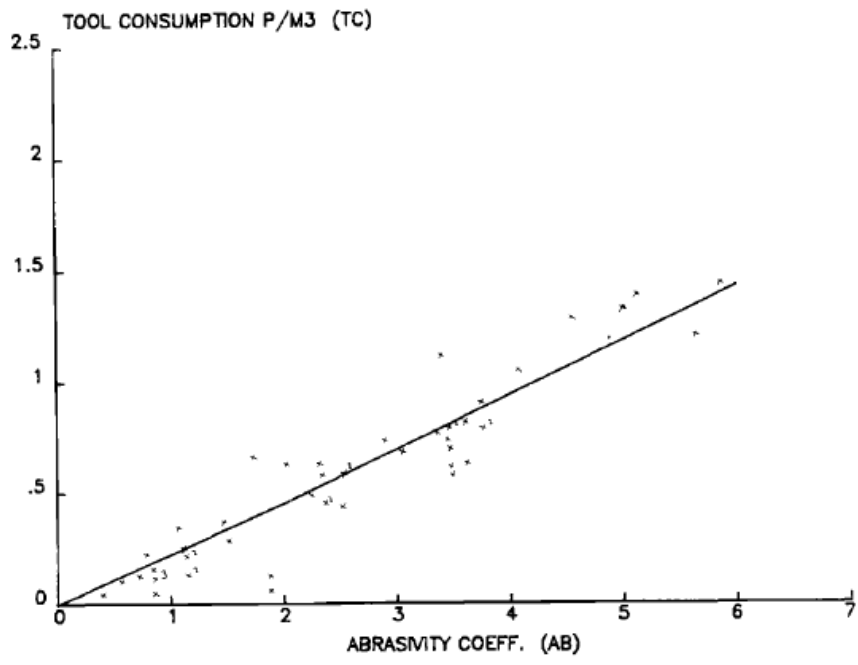
Figure 2.9. Abrasivity coefficient against tool consumption (after Johnson and Fowell, 1986).

Fowell and Johnson (1991) presented a correlation between Abrasivity Coefficient (AB) obtained from modified CERCHAR test and tool consumption rates for light weight (L.W.), medium weight (M.W.) and heavy weight (H.W.) boom tunneling machines. Figure 2.10 shows higher tool consumption for the light weight category of machine as compared to heavy duty machines.
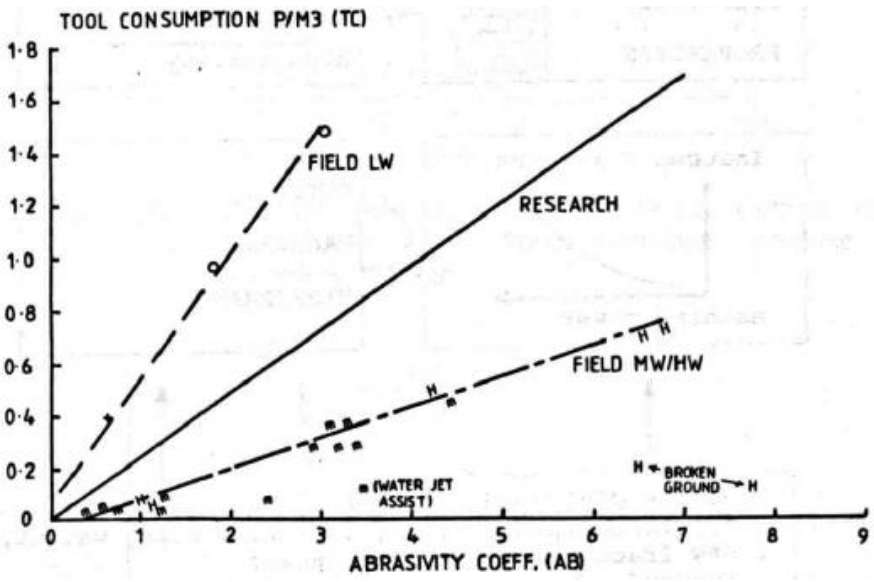
Figure 2.10. Abrasivity coefficient versus Tool consumption (after Fowell and Johnson, 1991).

Gehring (1995) explained that the 17 inch TBM disc cutter should be replaced when the weight loss of disc is approximately 3500 grams. The cited author also presented an empirical formula for the estimation of specific disc cutter weight loss as a function of the CERCHAR Abrasivity Index (CAI):

$$V_S = 0.74 \times CAI^{1.93} \tag{2.24}$$

Where;

V_S = Specific disc weight loss in mg/m rolling distance;

CAI = CERCHAR Abrasivity Index.

Maidl et al. (2001) developed a correlation (Figure 2.11) for TBM cutter life estimation, based on CAI and UCS of few common rock types including marlstone, weak molasse sandstone, limestones, gneiss and granites. Each curve shown in Figure 2.11 corresponds to a particular CAI value for a rock or group of rocks. For example CAI value of 2 designates group of rocks including weak molasse sandstone and limestones. In general the volume of rock excavated per disc cutter (m^3/disc) decreases with the corresponding increase in CAI and UCS values of the rocks and vice versa.
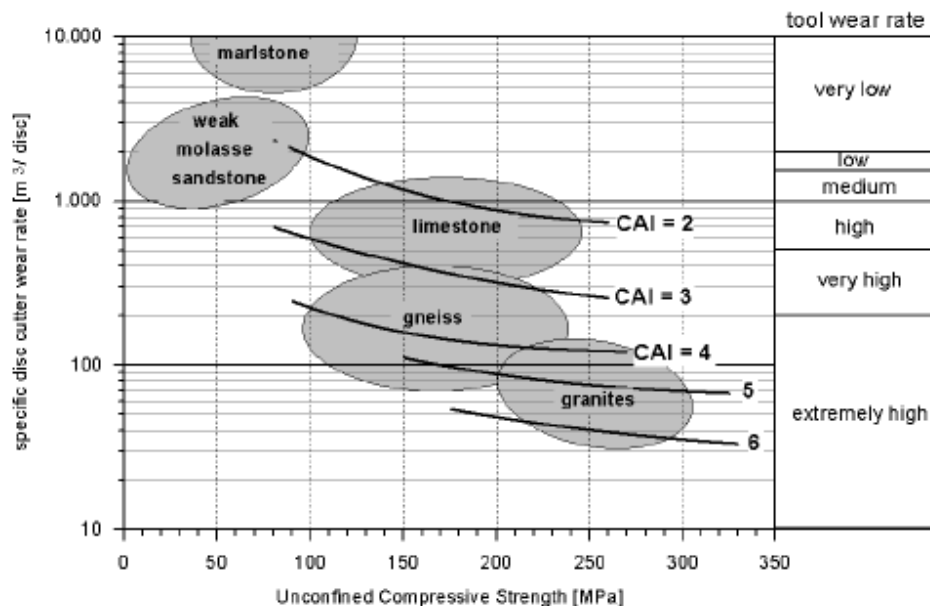
Figure 2.11. Correlation of TBM disc cutter lifetime (m^3/disc) with CAI and UCS of some common rock types (after Maidl et al., 2001).

Plinninger (2002 and 2008) proposed linear and exponential regression models (Figure 2.11) for the estimation of button drill bit (Ø 45mm) lifetime (m/bit) based on

CAI values. The cited author also warns that the proposed models presented in Figure 2.12 should be used for rough estimations with extreme caution.
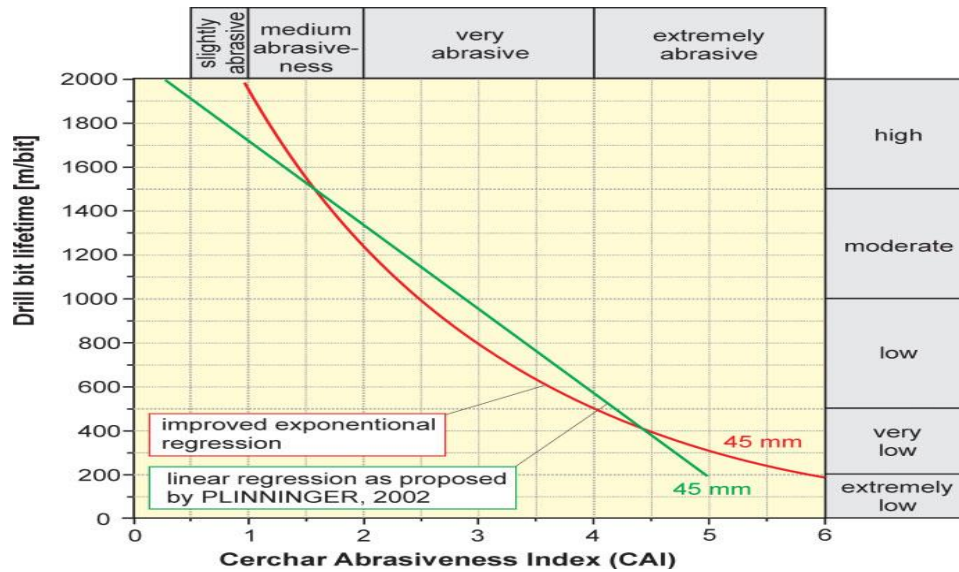
Figure 2.12. Correlations of 45 mm button bit lifetime with CAI (after Plinninger, 2002, 2008).

Rostami et al. (2005) suggested relationships for the prediction of cutting tool wear of mechanical excavators (roadheaders and TBMs) by utilizing the CERCHAR Abrasivity index (CAI). The bit consumption of roadheaders ranging from medium to heavy duty machine can be estimated by employing the following formula:

$$\text{Bit Consumption} = \frac{CAI}{4} \times k1 \times k2 \text{ (bits / ton of rock excavated)} \tag{2.25}$$

Where; CAI = CERCHAR Abrasivity Index;

k1 = constant ranging from 0.75 to 1, for cutter heads with water jet spray and jets effectiveness;

k2 = constant varying from 0.90 to 1, for low speed axial cutter heads to high speed transverse cutter heads.

For the estimation of disc cutter life for hard rock TBMs the cited authors have presented the following formula:

$$LF = \frac{6.75 \times D}{17 \times CAI} \tag{2.26}$$

Where; LF = disc life in linear feet of cutter travel on the tunnel face expressed in million feet;

D = disc diameter in inches;

CAI = CERCHAR Abrasivity Index.

While the cutter life in terms of volume of rock excavated per cutter disc change can be calculated as follows:

$$CL = \frac{6.75 \times D \times PR \times A}{1026 \times CAI \times RPM \times N \times D_{TBM}}$$ (2.27)

Where; CL = cutter life in ft^3 per cutter;

PR = rate of penetration in feet per hour;

A = surface area of the tunnel;

N = number of cutters mounted on the cutter head.

Yarali et al. (2008) proposed the following linear relationship between tool consumption (TC) and CERCHAR abrasivity index (CAI) of the coal measures rocks of Turkey:

TC = 0.2533 (CAI) – 0.0948;   (R^2 = 0.98) (2.28)

Farrokh et al. (2013) developed correlation charts between rock mass parameters (quartz content and UCS) and disc cutter life (m^3/cutter) for the initial prediction of cutter consumption using a database consisting of 135 TBM tunneling cases. The overall trends show an increase in the cutter life with the decreasing quartz content and UCS of rocks and vice versa. The cited authors also presented a modified form of formula already proposed by Rostami et al. (2005) for the estimation of TBM cutter life:

$$CL = \frac{720 \times d \times PR \times D}{CAI \times RPM \times N}$$ (2.29)

Where; CL = cutter life in m^3 per cutter;

PR = rate of penetration in meters per hour;

d = cutter diameter in inches;

D = tunnel diameter in meters;

N = number of cutters mounted on the cutter head;

RPM = rotational speed of TBM cutter head per minute;

CAI = CERCHAR Abrasivity Index.

2.2.2.2. The LCPC rock abrasivity test. The LCPC test was introduced by the Laboratoire Central des Ponts et Chaussees (LCPC) in France in the 1970s in order to investigate and classify abrasiveness related to rock crusher application (Plinninger and Restner, 2008). This test is regulated under the French standard AFNOR P18-579 (1990) and as mentioned in the published literature (Buchi et al., 1995; Thuro et al., 2007; Kasling and Thuro, 2010) finds application for the abrasivity measurement of rock and soil samples. For this test 500 grams of rock ground to a grading corresponding to the 4.0-6.3 mm fraction are used. The test sample is placed in a vertical cylindrical mould 100 mm in diameter. A steel insert (50 x 25 x 5 mm), placed in a horizontal plane at the end of a vertical metallic shaft, is immersed in the material. The shaft is aligned on the axis of the mould and driven by a motor at a speed of 4500 rpm (power 750 W). The test consists of turning the insert of grade XC 12 steel (Rockwell B hardness between 60 and 75 HRB) for 5 minutes and determining the mass it loses. The mass of the insert is accordingly measured before and after the test and the LCPC abrasivity coefficient, ABR (g/t) is stated as the ratio of loss of mass to initial mass in ten-thousandths (AFTES, 1982). The value of ABR varies between 0 and 2000 (g/t) for natural rock and soil samples (Thuro et al., 2007). After performing test the breakability or brittleness of the sample can be quantified by determining the weight of material passing 1.6 mm sieve. Its percentual weight share of the total sample provides information on the breakability, BR (%) of the sample. The LCPC breakability index, BR (%) could be correlative with the borability of the rock (Buchi et al., 1995). The classification of LCPC indices [ABR (g/t) and BR (%)] is presented in Table 2.7, whereas Figure 2.13 shows the LCPC testing setup.

Table 2.7. Classification of LCPC indices including ABR (g/t) and BR (%).

Thuro et al. (2006, 2007)		Buchi et al. (1995)			
ABR (g/t)	Abrasivity classification	ABR (g/t)	Abrasivity classification	BR (%)	Breakability classification
0-50	Not abrasive	<500	Very low	<25	Very low
50-100	Not very abrasive	500-1000	Low	25-50	Low
100-250	Slightly abrasive	1000-1500	Medium	50-75	Medium
250-500	Abrasive	1500-2000	High	75-100	High
500-1250	Very abrasive	>2000	Very high	>100	Very high
1250-2000	Extremely abrasive				

The LCPC test is applicable for both rock and loose material, especially for wear investigations on cutting tools as well as cutter head in the field of shield tunneling machines (hydro or EPB tunnelling), as it allows better evaluation of wear and costs due to relatively low metal hardness. Moreover statements can be made relating to the influence of wet and dry processing, as well as on the influence of bentonite suspension on the abrasivity (Buchi et al., 1995). The use of LCPC test is still not very common, while in the past few years its use for preliminary investigations for underground development projects has been reported in limited cases (Fowell and Abu Bakar, 2007). For applications in hard rock excavation the testing principle of LCPC test is not suitable to assign tool wear primarily because of destruction of some of the most important rock properties in the process of sample preparation and hence neglected in the measured ABR (g/t) value (Ewendt, 1989; Plinninger, 2002), therefore giving a rock abrasivity value identical for solid rock and for a loose heap of the same material (Kohler et al., 2011). Although in the recent past LCPC test is extensively being used for the abrasivity determination of soils and weak rocks, but it should be kept in mind that during sample preparation some of the most relevant soil parameters are also changed significantly or even discarded completely (Plinninger and Restner, 2008). Dullmann et al. (2014) further highlighted that LCPC test can at best reflect an approximation of the efficiency of the wear mechanism, but non-standardized testing apparatus and the testing materials can lead to inaccuracy in the results, which complicates quantitative measurement (weighing sensitivity of testing body) and the comparison of ABR (g/t) values from different testing organizations.

Figure 2.13. LCPC rock abrasivity testing device (after Nilsen et al., 2007).

The LCPC test is quite well researched method. Numerous investigations have compared the results of LCPC abrasivity index with CERCHAR abrasivity index (CAI). Similarly numerous other parameters affecting the results of LCPC test were also examined in detail by a number of researchers in the past and have been reported in the literature. These parameters include influence of rock water content, effect of test speed, effect of insert metallurgy, relationship with rock properties amongst others. The effects of different testing parameters on LCPC test results are discussed as follows:

2.2.2.2.1. Relationship of ABR (g/t) with CAI. In the past extensive work has been done comparing the results of two rock abrasivity measurement methods. Thuro and Kasling (2009) developed a comprehensive unified classification scale which is reproduced below (Table 2.8):

Table 2.8. Unified classification scale of ABR (g/t) and CAI (after Thuro and Kasling, 2009).

ABR (g/t)	CAI	Abrasivity classification	Tool wear potential	Examples for rock and components in soil	Soil
0-50	0-0.3	Not abrasive	Very low	Timber, peat	Silty clay and clayey silt, carbonate sands
50-100	0.3-0.5	Not very abrasive	Low	Clay-siltstone, mudstone, marl	
100-250	0.5-1.0	Slightly abrasive	Moderately	Slate, Fine grained sandstone with clay binder, dolomite, marble	Pure carbonate gravels
250-500	1.0-2.0	Medium abrasive	High	Sandy limestone, quartz bearing dolomite, sandstone, phyllites and schists	Quartz & crystalline rich sands, carbonate rich gravels
500-1250	2.0-4.0	Very abrasive	Very high	Quartzitic sandstone, quartz phyllite, porphyry, andesite, basalt, mica schist, weak amphibolite	Quartz & crystalline rich gravels, fine grained soils with quartz or crystalline gravels, pebbles or cobbles
1250-2000	4.0-6.0	Extremely abrasive	Extremely high	Vein quartz, quartzite, diorite, syenite, gneiss, eclogite, hard amphibolite	

Similarly numerous investigators have proposed correlations between the LCPC abrasivity coefficient and CERCHAR abrasivity index, which are summarized in Table 2.9. According to Kohler et al. (2011) LCPC test is only suitable for the abrasivity determination of graded loose material, while CERCHAR test is conducted on intact rock pieces, so that no correlation with CAI test can be possible.

Table 2.9. Correlations between ABR (g/t) and CAI values of rocks.

Sr. #	Correlations	Investigators
1)	ABR ≈ 300 (CAI)	Buchi et al. (1995)
2)	ABR = 303.70 (CAI) – 71.02	Thuro et al. (2007)
3)	Scatter plot showing poor correlation between the two indices for all rocks tested.	Fowell and Abu Bakar (2007)
4)	ABR = 273 (CAI); {based on data set of 74 rocks}	Thuro and Kasling (2009)
5)	ABR = 273 (CAI); [Modified from Thuro and Kasling (2009), based on data set of 83 rocks]	Kasling and Thuro (2010)

2.2.2.2.2. <u>Influence of water content.</u> The effect of water saturation on LCPC abrasivity coefficient has been a topic of research of some past investigations. These studies have shown that the presence of water in abrasive medium at certain moisture content generally increases abrasivity (Fowell and Abu Bakar, 2007; Drucker, 2011; Barzegari et al., 2015; Hashemnejad et al., 2015).

Fowell and Abu Bakar (2007) performed LCPC tests on seven selected highly abrasive rock samples by using 200 ml of water with 500 grams of crushed rock aggregate. They observed appreciable increase in the wear and hence in the corresponding ABR (g/t) values.

Drucker (2011) conducted tests on Danube gravel in dry state as well as by adding 75, 150 and 250 grams of tap water to the abrasive granular material before the start of LCPC test. The author reported that it was not possible to perform LCPC test with water content below 75 grams due to lack of interaction between the insert and grains, as a small portion of the test grains had already accumulated on the walls of the container. The tests carried out at water content of 75 grams showed 100% to 300% rise in ABR (g/t) value, compared to the performance of test with oven dried material. Further increase in water content caused the ABR (g/t) values to fall again and finally at 250 grams water content attained the same magnitude as in a dry test.

Barzegari et al. (2015) studied the effect of water saturation on LCPC abrasivity coefficient, by conducting tests on 24 selected rock and soil samples in the dry state as well as with the addition of 150 ml of water. In most of the cases the addition of water caused the increase of abrasivity, primarily due to formation of thick abrasive slurry, due to rotation of impeller firstly against intact rock pieces as well as in thick abrasive paste later and rotation of impeller into the particles most of the time. The cited authors also performed tests on eleven (11) selected samples with bentonite slurry. The test results showed that the presence of bentonite slurry in 55% of the sample enhanced the abrasivity. They explained that the addition of bentonite slurry caused the finer materials to create a cohesive paste holding the coarser grains and enhanced the steel wear. They also observed that the addition of clay to the sample enhanced the sample adhesion in the form of stickiness resulting in adhesive wear.

Hashemnejad et al. (2015) carried out tests on 27 different rock samples utilizing 0%, 10%, 20%, 30%, 40%, 50%, 65%, 80% and 100% water saturation. According to the test results the highest abrasivity of samples occurred at 25-40% water saturation. The cited authors developed the following relationship to find the LCPC abrasivity coefficient at 35% water saturation for rocks falling in the equivalent quartz content range of 75-100%:

$$\frac{LAC_{w=35}}{LAC_{w=0}} = 1.37 \ \times \ EQC_{(75-100)\%} \qquad\qquad (2.30)$$

Where; $LAC_{w=35}$ = LCPC abrasivity coefficient at 35% water saturation,

$LAC_{w=0}$ = LCPC abrasivity coefficient at 0% water saturation,

EQC = Eqivalent quartz content in the range of (75-100) %.

      2.2.2.2.3. <u>Influence of test speed.</u> This test did not gain much recognition among researchers, engineers and laboratories owing to the fact that it does not simulate the actual wear process that occurs in mechanized excavation, due to the high impeller rotational speed of 4500 ± 50 rpm as prescribed by the French standard (Normalisation Francaise NF P18-579, 1990). It appears that this extraordinary test speed has no logical relationship with the rotational speeds of rock excavation and drilling machines used in the mining and geo-technical industry, as well as the contact stresses between the crushed rock fraction and the LCPC insert are not analogous to those of in-situ field conditions (Abu Bakar et al., 2014). Also due to the high rotational speed of 4500 rpm, the wear produced within the LCPC test process is predominantly caused by a hitting impulse between the insert and rock grains (Nilsen et al., 2007; Ghasemi, 2010), while it has not a very important role in the wear mechanism of mechanical excavators, specifically, TBMs (Ghasemi, 2010). Moreover such a high speed is also difficult to attain and maintain in ordinary laboratory rotational devices used for LCPC testing (Abu Bakar, 2006). For example tunnel boring machine (TBM) utilized for hard rock application has an average cutter head speed of 9 rpm (Alber, 2008b) and the TBM tunnel drive used in soil or soft ground conditions, has a relatively low velocity of typically 1.5 to 2 rpm (Nilsen et al. 2007). Similarly, the roadheaders have in general two cutter head velocity settings; the low speed ranging from (25 to 35) rpm and the high speed starting from (50 to 70) rpm depending upon the rock conditions (Bilgin et al. 2014).

      As regards the speed of LCPC testing setup selected by the LCPC institute in 1970s, one has to bear in mind, that this model test was originally invented for hard rock application in the mineral processing industry (specifically for use with equipment including all kind of conveyors, crushers, sieves, etc.) and not developed for TBM/shield in loose soil applications. However, regarding the technical specifications (speed, insert hardness, sample grain size fraction, etc.) of the test it is in general of crucial importance

to very precisely define the testing circumstances of such a model testing setup in order to gain comparable results with other rock abrasivity testing setups. The latter being the aim of the national French AFNOR (NF P18-579, 1990) LCPC standard (Plinninger, 2015). According to West (1981) some past investigations also have reported relationships of LCPC abrasivity values (ABR, g/t) with the wear of quarry rock crusher parts.

At present limited work is available on investigation of the effect of LCPC test speed variation, on rock abrasivity results. Abu Bakar et al. (2014) report LCPC tests on selected rock types at two propeller speeds of 2250 rpm and 4500 rpm for 10 minutes and 5 minutes respectively. The propeller rotational speed of 2250 rpm was selected on the logic that the speed at 4500 rpm for test duration of 5 minutes makes 22500 rotations, which is equivalent to test revolutions at 2250 rpm performed for 10 minutes. The cited authors also proposed following statistical correlations for the conversion of ABR (g/t) values at the two speeds tested.

$$ABR_{4500\ rpm} = 1.8(ABR_{2250\ rpm}) - 12.8 \quad \text{[for igneous and metamorphic rocks, } R^2 = 95\%] \quad (2.31)$$

$$ABR_{4500\ rpm} = 1.8(ABR_{2250\ rpm})^{0.9} \qquad \text{[for sedimentary rocks, } R^2 = 72\%] \qquad (2.32)$$

2.2.2.2.4. <u>**Effect of insert metallurgy.**</u> The available French standard (Normalisation Francaise NF P18-579, 1990) regulating the LCPC test suggests the use of impellers having hardness in the range of (60 to 75) HRB. However, there are references in the literature that the LCPC abrasiveness test has deficiencies regarding its validity and reproducibility since the system only conditionally reproduces the actually effective tribological system in tunnelling regarding the loading configuration (acting forces, moments) and the geology (grain size, particle shape, consolidation) (Dullmann et al., 2014; Drucker, 2011; Jakobsen and Lohne, 2013, Kupferle et al., 2015). The previous literature show little work on examination of LCPC test from the perspective of insert metallurgy. The pioneer work was performed by Drucker (2011) by varying the steel type and hardness of the LCPC test impellers, including C15E (76.0 HRB) and S275JR (88.6 HRB) inserts. The performance of LCPC abrasivity tests with the two types of impellers (C15E and S275JR) showed unforeseen results; the harder steel impellers (88.6 HRB) exhibited on average 20% higher weight loss in comparison to the softer steel impellers (76.0 HRB). This phenomenon can be explained in terms of material science; that is the

steel hardness, its fracture toughness and the deformability of steel are important for its resistance to abrasive wear (Czichos and Habig, 2010; Sommer and Heinz, 2010).

Kupferle et al. (2015) investigated LCPC test from the view point of material science and the consequential problems caused in the assessment of rock abrasivity index, ABR (g/t). They performed tests by utilizing three different types of heat treated impellers; S275 (soft annealed, 68 HRB), C45 (soft annealed, 71 HRB) and S275 (normalized, 72 HRB) against two selected abrasive minerals including crushed Quartz (Moh's hardness: 7) and fused corundum (Moh's hardness: 9). Regardless of the impeller material structure the test results showed higher ABR values for the fused corundum than that of the less abrasive crushed quartz. Alternatively from the view point of impeller material structure it was found that in spite of almost same material hardness (S275 and C45) in each of the heat treatment states, a difference in ABR values of 216 (g/t) was obtained for crushed quartz while a difference of 159 (g/t) was obtained in case of fused corundum.

2.2.2.2.5. <u>Relationship with rock properties.</u> To date numerous studies have proposed correlations of LCPC abrasivity coefficient, ABR (g/t) with the petrographical parameters. However little work is available on exploring relationships of LCPC indices {ABR (g/t) and BR (%)} with the physical and mechanical rock properties. Table 2.10 summarizes the relationships of ABR (g/t) and BR (%) with rock properties developed by some previous investigators.

Table 2.10. Correlations of ABR (g/t) and BR (%) with Rock Properties.

Sr. No.	Parameters	Investigators	Correlations with ABR and BR
1	Quartz Content (%)	Dullmann et al. (2014)	Increasing quartz content (%) of prepared mixture between silligran and marble gravel increases ABR (g/t).
		Barzegari et al. (2015)	1) ABR = 0.0687 $(Q)^2$ + 10.395 (Q) – 20.811 (grain size = 4.0-6.3 mm) 2) ABR = 0.0916 $(Q)^2$ + 0.5129 (Q) + 21.524 (grain size = 2.0-4.0 mm) 3) ABR = 0.0601 $(Q)^2$ – 3.1517 (Q) + 33.357 (grain size = 0.5-2.0 mm)
2	Equivalent Quartz Content (%)	From Thuro and Kasling (2009) with ref. to Festl (2006)	ABR = 0.46 $(EQC)^{1.929}$

Sr. No.	Parameters	Investigators	Correlations with ABR and BR
		Beckhaus (2010)	$ABR = 0.455 \ (EQC)^{1.929}$
		Kohler et al. (2011)	Scatter plot between ABR (g/t) and quartz equivalent content.
		Hashemnejad et al. (2015)	$ABR = 16.25 \ (EQC)$
		Hashemnejad et al. (2015)	1) $ABR = 19 \ (EQC) + 7 \ (\omega) - 48 \ (Sh) + 66 \ (S) + 37 \ (A) - 580 \quad (0 \leq \omega \leq 35)$ 2) $ABR = 18 \ (EQC) + 0.75 \ (\omega) - 53 \ (Sh) + 72 \ (S) + 40 \ (A) - 595 \ (35 < \omega \leq 100)$
3	Abrasive Mineral Content (%)	Kahraman et al. (2016)	$ABR = 13.06 \ (AMC) + 181.30$
4	Aspect Ratio of Grains (AR)	Kahraman et al. (2016)	$ABR = 8.79 \ (AMC \times AR) + 193.70$
5	Roundness of Grains (R)	Kahraman et al. (2016)	$ABR = 19.30 \ (AMC \times R) + 140.60$
6	Average Grain Diameter (mm)	Kahraman et al. (2016)	$ABR = 1.77 \ (AMC \times D) + 114.00$
7	Shape and Size Coefficient (SSC)	Kahraman et al. (2016)	$ABR = 1.71 \ (AMC \times SSC) + 108.80$
8	Uniaxial Compressive Strength (MPa)	Buchi et al. (1995)	Scatter plot between ABR (g/t) and UCS
		Gonzalez et al. (2014)	$ABR = 6.30 \ (UCS) + 380$
		Gonzalez et al. (2014)	$BR = -1.5 \ \ln(UCS) + 57$
9	Brazilian Tensile Strength (MPa)	Gonzalez et al. (2014)	$ABR = 41 \ (BTS) + 338$
		Gonzalez et al. (2014)	$BR = 601 \ (BTS)^{-0.05}$
10	Dry Density (g/cc)	Gonzalez et al. (2014)	$ABR = 32 \ (\rho_d)^{3.2}$
11	Water Content (%)	Gonzalez et al. (2014)	$ABR = 843 \ e^{-0.095W}$
		Gonzalez et al. (2014)	$BR = 1.6 \ (W) + 42$
12	Friction Angle (°)	Gonzalez et al. (2014)	$ABR = 16.5 \ e^{0.096(°)}$
		Gonzalez et al. (2014)	$BR = -0.5 \ (°) + 75$
13	Shape index (Sh)	Hashemnejad et al. (2015)	Larger grains show higher abrasivity.
14	Grain Size (mm)	Thuro et al. (2006)	The ABR (g/t) values increase more than linear with increasing grain size. Also sand, silt and clay do not play a significant role on abrasion even at high quartz content.
		Drucker (2011)	Linear increase in ABR (g/t) values with corresponding increase in average grain sizes (dm) of 3mm, 5.15mm, 6mm and 7.15 mm. However this linearity is contradicted by the results of the tests using the abrasive material broken down to the test size and then remixed (4 – 31.5mm, dm = 14.3mm).

Sr. No.	Parameters	Investigators	Correlations with ABR and BR
		Barzegari et al. (2015)	By increasing soil particle size the soil abrasivity increased significantly.
		Hashemnejad et al. (2015)	Increasing effective grain size increases impeller wear and abrasion.
15	Grain Angularity (*A*)	Dullmann et al. (2014)	The increase in grain angularity causes corresponding rise in ABR (g/t) value.
		Hashemnejad et al. (2015)	Angular grains cause more abrasion to the impeller surface and increase the ABR (g/t) value.

UCS- Uniaxial compressive strength; BTS- Brazilian tensile strength; ρ_d - Dry density; Q- Quartz content (%); EQC-Quartz equivalent content (%); ω- Water saturation; AMC- Abrasive mineral content; D- Average grain diameter; W- Water content; Sh- Shape index; *S*- Effective size; *A*- Grain angularity

2.2.2.2.6. <u>Estimation of rock cutting tool wear using LCPC test.</u> Gonzalez et al. (2015) in a study reported and analyzed the database of 33 km of Earth Pressure Balanced (EPB) tunnel drive records of recent underground Metro network projects (Linea 9 and Terrassa FGC) in the Barcelona area, from the geotechnical (abrasivity and strength) and maintenance (specifically tool wear) perspectives. The equivalent abrasivity (Abreq[TRDC]) of the mixed face was determined by using LCPC abrasivity index as the weighted average of the different materials appearing in the respective maintenance stretches (TRDC) taking into account their intersections with different geotechnical stretches (TG). A TRDC defines the length or space of tunnel between two stoppages of TBM for tool replacement purposes. The normalized consumption of tools (discs, scrapers and picks) was computed for each maintenance stretch (TRDC) by using the formula below:

$$CRH = \frac{L[TRDC]}{\left(\frac{N_{H[TRDC]}}{N_{H0}}\right) \times 100} \qquad (2.33)$$

Where; CRH = normalized tool consumption in meters per % of all category tools consumed (m/%H),

$L[TRDC]$ = length of the maintenance stretch where tool(s) replacement was recorded,

$N_{H[TRDC]}$ = number of tools replaced including discs, scrapers and picks,

N_{H0} = number of tool positions on the cutter head.

The cited authors also developed a correlation (Figure 2.14) between normalized tool consumption (CRH) and equivalent abrasivity (Abreq[TRDC]) which shows a decrease in CRH with the corresponding increase in material abrasivity and vice versa.
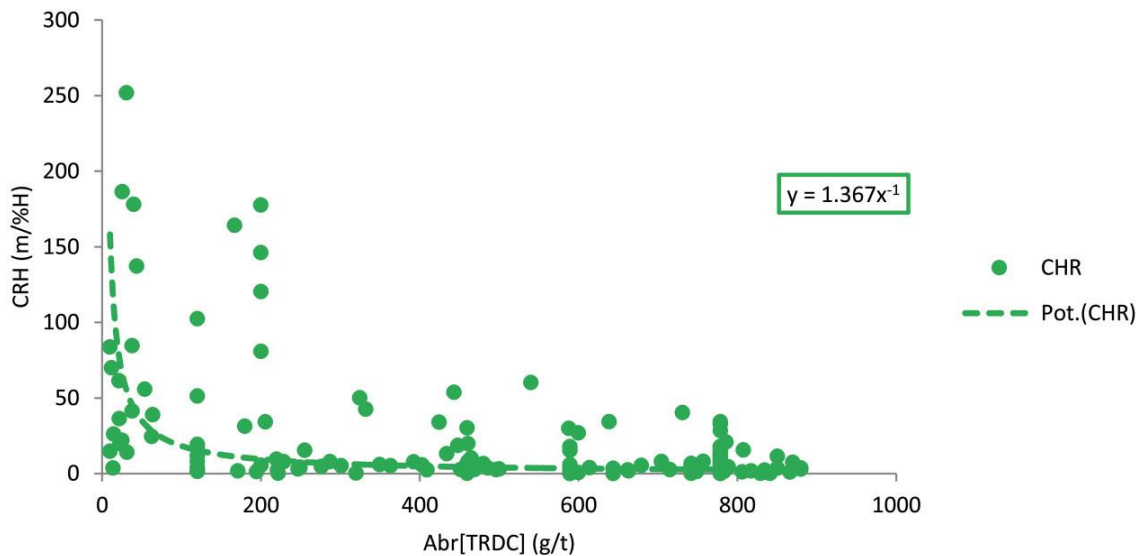
Figure. 2.14. Plot of CRH versus Abreq[TRDC] (after Gonzalez et al. (2015)).

2.2.2.3. The NTNU/SINTEF drillability test method. This test method, previously known as NTH method (Selmer-Olsen and Lien, 1960) was developed back in 1958-1961 for the drillability assessment of rocks by percussive drilling (Dahl et al., 2012). In recent years this method has been used in major international mechanized underground construction projects, and is considered as one of the most recognized and widely used methods for the performance prediction of Tunnel Boring Machines (TBMs) (Dahl et al., 2007). NTNU/SINTEF test method comprises of a set of drillability tests [Brittleness value (S_{20}) test, Sievers'J-value (SJ) test, Abrasion value (AV) test and Abrasion Value Steel (AVS) test] and three different drillability indices (DRI, BWI and CLI). These indices including Drilling Rate Index[TM] (DRI), Bit Wear Index[TM] (BWI) and Cutter Life Index[TM] (CLI) provide indirect measures for the drillability of rocks (Zare and Bruland, 2012) and are described as follows:

2.2.2.3.1. The Drilling rate index (DRI). The DRI was developed at the Department of Geology and Mineral Resources Engineering at NTNU in the year 1958-1961 (Selmer-Olsen and Lien, 1960). The DRI is described as the Brittleness Value corrected for the rock surface hardness (Dahl, 2003). It is evaluated on the basis of two laboratory tests consisting of the Brittleness Value (S_{20}) test and Sievers'J-Value (SJ) miniature drill test (Selmer-Olsen and Lien, 1970).

2.2.2.3.2. <u>The Brittleness value (S_{20}) test.</u> This test was originally developed in Sweden by Matern and Hjelmer (1943) for determining the strength properties of aggregates. Later on several modified versions of this test have been developed for different purposes. The version of S_{20} test (Figure 2.15) utilised by NTNU/SINTEF has been used since the end of the 1950s for the determination of drillability of rock (Dahl et al., 2012).
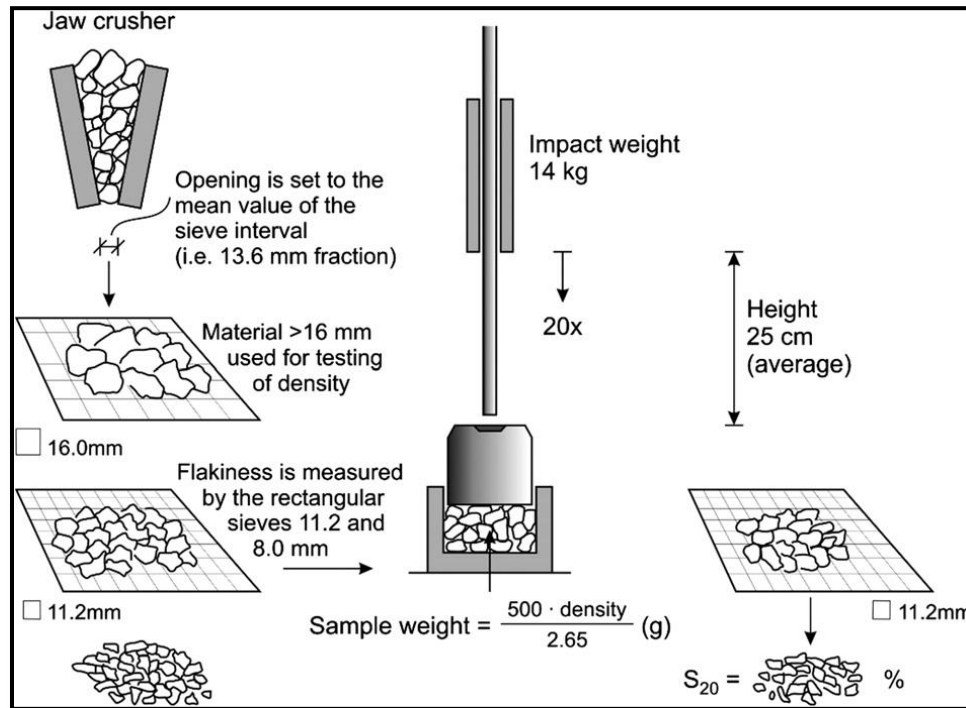
Figure 2.15. Schematic view of the Brittleness Value (S_{20}) test (after Dahl et al., 2012).

This test gives a measure of the mechanical properties of a rock sample including flakiness number (*f*) and brittleness value (S_{20}) (Dahl, 2003). The test sample consists of crushed rock fraction with size ranging between 16mm and 11.2mm sieves. The sample weight is an equivalent of 500 grams for a rock density of 2.65, adjusted with the sample density (Bruland, 1998). The Brittleness Value (S_{20}) is equal to the percentage of sample material passing 11.2mm sieve, after the aggregate sample of the 11.2-16 mm fraction has been crushed by 20 blows in a steel mould. Then S_{20} is the average value of 3 to 5 parallel tests (Zare and Bruland, 2013).

2.2.2.3.3. <u>The Sievers' J-value (SJ) test.</u> The Sievers'J miniature drill test was initially developed by Sievers in the 1950s (Dahl, 2003). It provides a measure of the

rock surface hardness or resistance to indentation of the rock. The SJ is the average value of the measured drill hole depths in 1/10 mm, after 200 revolutions of the 8.5 mm miniature drill bit (Figure 2.16).
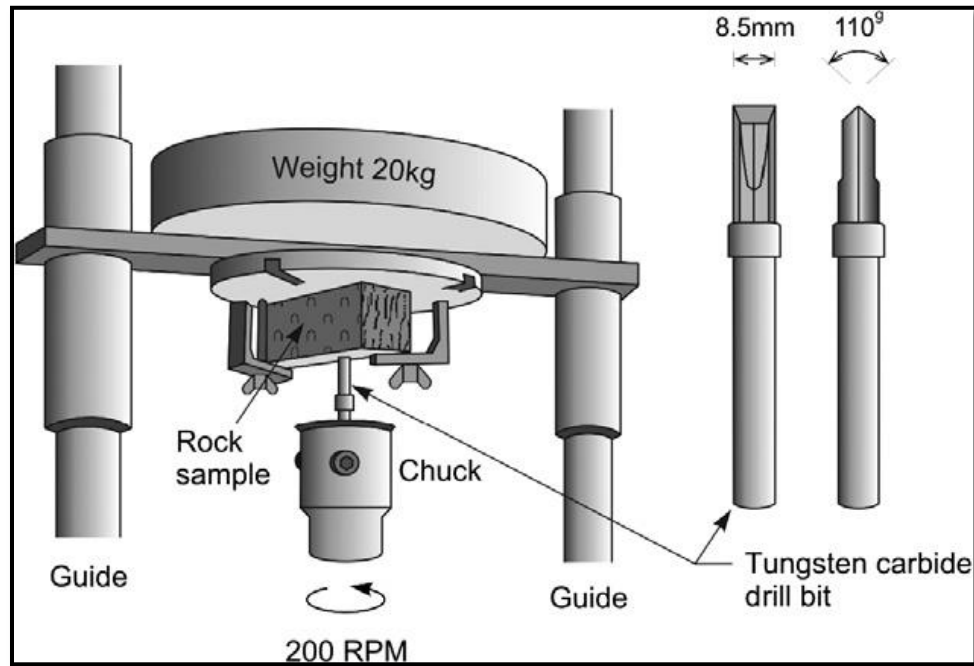
Figure 2.16. Schematic view of the Sievers' J-Value (SJ) Miniature Drill test (after Dahl et al., 2012).

The SJ test is conducted on a pre-cut surface of the rock sample, which is perpendicular to the foliation of the rock. Sievers'J-Value is therefore measured parallel to the rock foliation. This test is carried out normally as 4-8 drillings, depending upon the textural variations of the rock sample, and reported as the mean value of the performed drillings. The SJ value is influenced by a number of factors including the mineralogical composition, grain size, grain cementation, degree of weathering or alteration, micofracturing and foliation of the rock (Dahl et al., 2012).

Dahl et al. (2012) developed a classification table (Table 2.11), based on the distribution of the recorded Sievers'J-Values of 3046 rock samples present in the NTNU/SINTEF database. Recently Ko et al. (2016) citing Dahl et al. (2012) have reported following correlation between SJ and CAI values:

$$SJ = 126.1 - 73.18(CAI) + 17.53(CAI^2) - 1.996(CAI^3) + 0.08876(CAI^4) \qquad (2.34)$$

Table 2.11. Classification of rock surface hardness (after Dahl et al., 2012).

Category (Surface Hardness)	SJ value (mm/10)	Cumulative percentage (%)
Extremely high	≤ 2.0	0-5
Very high	2.1-3.9	5-15
High	4.0-6.9	15-35
Medium	7.0-18.9	35-65
Low	19.0-55.9	65-85
Very low	56.0-85.9	85-95
Extremely low	≥ 86.0	95-100

2.2.2.3.4. <u>The Bit wear index (BWI).</u> Bit Wear Index is applied to assess the lifetime of drill bits used in rock drilling (Dahl, 2003). BWI is computed on the basis of two drillability tests namely DRI and the Abrasion Value (AV). The Abrasion Value (AV) test was introduced by the Department of Geology at NTH in the beginning of the 1960s (Dahl et al. 2013) and is a measure of time dependent abrasion on a tungsten carbide test bit from crushed rock powder (Zare and Bruland, 2013). The schematic of NTNU/SINTEF abrasion test set up is shown in Figure 2.17. In this test the abrasion powder finer than 1mm screen size passes under a tungsten carbide test piece, loaded with a static weight of 10 kg. The Abrasion Value is the weight loss in milligrams of the tungsten carbide bit after 100 revolutions of the steel disc rotating at the speed of 20 revolutions per minute. Therefore 100 revolutions of the steel disc is equivalent to 5 minutes of total testing time. The reported AV is an average value of 2 to 4 parallel tests (Dahl, 2003).

2.2.2.3.5. <u>The Cutter life index (CLI).</u> The Cutter Life Index was developed in the years 1980-1983, based on the original NTH test method. CLI is used to estimate the life in boring hours of TBM disc cutter rings. The CLI is computed on the basis of SJ value and the Abrasion Value Cutter Steel (AVS). The AVS test employs test bits of steel prepared from actual TBM disc cutter rings with specified properties (Dahl et al., 2012). The AVS is measured using the same test setup and procedure as for the Abrasion Value test (Figure 2.17). However the testing time for AVS test is one (01) minute, which corresponds to 20 revolutions of the steel disc. The AVS is calculated as the average value of the measured weight loss in milligrams after 1 minute testing time. The reported AVS is a mean value of 2 to 4 parallel tests. Dahl et al. (2012) have established a

classification table (Table 2.12), based on the statistical distribution of the recorded AVS test values of 1590 rock samples present in the NTNU/SINTEF database.
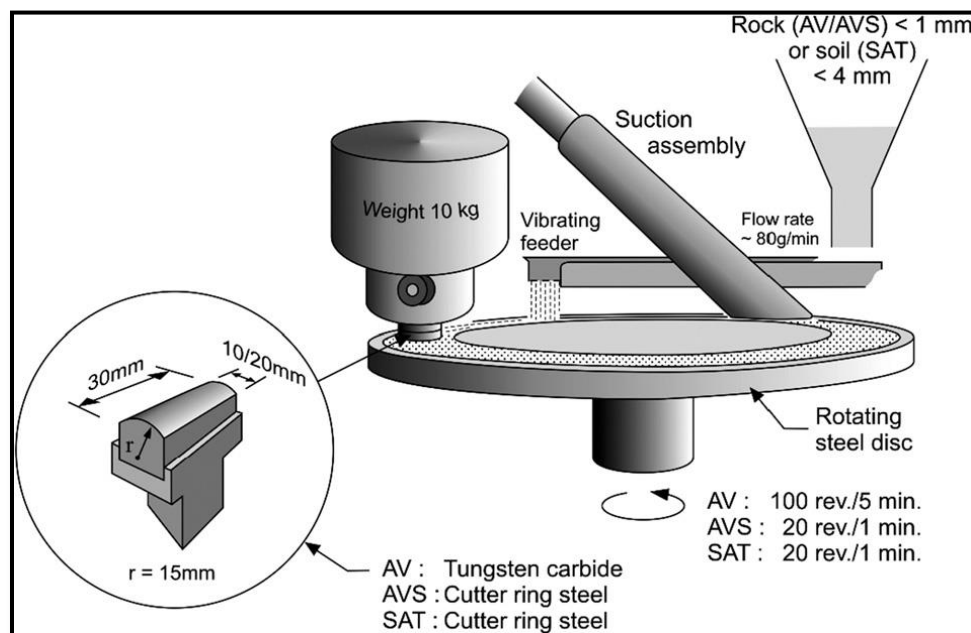
Figure 2.17. Outline of NTNU/SINTEF abrasion test setup (after Dahl et al., 2012).

Table 2.12. Classification of rock abrasivity on cutter steel test bit (after Dahl et al., 2012).

Category (cutter steel abrasion)	AVS (mg)	Cumulative percentage (%)
Extremely high	≥ 44.0	95-100
Very high	36.0-44.0	85-95
High	26.0-35.9	65-85
Medium	13.0-25.9	35-65
Low	4.0-12.9	15-35
Very low	1.1-3.9	5-15
Extremely low	≤ 1.0	0-5

The Sievers' J-value (SJ) and the Abrasion Value Steel (AVS) expresses the CLI by the following relationship   (Dahl, 2003):

$$\text{CLI} = 13.84 \left(\frac{\text{SJ}}{\text{AVS}}\right)^{0.3847} \tag{2.35}$$

In the Cutter Life Index equation 2.35, the component AVS explains how rapidly crushed rock and rock chips will abrade the ring, whereas the component SJ describes the surface hardness of the rock or alternatively how deep a TBM disc cutter ring will

indent into the rock face. Low SJ value means hard rock and depicts less indentation depth of the disc cutter resulting in mainly tip wear. High SJ value means less hard rock which in turn allows high cutter ring indentation into the rock face, resulting in wear at the tip as well as on the sides of the disc cutter (Zare and Bruland, 2013). It is worth mentioning that the test results of about 3200 rock samples from numerous rock excavation projects around the globe are present in the NTNU/SINTEF database and are continuously being updated (Dahl et al., 2012). However it should be noted that the drillabilty indices especially BWI and CLI is based on costly, time consuming, laborious and complex drillability tests (SJ, AV and AVS). Moreover these tests require rock sample in significant quantities. At present very limited work is published on the relationships of AVS and CLI with CAI and other rock parameters comprising UCS and quartz content among others, which is cited in Table 2.13 below:

Table 2.13. Correlations of CLI with Rock Parameters.

Sr. #	Parameters	Investigators	Correlations with AVS and CLI
1	CERCHAR Abrasivity Index	Bruland (1998)	$CLI = 2.87(CAI^2) - 35.62(CAI) + 112.9$ (Recommended for rough assessment purposes)
		Dahl et al. (2012)	1) $AVS = 6.186 (CAI) - 8.317$ 2) $CLI = 115.24(CAI^{-1.724})$
		Ko T.Y. et al. (2016)	$CLI = -8.725 \times \ln(CAI) + 18.898$
2	Quartz Content (%)	Ko T.Y. et al. (2016)	$CLI = 16.519(Q^{-0.272})$
3	Uniaxial Compressive Strength (MPa)	Ko T.Y. et al. (2016)	1) $CLI = -3.442 \times \ln(UCS) + 23.851$ 2) $19.029 - 1.515(CAI) - 0.0796(Q) - 0.02654(UCS)$
CAI- CERCHAR abrasivity index; Q- Quartz content (%); UCS- Uniaxial compressive strength			

2.2.2.4. Schimazek's Pin-on-Disc test. According to Verhoef (1997) this test developed by Schimazek and Knatz (1970) was performed by using a turning table generally applied in grinding and polishing. A rock disc is placed on the turning table as shown in Figure 2.18. In the beginning of test the rock surface is first polished with 240 SiC powder. A 10 mm diameter pin prepared from readily wearing St 50 wedge steel having 700 MPa tensile strength with a 90° conical point flattened to 0.3 mm, is placed in a holder and loaded with a mass of 4.5 kg. During a test the pin holder moves radially outward, which results in the pin describing a spiral path on the rock surface, cutting or scratching continuously in fresh rock. The distance between the cutting grooves is 0.5

mm and the number of revolutions of the disc is 100. The rate of rotation of disc is set at 25 rpm. The total distance travelled by the pin is 16 m. After a test the mass loss of the pin is determined. On each rock type 10 tests are conducted and the average mass loss is reported. It is pertinent to mention here that Schimazek and Knatz (1970) compared the measured mass loss of the pins with the variation in tensile strength, quartz content and grain size of an artificial rock (concrete with varying quartz content and grain size) and found a linear correlation called Schimazek's F-value.
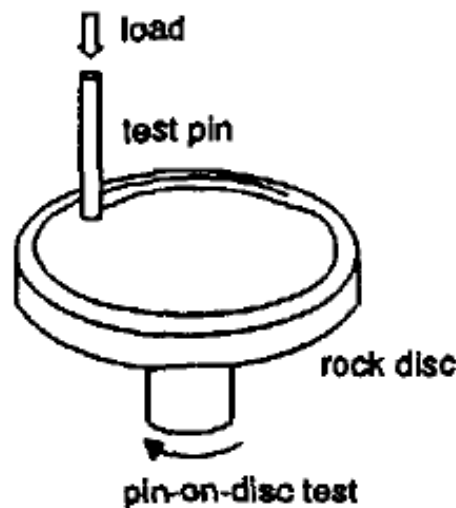
Figure 2.18. Schimazek's pin-on-disc test (after Verhoef, 1997).

Schimazek's pin-on disc test was further explored by Paschen (1980). He identified that the presence of loosened rock particles by the pin, interfere with the pin wearing process. Therefore paschen (1980) modified the Schimazek's pin-on disc test by using a lathe where the pin would horizontally press into the rotating rock disc as illustrated in Figure 2.19.
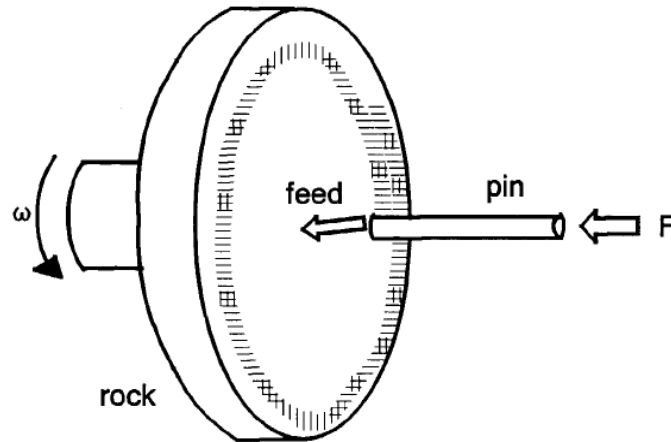
Figure 2.19.The principle of pin-on-disc test on lathe (Verhoef, 1997; after Paschen (1980)).

2.2.2.5. Modified Taber abrasion test. Tarkoy (1973) reports this test was developed over the several past years in the Civil Engineering Rock Mechanics Laboratory at the University of Illinois at Urbana-Champaign. An NX size, 0.6 cm thick rock disc, is secured to the rotating turntable of the abrasion machine (Figure 2.20). An Abraser wheel (Taber Calibrade H-22), on an axle allowing it to revolve freely is placed on the rock specimen as a rider. An additional weight of 250 grams is placed on the arm carrying the abraser wheel. As the turn table revolves, the main component of travel of the rock specimen is parallel to the axis of the abrading wheel causing it to be dragged along the rock surface with an abrading action. In order to make even wear possible of the abrading wheel, it is positioned so that it revolves slowly on its axle as the rock disc passes under it. Throughout testing, abrasion debris is continuously sucked from the rock surface and abrader wheel by a vacuum. A minimum of two rock discs are tested for each rock type. Each side of the rock disc is revolved 400 times, with a fresh abraser wheel on each side. The rock disc and its related two abrader wheels are weighted before and after the tests and the abrasive wheels are resurfaced before applying them to the next test.

Rock abrasivity is determined by measuring the loss in weight of the abraser wheels and is defined as the reciprocal of the average weight loss in grams. On the other hand the loss in mass of the rock disc is a measure of the rock abradability.

Figure 2.20. Modified Taber abrasion test (after Tarkoy, 1973).

2.2.2.6. Core cutting test. McFeat and Fowell (1977) report that the core cutting test was developed by Roxborough and Phillips (1974) to simulate the cutting action of a drag-pick tool and to measure the corresponding cutting properties of rock material (cutting and normal mean peak force components, specific energy, cutting wear and coarseness index). The cutting wear is produced by two simultaneously induced mechanisms namely chipping and abrasion. Verhoef (1997) describes that the test arrangement is placed on a shaper and consist of cutting a 12.7 mm wide and 5 mm deep groove along the surface length of a rock core sample parallel to its axis. The core is then rotated by 180° to make a similar parallel cut. If the core has not been broken, it may be rotated again to make a third and fourth cut. If the core is 250 mm long a maximum length of 1m can be tested. For each rock core tested a new tungsten carbide chisel shaped cutter insert is used (width: 12.7mm, front rake angle: 0° and back clearance angle: 5°). To determine cutting wear the tungsten carbide insert is weighted before and after the set of up to four cuts for its weight loss.

2.2.2.7. Core abrasion test. Roxborough (1987) developed the core abrasion test to examine the contribution of abrasive wear to the total chisel wear in the core cutting test. In this test the core is placed in a lathe rotating at 50 rpm and feeding the tungsten carbide insert at an angle of approximately 45° axially along the outer core surface as shown in Figure 2.21. The forward feed is controlled at 0.1 to 0.2 mm per revolution. In this way lengths of 25 up to 100 meter of rock surface may be abraded. The abrasive wear can be described as the ratio of loss in weight of tungsten carbide insert to the cutting length (mg/m).
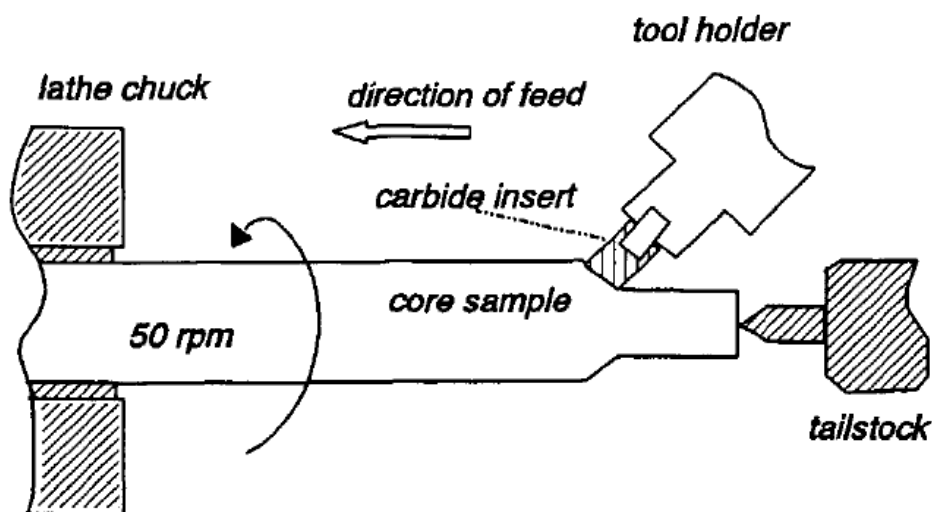
Figure 2.21. Experimental setup of core abrasion test (Verhoef, 1997; after Roxborough (1987)).

2.2.2.8. Deketh's scraping test. Deketh et al. (1998) describe the scrapping test to explore the transition of wear processes (from scraping process using chisel to cutting process) for different rock types at varying cutting depths. Figure 2.22 illustrates the test principle. The test is displacement controlled. A lathe machine is employed to rotate 140 mm diameter rock discs which are penetrated by the chisels with a constant feed rate. The chisels are either of the relatively soft Fe60 K steel (Vickers Hardness of 300 VH), or a hardened SRO 57N steel directly derived from dredger teeth (Vickers Hardness of 614 VH). In most cases the experiments were conducted with a cutting velocity of 0.4 m/sec. The loss in mass of the chisel and volume of the rock material excavated are measured and in the end the wear phenomenology of the chisel are described and photographed.
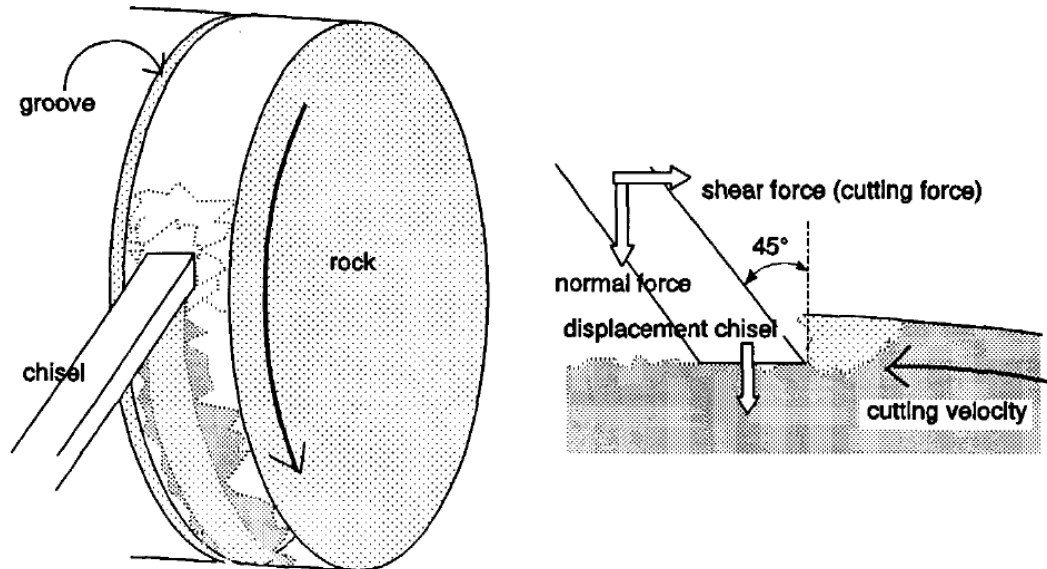
Figure 2.22. The principle of scraping test experiments (Verhoef, 1997; after Dekth (1995)).

2.2.2.9. The Gouging abrasion test. Labas et al. (2012) report this test was developed at advanced Manufacturing Technologies Centre, Australia. A rectangular rock sample, 80 ± 0.5 mm long, with flat and smooth wear surface is placed into the sample holder (Figure 2.23). A steel wear tool of hardness 40–42 HRC, with a 90° sharp conical point is fastened to the swinging pendulum arm of the abrasion tester and the arc of the pendulum travel is fine-tuned in such a way that the wear tool definitely contacts the flat surface of the rock sample as it swings past. Gouging Abrasion Index (Gi) is computed as the average diameter of the wear flat of wear tools in millimetres multiplied by a factor of 10. The reported Gi value is the mean of three to five parallel tests conducted on each rock sample. The Gouging Abrasion Index can be used for the estimation of wear rates of crushers, TBM disc cutters, hoppers and chute linings and ground engaging tools.
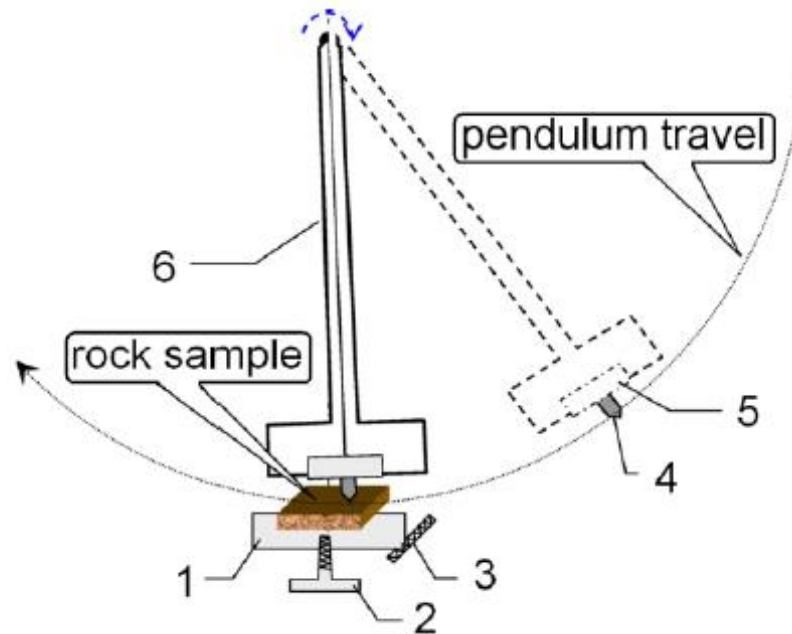
Figure 2.23. The Gouging abrasion test setup: 1- sample holder; 2- transmission screw assembly for vertical adjustment of sample holder; 3- spring loaded mechanism for horizontal adjustment of sample holder; 4- wear tool; 5- wear tool holder; 6- pendulum arm (Labas et al., 2012; after Golovanevsiky and Bearman, 2008).

2.2.2.10. Abrasionmeter according to ON441121 norm. Labas et al. (2012) report this abrasionmeter as per the ON441121 norm, was developed at the Institute of Geotechnics of Slovak Academy of Sciences. It is a rotating machine which provides constant revolutions of 100 rpm and applies a constant thrust force of 100 N on rock specimen during testing. Testing requires a set of normalized metal pins (number of pins relates to the number of tracks) of 3.0 mm diameter, 22mm length, 720 MPa strength and 210 HB hardness. A prepared rock specimen of minimal diameter of 59.0 mm is place centrally into the fixing jaws of the abrasionmeter (Figure 2.24) keeping the measured surface vertical and orthogonal to the axis of the installed normalized metal pin. The pre-weighted set of metal test pins is then fixed one after another into the slider of the machine. The measurements (with individual pins) are taken subsequently on the concentric tracks with diameters of 10, 20, 30, 40 and 50 mm, at constant thrust of 100N and defined number of revolutions n=32. The testing is finished when the metal pins complete a total track of 15.08 meters long. The tested set of pins utilized for one rock sample are reweighted to find the total weight loss and the abrasiveness F_v of tested rock body in milligrams per meter is computed by the following equation:

$$F_v = G/L \tag{2.26}$$

Where; F_v = rock abrasiveness in mg/m;

G = sum of total weight loss of the set of metal pins in mg;

L = length of total track of motion (15.08 meters).
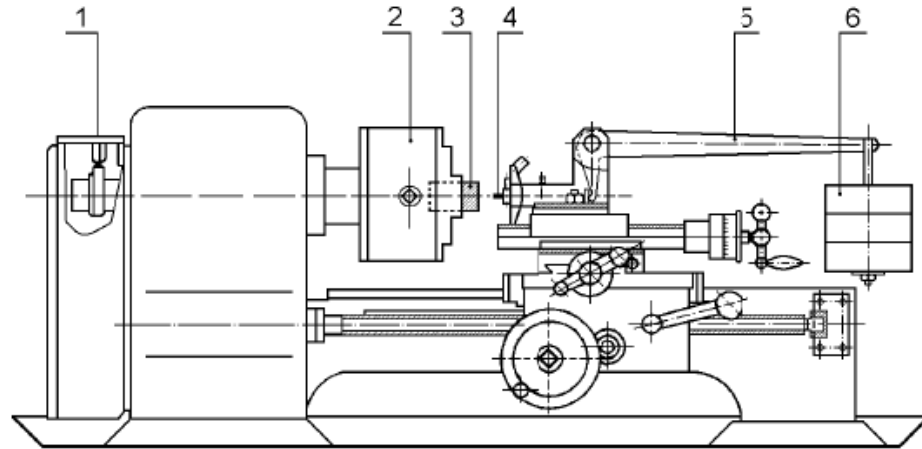
Figure 2.24. Schematic of abrasionmeter as per ON441121 norm: 1- revolution counter; 2- chuck for fixation of the test rock specimen; 3- rock sample; 4- metal test pin; 5- lever gear for constant thrust; 6- balance weight (after Labas et al., 2012).

2.2.2.11. New test equipment for rock abrasion measurement. Rostami et al. (2013) report the development of new prototype test equipment, which used a small machine shop lathe for preliminary testing. The device simply consists of a handle mounted on a frame, which can transfer a vertical applied dead load into the horizontal load applied on a pin which is guided through a cylinder and pressed against the rock surface on a rock sample that is held and rotated on chuck of the lathe machine as shown in Figure 2.25. Various loads can be applied on the pin by just changing the position of the dead load on the upper surface of the swinging arm. Therefore by varying the test duration, rock specimen rotational speed and distance from the core centre different scratch lengths can be obtained. For initial tests the cited authors utilized the same pins which are used in Cerchar testing (HRC 54/56).
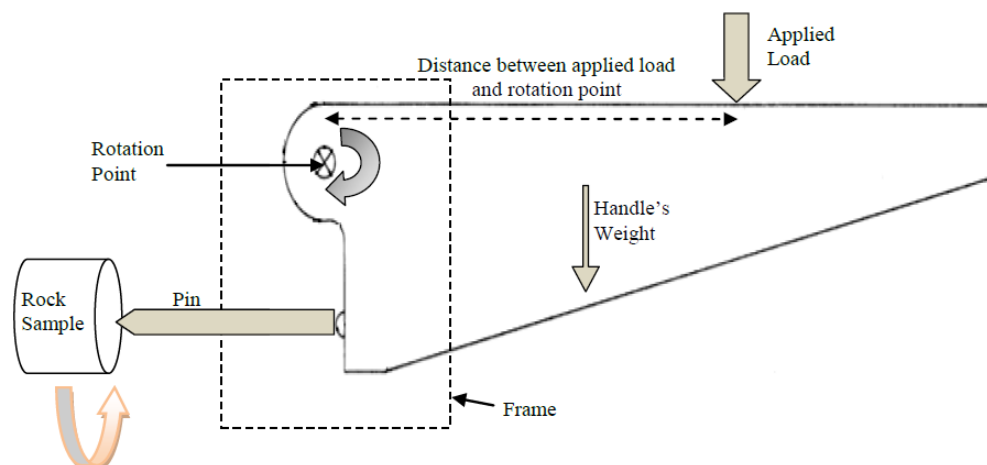
Figure 2.25. Schematic view of the new rock abrasion measurement test equipment (after Rostami et al., 2013).

2.2.2.12. The steel cube test. West (1981) reports that the steel cube test was initially developed to test the abrasiveness of rock debris generated by a full-face tunnelling machine, and later on it was utilized for the evaluation of the abrasiveness of rock aggregates used to manufacture concrete blocks for instrumented drilling trials. In this test a one-inch cube of bright mild steel is tumbled in a tumble polishing machine together with a water saturated rock aggregate sample of 900 grams, for three hours. The abrasiveness of rock is measured as the loss in weight per hour of the steel cube, expressed as a percentage of its original weight. The cited author also developed a correlation between replacement rate of disc cutter on full-face tunneling machine for a tunnel drive in Carboniferous rocks and rock abrasiveness measured by steel cube test.

2.2.2.13. Modified Schmidt hammer test. The unique feature of this test is its application directly in the field and in-situ rock conditions for the measurement of rock abrasivity. Janach and Merminod (1982) employed a modified version of type-M Schmidt hammer (impact energy 30 Joules), furnished with a steel roller bearing bit of Rockwell hardness 62 HRC to evaluate rock abrasiveness. The loss of mass of the bit after performing a number of hammer impacts on a particular rock surface is a measure of rock abrasivity. The results of Schmidt hammer are reported in mass loss per total impact energy which is the impact energy of hammer times the number of blows (mg/kJ).The cited authors found useful correlation between the result of modified Schmidt hammer and mini-disc wear test which is utilized to measure performance of

TBM. Verhoef (1997) reports the use of smaller N-type Schmidt hammer (impact energy 2.25 Joules) to find the rock abrasivity for his experiments. The N-type hammer was equipped with bits of weaker steel types (wedge steel, St 37 or hardened steel, C45) which plastically deformed under the impact of blows with no resulting mass loss of the bit.

2.2.2.14. The Hacksaw test. According to West (1981) the Hacksaw test developed by Fowell (1970) is conducted on a rock core sample employing a typical workshop reciprocating hacksaw equipped with a high speed cutting edge blade. The rock core is fastened in a vice holder orthogonally to the blade and ten strokes of the reciprocating arm are given. The rock specimen is moved along the vice and the procedure is repeated ten times. For each test repetition a new pre-weighted blade is used. The tested blades are then accurately weighted after the test. The loss in weight experienced by the blade is a measure of rock abrasivity which is expressed in mg. Test results range up to about 350 mg for abrasive sandstones.

2.2.2.15. Voest-Alpine rock cuttability index test. Bamford (1984) reports the rock abrasivity measurement with Voest-Alpine rock cuttability test. The testing procedure involves casting a rock lump with cement into a cubic mould having side lengths of 100 mm. After curing when the cement has set the block is cut into two halves. The abrasion is measured on the exposed one half saw cut rock surface. A 3.5 mm diameter steel pin is vertically loaded with a 100 N force onto the rock surface, and rotated along a circular path a sufficient number of revolutions so that the total distance traversed is 3 meters. 5 different pins are used each in a different holder with a different rotational diameter. The holder with the largest rotation diameter is 50mm. The rock abrasiveness or coefficient of wear (mg/m) is calculated by using the following formulae:

$$\text{Wear coefficient} = \frac{\Delta M}{\text{Total traverse distance of 5 pins}} \qquad (2.26)$$

Where; ΔM = Total loss in mass of the 5 pins;

Total traverse distance of 5 pins = 15m.

2.2.2.16. The rolling indentation abrasion test (RIAT). Macias et al. (2015) report the development of a new test method for the measurement of rock abrasivity by rolling disc

called as Rolling Indentation Abrasion Test (RIAT). Figure 2.26 illustrates the RIAT setup which comprises of two small replaceable rolling discs. The rotation, torque and vertical pull down pressure to the wear tool is provided by an appropriate motorized drive unit. During operation the miniature cutter discs penetrate the surface of rock specimen. The miniature discs have a hardness 50 ± 1 HRC, with constant tip width and are manufactured from alloy (AISI type H13 Hot Work Tool Steel) used for building the real TBM cutter discs. For RIAT testing a prepared (cut and surface ground) intact rock specimen of at least 100 mm diameter is recommended. The suggested rolling velocity is 40 rpm, vertical thrust is 1250 N and testing time is 30 minutes. After testing the loss in weight (mg) of the wear discs is a measure of rock abrasivity reported as RIAT Abrasivity Index (RIAT$_a$). Additionally the penetration depth of the rolling discs into the rock surface is given by the RIAT Indentation Index (RIAT$_i$).
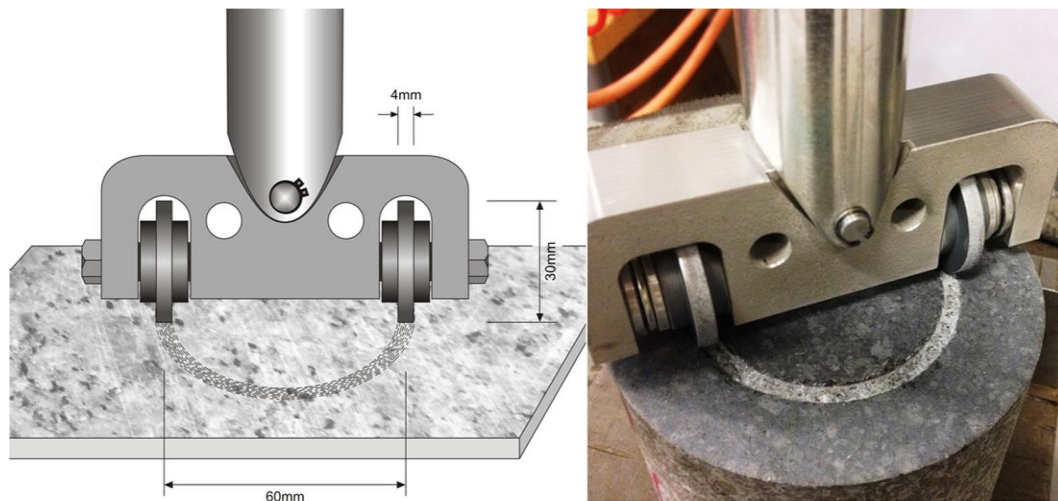
Figure 2.26. Schematic of Rolling Indentation Abrasion Test (RIAT) setup (after Macias et al., 2015).

2.3. SOIL ABRASIVITY MEASUREMENT METHODS

In recent years the increased application of shielded TBMs for soft ground tunneling projects in urban areas (underground metro lines, tubes, sever and drainage tunnels among others) has raised demand for the evaluation of wear and life of excavation tools as well as other machine components including cutter head structure, bulkhead, plunging wall structures, screw conveyors, slurry pipes, valves and pumps (Nilsen et al., 2007) coming in contact with soft ground and soils during the construction process. For soft ground applications, a variety of tunneling machines have been

introduced in the past few decades comprising of slurry shields and earth pressure balance (EPB) machines (Alavi Gharahbagh et al., 2011). At present different methods for the measurement of soil or soft ground abrasiveness have been developed which are discussed below:

2.3.1. NTNU/SINTEF Soil Abrasion Test (SAT^{TM}). According to Jakobsen et al. (2013) the new NTNU/SINTEF SAT test is developed from the existing NTNU/SINTEF abrasion tests. Figure 2.17 shows the schematic of the apparatus used for the SAT test as well as for Abrasion Value (AV) and Abrasion Value Cutter Steel (AVS) tests. The original SAT tests were conducted with an upper grain size limit of 1mm (Nilsen et al., 2006a to c) by employing the same test piece as used for AVS tests. But now the modified SAT test (Figure 2.27) utilizes a soil sample passing 4.0 mm sieve mesh, in comparison to the AVS test which uses a crushed rock powder of <1 mm size. In order to include soil particles up to 4.0 mm the original SAT test piece was also modified by increasing its width from 10 mm to 20 mm (Nilsen et al., 2007). With this modification now the SAT test can be applied to find the abrasivity of clay, silt and sand fractions. However the test is not valid for testing fragment sizes greater than 4 mm (Jakobsen et al., 2013).
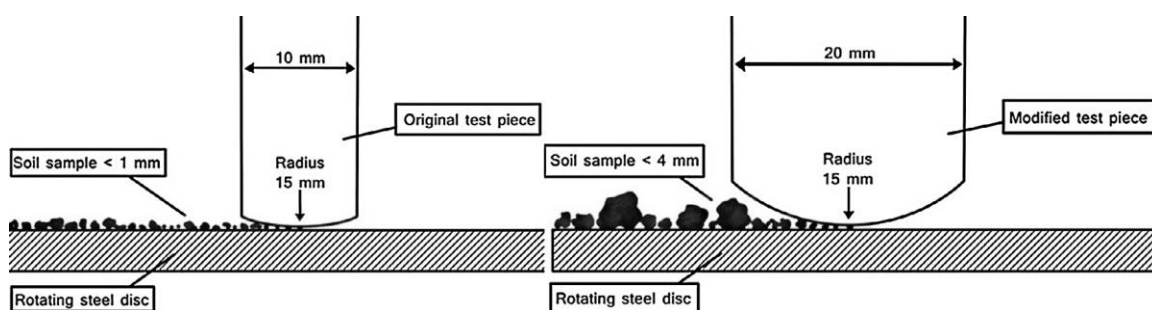
Figure 2.27. The original SAT test piece (left) and modified and recent test piece (right) (after Jakobsen et al., 2013).

2.3.2. The Penn State Soil Abrasion Testing Method. Alavi Gharahbagh et al. (2011) proposed this method for finding Penn-state Soil Abrasion Index (PSAI) which is measured by employing the Penn-state soil testing apparatus as shown in Figure 2.28. The test apparatus comprises of a cylindrical chamber of 14 inch diameter and 18 inch in height and a propeller coupled to a drive shaft which rotates within the testing chamber (partially filled with the soil sample). The complete assembly is mounted on a drill press

equipped with a 5 hp motor with variable rpm settings down to 60 rpm. The design of testing vessel allows test performances under ambient pressures of up to 10 bar. The test propeller of 150 mm radius has three blades that are welded at an angle of 120° on a cylindrical base. In order to protect propeller blades from severe wear and more accurate measurement of the weight loss on the tools, the blades are fitted with removable steel covers. To determine soil abrasion the covers are weighted before and after each test to calculate weight loss in grams during the test within a given time span.
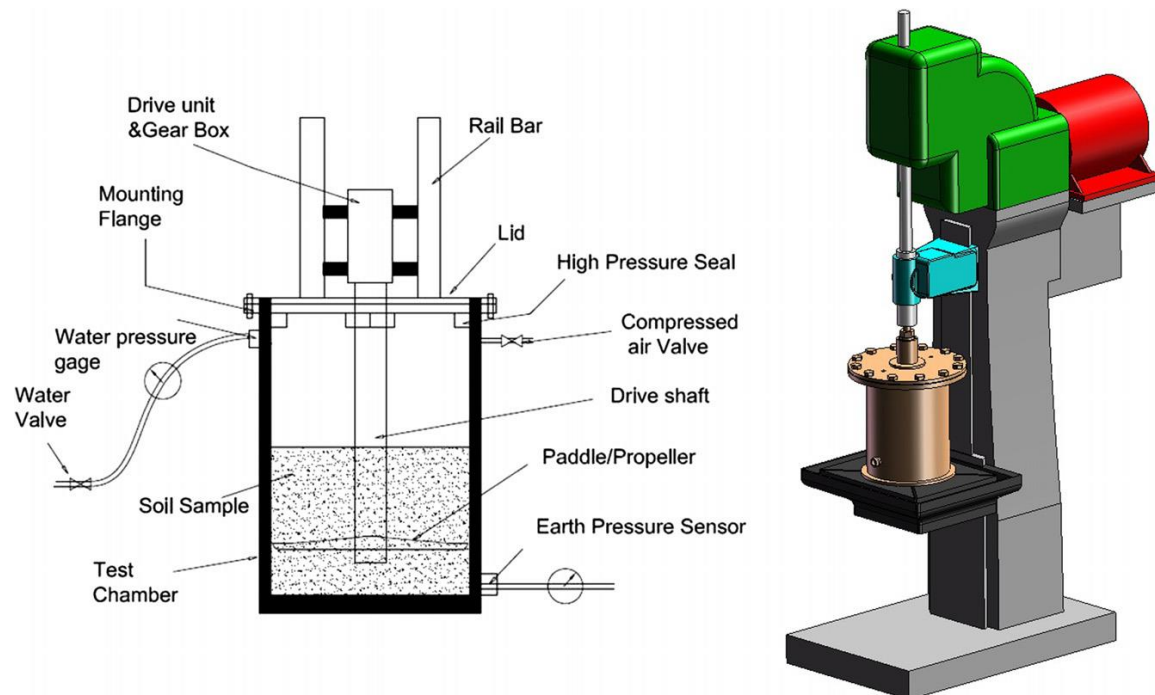
Figure 2.28. The schematic view of a Penn-state abrasion testing apparatus (after Alavi Gharahbagh et al., 2011).

2.3.3. The Soft Ground Abrasion Tester (SGAT). Jakobsen et al. 2013 report the SGAT device and the applied testing procedure were developed jointly by NTNU, SINTEF Rock Engineering and BASF Construction Chemicals for the estimation of in situ soil and soft ground abrasiveness. The SGAT apparatus (Figure 2.29) consists of a vertically mounted drive unit for imparting rotational movement to a shaft in the range between 0 to 100 rpm and a changeable wear tool comprising of two steel bars of Rockwell hardness HRC 20. The wear tool is attached to the shaft which rotates in a testing chamber containing soil sample. The use of two separate steels bars in the design of drilling tool offer an opportunity to differentiate between primary wear recorded on the

lower steel bar and secondary wear traced on the upper steel bar. The testing chamber provided with airtight lid is capable of creating a pressure of up to 6 bars. For introducing foam or conditioner in the test chamber a pump is provided.

The testing procedure of SGAT device consists of drying the soil sample at a temperature 30° for 48 hours in a ventilated oven before testing. After drying the soil grains coarser than 10mm are removed from the test sample and the sieved sample is properly mixed with water at the desired water content. However the soil sample already containing the desired water content can be directly tested without oven drying. In SGAT standard test procedure the penetration rate and rotational speed is fixed while the torque and thrust force varies. Alternatively it is possible to run tests at a fixed torque with varying vertical penetration rate or with varying rpm. The difference in weights of the testing tool measured before and after performing tests is a measure of soil abrasivity or wear reported as SGAT weight loss in mg.
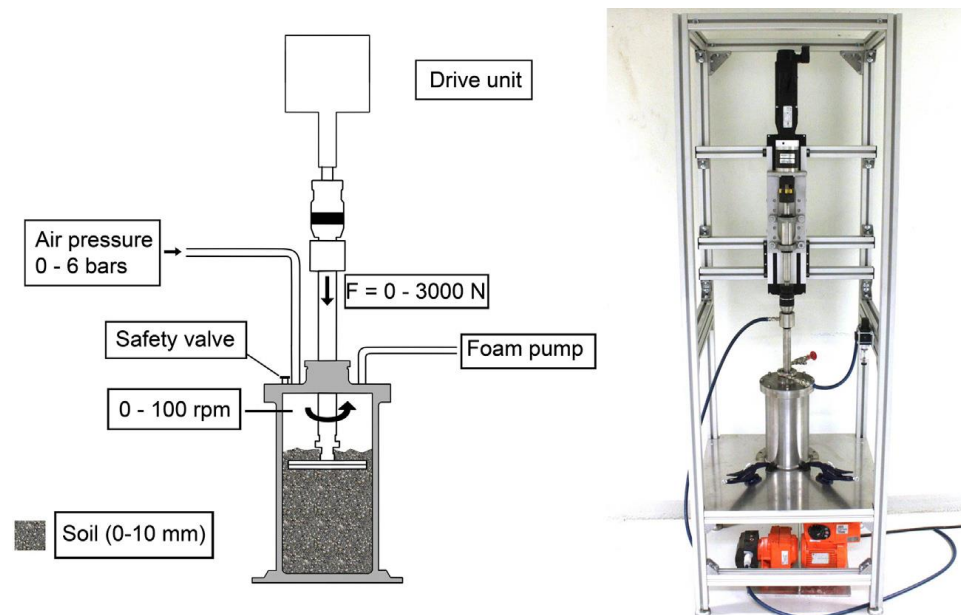
Figure 2.29. Schematic of Soft Ground Abrasion Tester (SGAT) (left) and picture of the test rig (right) (after Jakobsen et al., 2013).

2.3.4. The Soil Abrasion Testing Chamber (SATC). According to Barzegari et al. (2015) the SATC test apparatus (Figure 2.30) is designed to simulate the EPB-TBM chamber conditions in laboratory scale for the determination of soil abrasivity. The device consists of a gearbox coupled to a motor (750 W, power capacity) to rotate a wear plate at a speed of 20 rpm inside a cylindrical container. The soil container having 20 cm

diameter and 12 cm in height can test a variety of soils with particle sizes ranging from clay to silt to gravel up to 10 mm size. In order to provide real time soft ground tunnelling conditions the testing device contains a pneumatic pushing jack capable of exerting pressure up to 3 bars on the soil sample. The wear plate is a disc of 15cm diameter and consists of mild steel having hardness of 65-70 HRB. It is connected to a shaft to rotate inside at the bottom of soil chamber. Soil abrasiveness is determined by measuring the weight loss of the wear plate after rotating it for a period of 10 min under soil sample. Each test procedure utilizes a new wear plate for the measurement of soil abrasivity.
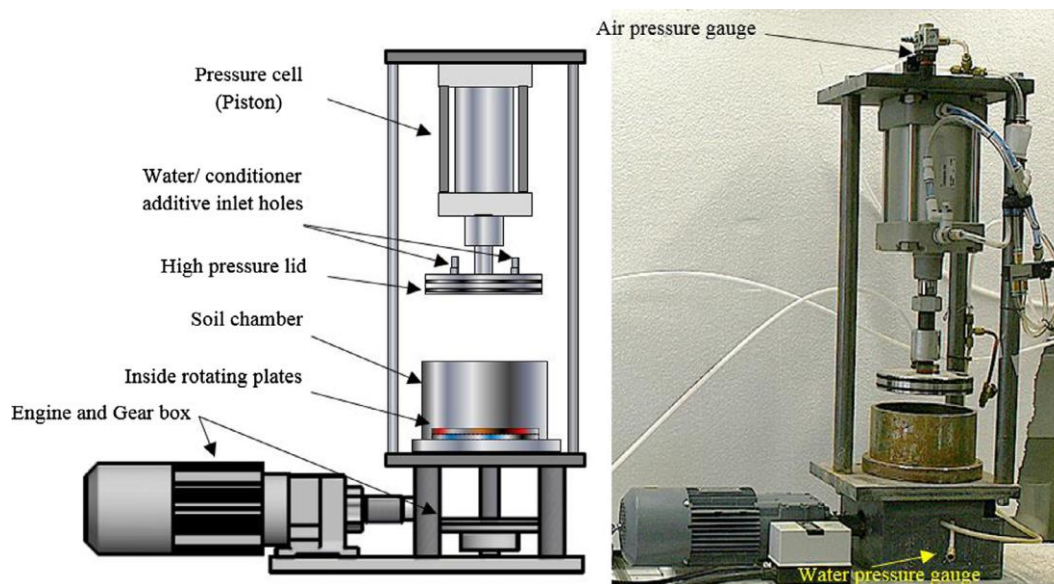
Figure 2.30. The outline and picture of soil abrasion testing chamber (SATC) device (after Barzegari et al., 2015).

2.3.5. The FAUT Method. Mirmehrabi et al. (2015) report the development of FAUT method and testing device (Figure 2.31) at the Ferdowsi University of Mashad, Iran for the evaluation of soil abrasion. This test device consists of a cylindrical chamber of 20 cm in diameter and utilizes four steel bolts (M8 type) as wear tools, each of 90 mm in length having Vickers Hardness of 179. The four steel bolts (wear tools) are fastened to a vertical shaft located in the test chamber. The shaft assembly is coupled with a 1.5 hp drive unit through a gear box system. The vertical center to center distance of one bolt to the next bolt is 20 mm and the lowest bolt is located 25 mm above the bottom of the chamber. To conduct test the cylindrical chamber is filled with approximately 6 kg of soil sample to a particular height (at least 10 cm) so that the maximum height of soil is some

centimeters above the top bolt. Subsequently the pre-selected dead load is applied on top of the soil sample to maintain a positive pressure and to engage the soil with the wear tools or bolts. To determine soil abrasiveness index the weight of all bolts before and after testing is measured accurately to register the weight loss. The summation of all four weight losses gives the proposed FUAT soil abrasivity index.
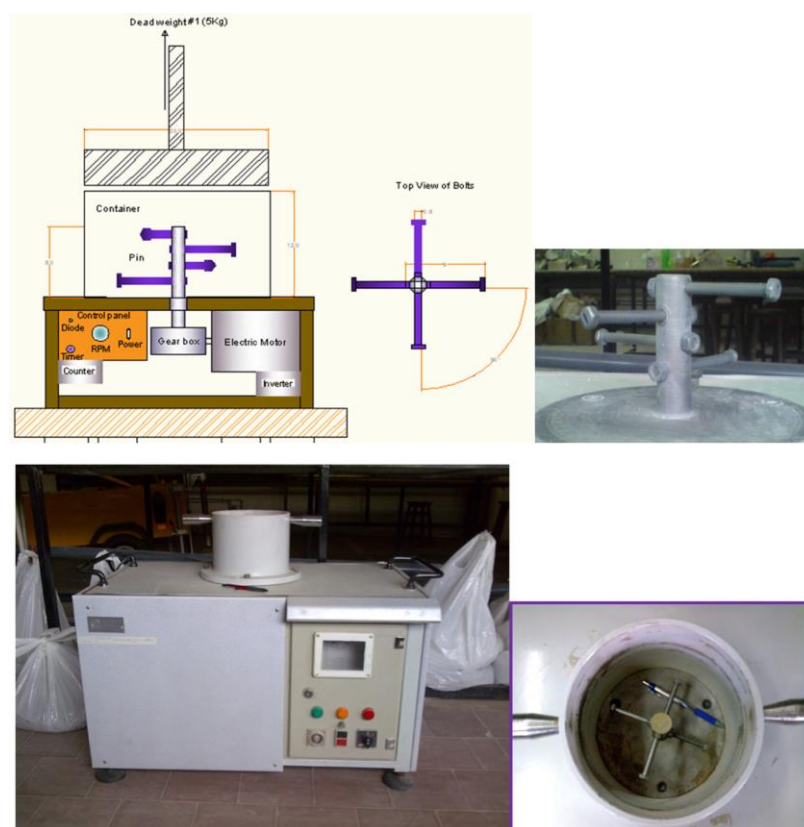
Figure. 2.31. The FUAT soil abrasivity testing setup: schematic outline of device (upper left) and its laboratory photograph (lower left); shaft side view (upper right) and top view of the shaft (lower right) (after Mirmehrabi et al., 2015).

2.3.6. The RUB Testing Device. Kupferle et al. (2016) report the development of a new tunneling apparatus and the test method at the Ruhr-University Bochum (RUB), to determine the abrasion of tools used for soil excavation. The RUB testing device (Figure 2.32) has a horizontal setup and simulates the real time excavation process through the soil, analogous to TBM tunneling. The RUB tunneling device consists of a container (750 mm in length and 195 mm in diameter) and operates on a lathe machine. Figure 2.33 shows that a shaft is clamped in the drill chuck and a star shaped cutting head equipped

with steel styli is mounted on the other end of same shaft. The steel wear pins are made of S275JR steel which is used in the construction of TBM cutting head rim. To support the excavated soil, a spring-seated PTFE liner is braced against the soil container lid. For running a test the whole assembly is horizontally mounted on a lathe machine (Figure 2.32). After each test run the container is disassembled and the worn out test styli by soil excavation are then analyzed to determine the wear. The cumulative loss in weight of the test pins (12 pins over the whole track radius or 24 for double track stocking) serves as a measure of wear.
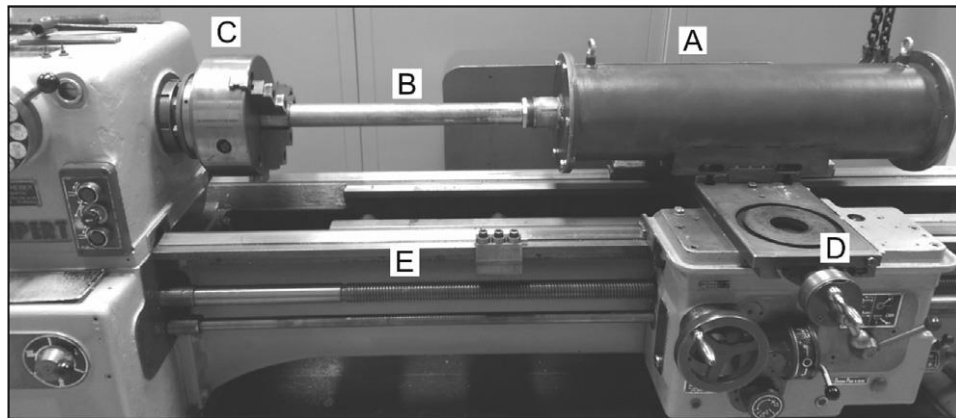
Figure. 2.32. The photograph of RUB Tunnelling Device mounted on a lathe machine. (A) The sealed container with soil. (B) Shaft equipped with cutting head. (C) The drill chuck. (D) Lathe carriage (E) Horizontal spindle (after Kupferle et al., 2016).
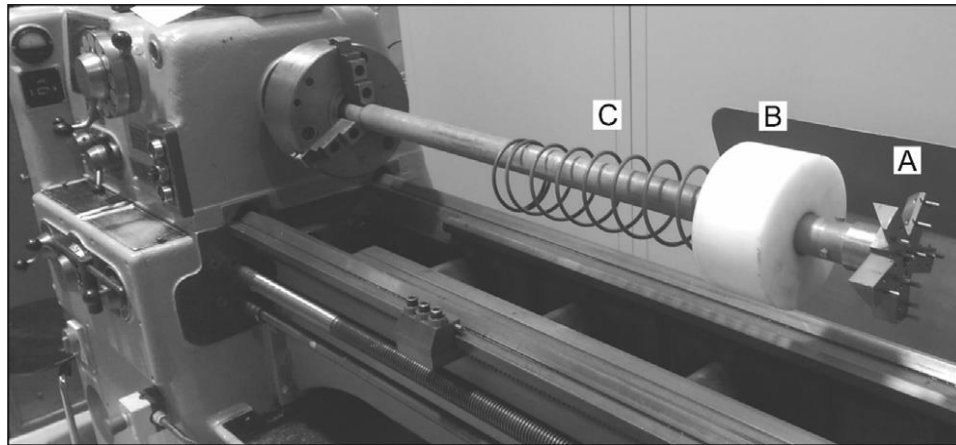
Figure. 2.33. The RUB Tunnelling Device mounted on a lathe machine without container. (A) Cutting head. (B) PTEF liner. (C) Spring (after Kupferle et al., 2016).

3. RESEARCH METHODOLOGY

This study comprises of a comprehensive testing program including the rock abrasivity tests, petrographic thin section analyses, mechanical strength tests including uniaxial compressive strength (UCS) and Brazilian tensile strength (BTS), density, pore volume, porosity and p-wave velocity tests. This section comprises the details pertaining to the rock samples included, as well as the description of test equipments and experimental procedures adopted for conducting this research work.

3.1. ROCK SAMPLE COLLECTION

51 rock types selected from 25 rock formations were collected from Punjab (Salt Range, Kirana Group and Surghar Range), Khyber Pakhtunkhwa (Sirban Hill Abbottabad, Hazara and Oogi) and Azad Jammu and Kashmir (Nelum Valley) regions of Pakistan, to provide a good representation of rocks with various abrasion characteristics. Table 3.1 summarizes the details of rock groups and sampling sites. The geological description of the selected rock samples along with their formations are presented in Table 3.2 (Shah, 2009).

Table 3.1. List of selected rocks.

Sr. No.	Rock	Rock Group	Location (in Pakistan)
1	Dolerite-1	Igneous	Kayan, Azad Jammu and Kashmir
2	Dolerite-2	Igneous	Chugian, Azad Jammu and Kashmir
3	Dolerite-3	Igneous	Jhugian, Azad Jammu and Kashmir
4	Dolerite-4	Igneous	Sillanwali, Punjab Province, (Latitude 31°45′ 30″ N; Longitude 72°29′ 50″ E)
5	Granite-1	Igneous	Jura, Azad Jammu and Kashmir
6	Granite-2	Igneous	Sandok, Azad Jammu and Kashmir
7	Granite-3	Igneous	Sarsangar, Azad Jammu and Kashmir
8	Granite-4	Igneous	Keran, Azad Jammu and Kashmir
9	Granite-5	Igneous	Oogi, Khyber Pakhtunkhwa (KPK) Province
10	Granite-6	Igneous	Khewra Gorge, Punjab Province
11	Migmatite	Igneous	Kelseri, Azad Jammu and Kashmir
12	Andesite	Igneous	Nelum Valley, Azad Jammu and Kashmir
13	Granitic Gneiss-1	Metamorphic	Leswa, Azad Jammu and Kashmir
14	Granitic Gneiss-2	Metamorphic	Nelum Valley, Azad Jammu and Kashmir
15	Phyllite	Metamorphic	Abottabad, Khyber Pakhtunkhwa Province
16	Quartzite-1	Metamorphic	Abottabad, Khyber Pakhtunkhwa Province
17	Quartzite-2	Metamorphic	Tobar Village, Punjab Province
18	Siltstone-1	Sedimentary	Nelum Jehlum Hydro Power Project, Azad Jammu and Kashmir, (Latitude 34°23′ 34″ N; Longitude 73°43′ 08″ E)
19	Siltstone-2	Sedimentary	Khewra Gorge, Punjab Province
20	Sandstone-1	Sedimentary	Khewra Gorge, Punjab Province
21	Sandstone-2	Sedimentary	Khewra Gorge, Punjab Province
22	Sandstone-3	Sedimentary	Nelum Jehlum Hydro Power Project, Azad Jammu and Kashmir, (Latitude 34°23′ 34″ N; Longitude 73°43′ 08″ E)
23	Sandstone-4	Sedimentary	Tobar Village, Punjab Province
24	Sandstone-5	Sedimentary	Dandot Village, Punjab Province
25	Sandstone-6	Sedimentary	Zaluch Nala, Punjab Province
26	Sandstone-7	Sedimentary	Zaluch Nala, Punjab Province

Sr. No.	Rock	Rock Group	Location (in Pakistan)
27	Sandstone-8	Sedimentary	Jan Sukh Nala, Warcha, Punjab Province
28	Sandstone-9	Sedimentary	Makerwal, Punjab Province
29	Sandstone-10	Sedimentary	Makerwal, Punjab Province
30	Sandstone-11	Sedimentary	Zaluch Nala, Punjab Province
31	Sandstone-12	Sedimentary	Jansukh Nala, Warcha, Punjab Province
32	Sandstone-13	Sedimentary	Zaluch Nala, Punjab Province
33	Sandstone-14	Sedimentary	Balkasar, Punjab Province
34	Sandstone-15	Sedimentary	Khewra Gorge, Punjab Province
35	Sandstone-16	Sedimentary	Abottabad, Khyber Pakhtunkhwa (KPK) Province
36	Sandstone-17	Sedimentary	Jansukh Nala, Warcha, Punjab Province
37	Sandstone-18	Sedimentary	Herighal Majeed Gala, Hydro Power Project, Azad Jammu and Kashmir, (Latitude 33°56′ 37.03″ N; Longitude 73°41′ 56.21″ E)
38	Chamositic Siderite	Sedimentary	Zaluch Nala, Punjab Province
39	Dolomite-1	Sedimentary	Zaluch Nala, Punjab Province
40	Dolomite-2	Sedimentary	Khewra Gorge, Punjab Province
41	Dolomite-3	Sedimentary	Sirban Hills, Abottabad, Khyber Pakhtunkhwa (KPK) Province
42	Dolomite-4	Sedimentary	Khewra Gorge, Punjab Province
43	Limestone-1	Sedimentary	Bestway Cement Quarry, Kattas, Punjab, (Latitude 32°43′ 13.44″ N; Longitude 72°56′ 6″ E)
44	Limestone-2	Sedimentary	D.G.Khan Cement Quarry, Kattas, Punjab, (Latitude 32°42′ 54″ N; Longitude 72°49′ 30″ E)
45	Limestone-3	Sedimentary	Bestway Cement Quarry, Hattar, Khyber Pakhtunkhwa (KPK) Province, (Latitude 33°50′ 30.88″ N; Longitude 72°52′ 24.12″ E)
46	Limestone-4	Sedimentary	Namal Gorge, Punjab Province
47	Limestone-5	Sedimentary	Makerwal, Punjab Province
48	Limestone-6	Sedimentary	Mustahkam Cement Quarry, Hattar, Khyber Pakhtunkhwa (KPK) Province, (Latitude 33°49′ 19.20″ N; Longitude 72°50′ 19.68″ E)
49	Limestone-7	Sedimentary	Nammal Gorge, Punjab Province
50	Rock Gypsum	Sedimentary	Khewra Gorge, Punjab Province
51	Marl	Sedimentary	Khewra Gorge, Punjab Province

Table 3.2. Geological description of selected rocks (Shah, 2009)

Sr. No.	Rock	Formation Name	Age	Description of Rock and Formation
1	Dolerite-1	Salkhala (Metabasites)	Precambrian	Very hard, compact, green to greyish green in color. The three major lithostratigraphic units of Nelum valley including Naril Group, Kundalshahi Group and Surgun Group are intruded by metabasites (dolerites now metamorphosed to amphibolites) dykes (Malik et al., 1996).
2	Dolerite-2	Salkhala (Metabasites)	Precambrian	Very hard, compact, green to greyish green in color. The three major lithostratigraphic units of Nelum valley including Naril Group, Kundalshahi Group and Surgun Group are intruded by metabasites (meta-dolerites and amphibolites) dykes (Malik et al., 1996).
3	Dolerite-3	Salkhala (Metabasites)	Precambrian	Very hard, compact, green to greyish green in color. The three major lithostratigraphic units of Nelum valley including Naril Group, Kundalshahi Group and Surgun Group are intruded by metabasites (meta-dolerites and amphibolites) dykes (Malik et al., 1996).
4	Dolerite-4	Kirana Complex (Hachi Volcanic)	Precambrian	This rock unit is hard, massive and has greenish grey color. It belongs to the Hachi Volcanic of the Kirana Complex, Punjab. The Kirana Complex comprising of Machh Super Group and Hachi Volcanic refers to the oldest rock sequence exposed in the Punjab and contains the most northerly exposures of the Indian shield. Hachi Volcanic mainly consists of dolerites, andesite, dacite, dacitic tuff, rhyolite and rhyolitic tuff with interbedded slates. Whereas Machh Super Group includes conglomerates, calcareous quartzite and slates (Chaudary et al., 1999).
5	Granite-1	Salkhala (Leucogranite)	Precambrian	Compact, medium hard, abrasive, white granite. The rock unit is mega crystic just like Mansehra granite. The three major lithostratigraphic units of Nelum valley including Naril Group, Kundalshahi Group and Surgun Group are intruded by leucogranite (Malik et al., 1996).

Sr. No.	Rock	Formation Name	Age	Description of Rock and Formation
6	Granite-2	Salkhala (Leucogranite)	Precambrian	Compact, medium hard, abrasive, white granite. The rock unit is mega crystic just like Mansehra granite. The three major lithostratigraphic units of Nelum valley including Naril Group, Kundalshahi Group and Surgun Group are intruded by leucogranite (Malik et al., 1996).
7	Granite-3	Salkhala (Leucogranite)	Precambrian	Compact, medium hard, abrasive, white granite. The rock unit is mega crystic just like Mansehra granite. The three major lithostratigraphic units of Nelum valley including Naril Group, Kundalshahi Group and Surgun Group are intruded by leucogranite (Malik et al., 1996).
8	Granite-4	Salkhala (Leucogranite)	Precambrian	Compact, medium hard, abrasive, white granite. The rock unit is mega crystic just like Mansehra granite. The three major lithostratigraphic units of Nelum valley including Naril Group, Kundalshahi Group and Surgun Group are intruded by leucogranite (Malik et al., 1996).
9	Granite-5	Mansehra Granite	Cambrian	Also called Swat and Mansehra granite complex which lie in the Peshawar-Kashmir zone. The age of Mansehra granite is 516 ± 16 MA (Geological Survey of Pakistan, 1993). The rock unit is fine to medium grained, massive, hard and compact with Greyish black color.
10	Granite-6	Tobra	Permian	Tobra formation exhibits varied lithology including Tillitic, Freshwater and Complex facies. This rock unit also called the Nagar Parkar pink granite of Precambrian age exists as boulders in the Tillitic facies of Tobra formation. This Pink granite is composed of coarse grains of orthoclase, quartz and few mafic minerals. The type locality is Tobar village in eastern part of the Salt Range Punjab, where the formation thickness is about 20 meters.
11	Migmatite	Salkhala (Naril Group)	Precambrian	This rock unit is medium hard, compact and has light colored granitic composition (Leucosome). The pre-cambrian Naril group forms the pre-Himalayan basement (Malik et al., 1996).
12	Andesite	Salkhala (Sharda Group)	Precambrian	Greyish black, very hard and compact rock belonging to Nelum valley. Wadia (1931 and 1934) included the lithological units occurring in Nelum valley as the Salkhala series. Later Ghazanfar et al. (1983) have classified the rock units outcropping in the north of Lawat as Sharda group. The Sharda group includes garnet mica schist, gneisses, minor graphite schists, marbles, calc-schists, garnet amphibole and calc-gneisses. In Sharda area the common rock units exposed are sharda gneisses and changan marbles.
13	Granitic Gneiss-1	Salkhala (Naril Group)	Precambrian	Acidic granulitic gneiss, medium strength, abrasive and banded rock. Contains mainly quartz, feldspar, biotite and garnet minerals. The pre-cambrian Naril group forms the pre-Himalayan basement (Malik et al., 1996).
14	Granitic Gneiss-2	Salkhala (sharda Group)	Precambrian	Acidic granulitic gneiss, medium strength, abrasive and banded rock. Contains mainly quartz, feldspar, biotite and garnet minerals. Wadia (1931 and 1934) included the lithological units occurring in Nelum valley as the Salkhala series. Later Ghazanfar et al. (1983) have classified the rock units outcropping in the north of Lawat as Sharda group. The Sharda group includes garnet mica schist, gneisses, minor graphite schists, marbles, calc-schists, garnet amphibole and calc-gneisses. In Sharda area the common rock units exposed are sharda gneisses and changan marbles.
15	Phyllite	Abbottabad	Cambrian	Abbottabad formation is mainly composed of dolomite, quartzite and Phyllite (Calkins et al., 1969). The type section is Sirban Hill near Abbottabad town, where the formation thickness is around 660 meters. Phyllite of this area has fine to medium grain in texture, light grayish-green color, which changes to brownish green upon weathering. Due to its phyllitic texture the weathered part readily crumbles and also the rock is difficult to core.

Sr. No.	Rock	Formation Name	Age	Description of Rock and Formation
16	Quartzite-1	Abbottabad	Cambrian	Abbottabad formation is mainly composed of dolomite, quartzite and Phyllite rocks (Calkins et al., 1969). The type section is Sirban Hill near Abbottabad town, where the formation thickness is around 660 meters. Quartzite is fine grained, pure white to creamish- white in color, which changes at some places to creamish-brown color. Compact, hard and abrasive rock which contains visible flaws or cracks due to structural disturbance.
17	Quartzite-2	Tobra	Permian	This rock unit is a member of the tillitic facies of Tobra formation and exists as quartzite boulders of grey color in the conglomeratic bed. The boulders are generally rounded and polished. The type locality is Tobra village in the eastern Salt Range Punjab.
18	Siltstone-1	Murree	Miocene	This rock unit is referred as the reddish brown hard siltstone of Murree formation. The Murree formation mainly contains monotonous sequence of sandstone with interbeds of siltstone, conglomerate lenses and shale. The type section is exposed to the north of Dhok Maiki in the Campbellpur district.
19	Siltstone-2	Tobra	Permian	The type locality is positioned near Tobra village in the Eastern Salt Range Punjab. Tobra siltstone is light cream in color and belongs to the Freshwater facies of Tobra formation. The depositional environment of the formation was Lacustrine (Teichert, 1967).
20	Sandstone-1	Tobra	Permian	This sandstone belongs to Complex marine conglomeratic facies of Tobra formation. The facies is composed of dark green, grey clay and sandstone with pebbles and boulders.
21	Sandstone-2	Khewra Sandstone	Cambrian	Khewra Sandstone consists of fine grained, purple to brown or yellowish brown sandstone. It is extensively present throughout the Salt Range area. The type locality is in Khewra Gorge, located near Khewra town. The thickness of the bed at type locality is around 150 meters.
22	Sandstone-3	Murree	Miocene	This rock unit belongs to the medium grained and grey colored variety of Murree sandstone. The type section is exposed to the north of Dhok Maiki in the Campbellpur district.
23	Sandstone-4	Tobra	Permian	This rock unit consists of Complex facies of Tobra formation. The facies is composed of medium to coarse grained, thick bedded, dark to light olive grey sandstone. The type locality is Tobra village in the eastern Salt Range Punjab.
24	Sandstone-5	Dandot	Permian	Dandot formation is generally exposed in the eastern Salt Range, Punjab. The type section is located near Dandot Village, eastern Salt Range, Punjab. At the type locality the lithology consists of light grey to olive green yellowish sandstone.
25	Sandstone-6	Tobra	Permian	This sandstone belongs to the lower part of Tobra formation in the western Salt Range at Zaluch nala, Punjab. The lower part is composed of a brownish green massive unit. At Zaluch nala the overall thickness of Tobra formation becomes more than 133 m.
26	Sandstone-7	Chidru	Permian	Chidru formation consists of three beds (the top most, the middle and the basal bed) with a total thickness of 64 meters. This rock unit is present at the top most part of Chidru formation having white color with ripple marks as characteristic distinguishing feature. The sandstone is medium to fine grained in texture. It contains quartz and feldspar as major minerals while muscovite, biotite and iron oxide as minor minerals.
27	Sandstone-8	Warchha Sandstone (Speckled)	Permian	Arkosic cross bedded sandstone with medium to coarse grains, and light pink color. It is largely composed of pink granite and Quartzite grains or pebbles. Warchha Sandstone is widely distributed in the Salt Range and type section is positioned at Warchha Gorge.
28	Sandstone-9	Lumshiwal	Mesozoic (Cretaceous)	Current-bedded , massive sandstone with light greyish yellow colour. The rock unit is feldspathic, ferruginous and also contains carbonaceous material. At the type locality (one km north of Lumshiwal nala) the formation thickness varies from 80 to 120 meters.

Sr. No.	Rock	Formation Name	Age	Description of Rock and Formation
29	Sandstone-10	Hangu	Cainozoic (Tertiary-Paleocene)	Dark grey, rarely variegated sandstone. The reference section is located at Dhak pass in Salt Range, Punjab, where the formation thickness is 45 meter.
30	Sandstone-11	Datta	Mesozoic (Jurassic)	Variegated (red, maroon , grey, green and white) sandstone. Formation is extensively distributed in the Salt Range as well as in the Trans-Indus ranges. The Type section is positioned at Datta Nala in the Surghar Range.
31	Sandstone-12	Warchha Sandstone	Permian	Arkosic cross bedded sandstone with medium to fine size grains having light pink in color. Warchha Sandstone is widely distributed in the Salt Range and type section is located at Warchha Gorge.
32	Sandstone-13	Amb	Permian	Medium grained, brownish grey and calcareous sandstone. The formation is fully developed in the western part of Salt Range and thins out east wards. The reference section is Amb village in the central Salt Range Punjab, where its thickness is 80 meters.
33	Sandstone-14	Nagri	Miocene	The Nagri formation mainly consists of medium to coarse grained, greenish grey, cross bedded and massive sandstone. The rock unit is moderately to poorly cemented. The formation is extensively present in the Indus Basin and the Calcareous Zone of the northern Axial Belt (Quetta region).
34	Sandstone-15	Kussak	Cambrian	Greenish-grey, glauconitic and micaceous sandstone. The type section is present near Kussak Fort, in the eartern Salt Range, Punjab where the formation exposure is 70 meters. It is widely distributed all over the Salt Range.
35	Sandstone-16	Hazira	Cambrian	Yellowish brown to reddish brown, shaly and compact hard sandstone. The formation exposed at Hazira village in Hazara area has been declared as the type section. The hazira formation attains a maximum thickness of 300 m.
36	Sandstone-17	Warchha Sandstone (Red)	Permian	Arkosic cross bedded sandstone with coarse grains, and red to purple in color. It is largely composed of pebbles of pink granite and Quartzite. Warchha Sandstone is widely distributed in the Salt Range and type section is positioned at Warchha Gorge.
37	Sandstone-18	Murree	Miocene	This rock unit belongs to the medium grey, fine grained variety of Murree sandstone. The type section is exposed to the north of Dhok Maiki in the Campbellpur district.
38	Chamositic Siderite	Chichali	Mesozoic (Cretaceous)	The rock unit is greenish grey, rusty brown (weathering) , glauconitic, chamositic and unfossiliferous marine sandstone. Compact and hard iron ore with iron content ranging from 32% to 36%. The type locality is Chichali pass, Surghar Range, where formation thickness varies from 55 to 70 meters.
39	Dolomite-1	Kingriali	Mesozoic (Triassic)	Massive, light grey, coarse textured dolomite. Formation is well exposed in Zaluch Nala in the western Salt Range and varies in thickness from 76 to 106 meters.
40	Dolomite-2	Jutana	Cambrian	Jutana formation mainly consists of rock dolomite. The reference locality is Jutana village in the eastern Salt Range, Punjab where the thickness of formation is 80 meters. This rock unit belongs to light grayish-green, massive, hard and partly sandy variety of Jutana formation.
41	Dolomite-3	Abbottabad (Pink)	Cambrian	Abbottabad formation is mainly composed of dolomite, quartzite and Phyllite rocks (Calkins et al., 1969). The type section is Sirban Hill near Abbottabad town, where the formation thickness is around 660 meters. Abbottabad dolomite is found in pink and grey varieties. Compact, hard and massive rock which contains considerable cracks due to structural deformation.
42	Dolomite-4	Jutana	Cambrian	Jutana formation mainly consists of rock dolomite. The reference locality is Jutana village in the eastern Salt Range, Punjab, where the thickness of formation is 80 meters. This rock unit belongs to the dirty white or creamish, massive, hard and partly sandy variety of Jutana formation.

Sr. No.	Rock	Formation Name	Age	Description of Rock and Formation
43	Limestone-1	Sakesar Limstone	Cainozoic (Tertiary-Eocene)	The current rock sample is collected from Bestway Cement quarry, eastern Salt Range Punjab. It is compact, very hard and cream to light grey in color. The rock unit has fossils in abundance. The type locality is Sakesar peak in the Central Salt Range, Punjab. The formation is massive widely distributed in the Salt Range where its thickness varies from 70 meters to 150 meters.
44	Limestone-2	Sakesar Limstone	Cainozoic (Tertiary-Eocene)	This rock sample is collected from D.G. Cement quarry, eastern Salt Range Punjab. It is compact, very hard and cream to light grey in color. The rock unit has fossils in abundance. The type locality is Sakesar peak in the Central Salt Range, Punjab. The formation is massive and widely distributed in the Salt Range, where its thickness varies from 70 meters to 150 meters.
45	Limestone-3	Samana Suk	Mesozoic (Jurassic)	This rock sample is collected from Bestway Cement quarry, Samana Range, KPK. It is massive, compact, very hard and grey to dark grey in color. The type locality is Shinawari in the Western part of Samana Range, where its thickness is186 meters. The formation is out cropped at a number of places in the Kala Chitta, Hazara, Kohat, Western Salt Range and Trans-Indus ranges.
46	Limestone-4	Wargal Limestone	Permian	Fossiliferous, compact, hard and cream to light brown in color. The type section is positioned close to Wargal village in the Central part of Salt Range, Punjab. The standard section of the formation is present at Zaluch Nala, where its thickness is 183 meters.
47	Limestone-5	Sakesar Limstone	Cainozoic (Tertiary-Eocene)	This rock sample is collected from Makerwal, Western Salt Range Punjab. It is compact, very hard and cream to light grey in color. The rock unit has fossils in abundance. The type locality is Sakesar peak in the Central Salt Range, Punjab. The formation is massive and widely distributed in the Surghar Range, where its thickness is around 300 meters.
48	Limestone-6	Samana Suk	Mesozoic (Jurassic)	This rock sample is collected from Mustahkam Cement quarry, Samana Range, KPK. It is massive, compact, very hard and grey to dark grey in color. The type locality is Shinawari in the Western part of Samana Range, where its thickness is186 meters. The formation is out cropped at a number of places in the Kala Chitta, Hazara, Kohat, Western Salt Range and Trans-Indus ranges.
49	Limestone-7	Nammal	Cainozoic (Tertiary-Eocene)	This rock sample is argillaceous, compact, medium hard and creamish to light grey in color. The reference section is located at Nammal Gorge, Central Salt Range Punjab, where its thickness is 100 meters. The existence of abundant fossils has been reported in the formation.
50	Rock Gypsum	Salt Range	Precambrian	White to light grey colored, soft rock mainly consists of and massive gypsum with minor beds of dolomite and clay. The Salt Range formation contains three members including Sahwal Marl Member, Bhandar Kas Gypsum and Billianwala Salt Member. The type section is Khewra Gorge, where formation thickness is more than 830 meters.
51	Marl	Salt Range	Precambrian	Red colored, soft rock mainly consists of clay, gypsum and dolomite along with some quartz grains. The Salt Range formation contains three members including Sahwal Marl Member, Bhandar Kas Gypsum and Billianwala Salt Member. The type section is Khewra Gorge, where formation thickness is more than 830 meters.

3.2. ROCK ABRASIVITY MEASUREMENT EXPERIMENTS

3.2.1. CERCHAR Abrasivity Tests. The CERCHAR abrasivity tests were performed compliant with the ASTM-D7625-10 standards and ISRM suggested method (Alber et al. 2014) by utilizing a locally fabricated CERCHAR test apparatus (Figure 3.1

a), similar to the equipment developed by the Colorado School of Mines (CSM). The steel used for the fabrication of test pins was of 200 kg/mm^2 tensile strength and the styli were sharpened at one end to a conus angle of 90° before heat treatment (West, 1989) to attain a Rockwell hardness of 54-56 HRC according to the original specifications given by CERCHAR (1986), ASTM-D7625-10 standard and ISRM suggested method (Alber et al., 2014). As cautioned by (Alber et al., 2014) in ISRM suggested method, after heat treatment the actual hardness of each stylus was also measured and recorded prior to its first test application. Similarly a cooling fluid was used for subsequent grindings of tested or used pins (Figure 3.2) in order to prevent any alteration in their standard Rockwell hardness of 54-56 HRC. The CERCHAR tests were conducted on air dried freshly broken as well as sawn rock surfaces (Figure 3.1 b) by utilizing rock core or block samples. To carry out CERCHAR test, the rock sample was clamped to the vice of the apparatus in such a way that the test surface was approximately aligned with the horizontal. Thereafter a sharpened stylus was clamped into the pin holder attached with the 7 Kg static load. The test stylus was then carefully lowered until it rests orthogonal to the rock surface in a gentle manner in order to protect pin tip from any damage. The articulated hand lever was subsequently pulled to scratch pin tip across the rock surface for a distance of 10 mm within about 1 second sliding time. During test performance the stylus was carefully monitored for its constant contact with the rock surface. After testing the static load was lifted carefully to unclamp the pin. This test procedure was repeated with at least five CERCHAR pins to obtain an average CAI value for that particular rock sample.
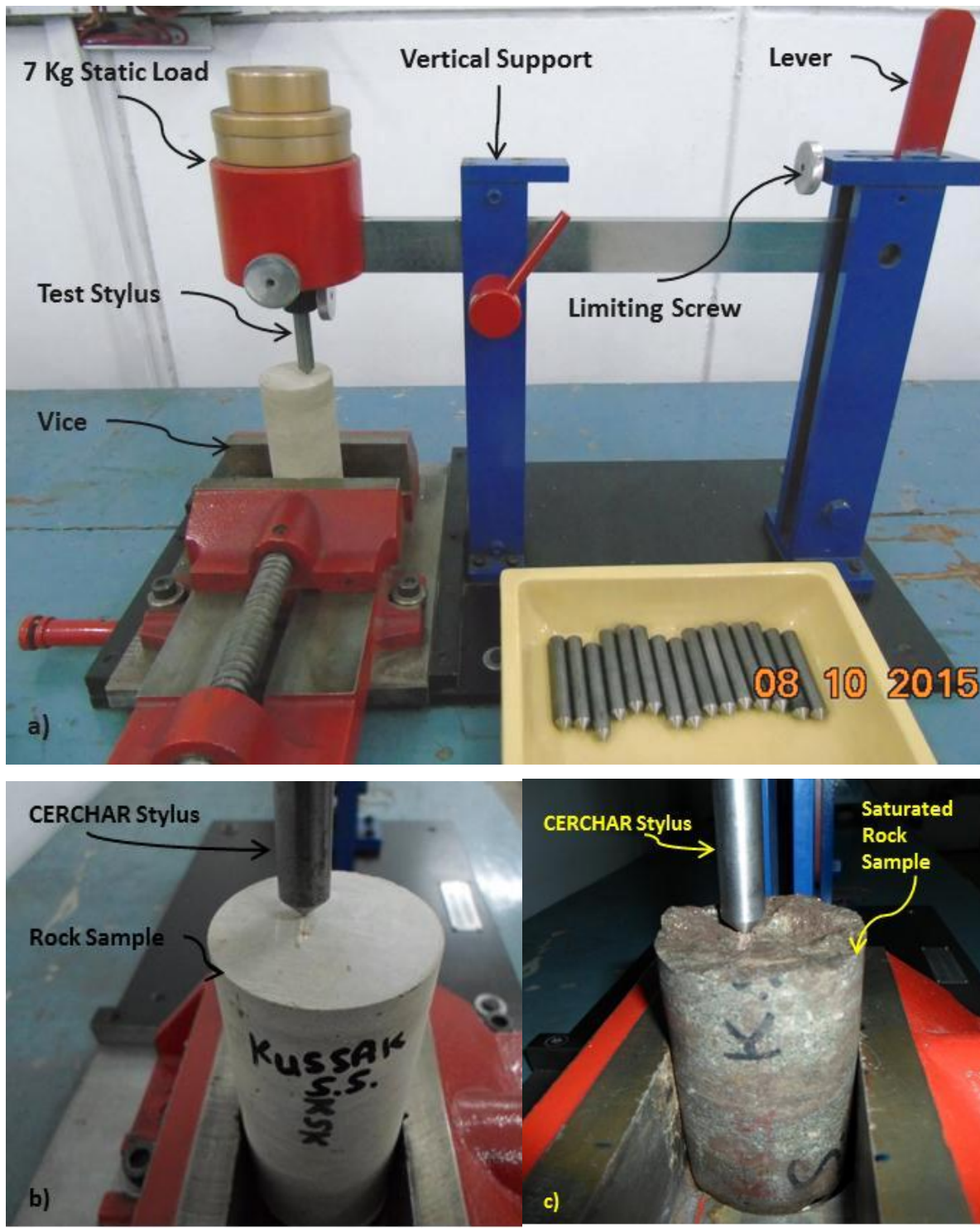
Figure 3.1(a) CERCHAR rock abrasivity measurement setup (b) view of a test performed on a saw cut, dry Kussak sandstone sample (c) view of a test conducted on a freshly broken fully water saturated sandstone sample.
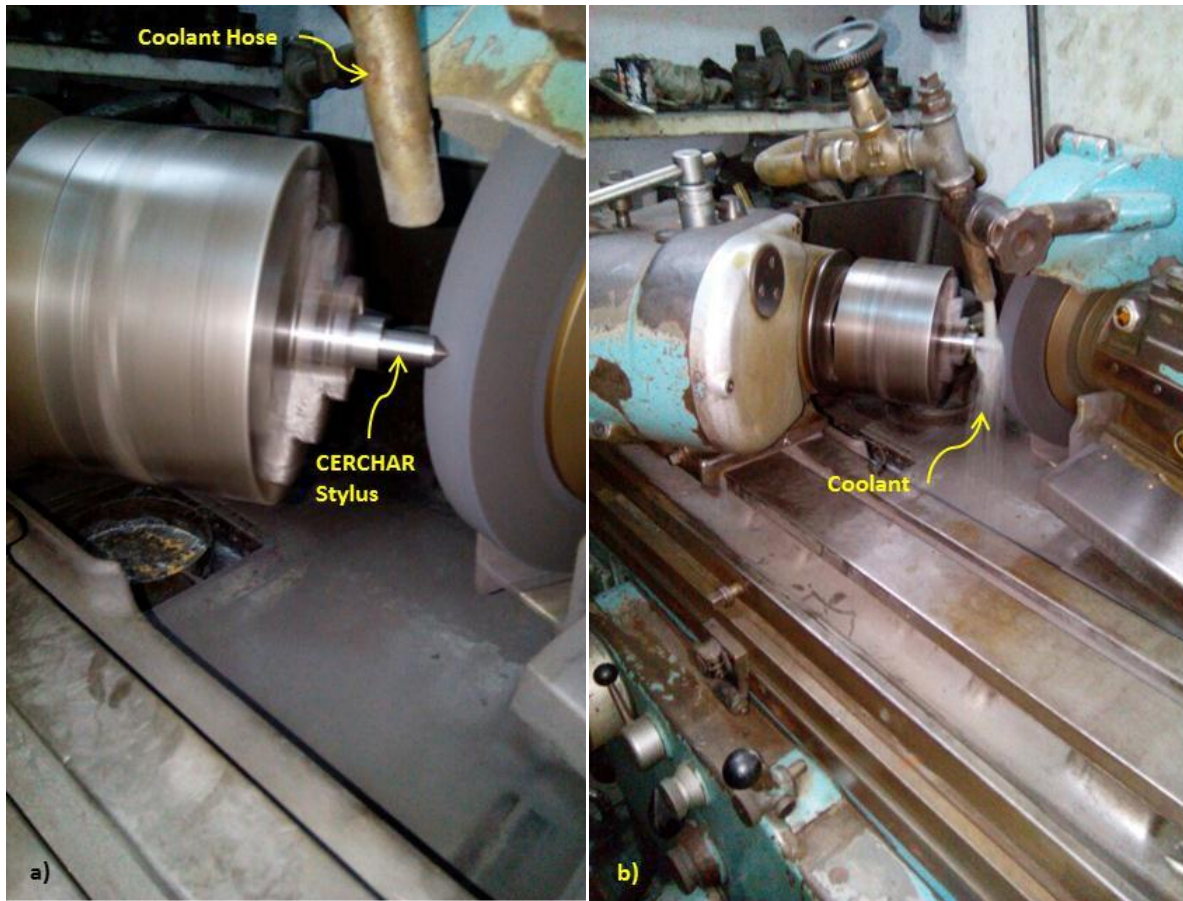
Figure 3.2. (a) Positioning of a tested CERCHAR stylus on a cylindrical grinding machine for re-sharpening (b) view of a CERCHAR stylus during grinding process by using cooling fluid.

Additionally, CERCHAR testing on both saw cut and rough rock surfaces was also performed on fully saturated sedimentary rock samples for that purpose 33 rock samples were selected from initially selected 51 rock specimens included in the data bank (Figure 3.1 c). This was done to evaluate the influence of water saturation on the measured CERCHAR abrasivity indices. For the measurement of flat styli end produced, a tool maker's microscope (Chien Wei CE-4450DV, equipped with built-in camera and 70x magnification power) was used. In this study both the top and side view wear flat measurement methods of CERCHAR stylus were used to compute the CAI values (Figures 3.3 a, b). For top measurement (Figure 3.3 a), the width or diameter of wear flat was determined by obtaining the arithmetic mean of two mutually perpendicular diameters of the wear surface at the stylus tip for each of the five test stylus used in accordance with the ASTM-D7625-10 standard and adopting the optical measurement

procedure laid down in ISRM suggested method (Alber et al., 2014). The measurement of wear flat using side view setting of the test stylus (Figure 3.3 b) was conducted in accordance with the procedure laid down in ISRM suggested method (Alber et al., 2014). For this purpose diameter of the stylus tip was measured horizontally four times, each at 90° rotation. The mathematical average of these four measurements was obtained to calculate the CAI value. Figures 3.4 (a) and (b) show a view of tool maker's microscope measuring the wear flat of a tested CERCHAR stylus by adopting top viewing and side viewing wear flat measurement techniques respectively.
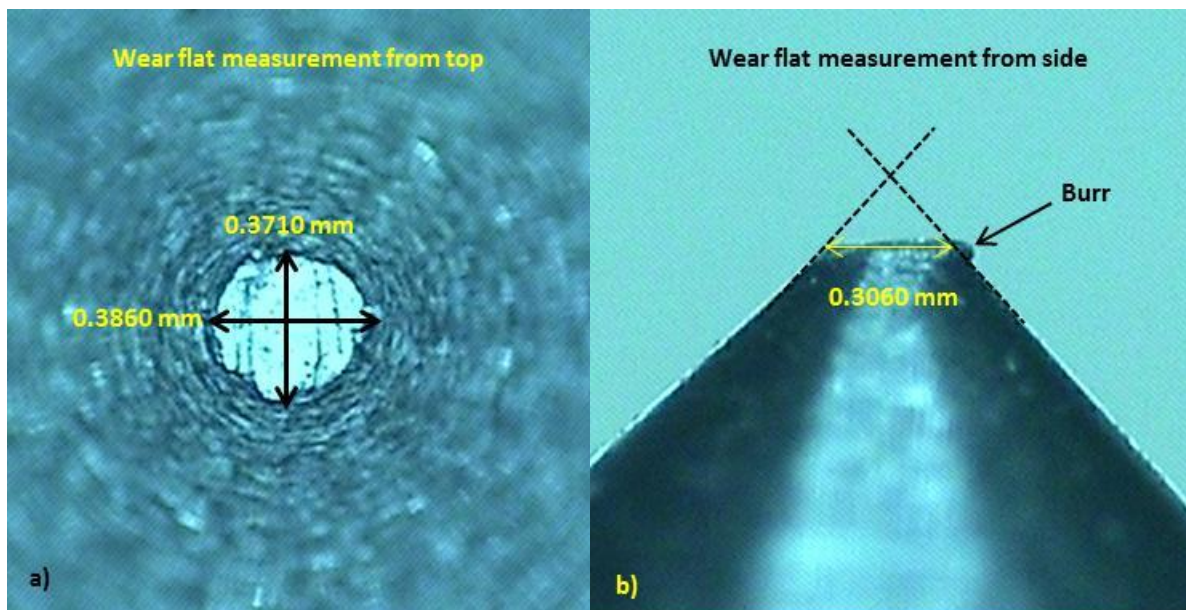
Figure 3.3 Views of wear flat measurement at CERCHAR styli tips (a) from top (b) from side for a saw cut Warchha (Red) sandstone sample.
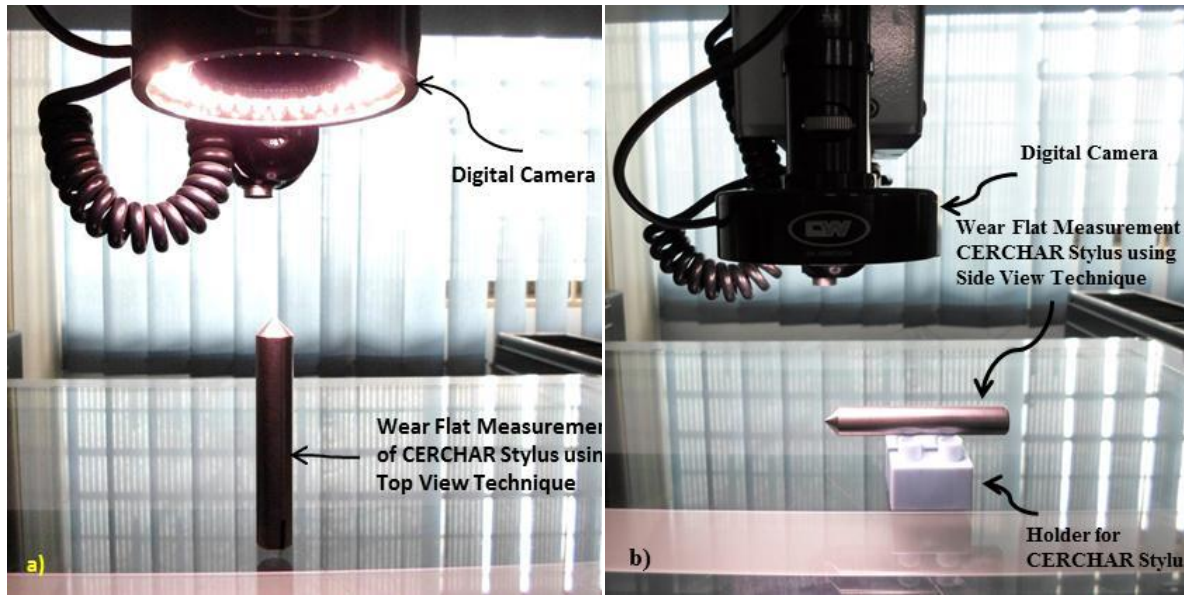
Figure 3.4 Views of wear flat measurements of CERCHAR styli on tool maker's microscope (Chien Wei CE-4450DV) (a) by using top viewing method (b) by using side viewing method.

3.2.2. LCPC Abrasivity Tests. In this research work the LCPC tests were carried out by using an indigenously fabricated machine (Figure 3.5) according to the design specifications provided in AFTES (1982). The LCPC test inserts having dimensions of 50mm x 25mm x 5mm, were manufactured from carbon steel (grade XC 12) of Rockwell hardness lying between 60 to 75 HRB. The whole batch of fabricated test inserts was checked for Rockwell hardness accuracy (Figure 3.6) before its application to the testing procedure (AFTES, 1982). The French regulation NF P18-579 (ANFOR, 1990) was adopted as the standardized LCPC testing procedure. The test fraction was prepared by reducing the size of rock lumps in steps through jaw crusher and rolls crusher. The crushed rock so obtained was thereafter sieved to a grading corresponding to the 4/6.3-mm size fraction. To carry out test a pre-weighted, new LCPC insert was fastened to the end of steel shaft. After clamping mould to the machine base the test insert was positioned near the bottom of the mould by lowering it with the help of a spring loaded hand lever provided at right hand side of the machine. A pre-weighted 500 grams of prepared rock fraction (4/6.3-mm) was poured into the LCPC mould and the impeller was rotated into the granular fraction at the specified speed of 4500 RPM for five minutes. The insert was un-screwed from the steel shaft and re-weighted carefully to find the loss

in mass of the insert before and after testing. Figure 3.7 (a) shows a view of prepared rock fraction of 500 grams before testing and Figure 3.7 (b) presents the milled rock fraction after test performance.

Figure 3.5. The LCPC rock abrasivity measurement apparatus (a) side view (b) front view.

Figure 3.6. A view of Rockwell hardness testing machine captured while testing hardness of a LCPC test insert.

Figure 3.7. (a) A view of prepared rock fraction before LCPC test (b) a view of rock fraction after LCPC test, where the rock breakability effect can be noticed.

For the determination of rock abrasiveness the difference of weight of metallic test piece before and after LCPC test performance was further utilized in Equation 3.1 (Thuro et al., 2007), and the LCPC abrasivity coefficient (ABR) was calculated in grams per ton. Figure 3.8 shows an example of a new and some used test pieces on which the effects of deformation and abrasion due to their interaction with the rock fraction can be noted. In order to find the breakability or brittleness of rock, the tested rock fraction was further sieved to find the mass of fraction passing 1.6 mm mesh screen. The LCPC breakability index (BR %), was then calculated by using equation 3.2 (Thuro et al., 2007).

$$ABR = \frac{(m_o - m)}{M} \qquad (3.1)$$

Where;

ABR = LCPC abrasivity coefficient measured in grams/ton;

m_o = Mass of LCPC insert before test in grams;

m = Mass of LCPC insert after test in grams;

M = Mass of prepared sample (-6.3 mm + 4.0 mm) in tons.

$$BR = \frac{M_{1.6} \times 100)}{M} \qquad (3.2)$$

Where;

$M_{1.6}$ = Mass of tested rock fraction passing 1.6 mm sieve after LCPC test in grams;

M = Mass of prepared sample (-6.3 mm + 4.0 mm) in grams.

Figure 3.8. LCPC inserts before and after test performance. 57- new test piece, 49- tested on Limestone-3 (ABR= 8 g/t), 11- tested on Sandstone-2 (ABR= 62 g/t), 48- tested on Dolomite-3 (ABR= 336 g/t), 51- tested on Quartzite-1(ABR= 498.50 g/t), 38- tested on Sandstone-16 (ABR= 1444.56 g/t).

In addition to the dry tests, LCPC tests were also performed on 20 selected rock samples by varying the water content of the test fraction, in order to explore the impact of moisture quantity on the computed rock abrasivity value (ABR). For this purpose water was added to the rock fraction prior to the start of test in quantities of 75grams (15% by weight), 150 grams (30% by weight), 225 grams (45% by weight) and 300 grams (60% by weight). Figures 3.9 a-d, show photographs of the tested fractions of sandstone-5 rock sample at the specified water contents.

Figure 3.9. LCPC saturated tests performed on Sandstone-5 rock sample (a) at 15% water content; (b) at 30% water content; (c) at 45% water content; (d) at 60% water content.

3.2.3. NTNU/SINTEF Abrasivity Tests. The NTNU/SINTEF abrasivity tests comprising of Sievers' J Miniature Drill test and Abrasion Value Steel Cutters (AVS) test were performed by employing locally manufactured testing setups according to the standardized specifications provided in the "Draft: DRI, BWI, CLI standard" Dahl (2003). For Sievers'J test, miniature drill bits of tungsten carbide were prepared (Figure 3.10 b) in accordance with the NTNU/SINTEF specifications shown in Figure 3.10 (a). The Sievers'J tests were performed on 10 selected rock samples, by adopting the standard

test procedure suggested in Dahl (2003). As specified the pre-cut rock sample (slab or disc) was marked for 4 to 8 drill dots prior to actual drilling keeping in view the heterogenity of the rock. Before holding the bit into the drill chuck, the drill bit edge was checked visually for its accuracy with the help of a hand lens of 10X magnification. The prepared Sievers'J rock sample was then fastened to the 20 kg weight and carefully lowered until one of the marked drill spot rests onto the drill bit edge. The test was run for 200 revolutions of the drill bit and the same procedure was repeated to drill the rest of marked drill spots. The Sievers'J Value (SJ) was calculated as the mean value of the miniature drill holes depth measured in 1/10 mm. Figure 3.11 (a) illustrates the Sievers'J test machine whereas Figure 3.11 (b) and (c) show drilled rock samples of Dolerite-3 and Sandstone-16 respectively.
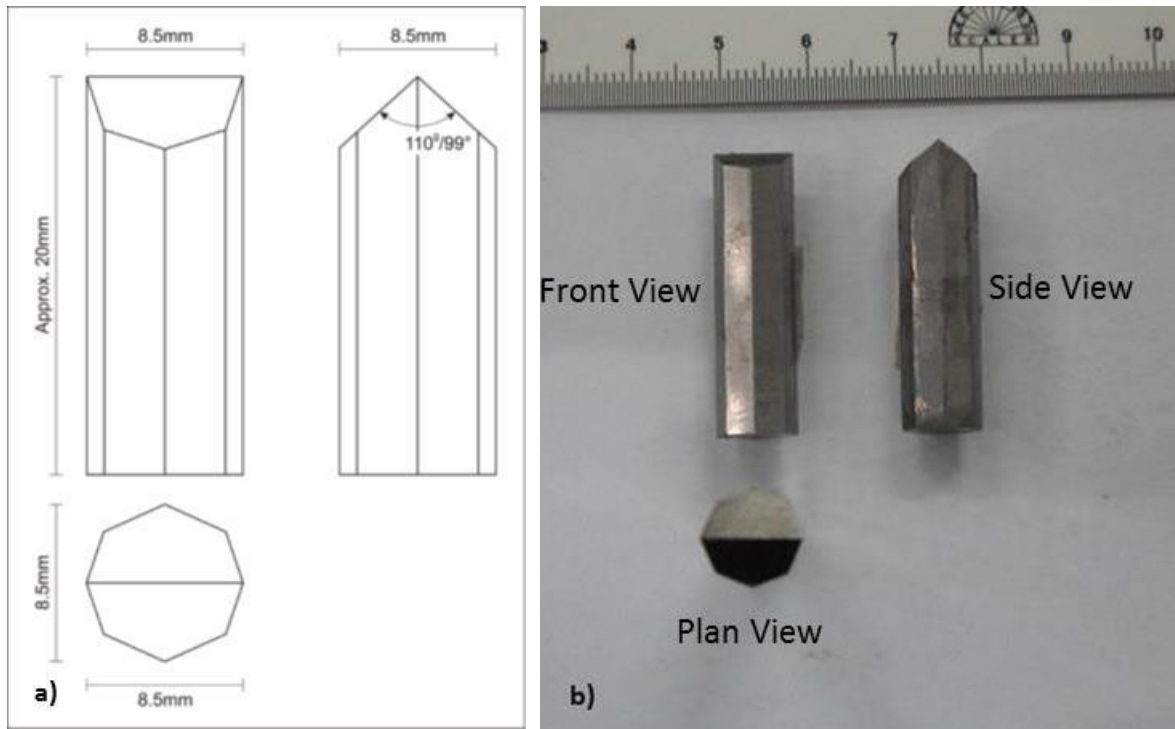
Figure 3.10. (a) Sievers'J Miniature tungsten carbide drill bit specification (after Dahl, 2003) (b) the tungsten carbide miniature drill bits fabricated in this research as per standard.

The Abrasion Value Steel Cutters (AVS) test apparatus used in this research is presented in Figure 3.12. The cutter steel test pieces as per NTNU/SINTEF specifications (Dahl, 2003) were prepared from the worn out TBM disc cutter ring of 17 inch diameter.

At present two TBMs supplied by Herrenknecht Company to the Water and Power Development Authority (WAPA) of Pakistan, are engaged in the construction of 19.6 Km long twin tunnels each having 52 m^2 cross sectional area, at Nelum Jehlum Hydro Power Project, Azad Jamu and Kashmir, Pakistan. Figure 3.13 shows the side view and lateral view of the fabricated test pieces. The AVS tests were also performed on the same set of rock sample selected for the Sievers'J tests. The experimental matrix for AVS test was designed keeping in consideration two important test parameters namely the size fraction of the rock abrasion powder, as well as the rotational speed of the steel disc.
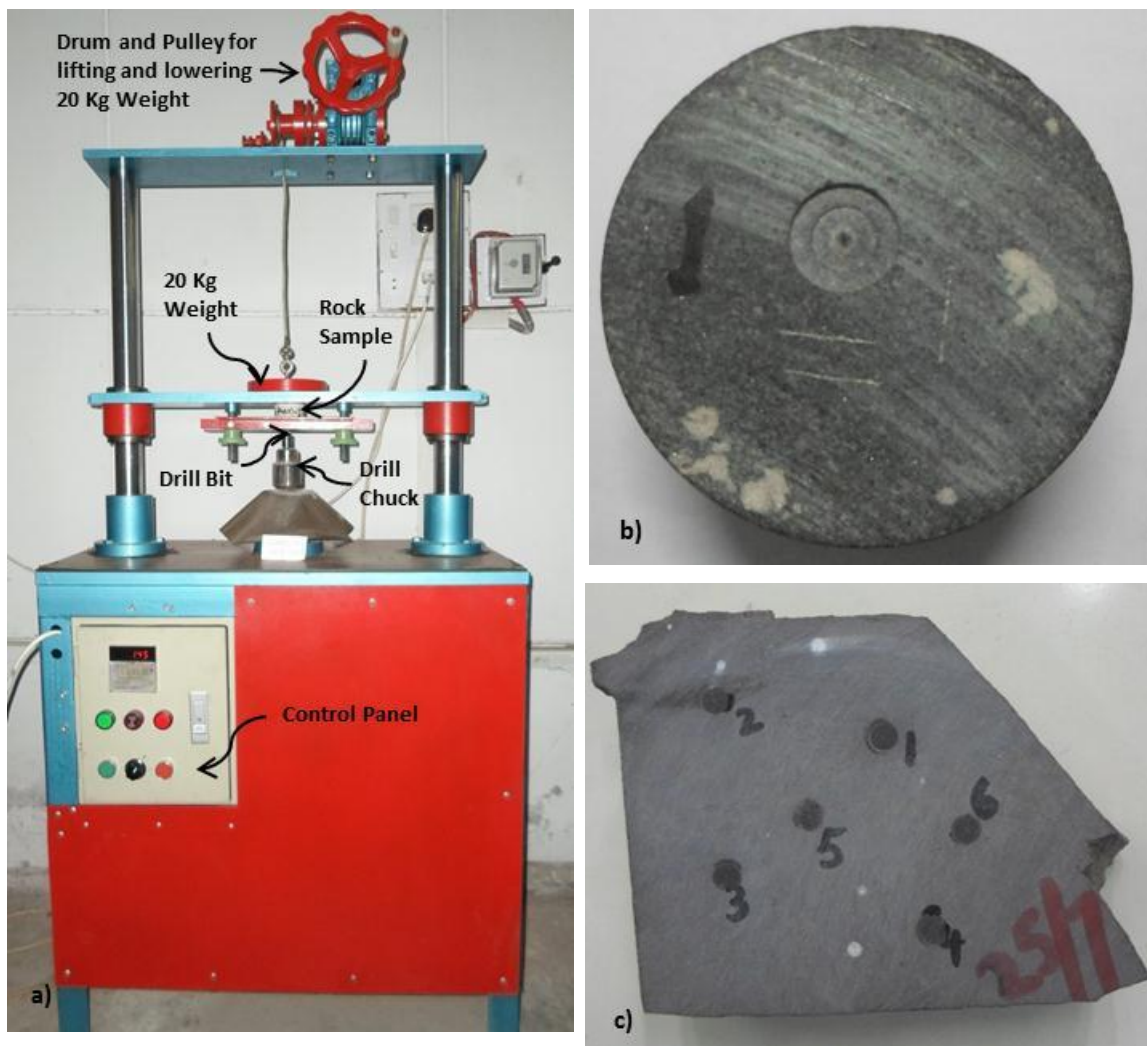
Figure 3.11. (a) Sievers'J Miniature drill test apparatus (b) Tested Dolerite-3, rock sample (c) view of drilled Sandstone-16 rock sample. Notice the drilled holes visible on the rock samples.

The first series of experiments were conducted by varying the grain size of standard abrasion powder [99% < 1mm and (70 ± 5) % < 0.50 mm] as specified by Dahl (2003), keeping the boundary conditions similar. Meaning the upper limit for grain size of all the rock fractions incorporated in this research study is passing 1mm sieve mesh. Therefore, the crushed rock powder passing 1mm sieve size was processed to make abrasion powders with three different size fraction combinations (Table 3.3) in addition to the standard size fraction. The rock abrasion powders were prepared by reducing the size of rock lumps through several crushing and sieving steps.

Table 3.3. Different size fraction combinations used for AVS testing.

Test Fraction Combination	Grain Size Distribution
Coarser	99% < 1mm and (70 ± 5) % < 0.71 mm
Standard	99% < 1mm and (70 ± 5) % < 0.50 mm
Fine	99% < 1mm and (70 ± 5) % < 0.25 mm
Finer	99% < 1mm and (70 ± 5) % < 0.15 mm

Before starting each AVS test, the flow rate of the rock abrasion powder was carefully adjusted so that the quantity of powder fed onto the steel disc was approximately 80 grams/min. The ground and polished test piece was accurately weighted to the nearest 0.001 g. The test piece was clamped to the 10 Kg mass and gently rested on the steel disc in middle of the track. The test was performed for 1 minute i.e. 20 revolutions. The worn out test piece was unclamped from the 10 Kg mass and was rinsed with water before weighing on a sensitive balance. The AVS in mg was reported as the average of 2 to 4 parallel tests.

Figure 3.12. NTNU/SINTEF Abrasion Value Steel Cutters (AVS) test apparatus
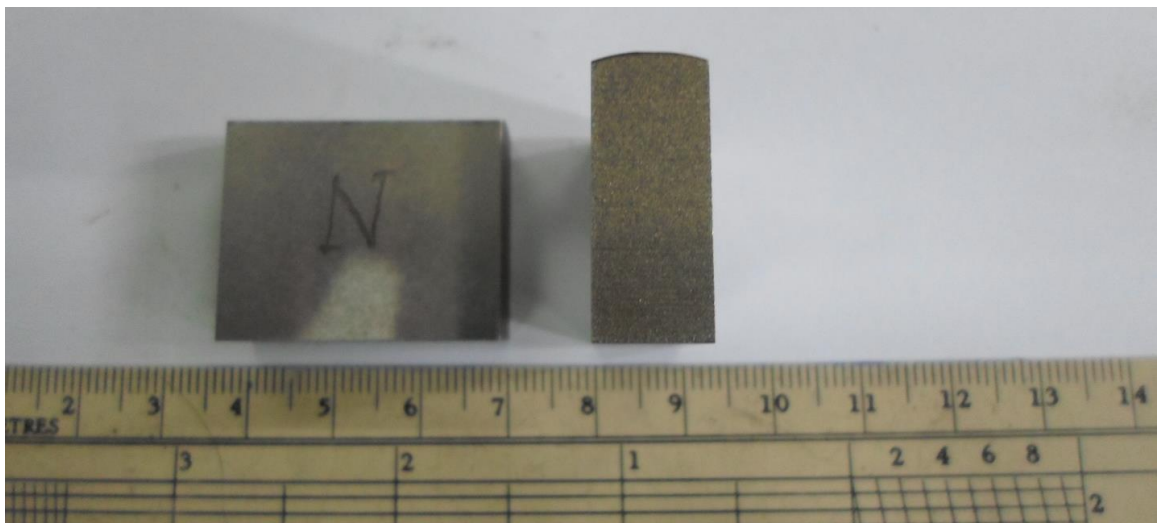
Figure 3.13. View of AVS test pieces used in this research work.

The second series of AVS experiments were conducted on the same set of 10 rock samples used in Sievers'J tests by using the standard test fraction [99% < 1mm and (70 ± 5) % < 0.50 mm] at the disc speed of 10 rpm i.e. half the suggested speed of 20 rpm. The experimental matrix was designed in such a way that at both the test speeds of 20 rpm and 10 rpm the cutter steel test piece is exposed to the similar test conditions including total rotations of the steel disc as well as the total amount of rock abrasion powder interacted. The matrix of experiments is presented in Table 3.4. Figure 3.14 (a) shows a view of steel disc during testing of Quartzite-1 rock sample at the speed of 10 rpm, whereas Figure 3.14 (b) shows the used test pieces tested on the same rock sample.

Table 3.4. Experimental matrix for variation in test speed.

Test Speed (RPM)	Grain Size Distribution	Testing Time (Min)	Sample Flow Rate (g/min)
20	Standard	1	80 ± 5
10	Standard	2	40 ± 2.5
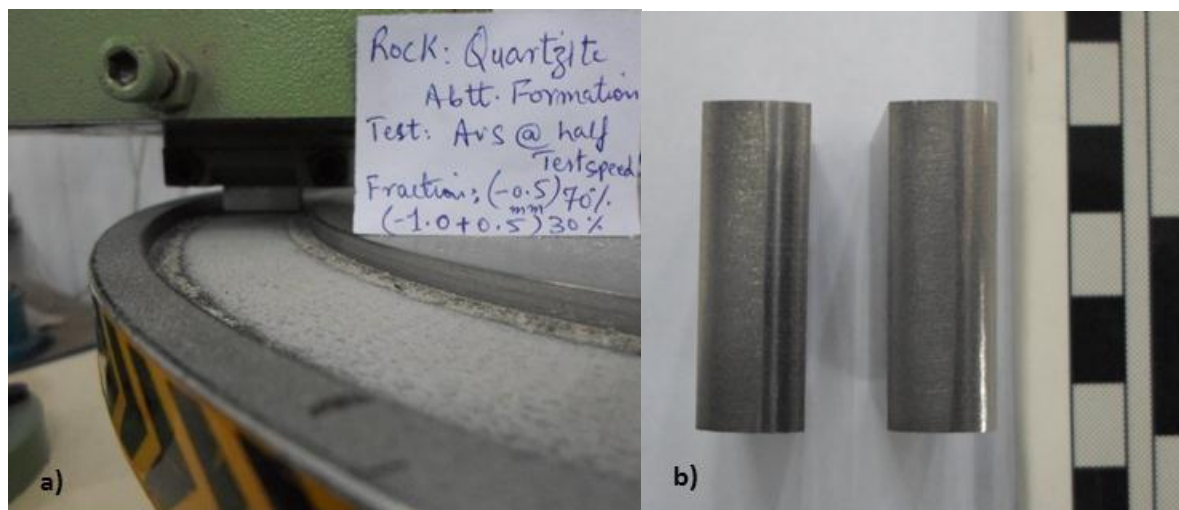
Figure 3.14. (a) Picture of steel disc and test piece during testing of a Quartzite-1 rock abrasion powder (b) view of AVS test pieces used on Quartzite-1 rock sample.

3.3. PETROGRAPHICAL STUDIES

To calculate the wear indices including Schimazek's F-values and Rock Abrasivity Index (RAI) thin sections of the rock samples were prepared and analyzed for their quantitative mineral content and grain sizes. Thin sections were prepared from the same rock blocks on which rock abrasivity as well as mechanical and physical properties

tests were carried out. The mineral content and the grain sizes were determined using a petrographic microscope (Russian MNH-8 polarized light microscope) (Figure 3.15). The grain size measurements were carried out by using the mean intersection length method as suggested by Paschen (1980). Mineral contents were determined by counting grains from thin section under the polarizing microscope.

All thin sections were described according to the ISRM Suggested Method for Petrographic Description of Rocks (Brown, 1981) and rocks were described according to BS 5930:1999 (Code of Practice for Site Investigations). An example of the grain size calculation is presented in Figure 3.16. Detailed petrographic descriptions for each rock sample are displayed in Appendix-E.

Figure 3.15. MNH-8 Russian, polarized light microscope used in the petrographic study.
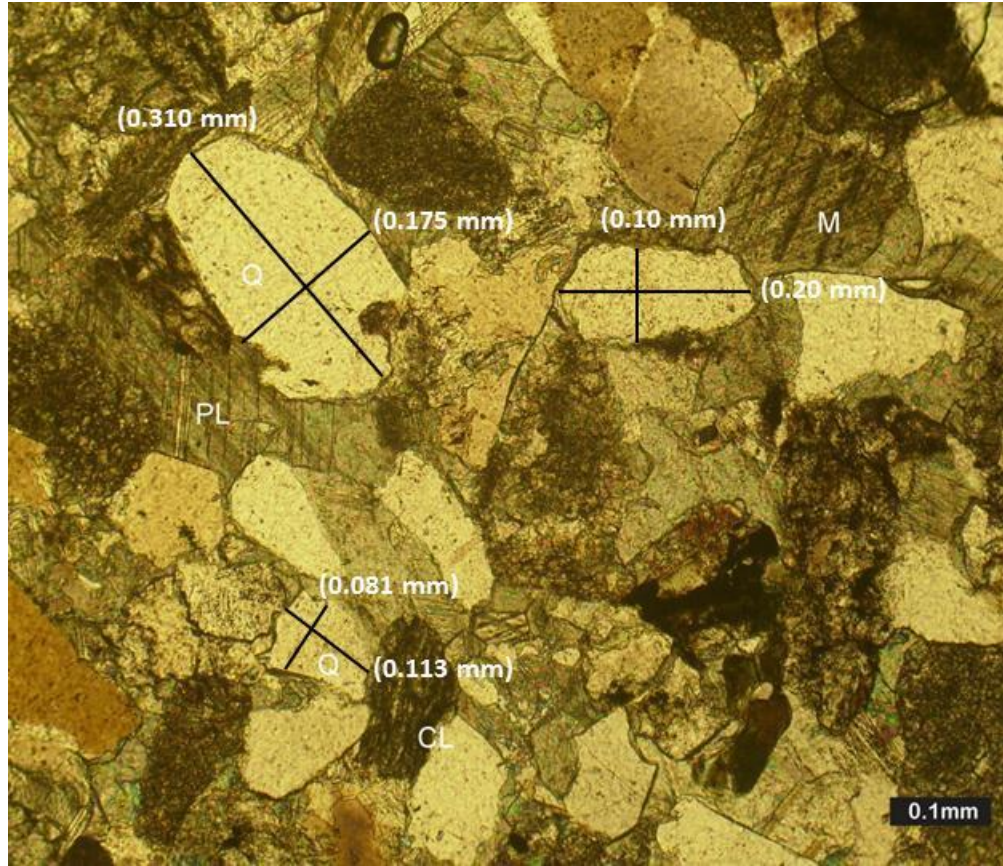
Figure 3.16. Example of grain size calculation for a Sandstone -3 rock sample.

3.4. CALCULATION OF SCHIMAZEK'S F-VALUE AND RAI

The results obtained from the thin section analysis were further used for the computation of Schimazek's F-value (Schimazek and Knatz, 1970) and Rock Abrasivity Index (RAI) (Plinninger, 2002). Schimazek's F-value was determined by using the following equation defined by Schimazek and Knatz (1970) based on Schimazek's pin-on-disc test cited in Verhoef (1997):

$$F = \frac{Qtz.eq \times \O \times BTS}{100} \ (N/mm) \tag{3.3}$$

Where;

Qtz. eq = Mineral content expressed in hardness of Quartz using Rosiwal's hardness scale (in vol.%);

$\O$ = Mean diameter of mineral grains (mm);

BTS = Brazilian tensile strength (MPa).

Table 3.5 shows a sample calculation of Schimazek's F-value for the Granitic Gneiss-1 (Leswa, AJK) wherein Qtz.eq is computed by the following equation adopted from Abu Bakar (2006):

$$Qtz.\,eq \; = \; \sum_{i=1}^{n} V_i.\,R_i \qquad\qquad (3.4)$$

Where;

V = Mineral quantity (%);

R = Rosiwal hardness.

The RAI values were computed by multiplying the Qtz.eq with the UCS values of each rock sample (Plinninger, 2002; Plinninger et al., 2004). Table 3.5 also shows a sample calculation of RAI for the same granitic gneiss.

Table 3.5. Sample calculation of Schimazek's F-value and RAI for Granitic Gneiss-1 (Leswa, AJK) having UCS = 69.22 MPa and BTS = 4.07 MPa.

Minerals	Quantity (%)	Grain Size (mm)	Rosiwal Hardness	Quartz Equivalent (%)	Schimazek's F-value (N/mm)	RAI
Quartz	73	0.565	100	73.00		
Potassium -Feldspars	13	1.375	35	4.55		
Plagioclase	8	1.247	35	2.80		
Muscovite	3.5	0.654	4	0.14	2.1	57.041
Biotite	2	0.798	4	0.08		
Zircon	0.5	0.162	367	1.84		
Total Quartz Equivalent Content				82.41		
$F = \dfrac{[(0.73 \times 100 \times 0.56) + (0.13 \times 35 \times 1.37) + (0.08 \times 35 \times 1.24) + (0.035 \times 4 \times 0.65) + (0.02 \times 4 \times 0.79) + (0.005 \times 367 \times 0.16)] \times 4.07}{100}$						
RAI = 82.41 × 69.22						

3.5. MECHANICAL AND PHYSICAL ROCK PROPERTIES TESTS

For conducting mechanical and physical properties tests, rock cores were drilled perpendicular to the bedding of the collected rock blocks by using 54 mm and 42 mm diamond core barrels. Core specimen preparation was performed in accordance with the ASTM-D4543 (2008) standards. In addition to the tests performed on all 51 air dried rock samples, mechanical tests including UCS and BTS were also conducted on fully saturated 33 sedimentary rock samples. For saturated tests, the prepared samples were saturated by adopting the progressive saturation technique developed by the US Army Corps of Engineers (1995). The past studies (Roxborough and Rispin, 1973; Mammen et al., 2009) performed for instrumented rock cutting tests, report full immersion of rock samples in

water to achieve saturation, but this method of rock saturation generally leaves dry segments or zones inside the samples mainly due to the trapping of pore air within these zones. This is avoided by progressive saturation, which starts with the base of the sample placed in a few centimeters of water. As the saturation line becomes visible in the rock fabric due to capillary action, the water level in the container is accordingly raised to bring it approximately halfway up to the saturation line. This procedure is repeated till the saturation line reaches top of the sample (Abu Bakar and Gertsch, 2011; 2013). Figure 3.17 shows the prepared cores of Sandstone-14 rock sample, placed for achieving full water saturation according to the progressive saturation technique.
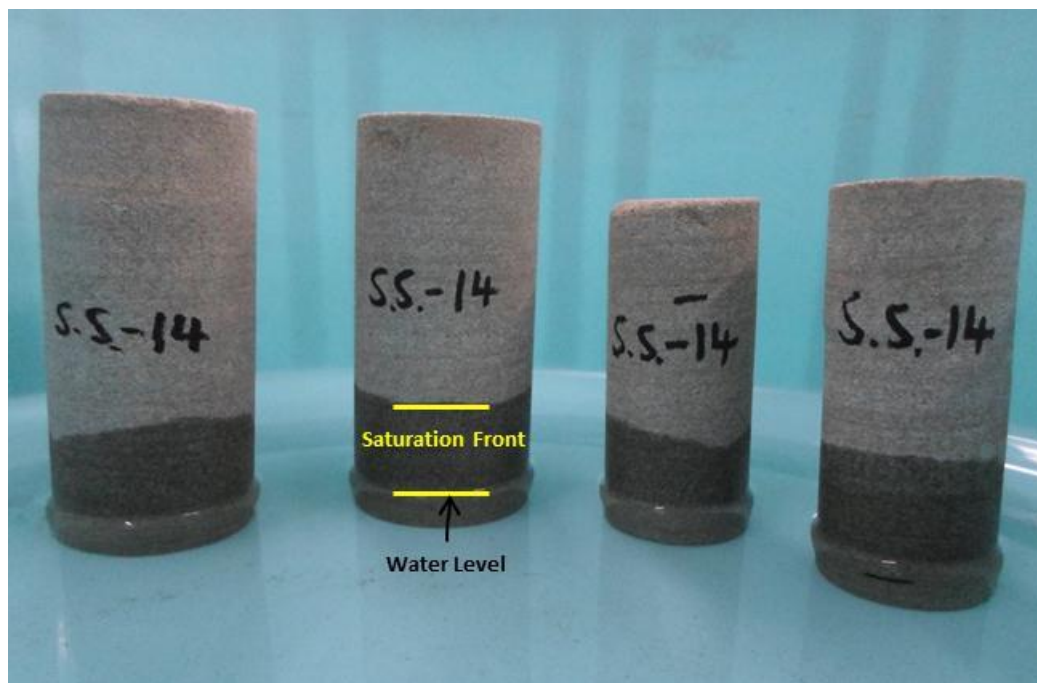
Figure 3.17. Rock cores placed for full water saturation adopting the progressive saturation technique. Notice the water saturation front advancing progressively towards the top of the rock core.

3.5.1. Mechanical Rock Properties (UCS and BTS) Tests. The UCS tests were conducted in accordance with the experimental procedures laid down in the ISRM suggested methods (1979a). The Shimadzu 200 tons universal testing machine (Figure 3.18) was used to compress trimmed and lapped rock cores having length to diameter ratio of approximately 2.5:1 till failure (Figure 3.19). UCS of the specimen was calculated by utilizing equation 3.5:

$$\sigma = \frac{P}{A_\circ} \qquad\qquad (3.5)$$

Where;

σ = UCS of the rock specimen;

P = Maximum load bearing capacity of the rock specimen during test performance;

$A_\circ$ = Original cross-sectional area of the rock specimen.

Figure 3.18. A view of Shimadzu 200 tons universal testing machine used for performing mechanical rock properties tests.

Figure 3.19. View of rock cores after performing UCS tests (a) Limestone-4 rock core tested in the dry state (b) a fully saturated core of Sandstone-18 rock sample after failure.

The BTS tests were performed in accordance with the guidelines of ISRM suggested methods (1978a). The prepared rock discs of NX size (54.00 mm) diameter with thickness to diameter ratio of approximately 0.5 were loaded till failure between the platens of the Shimadzu 200 tons universal testing machine (Figure 3.20). BTS of the specimen was determined by employing equation 3.6:

$$\sigma_t = \frac{0.636 \times P}{D \times t} \tag{3.6}$$

Where;

σ_t= BTS of the rock specimen;

P = Maximum load bearing capacity of the rock specimen during test performance;

D = Diameter of the test specimen;

t = Thickness of the test specimen.

Figure 3.20. View of rock disc after performing BTS tests (a) a failed disc of Sandstone-7 rock sample tested in the dry condition (b) a fully saturated disc of Siltstone-2 rock sample after failure.

3.5.2. Physical Rock Properties Tests. The physical rock properties included in this research work comprise sonic velocity (Vp), density (both dry and saturated), porosity and pore space volume. Primary waves velocity (Vp) was determined as per ISRM (1978b) suggested methods, by using Portable Ultrasonic Non-destructive Indication Tester (PUNDIT) shown in Figure 3.21. Sonic pulses were passed through rock specimens by positioning PUNDIT transducers at the greased ends of cores to measure sonic waves travel time. Vp was computed by using equation 3.7:

$$v_p = \frac{d}{t_p} \tag{3.7}$$

Where;

v_p = Velocity of primary wave through the rock specimen;

d = Distance between the PUNDIT transducers;

t_p = Time of P-wave to travel distance d.

Figure 3.21. View of measuring P-wave velocity of a Sandstone -16 rock sample using PUNDIT.

Density of dry rock is the ratio of solid mass component of the sample to its total volume, whereas saturated rock density is the ratio of rock specimen's mass including the grains and pore water to its total volume. Rock porosity can be expressed as the ratio of void space volume to the total specimen volume. According to Karakus et al. (2005) a variety of methods are present to determine the density, porosity and related properties of rocks but saturation and caliper method and saturation and buoyancy method are the most frequently utilized techniques. In the present research work the density and porosity tests were performed by employing the saturation and caliper technique of ISRM suggested methods (1979b) valid only for the rock samples of regular dimensions. Therefore, prepared rock discs were utilized for these tests. The bulk volume of rock discs was determined by averaging out several caliper measurements for each dimension. Specimen saturation was achieved by using the progressive saturation method adopted from the US Army Corps of Engineers (1995). The saturated rock discs were weighted to determine their saturated surface dried mass (M_{sat}) and then specimens were placed in an oven at a temperature of 105°C for 24 hours to measure their dried grain mass (M_s). Pore space

volume of rock samples were computed by utilizing equation 3.8. Dry density, saturated density and porosity of rock samples were determined by using equations 3.9, 3.10 and 3.11 respectively:

$$V_v = \frac{M_{sat} - M_s}{\rho_w} \qquad (3.8)$$

Where;

V_v = Pore volume of the specimen;

M_{sat} = Saturated surface dried mass of the specimen;

M_s = Oven dried grain mass of the specimen;

ρ_w = Unit weight of water.

$$\rho_d = \frac{M_s}{V} \qquad (3.9)$$

Where;

ρ_d = Dry density of the rock specimen;

M_s = Oven dried grain mass of the specimen;

V = Specimen bulk volume.

$$\rho_{sat} = \frac{M_s + (\rho_w) V_v}{V} \qquad (3.10)$$

Where;

ρ_{sat} = Saturated density of the rock specimen;

M_s = Oven dried grain mass of the specimen;

ρ_w = Unit weight of water;

V_v = Pore volume of the specimen;

V = Specimen bulk volume.

$$n = \frac{V_v \times 100}{V} \qquad (3.11)$$

Where;

n = Porosity of the rock specimen;

V_v = Specimen pore volume;

V = Specimen bulk volume.

4. EXPERIMENTAL RESULTS

This chapter includes the results of experiments performed in this research work which are summarized in Chapter 3. Further the parameters computed from the test results are also described here.

4.1. PETROGRAPHICAL ANALYSES OF ROCK SAMPLES

Out of initially selected 51 rock samples, 48 abrasive and non-abrasive rocks were selected for petrographic studies. Thin sections of these rocks were prepared and analyzed for their quantitative mineral content and grain sizes. The results obtained from the thin section analyses were further used for the computation of Schimazek's F-value (Schimazek and Knatz, 1970) and Rock Abrasivity Index (RAI) (Plinninger, 2002). Schimazek's F-value was determined by using the following equation defined by Schimazek and Knatz (1970) based on Schimazek's pin-on-disc test cited in Verhoef (1997):

$$F = \frac{Qtz.eq \times \emptyset \times BTS}{100} \ (N/mm) \tag{4.1}$$

Where;

$Qtz.\,eq$ = Quartz equivalent content defined as mineral content expressed in hardness of Quartz using Rosiwal's hardness scale (in volume %);

$\emptyset$ = Mean diameter of mineral grains (mm);

BTS = Brazilian tensile strength (MPa).

The quartz equivalent content (Qtz.eq) was computed by adopting the following procedure (Equation 4.2) as explained by Schimazek and Knatz (1970):

$$Qtz.\,eq \ = \ \sum_{i=1}^{n} V_i.\,R_i \tag{4.2}$$

Where;

V = Mineral quantity (%);

R = Rosiwal hardness.

The RAI values were computed by multiplying the Qtz.eq with the UCS values of each rock sample (Plinninger, 2002; Plinninger et al., 2004). Calculation procedure of Schimazek's F-value and RAI has already been illustrated in Table 3.5 for a Granitic

Gneiss-1 (Leswa, AJK) rock sample. The complete results of petrograhical analyses including quartz content (Qtz, %), quartz equivalent content (Qtz.eq, %), quartz grain size (Ø-Qtz, mm), overall grain size (Ø, mm), Schimazek's F-value (N/mm) and RAI are listed in Table 4.1. The detailed calculations of Schimazek's F-value (N/mm) and RAI for dry rock samples are presented in Appendix-H.

Table 4.1. Results of petrographic analyses along with computed values of Schimazek's F and RAI.

Sr. No.	Rock Sample	Qtz (%)	Qtz.eq (%)	Ø-Qtz (mm)	Ø (mm)	Schimazek's F-value (N/mm)	RAI
1	Dolerite-1	5.00	37.39	0.22	0.33	0.94	80.19
2	Dolerite-3	7.00	40.96	0.23	0.49	3.33	81.63
3	Dolerite-4	18.00	53.76	0.36	0.35	2.89	75.54
4	Granite-2	74.00	81.86	1.10	1.14	3.07	68.61
5	Granite-3	65.00	73.89	1.30	1.11	3.62	57.35
6	Granite-4	67.00	78.45	1.19	1.72	2.19	42.28
7	Granite-5	73.00	82.06	0.39	0.85	7.70	190.38
8	Granite-6	24.60	58.85	2.50	1.54	2.22	26.37
9	Migmatite	70.00	79.58	1.22	1.35	2.44	45.17
10	Andesite	10.00	36.42	0.18	0.60	3.44	84.30
11	Granitic Gneiss-1	73.00	82.41	0.57	0.80	2.10	57.04
12	Phyllite	50.00	53.95	0.14	0.78	0.32	29.31
13	Quartzite-1	90.60	96.78	0.74	0.32	3.01	54.57
14	Quartzite-2	70.80	75.38	0.54	0.30	4.26	110.82
15	Siltstone-1	15.20	23.42	0.23	0.29	0.48	11.55
16	Siltstone-2	22.00	36.31	0.15	0.21	0.52	21.02
17	Sandstone-1	68.00	72.27	0.41	0.73	0.59	28.77
18	Sandstone-2	67.00	77.50	0.24	0.20	0.09	32.20
19	Sandstone-3	64.00	79.36	0.59	0.58	2.87	101.26
20	Sandstone-4	78.00	84.26	0.39	0.39	0.47	22.52
21	Sandstone-5	62.30	76.63	0.51	0.48	1.10	33.72
22	Sandstone-6	70.10	89.70	0.72	0.81	5.55	98.43
23	Sandstone-7	67.50	89.69	0.11	0.26	1.27	55.17
24	Sandstone-8	55.50	69.31	0.41	0.82	0.38	7.65
25	Sandstone-9	78.00	84.47	0.59	0.67	0.91	24.53
26	Sandstone-10	75.00	76.91	0.45	0.37	0.24	12.84
27	Sandstone-11	73.00	82.43	0.58	0.59	0.96	17.46
28	Sandstone-12	55.00	64.62	0.24	0.38	0.25	17.50
29	Sandstone-13	77.00	85.33	0.27	0.60	0.37	39.59
30	Sandstone-14	72.50	83.90	0.43	0.54	0.31	14.32
31	Sandstone-15	78.00	84.26	0.09	0.25	0.48	58.17
32	Sandstone-16	95.00	96.22	0.27	0.26	5.91	124.88
33	Sandstone-17	56.00	68.09	0.73	0.53	2.04	38.65
34	Sandstone-18	61.00	71.42	0.25	0.25	1.05	59.12
35	Chamositic-Siderite	13.00	15.61	0.08	0.17	0.13	8.07
36	Dolomite-1	1.00	6.01	0.05	0.17	0.04	3.71
37	Dolomite-2	2.00	7.04	0.05	0.24	0.16	10.17
38	Dolomite-3	2.50	7.32	0.35	0.43	0.25	7.32
39	Dolomite-4	10.00	17.77	0.18	0.21	0.19	23.58
40	Limestone-1	0.00	2.62	0.00	0.49	0.05	1.71
41	Limestone-2	0.00	2.60	0.00	0.49	0.04	2.49
42	Limestone-3	0.00	3.44	0.00	1.51	0.19	2.77
43	Limestone-4	0.00	2.03	0.00	0.70	0.09	1.35
44	Limestone-5	0.00	2.22	0.00	0.44	0.01	2.22
45	Limestone-6	0.00	3.32	0.00	0.75	0.04	2.32
46	Limestone-7	0.00	3.01	0.00	0.13	0.03	0.60
47	Rock gypsum	0.00	0.55	0.00	0.36	0.00	0.07
48	Marl	21.00	24.20	0.10	0.17	0.02	1.29

4.2. THE CERCHAR TESTS

The CERCHAR tests were conducted on 51 rock samples both on freshly broken and saw cut air dried rock surfaces. Additionally, the tests using fully saturated freshly broken and sawn rock samples were also performed on 33 sedimentary rocks incorporated in this research work. The CERCHAR abrasivity index (CAI) values were computed by measuring the wear flat of styli under a tool maker's microscope by adopting the top viewing method (CERCHAR, 1986; ASTM-D7625-10; Alber et al., 2014) as well as the technique of side viewing as per ISRM suggested method (Alber et al., 2014). Tables 4.2 and 4.3 illustrate example calculations of CAI values for CERCHAR tests conducted on dry, saw cut rock sample (Sandstone-17) both by utilizing the side and top viewing measurement methods of wear plane at the stylus tip. The mean values of CAI computed from CERCHAR tests carried out on dry rock surfaces are presented in Table 4.4, whereas the mean CAI values of tests conducted on saturated sedimentary rocks are displayed in Table 4.5. Appendix-A presents the detailed results of CERCHAR tests for dry sawn and freshly broken rock surfaces, while Appendix-B displays the complete results of CERCHAR testing conducted on saturated saw cut and freshly broken rock surfaces.

Table 4.2. Example calculation of CAI value measured on a saw cut Sandstone-17 rock sample by utilizing side viewing wear flat measurement method.

Test No.	1st Wear Flat Measurement (mm)	2nd Wear Flat Measurement at 90° Rotation (mm)	3rd Wear Flat Measurement at 90° Rotation (mm)	4th Wear Flat Measurement at 90° Rotation (mm)	Average Wear Flat Measurement (d) mm	CAI $_{(SIDE)}$ (d x 10)	Avg. CAI $_{(SIDE)}$
1	0.302	0.278	0.313	0.286	0.295	2.95	
2	0.294	0.303	0.259	0.283	0.285	2.85	
3	0.306	0.315	0.281	0.307	0.302	3.02	2.88
4	0.287	0.263	0.300	0.256	0.277	2.77	
5	0.277	0.305	0.273	0.273	0.820	2.82	

Table 4.3. Example calculation of CAI value measured on a saw cut Sandstone-17 rock sample by utilizing top viewing wear flat measurement method.

Test No.	1st Wear Flat Measurement (mm)	2nd Wear Flat Measurement at 90° Rotation (mm)	Average Wear Flat Measurement (d) mm	CAI $_{(TOP)}$ (d x 10)	Avg. CAI $_{(TOP)}$
1	0.303	0.394	0.348	3.48	
2	0.391	0.377	0.384	3.84	
3	0.371	0.386	0.379	3.79	3.67
4	0.349	0.402	0.376	3.76	
5	0.351	0.351	0.351	3.51	

Table 4.4. Test results of CERCHAR abrasivity index conducted on dry rock samples.

Sr. No.	Rock Sample	$CAI_{s(Top)}$	$CAI_{s(Side)}$	$CAI_{fb(Top)}$	$CAI_{fb(Side)}$
1	Dolerite-1	3.237	2.816	3.627	3.083
2	Dolerite-2	3.015	2.673	4.074	3.150
3	Dolerite-3	3.540	2.990	4.650	3.850
4	Dolerite-4	3.220	2.220	4.450	3.590
5	Granite-1	4.500	3.577	5.273	4.502
6	Granite-2	4.610	4.040	4.980	4.110
7	Granite-3	4.184	3.634	5.283	4.150
8	Granite-4	3.907	3.111	5.081	4.031
9	Granite-5	3.590	2.820	4.480	3.450
10	Granite-6	3.902	3.490	4.987	4.687
11	Migmatite	4.320	3.550	3.600	3.210
12	Andesite	3.528	3.250	5.154	4.425
13	Granitic Gneiss-1	3.650	2.870	3.570	3.270
14	Granitic Gneiss-2	4.952	4.262	5.025	4.164
15	Phyllite	1.433	1.189	2.677	2.184
16	Quartzite-1	4.394	3.930	4.703	3.932
17	Quartzite-2	4.134	3.394	4.594	3.652
18	Siltstone-1	1.150	0.990	1.440	1.250
19	Siltstone-2	2.216	1.536	2.302	1.872
20	Sandstone-1	1.783	1.524	2.067	1.764
21	Sandstone-2	0.620	0.710	1.250	0.860
22	Sandstone-3	3.920	3.240	3.550	2.840
23	Sandstone-4	1.410	1.054	1.540	1.220
24	Sandstone-5	3.038	2.437	2.931	2.275
25	Sandstone-6	3.300	2.840	3.210	3.210
26	Sandstone-7	2.030	1.670	1.680	1.380
27	Sandstone-8	1.430	1.420	1.140	1.250
28	Sandstone-9	2.320	2.380	2.690	2.610
29	Sandstone-10	1.394	1.403	1.570	1.443
30	Sandstone-11	1.950	1.480	1.930	1.490
31	Sandstone-12	1.621	1.589	1.281	1.147
32	Sandstone-13	1.640	1.400	2.160	1.810
33	Sandstone-14	1.260	1.300	1.230	1.310
34	Sandstone-15	1.940	1.600	1.700	1.450
35	Sandstone-16	3.973	3.664	6.355	5.532
36	Sandstone-17	3.675	2.881	3.820	2.913
37	Sandstone-18	3.192	2.339	3.481	2.385
38	Chamositic-Siderite	1.066	0.926	1.837	1.018
39	Dolomite-1	2.121	2.082	1.568	1.608
40	Dolomite-2	2.223	1.818	1.979	1.787
41	Dolomite-3	2.445	2.041	2.052	1.895
42	Dolomite-4	2.500	2.125	2.410	2.149
43	Limestone-1	1.017	0.571	1.260	1.062
44	Limestone-2	1.102	0.906	1.207	0.938
45	Limestone-3	1.478	1.400	1.631	1.455
46	Limestone-4	0.958	1.098	0.961	1.188
47	Limestone-5	1.161	1.109	1.051	1.130
48	Limestone-6	1.002	0.863	0.912	0.689
49	Limestone-7	0.306	0.229	0.335	0.252
50	Rock Gypsum	0.731	0.435	0.809	0.503
51	Marl	0.278	0.194	0.206	0.186

$CAI_{s(Top)}$ - CAI value for sawn rock surface measured using top viewing method at the stylus tip, $CAI_{s(Side)}$ - CAI value for sawn rock surface measured using side viewing method at the stylus tip, $CAI_{fb(Top)}$ - CAI value for freshly broken rock surface measured using top viewing method at the stylus tip, $CAI_{fb(Side)}$ - CAI value for freshly broken rock surface measured using side viewing method at the stylus tip.

Table 4.5. Test results of CERCHAR abrasivity index conducted on saturated sedimentary rock samples.

Sr. No.	Rock Sample	$CAI_{ss(Top)}$	$CAI_{ss(Side)}$	$CAI_{fbs(Top)}$	$CAI_{fbs(Side)}$
1	Siltstone-1	1.147	0.837	1.346	1.034
2	Siltstone-2	2.488	2.057	2.124	1.569
3	Sandstone-1	1.423	1.210	1.401	1.309
4	Sandstone-2	1.276	0.816	1.326	0.944
5	Sandstone-3	2.653	2.151	3.457	2.679
6	Sandstone-4	1.371	1.093	1.438	1.043
7	Sandstone-5	3.292	2.870	3.554	2.327
8	Sandstone-6	2.940	2.644	2.655	2.368
9	Sandstone-7	1.474	1.282	1.830	1.693
10	Sandstone-8	1.426	1.117	1.348	1.194
11	Sandstone-9	2.221	1.893	2.450	2.165
12	Sandstone-10	1.321	1.044	1.323	1.260
13	Sandstone-11	1.682	1.312	2.351	1.806
14	Sandstone-12	1.148	1.033	1.371	1.243
15	Sandstone-13	1.805	1.442	1.573	1.325
16	Sandstone-14	1.140	0.984	1.284	1.046
17	Sandstone-15	1.836	1.611	1.603	1.373
18	Sandstone-17	2.675	2.054	3.280	2.156
19	Sandstone-18	2.761	2.046	2.685	1.559
20	Chamositic Siderite	1.152	1.051	1.137	0.986
21	Dolomite-1	2.126	1.739	1.866	1.399
22	Dolomite-2	1.928	1.703	1.859	1.609
23	Dolomite-3	2.096	1.942	2.665	2.177
24	Dolomite-4	2.082	1.756	1.628	1.363
25	Limestone-1	1.355	1.121	0.919	0.866
26	Limestone-2	1.316	1.190	1.106	0.814
27	Limestone-3	1.115	0.901	1.153	0.990
28	Limestone-4	1.181	1.100	1.323	1.174
29	Limestone-5	1.141	1.006	1.285	1.137
30	Limestone-6	0.621	0.480	0.702	0.534
31	Limestone-7	0.244	0.188	0.277	0.211
32	Rock Gypsum	0.168	0.128	0.167	0.142
33	Marl	0.223	0.145	0.164	0.111

$CAI_{ss(Top)}$ - CAI value for saturated sawn rock surface measured using top viewing method at the stylus tip, $CAI_{ss(Side)}$ - CAI value for saturated sawn rock surface measured using side viewing method at the stylus tip, $CAI_{fbs(Top)}$ - CAI value for saturated freshly broken rock surface measured using top viewing method at the stylus tip, $CAI_{fbs(Side)}$ - CAI value for saturated freshly broken rock surface measured using side viewing method at the stylus tip.

4.3. THE LCPC TESTS

The LCPC tests were performed on 51 dry rock samples, comprising of all three generic rock types. The LCPC abrasivity co-efficient (ABR) was calculated by carefully determining the loss of mass in grams of the metallic test piece (before and after the test performance) per ton of rock sample material (Büchi et al., 1995). The breakability, grindability or brittleness of the rock material known as LCPC breakability index (BR) can also be assessed with the help of LCPC abrasivity test (Thuro et al., 2007). The LCPC breakability index (BR) was calculated as the ratio of mass of the tested rock sample particles less than 1.6 mm in size to the initial sample mass expressed in

percentage (Büchi et al., 1995). The test results of LCPC abrasivity co-efficient (ABR) and LCPC breakability index (BR) for dry rock samples are presented in Table 4.6.

Table 4.6. Test results of LCPC abrasivity co-efficient and LCPC breakability index conducted on dry rock samples.

Sr. No.	Rock Sample	$ABR_{(dry)}$ (g/t)	$BR_{(dry)}$ (%)
1	Dolerite-1	616.00	33.70
2	Dolerite-2	235.53	30.76
3	Dolerite-3	186.00	29.20
4	Dolerite-4	1391.28	18.99
5	Granite-1	359.64	75.42
6	Granite-2	319.36	50.90
7	Granite-3	415.58	79.22
8	Granite-4	477.52	67.43
9	Granite-5	1534.50	17.30
10	Granite-6	1273.00	50.75
11	Migmatite	301.40	67.76
12	Andesite	1385.00	26.30
13	Granitic Gneiss-1	171.66	58.68
14	Granitic Gneiss-2	429.00	71.45
15	Phyllite	80.00	58.25
16	Quartzite-1	498.50	51.05
17	Quartzite-2	1208.00	30.70
18	Siltstone-1	63.00	42.65
19	Siltstone-2	476.00	43.20
20	Sandstone-1	218.00	58.90
21	Sandstone-2	102.00	61.53
22	Sandstone-3	744.00	65.80
23	Sandstone-4	159.93	67.07
24	Sandstone-5	228.00	75.60
25	Sandstone-6	474.00	73.00
26	Sandstone-7	226.00	58.50
27	Sandstone-8	186.00	64.80
28	Sandstone-9	406.00	73.60
29	Sandstone-10	260.00	66.80
30	Sandstone-11	134.00	72.00
31	Sandstone-12	91.00	60.70
32	Sandstone-13	232.00	53.80
33	Sandstone-14	57.00	58.30
34	Sandstone-15	424.00	35.00
35	Sandstone-16	1444.56	40.36
36	Sandstone-17	633.00	60.85
37	Sandstone-18	740.00	48.90
38	Chamositic-Siderite	4.00	46.20
39	Dolomite-1	642.00	46.50
40	Dolomite-2	304.00	39.00
41	Dolomite-3	336.00	40.40
42	Dolomite-4	208.00	60.40
43	Limestone-1	6.00	40.10
44	Limestone-2	7.00	43.88
45	Limestone-3	8.00	47.90
46	Limestone-4	8.01	52.35
47	Limestone-5	4.01	37.27
48	Limestone-6	20.00	46.30
49	Limestone-7	7.98	53.69
50	Rock Gypsum	8.00	54.80
51	Marl	32.99	58.52

Further, LCPC tests were also conducted on 20 selected rock samples out of total 51 samples, by varying the water content at 15%, 30%, 45% and 60% by mass of the total sample material or fraction. To determine the LCPC breakability index (BR) of tests

conducted on 20 rock samples with the addition of water (15%, 30%, 45% and 60%), the tested wet rock fractions were further processed after drying completely in the laboratory oven. Table 4.7 outlines the LCPC abrasivity coefficient (ABR) values for the above mentioned saturated tests, whereas Table 4.8 displays the corresponding values of LCPC breakability index (BR). The complete results of LCPC dry and saturated tests for each rock sample can be viewed in Appendix-C.

Table 4.7. Test results of LCPC abrasivity co-efficient performed on saturated rock samples.

Sr. No.	Rock Sample	$ABR_{(15\%)}$ (g/t)	$ABR_{(30\%)}$ (g/t)	$ABR_{(45\%)}$ (g/t)	$ABR_{(60\%)}$ (g/t)
1	Dolerite-3	882.00	1086.00	1032.00	942.00
2	Dolerite-4	1934.00	1814.00	1836.00	1714.00
3	Granite-4	478.00	788.00	560.00	484.00
4	Granite-5	1862.00	1758.00	1874.00	1770.00
5	Granite-6	1660.00	1642.00	1548.00	1342.00
6	Andesite	2008.00	1856.00	1778.00	1798.00
7	Granitic Gneiss-1	516.00	606.00	420.00	356.00
8	Granitic Gneiss-2	156.00	620.00	426.00	394.00
9	Phyllite	306.00	200.00	98.00	82.00
10	Siltstone-1	372.00	346.00	322.00	266.00
11	Sandstone-2	40.00	270.00	132.00	108.00
12	Sandstone-3	848.00	986.00	791.17	666.00
13	Sandstone-4	42.00	358.00	158.00	102.00
14	Sandstone-5	214.00	384.00	206.00	200.00
15	Sandstone-12	26.00	252.00	118.00	84.00
16	Sandstone-14	10.00	142.00	132.00	56.00
17	Sandstone-15	930.00	886.00	798.00	670.00
18	Sandstone-17	1330.00	1108.00	854.00	816.00
19	Limestone-3	14.00	24.00	22.00	12.00
20	Marl	8.00	92.00	42.00	28.00

Table 4.8. Test results of LCPC breakability index conducted on saturated rock samples.

Sr. No.	Rock Sample	$BR_{(15\%)}$ (%)	$BR_{(30\%)}$ (%)	$BR_{(45\%)}$ (%)	$BR_{(60\%)}$ (%)
1	Dolerite-3	23.80	16.60	16.60	17.20
2	Dolerite-4	15.50	13.10	12.30	12.60
3	Granite-4	46.00	46.7	39.00	38.50
4	Granite-5	15.00	13.60	11.00	13.40
5	Granite-6	29.60	19.80	21.80	17.20
6	Andesite	19.60	16.20	12.80	14.60
7	Granitic Gneiss-1	54.80	55.60	43.00	41.80
8	Granitic Gneiss-2	38.80	55.00	44.60	42.20
9	Phyllite	31.40	46.50	41.70	37.70
10	Siltstone-1	26.80	21.20	19.00	21.00
11	Sandstone-2	39.30	86.70	60.40	53.30
12	Sandstone-3	34.80	30.60	27.31	27.60
13	Sandstone-4	33.00	71.20	53.80	14.80
14	Sandstone-5	39.50	43.40	37.00	38.20
15	Sandstone-12	37.50	80.80	61.20	52.40
16	Sandstone-14	36.80	70.80	73.20	62.80
17	Sandstone-15	30.20	23.00	22.50	20.10
18	Sandstone-17	34.80	32.80	28.40	29.00
19	Limestone-3	39.40	24.00	22.40	22.30
20	Marl	20.00	53.40	35.40	30.60

4.4. THE NTNU/SINTEF TESTS

To find the Cutter Life Index (CLI), NTNU/SINTEF tests including Sievers'J-Value (SJ) test and Abrasion Value Steel (AVS) tests were conducted on ten selected rock samples out of the initially included 51 rock samples in this research work. The Sievers'J Miniature Drill test provides a quantification of the surface hardness or resistance against penetration of the drill bit into the rock surface (Zare and Bruland, 2013). Sievers'J-Values for rock samples were calculated as the mean depth of 4 to 8 miniature holes drilled by using a standard 8.5 mm drill bit after 200 rotations, expressed in tenths of a millimeter. Tables 4.9 demonstrate an example calculation of Sievers'J-Value for miniature drill tests conducted on Sandstone-16, rock sample. The complete Sievers'J test results are shown in Table 4.10.

Table 4.9. Example calculation of Sievers'J Value for Hazira Sandstone (Sandstone-16) rock sample.

Depth of Drill Hole #1 (mm)	Depth of Drill Hole #2 (mm)	Depth of Drill Hole #3 (mm)	Depth of Drill Hole #4 (mm)	Depth of Drill Hole #5 (mm)	Depth of Drill Hole #6 (mm)	Average Depth (mm)	Sievers'J Value (1/10) mm
0.15	0.13	0.06	0.16	0.15	0.11	0.1266	1.27

The Abrasion Value Steel (AVS) tests were conducted on the same set of ten rock samples utilized for the determination of Sievers'J-Values. According to the standard test procedure (Dahl, 2003) the AVS was calculated by determining the mass loss of the cutter steel test pieces after completing 20 revolutions of the rotating steel disc in 1 minute of testing time. The reported AVS value in mg is the average of 2 to 4 parallel tests conducted on the same rock sample. Table 4.11 lists the AVS test results conducted on four different rock abrasion powders prepared by varying the grain size of rock powder finer than 1 mm sieve size, according to the pre-defined experimental matrix mentioned in Chapter 3. Further Table 4.12 displays the results of AVS tests carried out by varying the test speed of the rotating steel disc using standard abrasion powder [99% < 1mm and (70 ± 5) % < 0.50 mm] in accordance with the pre-defined experimental matrix also described in Section 3.

The results of Sievers'J-Value and AVS tests were utilized to compute the Cutter Life Index (CLI) for the selected rock samples by adopting equation 4.1 (Dahl, 2003).

CLI is the life of TBM disc cutter rings expressed in boring hours (Zare and Bruland, 2013). Table 4.13 presents the computed CLI values of the tested rock samples.

$$\text{CLI} = 13.84 \left(\frac{\text{SJ}}{\text{AVS}}\right)^{0.3847} \tag{4.1}$$

Where;

SJ = Sievers'J-Value;

AVS = Abrasion Value Steel Cutters.

The comprehansive results of NTNU/SINTEF abrasivity tests (Sievers' J-Value and AVS) for each rock sample can also be examined in Appendix-D.

Table 4.10. Results of Sievers'J-Value test.

Sr. No.	Rock Sample	SJ-Value
1	Dolerite-3	6.45
2	Dolerite-4	12.58
3	Granite-6	3.63
4	Andesite	2.36
5	Granitic Gneiss-2	56.57
6	Quartzite-1	2.06
7	Sandstone-2	110.54
8	Sandstone-3	67.30
9	Sandstone-14	109.44
10	Sandstone-16	1.27

Table 4.11. Results of Abrasion Value Steel (AVS) tests using four different rock abrasion powders keeping the other test parameters as standard.

Sr. No.	Rock Sample	AVS (mg) for Fraction [99% < 1mm and (70 ± 5) % < 0.71 mm]	AVS (mg) for Fraction [99% < 1mm and (70 ± 5) % < 0.50 mm]	AVS (mg) for Fraction [99% < 1mm and (70 ± 5) % < 0.25 mm]	AVS (mg) for Fraction [99% < 1mm and (70 ± 5) % < 0.15 mm]
1	Dolerite-3	10.0	8.0	5.5	3.5
2	Dolerite-4	11.0	9.3	8.5	6.0
3	Granite-6	30.5	26.5	24.0	12.5
4	Andesite	5.3	4.0	3.0	1.5
5	Granitic Gneiss-2	36.5	33.5	29.5	26.0
6	Quartzite-1	40.0	37.0	34.0	32.0
7	Sandstone-2	26.0	25.0	23.5	21.0
8	Sandstone-3	20.0	19.0	13.0	9.0
9	Sandstone-14	21.0	18.0	15.0	8.0
10	Sandstone-16	20.0	17.5	8.0	7.0

Table 4.12. Results of Abrasion Value Steel (AVS) tests by varying the test speed using the standard rock fraction [99% < 1mm and (70 ± 5) % < 0.50 mm].

Sr. No.	Rock Sample	AVS (mg) @ the Speed of 20 RPM	AVS (mg) @ the Speed of 10 RPM
1	Dolerite-3	8.0	11.5
2	Dolerite-4	9.3	10.5
3	Granite-6	26.5	35.7
4	Andesite	4.0	6.0
5	Granitic Gneiss-2	33.5	35.0
6	Quartzite-1	37.0	38.5
7	Sandstone-2	25.0	29.0
8	Sandstone-3	19.0	21.5
9	Sandstone-14	18.0	19.5
10	Sandstone-16	17.5	24.5

Table 4.13. Cutter Life Index (CLI) values computed from Sievers'J-Values and AVS.

Sr. No.	Rock Sample	CLI for Fraction [99% < 1mm and (70 ± 5) % < 0.71 mm]	CLI for Fraction [99% < 1mm and (70 ± 5) % < 0.50 mm]	CLI for Fraction [99% < 1mm and (70 ± 5) % < 0.25 mm]	CLI for Fraction [99% < 1mm and (70 ± 5) % < 0.15 mm]
1	Dolerite-3	11.7	12.7	14.7	17.5
2	Dolerite-4	14.6	15.6	16.1	18.4
3	Granite-6	6.1	6.4	6.7	8.6
4	Andesite	10.4	11.3	12.6	16.5
5	Granitic Gneiss-2	16.4	16.9	17.8	18.7
6	Quartzite-1	4.4	4.6	4.7	4.8
7	Sandstone-2	24.2	24.5	25.1	26.2
8	Sandstone-3	22.1	22.5	26.1	30.0
9	Sandstone-14	26.1	27.7	29.7	37.9
10	Sandstone-16	4.8	5.0	6.8	7.2

4.5. MECHANICAL AND PHYSICAL ROCK PROPERTIES TESTS

The mechanical rock properties include uniaxial compressive strength (UCS) and Brazilian tensile strength (BTS) tests, whereas physical rock properties comprise of dry density (ρ_d), saturated density (ρ_s), pore space volume (V_v), porosity (n) and compressional wave velocity (V_p) tests. Table 4.14 lists the average values of the mechanical and physical rock properties tests conducted on 51 rock samples included in the data base. In addition, rock properties tests including $UCS_{(Sat)}$, $BTS_{(Sat)}$ and $V_{p(Sat)}$ were also conducted on fully saturated, 33 sedimentary rocks included in the sample data base which are presented in Table 4.15. The complete results of mechanical tests (UCS and BTS) for both dry and saturated rock samples are presented in Appendix-F and Appendix-G respectively.

Table 4.14. Results of mechanical and physical rock properties tests.

Sr. No.	Rock Sample	UCS (MPa)	BTS (MPa)	ρ_d (g/cc)	ρ_{sat} (g/cc)	V_v (cc)	n (%)	V_p (km/s)
1	Dolerite-1	214.50	6.76	2.91	2.91	0.24	0.51	6.54
2	Dolerite-2	212.10	8.16	3.09	3.10	0.48	0.82	4.95
3	Dolerite-3	199.30	9.82	3.12	3.13	0.24	0.52	8.19
4	Dolerite-4	140.50	13.73	3.05	3.06	0.07	0.12	7.22
5	Granite-1	40.21	1.60	2.76	2.77	0.33	1.07	3.31
6	Granite-2	83.81	3.37	2.62	2.62	0.26	0.67	3.29
7	Granite-3	77.61	3.69	2.71	2.72	0.29	1.16	4.22
8	Granite-4	53.90	2.23	2.70	2.71	0.30	0.88	3.67
9	Granite-5	231.99	18.65	3.07	3.07	0.33	0.53	6.28
10	Granite-6	44.80	2.30	2.55	2.56	0.99	1.40	3.69
11	Migmatite	56.76	2.27	2.62	2.64	0.37	1.24	3.31
12	Andesite	231.46	14.07	3.00	3.01	0.27	0.40	5.98
13	Granitic Gneiss-1	69.22	4.07	2.65	2.66	0.24	0.86	0.94
14	Granitic Gneiss-2	54.53	3.19	2.58	2.59	0.72	1.07	1.78
15	Phyllite	54.33	4.10	2.42	2.50	3.62	7.68	4.97
16	Quartzite-1	56.39	4.35	2.45	2.48	2.34	3.27	3.15
17	Quartzite-2	147.03	14.58	2.73	2.73	0.22	0.40	5.82
18	Siltstone-1	49.30	7.36	2.69	2.71	0.73	1.03	5.31
19	Siltstone-2	57.88	9.02	2.60	2.64	2.22	3.63	5.60
20	Sandstone-1	39.80	1.85	2.63	2.70	3.90	6.87	3.79
21	Sandstone-2	41.55	0.48	2.18	2.30	7.26	11.73	2.29
22	Sandstone-3	127.60	6.38	2.62	2.63	0.90	1.17	5.85
23	Sandstone-4	26.73	1.45	2.25	2.37	7.93	12.22	2.64
24	Sandstone-5	44.00	2.84	2.53	2.56	1.94	3.12	3.38
25	Sandstone-6	109.73	6.03	2.56	2.62	2.95	4.73	4.85
26	Sandstone-7	61.51	7.32	2.59	2.61	3.00	4.79	6.64
27	Sandstone-8	11.04	1.31	2.28	2.38	6.76	10.70	2.59
28	Sandstone-9	29.04	1.87	2.11	2.26	9.12	15.05	2.78
29	Sandstone-10	16.69	0.70	3.16	2.26	7.51	10.26	2.05
30	Sandstone-11	21.18	2.05	2.19	2.31	7.37	12.10	2.73
31	Sandstone-12	27.09	1.61	2.29	2.40	6.19	10.83	2.06
32	Sandstone-13	46.40	1.60	2.19	2.33	6.72	11.40	4.41
33	Sandstone-14	17.07	0.86	2.51	2.61	7.43	12.77	1.98
34	Sandstone-15	69.04	6.10	2.49	2.57	4.44	6.82	4.38
35	Sandstone-16	129.79	22.67	2.64	2.66	1.11	1.63	3.64
36	Sandstone-17	56.76	4.20	2.60	2.64	2.26	3.61	5.12
37	Sandstone-18	82.77	6.01	2.63	2.65	0.94	2.82	5.58
38	Chamositic- Siderite	51.72	8.08	2.62	2.82	12.97	20.02	3.61
39	Dolomite-1	61.84	6.54	2.57	2.64	3.94	6.15	6.29
40	Dolomite-2	144.43	11.96	2.77	2.78	0.83	1.23	5.90
41	Dolomite-3	99.93	12.53	2.81	2.82	0.25	0.38	7.26
42	Dolomite-4	132.70	6.65	2.50	2.56	4.11	6.43	5.77
43	Limestone-1	65.26	5.01	2.61	2.64	0.98	3.48	6.36
44	Limestone-2	95.78	4.60	2.67	2.68	0.49	0.80	6.12
45	Limestone-3	80.70	5.62	3.17	3.20	0.66	2.81	6.66
46	Limestone-4	66.45	5.39	2.69	2.70	0.78	1.17	7.49
47	Limestone-5	92.75	7.89	2.50	2.54	4.11	7.15	5.41
48	Limestone-6	69.89	3.31	2.65	2.66	0.86	1.37	6.47
49	Limestone-7	20.08	7.83	2.50	2.57	4.13	6.53	4.78
50	Rock Gypsum	13.53	1.33	2.07	2.25	10.70	18.37	5.38
51	Marl	5.35	0.78	2.00	2.25	14.95	24.70	2.29

ρ_d - dry density of rock specimen, ρ_{sat} - saturated density of rock specimen, V_v - Speciemn pore volume, n - Porosity of rock specimen, V_p - Primary wave velocity through rock specimen.

Table 4.15. Results of mechanical and physical rock properties tests conducted on fully saturated sedimentary rock samples.

Sr. No.	Rock Sample	UCS$_{(Sat)}$ (MPa)	BTS$_{(Sat)}$ (MPa)	V$_{p (Sat)}$ (km/s)
1	Siltstone-1	17.30	2.05	5.17
2	Siltstone-2	56.07	6.77	5.88
3	Sandstone-1	19.10	2.11	4.95
4	Sandstone-2	26.20	0.11	1.90
5	Sandstone-3	85.33	2.46	5.25
6	Sandstone-4	13.57	0.91	3.01
7	Sandstone-5	40.27	2.74	4.94
8	Sandstone-6	66.30	1.20	4.44
9	Sandstone-7	58.03	2.56	5.87
10	Sandstone-8	17.55	0.98	3.17
11	Sandstone-9	14.15	1.78	2.71
12	Sandstone-10	13.04	1.00	2.93
13	Sandstone-11	19.74	1.96	3.28
14	Sandstone-12	23.60	1.41	1.86
15	Sandstone-13	30.65	1.75	3.86
16	Sandstone-14	4.84	0.88	2.58
17	Sandstone-15	43.73	3.91	4.91
18	Sandstone-17	60.90	1.37	5.27
19	Sandstone-18	61.97	3.94	5.84
20	Chamositic- Siderite	38.79	4.15	3.89
21	Dolomite-1	33.50	3.86	5.97
22	Dolomite-2	67.75	8.22	6.48
23	Dolomite-3	55.52	4.66	7.29
24	Dolomite-4	57.94	3.83	5.77
25	Limestone-1	60.85	1.22	6.42
26	Limestone-2	48.74	2.64	6.08
27	Limestone-3	29.64	5.42	7.00
28	Limestone-4	37.21	3.11	6.30
29	Limestone-5	80.79	5.13	5.06
30	Limestone-6	32.25	2.77	6.40
31	Limestone-7	32.13	0.76	5.09
32	Rock Gypsum	8.48	1.36	5.18
33	Marl	2.10	0.33	2.06

4.6. RESULTS OF WEAR INDICES OF SATURATED ROCK SAMPLES

The test results of petrographic analyses (Table 4.1) and mechanical properties including UCS and BTS in the saturated state (Table 4.15) of 33 sedimentary rock samples were also utilized to determine wear indices such as Schimazek's F-value$_{(sat)}$ and RAI$_{(sat)}$ which are presented in Table 4.16. The calculation details of Schimazek's F-value (N/mm) and RAI for fully saturated rock samples can be examined in Appendix-H.

Table 4.16. Results of wear indices computed from petrographical analyses and mechanical rock properties of fully saturated sedimentary rock samples.

Sr. No.	Rock Sample	Schimazek's F-value$_{(Sat)}$ (N/mm)	RAI$_{(Sat)}$
1	Siltstone-1	0.135	4.050
2	Siltstone-2	0.390	20.360
3	Sandstone-1	0.672	13.800
4	Sandstone-2	0.020	20.310
5	Sandstone-3	1.106	76.717
6	Sandstone-4	0.294	11.434
7	Sandstone-5	1.062	30.860
8	Sandstone-6	1.107	59.470
9	Sandstone-7	0.440	52.050
10	Sandstone-8	0.283	12.162
11	Sandstone-9	0.870	11.955
12	Sandstone-10	0.344	10.028
13	Sandstone-11	0.916	16.663
14	Sandstone-12	0.218	15.251
15	Sandstone-13	0.405	26.151
16	Sandstone-14	0.313	4.065
17	Sandstone-15	0.305	36.847
18	Sandstone-17	0.665	41.467
19	Sandstone-18	0.687	44.258
20	Chamositic- Siderite	0.067	6.055
21	Dolomite-1	0.024	2.012
22	Dolomite-2	0.111	4.768
23	Dolomite-3	0.093	4.065
24	Dolomite-4	0.111	10.292
25	Limestone-1	0.011	1.595
26	Limestone-2	0.024	1.268
27	Limestone-3	0.182	1.018
28	Limestone-4	0.054	0.754
29	Limestone-5	0.007	1.794
30	Limestone-6	0.034	1.069
31	Limestone-7	0.002	0.966
32	Rock Gypsum	0.003	0.046
33	Marl	0.009	0.508

5. DISCUSSION: ABRASIVITY EVALUATIONS UTILIZING CERCHAR ABRASIVITY TESTING METHOD

This chapter presents discussion on CERCHAR abrasivity measurements performed on selected rock units belonging to various startigraphic formations of Pakistan. The CERCHAR tests are performed on all 51 rock units included in this research work. However this section utilizes the experimental results of 46 rock samples (Table 5.1) out of the initially selected 51 rocks, for the evaluation of CERCHAR abrasivity indices with the petrographical, mechanical and physical properties of rocks. The petrographic studies of 40 abrasive and non-abrasive rocks selected out of the total 51 rock samples are used for analyses with CERCHAR abrasivity index (CAI), which are presented in Table 5.2. The experimental methodology is outlined in Section 3, whereas the complete results of the experiments conducted are summarized in Section 4. In this section the discussion of results is mainly focused on evaluating the effects of wear flat measurement methods and test surface conditions on the CAI values. Moreover, the dependence of CERCHAR abrasivity index on petrographic parameters, the wear factors (Schimazek's F-value and RAI) and the physical and mechanical properties of rocks are also discussed.

Table 5.1. The CAI and the properties of the tested rocks.

Sr. No.	Rock Sample	CAI s(Top)	CAI s(Side)	CAI fb(Top)	CAI fb(Side)	UCS (MPa)	BTS (MPa)	Dry Density (g/cc)	Porosity (%)	Vp (Km/s)
1	Dolerite-1	3.237	2.816	3.627	3.083	214.500	6.761	2.908	0.512	6.544
2	Dolerite-2	3.015	2.673	4.074	3.150	212.100	8.161	3.091	0.819	4.955
3	Dolerite-3	3.540	2.990	4.650	3.850	199.300	9.820	3.120	0.520	8.190
4	Dolerite-4	3.220	2.220	4.450	3.590	140.500	13.730	3.050	0.120	7.220
5	Granite-1	4.500	3.577	5.273	4.502	40.210	1.600	2.761	1.071	3.315
6	Granite-2	4.610	4.040	4.980	4.110	83.810	3.370	2.620	0.670	3.290
7	Granite-3	4.184	3.634	5.283	4.150	77.614	3.690	2.711	1.157	4.220
8	Granite-4	3.907	3.111	5.081	4.031	53.895	2.234	2.703	0.881	3.674
9	Granite-5	3.590	2.820	4.480	3.450	231.990	18.650	3.070	0.530	6.280
10	Granite-6	3.900	3.490	4.987	4.687	44.800	2.300	2.550	1.400	3.690
11	Migmatite	4.320	3.550	3.600	3.210	56.760	2.270	2.620	1.240	3.310
12	Andesite	3.528	3.250	5.154	4.425	231.462	14.065	3.004	0.398	5.983
13	Granitic Gneisse-1	3.650	2.870	3.570	3.270	69.220	4.070	2.650	0.860	0.940
14	Granitic Gneisse-2	4.952	4.262	5.025	4.164	54.532	3.190	2.582	1.070	1.775
15	Phyllite	1.433	1.189	2.677	2.184	54.330	4.100	2.423	7.683	4.973
16	Quartzite-1	4.390	3.930	4.703	3.932	56.390	4.350	2.450	3.270	3.150
17	Quartzite-2	4.134	3.394	4.594	3.652	147.027	14.583	2.731	0.399	5.818
18	Siltstone-1	1.150	0.990	1.440	1.250	49.300	7.360	2.690	1.030	5.310
19	Siltstone-2	2.216	1.536	2.302	1.872	57.880	9.016	2.600	3.634	5.601
20	Sandstone-1	1.783	1.524	2.067	1.764	39.800	1.846	2.627	6.866	3.786
21	Sandstone-2	0.620	0.710	1.250	0.860	41.550	0.480	2.180	11.730	2.290
22	Sandstone-3	3.920	3.240	3.550	2.840	127.600	6.380	2.620	1.170	5.850
23	Sandstone-4	1.410	1.050	1.540	1.220	26.730	1.447	2.250	12.220	2.640

Sr. No.	Rock Sample	CAI s(Top)	CAI s(Side)	CAI fb(Top)	CAI fb(Side)	UCS (MPa)	BTS (MPa)	Dry Density (g/cc)	Porosity (%)	Vp (Km/s)
24	Sandstone-5	3.038	2.437	2.931	2.275	44.003	2.839	2.533	3.116	3.381
25	Sandstone-6	3.300	2.840	3.210	3.210	109.730	6.030	2.560	4.727	4.850
26	Sandstone-7	2.030	1.670	1.680	1.380	61.510	7.320	2.590	4.792	6.640
27	Sandstone-8	1.430	1.420	1.140	1.250	11.040	1.310	2.280	10.703	2.590
28	Sandstone-9	2.320	2.380	2.690	2.610	29.040	1.870	2.110	15.054	2.780
29	Sandstone-10	1.394	1.403	1.570	1.443	16.690	0.700	3.161	10.256	2.046
30	Sandstone-11	1.950	1.480	1.930	1.490	21.180	2.050	2.190	12.099	2.730
31	Sandstone-12	1.621	1.589	1.281	1.147	27.085	1.610	2.292	10.835	2.061
32	Sandstone-13	1.640	1.400	2.160	1.810	46.400	1.600	2.190	11.402	4.410
33	Sandstone-14	1.260	1.300	1.230	1.310	17.070	0.860	2.510	12.770	1.980
34	Sandstone-15	1.940	1.600	1.700	1.450	69.040	6.100	2.490	6.820	4.380
35	Sandstone-16	3.973	3.664	6.355	5.532	129.793	22.666	2.643	1.629	3.643
36	Chamositic-Siderite	1.066	0.926	1.837	1.018	51.715	8.080	2.621	20.021	3.614
37	Dolomite-1	2.121	2.082	1.568	1.608	61.840	6.540	2.575	6.152	6.287
38	Dolomite-2	2.223	1.818	1.979	1.787	144.425	11.958	2.771	1.230	5.898
39	Dolomite-3	2.445	2.041	2.052	1.895	99.928	12.530	2.813	0.376	7.257
40	Dolomite-4	2.500	2.125	2.410	2.149	132.704	6.653	2.499	6.431	5.767
41	Limestone-1	1.017	0.571	1.260	1.062	65.257	5.008	2.609	3.475	6.358
42	Limestone-2	1.102	0.906	1.207	0.938	95.776	4.604	2.672	0.798	6.123
43	Limestone-3	1.478	1.400	1.631	1.455	80.700	5.618	3.169	2.809	6.665
44	Limestone-4	0.958	1.098	0.961	1.188	66.450	5.390	2.690	1.170	7.491
45	Limestone-5	1.161	1.109	1.051	1.130	92.745	7.890	2.496	7.146	5.413
46	Rock Gypsum	0.731	0.435	0.809	0.503	13.525	1.332	2.067	18.372	5.382

$CAI_{s(Top)}$ - CAI value for sawn rock surface measured using top viewing method at the stylus tip, $CAI_{s(Side)}$ - CAI value for sawn rock surface measured using top viewing method at the stylus tip, $CAI_{fb(Top)}$ - CAI value for freshly broken rock surface measured using top viewing method at the stylus tip, $CAI_{fb(Side)}$ - CAI value for freshly broken rock surface measured using side viewing method at the stylus tip.

Table 5.2. Petrographic analysis of selected rocks.

Sr. No.	Rock Sample	Qtz (%)	Qtz-eq (%)	Ø-Qtz (mm)	Ø (mm)	Schimazek's F-value (N/mm)	RAI
1	Dolerite-1	5.000	37.385	0.224	0.334	0.939	80.191
2	Dolerite-3	7.000	40.957	0.226	0.494	3.326	81.627
3	Dolerite-4	18.000	53.762	0.363	0.352	2.890	75.535
4	Granite-2	74.000	81.860	1.103	1.144	3.069	68.607
5	Granite-3	65.000	73.890	1.303	1.113	3.623	57.349
6	Granite-4	67.000	78.453	1.194	1.721	2.193	42.282
7	Granite-5	73.000	82.063	0.386	0.845	7.697	190.377
8	Granite-6	24.600	58.852	2.496	1.537	2.224	26.366
9	Migmatite	70.000	79.580	1.215	1.352	2.440	45.170
10	Andesite	10.000	36.420	0.180	0.599	3.437	84.298
11	Granitic Gneiss-1	73.000	82.405	0.565	0.800	2.095	57.041
12	Phyllite	50.000	53.945	0.139	0.784	0.324	29.308
13	Quartzite-1	90.600	96.775	0.737	0.318	3.009	54.571
14	Quartzite-2	70.800	75.377	0.538	0.304	4.257	110.824
15	Siltstone-1	15.200	23.424	0.225	0.290	0.484	11.548
16	Siltstone-2	22.000	36.308	0.154	0.206	0.517	21.015
17	Sandstone-1	68.000	72.274	0.413	0.729	0.588	28.765
18	Sandstone-2	67.000	77.505	0.237	0.204	0.086	32.203
19	Sandstone-3	64.000	79.360	0.588	0.575	2.870	101.263
20	Sandstone-4	78.000	84.255	0.392	0.389	0.468	22.521
21	Sandstone-5	62.300	76.633	0.513	0.480	1.099	33.720
22	Sandstone-6	70.100	89.700	0.716	0.812	5.554	98.427
23	Sandstone-7	67.500	89.691	0.106	0.263	1.270	55.169
24	Sandstone-8	55.500	69.306	0.414	0.815	0.380	7.651
25	Sandstone-9	78.000	84.473	0.588	0.674	0.909	24.531
26	Sandstone-10	75.000	76.907	0.452	0.366	0.241	12.836
27	Sandstone-11	73.000	82.425	0.581	0.589	0.958	17.458
28	Sandstone-12	55.000	64.617	0.240	0.376	0.249	17.501
29	Sandstone-13	77.000	85.328	0.273	0.597	0.370	39.592
30	Sandstone-14	72.500	83.900	0.431	0.542	0.305	14.322
31	Sandstone-15	78.000	84.255	0.090	0.246	0.476	58.170
32	Sandstone-16	95.000	96.217	0.272	0.257	5.907	124.883

Sr. No.	Rock Sample	Qtz (%)	Qtz-eq (%)	Ø-Qtz (mm)	Ø (mm)	Schimazek's F-value (N/mm)	RAI
33	Dolomite-1	1.000	6.006	0.053	0.173	0.041	3.714
34	Dolomite-2	2.000	7.039	0.047	0.235	0.162	10.166
35	Dolomite-3	2.500	7.322	0.345	0.426	0.249	7.317
36	Dolomite-4	10.000	17.765	0.175	0.214	0.193	23.575
37	Limestone-2	0.000	2.601	0.000	0.485	0.042	2.491
38	Limestone-3	0.000	3.436	0.000	1.512	0.189	2.773
39	Limestone-4	0.000	2.026	0.000	0.698	0.093	1.346
40	Limestone-5	0.000	2.220	0.000	0.436	0.012	2.059

5.1. EFFECT OF WEAR FLAT MEASUREMENT PROCEDURE ON CAI VALUE

In this research work the CERCHAR tests were performed using the freshly broken and sawn rock surfaces to evaluate their influence on the measured CAI values. Both the top and side measurement techniques were adopted in order to compare the results obtained. Top and side view wear flat measurements at the stylus tip were conducted in accordance with the ASTM-D7625-10 standard and ISRM suggested method (Alber et al., 2014). However, for side measurement of the wear flat, the technique suggested by Alber et al. (2014) could not be fully followed due to unavailability of some features required for the measurement of the tip angle in the tool maker's microscope used. Therefore, side viewing of the tips was done by carefully disregarding the splinters or burrs produced as suggested by West (1989). Figures 5.1a, 5.1b and 5.1c show both the top and side views of a stylus tested over a freshly broken surface of a Tobra siltstone (Siltstone-2) specimen. Burr or splinter is clearly visible on the tip of the stylus (Figures 5.1b and 5.1c) giving a measurement of 0.3210 mm along one diameter of test stylus both from the top view (Figure 5.1a) and from the side view (Figure 5.1c) without disregarding the burr. When the test stylus was viewed from the side by disregarding the splinter (Figure 5.1b) gave a measurement of 0.2000 mm of the same stylus diameter.

To establish whether the CAI values obtained by measuring the wear flats of steel styli from top or side views under a microscope, are really dissimilar, hypothesis testing about the means was carried out. For this purpose the t-test statistics was adopted with the assumption that the population distributions are normal (Gaussian) and have equal variances. In t-statistics when population variance is not known it is estimated by pooling

the independent sample variances. T-score is calculated by using equation 5.1 (Samaranayake, 2009; Lyman and Longnecker, 2010):
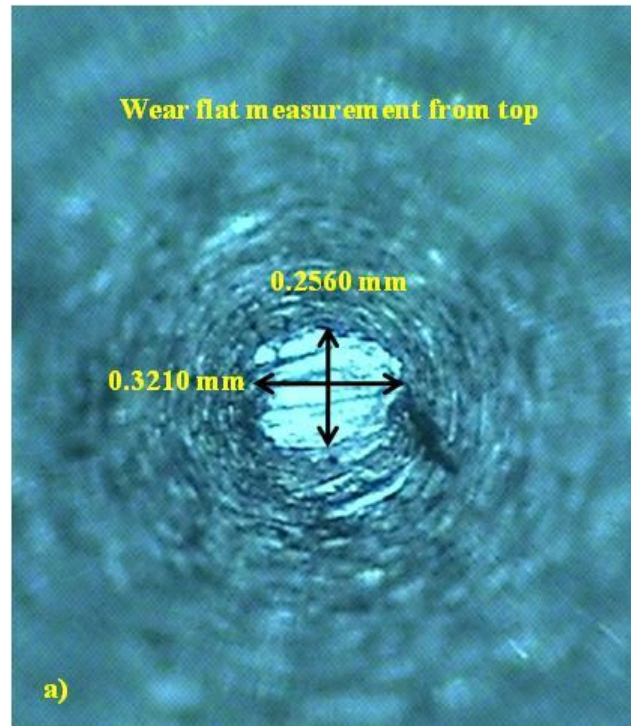
Figure 5.1(a) Wear flat measurement at stylus tip from top for Siltstone-2 sample.
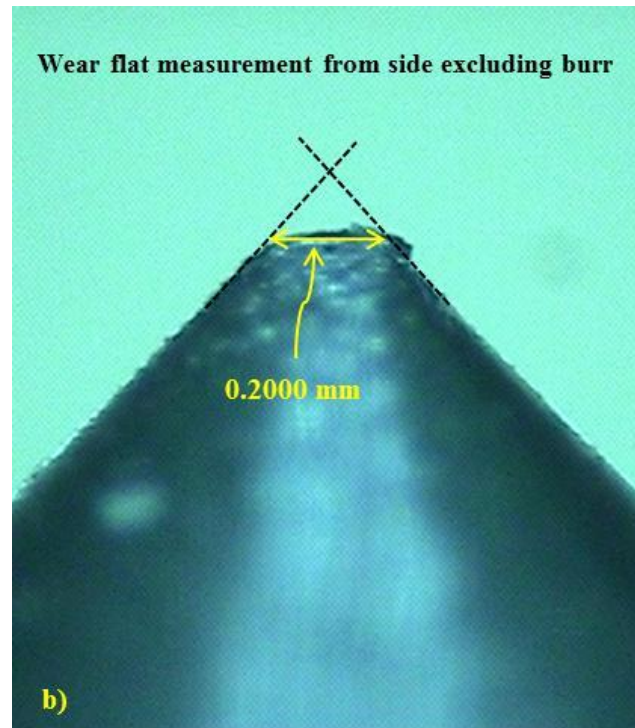
Figure 5.1(b) Wear flat measurement at stylus tip from side excluding burr for Siltstone-2 sample. Notice the difference in the wear flat values measured in mm (Figure 5.1a, c).
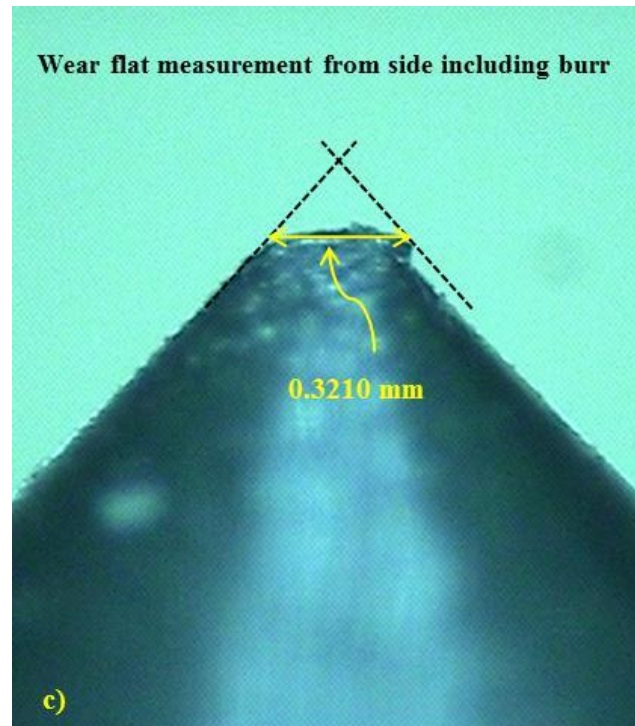
Figure 5.1(c) Wear flat measurement at stylus tip from side including burr for Siltstone-2 sample.

$$T = \frac{(\bar{X} - \bar{Y}) - \mu_0}{S_P \sqrt{\frac{1}{n_1} + \frac{1}{n_2}}} \qquad (5.1)$$

Where;

S_P = Pooled variance i.e. weighted average of the independent population variances;

n_1 = First population sample size;

n_2 = Second population sample size;

$\overline{X}$ = Average value of first population;

$\overline{Y}$ = Average value of second population.

The T-statistics scores were calculated for contrasts in the values of individual CAI means of the top and side stylus measurements for both sawn (CAI_s) and freshly broken (CAI_{fb}) rock surfaces. The significance level for t-test was fixed at $\alpha = 0.1$ (90 % confidence level). To determine the statistical significance of test results, p-values were also calculated for the means comparison. p-value is the probability of obtaining a test statistics at least as large as the one in the sample population with the assumption that null hypothesis (H_0) is true. A p-value smaller than or equal to α- value provides strong evidence to reject the null hypothesis and to accept the alternate or new hypothesis (H_1) (Abu Bakar and Gertsch, 2012). The null hypothesis (Equations 5.2 and 5.3) for this study was based on the fact that the calculated mean value of CAI is equal if measured from top or side for both sawn and freshly broken rock surfaces respectively. On the other hand the alternate hypothesis (Equations 5.2 and 5.3) was that the CAI value would be different for both the top and side measurements.

$$H_0 = \mu_{\text{side}} - \mu_{\text{top}} = 0 \qquad \begin{bmatrix} For \\ Sawn\ Surface \end{bmatrix} \qquad (5.2)$$
$$H_1 = \mu_{\text{side}} - \mu_{\text{top}} \neq 0$$

$$H_0 = \mu_{\text{side}} - \mu_{\text{top}} = 0 \qquad \begin{bmatrix} For \\ Freshly\ Broken\ Surface \end{bmatrix} \qquad (5.3)$$
$$H_1 = \mu_{\text{side}} - \mu_{\text{top}} \neq 0$$

The p-values calculated from the T-score of corresponding sample populations for sawn (CAI_s) and rough (CAI_{fb}) rock surfaces when read from both top and side are listed

in Table 5.3. It can be seen that 63% of p-values were found statistically significant at $\alpha = 0.1$ for both CAI_s and CAI_{fb} thereby rejecting the null hypothesis. It shows that most of the wear flat measurements made from the top side of the styli were higher than the measurement made from the side of the test styli. This fact can be seen in Figures 5.2 and 5.3, where majority of the CAI values when measured from top side (regardless of the statistical significance specified) lie above the 1:1 line. A few exceptions can be seen, where the CAI values measured both from the top and side coincided. The results of the statistical analyses support the findings of the earlier investigations (West, 1989; Rostami et al., 2005; Gharahbagh et al., 2011; Rostami et al., 2013; Alber et al., 2014) where the difference of top and side measurements was attributed to the creation of burrs or splinters, usually concealed in the top measurements.

It can be noticed that the correlation equations (Figures 5.2 and 5.3) developed for sawn and freshly broken rock surfaces using top and side view measurements, show a significant increase of 17% and 19% respectively in CAI values when measured from the top of the stylus. The CERCHAR test is widely used in tender documents of rock excavation projects for estimating the life and cost of cutting tools. The practical implications of using higher CAI values based on top measurements of wear flat could be the exaggeration of the rock behavior towards wear of rock cutting tools and consequently over estimation of the cost, replacement rate of the cutting tools and the machine down time. Therefore, it is prudent to normalize the CAI values measured from top view of the styli to the side view values. Likewise, the ISRM suggested methods (Alber et al., 2014) also strongly recommend CAI measurements by side view of the stylus.

Table 5.3. p-values of means comparison for CAI-values using top and side views on sawn and freshly broken rock surfaces. Bold faced values show statistically different values at α=0.1 significant level.

Sr. No.	Rock	p-value (CAI$_s$)	p-value (CAI$_{fb}$)
1	Dolerite-1	**0.0645**	**0.0735**
2	Dolerite-2	**0.0255**	**0.0612**
3	Dolerite-3	**0.0488**	**0.0367**
4	Dolerite-4	**0.0003**	**0.0178**
5	Granite-1	**0.0063**	0.1283
6	Granite-2	**0.1728**	**0.0573**
7	Granite-3	**0.0734**	**0.0435**
8	Granite-4	0.2579	**0.0087**
9	Granite-5	**0.0259**	**0.0181**
10	Granite-6	**0.0594**	**0.0684**
11	Migmatite	**0.0295**	0.2466
12	Andesite	**0.0494**	**0.0576**
13	Granitic Gneisse-1	**0.0113**	0.2579
14	Granitic Gneisse-2	**0.0376**	0.1560
15	Phyllite	**0.0050**	**0.1032**
16	Quartzite-1	**0.2499**	**0.1090**
17	Quartzite-2	**0.0000**	**0.0040**
18	Siltstone-1	0.1814	0.1333
19	Siltstone-2	**0.0003**	**0.0199**
20	Sandstone-1	0.2879	0.1880
21	Sandstone-2	0.7784	**0.0003**
22	Sandstone-3	**0.0036**	**0.0343**
23	Sandstone-4	**0.0519**	**0.0119**
24	Sandstone-5	**0.0161**	**0.1081**
25	Sandstone-6	**0.0429**	0.5052
26	Sandstone-7	**0.0025**	0.1097
27	Sandstone-8	0.4834	0.7551
28	Sandstone-9	0.6406	0.4097
29	Sandstone-10	0.5174	**0.0648**
30	Sandstone-11	**0.0126**	**0.0013**
31	Sandstone-12	0.4088	0.2350
32	Sandstone-13	0.1107	**0.0482**
33	Sandstone-14	0.6012	0.8865
34	Sandstone-15	**0.0512**	**0.0224**
35	Sandstone-16	**0.0449**	**0.0036**
36	Chamositic Siderite	0.2160	0.1952
37	Dolomite-1	0.3411	0.6684
38	Dolomite-2	**0.0063**	**0.0679**
39	Dolomite-3	**0.0696**	0.1960
40	Dolomite-4	**0.0089**	**0.0216**
41	Limestone-1	**0.0839**	**0.0721**
42	Limestone-2	**0.0061**	**0.0290**
43	Limestone-3	0.3368	0.1818
44	Limestone-4	0.8731	0.9647
45	Limestone-5	0.2700	0.7656
46	Rock Gypsum	**0.0039**	**0.0360**
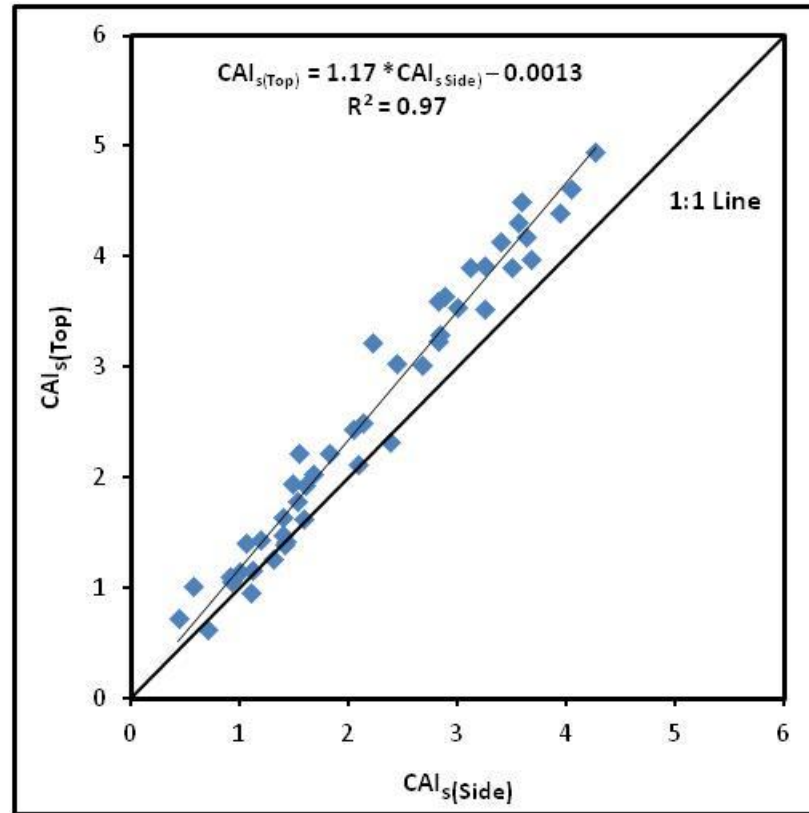
Figure 5.2. CAI$_s$ values measured from top and side views of the CERCHAR styli (after Majeed and Abu Bakar, 2015).
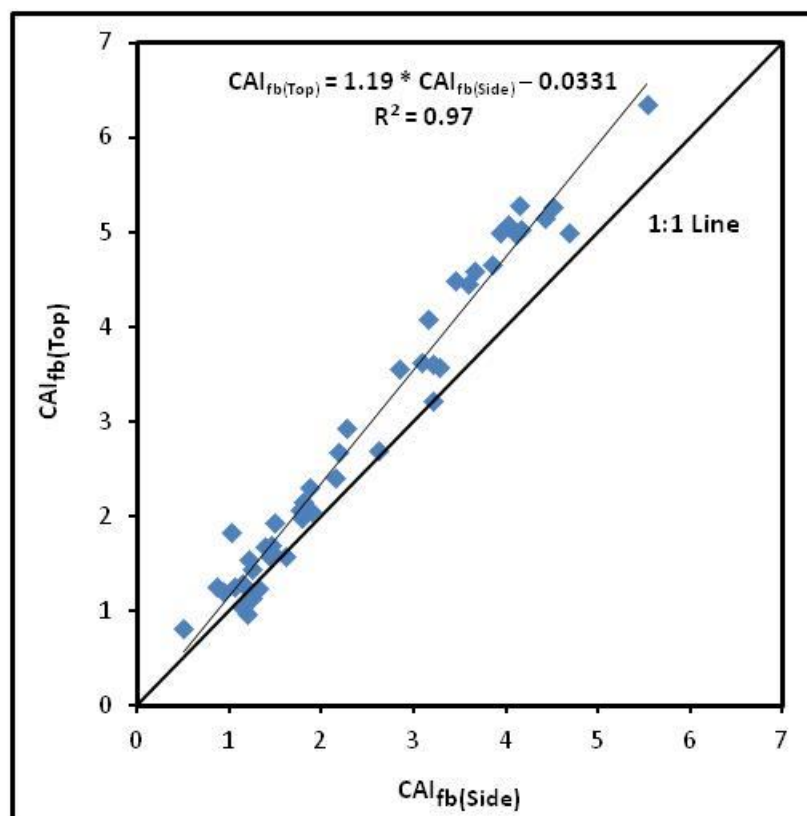
Figure 5.3. CAI_{fb} values measured from top and side views of CERCHAR styli (after Majeed and Abu Bakar, 2015).

Moreover, it was observed that the CERCHAR Abrasivity Index values obtained especially on freshly broken rock surfaces (CAI_{fb}) usually produced uneven wear flats and scratch grooves at the side of test tip due to initial burying of the test tip in the abrasive rocks. In the top viewing mode of stylus, these grooves sometimes were not easily distinguishable from the actual wear flat at the top of the stylus tip and were therefore, included in the wear flat readings. The same stylus when viewed from the side easily identified these scratch grooves and was excluded for the measurement of CAI values. Figure 5.4 shows both the top and side views of a stylus tested over a freshly broken surface of a Tobra quartzite sample. Scratch groove is clearly visible at the side of the stylus tip giving a measurement of 0.5150 mm along one diameter of test stylus from top view and when viewed from the side by excluding the scratch groove gave a measurement of 0.2650 mm of the same diameter of the test stylus.
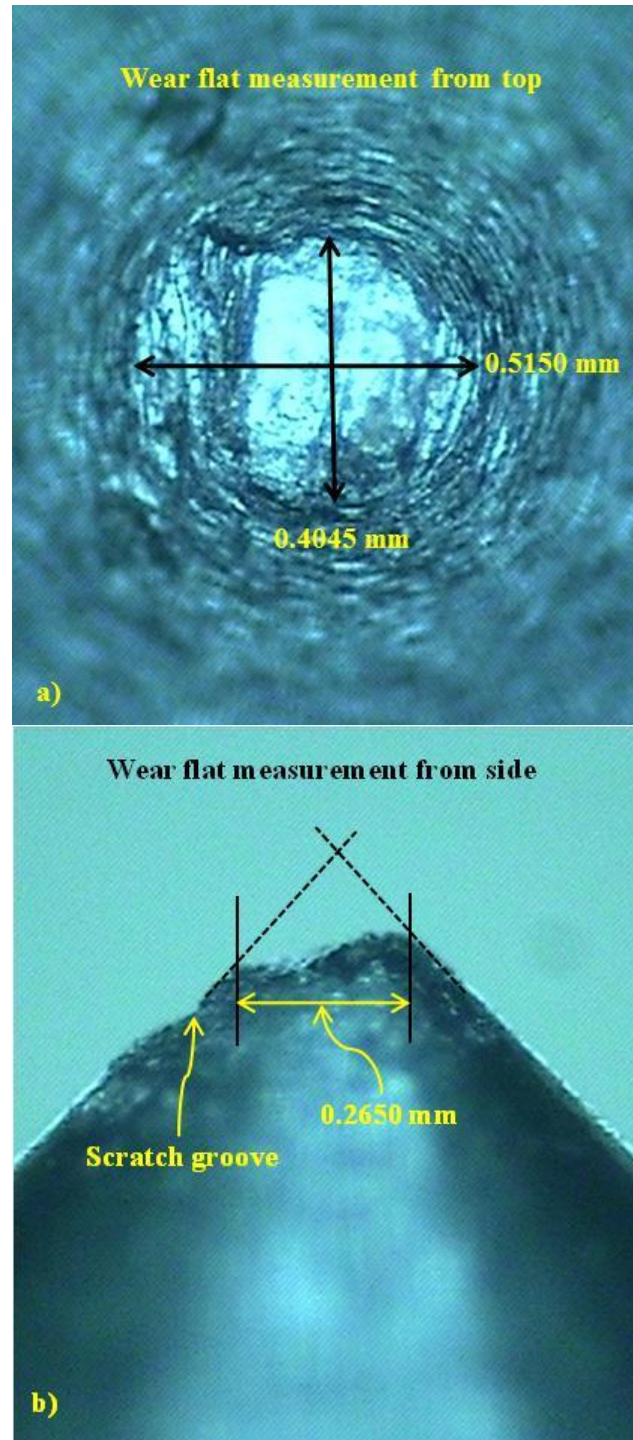
Figure 5.4. Wear flat measurement at stylus tip; (a) from top (b) from side for a Tobra Quartzite rock sample. Notice the difference in the wear flat values measured in millimeters (mm) when disregarding a scratch groove.

5.2. EFFECT OF SURFACE CONDITION OF ROCK ON CAI

The effect of surface condition for the measurement of CAI has been under discussion by several past investigators and has shown that the CAI when measured on freshly broken rough surfaces produces about 0.5 higher values of CAI (Plinninger et al., 2003). The CAI_{fb} and CAI_s values measured on freshly broken and sawn rock surfaces by using both the side and top views for all tested rock samples are shown in Figure 5.5 and Figure 5.6 respectively. It can be seen that significant linear correlations exist between the CAI values measured on standard freshly broken rock surfaces and the diamond sawn rock surfaces ($R^2 = 86\%$) by viewing the wear flat from both the top and side of the styli used. The equations developed (Eq. 5.4 and Eq. 5.5) closely match the already published equations (Al-Ameen and Waller, 1994; Plinninger et al., 2003; Fowell and Abu Bakar, 2007; ASTM-D7625-10; Kasling and Thuro, 2010). Recently Alber et al. (2014) in ISRM suggested methods have adopted the relationship developed by Kasling and Thuro (2010) for the conversion of CAI value measured on saw cut rock surfaces to the standard rough natural rock surfaces, which coincides completely with the correlations developed in this study. Therefore the proposed correlations (Eq. 5.4 and Eq. 5.5) confirm the work of earlier investigators.

$$CAI_{fb(Side)} = 1.14 \times CAI_{s(Side)} - 0.029 \qquad (5.4)$$

$$CAI_{fb(Top)} = 1.15 \times CAI_{s(Top)} - 0.047 \qquad (5.5)$$

For low to medium abrasive rocks (CAI=0.5-2.0), the CAI values are more or less consistent when tested on both the freshly broken and sawn rock surfaces as shown in Figure 5.5 and Figure 5.6. A significantly higher value of CAI_{fb} than the CAI_s was observed for a freshly broken metamorphic phyllite (UCS = 54.33 MPa). This increase in the CAI_{fb} is attributed to the uneven surface produced due to the phyllitic texture. For high to extremely abrasive rocks (CAI=2.0-6.0), higher values of the CAI can be observed on freshly broken rock surfaces. An exceptionally higher value of CAI_{fb} (CAI_{fb}-CAI_s difference of 2.40) was also observed for a Sandstone-16 rock sample of Hazira Formation (UCS = 130 MPa) which is also attributed to the uneven surface produced and its very high UCS. These findings are consistent with the work of previous investigators

(Al-Ameen and Waller, 1994; Plinninger et al., 2003; Rostami et al., 2005). The higher values of CAI for harder and abrasive rocks on freshly broken rock surfaces as explained by Rostami et al. (2013) are due to the inability of the stylus to penetrate into the hard rock surface and hence sliding of the stylus on the rock surface. Moreover, the stylus follows an uneven path on the freshly broken rock surface resulting in higher CAI values.
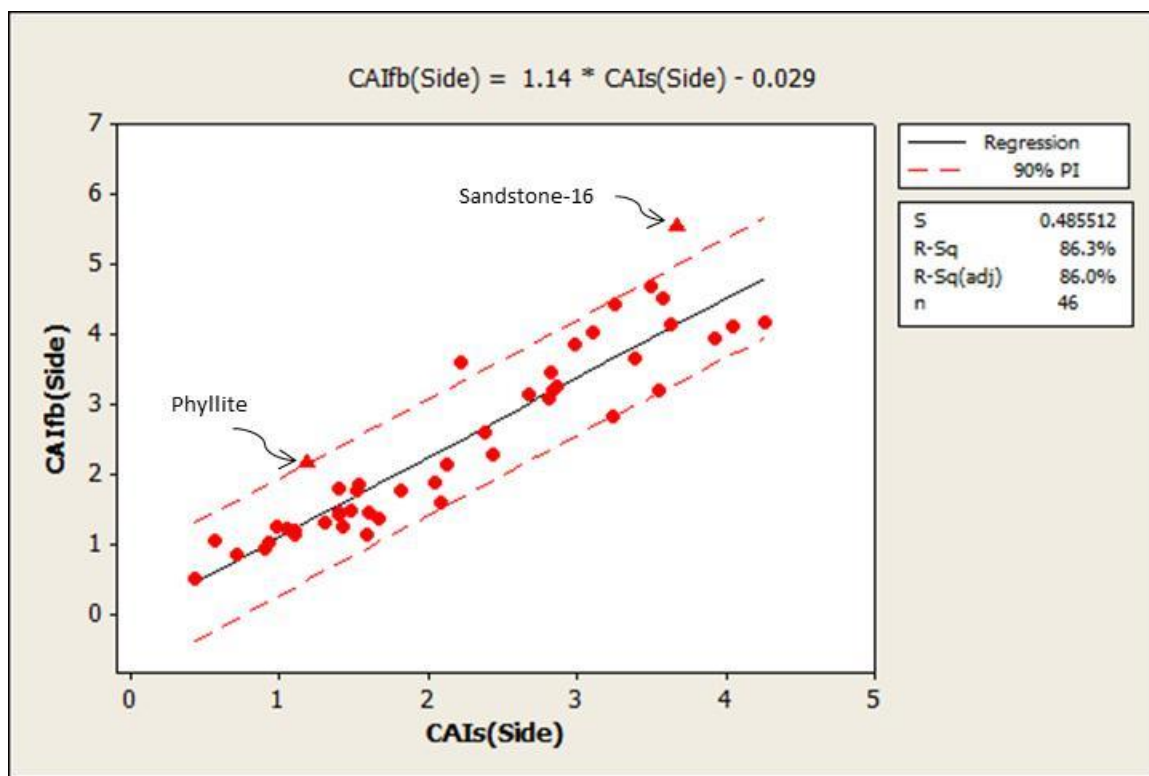
Figure 5.5. Regression plot between $CAI_{fb(Side)}$ and $CAI_{s(side)}$
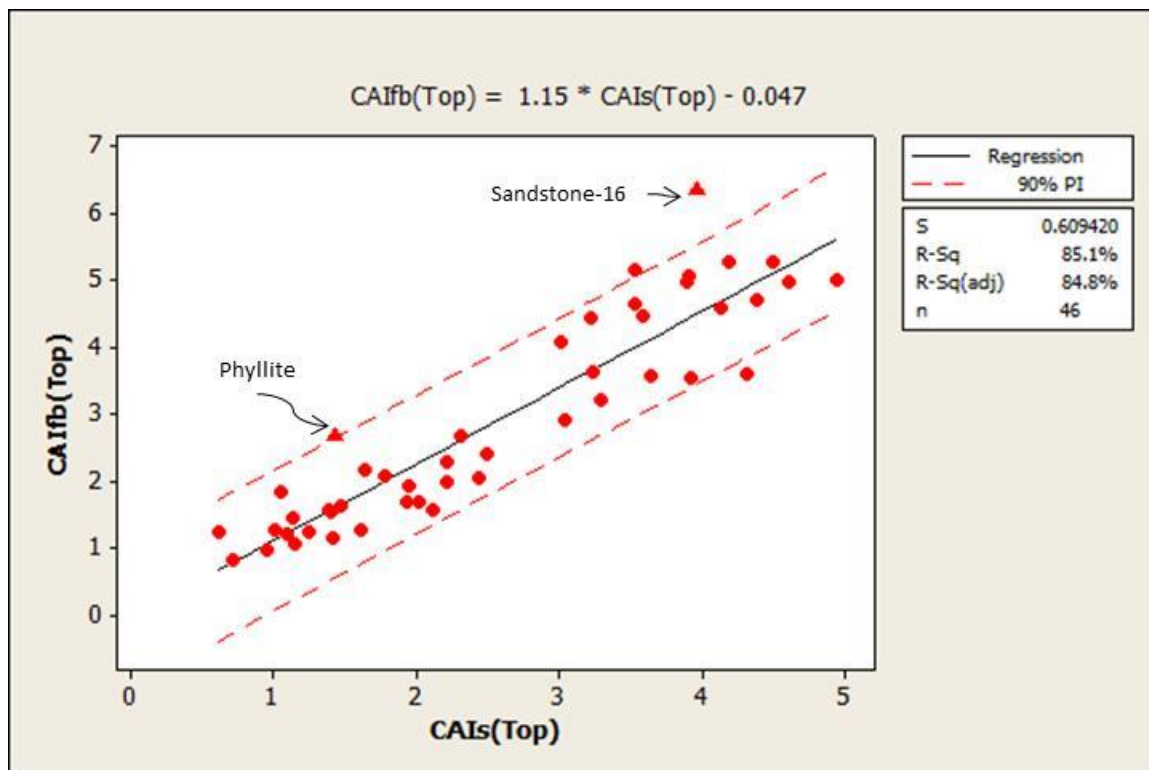
Figure 5.6. Regression plot between $CAI_{fb(Top)}$ and $CAI_{s(Top)}$

5.3. RELATIONSHIP OF CAI WITH PETROGRAPHICAL PROPERTIES

The petrographic thin section analyses results were used for the calculations of quartz content (Qtz), quartz equivalent content (Qtz.eq), average grain size of quartz (Ø-Qtz), average grain size of all minerals (Ø), Schimazek's *F* value and Rock Abrasivity Index (RAI). This section includes the correlations of CAI with geotechnical wear indices (Schimazek's *F* value and RAI) and with the petrographical properties including Qtz (%), Qtz.eq (%) and Ø-Qtz (mm).

5.3.1. CAI versus Rock Abrasivity Index (RAI). Figures 5.7a-d show relationships of CAI_s and CAI_{fb} values measured from top and side views of styli with RAI. A logarithmic increasing trend between CAI and RAI values can be observed in the presented relationships which closely coincide with the correlations already proposed by (Plinninger, 2002; Plinninger et al., 2004). However, the statistical results are somewhat different from the cube root function developed by Schumacher (2004). Plinninger (2002) also developed a prediction graph for the estimation of button drill bits life time (m/bit) based on RAI values from a number of conventional drill and blast tunneling projects in

Western Europe. The proposed prediction diagram illustrates that drill bit lifetime (m/bit) decreases in rocks of higher RAI values and vice versa.

It is interesting to note that there is a variation in the plotted values of CAI_s and CAI_{fb} around the RAI value of 60. These data points correspond to Sandstone-15, Sandstone-7, Granitic Gneiss-1, Granite-3 and Quartzite-1 rock samples, having UCS values falling in a close range from 56.39 MPa to 77.614 MPa. The scatter around RAI value of 60 may be attributed to the quartz equivalent content (ranging from 73.89% to 96.78%), which is directly affecting the values of RAI (being a multiplying factor with UCS in the calculation of RAI). The scatter in CAI values at or around RAI of 60 may also be attributed to the variation in the quartz content of these rock samples varying from 65% to 90.60%. Previous studies by West (1989) and Yarali et al. (2008) also noted that CAI values are dependent on the quartz content of the rock samples.

Further an exceptionally high RAI value of 190 with relatively lower CAI value can be observed (Figures 5.7a-d) for an igneous granite (UCS = 232 MPa). The lower values of CAI are probably due to considerably high rock strength imparting skidding effect to the stylus especially over the sawn test surface of the sample. The skidding effect has also been mentioned by Rostami et al. (2013).
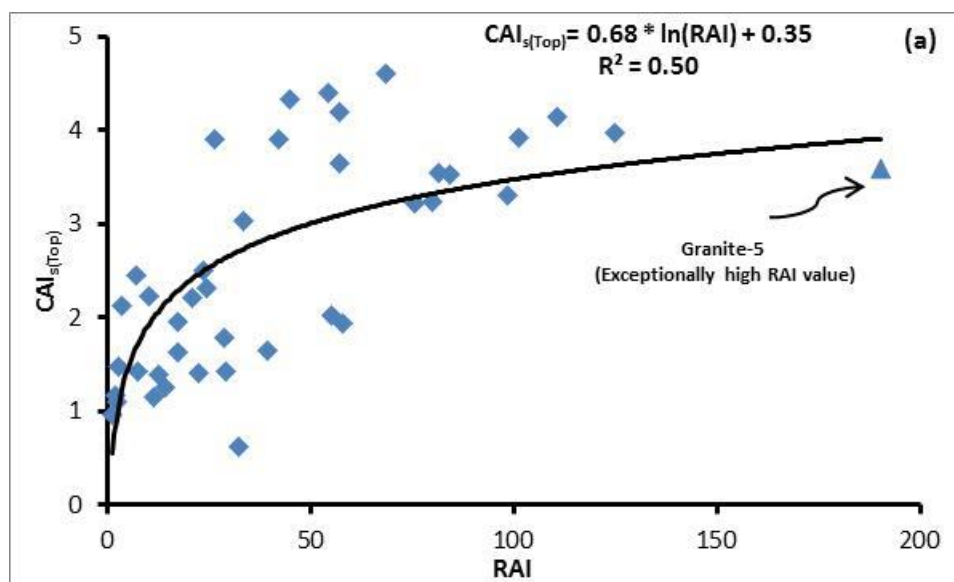
Figure 5.7. (a) Graph of CAI_s values measured from top view of the CERCHAR styli with RAI.
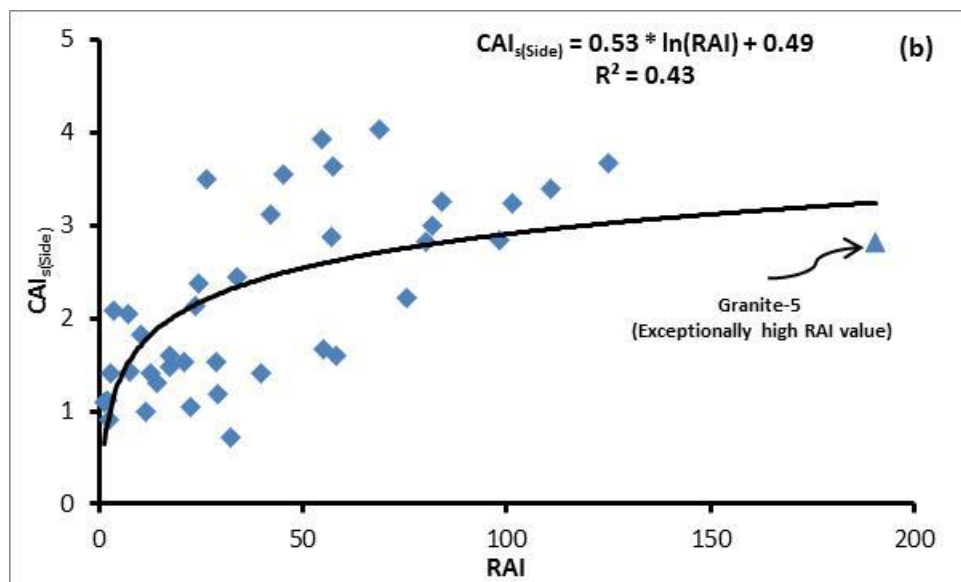
Figure 5.7. (b) Graph of CAI$_s$ values measured from side view of the CERCHAR styli with RAI.
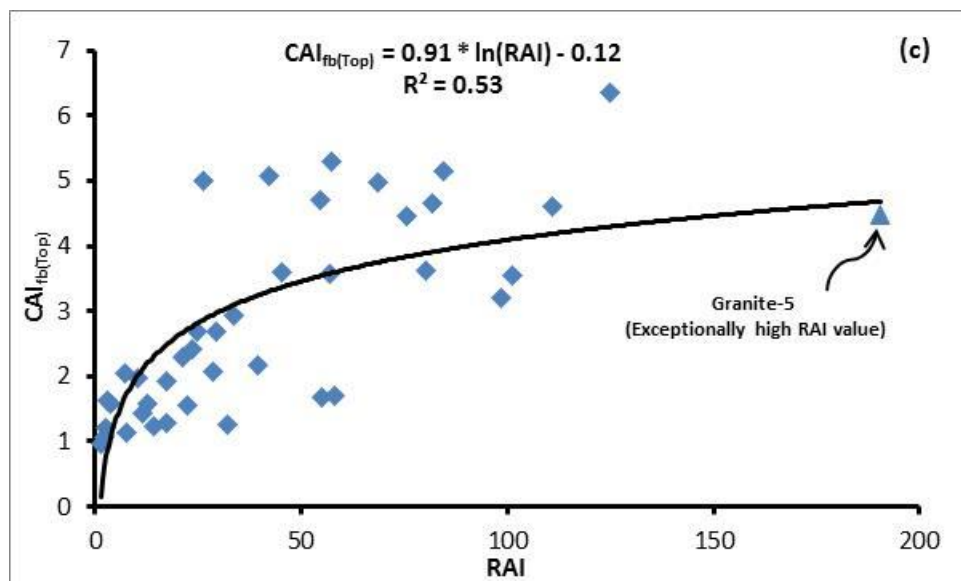
Figure 5.7. (c) Graph of CAI$_{fb}$ values measured from top view of the CERCHAR styli with RAI.
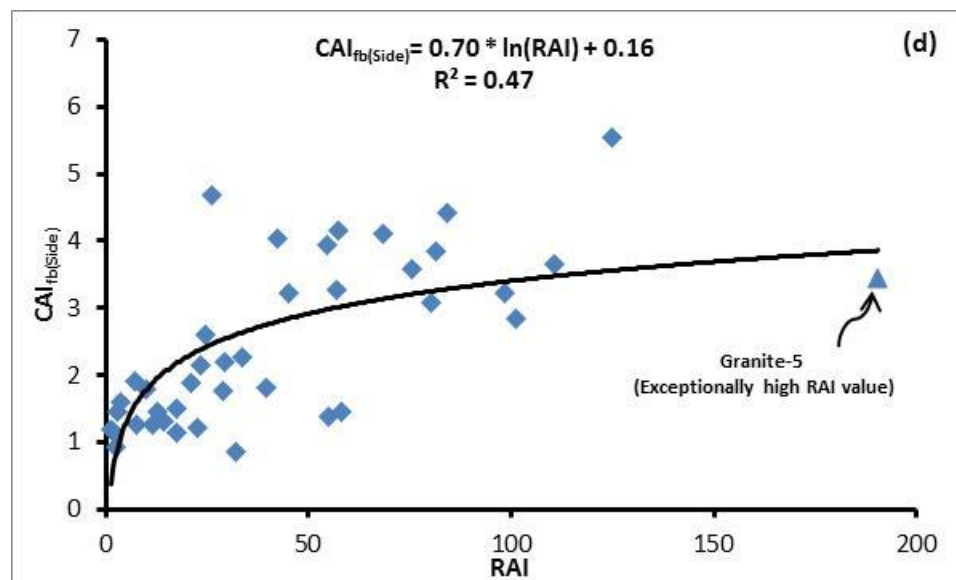
Figure 5.7. (d) Graph of CAI_{fb} values measured from side view of the CERCHAR styli with RAI.

5.3.2. CAI versus Schimazek's F-value. Figures 5.8a-d show the regression plots of $CAI_{s(Top)}$, $CAI_{s(Side)}$, $CAI_{fb(Top)}$ and $CAI_{fb(Side)}$ with the Schimazek's F-values. The graphs show fair power correlations of CAI_s and CAI_{fb} values using top and side view stylus measurement method with the Schimazek's F-values. Generally the proposed relationships show an increase in CAI values of the rocks tested with the corresponding increase in their Schimazek's F-values. In the past Becker and Lemmes (1984) developed a positively linear correlation between CERCHAR number and Schimazek's F-value for coal measures rocks. The results of this study are also consistent with the earlier reported investigations (Paschen, 1980; Verhoef et al., 1990; Deketh, 1991 and Bisschop, 1991) where the wear rate of instrumental test pieces also increased with corresponding increase in the Schimazek's F-values.

It is noteworthy that there is a vertical scatter in CAI_s and CAI_{fb} values in the plotted area, approximately near Schimazek's F-value of 3. These data points include Dolerite-4, Sandstone-3, Quartzite-1 and Granite-2 rock samples. The variation of CAI values around the Schimazek's F-value of 3 may be attributed to the quartz equivalent content (ranging in values from 53.76% to 96.77%) which has a direct impact on the values of Schimazek's F-value. Further some past investigations (Suana and Peters, 1981; Yarali et al., 2008; Gharahbagh et al., 2011) highlighted that there is an increase in CAI

values with the corresponding increase in quartz equivalent content of the rock samples. The scatter in CAI values at or about Schimazek's F-value of 3 may also be ascribed to the variation in the average mineral grain size (ranging from 0.352mm to 1.144mm) of these rock specimens. An extraordinary higher Schimazek's F-value of 8 with relatively lower CAI value can be noticed (Figures 5.8a-d) for an igneous granite rock (UCS = 232 MPa). This higher Schimazek's F-value with corresponding lower value of CAI is probably due to the same reason as explained for higher RAI with lower CAI values.
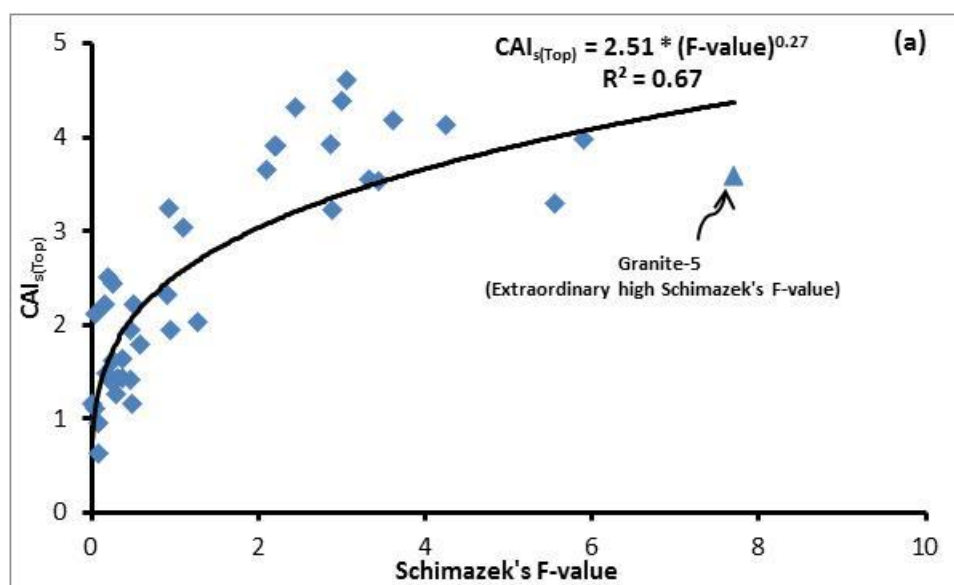
Figure 5.8. (a) Plot of CAI_s values measured from top view of the CERCHAR styli with Schimazek's F-value.
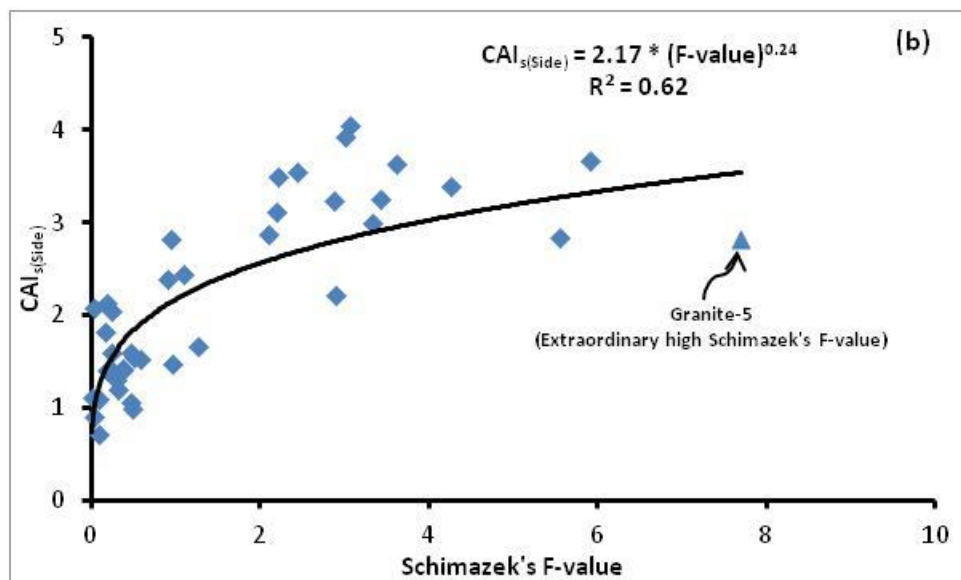
Figure 5.8. (b) Plot of CAI_s values measured from side view of the CERCHAR styli with Schimazek's F-value.
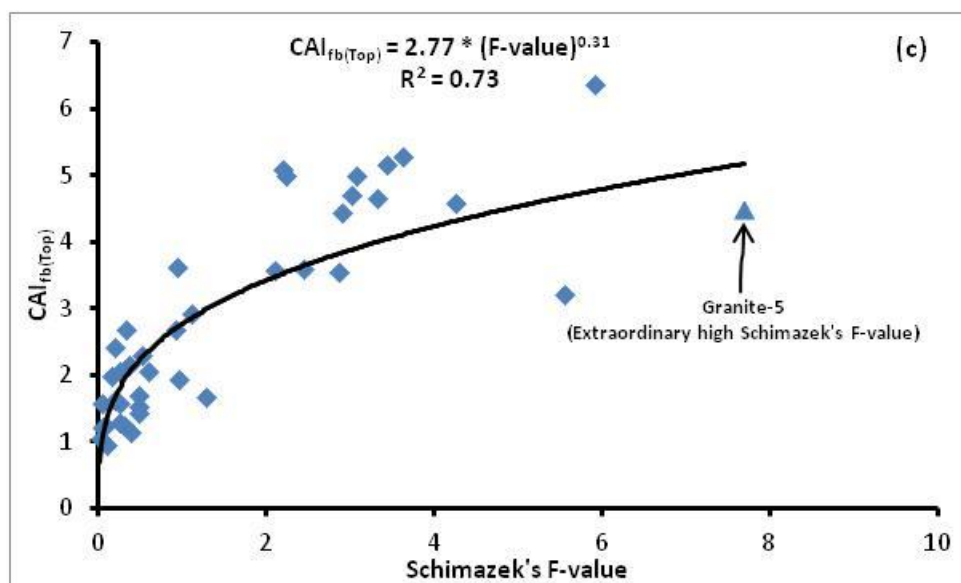
Figure 5.8. (c) Plot of CAI_{fb} values measured from top view of the CERCHAR styli with Schimazek's F-value.
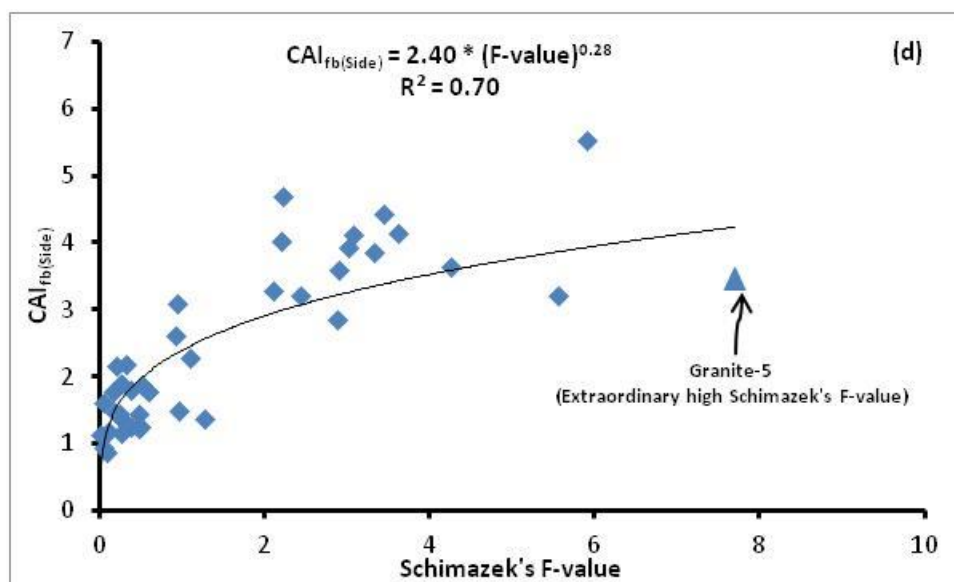
Figure 5.8. (d) Plot of CAI_{fb} values measured from side view of the CERCHAR styli with Schimazek's F-value.

5.3.3. CAI Versus Quartz Content (Qtz %). Figure 5.9 shows the scatter plot of $CAI_{fb(Side)}$ values against quartz content for all 40 rocks included, where no significant correlation between the dependent and independent variables can be identified. Alber (2008) also conducted several tests on four rock types and found no significant relationship between CAI and the quartz content. Similarly Ko et al. (2016) found no significant relationships between CAI and quartz content for igneous and metamorphic rock samples respectively. It is pertinent to mention here that contrary to the results of earlier reported investigations, Ko et al. (2016) reported negative linearly decreasing trend between CAI and quartz content.
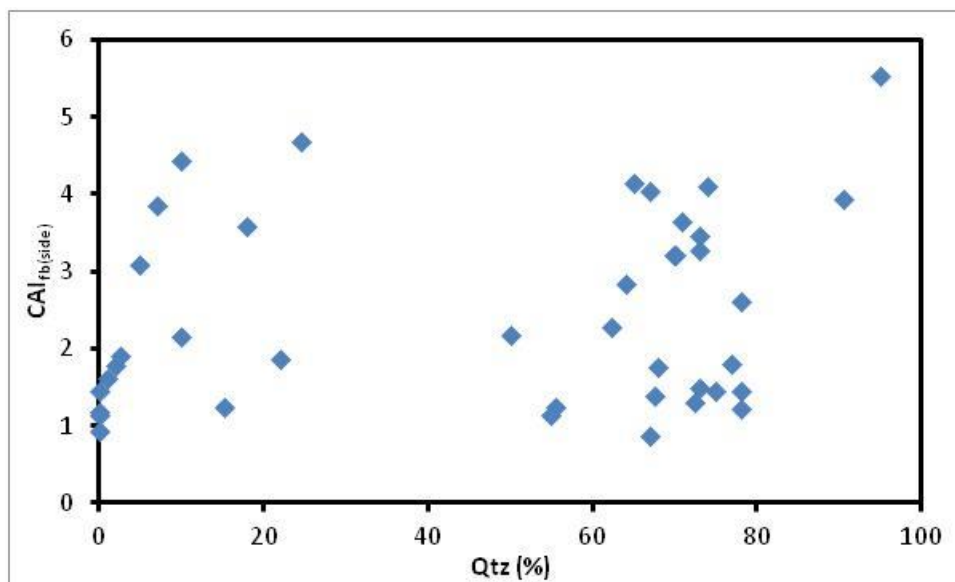
Figure 5.9. Scatter plot of $CAI_{fb(Side)}$ values with quartz content for all 40 rocks.

5.3.4. CAI Versus Equivalent Quartz Content (Qtz-eq %). The analysis of test results show (Figure 5.10) poor correlation of $CAI_{fb(Side)}$ with quartz equivalent content values for all rocks. The test results of this study are confirmed by the previous work of Kasling (2000) who conducted study on 109 different rock samples with a wide range of abrasiveness (CAI=0.3 to CAI=5.6) and found no correlation between CAI and equivalent quartz content. Similarly Alber (2008) reported non existence of significant correlation between the two parameters.
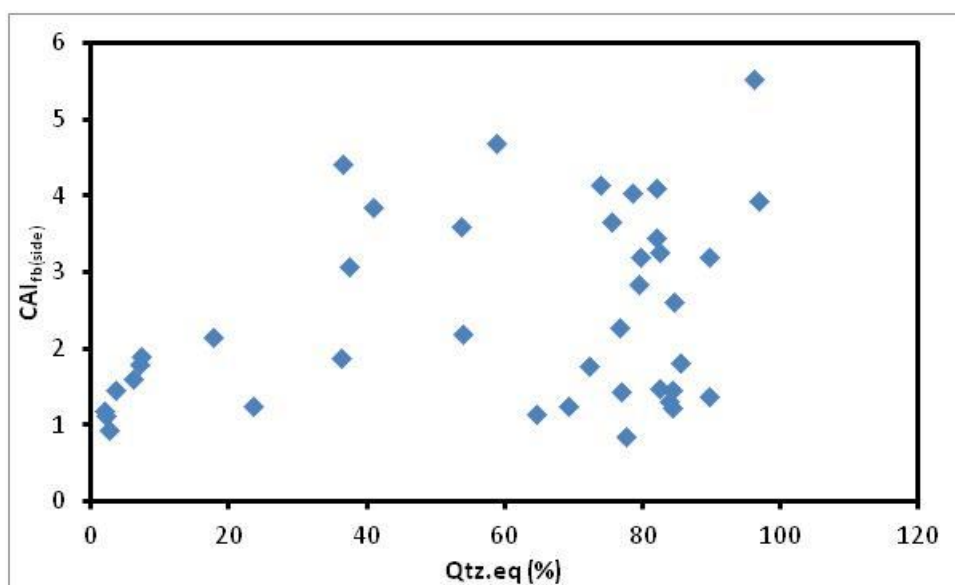
Figure 5.10. Scatter plot of $CAI_{fb(Side)}$ values with equivalent quartz content (Qtz-eq) for all 40 rocks.

5.3.5. CAI Versus Quartz Grain Size (Ø-Qtz). The effect of quartz grain size (Ø-Qtz, mm) on CERCHAR abrasivity index has been under discussion by few past investigators and has shown that a positive linear correlation exists between CAI and the average grain size of mineral quartz present in the rock samples. In this study when test results of rock samples were plotted (Figure 5.11) a positively linear correlation of weak quality was found between $CAI_{fb(Side)}$ and Ø-Qtz (mm). In Figure 5.11 a vertical scatter of $CAI_{fb(Side)}$ values can be noticed around quartz grain size (Ø-Qtz) of 0.25 mm. These data points correspond to Sandstone-16, Andesite and Dolerite-3 rock samples. This variation of $CAI_{fb(Side)}$ about the Ø-Qtz value of 0.25 mm, may be attributed to the UCS (ranging from 129.793 to 231.462 MPa) which has a direct impact on CAI values. The results observed in this study are supported by the studies of Yarali et al. (2008) and Er and Tugrul (2016).
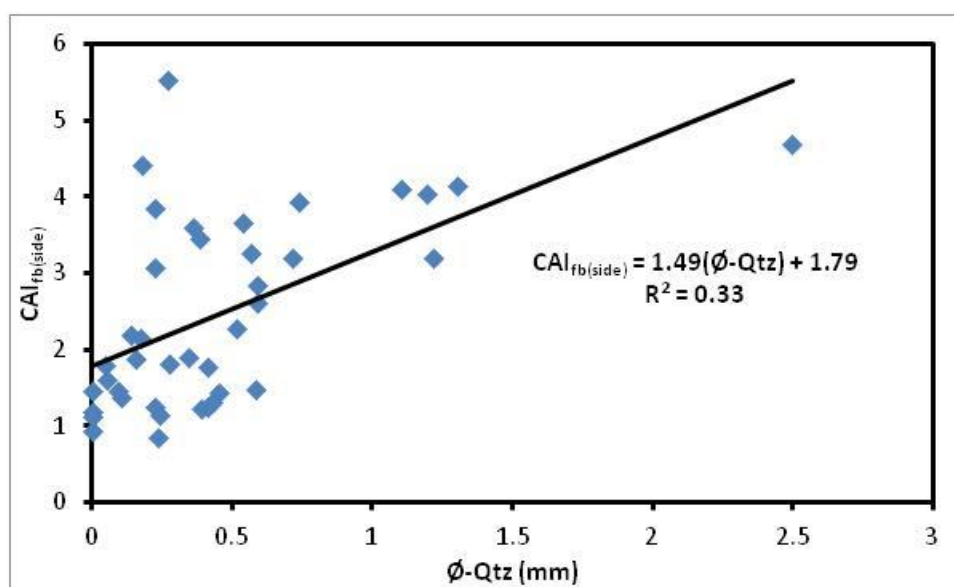
Figure 5.11. Plot of $CAI_{fb(Side)}$ with quartz grain size (Ø-Qtz) for all rocks.

5.4. RELATIONSHIP OF CAI WITH MECHANICAL AND PHYSICAL ROCK PROPERTIES.

Simple linear regression analyses for all rocks were conducted to investigate the relationships between CAI_s and CAI_{fb} values measured from top and side views of styli (dependent variables) and physico-mechanical rock properties (independent variables) as shown in Table 5.4.

Table 5.4. Correlation matrix of CAI with physical and mechanical properties for all rocks.

	CAI_s (Top)	CAI_s (Side)	CAI_{fb} (Top)	CAI_{fb} (Side)	UCS (MPa)	BTS (MPa)	Dry Density (g/cc)	Porosity (%)	V_p (km/s)
$CAI_{s\ (Top)}$	1.00								
$CAI_{s\ (Side)}$	0.98	1.00							
$CAI_{fb\ (Top)}$	0.92	0.91	1.00						
$CAI_{fb\ (Side)}$	0.92	0.93	0.99	1.00					
UCS (MPa)	0.39	0.38	0.47	0.45	1.00				
BTS (MPa)	0.26	0.24	0.38	0.36	0.74	1.00			
Dry Density (g/cc)	0.33	0.31	0.38	0.37	0.65	0.51	1.00		
Porosity (%)	-0.63	-0.60	-0.59	-0.60	-0.57	-0.45	-0.65	1.00	
V_p (km/s)	-0.10	-0.13	-0.05	-0.06	0.60	0.55	0.47	-0.41	1.00

Weak positively linear correlations of $CAI_{s(Top)}$, $CAI_{s(Side)}$, $CAI_{fb(Top)}$ and $CAI_{fb(Side)}$ with UCS and BTS of rocks were observed for all rocks (Table 5.4). Numerous studies (Jaeger, 1988; Al-Ameen and Waller, 1994; Kahraman et al., 2010; Gharahbagh et al., 2011; Deliormanli, 2012; Dipova, 2012; Ko T.Y. et al., 2016; Er and Tugrul, 2016) correlating CAI with UCS and BTS have also reported similar positive correlations. It is worth mentioning that when correlation matrix (Table 5.5) was constructed for relations between CAI and mechanical properties (UCS and BTS) of sedimentary rocks, fair relationships were found probably due to similar rock type.

Table 5.5. Correlation matrix of CAI with mechanical properties for sedimentary rocks.

	$CAI_{s(Top)}$	$CAI_{s(Side)}$	$CAI_{fb(Top)}$	$CAI_{fb\ (Side)}$	UCS (MPa)	BTS (MPa)
$CAI_{s\ (Top)}$	1.00					
$CAI_{s\ (Side)}$	0.97	1.00				
$CAI_{fb\ (Top)}$	0.87	0.87	1.00			
$CAI_{fb\ (Side)}$	0.87	0.90	0.97	1.00		
UCS (MPa)	0.56	0.53	0.50	0.52	1.00	
BTS (MPa)	0.53	0.51	0.64	0.64	0.73	1.00

The test results for all rocks (Table 5.4) show weak positively linear correlations of CAI with dry density of the rocks. Limited literature reports are present on correlations of CAI with rock density. Er and Tugrul (2016) proposed moderately strong positive linear correlation between CAI and dry unit weight of granitic rocks which generally coincides with the correlation observed in this study. On the other hand Kahraman et al.

(2010) developed weak negatively linear correlation of CAI with rock density which is contrary to the findings of this work.

The highest correlation coefficients were calculated (Table 5.4) for porosity with negatively linear trends, which mean that CAI appears to be high when rocks are less porous and vice versa. This result is supported by the past investigations of Alber (2008) and Er and Tugrul (2016).

Finally the results of this study shows (Table 5.4) poor negatively linear correlations of $CAI_{s(Top)}$, $CAI_{s(Side)}$, $CAI_{fb(Top)}$ and $CAI_{fb(Side)}$ with P-wave velocity (V_p) of the rocks tested. These results are contrary to the past investigations (Kahraman et al., 2010; Khandelwal and Ranjith, 2010; Er and Tugrul, 2016) where positively linear trends have been proposed between CAI and P-wave velocity of rocks.

5.5. MULTIPLE REGRESSION MODEL

To explain the variation and dependence of CAI values on the physical, mechanical and petrographic characteristics of the rocks, a stepwise multiple linear regression model was developed by using SPSS 21.0 statistical software. $CAI_{fb(Side)}$ was taken as the dependent or response variable, whereas quartz content (Qtz %), quartz equivalent content (Qtz-eq %), average quartz grain size (Ø-Qtz), mean diameter of mineral grains (Ø), Schimazek's F-value, RAI, UCS, BTS, dry density, porosity and Vp were taken as independent variables or regressors. Stepwise multiple regression method is hybrid of forward selection and backward elimination methods. This method allows independent variables to enter in the model one by one in descending order of their partial F statistics values as long as they are significant at a pre-defined significance level of entry (SLE). At each step when a variable is entered to the model, the equation is evaluated and the variable with the lowest partial F statistics value is checked at the pre-defined significance level to stay (SLS) and deleted if found insignificant. This process is repeated until the selection of an additional variable does not increase the R^2 value by a considerable amount at the pre-defined level of significance (Samaranayake, 2009).

Equation (5.6) gives the best explanatory model (F-value = 44.302, P-value < 0.0001 at α=0.1) explaining the dependence of $CAI_{fb(Side)}$ on Schimazek's F-value, quartz grain size (Ø-Qtz) and uniaxial compressive strength (UCS).

$$CAI_{fb(Side)} = 0.811 + 0.289 \times (\text{F-value}) + 1.285 \times (\text{Ø-Qtz}) + 0.007 \times (\text{UCS}); \quad (R^2 = 0.79) \qquad (5.6)$$

Where;

$CAI_{fb(Side)}$ = Cerchar abrasivity index computed by using side view wear flat measurement technique, tested on freshly broken rock surface;

F-value = Schimazek's F-value (N/mm);

Ø-Qtz = Quartz average grain size (mm);

UCS = Uniaxial compressive strength (MPa).

The statistical import of the derived model (equation 5.6) was assessed by employing a few test statistics. The coefficient of determination (R-squared) is the percentage of variance in the dependent variable and the coefficient of correlation (R) is the relationship between observed and estimated values of dependent variable. The standard error of the estimate or the root mean square error, is the standard deviation of the error term and is the square root of the mean square residual (Yilmaz et al., 2007). The computed R-squared value for this model (R^2 = 0.79) shows that 79 % of the variance in $CAI_{fb(Side)}$ can be expected from the explanatory variables (Schimazek's F-value, Ø-Qtz and UCS). The determined value of correlation coefficient (R = 0.89) specifies a strong relationship between the response variable and the independent variables. The standard error of estimate for the derived model (equation 5.6) indicates that the standard deviation of the residuals is 0.59 and finally the adjusted R^2 value suggests that the proposed explanatory model accounts for 76.90 % of the total variation in $CAI_{fb(Side)}$ values.

Table 5.6 gives the details of Analysis of Variance (ANOVA) which is the most commonly used technique for the statistical analysis of quantitative data (Deliormanli, 2012). The hypotheses testing for the explanatory model (Equation, 5.6) was implemented with an F-test in ANOVA. The null hypothesis (H_o) represents that there is no relationship or dependence between $CAI_{fb(Side)}$ and the three explanatory variables namely Schimazek's F-value, Ø-Qtz and UCS. The alternate or new hypothesis (H_1) is the reverse of null hypothesis. The null and alternate hypotheses are explained as below:

If $F_{(model)} < F_{(table)}$ then accept H_o and reject H_1, OR alternately

If $F_{(model)} > F_{(table)}$ then reject H_o and accept H_1

Using F-distribution table at ($\alpha = 0.1$; $df_1 = 3$; $df_2 = 36$) the $F_{(table)}$ value of 2.24, was computed which is smaller than the $F_{(model)}$ value of 44.302, thereby rejecting the null hypothesis. This indicates the presence of a linear relationship between the $CAI_{fb(Side)}$ and the three explanatory variables. Table 5.7 presents the coefficients and summary of other parameters for the dependant variable $CAI_{fb(Side)}$. It may be noticed (Table 5.8) that p-values of independent variables Schimazek's F-value, Ø-Qtz and UCS are 0.000, 0.000 and 0.003 respectively and hence are the most significant parameters in explaining the dependency of $CAI_{fb(Side)}$ under the given experimental conditions. The independent variables (Qtz %, Qtz-eq %, Ø, RAI, UCS, BTS, dry density, porosity and Vp) are excluded from the regression model (Equation 5.6) due to their statistical insignificance at the selected level of significance i.e. $\alpha = 10\%$.

Furthermore, the multicollinearity option was also checked in the stepwise regression analysis in the SPSS software. The multiple regression models usually contain multicollinearity to some extent, which exists when two or more independent variables are very much correlated and the most commonly used tools for the detection of severity of multicollinearity is the variance inflation factor (VIF) (Yilmaz et al., 2006). A value of 10 is recommended as the upper limit for VIF in multiple regression analysis (Kennedy, 2008; Hair et al., 2009). The VIF values for Schimazek's F-value, Ø-Qtz and UCS are 2.105, 1.498 and 1.936 which are quite less than the allowed VIF factor of 10 which confirms that Equation (5.6) does not suffer from a high level of multicollinearity. Finally, it can be inferred from the explanatory model obtained that $CAI_{fb(Side)}$ is mainly dependent on mean quartz grain size (Ø-Qtz), uniaxial compressive strength (UCS) and the Schimazek's F-value which includes petrographic parameters (Qtz-eq %, Ø) and the tensile strength (BTS) of the rocks tested in this research program.

Some past investigators (Fowell and Abu Bakar, 2007; Gharahbagh et al., 2011; Rostami et al., 2013) have also proposed multiple regression models correlating CAI with rock properties including petrographic, physical and mechanical parameter. A review of these relationships is provided in chapter 2. Most of these models show the dependence

of CAI values on the quartz equivalent content, quartz grain size and UCS, whereas the model developed herein includes an additional parameter of Schimazek's F-value which is a combination of a number of parameters as explained earlier. Therefore, this model covers more rock parameters as compared to the previously developed models.

Table 5.6. ANOVA for dependent variable $CAI_{fb(Side)}$.

Model	Sum of squares	Df	Mean square	F	Sig.
Regression	47.469	3	15.823	44.302	0.000
Residual	12.858	36	0.357		
Total	60.326	39			

Table 5.7. Coefficients and summary of some parameters affecting the quality of model for dependent variable $CAI_{fb(Side)}$.

Parameter	Unstandardised Coefficients		t	Sig.	Variance Inflation Factor (VIF)
	B	Std. error			
Constant	0.811	0.216	3.754	0.001	
Schimazek's F-value	0.289	0.074	3.883	0.000	2.105
Ø-Qtz	1.285	0.247	5.198	0.000	1.498
UCS	0.007	0.002	3.169	0.003	1.936

5.6. SUMMARY OF PROPOSED CORRELATIONS

Table 5.8 lists the correlations of CERCHAR abrasivity index values measured on both sawn and freshly broken rock surfaces using top viewing wear flat method [$CAI_{s(Top)}$ and $CAI_{fb(Top)}$] with measurements conducted by utilizing the side viewing wear flat technique [$CAI_{s(Side)}$ and $CAI_{fb(Side)}$] respectively. Similarly the relationships showing impact of rock surface condition including $CAI_{fb(Top)}$ against $CAI_{s(Top)}$ and $CAI_{fb(Side)}$ against $CAI_{s(Side)}$ are displayed. Moreover the correlations developed in this research work showing dependence of CAI values on wear indices (RAI and Schimazek's F-value) and rock properties are also presented.

Table 5.8. List of correlations developed in this study.

Sr. No.	Correlation
1	$CAI_{s(Top)} = 1.17 \times CAI_{s(Side)} - 0.0013$; ($R^2 = 0.97$)
2	$CAI_{fb(Top)} = 1.19 \times CAI_{fb(Side)} - 0.0331$; ($R^2 = 0.97$)
3	$CAI_{fb(Side)} = 1.14 \times CAI_{s(Side)} - 0.029$; ($R^2 = 0.86$)
4	$CAI_{fb(Top)} = 1.15 \times CAI_{s(Top)} - 0.047$; ($R^2 = 0.85$)
5	$CAI_{s(Top)} = 0.68 \times \ln(RAI) + 0.35$; ($R^2 = 0.50$)
6	$CAI_{s(Side)} = 0.53 \times \ln(RAI) + 0.49$; ($R^2 = 0.43$)
7	$CAI_{fb(Top)} = 0.91 \times \ln(RAI) - 0.12$; ($R^2 = 0.53$)
8	$CAI_{fb(Side)} = 0.70 \times \ln(RAI) + 0.16$; ($R^2 = 0.47$)
9	$CAI_{s(Top)} = 2.51 \times (F\text{-value})^{0.27}$; ($R^2 = 0.67$)
10	$CAI_{s(Side)} = 2.17 \times (F\text{-value})^{0.24}$; ($R^2 = 0.62$)
11	$CAI_{fb(Top)} = 2.77 \times (F\text{-value})^{0.31}$; ($R^2 = 0.73$)
12	$CAI_{fb(Side)} = 2.40 \times (F\text{-value})^{0.28}$; ($R^2 = 0.70$)
13	$CAI_{fb(Side)} = 1.49 \times (Ø\text{-}Qtz) + 1.79$; ($R^2 = 0.33$)
14	$CAI_{fb(Side)} = 0.811 + 0.289 \times (F\text{-value}) + 1.285 \times (Ø\text{-}Qtz) + 0.007 \times (UCS)$; ($R^2 = 0.79$)

5.7. ABRASIVITY CHARACTERIZATION OF TESTED ROCK SAMPLES BASED ON CERCHAR TESTS

This section presents the abrasivity characterization of all 51 rock samples included in this research collected from various rock formations of Pakistan based on CERCHAR test. As CERCHAR test is the only standardized rock abrasivity measurement method therefore, the abrasivity classifications suggested by both ASTM-D7625-10 and ISRM suggested methods by Alber et al. (2014) have been adopted to characterize the $CAI_{fb(side)}$ values measured in this study. The proposed abrasivity classification criteria [ASTM-D7625-10 and ISRM suggested methods (Alber et al., 2014)] based on CAI values have already been presented in Chapter 2. Tables 5.9, 5.10 and 5.11 lists the abrasivity characterization of measured $CAI_{fb(side)}$ values for igneous, metamorphic and sedimentary rocks respectively. Whereas figures 5.12, 5.13 and 5.14 presents the column charts for igneous, metamorphic and sedimentary rock samples respectively showing $CAI_{fb(side)}$ values arranged in ascending order.

Table 5.9. Characterization of CERCHAR abrasivity index, (CAI) values of selected igneous rocks of Pakistan.

Sr. No.	Rock Sample	CAI$_{fb(side)}$	Abrasivity Classification as per ASTM-D7625-10	Abrasivity Classification as per ISRM suggested methods (Alber et al., 2014)
1	Dolerite-1	3.083	High Abrasiveness	High
2	Dolerite-2	3.150	High Abrasiveness	High
3	Dolerite-3	3.850	High Abrasiveness	High
4	Dolerite-4	3.590	High Abrasiveness	High
5	Granite-1	4.502	Extreme Abrasiveness	Very High
6	Granite-2	4.110	Extreme Abrasiveness	Very High
7	Granite-3	4.150	Extreme Abrasiveness	Very High
8	Granite-4	4.031	Extreme Abrasiveness	Very High
9	Granite-5	3.450	High Abrasiveness	High
10	Granite-6	4.687	Extreme Abrasiveness	Very High
11	Migmatite	3.210	High Abrasiveness	High
12	Andesite	4.425	Extreme Abrasiveness	Very High

Table 5.10. Characterization of CERCHAR abrasivity index, (CAI) values of selected metamorphic rocks of Pakistan.

Sr. No.	Rock Sample	CAI$_{fb(side)}$	Abrasivity Classification as per ASTM-D7625-10	Abrasivity Classification as per ISRM suggested methods (Alber et al., 2014)
1	Granitic Gneisse-1	3.270	High Abrasiveness	High
2	Granitic Gneisse-2	4.164	Extreme Abrasiveness	Very High
3	Phyllite	2.184	High Abrasiveness	Medium
4	Quartzite-1	3.932	High Abrasiveness	High
5	Quartzite-2	3.652	High Abrasiveness	High

Table 5.11. Characterization of CERCHAR abrasivity index, (CAI) values of selected sedimentary rocks of Pakistan.

Sr. No.	Rock Sample	CAI$_{fb(side)}$	Abrasivity Classification as per ASTM-D7625-10	Abrasivity Classification as per ISRM suggested methods (Alber et al., 2014)
1	Siltstone-1	1.250	Medium Abrasiveness	Low
2	Siltstone-2	1.872	Medium Abrasiveness	Low
3	Sandstone-1	1.764	Medium Abrasiveness	Low
4	Sandstone-2	0.860	Low Abrasiveness	Very Low
5	Sandstone-3	2.840	High Abrasiveness	Medium
6	Sandstone-4	1.220	Medium Abrasiveness	Low
7	Sandstone-5	2.275	High Abrasiveness	Medium
8	Sandstone-6	3.210	High Abrasiveness	High
9	Sandstone-7	1.380	Medium Abrasiveness	Low
10	Sandstone-8	1.250	Medium Abrasiveness	Low
11	Sandstone-9	2.610	High Abrasiveness	Medium
12	Sandstone-10	1.443	Medium Abrasiveness	Low
13	Sandstone-11	1.490	Medium Abrasiveness	Low
14	Sandstone-12	1.147	Medium Abrasiveness	Low
15	Sandstone-13	1.810	Medium Abrasiveness	Low
16	Sandstone-14	1.310	Medium Abrasiveness	Low
17	Sandstone-15	1.450	Medium Abrasiveness	Low
18	Sandstone-16	5.532	Extreme Abrasiveness	Extremely High
19	Sandstone-17	2.913	High Abrasiveness	Medium
20	Sandstone-18	2.385	High Abrasiveness	Medium
21	Chamositic Siderite	1.018	Medium Abrasiveness	Low
22	Dolomite-1	1.608	Medium Abrasiveness	Low
23	Dolomite-2	1.787	Medium Abrasiveness	Low
24	Dolomite-3	1.895	Medium Abrasiveness	Low
25	Dolomite-4	2.149	High Abrasiveness	Medium
26	Limestone-1	1.062	Medium Abrasiveness	Low
27	Limestone-2	0.938	Low Abrasiveness	Low
28	Limestone-3	1.455	Medium Abrasiveness	Low
29	Limestone-4	1.188	Medium Abrasiveness	Low
30	Limestone-5	1.130	Medium Abrasiveness	Low
31	Limestone-6	0.689	Low Abrasiveness	Very Low
32	Limestone-7	0.252	Very Low Abrasiveness	Extremely Low
33	Rock Gypsum	0.503	Low Abrasiveness	Very Low
34	Marl	0.186	Very Low Abrasiveness	Extremely Low
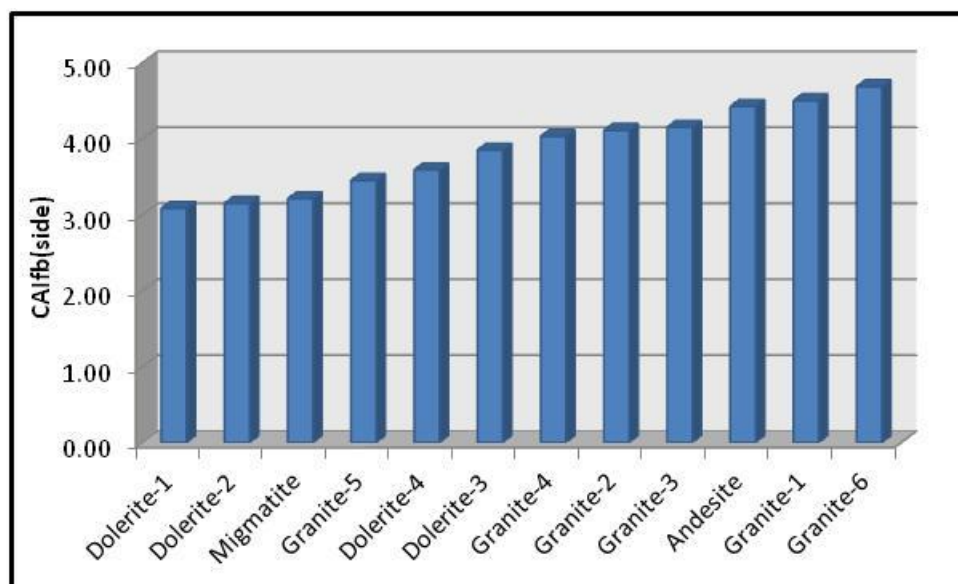
Figure 5.12. Column chart of $CAI_{fb(side)}$ values of igneous rock samples arranged in ascending order.
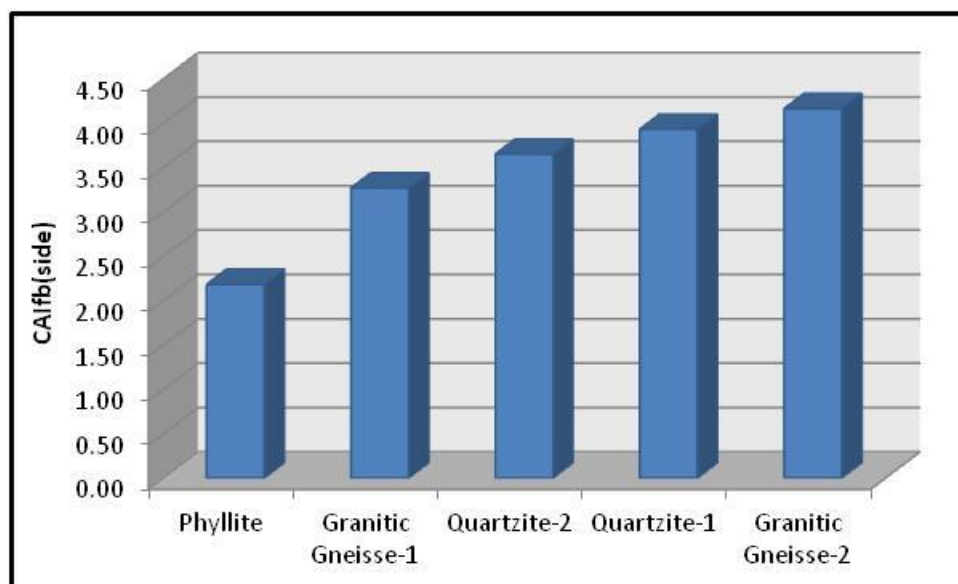
Figure 5.13. Column chart of $CAI_{fb(side)}$ values of metamorphic rock samples arranged in ascending order.
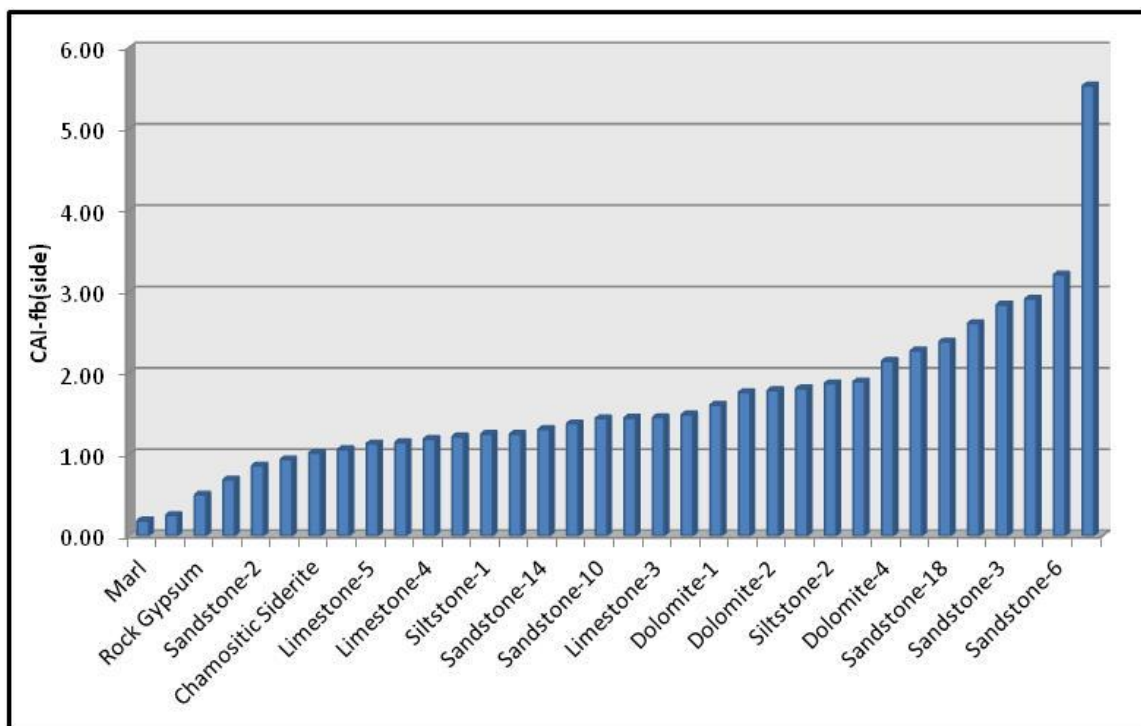
Figure 5.14. Column chart of $CAI_{fb(side)}$ values of sedimentary rock samples arranged in ascending order.

6. DISCUSSION: ROCK SATURATION EFFECTS ON CERCHAR ABRASIVITY INDEX

This chapter presents discussion concerning the influence of rock saturation on the measured CERCHAR Abrasivity Index (CAI) values as compared to the CERCHAR abrasivity tests conducted on air dried rock samples. In this section 33 sedimentary rock samples included in the total data base of 51 rock units are utilized for the evaluation of CERCHAR abrasivity indices on dry and saturated, sawn as well as freshly broken rock surfaces. The experimental methodology is outlined in Chapter 3, whereas complete results of the experiments conducted are summarized in Chapter 4. The discussion of results in this Chapter is mainly focused on evaluating the effects of rock saturation on the CERCHAR abrasivity test results. Moreover, the dependence of CERCHAR abrasivity index values (CAI_{sat}), for saturated freshly broken rock surfaces obtained using the side viewing wear flat measurement technique on the petrographic parameters [quartz content (QC %), equivalent quartz content (EQC %)], the wear factors [Schimazek's F-value$_{(sat)}$ and RAI$_{(sat)}$] and the physical and mechanical rock properties (UCS$_{(sat)}$, BTS$_{(sat)}$, density$_{(sat)}$, porosity, and Pore-space Volume) in saturated conditions are also discussed.

6.1. BACK GROUND

Production of minerals in the mining industry, construction of underground and surface structures increasingly involves the use of various types of mechanical excavators such as tunnel boring machines (TBM), Roadheaders, roadmilling machines, or similar equipment. In most of these cases the host rock is moist and in some cases is fully saturated with water. Moreover, in specialized applications including off-shore drilling, construction of harbor, dredging of hard formations, and construction of structures underneath bodies of water, rock excavation is generally carried out in saturated rock. All the excavators used for such applications employ bits or other cutting tools to excavate rocks both in dry and saturated environments, which in turn affect the bit wear rate, bit life, cutting forces, and specific energy. Laboratory testing of rock samples for estimation of performance and production rate of these excavators is usually conducted on air dried rock samples. This can result in over/under estimation of cutting forces and rock abrasivity, and in turn affects overall technical/operational feasibility of the proposed

systems and economics of the project. A quick review of the literature on rock behavior (abrasiveness, cutting forces, specific energy and strength etc.) clearly indicates that rock behavior changes at various moisture contents and perhaps under saturated conditions these changes can impact the production rate and tool consumption of any excavation machine (Abu Bakar and Gertsch, 2013). At present CERCHAR Abrasivity Index is the most commonly used test for the assessment of wear rate of rock cutting tools (disc and drag picks) employed on mechanical excavation machines. Therefore, any abrasivity evaluation based on entirely air dried rocks can affect the machine performance and eventually the overall economy of rock excavation operations.

6.2. EFFECT OF WATER CONTENT OF ROCK ON MEASURED CAI VALUES

In this study both top and side view wear flat measurement methods of CERCHAR stylus were used to compute the CAI values. However the past studies conducted by Rostami et al. (2005, 2013) and ISRM suggested method by Alber et al. (2014) strongly recommend to measure CAI values by employing the side viewing wear flat measurement technique initially developed at NTNU/SINTEF, Norway (Bruland, 2000). These findings of earlier studies have already been statistically confirmed in Chapter 5 and it was also concluded that CAI measurements made from the side view of the stylus are more reliable owing to the fact that the measured values are free from burrs and scratch grooves. Moreover, the CERCHAR (1986) guidelines, ASTM D7625-10 standards and ISRM suggested methods (Alber et al. 2014) only suggest freshly broken rock surfaces for CERCHAR tests. However in exceptional cases of heterogeneous rock types including conglomerates, coarse grained granites or rocks with schistose planes, where appropriate naturally broken rock surfaces are difficult to achieve through hammer blows, the CERCHAR test can be performed on saw cut surfaces. In these circumstances the CAI values obtained on sawn rock surfaces before utilization, should be corrected as suggested by ASTM-D7625-10 standards and ISRM suggested method (Alber et al. 2014). Therefore, in view of above recommendations the CERCHAR Abrasivity Index values for freshly broken rock surfaces obtained by using side viewing wear flat measurement technique (CAI_{sat} and CAI_{dry}) are utilized for further analysis in this Chapter.

Figures 6.1(a) and (b) show the results of CERCHAR testing carried out on a dry and saturated Sandstone-17 (Warchha (Red) sandstone) rock sample using side viewing technique of the stylus. It is interesting to note the difference between the wear flat measurement readings of 0.2960 mm ($CAI_{(dry)}$ = 2.96) and 0.1960 mm ($CAI_{(sat)}$ = 1.96) for styli tested on dry and saturated rock surfaces respectively.
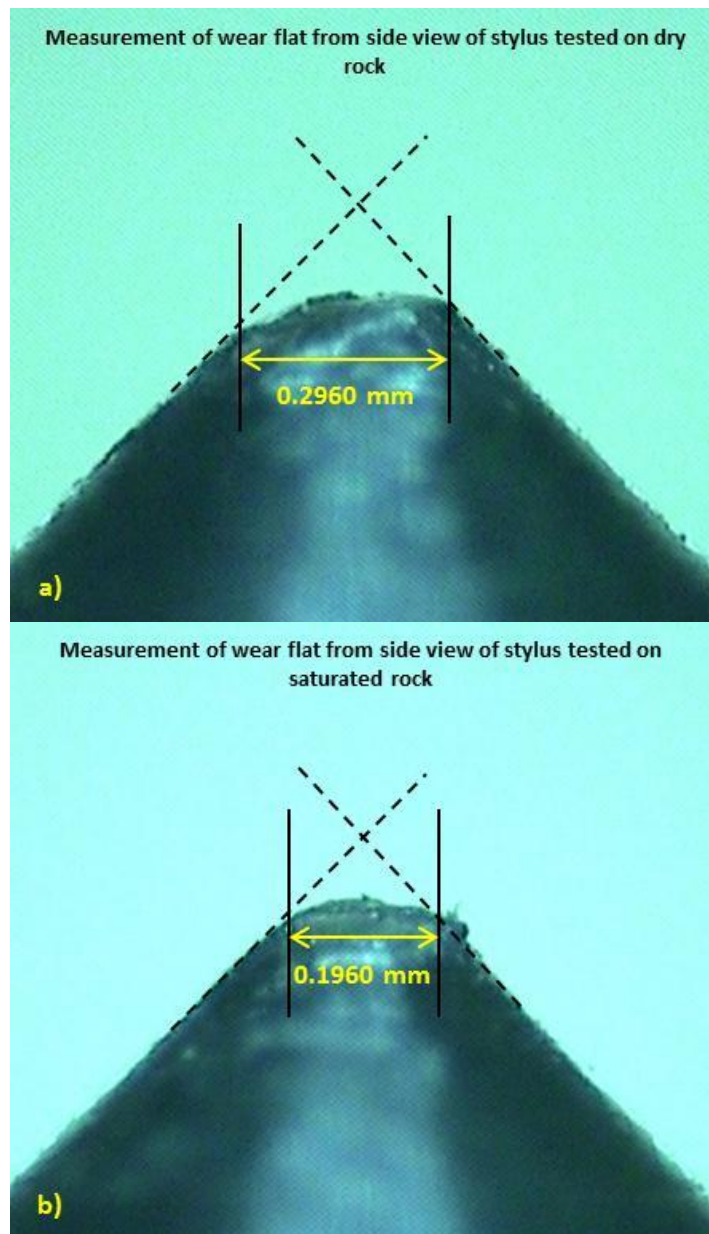
Figure 6.1. (a) Wear flat measurement from side of stylus tested on a dry and (b) saturated Warchha (Red) Sandstone rock sample.

In order to examine whether the CAI values obtained from scratch tests on both dry and water saturated rock surfaces, are truly different, hypothesis testing about corresponding population means was conducted. For this purpose the statistical technique of single factorial, analysis of variance (ANOVA) with completely randomized design was adopted (means model). The assumptions for experimental design include that there are t different populations from which independent samples of sizes n_1, n_2, ….. , n_t , are drawn respectively. Further the experimental units (n_1, n_2, ….. , n_t) are homogeneous and treatments are allocated randomly to these experimental units (Samaranayake, 2009; Lyman and Longnecker, 2010). To explain a completely randomized design with a single factor, the CAI values measured on dry and saturated rock surfaces of a Siltstone-2 (Tobra Siltstone) rock sample are shown in Table 6.1, where y_{ij}s are replications on " j " number of CERCHAR styli receiving " i " treatments on dry and saturated rock surfaces and $\overline{y}_i$. are replication averages on " j " number of CERCHAR styli. The structure of a one way ANOVA table, based on a sample calculation for the same rock is given in Table 6.2.

Table 6.1. Example showing a completely randomized design using CAI value tested on a Tobra Siltstone rock sample.

Rock surface treatments (*i*)	CAI values					Mean
Dry rock surface	$Y_{11} = 1.697$	$Y_{12} = 1.735$	$Y_{13} = 2.071$	$Y_{14} = 1.930$	$Y_{15} = 1.925$	$\overline{y}_1$. = 1.872
Saturated rock surface	$Y_{21} = 1.975$	$Y_{22} = 1.547$	$Y_{23} = 1.402$	$Y_{24} = 1.515$	$Y_{25} = 1.405$	$\overline{y}_2$. = 1.569
Overall mean						$\overline{y}_{..}$ = 1.720

Table 6.2. One way analysis of variance (ANOVA) table

Source	Sum of squares	Degree of freedom	Mean square	F-ratio
Treatments	SSTreatment = 0.229	$df_1 = 1$	MST = 0.229	5.772
Error	SSE = 0.318	$df_2 = 8$	MSE = 0.040	
Total	SSTotal = 0.547	9		

Where;

Sum of squares treatment (SSTreatment) = n $(\sum_i(\overline{y}_i.)^2) - N(\overline{y}_{..})^2$: is a measure of the variability in the y'_{ij}s due to differences between the dry and saturated rock surfaces treatment averages u'_is (i th treatment mean);

Total sum of squares (SSTotal) = $\sum_{ij} y_{ij}^2 - N(\overline{y_{..}})^2$: Shows the measurements about the overall average;

Sum of square for error (SSE) = SST − SSTreatment;

df_1 = Total treatments (t) − 1;

df_2 = Total number of scenarios (N) − t;

Mean squares treatment (MST) = SST/(t − 1);

Mean squares error (MSE) = SSE/(N − t);

F-ratio = MST/MSE.

The F-ratios were calculated for the individual CAI values means carried out on both dry and saturated freshly broken rock surfaces. The significance level for ANOVA test was fixed at α = 0.15 (85 % confidence level). To determine the statistical significance of test results, p-values were also computed for corresponding F values. p-value is the probability of obtaining a test statistics at least as large as the one in the sample population with the assumption that null hypothesis (H_0) is true. A p-value smaller than or equal to α- value provides strong evidence to reject the null hypothesis and to accept the alternate or new hypothesis (H_a) (Samaranayake, 2009; Abu Bakar and Gertsch, 2012). For this study the null hypothesis (Equation 6.1) was based on the fact that the calculated mean value of CAI is equal if measured on both dry and saturated freshly broken rock surfaces respectively. On the other hand the alternate hypothesis (Equation 6.2) was that the CAI value would be different for both the dry and saturated measurements.

$H_0 : \mu_{dry} = \mu_{sat}$ (6.1)

$H_a : \mu_{dry} \neq \mu_{sat}$ (6.2)

Table 6.3 presents the p-values calculated from the F-ratios of corresponding sample populations for dry and saturated rock surfaces. It can be observed that 52% of p-values were found statistically significant at α = 0.15 for both CAI_{dry} and CAI_{sat} thereby rejecting the null hypothesis. It shows that majority of the CAI measurements made on dry rock surfaces were higher as compared to the measurement made on the saturated rock surfaces. This fact can be seen in Figure 6.2, where 79% of the CAI_{dry} values lie below the 1:1 line. In few exceptional cases the CAI values measured on both dry and

saturated rock surfaces coincided. These results are consistent with the findings of earlier investigation carried out by Mammen et al., (2009) where a reduction of 13% was recorded in CAI values when measured on dry and fully saturated sandstone rock sample.

Table 6.3. p-values of means comparison for CAI-values measured on dry and saturated freshly broken rock surfaces. Highlighted and bold faced values show statistically different values at α=0.15 significance level.

Sr. No.	Rock Sample	p-value (CAI)
1	Siltstone-1	0.2207
2	Siltstone-2	**0.0430**
3	Sandstone-1	**0.1500**
4	Sandstone-2	0.4377
5	Sandstone-3	0.5891
6	Sandstone-4	**0.1410**
7	Sandstone-5	0.8681
8	Sandstone-6	**0.0135**
9	Sandstone-7	**0.0241**
10	Sandstone-8	0.5553
11	Sandstone-9	0.2379
12	Sandstone-10	**0.0044**
13	Sandstone-11	**0.1771**
14	Sandstone-12	0.3702
15	Sandstone-13	**0.0202**
16	Sandstone-14	**0.0004**
17	Sandstone-15	0.5453
18	Sandstone-17	**0.0520**
19	Sandstone-18	**0.0095**
20	Chamositic Siderite	0.8752
21	Dolomite-1	**0.0802**
22	Dolomite-2	0.3562
23	Dolomite-3	0.2947
24	Dolomite-4	**0.0000**
25	Limestone-1	**0.1469**
26	Limestone-2	0.4257
27	Limestone-3	**0.0089**
28	Limestone-4	0.9044
29	Limestone-5	0.8735
30	Limestone-6	**0.0840**
31	Limestone-7	0.4994
32	Rock Gypsum	**0.0023**
33	Marl	**0.0237**

Further Figure 6.2, shows a relationship between CERCHAR abrasivity index values measured on saturated and dry rock surfaces which is presented below:

$$CAI_{sat} = 0.782 \times CAI_{dry} + 0.128; (R^2 = 0.83) \tag{6.3}$$

The proposed correlation (Equation 6.3) explains that CAI_{sat} is about 80% of the CAI_{dry} value. At present CERCHAR test is widely used for assessing the tool wear life and cost for cutting tools of TBM's, Roadheaders and similar machines and it is based on the CAI values measured on dry rock surfaces. Since these machines usually encounter both dry as well as wet rock strata along the proposed route of excavation, it makes sense to use

proper CAI values for estimation of tool cost based on the conditions present at the site relative to water content of the rock. This could also lead to better correlation between the estimated tool life and cost and CERCHAR values which from time to time is somewhat inaccurate.
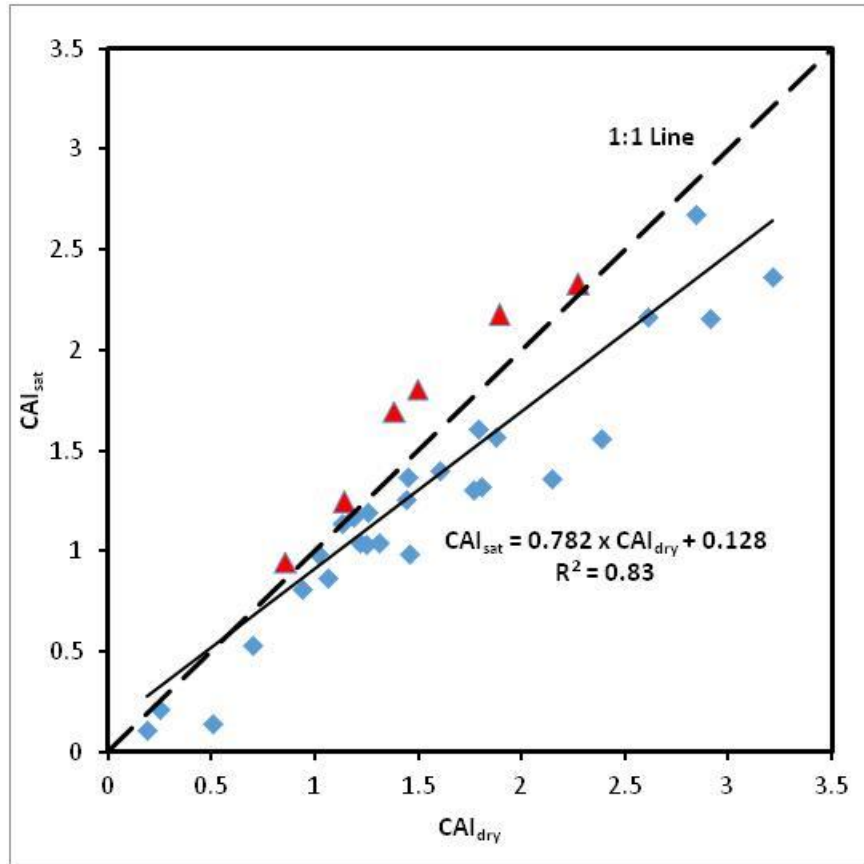
Figure 6.2. Plot of CAI_{sat} versus CAI_{dry} (The red triangles correspond to the higher $CAI_{(sat)}$ values) (after Abu Bakar et al. 2016).

The previous literature reports change in tool wear and hence in their replacement rate with variation in moisture content. For example Mammen et al. (2009) conducted rock cutting tests employing a modified linear shaping machine on argillaceous quartz sandstone by varying the moisture content of test sample in six increments starting from dry (0% moisture) to fully saturated (4.6% moisture) conditions. They found that the wear of rock cutting tool in saturated sample was about 20% of that obtained in cutting the sample in dry state. Similarly in another study Abu Bakar and Gertsch (2013) performed full-scale cutting experiments using a chisel type drag pick on Roubidoux

sandstone in both dry and fully saturated conditions. When cutting rock in dry state, the drag picks experienced failure of tungsten carbide tips, mainly due to thermal fatigue; frequent observation of this phenomenon corresponds to premature failure and repeated replacement of picks. On the other hand while conducting cutting tests in saturated rock blocks no pick failure was reported, this showed that water saturation resulted in reduction in thermal fatigue.

The reduction in CAI_{sat} may be attributed to the weakening of the rock cementing material holding the mineral grains together within the rock matrix. The reduction in CAI values upon saturation could also be ascribed to the lubricating effect imparted by saturated water between the CERCHAR stylus and the rock surface thereby reducing the friction between the two surfaces. In other words lubrication provided by the rock water content aids in cooling the temperature at CERCHAR stylus tip and therefore reduction in its wear. This fact was also noticed in the investigation of Phillips and Roxborough (1981), where significant reduction in the tool wear rate was noted while cutting saturated Bunter sandstone compared to the wear observed in cutting dry rock primarily due to the cooling of cutting tool. This cooling effect of water through heat dissipation was very much evident from the production of large volumes of steam during the wear tests. Ford and Friedman (1983) also attributed reduction in the drag tools cutting forces to the lubrication of tool/rock interface due to the water induced by high pressure water-jets thereby lowering the frictional forces. Rostami et al. (2012) and Mosleh et al. (2013) have made similar observation when examining the abrasion of soil in dry, wet and saturated conditions. Their studies show that the abrasivity of soil will increase to a peak which could be up to two order of magnitude higher than the dry conditions at (7-10) % water content, due to increase in cohesion between the grains and thus soil is more prone to compaction (as shown in Proctor tests), and thus to higher strength, leading to higher abrasion. As the amount of water in the mixture increases beyond the maximum compaction (Proctor), the abrasivity of the soil-water mixture reduces to the point that saturated soil is less abrasive than dry soil. This also was attributed to the impact of water in lubricating the contact area between steel and grains as well as grain-grain contact and beginning of building pore pressure.

A few exceptions can be noted in Figure 6.2, where the CAI_{sat} were higher than the values measured on dry rocks. These rock samples include some sandstone (Khewra, Dandot, Chhidru, Warchha and Datta formations) and a dolomite (Abottabad formation). The rock properties of these specimens show quartz equivalent content (EQC) of (7.3 to 89.7) %, rock matrix (clay and carbonate) of (1.5 to 92) %, mean grain size of (0.204 to 0.589) mm and a loss in strength (UCS) on saturation in the range of (5.66 to 44.44) %. The increase in CAI_{sat} values may be due to the petrographic characteristics as well as the intrinsic physical properties of the rock samples. This phenomenon can be explained according to the past findings of Al-Ameen and Waller (1994) who suggested that the development of wear flat at stylus tip in the beginning of test (i.e. $\approx$ 1mm scratch distance) is due to its initial burial into the rock surface, deformation and shear failure under the applied static load of 7 kg and not on the amount of abrasive mineral content of the rock. If the rock tested is a sedimentary rock, the shear failure at the stylus tip will be primarily related to the rock strength and particle size. For the remaining (2-10) mm scratch distance, the wear flat will increase in diameter depending on the inherent physical characteristics and mineralogy of rock samples. In the case of softer and abrasive sedimentary rocks the CERCHAR stylus tip will indent deeper into the rock sample resulting in more abrasion, due to its continuous contact with the rough surface texture. In contrast if abrasive minerals are absent in the host rock the wear flat diameter will not increase with the increased sliding distance. Moreover it is also known from the earlier investigations that CAI value is not much influenced by the mineral grain size in the range between 50 μm to 1000 μm (Suana and Peters, 1982; Al-Ameen and Waller, 1992b). The observation on the size of the wear flat and its indentation into the rock surface noted above was measured with high degree of accuracy by Hamzaban et al. (2014a, 2014b). They showed that the size of wear flat increases with the length of the scratch in extremely hard and abrasive rocks using a precise measurement of the length of the scratch, pin penetration into the face, and shearing forces. The result of testing shows that the effect of mineral grain size was negligible in producing higher CAI_{sat} values, because of mean grain sizes of the concerned rocks (0.204mm to 0.589mm) was below 1.0 mm, as suggested by Suana and Peters (1982) and Al-Ameen and Waller (1992b; 1993b).

The softening of the rocks is also visible in Figure 6.3, where significant reduction (overall 50%) in uniaxial compressive strength was observed for majority of the rocks tested upon full saturation, compared to dried samples, as reported in the previous studies (Colback and Wiid, 1965; Wiid, 1970; Kitaowa et al., 1977; Bell, 1978; Hassani et al., 1979; Ferreira et al., 1981; Priest and Selvakumar, 1982; Koshima et al., 1983; Pells and Ferry, 1983; Dobereiner, 1984; Dyke, 1984; Gunsallus and Kulhawy, 1984; Denis et al., 1986; Howarth, 1987; Dyke and Dobereiner, 1991; Hawkins and McConnell, 1992; Pells, 2004; Erguler and Ulusay, 2009; Yilmaz, 2010; Hui et al., 2014 among others).

Table 6.4 presents the detailed results of loss of strength in uniaxial compressive strength (UCS) and Brazilian tensile strength (BTS) tests, occurred on complete saturation of 33 sedimentary rock samples from the air dried condition.
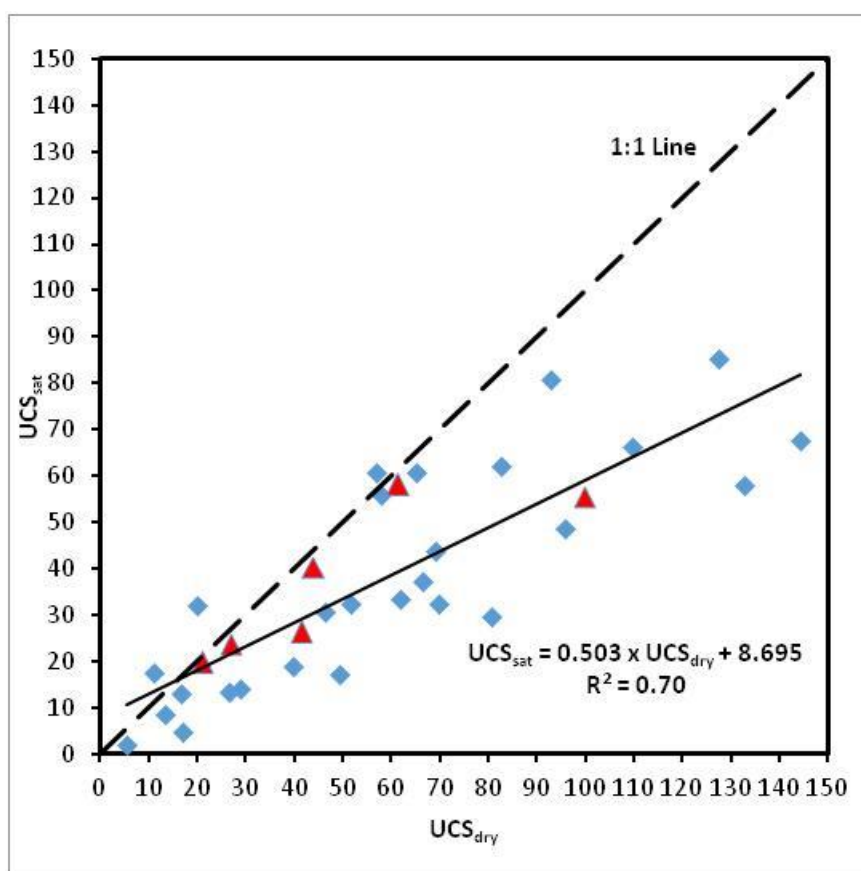
Figure 6.3. Relationship between UCS_{dry} and UCS_{sat} for the rocks tested. The red triangles correspond to the higher $CAI_{(sat)}$ values (after Abu Bakar et al. 2016).

Table 6.4. Test results of reduction in strength of sedimentary rock samples upon full saturation.

Sr. No.	Rock Sample	Strength Loss in UCS		Strength Loss in BTS	
		(MPa)	(%)	(MPa)	(%)
1	Siltstone-1	32.00	64.89	5.31	72.18
2	Siltstone-2	1.81	3.125	2.25	24.91
3	Sandstone-1	20.70	52.01	-0.26	-14.35
4	Sandstone-2	15.35	36.95	0.37	76.37
5	Sandstone-3	42.27	33.13	3.92	61.50
6	Sandstone-4	13.16	49.24	0.54	37.21
7	Sandstone-5	3.73	8.48	0.10	3.37
8	Sandstone-6	43.43	39.58	4.83	80.06
9	Sandstone-7	3.48	5.66	4.76	65.07
10	Sandstone-8	-6.51	-58.95	0.33	25.40
11	Sandstone-9	14.89	51.26	0.09	4.64
12	Sandstone-10	3.65	21.87	-0.30	-42.76
13	Sandstone-11	1.44	6.81	0.09	4.33
14	Sandstone-12	3.48	12.86	0.20	12.63
15	Sandstone-13	15.75	33.95	-0.15	-9.50
16	Sandstone-14	12.23	71.62	-0.02	-2.29
17	Sandstone-15	25.31	36.65	2.19	35.90
18	Sandstone-17	-4.14	-7.29	2.83	67.38
19	Sandstone-18	20.80	25.13	2.06	34.37
20	Chamositic Siderite	12.92	24.99	3.93	48.68
21	Dolomite-1	28.34	45.82	2.68	40.96
22	Dolomite-2	76.68	53.09	3.74	31.25
23	Dolomite-3	44.41	44.44	7.87	62.78
24	Dolomite-4	74.77	56.34	2.82	42.41
25	Limestone-1	4.41	6.75	3.79	75.68
26	Limestone-2	47.03	49.11	1.96	42.64
27	Limestone-3	51.06	63.28	0.20	3.55
28	Limestone-4	29.24	44.00	2.28	42.24
29	Limestone-5	11.95	12.89	2.76	34.93
30	Limestone-6	11.95	12.89	2.76	34.93
31	Limestone-7	-12.06	-60.05	7.07	90.27
32	Rock Gypsum	5.05	37.34	-0.03	-2.05
33	Marl	3.25	60.75	0.45	57.44

6.3. MULTIPLE REGRESSION ANALYSIS

Multiple regression analysis was carried out to develop an empirical model for the prediction of CAI_{sat} from rock properties, normally measured in laboratory testing. SPSS-21.0 statistical software package was used for the statistical analysis with CAI_{sat} as the response variable and UCS, BTS, density, Schimazek's F-value, RAI in saturated conditions, quartz content (QC %), equivalent quartz content (EQC %), porosity, pore-space volume, mean quartz grain size (Ø-Qtz), average grain size of minerals (Ø), as independent variables. In order to evaluate all possible regression models, a stepwise multi variable regression technique was selected. This method is a combination of forward selection and backward elimination. In this technique the regressors are entered in the model individually in descending order of their partial *F*-statistics values, provided that they remain significant at a pre-fixed significance level of entry (SLE). The equation

is evaluated at each step when an independent variable is entered to the model, and the variable with the smallest partial *F*-statistics value is checked at the pre-defined significance level to stay (SLS) and removed if established insignificant. This procedure is followed by iteration of the steps until the selection of an additional regressor does not increase the R^2 value by a substantial amount at the pre-fixed level of significance (Samaranayake, 2009). Accordingly, the variables Schmizek's F-value$_{sat}$, UCS$_{sat}$, Ø-Qtz and BTS$_{sat}$ were incorporated in the regression equation and the independent variables including density$_{sat}$, RAI$_{sat}$, QC (%), EQC (%), Ø, porosity, pore-space volume were excluded from the model due to their lack of statistical significance at α = 0.1. Equation 6.4, presents the results of best fit regression model (*F* statistics value = 50.543, *p* value < 0.0001 at α = 0.10).

$$CAI_{sat} = 0.111 + 0.431 \text{ x (F-value}_{sat}) + 0.008 \text{ x (UCS}_{sat}) + 1.753 \text{ x (Ø-Qtz)} + 0.117 \text{ x (BTS}_{sat}); \quad (6.4)$$

$$(R^2 = 0.88)$$

To check the validity and statistical significance of the current derived equation, standard test statistics were employed. The value of co-efficient of determination ($R^2 = 0.88$) for this model (Equation 6.4) indicates that 88% of the variance in CAI$_{sat}$ can be predicted from the variables (Schmizek's F-value$_{sat}$, UCS$_{sat}$, Ø-Qtz and BTS$_{sat}$). The computed value of correlation coefficient (R = 0.94) shows a strong relationship between the response and independent variables. The standard error of the estimate also called the root mean square error, is the standard deviation of the error term, and is the square root of the mean square residual (Yilmaz et al., 2007). For Equation 6.4, the standard error of the estimate specifies that the standard deviation of the residuals is 0.23. The adjusted R^2 value suggests that the proposed model accounts for 86.20 % of total variation in the CAI$_{sat}$ values.

Moreover the regression model was also checked for collinearity. The variance inflation factor (VIF) is the most commonly used tool for finding the severity of collinearity. The VIF is the coefficient of determination of each independent variable with all others. For example a VIF value of 1 shows no linear dependency (Yilmaz et al., 2007). On the other side a VIF of 10 is proposed as the upper limit in regression analysis (Kennedy, 2008; Hair et al., 2009). The VIF values for independent parameters in

Equation 6.4 were calculated using the built in option provided in SPSS software as: Schmizek's F-value$_{sat}$ (3.746), UCS$_{sat}$ (1.572), Ø-Qtz (4.002) and BTS$_{sat}$ (1.721). Accordingly it was concluded that Equation 6.4, is free from high level of collinearity.

The results of ANOVA are presented in Table 6.5. The overall utility or prediction accuracy of regression model (Equation 6.4) was checked by implementing the relevant F-test:

$$MS_{(regression)} = \frac{SS_{(regression)}}{K-1} = \frac{11.015}{5-1} = 2.754;$$

$$S^2 = \frac{SS_{(residual)}}{n-k} = \frac{1.518}{33-5} = 0.054;$$

$$F_{(model)} = \frac{MS_{(regression)}}{S^2} = 50.802;$$

$$F_{(critical)} = F_{[\propto]}^{(k-1,n-k)} = F_{[0.10]}^{(4,28)} = 2.16.$$

Where;

MS$_{(regression)}$ = Mean square regression;

SS$_{(regression)}$ = Sum of squares regression which gives the explained variation;

K = Number of parameters;

S^2 = Model variance;

SS$_{(residual)}$ = Sum of squares residuals which gives the unexplained variation;

n = Number of samples;

α = Pre-fixed Level of significance (0.10).

The hypothesis testing for the prediction model (Equation 6.4) was also implemented. The null hypothesis (H$_o$) implies that there is no association between the dependent variable, CAI$_{sat}$ and the independent variables (Schmizek's F-value$_{sat}$, UCS$_{sat}$, Ø-Qtz and BTS$_{sat}$). On the other hand the new or alternate hypothesis (H$_a$) is the reverse of null hypothesis. As F$_{(model)}$ > F$_{(critical)}$ therefore, we can reject null hypothesis (H$_o$) and accept the alternate hypothesis (H$_a$) which implies that there is a relationship between the independent and dependent variable. It can be noted that the p-value of the model (Table 6.5) is also less than the pre-defined significance level (α) of 0.10, suggesting that there exists a statistically significant correlation between CAI$_{(sat)}$ and Schmizek's F-value$_{sat}$, UCS$_{sat}$, Ø-Qtz and BTS$_{sat}$ at 90% confidence level and the derived model is statistically valid.

Table 6.5. Analysis of variance (ANOVA) for dependent variable CAI$_{(sat)}$

Model	Sum of squares (SS)	Df	Mean square (MS)	F-ratio	Sig.
Regression	11.015	4	2.754	50.802	0.000
Residual	1.518	28	0.054		
Total	12.532	32			

Coefficient of correlation (R) = 0.94

Coefficient of determination (R^2) = 0.88

Adjusted R^2 = 0.862

Standard error of the estimate = 0.233

An attempt is also made to utilize the saturated rock properties (UCS$_{sat}$, BTS$_{sat}$, Schimazek's F-value$_{sat}$) measured in this work, in the already published CAI prediction models incorporating physical and petrographical properties of dry rocks (Rostami et al., 2013 and Majeed and Abu Bakar, 2015). Table 6.6 presents the selected models used for validation.

Table 6.6. Statistical models for the prediction of CAI values from physical and petrographical properties of rock.

Reference	Rock type	Regression model
Rostami et al. (2013)	Equations (A) and (B) are developed using igneous, metamorphic and sedimentary rock types, utilizing a dataset of 15 and 34 rocks respectively.	(A) CAI 54$_{HRC\text{-}Rough}$ = 0.0151 x UCS$^{0.788}$ x EQC$^{0.377}$ (R^2 = 89.9 %) (B) CAI 55$_{HRC\text{-}Rough}$ = 0.056 x UCS$^{0.431}$ x EQC$^{0.448}$ (R^2 = 79.6 %)
Majeed and Abu Bakar (2015)	Developed using all three generic rock types based on a dataset of 46 rocks.	CAI$_{fb(Side)}$ = 0.811 + 0.289 (F-value) + 1.285(ϕ-Qtz) + 0.007(UCS) (R^2 = 79.0 %)
UCS- uniaxial compressive strength, EQC- equivalent quartz content, F-value- schimazek's F-value, ϕ-Qtz- quartz grain size		

Table 6.7 presents the actual CAI$_{sat}$ values along with the predicted CAI$_{sat}$ values using equations listed in Table 6.6. The actual CAI$_{sat}$ and predicted CAI$_{sat}$ (from the three prediction models listed in Table 6.6) are plotted in Figure 6.4. The results of Table 6.7 and Figure 6.4 show that CAI$_{sat}$ values estimated from the equation proposed by Majeed and Abu Bakar (2015) are showing better agreement with the actual CAI$_{sat}$ values probably due to the fact that the prediction model was developed based on higher number of data sets (46 rock samples) thereby increasing its statistical reliability, as compared to the relatively limited number of data sets utilized in deriving equations (A) and (B) suggested by Rostami et al. (2013). Moreover, the formulas offered by previous studies

did not include water content and were only applicable to dry samples to begin with. However it is pertinent to mention here that all the three prediction models under comparison (Table 6.6) have fairly good co-efficient of determination (R^2) values.

Table 6.7. Comparison of actual and predicted CAI$_{sat}$ values.

Sr. No.	Rock sample	Actual CAI$_{sat}$	Predicted CAI$_{sat}$		
		(Measured in this work)	Rostami et al. (2013) [CAI 54$_{HRC-Rough}$]	Rostami et al. (2013) [CAI 55$_{HRC-Rough}$]	Majeed and Abu Bakar (2015)
1	Siltstone-1	1.569	1.397	1.588	1.513
2	Siltstone-2	1.035	0.469	0.786	1.260
3	Sandstone-1	1.309	0.775	1.359	1.670
4	Sandstone-2	0.945	1.021	1.607	1.305
5	Sandstone-3	2.679	2.611	2.701	2.484
6	Sandstone-4	1.043	0.627	1.256	1.495
7	Sandstone-5	2.327	1.426	1.924	2.059
8	Sandstone-6	2.368	2.241	2.559	2.515
9	Sandstone-7	1.693	2.018	2.416	1.482
10	Sandstone-8	1.194	0.714	1.286	1.548
11	Sandstone-9	2.165	0.649	1.281	1.916
12	Sandstone-10	1.260	0.587	1.185	1.583
13	Sandstone-11	1.806	0.836	1.462	1.961
14	Sandstone-12	1.243	0.878	1.416	1.347
15	Sandstone-13	1.325	1.198	1.795	1.493
16	Sandstone-14	1.046	0.278	0.804	1.489
17	Sandstone-15	1.373	1.577	2.080	1.321
18	Sandstone-17	2.156	1.938	2.211	2.381
19	Sandstone-18	1.559	1.950	2.245	1.759
20	Chamositic-Siderite	0.986	0.760	0.928	1.203
21	Dolomite-1	1.399	0.472	0.568	1.121
22	Dolomite-2	1.609	0.873	0.826	1.378
23	Dolomite-3	2.177	0.758	0.772	1.670
24	Dolomite-4	1.363	1.095	1.169	1.474
25	Limestone-1	0.866	0.553	0.507	1.240
26	Limestone-2	0.814	0.463	0.459	1.159
27	Limestone-3	0.990	0.347	0.419	1.071
28	Limestone-4	1.174	0.341	0.365	1.087
29	Limestone-5	1.137	0.649	0.531	1.379
30	Limestone-6	0.534	0.366	0.428	1.047
31	Limestone-7	0.211	0.352	0.409	1.037
32	Rock Gypsum	0.142	0.065	0.107	0.871
33	Marl	0.111	0.090	0.321	0.958
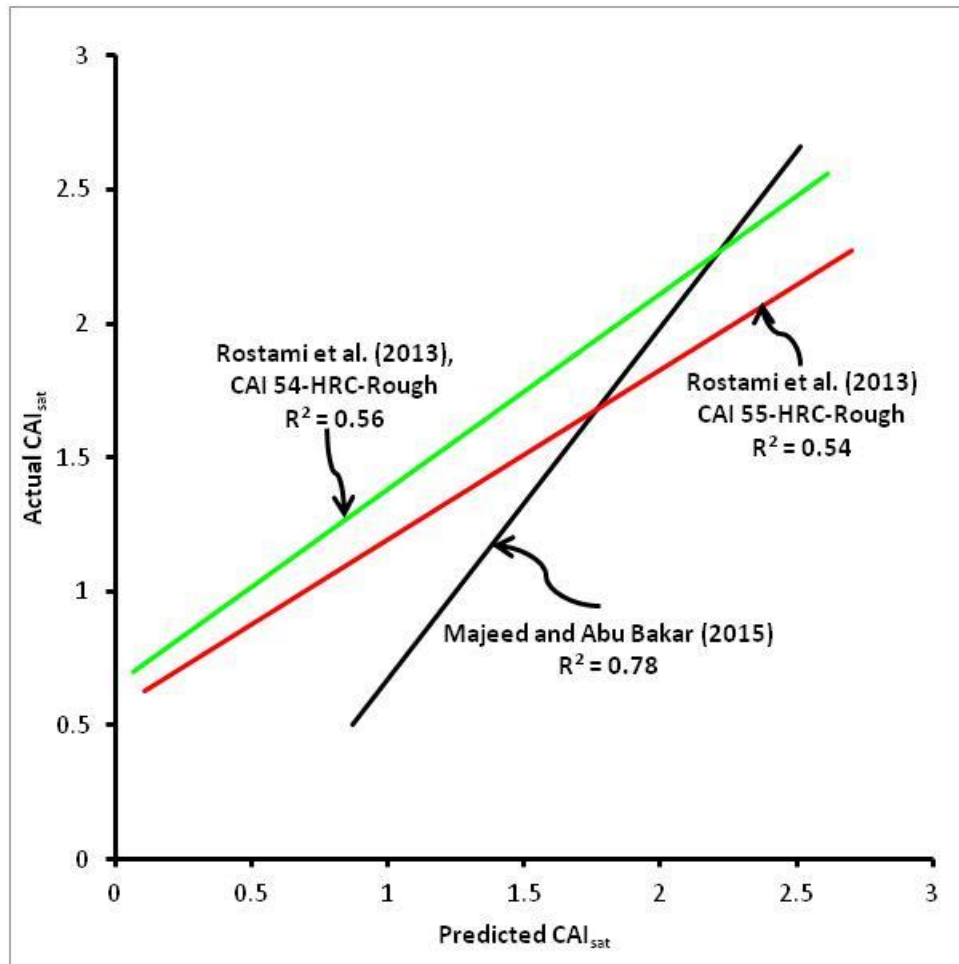
Figure 6.4. Actual and predicted CAI$_{sat}$ values by different regression models (after Abu Bakar et al. 2016).

In order to further investigate the estimation performance of the selected models (Table 6.6), the variance account for (VAF) and the root mean square (RMSE) statistical performance analysis techniques were employed:

$$VAF = \left(1 - \frac{Variance\ (y_i - \hat{y}_i)}{Variance\ (y_i)}\right) \times 100\ \%$$ (6.5)

$$RMSE = \sqrt{\frac{1}{N} \sum_{i=1}^{N}(y_i - \hat{y}_i)^2}$$ (6.6)

Where;

y_i = actual or measured value;

$\hat{y}_i$ = predicted or estimated value;

N = total number of samples.

The analytical interpretation of the performance indices (VAF) and (RMSE) is that higher value of VAF shows that the regression model is providing better prediction results. For instance, a VAF value of 100% means that the measured output has been predicted exactly, whereas a VAF value of 0% means that the model performs as poorly as a predictor using simply the mean value of the data. The lower value of RMSE shows the better prediction performance of the model. Contrary to VAF, RMSE also accounts for a bias in the model (Alvarez and Babuska, 1999; Gokceoglu, 2002; Gokceoglu and Zorlu, 2004; Yilmaz et al., 2007). By using the same data provided in Table 6.7, the VAF (%) and RMSE values were computed for the selected models and presented as follows in Table 6.8.

Table 6.8. Comparison of VAF and RMSE values computed for the selected models.

Model	VAF (%)	RMSE
Rostami et al. (2013) [CAI $54_{HRC-Rough}$]	48.20	0.60
Rostami et al. (2013) [CAI $55_{HRC-Rough}$]	35.96	0.51
Majeed and Abu Bakar (2015)	73.37	0.36

The results in Table 6.8 show validity of the model by various statistical measures and reliability of the models for reasonable prediction of CAI_{sat}.

7. DISCUSSION: ROCK ABRASIVITY EVALUATIONS UTILIZING LCPC ROCK ABRASIVITY TEST METHOD

This section discusses the LCPC rock abrasivity tests conducted on 51 rock samples collected from various locations of Pakistan. The testing methodology is provided in chapter 3 whereas the detailed test results are presented in chapter 4.

The discussion of results in this section is confined to the effect of changing water content on LCPC test results, the correlations of LCPC abrasivity coefficient, ABR (g/t) with CERCHAR abrasivity index (CAI), physico-mechanical and petrographical rock parameters. In addition, the LCPC breakability index, BR (%) is also correlated with the physical and mechanical rock properties.

7.1. EFFECT OF WATER CONTENT ON LCPC ABRASIVITY COEFFICIENT

Rock excavation either by conventional drill and blast system or by mechanized excavators mostly encounters rocks in saturated conditions. In addition, nearly all the mechanical rock cutting machines (Roadheaders and TBMs) use high pressure waterjets to suppress the dust produced during excavation as well as to lubricate and cool the rock cutting tools. Moreover, the metropolitan underground tunnelling or construction activity conducted in soft grounds especially beneath the groundwater table is usually carried out by the application of earth pressure balanced (EPB) tunnelling machines. Numerous previous studies (Fowell and Abu Bakar, 2007; Drucker, 2011; Drucker, 2013; Barzegari et al., 2015; Hashemnejad et al., 2015) have investigated the influence of moisture content variations on LCPC abrasivity coefficient, ABR (g/t). In this research, to simulate the rock cutting process in wet and saturated ground conditions, the LCPC tests were performed on 20 selected rock samples by adding varying amounts of fresh tap water with 500 grams of sieved rock aggregate prior to the start of test. A minimum moisture content level of 15% was selected, since an amount of water less than this level accumulates rock grains on the walls of the mould thereby allowing the rotating impeller to rotate freely without any contact with the crushed rock. A similar moisture content level has also been suggested in a study conducted by Drucker (2011). The selected water contents and test results are outlined in Table 7.1.

Table 7.1. LCPC abrasivity coefficient, ABR (g/t) values at different water contents.

Sr. No.	Water Content (%)	0	15	30	45	60
	Water Mass (grams)	0	75	150	225	300
	Rock	ABR (g/t)				
1	Dolerite-3	186.00	882.00	1086.00	1032.00	942.00
2	Dolerite-4	1391.28	1934.00	1814.00	1836.00	1714.00
3	Granite-4	477.00	478.00	788.00	560.00	484.00
4	Granite-5	1534.50	1862.00	1758.00	1874.00	1770.00
5	Granite-6	1273.00	1660.00	1642.00	1548.00	1342.00
6	Andesite	1385.00	2008.00	1856.00	1778.00	1798.00
7	Granitic Gneiss-1	172.00	516.00	606.00	420.00	356.00
8	Granitic Gneiss-2	429.00	156.00	620.00	426.00	394.00
9	Phyllite	80.00	306.00	200.00	98.00	82.00
10	Siltstone-1	63.00	372.00	346.00	322.00	266.00
11	Sandstone-2	102.00	40.00	270.00	132.00	108.00
12	Sandstone-3	744.00	848.00	986.00	791.17	666.00
13	Sandstone-4	159.93	42.00	358.00	158.00	102.00
14	Sandstone-5	228.00	214.00	384.00	206.00	200.00
15	Sandstone-12	91.00	26.00	252.00	118.00	84.00
16	Sandstone-14	57.00	10.00	142.00	132.00	56.00
17	Sandstone-15	424.00	930.00	886.00	798.00	670.00
18	Sandstone-17	633.00	1330.00	1108.00	854.00	816.00
19	Limestone-3	8.00	14.00	24.00	22.00	12.00
20	Marl	32.99	8.00	92.00	42.00	28.00

The analyses of test results (Figure 7.1 a, b) show two distinct trends of LCPC abrasivity co-efficient ABR (g/t) with variation in the water content. The influence of water saturation on rock abrasivity can be summarized as follows:

7.1.1. Effect on ABR (g/t) at 15% Water Content. Figure 7.1 (a) shows the trends of 7 rock samples. There is a reduction in ABR (g/t) values ranging from 6% (Sandstone-5) to 83% (Sandstone-14) when comparing these test results conducted on dry (0% water saturation) rock samples. The likely explanation of this reduction in ABR (g/t) is the considerably high porosity (10.84% to 24.70%) of the rock samples with the exception of Sandstone-5 (n = 3.12%) and Granitic Gneiss-2 (n = 1.10%) rock samples, where the decrease in ABR (g/t) values is probably due to their low BTS values. It is conceivable that the addition of 15% water content to high porosity granular rock material present in the LCPC mould, resulted in complete absorption within the pore

recesses of rock grains and produced adhesive paste in the start of test which subsequently aligned rock grains along the walls of test mould beyond the reach of rotating impeller as can be seen in Figure 7.2 (a). Drucker (2011, 2013) also observed similar behavior at water content below 15%. Lemmerhofer (2010) reported that earth-damp abrasive material forms a compact slurry in the LCPC test and no further repeatable results can be achieved.
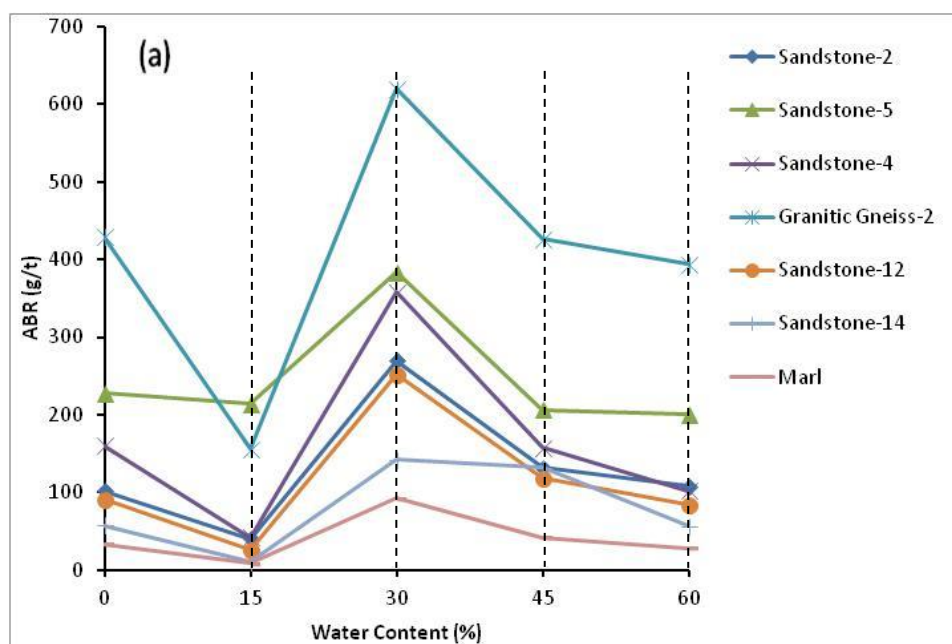
Figure 7.1. (a) Effect of water content on the LCPC abrasivity co-efficient for tested rock samples of relatively high porosity.
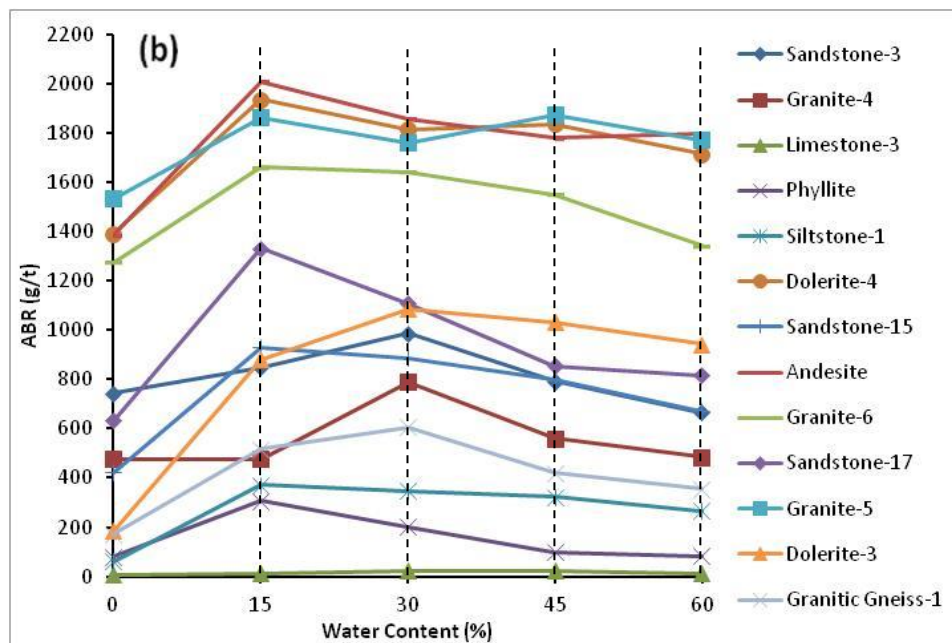
Figure 7.1. (b) Effect of water content on the LCPC abrasivity co-efficient for tested rock samples of relatively low porosity.
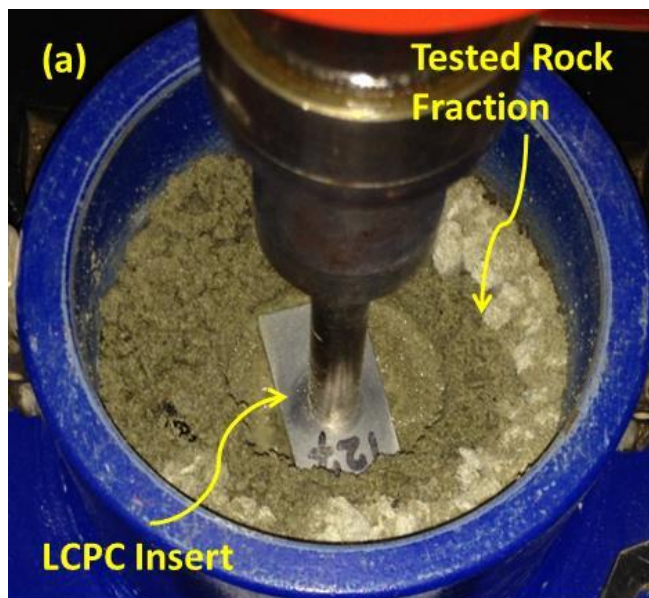
Figure 7.2. (a) A view of Sandstone-14 rock sample tested at 15% water content. Notice the alignment of material along the walls of the LCPC test container.

Figure 7.1 (b) shows the trends of 13 rock samples where the LCPC abrasivity co-efficient, ABR (g/t) values show an overall increase at 15% moisture content level in comparison to dry rock tests. This phenomenon may be attributed to the low porosity of the majority of rock samples (ranging from 0.12% to 3.61%) resulting in a water film

coating around the rock grains with little absorption in the pore spaces. However, Sandstone-15 (n = 6.82%) and Phyllite (n = 7.68%) are the exceptional cases where increase in ABR values is probably due to their relatively higher BTS values. It is noteworthy that in most cases (8 samples out of 13) the ABR (g/t) attained peak values ranging from 21% (Granite-5) to 490% (Siltstone-1) at 15% water content. Similar behavior was observed by Drucker (2011, 2013) where LCPC abrasivity coefficient also achieved its peak values at 15% water content. This increase in wear is explained by the bonding forces between the pore water and the concomitant water envelope around the grains of the abrasive material, resulting in more resistance to the movement of the wearing body through the material (Wellinger and Uetz, 1955). The same fact can also be noted in Figure 7.2. (b), where except few rock grains sticking with walls of the LCPC test container a large percentage of water-solid mixture is in suspension, which offers a great resistance to the rotation of impeller at high speed of 4500 rpm.
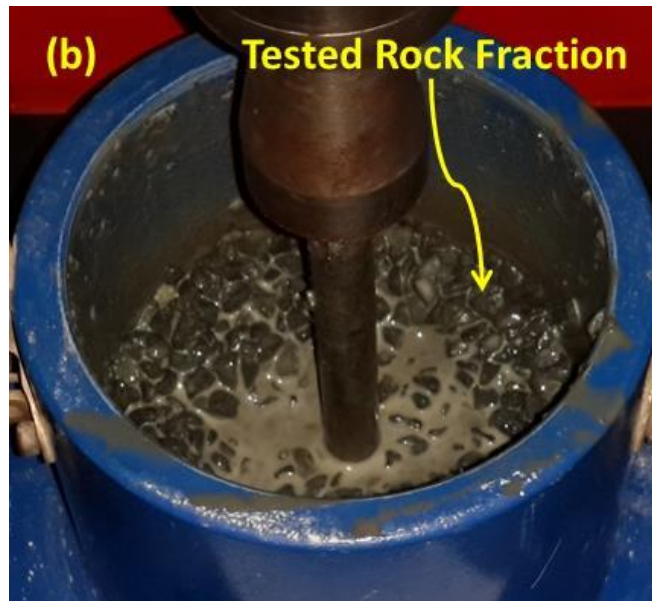
Figure 7.2. (b) Picture of a tested Dolerite-4 rock sample at 15% water content, where the material is in high density solid-water suspension.

However, Figure 7.1 (b) also shows the trends of 5 rock samples (Limestone-3, Granitic Gneiss-1, Granite-4, Dolerite-3 and Sandstone-17) where the ABR (g/t) values show increase at 15% water quantity relative to the dry test values, but do not attain the peak values. They are attaining their peak levels at 30% water content. The similar trend was reported by Hashemnejad et al. (2015) in their research.

7.1.2. Effect on ABR (g/t) at 30% Water Content. The test results (Figure 7.1 a) show the peak values of LCPC abrasivity co-efficient with an increase ranging from 45% (Granitic Gneiss-2) to 179% (Marl) compared to the tests conducted at 0% moisture content. This is probably due to rotation of LCPC test impeller in thick paste formed by the grinding and crushing of rock grains in water. Hashemnejad et al. (2015) reported peak values of abrasivity at 30% moisture content. However, the overall increase in ABR (g/t) values at 30% water quantity as compared to dry test values has also been reported in some past investigations (Drucker, 2011; Drucker, 2013; Barzegari et al., 2015).

Figure 7.1 (b) shows the decrease in ABR (g/t) values at 30% moisture content for the majority of cases (eight rock samples out of 13) after reaching the peak ABR (g/t) values at the water content of 15%. These results are in total agreement with the experimental findings of Drucker (2011). On the other hand five rock samples (Limestone-3, Granitic Gneiss-1, Granite-4, Sandstone-3 and Dolerite-3) experienced increase in ABR (g/t) values at 15% water content and attained peak values of ABR (g/t) ranging from 33% (Sandstone-3) to 484% (Dolerite-3) at the water content of 30%. This phenomenon is similar to the experimental observations of Hashemnejad et al. (2015).
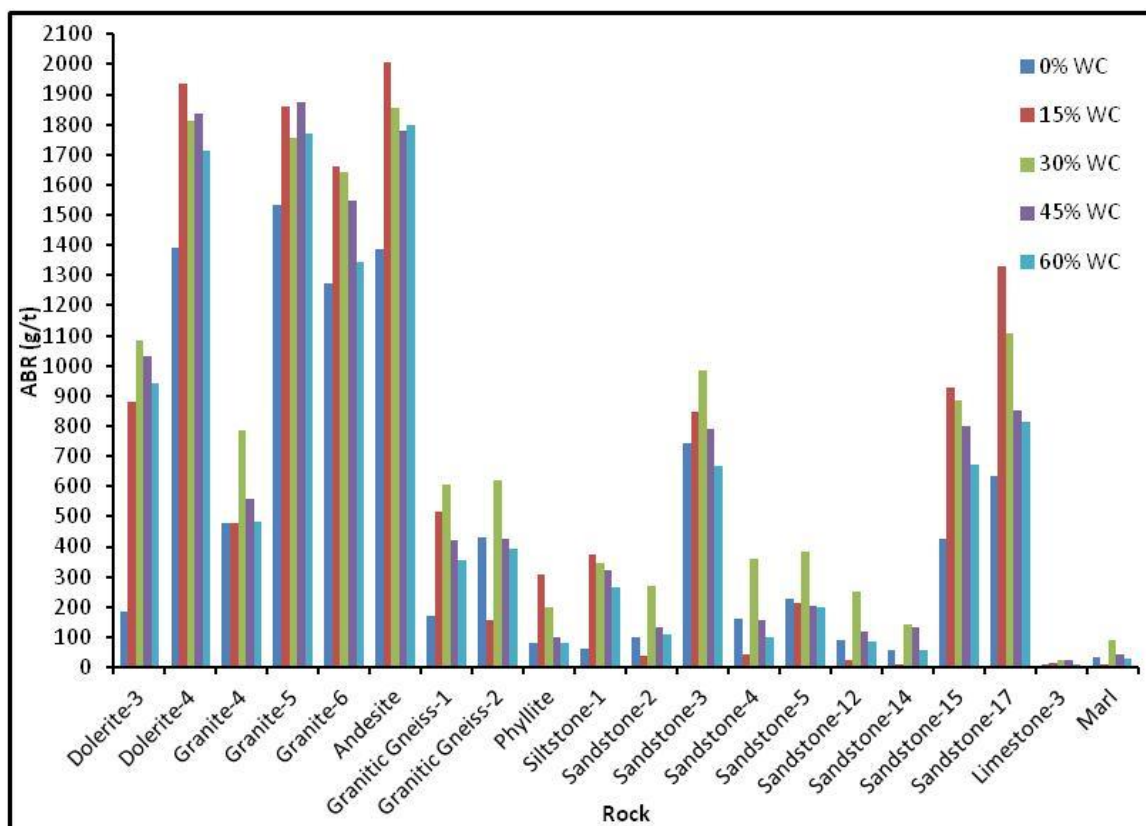
Figure 7.3. Comparison of ABR (g/t) values for the tested rocks at different water content levels.

7.1.3. Effect on ABR (g/t) at 45% and 60% Water Contents. Finally it can be seen in Figures 7.1 (a, b) and 7.3, that as the water content was further increased to 45% the LCPC abrasivity coefficient values dropped gradually but in most cases still remaining higher than the dry test values and approximately attained the dry test values at the water content of 60% in the case of 13 out of total 20 rock samples tested. These results are in agreement with the findings of previous studies (Fowell and Abu Bakar, 2007; Drucker, 2011; Drucker, 2013; Hashemnejad et al., 2015). According to Heinrich (1995) and Wellinger and Uetz (1955) the further increase of water content however reduces the abrasivity as the pore water becomes increasingly mobile and leads to growing propensity of the soil to flow, which lowers the friction between the wearing body and the opposing material. This drop in abrasivity with increasing water content can also be ascribed at first to the decrease of water-soil suspension density due to buoyant forces resulting in excessive water at the propeller-rock grains interface (Drucker, 2011)

and secondly to the lubrication and cooling effect of excessive water to the rotating propeller at high speed (Hashemnejad et al., 2015).

In LCPC tests performed with varying water contents, it is imaginable that the dominant wear process involved is the flowing motion of water and solid rock grains wearing the LCPC test piece through abrasion and surface fatigue mechanisms as suggested by Zum Gahr (1987) and DIN 50 320 (1979). This fact is evident from the examination of tested LCPC inserts in dry and wet states as shown in Figures 7.4 (a-e). In dry test (Figure 7.4, a) the worn out insert shows deformation and rounding at the edges, at first due to the impact of dry intact rock pieces and finally owing to the rotation in the milled rock powder. This milled rock powder actually provides a cushioning effect to the rotating impeller, as well as hinders further interaction with the remaining rock grains, as some intact rock fraction is compacted along the bottom walls of the container underneath it (Fowell and Abu Bakar, 2007). In wet tests (Figures 7.4 b-e) the wear pattern of insert clearly shows a tapered outline of material loss at the diagonally opposite corners under attack due to the initial contact with wet intact rock grains and later its interaction against the mixture of broken grains and paste of rock. This observation closely matches with the findings of Drucker (2011) and Barzegari et al. (2015).

In tunnel construction work the use of tunnel boring machines (TBMs) has become increasingly common in recent years (Nilsen et al., 2007). The type of TBM to be utilized depends upon the geological conditions of the tunneling site and particularly for soft grounds and soils, slurry shield and earth pressure balance (EPB) machines are applied. The efficiency and operating cost of these machines heavily depend upon the abrasivity evaluations of the rock or soil, keeping in view the true in-situ conditions of the site; the abrasiveness of the material as well as its moisture content level.

Figure 7.4. LCPC inserts tested on Andesite rock sample (a) in dry state (b) at 15% water content (c) at 30% water content (d) at 45% water content (e) at 60% water content.

In recent years the LCPC abrasivity testing method has been utilized in selected tunneling projects for initial investigation of rock abrasivity (Buchi et al., 1995). Its application has become more common in rocks and soil testing in the last decade in Europe (Plinninger and Restner, 2008; Kasling and Thuro, 2010). In this perspective the practical implications of using LCPC abrasivity coefficient ABR (g/t) values based on dry tests only, could be an over/under estimation of rock or soil abrasivity potential depending upon the moisture content level of the ground. If wrongly estimated it can impact TBM parts in two ways; the primary wear on the excavation tools such as disc

cutters, drag bits, scrapers and buckets and the secondary wear on the cutterhead structure, on bulkhead and plunging wall structures, on debris conveyance devices including conveyors on EPB-TBMs or slurry pipes, valves and pumps on Slurry-TBMs (Nilsen et al., 2007). Past investigations also have reported numerous TBM tunneling applications around the globe where severe damage to the cutterhead was observed mainly due to secondary wear including ECIS project in Los Angeles, the Elbe tunnel project in Germany, the Porto Metro in Portugal, the MTA in Singapore (Nilsen et al., 2007), the Brightwater tunnel project in Seattle, WA (Gwildis et al., 2010) and Isfahan Metro in Iran (Tarigh Azali and Moammeri, 2012).

The mechanical excavators used in mining and tunneling operations normally require the addition of water through high pressure waterjets (5 to 10% of the weight of rock debris) particularly for the control of dust at working face, reduction in production of frictional sparks and cooling of the cutting tools; which can substantially increase the abrasivity of the excavated muck produced during rock cutting process (Gharahbagh et al., 2014). However, in some instances the rock mass may also contain porewater content. The test results of this research showed rapid increase in the LCPC abrasivity coefficient (ABR) values of rock samples at water contents ranging from 15% to 30% in the case of less porous rocks, while for highly porous rocks 30% water content produced the peak abrasion values. Therefore, during the course of rock excavation moisture content of the rock debris can be examined. In case the water content at the working face is near the critical water content value (15 to 30%) for the particular rock type, addition of extra water to the muck can be beneficial in terms of increase in the water content and reduction of rock abrasivity as well as wear on the muck transportation contrivances especially the conveyors, loaders and hoppers. However, the increased water content of the muck might result in environmental nuisance and greater maintenance of rock debris conveying systems. Moreover, if the rock encountered during excavation is considerably porous, the amount of water sprayed through high pressure waterjets can be increased so that the overall water content at the working face approaches around 15% moisture level. This may help to reduce the abrasion and wear on the rock cutting tools.

Similar investigations exist where the reduction in abrasive wear of the testing tools has been reported by the addition of conditioning agents to the soil abrasion testing

systems. In one case history tunnel muck from a small open type hard rock TBM excavating abrasive granitic rock was tested using Penn State Soil Abrasion Tester. When the rock was tested at water content of 10% without conditioner, substantial weight loss of wear covers (41.553 grams) was observed in 5.5 minutes of testing. Whereas when appropriate conditioning additive (3% concentration solution 1, at Foam Injection Ratio (FIR) of 50% and Foam Expansion Ratio (FER) of 10) was applied at the same water content (W = 10%) the abrasion of wear tools was drastically reduced to about 1 gram in 30 minutes of testing time; a reduction in wear by a factor of around 250 times (Gharahbagh et al., 2014).

7.2. EFFECT OF WATER CONTENT ON LCPC BREAKABILITY INDEX

The initially selected 20 rock samples for the performance of LCPC tests at the pre-defined moisture contents, were further processed by oven drying to explore the influence of water content variation on LCPC breakability index BR (%) of rocks. The test results are presented in Table 7.2.   The present investigation (Figures 7.5 a,b) depicts two different trends of LCPC breakability index BR (%) with variation in the water content. Figure 7.5 (a) shows the test results of 8 rock samples which can be summed up as under:

7.2.1. Effect on BR (%) at 15% Water Content. In the first step at 15% water content there is a significant decrease in breakability ranging from 36.13% (Sandstone-2) to 65.82% (Marl) in contrast to the breakability at 0% moisture content. This behavior can be explained with reference to significantly high porosity of the test samples resulting in the alignment of moistened rock aggregate along the wall of LCPC test mould above the reach of impeller as shown in Figure 7.2 (a).

7.2.2. Effect on BR (%) at 30% Water Content. It is interesting to notice that at 30% water content there is an abrupt rise in BR (%) as compared to the breakability at 15% water content which clearly shows complete interaction between the rock fraction and test propeller. This behavior showing initial decrease (15% water content) and afterwards increase (30% water content) in LCPC breakability, is in contradiction to the experimental findings of Drucker (2011, 2013). According to Drucker (2011) the higher

is the water content of the test mixture, the lower is the breaking effect of the rotating impeller on the abrasive rock fraction, which is shown by the reduction of the LCPC breakability index. However it is worth mentioning (Figure 7.5 a) that at 30% water content three rock samples including Marl, Granitic Gneiss-2, Phyllite and Sandstone-5 showed decreases of 8.75%, 23.02%, 20.17% and 42.59% respectively, in BR (%) which is in accordance to the past investigations of Drucker (2011, 2013).

Table 7.2. LCPC breakability index, BR (%) values at different water contents.

Sr. No.	Water Content (%)	0	15	30	45	60
	Water Mass (grams)	0	75	150	225	300
	Rock	BR (%)				
1	Dolerite-3	29.20	23.80	16.60	16.60	17.20
2	Dolerite-4	18.99	15.50	13.10	12.30	12.60
3	Granite-4	67.43	46.00	46.7	39.00	38.50
4	Granite-5	17.30	15.00	13.60	11.00	13.40
5	Granite-6	50.75	29.60	19.80	21.80	17.20
6	Andesite	26.30	19.60	16.20	12.80	14.60
7	Granitic Gneiss-1	58.68	54.80	55.60	43.00	41.80
8	Granitic Gneiss-2	71.45	38.80	55.00	44.60	42.20
9	Phyllite	58.25	31.40	46.50	41.70	37.70
10	Siltstone-1	42.65	26.80	21.20	19.00	21.00
11	Sandstone-2	61.53	39.3	86.70	60.40	53.30
12	Sandstone-3	65.80	34.80	30.60	27.31	27.60
13	Sandstone-4	67.07	33.00	71.20	53.80	14.80
14	Sandstone-5	75.60	39.50	43.40	37.00	38.20
15	Sandstone-12	60.70	37.50	80.80	61.20	52.40
16	Sandstone-14	58.30	36.80	70.80	73.20	62.80
17	Sandstone-15	35.00	30.20	23.00	22.50	20.10
18	Sandstone-17	60.85	34.80	32.80	28.40	29.00
19	Limestone-3	47.90	39.40	24.00	22.40	22.30
20	Marl	58.52	20.00	53.40	35.40	30.60
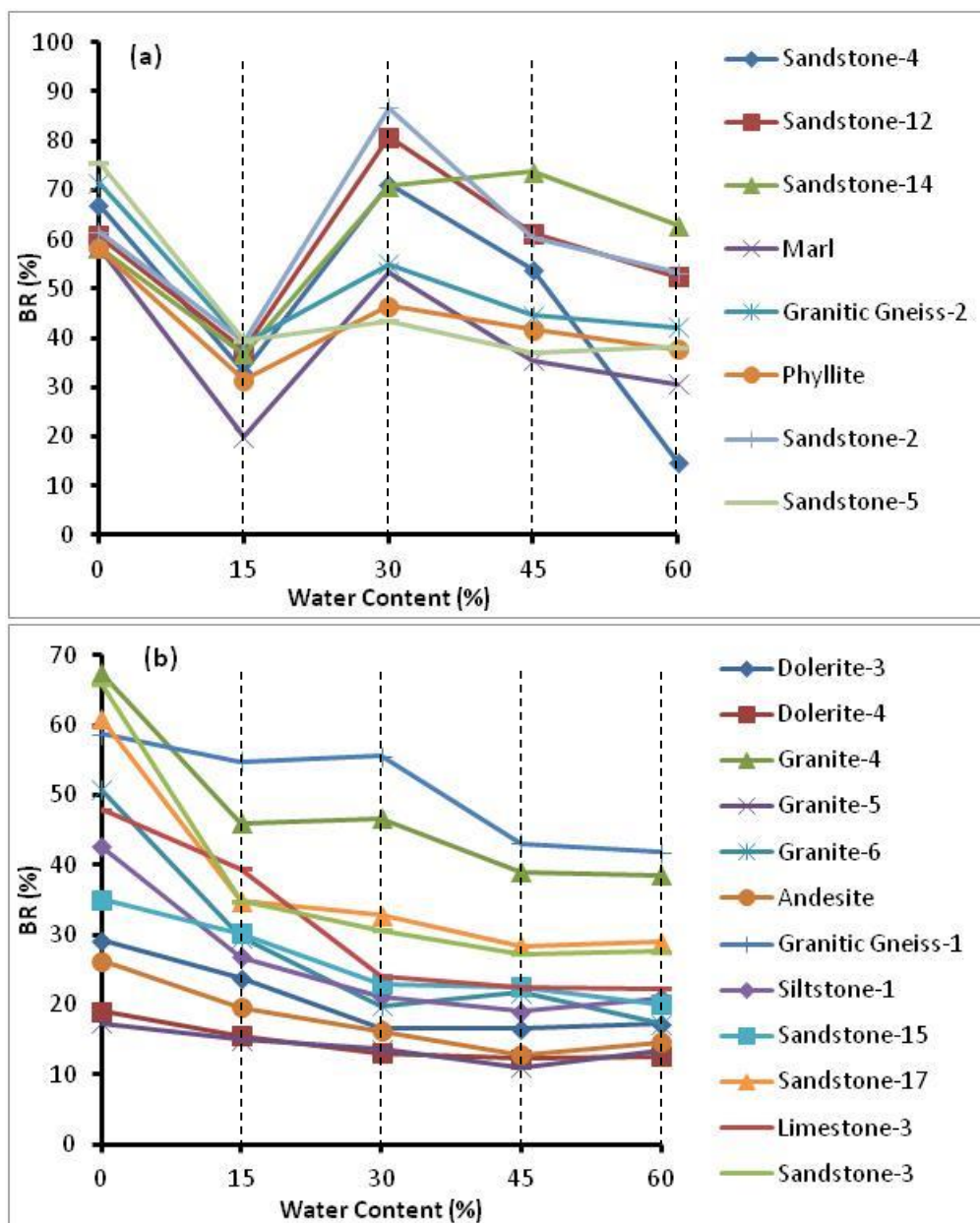
Figure 7.5. (a, b) Effect of water content on the LCPC breakability index for different rock samples tested.

7.2.3. Effect on BR (%) at 45% and 60% water contents. Finally at the water contents of 45% and 60%, the LCPC breakability index decreases gradually in comparison to the breakability of dry tests (Figure 7.5 a) which validate the past studies of Drucker (2011, 2013).

Similarly Figure 7.5 (b) includes the test results of 10 rock samples, where the LCPC breakability index shows a decreasing trend with the highest BR (%) achieved at

dry tests and gradually diminishing in tests conducted at 15% to 60% water contents. This is probably due to low porosity and relatively high BTS values of the rock samples tested. These results are in total agreement with the earlier findings of Drucker (2011, 2013).

7.3. CORRELATION OF LCPC TEST RESULTS WITH ROCK PROPERTIES

Numerous past investigations have evaluated LCPC indices (ABR (g/t), BR (%)) with other rock properties. This section includes possible correlations of LCPC test results with the CERCHAR abrasivity index (CAI), the petrographical and physico-mechanical parameters of the rocks tested.

7.3.1. Relationship of LCPC Abrasivity Co-efficient with CAI. The correlation of LCPC abrasivity co-efficient (ABR, g/t) with CERCHAR abrasivity index (CAI) has been a point of discussion of many previous investigations and it has been identified that one index point of the CAI corresponds to a LCPC abrasivity co-efficient of roughly about 300 (g/t) (Buchi et al., 1995).Whereas, according to Thuro and Kasling (2009) one degree of CAI corresponds to an average ABR value of 275 (g/t) approximately. The CAI_{fb} values (measured on freshly broken rock surfaces by adopting the side viewing stylus measurement method) and the related ABR (g/t) for all tested rocks are displayed in Figure 7.6. As expected a reasonable linear upward trend can be seen between the ABR and $CAI_{fb(side)}$ values. It is interesting to note that for low to medium abrasive rocks (CAI = 0.5 - 2.0) the ABR (g/t) values are relatively consistent, however the scatter increases towards very abrasive to extremely abrasive rocks (CAI = 2.5 − 5.0). For instance, extraordinary higher values of ABR (g/t) than the $CAI_{fb(side)}$ can be observed for Granite-5 (UCS = 232 MPa) and Dolerite-4 (UCS = 141 MPa), mainly due to their higher uniaxial compressive strength values. On the other hand some rock samples are showing lower ABR (g/t) values than their corresponding $CAI_{fb(side)}$ values including Granitic Gneiss-1 (UCS = 69.22 MPa; Qtz.eq = 82.405%), Granite-2 (83.80 MPa; Qtz.eq = 81.860%), Granite-3 (UCS = 77.614; Qtz.eq = 73.890%), Granite-1 (UCS = 40.21 MPa), Dolerite-2 (UCS = 212.10 MPa) and Dolerite-3 (UCS = 199.30 MPa; Qtz.eq = 40.957%) rocks among others. In the case of Gneiss and Granitic rocks this phenomenon may be ascribed due to their higher quartz equivalent content and their relatively lower UCS

values. While in the case of Dolerite-2 and Dolerite-3 rock samples this phenomenon may be attributed to the fact that during the process of sample preparation for LCPC test, some of the main rock features (especially the overall strength of rock fabric) are destroyed and hence are neglected in the measured LCPC abrasivity co-efficient (Plinniger and Restner, 2008; Kohler et al., 2011).
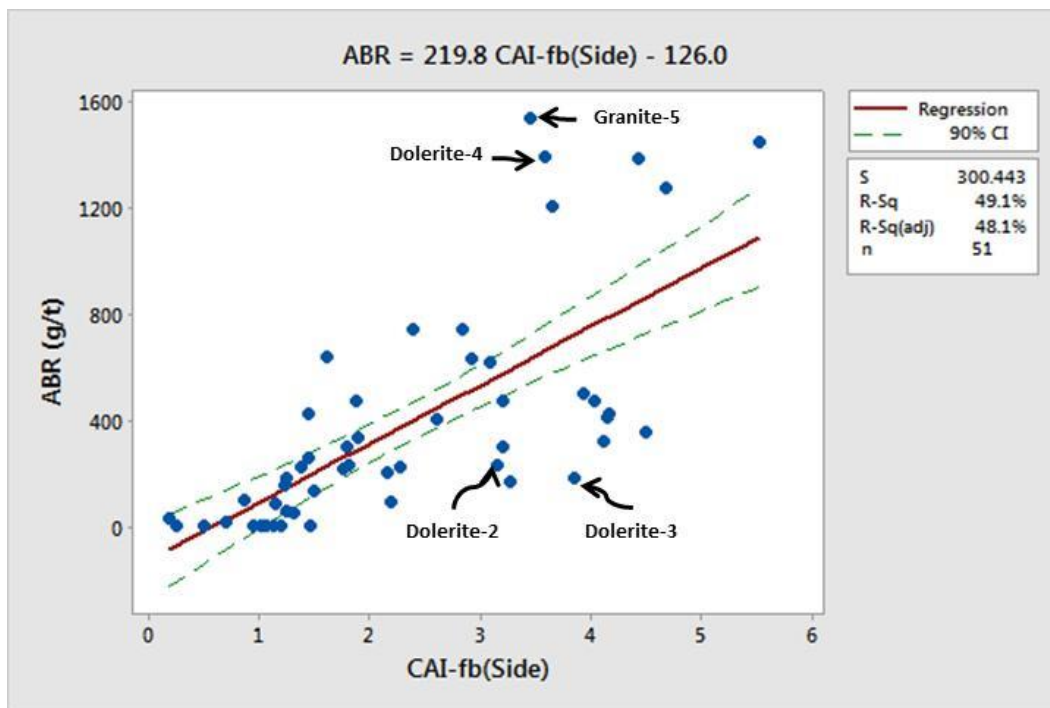
Figure 7.6. Relationship of LCPC abrasivity co-efficient with CERCHAR abrasivity index for all rocks.

According to Buchi et al. (1995) the correlation between the two test methods (LCPC and CERCHAR abrasivity indices) was not good for all groups of rocks. Rocks with similar mineralogical composition can lead to identical values in the case of one test, in the other they result in a considerable difference in their abrasivity class. In the present study when the LCPC and CERCHAR abrasivity indices for sedimentary rocks were plotted (Figure 7.7) a fairly good correlation (R^2 = 78.50 %) was found. It is interesting to note that the developed equation (Figure 7.7) closely coincides with the correlations already published in the literature (Buchi et al., 1995; Thuro et al., 2007; Thuro and Kasling, 2009; Kasling and Thuro, 2010). When the LCPC and CERCHAR abrasivity indices for igneous and metamorphic rocks were correlated (Figure 7.8) a poor correlation was found. The anomalous scatter of data points can be seen in Figure 7.8, showing higher values of ABR (g/t) against relatively lower values of CAI_{fb} and vice

versa. The probable reason for this scatter could be the higher UCS values of these rocks affecting the ABR (g/t) values.
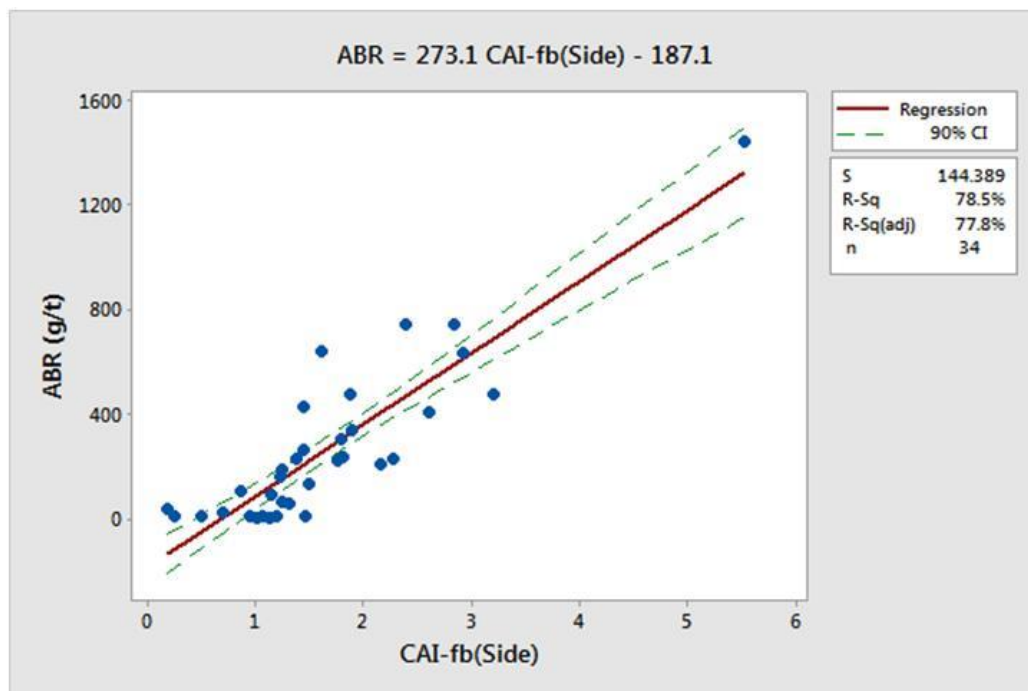
Figure 7.7. Relationship of LCPC abrasivity co-efficient with CERCHAR abrasivity index for sedimentary rocks only.
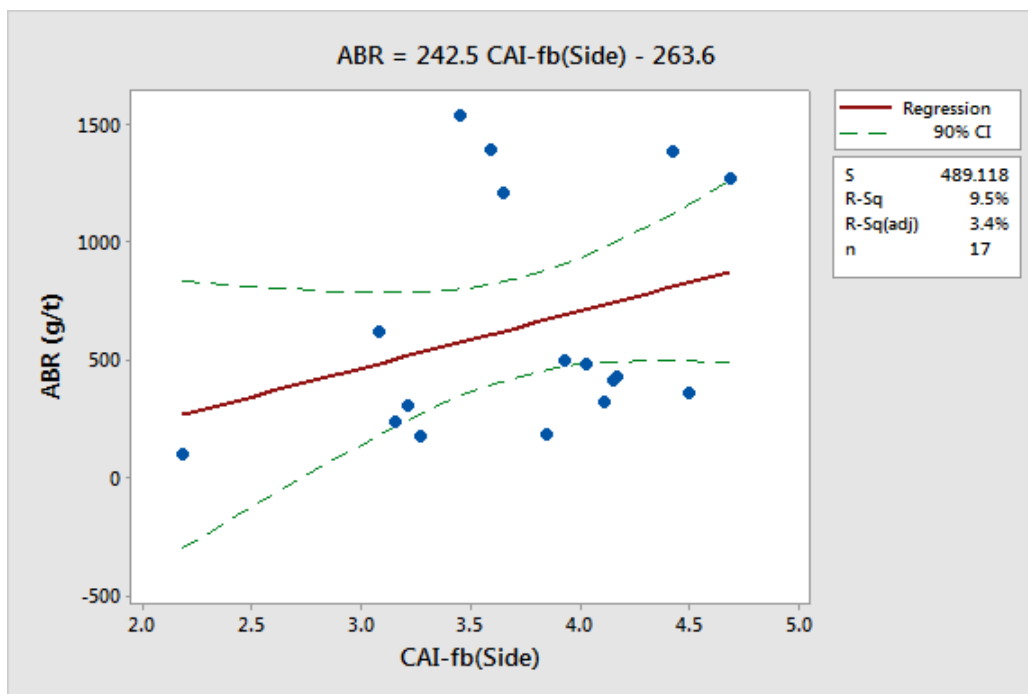
Figure 7.8. Relationship of LCPC abrasivity co-efficient with CERCHAR abrasivity index for igneous and metamorphic rocks only.

7.3.2. Influence of Rock Strength on LCPC Abrasivity Co-efficient. Published literature show a general upward trend of LCPC abrasivity coefficient (ABR, g/t) with the corresponding increase in the rock strength. Similarly, in this work the increase in both uniaxial compressive strength (UCS) and Brazilian tensile strength (BTS) of rocks (Figures 7.9 and 7.10) shows an overall linear increase in the ABR (g/t) values. The scatter plot between LCPC abrasivity coefficient, ABR (g/t) and UCS earlier proposed by Buchi et al. (1995) also illustrates a very limited degree of correlation as developed here in this work. The cited author further explained that a good correlation can only be expected within the same rock type (for example sandstone) with however different strengths, as well as for rock types of similar mineralogical composition (quartz content and equivalent quartz content). Moreover, the equations developed (Figures 7.9 and 7.10) also approximately match with the correlations already proposed by Gonzalez et al. (2014).

An anomalous data point showing low strength values (UCS = 44.80; BTS = 2.30) with considerably high LCPC abrasivity coefficient (ABR = 1273 g/t) can be noticed in Figures 7.9 and 7.10, which corresponds to a granitic rock of Tobra Formation (Granite-6). The likely reason for this low strength may be the weathering of these boulders beds involved during the depositional process (tillite), by an inland ice sheet (local glaciation) in the Tobra Formation of Eastern Salt Range, Punjab (Shah, 2009). Additionally, large variability or scatter of data is also evident in these plots depicting the effect of natural heterogeneity present in rocks.
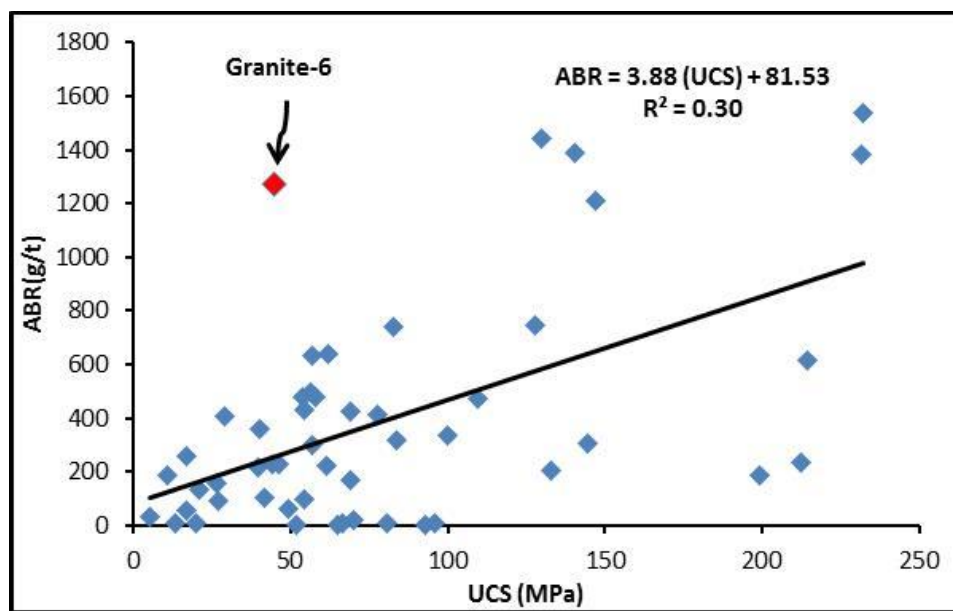
Figure 7.9. Relation between LCPC abrasivity coefficient and UCS of the rocks tested.
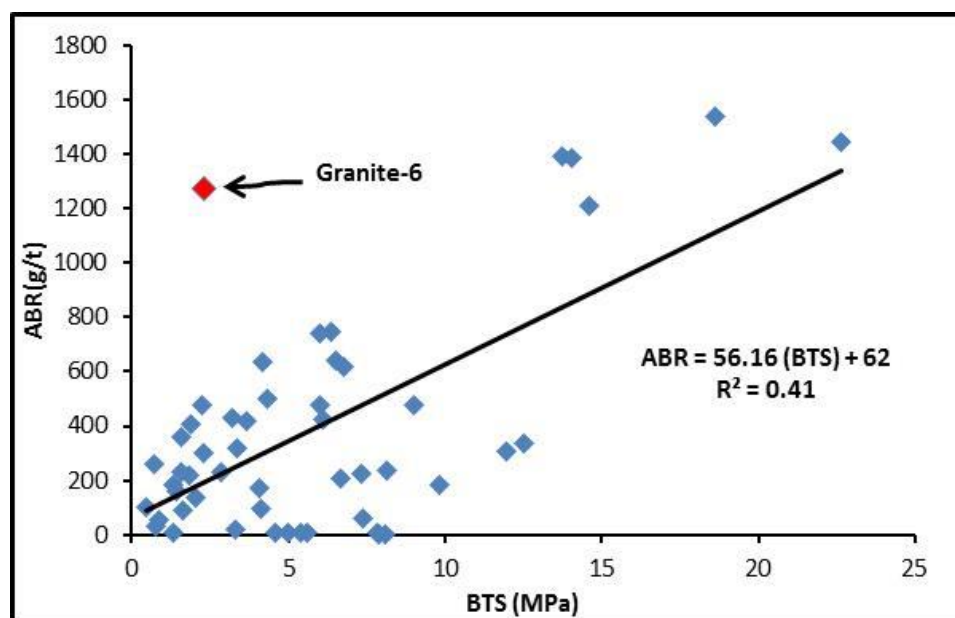
Figure 7.10. Relation between LCPC abrasivity coefficient and BTS of the rocks tested.

7.3.3. Influence of Rock Strength on LCPC Breakability Index. The effect of rock strength (UCS and BTS) on the LCPC breakability index, BR (%) is illustrated in Figures 7.11 and 7.12. The decrease in breakability or grindability of rock with the increase in uniaxial compressive strength and Brazilian tensile strength is expected as shown in the regression plots. The plots show moderate exponential decreasing correlations between the LCPC breakability index and rock strength including UCS and BTS. The results of this study are in total agreement with the past investigations (Buchi

et al., 1995; Gonzalez et al., 2014). In Figure 7.12, an exceptionally higher value of breakability (BR = 40.36 %) was observed for a Sandstone-16 rock sample of Hazira Formation with also a higher Brazilian tensile strength (BTS) of 22.67 MPa. This extraordinary higher BTS value of 22.67 MPa may be ascribed to the thinly bedded nature of Sandstone-16 rock sample. The phenomenon of higher breakability value (BR = 40.36 %) of this sandstone could also be due to the fact that the strength of overall rock matrix is not considered in the LCPC test and the sample material is broken down to a grain size range of 4 to 6.3 mm (Kohler et al., 2011).
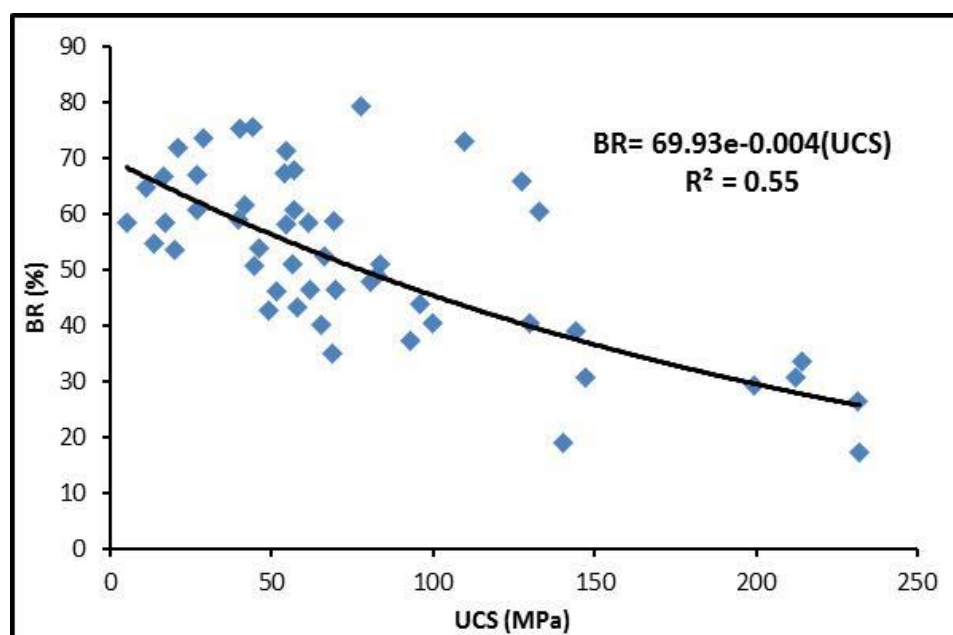
Figure 7.11. Correlation between LCPC breakability index and UCS of the rocks tested.
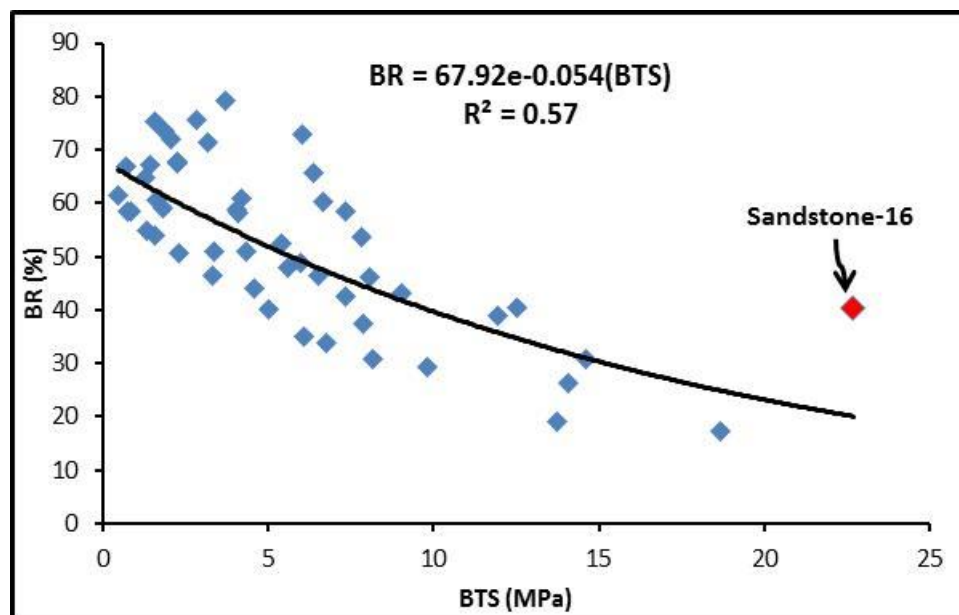
Figure 7.12. Correlation between LCPC breakability index and BTS of the rocks tested.

7.3.4. Correlation of LCPC Abrasivity Coefficient with Geotechnical Wear Indices. This part includes the relationships of ABR (g/t) with most commonly applied geotechnical wear indices including Quartz Content, Quartz Equivalent Content, Schimazek's F-value and Rock Abrasivity Index (RAI). Rather than testing specific wear systems, these wear indices relate to standard inherent rock properties and therefore use a different approach for the evaluation of rock abrasivity (Plinninger and Restner, 2008).

7.3.4.1. LCPC abrasivity coefficient versus Schimazek's F-value. Figure 7.13 shows the regression plot of ABR (g/t) with the Schimazek's F-value where a fair quality power function correlation is found. The proposed equation in general shows an increase in LCPC Abrasivity Coefficient values of the tested rocks with the corresponding increase in their Schimazek's F-values. The result of this work is completely in accordance with the published past investigations (Paschen, 1980; Verhoef et al., 1990; Deketh, 1991; Bisschop, 1991) conducted on pin-on-disc tests and shaper cutting and abrasion tests, where the wear rate of instrumental test pieces (mass loss of pin, wear of chisel) also increased with corresponding increase in the Schimazek's F-value (Verhoef, 1997).

It is noteworthy that there is a vertical scatter in the values of ABR (g/t) in the plotted area (Figure 7.13) around Schimazek's F-values in the range of 2 to 3.5 (N/mm). These data points correspond to Granite-6, Granitic Gneiss-1, Dolerite-4, Andesite and Dolerite-3 rock samples. This variation of ABR (g/t) values may be attributed to the quartz equivalent content values ranging from 36.42% to 82.41% which has a direct influence on the Schimazek's F-values. Moreover, some previous studies demonstrated that there is an increase in ABR (g/t) values with the corresponding increase in quartz equivalent percentage of the rock samples (Thuro et al., 2006; Thuro et al., 2007; Beckhaus, 2010; Hashemnejad et al., 2015). The scatter in ABR (g/t) values at Schimazek's F-values in the range of 2 to 3.5 (N/mm), may also be attributed to the BTS values ranging from 2.30 to 14.06 MPa which are directly affecting the Schimazek's F-values (being a multiplying factor with quartz equivalent content in the computation of Schimazek's F-value).
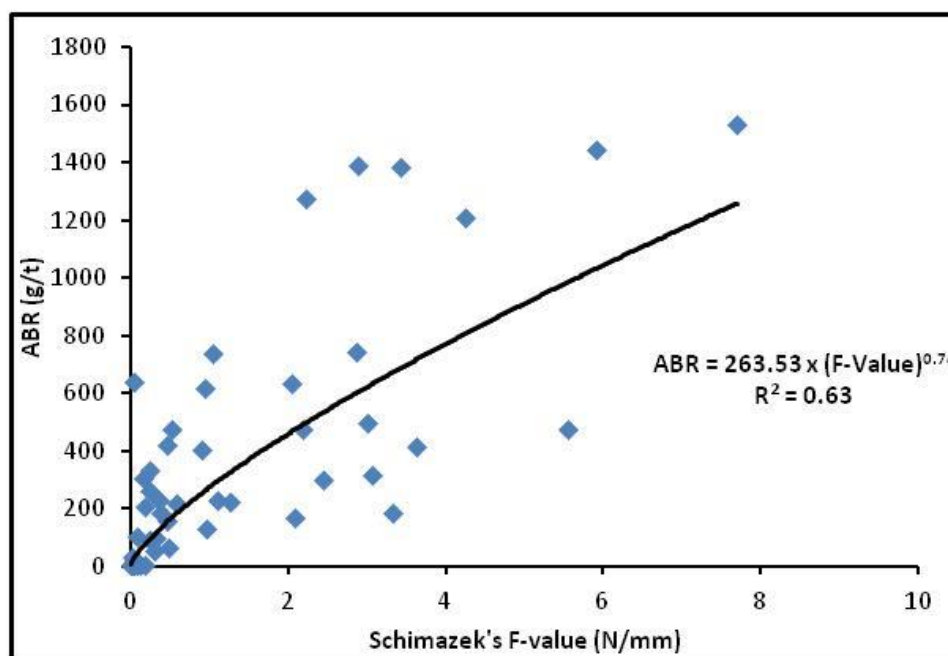
Figure 7.13. Correlation between LCPC abrasivity coefficient and Schimazek's F-value of rock samples.

7.3.4.2. LCPC abrasivity coefficient versus rock abrasivity index (RAI). Figure 7.14 shows relationship of LCPC abrasivity coefficient (ABR, g/t) values with RAI. A fair power function increasing trend can be observed in the presented correlation. No work is published to date correlating the results of LCPC abrasivity coefficient with

RAI. However, the correlations of CAI with RAI are available in the literature which shows a logarithmic increase between CAI and RAI values (Plinninger, 2002; Plinninger et al., 2004; Majeed and Abu Bakar, 2015).

It is interesting to note that there is an anomalous scatter of plotted data (Figure 7.14) around the RAI value of 80. These data points include Dolerite-3, Dolerite-4 and Andesite rock samples having equivalent quartz content (EQC) in a close range from 36.42 to 53.76 %. This variation around the RAI value of about 80 may be attributed to the UCS (ranging from 140.50 to 231.46 MPa), which is directly impacting the RAI values (being a multiplying factor with EQC in the calculation of RAI). Additionally, an extraordinary high ABR value of 1273 (g/t) with relatively lower RAI value of 81.63 can be noticed (Figure 7.14) for an igneous Granite-6 rock sample (UCS = 44.80 MPa). The likely reason for its lower RAI value of 81.63 could be its significantly lower UCS value.
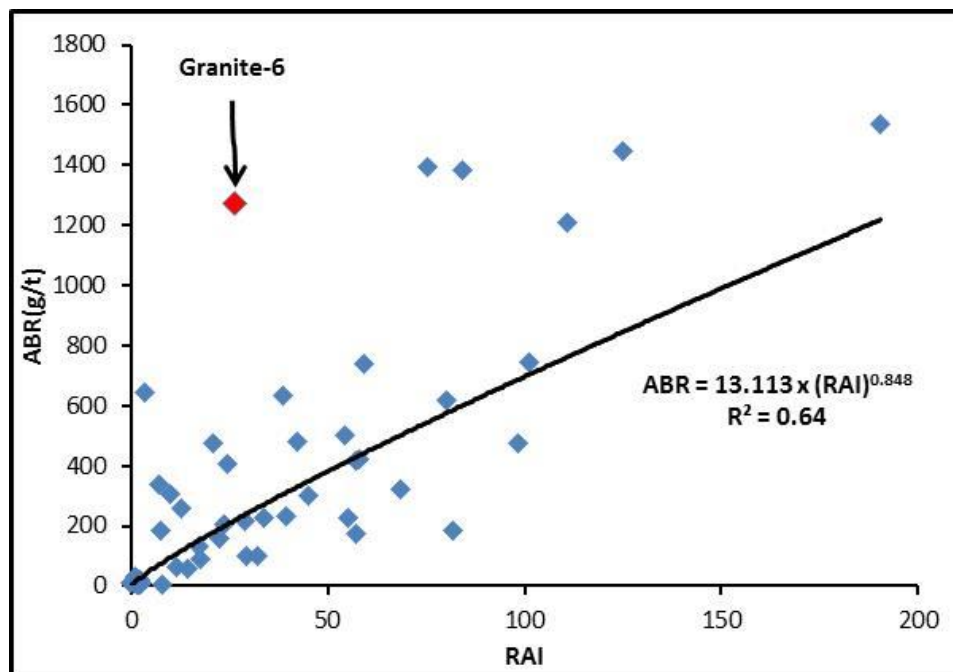
Figure 7.14. Correlation between LCPC abrasivity coefficient and RAI of rock samples.

7.3.4.3. LCPC abrasivity coefficient versus quartz and equivalent quartz content. Figures 7.15 and 7.16 show the scatter plots of ABR (g/t) with quartz content and equivalent quartz content respectively. No reasonable correlation is visible. Results obtained in the present study are confirmed by the findings of Kohler et al., (2011), where ABR (g/t) and equivalent quartz content (%) of 22 carbonate-crystalline fluvial

gravel samples were evaluated and no correlation was found between the two parameters. It is probably due to the existence of intrinsic heterogeneity and anisotropy present in natural materials and rocks. It may also be attributed to the rocks belonging to the three generic types having different characteristics. In contrast, numerous investigations (Festl, 2006; Thuro et al., 2006; Barzegari et al., 2015; Dullmann et al., 2014; Hashemnejad et al., 2015) have confirmed the existence of good correlation between ABR (g/t) and equivalent quartz content (%). It is however, pertinent to mention here that in studies conducted by Dullmann et al. (2014) and Barzegari et al. (2015), these correlations (ABR (g/t) versus EQC) were found by utilizing the pre-defined mixtures of soils with different quartz contents, which in actuality is a deviation from the behavior of natural materials like rocks.
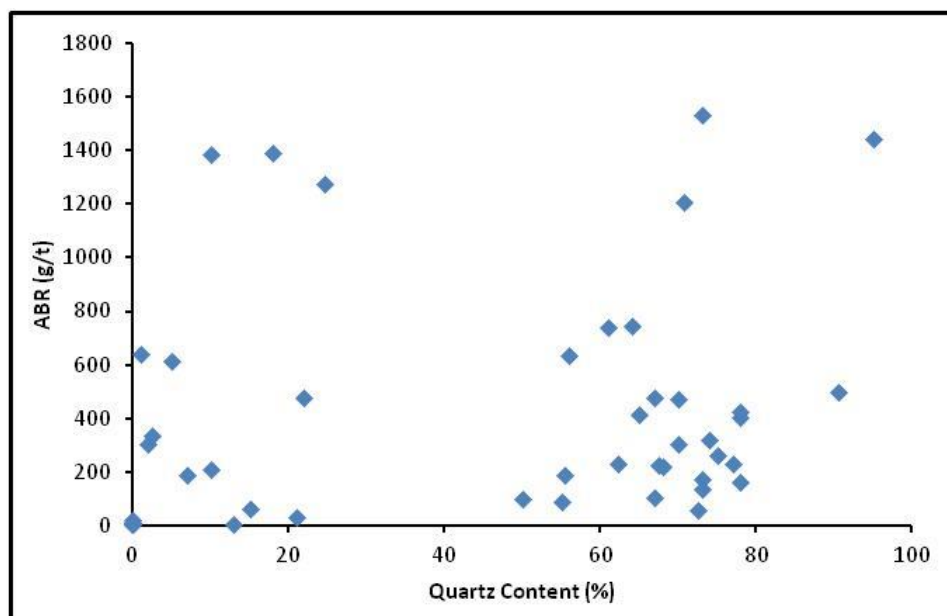
Figure 7.15. Scatter plot of ABR(g/t) against Quartz Content (%).
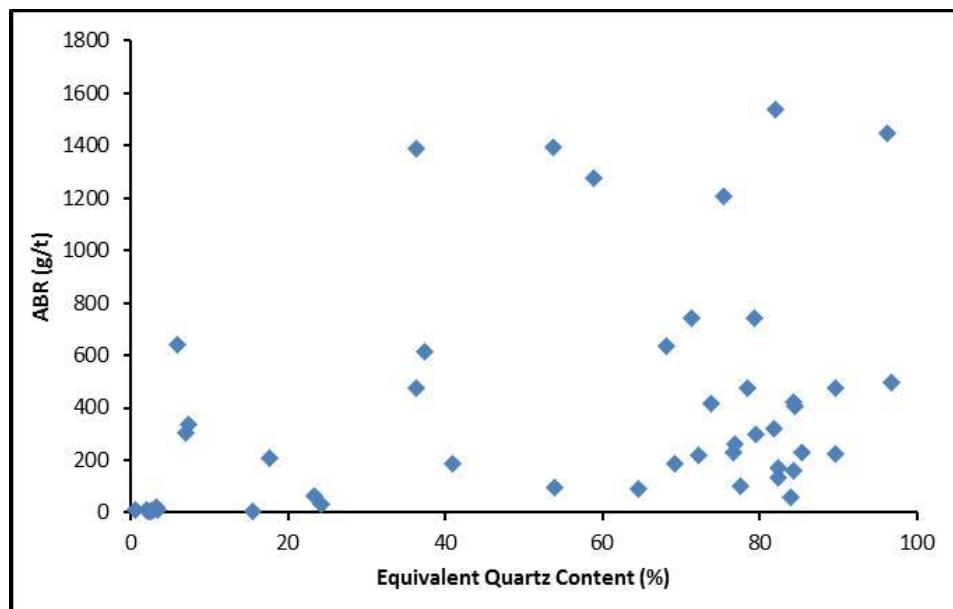
Figure 7.16. Scatter plot of ABR(g/t) against Equivalent Quartz Content (%).

7.3.5. Correlation of LCPC Abrasivity Coefficient with Rock Physical Properties. This section comprises the relationships of ABR (g/t) with commonly utilized physical properties of rocks including dry density, porosity and sonic wave velocity (v_p). At present very little work is published relating ABR (g/t) with the physical rock properties. Figures 7.17, 7.18 and 7.19 show the relationships between ABR (g/t) and dry density, porosity and sonic velocity (V_p) for all rocks respectively. Expectedly the ABR (g/t) increases with increasing dry density of rocks as shown in Figure 7.17. This trend is in agreement with the earlier findings of Gonzalez et al. (2014), where the LCPC abrasivity coefficient increased with increasing rock density. Figure 7.18 shows a logarithmic decreasing trend of ABR (g/t) with the increasing porosity of rocks ($R^2 = 0.28$). ABR (g/t) when plotted against the sonic velocity (V_p) a linear upward relationship was found (Figure 7.19) giving a very weak correlation ($R^2 = 0.034$). It is interesting to note that in all the three graphs presented below there is a separate cluster of data points having ABR (g/t) values ranging from 1208 to 1534.5 (g/t) which correspond to the Quartzite-2, Granite-6, Andesite, Dolerite-4, Sandstone-16 and Granite-5 rock samples. The likely explanation for this observable fact is the geomechanical property (UCS) influencing the ABR (g/t) values.
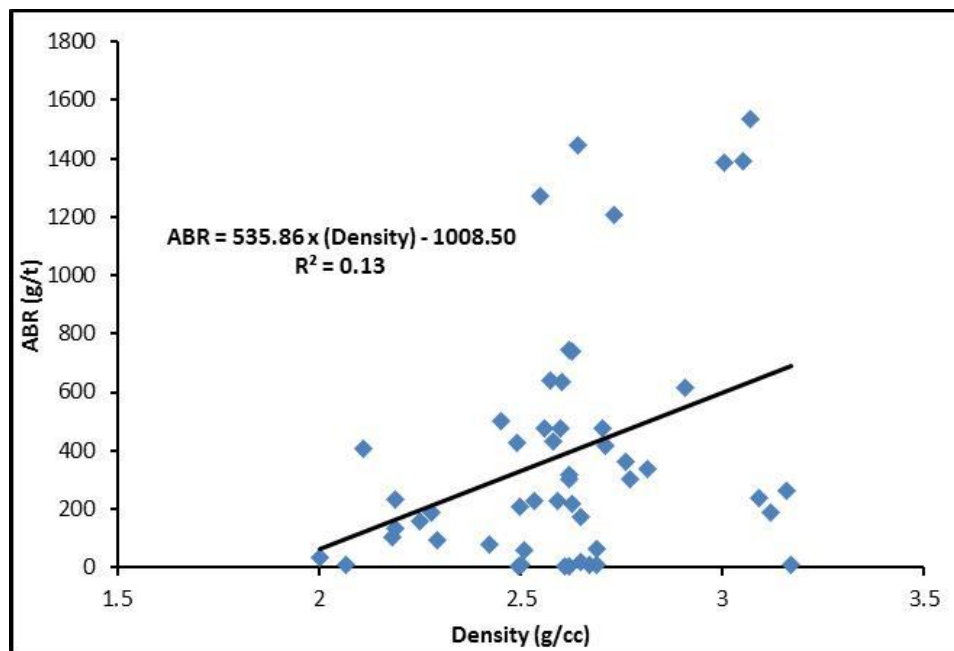
Figure 7.17. Graph of ABR (g/t) versus dry density (g/cc).
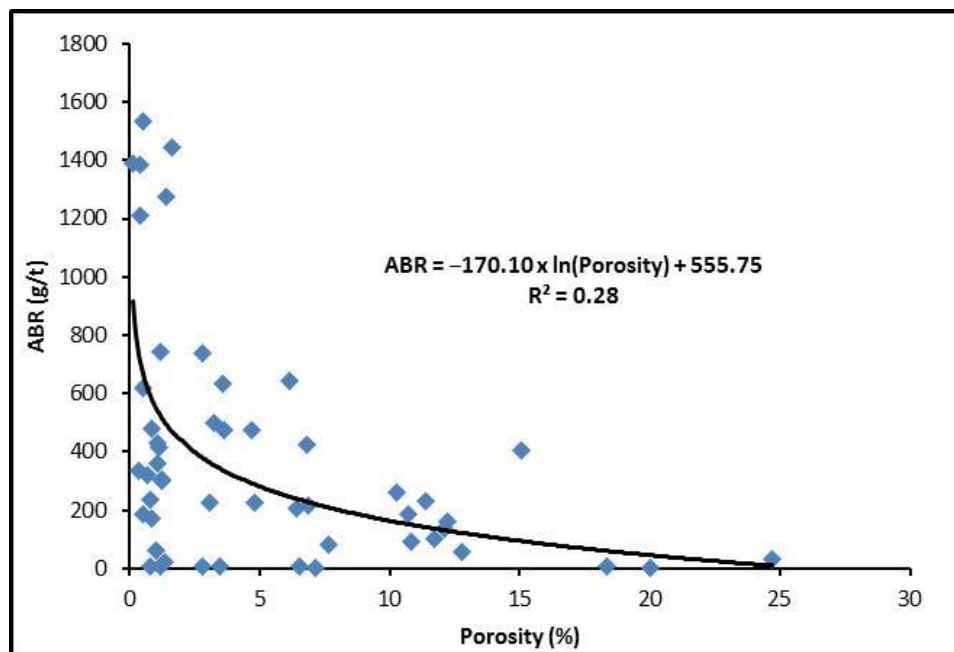
Figure 7.18. Graph of ABR (g/t) versus porosity (%).
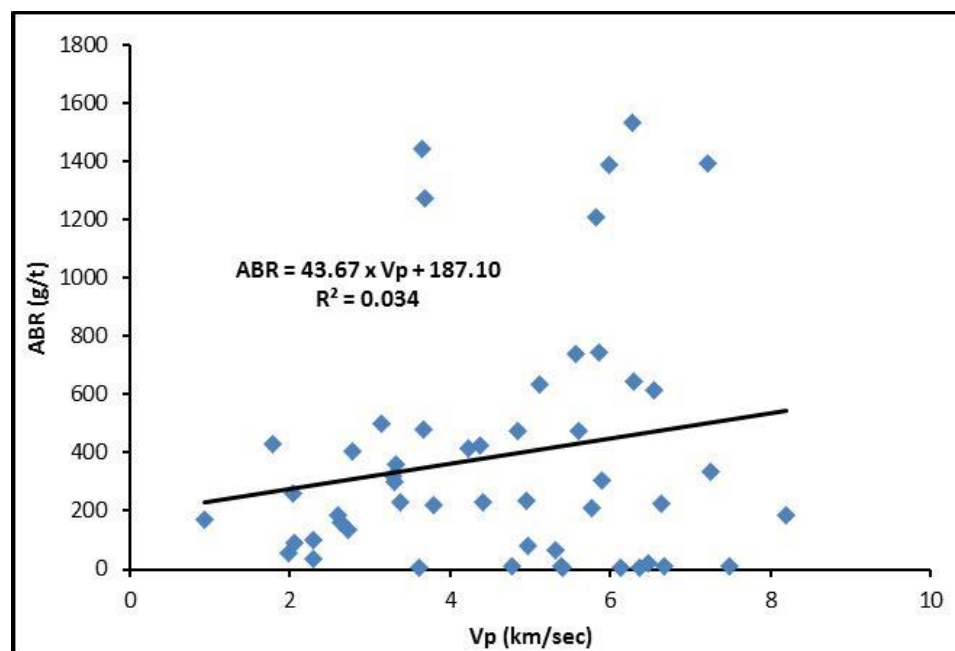
Figure 7.19. Graph of ABR (g/t) versus V_p (km/sec).

7.3.6. Correlation of LCPC Breakability Index with Physical Rock Properties. The correlations between BR (%) and physical properties [dry density, porosity and sonic velocity (V_p)] for all rocks are shown in Figures 7.20, 7.21 and 7.22 respectively. Figure 7.20 illustrates a decreasing exponential trend between the LCPC breakability index and dry density of rocks. Contrary to that the empirical relation proposed by Gonzalez et al. (2014) is a polynomial function with an inverted convex fit. Figure 7.21 shows a power function increasing trend of BR (%) with the rock porosity. A vertical scatter of plotted values of LCPC breakability index (BR, %) about the porosity of (0.1 to 1.5 %) can be noticed. These data points of BR (%) lying in the range of 50 to 80 % include Granitic Gneiss-1, Granite-1, Granite-2, Granite-3, Granite-4 and Migmatite rock samples having relatively lower UCS values (40 to 83 MPa) and hence possibly giving higher breakability values. On the other hand the data points of LCPC breakability index (Figure 7.21) lying in the range of 17 to 34 % include Dolerite-1, Dolerite-2, Dolerite-4, Granite-5 and Andesite rock samples having considerably higher UCS values (141 to 232 MPa) and therefore are giving lower breakability values. As expected when plotted BR (%) against V_p (km/sec) in Figure 7.22, a negative linear curve was observed with a reasonable correlation coefficient (R= 62%).
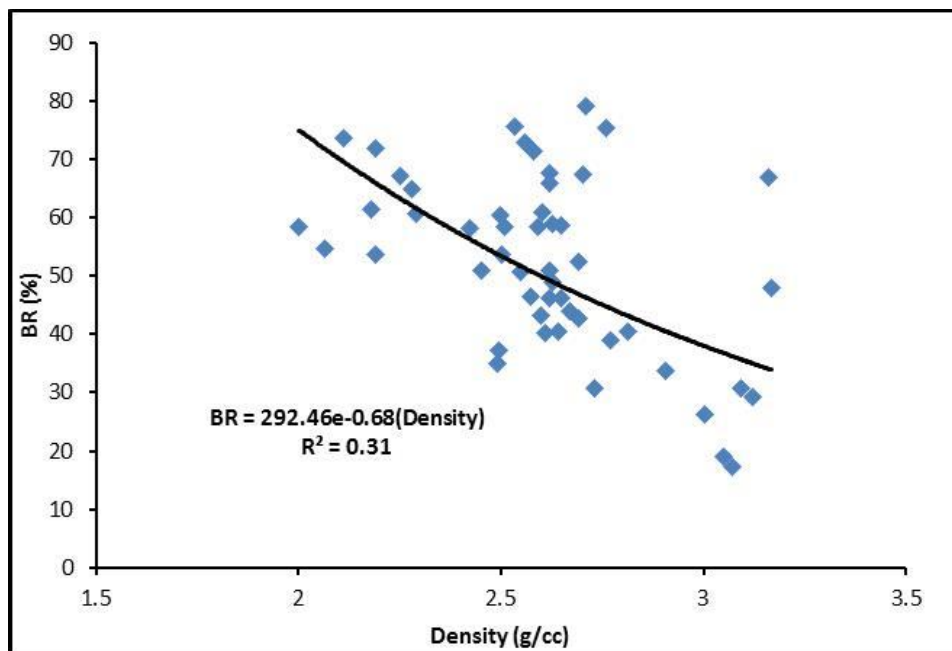
Figure 7.20. Graph of BR (%) versus dry density (g/cc).
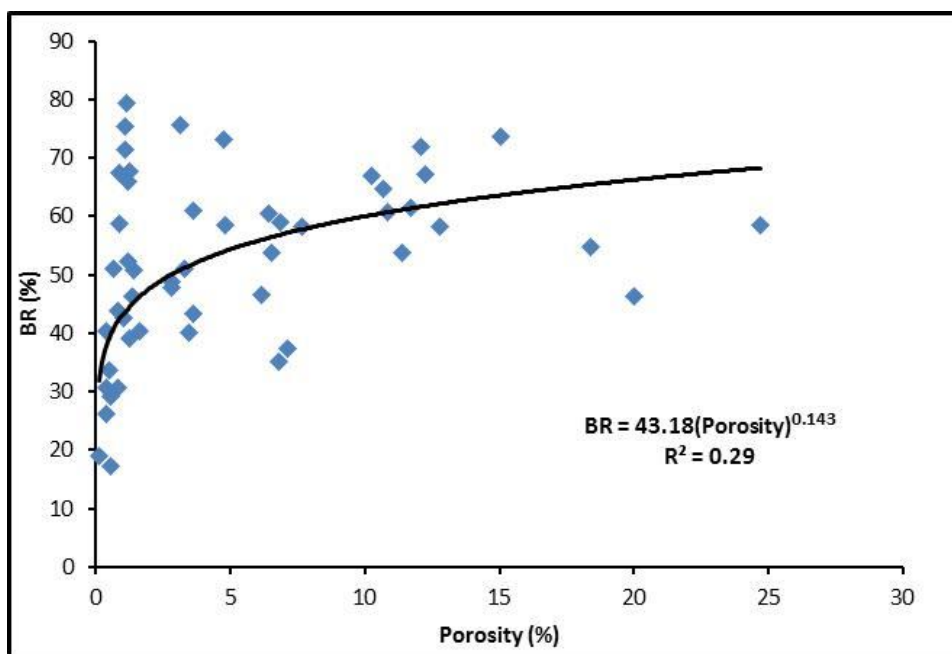
Figure 7.21. Graph of BR (%) versus porosity (%).
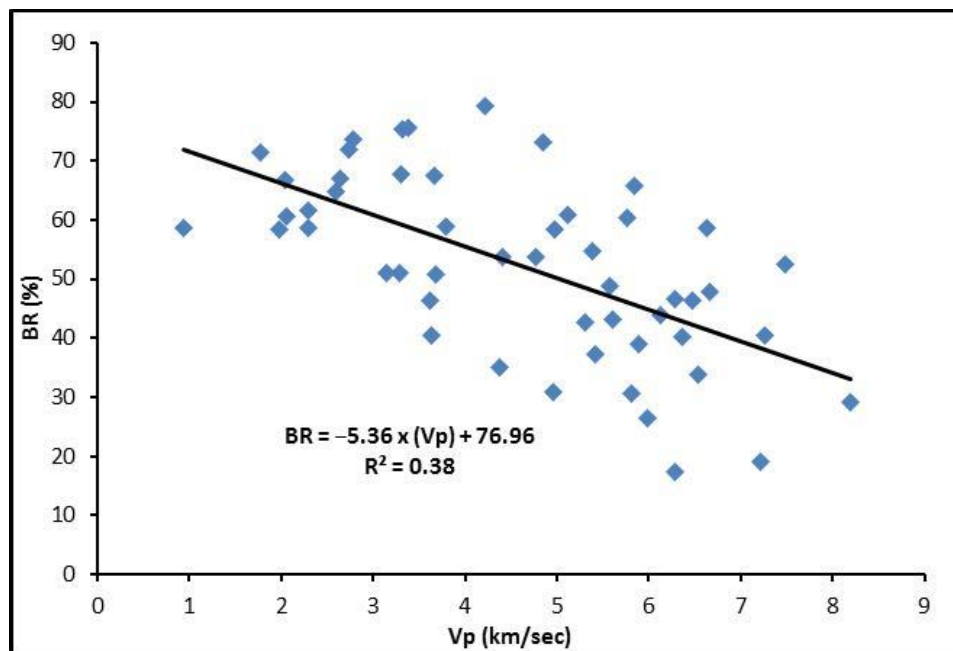
Figure 7.22. Graph of BR (%) versus V_p (km/sec).

7.3.7. Summary of Correlations of LCPC Test Results with Rock Properties.
Table 7.3 lists the correlations of LCPC abrasivity coefficient (ABR) and LCPC breakability index (BR) with rock properties, developed in this research work. The LCPC test results (Table 7.3) in most cases do not show fair relationships especially with the petrographical parameters (Quartz content and quartz equivalent content) and physico-mechanical properties of rocks. The shortcomings of this test have already been highlighted in the past literature. According to Köhler et al. (2011) rock breaking and sample preparation processes have not yet been standardized and different laboratories quote different values of ABR for the same sample. Moreover during sample preparation process for the LCPC test the rock material is broken down to a grain size of 4 to 6.3 mm and the overall strength of rock matrix is not considered in the obtained ABR (g/t) value. Plinninger and Restner (2008) also highlighted that to date no relationships are present for the prediction of tool wear rate in hard rock drilling or cutting based on LCPC abrasivity coefficient. However the LCPC test finds main application for the abrasivity testing of in soils and very soft rocks. The cited authors further cautioned that even in the case of soils the most significant soil properties are either changed or even discarded during sample preparation. Therefore there is an urgent need for the LCPC test to be

standardized by international standardization bodies including ASTM or ISRM suggested methods.

Table 7.3. List of correlations developed in this study.

Sr. No.	Correlation
1	$ABR = 219.8 \times CAI_{fb(side)} - 126.0$ [for all 51 rock samples]; ($R^2 = 0.49$)
2	$ABR = 273.1 \times CAI_{fb(side)} - 187.1$ [for all 34 sedimentary rock samples]; ($R^2 = 0.79$)
3	$ABR = 3.88 \times UCS + 81.53$; ($R^2 = 0.30$)
4	$ABR = 56.1 \times BTS + 62$; ($R^2 = 0.41$)
5	$BR = 69.93 \times e^{-0.004(UCS)}$; ($R^2 = 0.55$)
6	$BR = 67.92 \times e^{-0.054(BTS)}$; ($R^2 = 0.57$)
7	$ABR = 263.53 \times (F\text{-value})^{0.74}$; ($R^2 = 0.63$)
8	$ABR = 13.113 \times (RAI)^{0.848}$; ($R^2 = 0.64$)
9	$ABR = 535.86 \times (Density) - 1008.50$; ($R^2 = 0.13$)
10	$ABR = -170.10 \times \ln(Porosity) + 555.75$; ($R^2 = 0.28$)
11	$BR = 292.46 \times e^{-0.68(Density)}$; ($R^2 = 0.31$)
12	$BR = 43.18 \times (Porosity)^{0.143}$; ($R^2 = 0.29$)
13	$BR = -5.36 \times (Vp) + 76.96$; ($R^2 = 0.38$)

7.4. ABRASIVITY CHARACTERIZATION OF TESTED ROCK SAMPLES BASED ON LCPC TESTS

This section presents the abrasivity characterization of all 51 rock samples included in this research collected from various rock formations of Pakistan based on LCPC test. The review of literature shows that rock abrasivity classifications based on ABR (g/t) values have been proposed by Buchi et al. (1995) and Thuro et al. (2006, 2007), which are displayed in Chapter 2. Tables 7.4, 7.5 and 7.6 lists the abrasivity characterization of LCPC test results of rock samples included in this research work in accordance with the earlier proposed classifications (Buchi et al., 1995 and Thuro et al., 2006, 2007) for igneous, metamorphic and sedimentary rocks respectively. Whereas figures 7.23, 7.24 and 7.25 presents the column charts for igneous, metamorphic and sedimentary rock samples respectively showing ABR (g/t) values arranged in ascending order.

Table 7.4. Characterization of LCPC abrasivity coefficient, ABR (g/t) values of selected sedimentary rocks of Pakistan.

Sr. No.	Rock Sample	ABR (g/t)	Abrasivity Classification as per Buchi et al. (1995)	Abrasivity Classification as per Thuro et al. (2006, 2007)
1	Siltstone-1	63.00	Very Low	Not Very Abrasive
2	Siltstone-2	476.00	Very Low	Medium Abrasive
3	Sandstone-1	218.00	Very Low	Slightly Abrasive
4	Sandstone-2	102.00	Very Low	Slightly Abrasive
5	Sandstone-3	744.00	Low	Very Abrasive
6	Sandstone-4	159.93	Very Low	Slightly Abrasive
7	Sandstone-5	228.00	Very Low	Slightly Abrasive
8	Sandstone-6	474.00	Very Low	Medium Abrasive
9	Sandstone-7	226.00	Very Low	Medium Abrasive
10	Sandstone-8	186.00	Very Low	Slightly Abrasive
11	Sandstone-9	406.00	Very Low	Medium Abrasive
12	Sandstone-10	260.00	Very Low	Medium Abrasive
13	Sandstone-11	134.00	Very Low	Slightly Abrasive
14	Sandstone-12	91.00	Very Low	Not Very Abrasive
15	Sandstone-13	232.00	Very Low	Slightly Abrasive
16	Sandstone-14	57.00	Very Low	Not Very Abrasive
17	Sandstone-15	424.00	Very Low	Medium abrasive
18	Sandstone-16	1444.56	Medium	Extremely Abrasive
19	Sandstone-17	633.00	Low	Very Abrasive
20	Sandstone-18	740.00	Low	Very Abrasive
21	Chamositic Siderite	4.00	Very Low	Not Abrasive
22	Dolomite-1	642.00	Low	Very Abrasive
23	Dolomite-2	304.00	Very Low	Medium Abrasive
24	Dolomite-3	336.00	Very Low	Medium Abrasive
25	Dolomite-4	208.00	Very Low	Slightly Abrasive
26	Limestone-1	6.00	Very Low	Not Abrasive
27	Limestone-2	7.00	Very Low	Not Abrasive
28	Limestone-3	8.00	Very Low	Not Abrasive
29	Limestone-4	8.01	Very Low	Not Abrasive
30	Limestone-5	4.01	Very Low	Not Abrasive
31	Limestone-6	20.00	Very Low	Not Abrasive
32	Limestone-7	7.98	Very Low	Not Abrasive
33	Rock Gypsum	8.00	Very Low	Not Abrasive
34	Marl	32.99	Very Low	Not Abrasive

Table 7.5. Characterization of LCPC abrasivity coefficient, ABR (g/t) values of selected igneous rocks of Pakistan.

Sr. No.	Rock Sample	ABR (g/t)	Abrasivity Classification as per Buchi et al. (1995)	Abrasivity Classification as per Thuro et al. (2006, 2007)
1	Dolerite-1	616.00	Low	Very Abrasive
2	Dolerite-2	235.53	Very Low	Slightly Abrasive
3	Dolerite-3	186.00	Very Low	Slightly Abrasive
4	Dolerite-4	1391.28	Medium	Extremely Abrasive
5	Granite-1	359.64	Very Low	Medium Abrasive
6	Granite-2	319.36	Very Low	Medium Abrasive
7	Granite-3	415.58	Very Low	Medium Abrasive
8	Granite-4	477.52	Very Low	Medium Abrasive
9	Granite-5	1534.50	High	Extremely Abrasive
10	Granite-6	1273.00	Medium	Extremely Abrasive
11	Migmatite	301.40	Very Low	Medium Abrasive
12	Andesite	1385.00	Medium	Extremely Abrasive

Table 7.6. Characterization of LCPC abrasivity coefficient, ABR (g/t) values of selected metamorphic rocks of Pakistan.

Sr. No.	Rock Sample	ABR (g/t)	Abrasivity Classification as per Buchi et al. (1995)	Abrasivity Classification as per Thuro et al. (2006, 2007)
1	Granitic Gneisse-1	171.66	Very Low	Slightly Abrasive
2	Granitic Gneisse-2	429.00	Very Low	Medium Abrasive
3	Phyllite	80.00	Very Low	Not Very Abrasive
4	Quartzite-1	498.50	Very Low	Medium Abrasive
5	Quartzite-2	1208.00	Medium	Very Abrasive
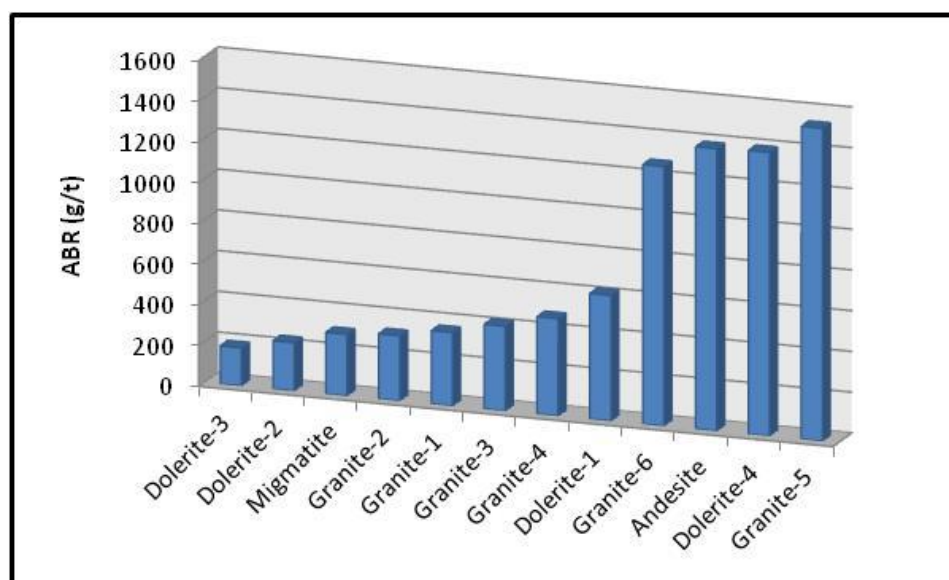
Figure 7.23. Column chart of ABR (g/t) values of igneous rock samples arranged in ascending order.
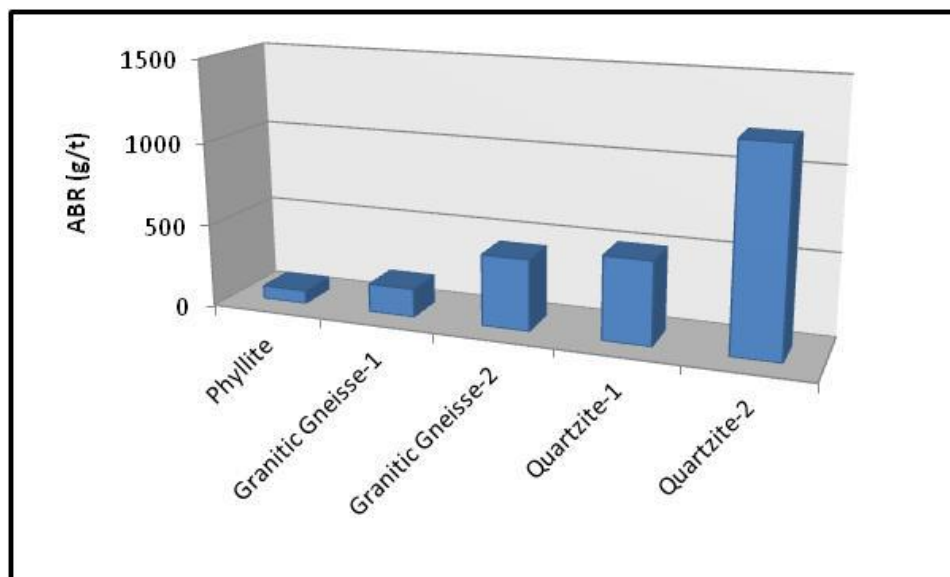
Figure 7.24. Column chart of ABR (g/t) values of metamorphic rock samples arranged in ascending order.
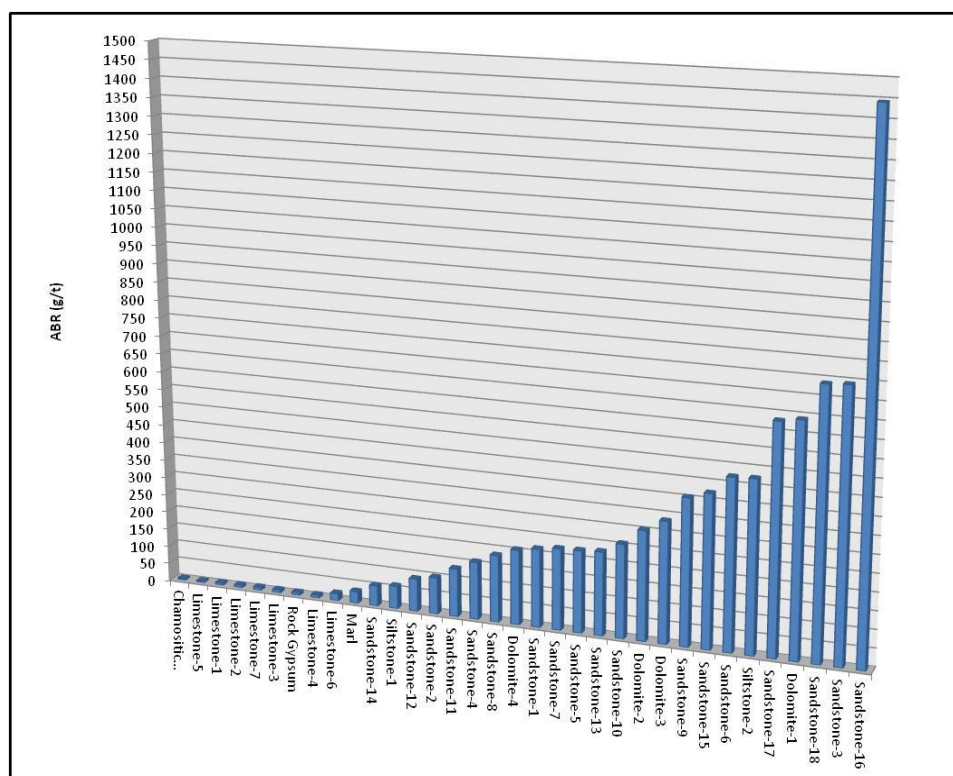
Figure 7.25. Column chart of ABR (g/t) values of sedimentary rock samples arranged in ascending order.

8. DISCUSSION: PARAMETRIC STUDY OF NTNU/SINTEF CUTTER LIFE INDEX

This section discusses the NTNU/SINTEF Abrasion Value Steel (AVS) tests and the computed Cutter Life Index (CLI) values for 10 rock samples selected out of a total data base of 51 rocks collected from various locations of Pakistan. The testing methodology is provided in chapter 3 whereas the detailed test results are presented in chapter 4.

The discussion of results in this section is confined to the effect of variations in the fraction size of rock abrasion powder utilized for the determination of AVS and the effect of change in disc speed of the test apparatus on AVS test results. Moreover the relationship of CLI with CERCHAR abrasivity index (CAI), LCPC abrasivity coefficient (ABR, g/t) and mechanical rock parameters are also discussed.

8.1. BACK GROUND

The NTNU/SINTEF Cutter Life Index (CLI) was developed in the years 1980-1983, for the estimation of cutter life in boring hours in relation with mechanized rock excavation using TBM. CLI is computed on the basis of NTNU drillability tests including Sievers'J-value (SJ) and Abrasion Value Steel (Zare and Bruland, 2013). The standardized testing procedures of SJ and AVS tests are provided in the "draft of DRI, BWI, CLI standard" (Dahl, 2003). Later on the AVS test is further modified for the development of NTNU, Soil Abrasion Test (SAT) which is also performed on the same apparatus as utilized for AVS testing. In comparison to AVS test, the SAT test utilizes soil sample passing 4.0 mm sieve size instead of crushed rock powder having fraction size less than 1.0 mm. The original SAT test used the same cutter steel wear piece as used for AVS test but afterwards a modification in the size of SAT test piece has been made (Nilsen et al., 2007).

Some irregularities and deficiencies in the testing procedure of SAT device have been reported by Barzegari et al. (2015), which are described below:

1) During test performance the soil particles are powdered after passing and crushing under the test piece carrying a static weight of 10 kg. The powdering of soil grains cover

the track on rotating disc immediately under the test piece and hinders the interaction between the fresh soil particles and the test piece.

2) The well-rounded particles escape out of the testing track because of the centrifugal force of the rotating disc and also due to the contact between test piece and soil grains.

3) It is difficult to control the feed flow at the specified rate of approximately 80 g/min and gathering of soil heaps behind the test piece.

4) At the specified feed flow rate of 80 g/min, there is tendency for soil particles to pass through the sides of the wear piece.

The main irregularities of the SAT test highlighted by Barzegari et al. (2015) are also valid for AVS test due to the same testing device and procedure involved. According to Bruland (2016) "the flow rate of approx. 80 g/min is controlled by varying it according to how the powder is travelling under the test piece. If the test piece is "plowing" the powder, i.e. much powder is passing on the sides of the test piece, the flow rate is reduced. If no powder is passing on the sides of the test piece, the flow rate is increased until just a small amount of powder is passing the sides of the test piece. The meaning of this is that the wear should occur between the test piece and the rotating plate, not on the sides of the test piece". In this current work the two main parameters affecting the AVS test results including the particle size of rock abrasion powder and speed of the turn table are further investigated to resolve the irregularities or deficiencies highlighted earlier.

8.2. IMPACT OF PARTICLE SIZE OF ROCK ABRASION POWDER ON AVS VALUES

The particle size distribution of the rock abrasion powder for the AVS test, prepared according to the standard specifications (Dahl, 2003) has an upper grain size limit of 1 mm, out of which (70 ± 5) % of the rock powder is less than 0.5 mm size. In order to investigate the impact of variation in particle size distribution of the crushed rock powder on the abrasion of AVS test pieces, four different particle size ranges were selected keeping the boundary conditions same. Meaning the upper grain size limit of all the fractions included in this study is less than 1mm size. The experimental matrix is presented in Table 8.1.

Table 8.1. Grain size distribution of the selected test fractions.

Sr. No.	Test Fraction	Grain Size Distribution	Standard Sieve Size as per Bunsekifurui Series (mm)
1	Coarser	99% < 1mm and (70 ± 5) % < 0.71 mm	0.710
2	Standard, as per NTNU/SINTEF	99% < 1mm and (70 ± 5) % < 0.50 mm	0.500
3	Fine	99% < 1mm and (70 ± 5) % < 0.25 mm	0.250
4	Finer	99% < 1mm and (70 ± 5) % < 0.15 mm	0.149

The AVS tests were conducted on ten selected rock samples to find the abrasion of wear pieces utilizing the four test fractions according to the experimental design (Table 8.1). Figure 8.1 illustrates the results of comparative study where the abrasion of cutter steel test pieces (AVS) was reduced as the grain size distribution of the test fractions became finer. The probable reason for the increase in AVS values in the case of relatively coarser rock fraction i.e. (70% <0.71 mm), is that the grains passing under the wear tool cut deep grooves on its working surface and also produce a wider wear flat strip, which is evident in the microscopic view of wear flat shown in Figure 8.2. Moreover, a crunching sound due to crushing of grains as they passed under the test piece was also observed during testing of 99% < 1mm and 70% <0.71 mm, rock fraction. Barzegari et al. (2015) also found increase in the abrasivity with increasing particle size of silica soils tested on Soil Abrasion Testing Chamber (SATC). To investigate the reason behind this phenomenon they analyzed the tested wear parts of SATC and explained that as the grain size dimension increases the scratches on wear piece becomes more obvious with more roughness in their direction. Similarly, Mirmehrabi et al. (2015) reported an increase in weight loss of wear tools (steel bolts) of Ferdowsi University Abrasion Test (FUAT) setup, with the corresponding increase in grain size of silica and orthoclase feldspar rock powders.

In the case of NTNU/SINTEF standard test fraction (99% < 1mm and (70 ± 5) % < 0.50 mm) the AVS values for all the rocks decreased in comparison with the 70% <0.71 mm, rock fraction which is primarily due to inclusion of less coarse particles in the standard test fraction and hence decreased interaction between the coarse rock grains and working surface of the test piece. This fact can also be observed in Figure 8.3 where the width of wear flat strip developed is also reduced as compared to the wear flat shown in

Figure 8.2. Another important observation (Figure 8.2) is the absence of deep cut grooves on the test piece used on standard fraction.
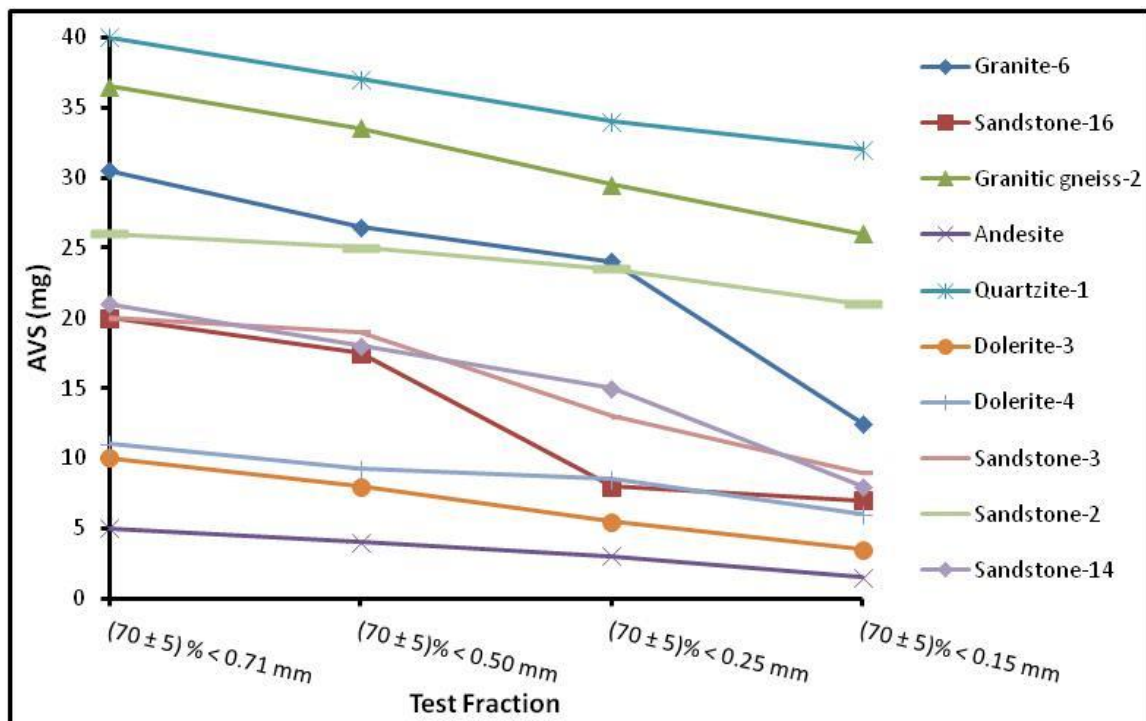
Figure 8.1. AVS test results by using different test fractions.

Figures 8.1 shows that as the test fraction becomes fine (70% <0.25 mm) the AVS values further decrease for all rocks as compared to the standard rock fraction tested. This can be explained due to the fact that in 70% <0.25 mm rock fraction, the proportion of fine particles is more which produced limited interaction with the test piece only at or near the point of contact with turn table. This phenomenon can be observed in Figure 8.4 where the size of wear flat strip is further reduced and the scratch grooves are also not visible. The AVS values of the finest rock fractions tested (70% <0.15 mm) are decreased further (Figure 8.1). This rock fraction contains majority of rock dust particles and therefore produced minimum abrasion on the AVS wear piece. The same fact is visible in Figure 8.5 where the wear flat strip size also decreased to the minimum among all other rock fractions tested. The decrease in the abrasivity with the increase in fine material proportion can be explained by quoting the results of few past investigations. Rostami et al. (2012) reported a decrease in weight loss and wear of propeller blades of Penn-state Soil Abrasion testing device when testing a finer grained clay sample, although the

abrasive minerals content of the tested sample was somewhat high. Mirmehrabi et al. (2015) conducted tests on FUAT device to study the influence of fine particles percentage on soil abrasivity. For this purpose they prepared six silica sand samples by mixing clay sized micro silica particles in different proportions to the crushed sand. The abrasivity of wear tools drastically decreased with the increasing percentage of fine micro silica particles in the test samples.

The preliminary test results of this study show increase in rock abrasivity (AVS) values with the increase in grain size distribution of the tested rock fractions as illustrated in Figure 8.1. This means that generally the AVS values determined by utilizing the coarser rock abrasion powder (99% < 1mm and (70 ± 5) % < 0.71 mm) are somewhat higher than what is reported in normal laboratory testing by using the NTNU/SINTEF standard rock abrasion powder (99% < 1mm and (70 ± 5) % < 0.50 mm). Alternatively it can be stated that the NTNU/SINTEF standard rock abrasion powder underestimates the rock abrasion values and hence can be normalized by performing AVS tests on the proposed test fraction (99% < 1mm and (70 ± 5) % < 0.71 mm). Obviously additional experiments are required to validate this conclusion.
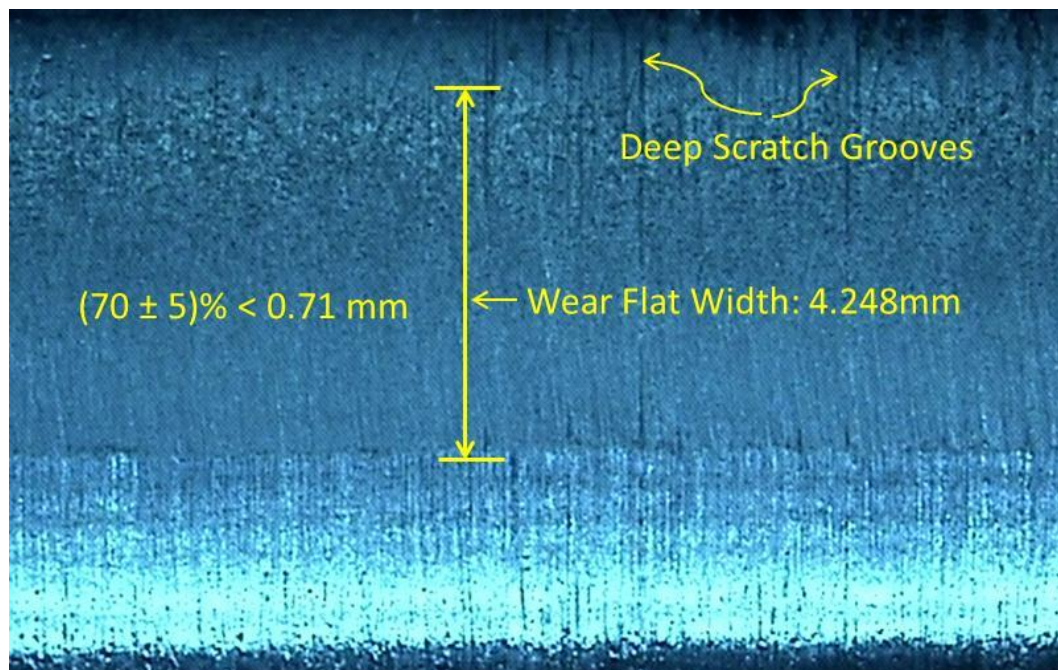
Figure. 8.2. Microphotograph of wear flat of AVS test piece tested on Dolerite-3 coarse rock powder.
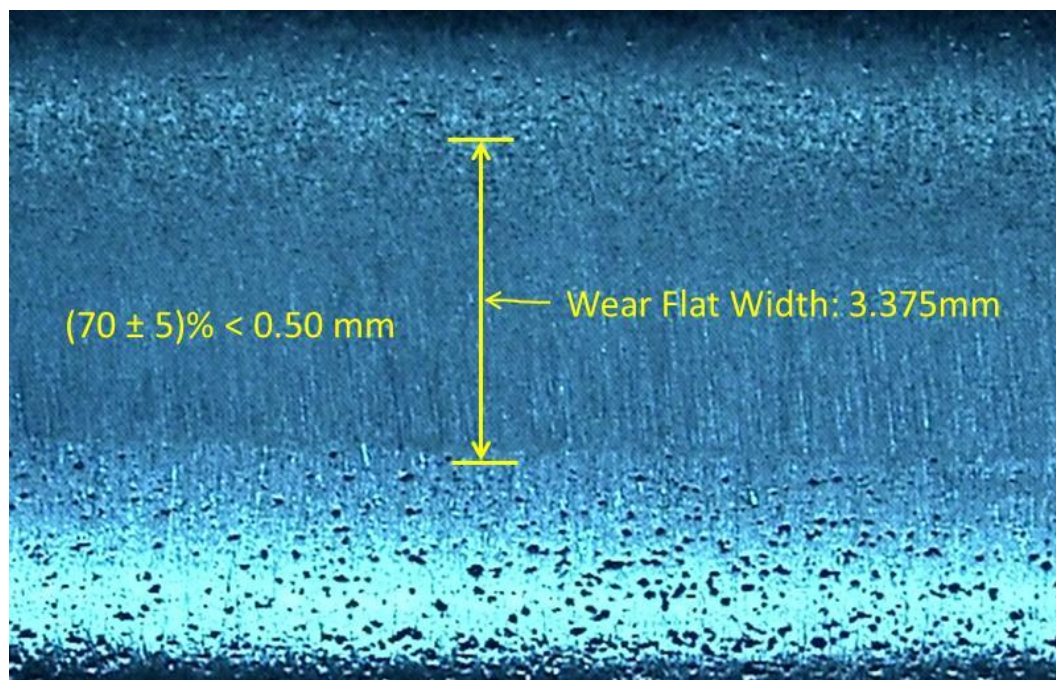
Figure. 8.3. Microphotograph of wear flat of AVS test piece tested on NTNU/SINTEF standard Dolerite-3 rock powder.
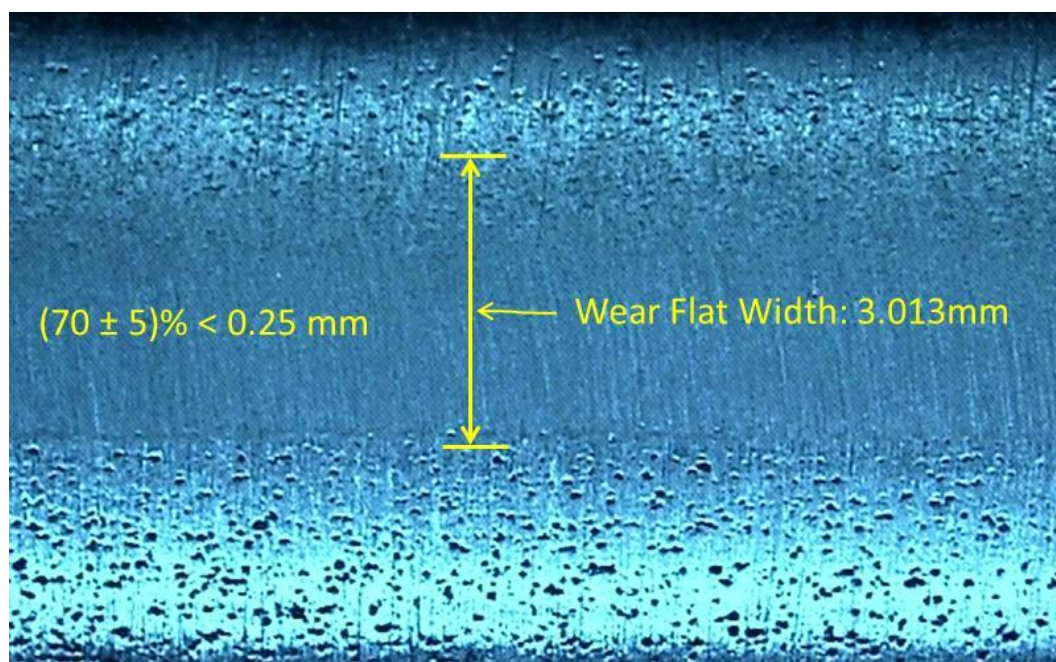
Figure. 8.4. Microphotograph of wear flat of AVS test piece tested on Dolerite-3 fine rock powder.
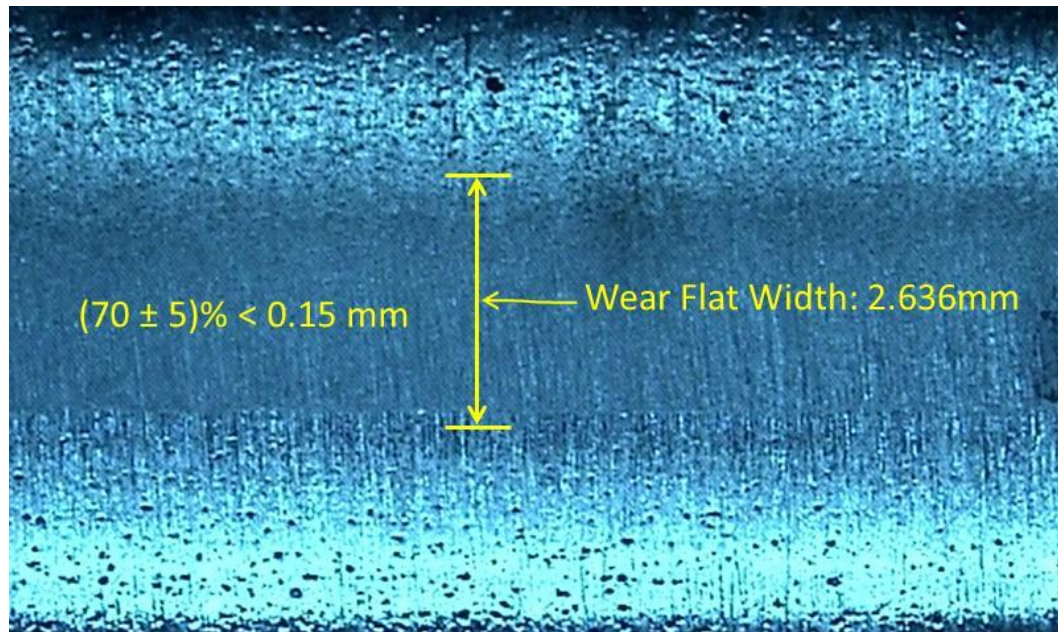
Figure. 8.5. Microphotograph of wear flat of AVS test piece tested on finer Dolerite-3 rock powder.

8.3. AFFECT OF ROTATIONAL SPEED OF ROTATING STEEL DISC ON AVS VALUES

The NTNU/SINTEF test was originally developed around 1960 for top hammer drilling using hard metal or tungsten carbide as test piece i.e. Abrasion Value (AV) test. The test speed of 20 rpm was decided by the available drive motor at the time the AV test was developed. Afterwards the same speed (20 rpm) was used when developing the AVS test using the AV test apparatus (Bruland, 2016). Dahl (2003) defines Abrasion Value Steel (AVS) as the mean value of measured weight loss of the cutter steel test pieces after 20 revolutions of the turn table for a testing time of one minute, thereby suggesting a speed of 20 rpm for the AVS test. Recently, Barzegari et al. (2015) have also reported the effect of centrifugal force in leaving the well rounded sample particles from the test track of SAT device at the suggested speed of 20 rpm.

The current study is aimed at exploring the effect of rotational speed of the steel disc on measured values of AVS. Therefore it was decided to run AVS tests using NTNU/SINTEF standard test fraction [99% < 1mm and (70 ± 5) % < 0.50 mm] at the disc speed of 10 rpm i.e. half the suggested speed of 20 rpm. The rationale behind selecting a speed of 10 rpm is to reduce the centrifugal effect of turn table on the grains

of rock sample so that they do not escape from the test track during test performance. The experimental design parameters are presented in Table 8.2. The experimental matrix is designed in such a way that at both the test speeds of 20 rpm and 10 rpm the cutter steel test piece is exposed to the similar test conditions including steel disc rotations as well as the total quantity of rock abrasion powder interacted.

Table 8.2. Experimental matrix for test speed variation.

Test Speed (RPM)	Grain Size Distribution	Testing Time (Min)	Sample Flow Rate (g/min)
20	Standard as per NTNU/SINTEF	1	80 ± 5
10	Standard as per NTNU/SINTEF	2	40 ± 2.5

Figure 8.6 shows the comparative results of AVS tests conducted on ten selected rock samples by varying the disc speeds at 20 rpm and 10 rpm. The detailed results are listed in Table 4.12. The wear of test pieces actually increased for all rocks when tested on 10 rpm speed of the turn table as compared to the AVS values obtained at the standard test speed of 20 rpm. The possible explanation for the increase in wear due to decrease in steel disc speed is the domination of three-body wear mode as explained by Verhoef (1997). In three-body wear phenomenon the hard rock particles cause abrasion between the two sliding surfaces and can be applied in the case of NTNU/SINTEF abrasion test setup where the abrasion powder acts between the test piece and the rotating steel disc. Therefore, when the turn table speed was set at 10 rpm, the rock particles found more time to interact and abrade the test piece and resulted in more pronounced abrasion as compared to the standard speed of 20 rpm.

Contrary to that, the past investigation of Krapivin et al. (1967) reported in Verhoef (1997) shows increase in wear (mm/km) at the critical velocity with the corresponding increase in cutting velocity (m/s) of the tool. The increase in cutting velocity imparts two effects; the increase in cutting forces and an increased generation of heat which in turn leads to the rise of tool temperature. According to Krapivin et al. (1967) at higher cutting velocities than the critical velocity, the increase in wear was due to the softening of the tool hardness with increasing temperature (1200-1400 °C). The critical velocity is related to the temperature reached at the tool-rock interface and for hard steel this temperature is 550-600 °C. Another probable reason is that in rock cutting

the two-body wear mode is generally dominant, therefore caused increased wear with increase in cutting speed.
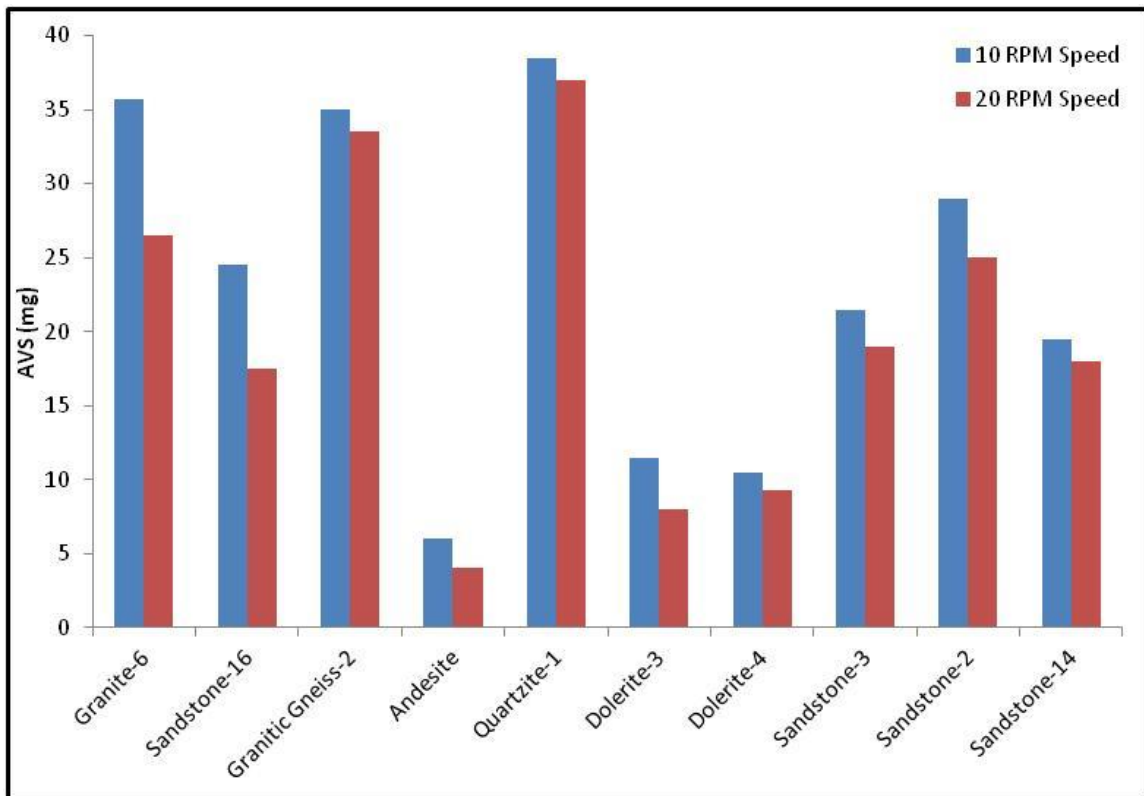
Figure 8.6. AVS test results conducted on 10 rpm and 20 rpm disc speeds using NTNU/SINTEF standard test fraction (99% < 1mm and (70 ± 5) % < 0.50 mm).

8.4. RELATIONSHIP OF CLI WITH CAI AND ABR (g/t)

The CLI computed from the AVS values of standard rock fractions and the related $CAI_{fb(Side)}$ values (measured on freshly broken rock surfaces by adopting the side viewing stylus measurement method) for ten selected rocks are shown in Figure 8.7. As expected a fair negatively linear trend can be seen between the CLI and $CAI_{fb(Side)}$ values, which shows that as the rock abrasiveness increases the cutter life in boring hours is reduced. To date a limited literature is available correlating CLI with CAI which generally coincides with the correlation presented in this work.

Bruland (1998) suggested a decreasing polynomial relationship for the rough estimation of CLI from CAI of rocks. Dahl et al. (2012) developed a trend following the power-law relationship where the CLI values drop with the corresponding rise in CAI of

rocks. Recently Ko et al. (2016) have proposed a logarithmic decreasing relationship between CLI and CAI of igneous and metamorphic rocks.
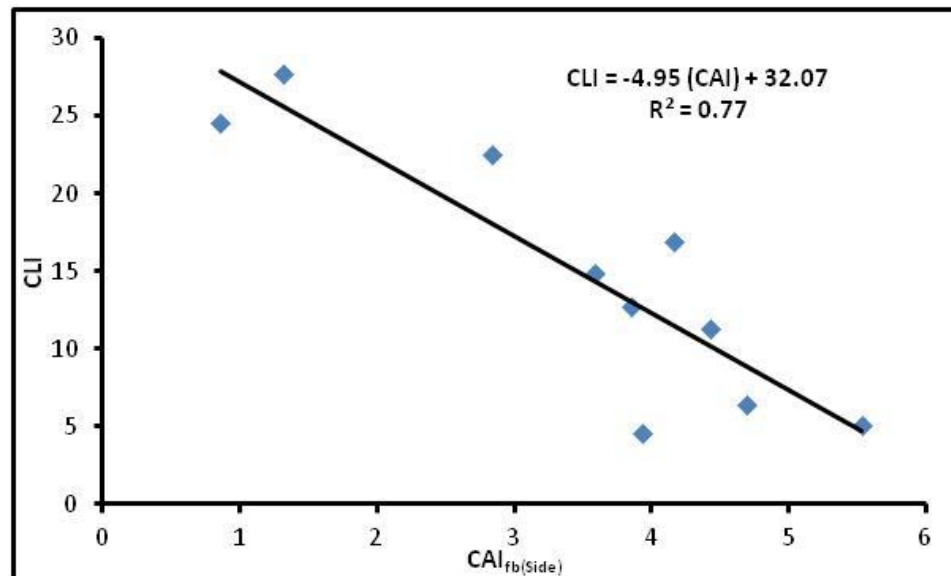
Figure 8.7. Correlation between CLI and $CAI_{fb(Side)}$.

Figure 8.8 illustrates a decreasing logarithmic relationship between CLI and ABR (g/t) values for the same set of rocks tested. Currently no work is present correlating the two rock abrasivity measurement methods. However, the general trend found in this study is in line with the trends established between CLI and CAI in some earlier investigations.

There is an anomalous data point (Figure 8.8) corresponding to Quartzite-1 rock sample, which shows a significantly low CLI value (4.58) in comparison to the LCPC abrasivity co-efficient of 498.50 (g/t). The inspection of test results used for the calculation of CLI depicts that the Sievers'J-value of 2.06 for Quartzite-1 rock sample is also very low and confirms that its surface hardness is high. However, the LCPC test is showing medium rock abrasivity (ABR = 498.50 g/t) as per classification of LCPC abrasivity co-efficient (Thuro et al., 2006). This anomaly can be explained in the light of inherent defect in the LCPC testing principle that it does not consider the overall strength of the rock matrix in the computed ABR (g/t) value due to crushing involved in the preparation of sample material (Kohler et al., 2011).
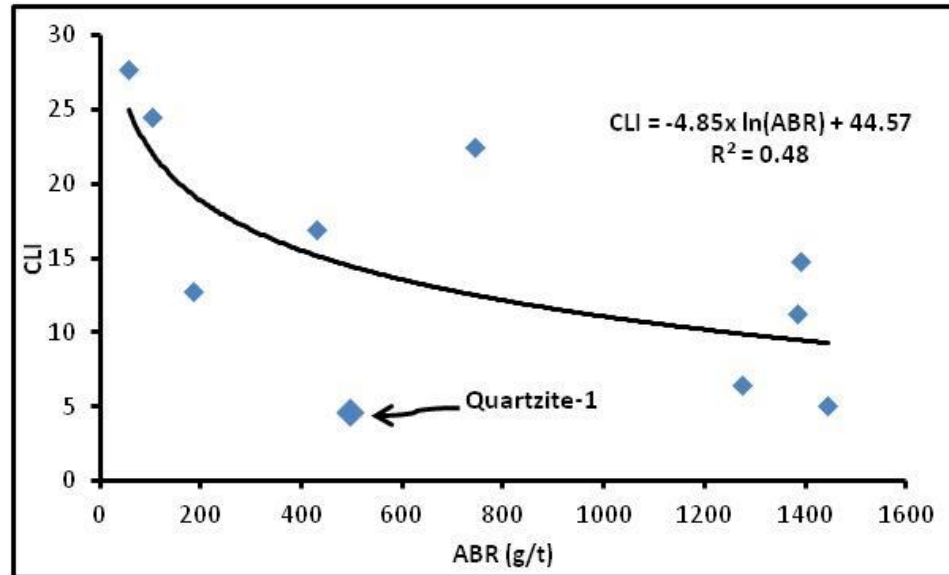
Figure 8.8. Correlation between CLI and ABR (g/t).

8.5. RELATIONSHIP OF CLI WITH MECHANICAL ROCK PROPERTIES

Regression analysis was performed to find possible correlations of CLI with uniaxial compressive strength (UCS) and Brazilian tensile strength of ten selected rocks. Figure 8.9 shows a logarithmic decreasing correlation between CLI and UCS of rocks tested which closely coincides with the relationship proposed by Ko et al. (2016). Figure 8.10 displays a linear inverse relationship between CLI and BTS of the rocks and shows that as the BTS of rocks increase the life of cutting tools decrease. It is pertinent to mention here that in both Figures 8.9 and 8.10 two data points pertaining to Granite-6 and Quartzite-1 rock samples have been omitted from regression and declared as potential outliers. The Granite-6 rock sample belongs to a granite of Tobra Formation which shows considerably low strength values (UCS = 44.80; BTS = 2.30) as well as low CLI value (6.44) which is an anomaly. The possible explanation for this low strength may be the weathering of these boulders beds involved during the deposition process (tillite), by an inland ice sheet (local glaciation) in the Tobra Formation of Eastern Salt Range, Punjab (Shah, 2009). The Quartzite-1 rock sample is also showing low strength values (UCS = 56.39; BTS = 4.35) along with low CLI value of 4.56. No plausible reason for showing this behavior can be explained and might be the effect of natural heterogeneity generally present in rocks.
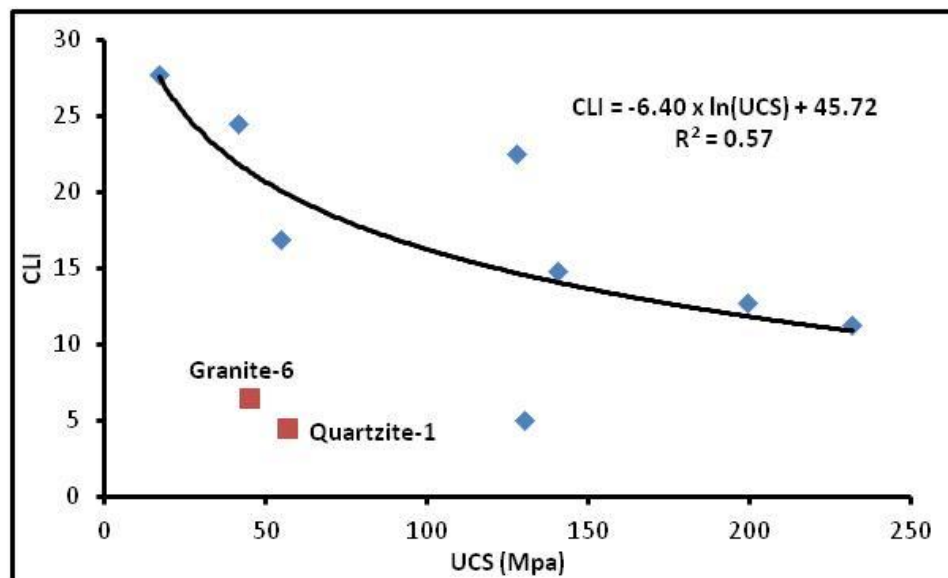
Figure 8.9. Correlation between CLI and UCS (MPa).
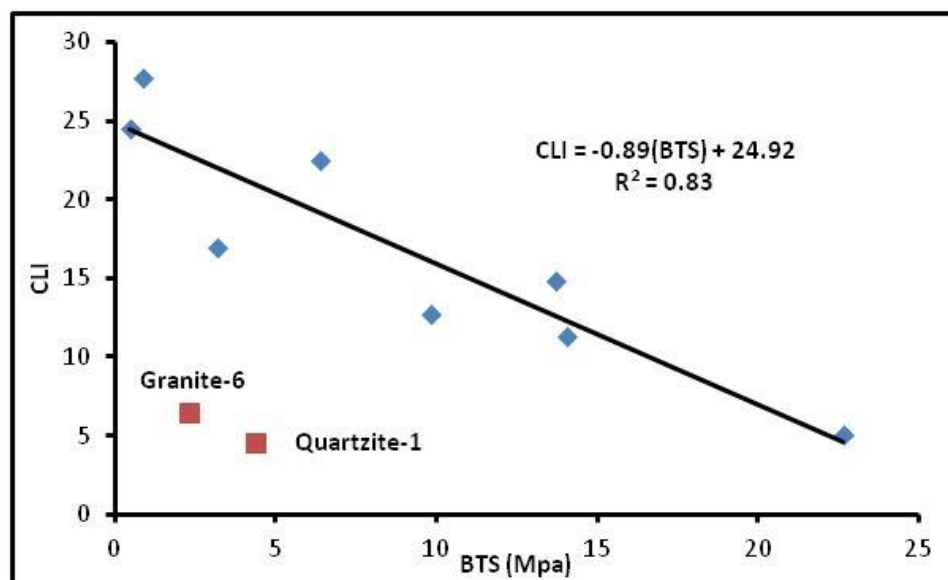
Figure 8.10. Correlation between CLI and BTS (MPa).

9. CONCLUSIONS AND RECOMMENDATIONS FOR FUTURE WORK

9.1. CONCLUSIONS

The research work presented in this dissertation was carried out to characterize the abrasivity potential of rocks as well as to evaluate different abrasivity measurement methods using selected rocks from various geological formations of Pakistan. For abrasivity measures three different rock abrasivity measurement methods including CERCHAR test, LCPC test and NTNU/SINTEF abrasivity test were selected. For abrasivity characterization 51 abrasive and non-abrasive rock samples were collected from 25 different rock formations of Pakistan. In mechanical rock cutting and conventional drill and blast operations these tests (CERCHAR, LCPC and NTNU) are frequently utilized for the estimation of abrasiveness of rocks (Perez et al., 2015). To further investigate the impact of water saturation on the results of these tests the CERCHAR and LCPC tests were also performed on selected rocks in saturated condition. For the determination of petrographical rock parameters [quartz content (Qtz), equivalent quartz content (Qtz.eq), mean quartz grain size (Ø-Qtz) and mean overall grain size of minerals (Ø)] analyses were conducted on 48 representative rock specimens. The petrographic rock parameters were further employed to calculate the wear indices including Schimazek's F- value and Rock Abrasivity Index (RAI). In order to explore the dependence of rock abrasivity on the engineering properties of rocks, the mechanical and physical properties tests comprising of UCS, BTS, primary wave velocity (V_p), density, porosity and pore-space volume were also performed. In addition to the mechanical and physical rock properties on dry samples, 33 fully saturated rock specimens were also subjected to the physical rock properties tests.

9.1.1. The CERCHAR Test. Abrasivity characterization of selected rocks of Pakistan by means of CERCHAR test and evaluation of this method was one of the major components of this study. The CERCHAR tests on saw cut and freshly broken dry rock surfaces were performed on all 51 rock units incorporated in this research work. The corresponding CERCHAR Abrasivity Index (CAI) values for both sawn and freshly broken rock surfaces were measured using the top and side view measurement methods of the CERCHAR test styli. The (CAI) values so obtained were utilized to develop

possible correlations with the mechanical and physical rock properties. Further the petrographic parameters as well as geo-technical wear indices (Rock Abrasivity Index (RAI) and Schimazek's F-value) of abrasive and non-abrasive rock samples were also used for analyses with CERCHAR abrasivity index (CAI).

In the first section of this study the effects of parameters such as wear flat measurement procedure and rock surface conditions were examined on the results of CERCHAR abrasivity test to validate the earlier research investigations. Hypothesis testing was performed to statistically validate that the test results of CAI_s and CAI_{fb} measured from top and side view of the test styli were truly different. For this purpose t-test statistics was adopted at a significance level (α) of 0.1 to calculate T scores for contrasts in the individual mean $CAI_{s(Top)}$ and $CAI_{fb(Top)}$ against $CAI_{s(Side)}$ and $CAI_{fb(Side)}$ values. The p-values calculated from respective T scores showed that 63% of CAI values for both saw cut and freshly broken rock surfaces were significantly different at the chosen level of significance ($\alpha = 0.1$) and were lower in value when measured using the side viewing technique suggested by Alber et al. (2014) as compared to the top view test stylus measurement method. Therefore, it was concluded that CAI measurements made from the side view of the stylus were more reliable due to fact that the measured wear flat values are free from burrs and scratch grooves. These findings totally confirm the conclusions of earlier studies carried out by Rostami et al. (2005); Rostami et al. (2013) and Alber et al. (2014). Similarly, the correlations of $CAI_{s(Top)}$ versus $CAI_{s(Side)}$ and $CAI_{fb(Top)}$ versus $CAI_{fb(Side)}$ show 17% and 19% increase respectively in CAI values when measured from top view setting of the stylus which practically is an overestimation of the abrasive capacity of the rock and in turn can increase the estimated cost of rock excavation including number of cutters to be replaced and wear of other machine components coming in contact with rock. In terms of the effect of freshly broken and sawn rock surfaces on CAI values, the results of this study illustrate that $CAI_{fb(Side)}$ and $CAI_{fb(Top)}$ values were higher than $CAI_{s(Side)}$ and $CAI_{s(Top)}$ by factors of about 1.14 and 1.15 respectively, which confirms the earlier findings of Kasling and Thuro (2010).

The second part of this study discusses the correlations of CAI values with rock properties (petrographic and physico-mechanical). The logarithmic correlations of

$CAI_{s(Top)}$, $CAI_{s(Side)}$, $CAI_{fb(Top)}$ and $CAI_{fb(Side)}$ with RAI presented herein closely match with the already proposed correlations developed by Plinninger et al. (2002). Similarly, the correlations of the form $CAI = k(F\text{-value})^n$ have been proposed between $CAI_{s(Top)}$, $CAI_{s(Side)}$, $CAI_{fb(Top)}$, $CAI_{fb(Side)}$ and Schimazek's F-value of the rock. Past investigations of Paschen (1980), Verhoef et al. (1990), Deketh (1991) and Bisschop (1991) only correlated Schimazek's F-value with the wear rate of experimental test pieces (loss in mass of pin and chisel) determined from Schimazek's pin-on-disc test, pin-on-disc test on a lathe machine and chisel abrasion test, where the wear rate of pin and chisel was increased with corresponding increase in the Schimazek's F-value. The variation of $CAI_{fb(Side)}$ with petrographic parameters including quartz content (Qtz %) and equivalent quartz content (Qtz-eq %) was not clear and no significant relationship could be observed due to considerable scatter present in the data. This was probably due to the inherent variability present in natural materials like rocks. Similar results were also reported in the past investigations of Kasling (2000), Alber (2008) and Ko et al. (2016). However, a linearly increasing correlation ($R^2 = 0.33$) was found between $CAI_{fb(Side)}$ and quartz grain size (Ø-Qtz, mm) which confirms the findings of earlier studies carried out by Yarali et al. (2008) and Er and Tugrul (2016).

No significant relationships of CAI for all rocks with mechanical and physical rock properties could be established in this study. CAI exhibits weak positively linear correlations with UCS and BTS of rock samples which may be attributed to different rock types having variety of strength values. Interestingly when correlations of CAI was established with mechanical rock properties (UCS and BTS) of sedimentary rocks only reasonable coefficient of determination (R^2) values of 0.31, 0.28, 0.25 and 0.27 were observed for $CAI_{s(Top)}$, $CAI_{s(Side)}$, $CAI_{fb(Top)}$ and $CAI_{fb(Side)}$ respectively most likely due to samples belonging to the same generic i.e. sedimentary rock type. Linear positive correlations though statistically weak in strength (R^2 ranging from 0.11 to 0.15) have been found between CAI and dry density of rocks, which are quite logical and generally coincide with the correlation proposed by Er and Tugrul (2016). However, Kahraman et al. (2010) found negatively linear trend between CAI and rock density in their study. Overall good correlations were found between CAI and rock porosity with the highest correlation of determination (R^2) value of -0.40 found between $CAI_{s(Top)}$ against porosity

which clearly shows that highly porous rocks are less abrasive than the rock samples having low porosity. Further negatively poor linear correlations were found between $CAI_{s(Top)}$, $CAI_{s(Side)}$, $CAI_{fb(Top)}$ and $CAI_{fb(Side)}$ with P-wave velocity (V_p) of the rocks tested which are in contradiction with the past investigations conducted by Kahraman et al. (2010), Khandelwal and Ranjith (2010) and Er and Tugrul (2016), where positive linear relationships have been proposed between CAI and P-wave velocity of rocks.

To explain the dependence of $CAI_{fb(Side)}$ on independent variables such as Schimazek's F-value, average quartz grain size (Ø-Qtz) and UCS of rocks, stepwise multiple regression technique was adopted to propose a linear model (Equation 9.1). This explanatory model accounts for 79% of total variation in the dependant variable ($CAI_{fb(Side)}$). The proposed model generally matches with the correlation equations developed by some previous researchers (Fowell and Abu Bakar, 2007; Gharahbagh et al., 2011; Rostami et al., 2013).

$$CAI_{fb(Side)} = 0.811 + 0.289 \times (\text{F-value}) + 1.285 \times (\text{Ø-Qtz}) + 0.007 \times (\text{UCS}); \quad (R^2 = 0.79) \tag{9.1}$$

9.1.2. Impact of Moisture Content on CERCHAR Abrasivity Index. A relatively new concept of CERCHAR Abrasivity Index has been further explored in this section which presents the effects of water saturation of rock samples on the CAI values. In mining and geotechnical applications rock excavators could work in a variety of strata conditions including dry, moist or fully saturated rocks. Moreover, in specialized cases (harbor construction, dredging, off-shore drilling and construction of underground structures under water bodies among others) the rock is generally cut under fully water saturated conditions. Review of literature shows that rock characteristics (abrasiveness, cutting forces, specific energy and strength) vary by the changing rock excavation scenarios i.e. dry and wet rock environments and water saturation could also influence the production rate as well as tool life of any rock cutting machine. At present the performance and production rate estimates of rock excavation machines are normally based on laboratory testing of air dried rock samples. Such test results can over or under estimate rock abrasivity and cutting forces which in turn affects overall technical/operational feasibility of the proposed systems and economics of the project. In

this study a set of 33 rock samples ranging from abrasive to non abrasive sedimentary rock units was subjected to a comprehensive laboratory testing program including CAI and rock mechanics testing in saturated conditions as well as computation of wear indices of wet rocks (Schimazek's F-value$_{sat}$ and RAI$_{sat}$) by utilizing petrographic parameters and saturated rock strength properties (UCS$_{sat}$ and BTS$_{sat}$). The CERCHAR tests were performed on saturated sawn and freshly broken rock surfaces. The corresponding CERCHAR Abrasivity Index (CAI) values were computed by employing both the top and side viewing wear flat measurement methods at the stylus tip. For analysis of the results the CAI values obtained from freshly broken rock surfaces, measured from the side view wear flat measurement technique (CAI$_{dry}$ and CAI$_{sat}$) being more reliable, were further utilized.

The test results of CAI$_{dry}$ and CAI$_{sat}$ were statistically examined and hypothesis testing was carried out to validate that the CAI values measured on dry and saturated rocks were actually dissimilar. To accomplish this, ANOVA test with completely randomized design was conducted at pre-defined significance level (α) of 0.15. To determine the statistical significance of test results, p-values were calculated from F-ratios of corresponding sample populations for dry and saturated rock surfaces and found that 52% of CAI$_{dry}$ and CAI$_{sat}$ were significantly different at the chosen level of significance ($\alpha = 0.15$). Further it was also found that overall 79% of the CAI$_{sat}$ were lower than CAI$_{dry}$ meaning that in 18% of the cases, CAI$_{sat}$ were higher than CAI$_{dry}$. This means that in general CAI values in saturated rocks are lower than what is reported in normal lab testing on dry rock samples. The reduction in CAI$_{sat}$ values in comparison to CAI$_{dry}$ values was probably due to the weakening of the sedimentary rock matrix upon saturation. This softening of rocks was also evident by the considerable decrease (50% overall) in the UCS of fully saturated rocks compared to air dried samples. The reduction in CAI$_{sat}$ values may also be attributed to lubrication affect of saturated water between the CERCHAR pin and the rock surface due to reduction in friction between the two surfaces as well as cooling of stylus tip during test performance. However, preliminary analysis of root causes for the exceptions based on study of other rock properties (i.e. quartz content and strength) did not offer a coherent explanation and additional studies are needed to find the reason for this deviation from general trend.

A correlation (Equation 9.2) was developed for the calculation of CAI_{sat} from CAI_{dry} that accounts for 83% of observations. The developed equation shows that CAI_{sat} is roughly 0.8 times the CAI_{dry} value, meaning approximately CAI_{sat} is 20% lower than the corresponding CAI_{dry}. Therefore, for practical purposes it is suggested to normalize the CAI values obtained by testing on dry rocks to account for the differences in saturated rock when estimating tool consumption. Obviously, a comparison of the CAI values and tools consumption in dry and saturated conditions is needed to validate this recommendation. It is pertinent to mention here that this phenomenon is well documented in soft ground tunnelling where moisture content of the soil and conditioned soil is often recorded. However, despite many observations in the field and some limited records in the lab, there is no study that relates the tool wear in saturated/dry rock to CAI_{dry}, and surely not to CAI_{sat} since this is a new use of the index. This study could be a prelude to this discussion and separation of bit life in various working conditions relative to the presence of water in the face and its impact on rock cutting tools.

$$CAI_{sat} = 0.782 \times CAI_{dry} + 0.128; (R^2 = 0.83) \tag{9.2}$$

Where;

CAI_{sat} = CAI value measured on saturated freshly broken rock surface using side viewing wear flat measurement method at the stylus tip;

CAI_{dry} = CAI value measured on dry freshly broken rock surface using side viewing wear flat measurement method at the stylus tip.

A multiple linear regression model was also developed (Equation 9.3) by adopting stepwise multivariate regression analysis, for the prediction of CAI_{sat} from the petrographical (Ø-Qtz) and geomechanical properties (F-value$_{sat}$, UCS$_{sat}$ and BTS$_{sat}$) of saturated rocks. This empirical model accounts for 88% of total variation in the dependant variable (CAI_{sat}) and can be employed for the estimation of CERCHAR abrasivity index in the saturated rock conditions from routine rock mechanics testing parameters.

$$CAI_{sat} = 0.111 + 0.431(F\text{-value}_{sat}) + 0.008(UCS_{sat}) + 1.753(Ø\text{-Qtz}) + 0.117(BTS_{sat}); \tag{9.3}$$

$$(R^2 = 0.88)$$

Finally the utility of existing CAI prediction models proposed by Rostami et al. (2013) and Majeed and Abu Bakar (2015) for the estimation of CAI_{sat} was checked statistically (in terms of performance indices such as VAF and RMSE) using the dataset of saturated rock properties (UCS_{sat}, BTS_{sat}, Schimazek's F-value$_{sat}$) generated in this research work. The performance comparison of these prediction models illustrate that the correlation equation developed by Majeed and Abu Bakar (2015) is statistically more significant.

9.1.3. The LCPC Test. The second important component of this research work was to determine the abrasivity of included rock samples by utilizing LCPC test method. The LCPC tests on dry rock fractions (4/6.3-mm) were conducted on all 51 rock samples incorporated in this study. The test results so obtained were further utilized to establish possible correlations with the CAI, rock wear indices (Schimazek's F-value and RAI), petrographical, mechanical and physical rock properties. Additionally, in order to simulate the rock excavation activity in wet grounds, the LCPC tests were also performed on 20 selected rock samples by introducing water. Water was added in fractions of 15%, 30%, 45% and 60% of 500 grams of sieved rock aggregate, in the beginning of each test.

The LCPC wet tests indicated two characteristic trends (Figure 7.1 a, b) towards rock abrasivity (ABR, g/t) apparently based on the porosity of tested rocks. At 15% moisture content seven rock samples mostly having high porosity (10.84% to 24.70%) showed an abrupt fall in abrasivity values (6% to 83%) while the remaining thirteen rock samples having relatively low porosity (0.12% to 3.61%) depicted an overall rise in ABR (g/t) values in comparison to the ABR values obtained in dry (0% saturation) LCPC tests. However, eight rock samples (low porosity) attained the peak values of abrasivity ranging from 21% (Granite-5) to 490% (Siltstone-1) at 15% water content (Figure 7.1 b). The decrease in ABR (g/t) values of high porosity rock samples at 15% moisture level was due to complete water absorption into the pore spaces of rock grains and production of adhesive paste in the beginning of test which aligned rock grains along the walls of the test container away from the contact of LCPC insert. Where as in the case of low porosity rocks the test fraction formed a high density suspension of water-solid mixture resulted in high resistance to the rotation of impeller. At 30% water content the high porosity rock specimens showed the peak values of LCPC abrasivity co-efficient with an increase

ranging from 45% to 179% compared to dry tests (Figure 7.1 a). This rise in ABR (g/t) values was due to the availability of excess water after getting absorbed into the rock pores for the formation of high density water-solid mixture which offered increased resistance and interaction of rotating impeller with rock grains. On the other hand low porosity group of rocks illustrated the decrease in ABR (g/t) values for the majority of cases (8 rocks out of 13), while five rock samples experienced further increase in abrasivity values (Figure 7.1 b). When the water content was further increased to 45%, abrasivity of all the rocks tested was gradually dropped and approximately attained the dry ABR (g/t) values at the water content of 60%. This gradual decrease in abrasivity at 45% and 60% water contents was probably due to decrease in the density of water-solid mixture with excessive water present at the interface of LCPC insert and rock grains, as well as the cooling and lubrication effect imparted by this excess water.

LCPC test has become popular for applications in rocks and soils abrasivity testing in the past ten years (Plinninger and Restner, 2008; Kasling and Thuro, 2010). Therefore, for practical purposes any rock abrasivity evaluations based on dry LCPC tests can over/under estimate the abrasivity potential of rock or soil depending upon the moisture content level of the ground. If wrongly estimated it can impact not only the cutting tools but also other parts of excavation machines coming in contact with ground. Generally, the rock excavation machines employed in mining and tunneling projects require the addition of water via high pressure waterjets (5 to 10% of the weight of rock debris) predominantly to control dust production at the working face as well as reduction in production of frictional sparks and cooling of the cutting tools; which can significantly increase the abrasivity of the excavated rock debris produced during cutting process (Gharahbagh et al., 2014). Therefore, during the course of rock excavation, moisture content of the rock debris can be examined. In case the water content at the working face is near the critical water content value (15 to 30%) for the particular rock type, addition of extra water to the muck can be beneficial in terms of increase in the water content and reduction of rock abrasivity as well as wear on the muck transportation devices particularly the conveyors, loaders and hoppers. However, the increased water content of the muck might result in environmental nuisance and greater maintenance of rock debris conveying systems. Moreover, if the rock encountered during excavation is considerably

porous, the amount of water sprayed through high pressure waterjets can be increased so that the overall water content at the working face approaches around 15% moisture level (as established in results of this work). This may help to reduce the abrasion and wear on the rock cutting tools.

In wet LCPC tests, another area of research was to find the impact of water saturation on breakability or grindability of tested rock samples. In the case of low porosity rock samples an overall decrease in LCPC breakability index (BR %) was noted with the peak values attained in dry tests and gradually decreasing in the tests performed at 15% to 60% water contents. This was probably due to low porosity and rather high tensile strength (BTS) values of the tested rock samples. Drucker (2011, 2013) also reported the same trends in her research work. Interestingly in the case of high porosity rock samples a significant decrease in breakability was noted at 15% water content compared to dry tests mainly due to lack of interaction between the water soaked rock fraction aligned with the walls of the mould and the rotating impeller. At 30% water content, the breakability was abruptly increased as compared to what was achieved at 15% water content, which clearly confirms full interaction between the granular rock fraction and the LCPC impeller during rotation. This trend showing preliminary decrease (at 15% water level) and subsequently increase (at 30% water level) in LCPC breakability is otherwise the research findings of Drucker (2011, 2013). Finally at 45% and 60% water contents the breakability decreased gradually in comparison to dry tests which confirms the experimental findings of Drucker (2011, 2013).

In the second part of this section, LCPC dry test results were related with the rock properties including CAI, petrography, wear factors (RAI and Schimazek's F-value) and physico-mechanical properties. The relationship of LCPC abrasivity coefficient (ABR, g/t) with CERCHAR abrasivity index (CAI) has been a topic of interest of numerous past studies. Expectedly, a reasonable positive linear correlation was observed (Equation 9.4) between $CAI_{fb(Side)}$ and ABR (g/t) for all rocks.

$$ABR = 219.8 \times CAI_{fb(Side)} - 126.0; \; (R^2 = 0.49) \qquad (9.4)$$

The proposed relationship (Equation 9.4) exhibited relatively consistent values of ABR (g/t) for low to medium abrasive rocks (CAI = 0.5 - 2.0) however, in the case of very abrasive to extremely abrasive rocks (CAI = 2.5 − 5.0) the scatter of plot generally increased (Figure 7.6). It was observed that some rock samples [Granite-5 (UCS = 232 MPa) and Dolerite-4 (UCS = 141 MPa)] showed remarkably higher values of ABR (g/t) than their corresponding $CAI_{fb(side)}$ probably due to higher UCS values. In contrast some Gneiss and Granitic rock samples showed lower ABR (g/t) values than their corresponding $CAI_{fb(side)}$ values possibly due to higher quartz equivalent content and relatively lower UCS values. The similar observation was reported by (Abu Bakar, 2006) in the case of a weak Penrith sandstone which showed relatively high abrasivity in CERCHAR test (CAI = 4.48) and Schimazek's F-value (2.39 N/mm) probably due to its high equivalent quartz content (61.57%) but in contrast exhibited very small abrasivity in LCPC test (ABR = 140 g/t) only due to its low strength (BTS = 3.88 MPa).

Interestingly when ABR (g/t) and $CAI_{fb(Side)}$ values were compared for sedimentary rocks only, a fairly good correlation (Equation 9.5) was established between the two abrasivity indices. The developed correlation closely matches with the correlations already published (Buchi et al., 1995; Thuro et al., 2007; Thuro and Kasling, 2009; Kasling and Thuro, 2010). However, when the LCPC and CERCHAR abrasivity indices for igneous and metamorphic rocks were plotted a poor correlation (R^2 = 0.095) was found and an anomalous scatter of data points (Figure 7.8) was also observed, showing higher values of ABR (g/t) against relatively lower values of $CAI_{fb(Side)}$ and vice versa. The probable reason for this scatter could be the higher UCS values of these rocks affecting the ABR (g/t) values. Likewise a considerable scatter can also be observed in the proposed correlation between LCPC and CERCHAR test results by Mathier and Gisiger (2003) specifically for igneous rocks.

$$ABR = 273.1 \times CAI_{fb(Side)} - 187.1; (R^2 = 0.79) \qquad (9.5)$$

Upward trends were observed between the LCPC abrasivity coefficient (ABR, g/t) and the mechanical rock properties including UCS and BTS of the tested rocks. In both cases (ABR vs. UCS and ABR vs. BTS) weak correlations were found with R^2 values of 0.30 and 0.41 respectively. The correlations so developed and the general trends

are totally confirmed by the previous studies of Büchi et al. (1995) and Gonzalez et al. (2014). The plots of ABR with UCS and BTS (Figures 7.9 and 7.10) both contain an anomalous data point showing low strength values (UCS = 44.80; BTS = 2.30) with considerably high LCPC abrasivity coefficient (ABR = 1273 g/t). This data point corresponds to a granitic rock of Tobra Formation (Granite-6). The probable reason for this low strength may be the weathering of these boulders beds involved during the depositional process in the Permian age (tillite), by an inland ice sheet (local glaciation) in the Tobra Formation of Eastern Salt Range, Punjab (Shah, 2009). Further, large variability of data can also be seen in both plots which clearly show the effect of natural heterogeneity present in rocks. Similarly, the effect of rock strength on LCPC breakability index (BR %) was also evaluated in this study. As expected, fair exponentially decreasing trends were found in both cases (BR vs. UCS and BR vs. BTS) with R^2 values of 0.55 and 0.57 respectively. The results of this study are in total agreement with the past investigations of Büchi et al. (1995) and Gonzalez et al. (2014).

Another important task of this research was to develop possible correlations of LCPC abrasivity coefficient (ABR, g/t) with rock wear factors such as Schimazek's F-value and RAI. Absolutely no such relationships exist in the past literature reports. When ABR (g/t) values were related with Schimazek's F-value a fair quality power function (Equation 9.6) correlation was found. This relationship generally illustrates an increase in ABR (g/t) values with the corresponding increase in the Schimazek's F-values. The results of this work are in complete agreement with the past published work (Paschen, 1980; Verhoef et al., 1990; Deketh, 1991; Bisschop, 1991) conducted on pin-on-disc tests and shaper cutting and abrasion tests, where the wear rate of instrumental test pieces (mass loss of pin, wear of chisel) also increased with corresponding increase in the Schimazek's F-value (Verhoef, 1997).

$$ABR = 263.53 \times (\text{F-value})^{0.74} \; ; (R^2 = 0.63) \tag{9.6}$$

Similarly, a fair power function relationship (Equation 9.7) was established between the LCPC abrasivity coefficient (ABR, g/t) and RAI values. An overall increasing trend was observed in the developed correlation. To date no published work is available in the literature correlating the results of ABR (g/t) with RAI.

$$\text{ABR} = 13.113 \times (\text{RAI})^{0.848} ; (\text{R}^2 = 0.64) \tag{9.7}$$

The proposed correlations of ABR (g/t) with Schimazek's F-value and RAI can be used as convertor equations to estimate ABR (g/t) from Schimazek's F-value and RAI or vice versa. Moreover the computation of Schimazek's F-value and RAI require determination of complex petrographic parameters including equivalent quartz content (Qtz-eq %) and mineral grain sizes.

The variation of ABR (g/t) with petrographic parameters including quartz content (Qtz %) and equivalent quartz content (Qtz-eq %) was not clear and no significant relationship could be defined due to substantial scatter present in the data plot. This was probably due to the intrinsic heterogeneity and anisotropy present in natural materials and rocks. Similar results were also reported by Kohler et al. (2011) where no relationship was established between ABR (g/t) and Qtz-eq (%). Alternatively, some earlier studies including Festl (2006), Thuro et al. (2006), Barzegari et al. (2014), Dullmann et al. (2014) and Hashemnejad et al. (2015) have established good correlations between ABR (g/t) and Qtz-eq (%).

Attempt was also made to establish correlations of ABR (g/t) with physical rock properties including dry density, porosity and sonic wave velocity (V_p). As expected a weak increasing linear trend ($R^2 = 0.13$) was observed between ABR (g/t) and dry density (g/cc) which seems logical. This trend also matches with the relationship proposed by Gonzalez et al. (2014). A reasonable decreasing logarithmic correlation ($R^2 = 0.28$) was found between ABR (g/t) and rock porosity (%) which describes decrease in ABR (g/t) values in corresponding rise in porosity of rocks. Finally a poor positively linear relationship ($R^2 = 0.034$) was observed between ABR (g/t) and V_p (km/sec). Again in this case the obtained trend line makes sense; meaning the rise in ABR values with corresponding rise in sonic wave velocity explains the fact that V_p is dependent on rock density and generally increases with increase in density. Keeping in view the results of regression analysis it can be stated that LCPC abrasivity coefficient, ABR (g/t) is not primarily dependent on physical properties of rocks (density, porosity and sonic wave velocity). The possible argument in the support of this conclusion is that rock crushing

process carried out for LCPC sample preparation (4.0/6.3 mm) actually destroys the physical rock properties as it does in the case of strength of rock matrix which is considered as the inherent flaw of LCPC testing method (Kohler et al., 2011).

Effort was also made to develop possible correlations of LCPC breakability index (BR %) with physical rock properties comprising of dry density, porosity and sonic wave velocity (V_p). As expected a reasonable exponentially decreasing trend ($R^2 = 0.31$) was found between BR (%) and dry density (g/cc) which is logical. In contrast Gonzalez et al. (2014) proposed a polynomial relationship between Br (%) and dry rock density with an inverted convex curve. A reasonable increasing power function ($R^2 = 0.29$) was observed between BR (%) and rock porosity (%) which defines increase in breakability with corresponding rise in rock porosity. Finally a reasonably fair linearly decreasing relationship ($R^2 = 0.38$) was found between BR (%) and V_p (km/sec). Finally it can be concluded that the LCPC breakability index, BR (%) is partially dependent on density, porosity and sonic wave velocity of tested rock samples and generally exhibits quite logical trends with physical rock properties

9.1.4. The NTNU/SINTEF Abrasivity Test. The last component of this research work was the evaluation of NTNU/SINTEF Abrasion Value Steel (AVS) test and the computation of corresponding Cutter Life Index (CLI) values. For this purpose AVS and Sievers' J-Value (SJ) miniature drill tests were conducted on ten selected potentially abrasive rock samples out of the total 51 rock samples incorporated in this study. The measured values from AVS and SJ tests were further utilized to calculate the respective CLI values of the included rock samples. The AVS test was evaluated based on two test parameters; (1) the effect of variations in the fraction size of rock abrasion powder and (2) the effect of change in the rotational speed of steel disc of AVS test setup. These parameters were evaluated due to some reported irregularities and deficiencies in the testing procedure (Barzegari et al., 2015). Additionally, the computed CLI values were also compared with the corresponding CAI, ABR and mechanical properties of tested rock samples.

To study the impact of variation in grain size distribution of rock abrasion powder on AVS values, four different particle size ranges were selected for the preparation of abrasion powders by keeping their upper grain size limit less than 1mm as in the case of NTNU/SINTEF standard test fraction [99% < 1mm and (70 ± 5)% < 0.50 mm] (Dahl, 2003). The four different test fractions used in this study are Coarser, NTNU/SINTEF Standard, Fine and Finer, all having upper grain size limit of passing 1mm sieve size out of which (70 ± 5)% of the abrasion powder is less than 0.71mm, 0.50mm, 0.25mm and 0.15mm size respectively. The details of experimental design are provided in Table 8.1. Therefore the AVS tests were performed to find the abrasion of wear pieces utilizing the four test fractions as per experimental design. The results of comparative study demonstrates (Figure 8.1) that the abrasion of cutter steel test pieces (AVS) was reduced as the particle size distribution of the test fractions became finer. In the case of Coarser abrasion powder [99% < 1mm and (70 ± 5)% < 0.71 mm] the higher AVS values for all the tested rock samples were measured. This was probably due to relatively coarse grains passing under the wear tool which cut deep grooves on its working surface accompanied by the development of wider wear flat. Furthermore, a crunching sound due to crushing of grains as they passed under the test piece was also noted during testing. In the case of NTNU/SINTEF standard test fraction [99% < 1mm and (70 ± 5) % < 0.50 mm] the AVS values for all the rock powders decreased as compared to coarser rock fraction [(70 ± 5) % <0.71 mm] which is primarily due to less coarse grains contained in the standard abrasion powder. Also a wear flat of lesser width was developed at the working surface of test piece in comparison to the wear flat width produced in the case of coarser test fraction. In the case of fine test fractions [99% < 1mm and (70 ± 5) % < 0.25 mm] the measured AVS values further decreased for all rock samples in comparison to the abrasion values obtained by testing NTNU/SINTEF standard abrasion powders. It was possibly due to proportion of more fine particles present in fine rock fraction [(70 ± 5) % <0.25 mm] which produced limited interaction with the test piece only at or near the point of contact with the steel disc. This phenomenon was very much clear due to further reduction in the width of wear flat developed at the working surface of cutter steel bit and the absence of scratch grooves. Finally in the case of finer rock fraction [99% < 1mm and (70 ± 5) % < 0.15 mm] the AVS values were further decreased probably due to the

presence of majority of fine rock particles and hence produced minimum abrasion on the AVS test piece. The same effect was visible on the working surface of the test piece where the size of wear flat width also decreased to the minimum among all other rock fractions tested. The preliminary test results of this study show increase in rock abrasivity (AVS) values with the increase in grain size distribution of the tested rock fractions as illustrated in Figure 8.1. This means that generally the AVS values determined by utilizing the coarser rock abrasion powder (99% < 1mm and (70 ± 5) % < 0.71 mm) are somewhat higher than what is reported in normal laboratory testing by using the NTNU/SINTEF standard rock abrasion powder (99% < 1mm and (70 ± 5) % < 0.50 mm). Alternatively, it can be stated that the NTNU/SINTEF standard rock abrasion powder underestimates the rock abrasion values and hence can be normalized by performing AVS tests on the proposed coarser test fraction [99% < 1mm and (70 ± 5) % < 0.71 mm]. Obviously additional experiments are required to validate this conclusion.

Another important research plan of this section was to examine the impact of variation in the rotational speed of steel disc on the measured AVS values. The NTNU/SINTEF Abrasivity test was initially originated around 1960 with the development of Abrasion Value (AV) test for top hammer drilling utilizing hard metal or tungsten carbide as wear piece. For AV test the 20 rpm rotational speed of steel disc was fixed primarily by the drive motor available at that time. Subsequently, the same speed of 20 rpm was adopted when developing the Abrasion Value Steel (AVS) test using the AV test device (Bruland, 2016). Further Barzegari et al. (2015) highlighted that round shaped grains of abrasion powder leave the testing track due to centrifugal force applied by 20 rpm rotational speed of the steel disc as well as also because of contact between the test bit and soil grain. Therefore, it was decided to conduct AVS tests on the same set of 10 selected rock samples using NTNU/SINTEF standard abrasion powder [99% < 1mm and (70 ± 5) % < 0.50 mm] at a speed of 10 rpm of the steel disc meaning half of the recommended speed of 20 rpm as specified in Dahl (2003). The justification behind selection of 10 rpm speed of steel disc is to lessen the centrifugal effect imparted by the standard rotational speed of steel disc (20 rpm) on the test fraction particles so that they do not escape out of the test track during test performance as reported by Barzegari et al. (2015). In the experimental design the test duration for 10 rpm rotational speed of disc

was set at two minutes as well as the flow rate of rock abrasion powder was fixed at 40 ± 2.5 (g/min) in contrast to the standard testing time of one minute and standard flow rate of 80 ± 5 (g/min) used for 20 rpm rotational disc speed. The details of experimental design parameters are presented in Table 8.2. The comparative results of AVS tests conducted by varying the disc speeds at 20 rpm and 10 rpm are shown in Figure 8.6. The wear of test pieces actually increased for all rocks when tested at 10 rpm disc speed as compared to the AVS values obtained at the standard test speed of 20 rpm. This increase in abrasion at the disc speed of 10 rpm can be explained by highlighting three-body wear mode (Verhoef, 1997), where hard rock particles cause abrasion between the two sliding surfaces. Therefore, at the reduced rotational speed of 10 rpm, the rock particles found more time to interact and abrade the cutter steel wear piece and resulted in more pronounced wear as compared to the standard speed of 20 rpm. The initial results obtained by reducing the test speed of steel disc to one half (10 rpm) of the standard test speed (20rpm) show an overall increase in rock abrasivity (AVS) values as demonstrated in Figure 8.6. It can be concluded that while using a test speed of 20 rpm in laboratory, testing on AVS apparatus there is a deviation in the reported value of abrasion from the actual field conditions involved in the wear of TBM disc cutters. The average speed of TBM cutter head is 9 rpm as reported by Alber (2008b). However, the standard speed of 20 rpm for AVS test closely simulates the other rock excavation machines including Roadheaders and boring equipment. According to Bilgin et al. (2014) the road headers have in general cutter head velocity ranging from 25 to 35 rpm at low speed settings. In this scenario the AVS values measured in the laboratory by using the standard test speed of 20 rpm seem to fulfill that purpose. Therefore, it is recommended that in the case of TBMs while reporting the abrasivity potential (AVS values) of rocks in the laboratory, the AVS test should be conducted on both the standard speed of 20 rpm as well as on 10 rpm speed so that the highest AVS value may be adopted for estimating tool consumptions. Obviously, further experiments are needed to confirm this conclusion.

When the AVS values measured from NTNU/SINTEF standard test fractions were related with $CAI_{fb(Side)}$ values a decreasing linear correlation (Equation 9.8) of fair strength was developed. The proposed relationship is useful for the conversion of CAI values to CLI in a logic that the computation of CLI is based on AVS and Sievers' J-

Value tests which are both costly and involve laborious procedures as compared to CERCHAR test.

$$CLI = -4.95 \times (CAI) + 32.07; (R^2 = 0.77) \tag{9.8}$$

Similarly, when AVS values were compared with ABR (g/t) values a logarithmic decreasing trend (Equation 9.9) was observed though weak in strength. At present no such relationship is available in the reported literature. Therefore the proposed relationship can be utilized for the prediction of CLI from ABR (g/t) values. Further the plot of CLI vs. ABR (Figure 8.5) shows scatter of data points which is probably due to the limited data points (10 rock samples) and can be improved by the addition of more test samples. This scatter of data may also be attributed to the inherent feature of LCPC testing principle, which does not consider the overall strength of rock matrix in the computed value of ABR (g/t).

$$CLI = -4.85 \times \ln(ABR) + 44.57; (R^2 = 0.48) \tag{9.9}$$

Finally, the regression analysis technique was also adopted to find relationships of CLI with rock strength properties (UCS and BTS) of tested rock samples. A logarithmic decreasing trend ($R^2 = 0.57$) was observed between CLI and UCS which closely matches with the correlation proposed by Ko et al. (2016). Similarly a strong relationship ($R^2 = 0.83$) was found between CLI and BTS. Both the relationships obtained are logical and show clearly the dependence of CLI on rock strength (UCS and BTS) i.e. decrease in cutter life in boring hours (CLI) with the corresponding increase in rock strength. However the authenticity and utility of proposed models can be enhanced by the addition of more test samples.

9.1.5. Abrasivity Characteristics of Rocks of Selected Formations of Pakistan. Finally the CERCHAR and LCPC test results were utilized to characterize the abrasivity of all 51 rock samples included in this research program. For this purpose the $CAI_{fb(Side)}$ values obtained from CERCHAR testing were characterized by employing the rock abrasivity classifications suggested by both ASTM-D7625-10 and ISRM Suggested Methods (Alber et al., 2014). The igneous rock samples generally fall (Table 5.9) in the

high abrasiveness to extreme or very high abrasiveness class (CAI 3.083 to 4.502). Similarly, metamorphic rocks are classed (Table 5.10) as medium or high abrasiveness to very high or extreme abrasiveness (CAI 2.184 to 4.164) range. Whereas, the sedimentary rock samples are characterized (Table 5.11) as very low or extremely low to high abrasiveness class (CAI 0.186 to 3.210), with the exception of Sandstone-16 which is falling in the extreme abrasivity class as per both standards.

The ABR (g/t) values obtained from LCPC tests were also used to characterize rock abrasivity by adopting the classifications suggested by Buchi et al. (1995) and Thuro et al. (2006). In general the igneous rock samples fall (Table 7.5) in the very low or slightly abrasive to high or extremely abrasive class. Similarly, the metamorphic rocks are classed (Table 7.6) as very low or not very abrasive to medium or very abrasive. The sedimentary rocks are classed (Table 7.4) as very low or not very abrasive to low or medium abrasive. However, the Sandstone-16 is falling in the medium / extreme abrasivity class according to both classifications as in the case of CERCHAR tests. The comparison of abrasivity characterization by LCPC method with its companion CERCHAR method shows that it (LCPC method) actually under estimates the abrasivity in the case of igneous as well as metamorphic rocks, the reasons for which are already discussed in the relevant sections of this dissertation.

9.2. RECOMMENDATIONS FOR FUTURE WORK

The conclusions of this dissertation highlight the need for extended probes into the rock abrasivity characterization along with the evaluation of rock abrasivity measurement methods on the remaining variety of geological rock formations of Pakistan. Keeping in view the findings of this research work, following are some suggested suitable research guidelines:

- Perform wear monitoring of rock cutting tools used on actual rock excavation machines in the field. The data pertaining to the consumption of rock cutting tools (disc cutters, picks, drill bits etc.) could be further utilized to correlate and validate the data generated through laboratory testing of CERCHAR test, LCPC test and NTNU/SINTEF rock abrasivity test. At present numerous rock excavation projects in

Pakistan are using mechanical excavators to cut rock. One such project is Neelum Jehlum Hydropower Project (Azad Jammu and Kashmir) utilizing two Herrenknecht TBMs to excavate 19.6 km long twin tunnels. Similarly, the defence related projects are utilizing Roadheaders for rock excavation. Moreover, a number of hydropower and geotechnical projects involving tunneling are expected to start in near future in the country. But there is a need to increase the liaison between the industry and academia.

- Effects of in-situ stresses on rock abrasion values should be evaluated.

- Validation of the proposed model (Equation 9.2) in the field for tool replacement rates with variation in strata moisture content. Tunnelling machines could work through a sequence of dry and wet conditions within the same rock formation. However currently, there is no study comparing the wear life of discs or other cutting tools to offer a conclusive discussion of the wear life of cutting tools in the dry and saturated conditions. Author hopes to continue this study with field data comparing the performance of both indices (CAI_{dry} and CAI_{sat}) when comparing cutter consumption in dry/wet rocks.

- Perform more CERCHAR tests at various moisture levels on sedimentary rocks as well as on porous varieties of metamorphic and igneous rocks of Pakistan to develop moisture content specific prediction models applicable to all generic rock types for the normalization of CAI_{dry} values to the CAI_{sat} values to estimate rock cutting tool consumption, in accordance with the actual water content encountered at the tunnelling face.

- Conduct CERCHAR tests by extending (in two increments of 2.5mm each) the standardized scratch length of 1.0 cm to 1.5 cm on all the three generic abrasive and non-abrasive rock types (igneous, metamorphic and sedimentary), to investigate its impact on the obtained CAI values.

- Conduct LCPC tests by varying the insert hardness of 60-75 HRB [as specified by the French standard NF P18-579 (1990)] to the actual hardness of disc cutters (54-56 HRC) used on TBMs. This study will help in simulating the abrasion and wear rate of real time cutters used for the excavation of particular rock or strata in the tunneling

and mining projects with the LCPC abrasivity co-efficient (ABR, g/t) determined in the laboratory testing of that rock.

- Perform LCPC tests by varying the particle size range of 4.0/6.3 mm, as specified by the French standard NF P18-579 (1990). This research direction will be helpful in finding the impact of rock grain size on the value of LCPC Abrasivity Co-efficient (ABR, g/t) determined in laboratory. Also the optimum size fraction could be suggested.

- Explore the impact of water pH level on the LCPC abrasivity co-efficient (ABR, g/t) to propose cost effective and economical additives other than the costly foams being used during rock excavation operations especially in Earth Pressure Balanced (EPB) tunnelling machines.

- Perform more tests on NTNU/SINTEF rock abrasivity apparatus to extend the existing data base in order to validate and confirm the trends of Abrasion Value Steel (AVS) proposed in this study by varying the grain size distribution of the standard rock abrasion powder as well as by reducing the rotational speed of steel disc to one half of the standard test speed.

- Conduct Sievers'-J tests on saturated rock samples at varying moisture content levels in order to compute saturated Cutter Life Index (CLI_{sat}) values for the evaluation of tool wear rates in wet ground conditions.

- Perform Soil Abrasion Tests (SAT) by utilizing the NTNU/SINTEF abrasivity test on selected soils of Pakistan. Currently, due to massive urbanization in mega cities of Pakistan a number of soft ground projects including underground metro lines, underground sever conveyance tunnels and small diameter bores for underground pipes etc. are expected to start in near future. Therefore, evaluation of the abrasivity potential of soils could be useful in mechanized soft ground tunneling projects. Moreover, many such tunneling projects may also be designed under bodies of water or in ground water table hence requiring earth pressure balanced (EPB) tunneling machines for boring.

APPENDIX A.

CERCHAR ROCK ABRASIVITY TEST RESULTS FOR DRY ROCKS

CERCHAR abrasivity index (CAI) for saw cut rock surfaces measured at top of the stylus tip.

Sr. No.	Rock Sample	Test No.	1st Wear Flat Measurement (TOP) mm	2nd Wear Flat Measurement at 90° Rotation (TOP) mm	$CAI_{s(Top)}$ (0.1 mm)	Avg. $CAI_{s(Top)}$
1	Dolerite-1	1	0.304	0.307	3.055	3.237
		2	0.334	0.291	3.125	
		3	0.314	0.267	2.905	
		4	0.365	0.362	3.635	
		5	0.364	0.329	3.465	
2	Dolerite-2	1	0.343	0.303	3.23	3.015
		2	0.314	0.273	2.935	
		3	0.285	0.271	2.78	
		4	0.324	0.341	3.325	
		5	0.280	0.281	2.805	
3	Dolerite-3	1	0.363	0.344	3.535	3.540
		2	0.265	0.285	2.750	
		3	0.343	0.347	3.450	
		4	0.428	0.423	4.253	
		5	0.374	0.395	3.845	
		6	0.325	0.351	3.380	
4	Dolerite-4	1	0.323	0.351	3.370	3.220
		2	0.302	0.332	3.171	
		3	0.322	0.299	3.107	
		4	0.333	0.335	3.340	
		5	0.300	0.323	3.112	
5	Granite-1	1	0.521	0.449	4.850	4.500
		2	0.491	0.365	4.280	
		3	0.422	0.452	4.370	
		4	0.390	0.492	4.410	
		5	0.479	0.439	4.590	
6	Granite-2	1	0.491	0.445	4.680	4.610
		2	0.530	0.529	5.295	
		3	0.412	0.495	4.535	
		4	0.424	0.426	4.250	
		5	0.425	0.435	4.300	
7	Granite-3	1	0.544	0.439	4.917	4.184
		2	0.345	0.358	3.515	
		3	0.404	0.425	4.145	
		4	0.404	0.428	4.160	
		5	0.418	0.419	4.185	
8	Granite-4	1	0.524	0.432	4.780	3.907
		2	0.263	0.344	3.034	
		3	0.440	0.511	4.755	
		4	0.324	0.461	3.925	
		5	0.268	0.341	3.045	
9	Granite-5	1	0.325	0.319	3.220	3.590
		2	0.396	0.402	3.990	
		3	0.370	0.347	3.585	
		4	0.359	0.363	3.610	
		5	0.345	0.364	3.545	

CERCHAR abrasivity index (CAI) for saw cut rock surfaces measured at top of the stylus tip.
Sr. No.	Rock Sample	Test No.	1st Wear Flat Measurement (TOP) mm	2nd Wear Flat Measurement at 90º Rotation (TOP) mm	$CAI_{s(Top)}$ (0.1 mm)	Avg. $CAI_{s(Top)}$
---	---	---	---	---	---	---
10	Granite-6	1	0.465	0.429	4.470	3.902
		2	0.355	0.369	3.618	
		3	0.363	0.328	3.455	
		4	0.391	0.398	3.945	
		5	0.379	0.426	4.025	
11	Migmatite	1	0.405	0.400	4.025	4.320
		2	0.498	0.451	4.747	
		3	0.437	0.399	4.178	
		4	0.398	0.447	4.225	
		5	0.436	0.449	4.425	
12	Andesite	1	0.363	0.368	3.655	3.528
		2	0.369	0.372	3.705	
		3	0.327	0.304	3.155	
		4	0.359	0.347	3.530	
		5	0.369	0.350	3.595	
13	Granitic Gneiss-1	1	0.309	0.384	3.466	3.650
		2	0.364	0.415	3.893	
		3	0.395	0.322	3.583	
		4	0.342	0.378	3.600	
		5	0.368	0.374	3.710	
14	Granitic Gneiss-2	1	0.401	0.503	4.520	4.952
		2	0.482	0.443	4.625	
		3	0.470	0.478	4.740	
		4	0.561	0.572	5.665	
		5	0.481	0.561	5.208	
15	Phyllite	1	0.162	0.153	1.573	1.433
		2	0.133	0.149	1.410	
		3	0.119	0.140	1.295	
		4	0.143	0.148	1.455	
		5	0.144	0.143	1.435	
16	Quartzite-1	1	0.495	0.486	4.906	4.394
		2	0.337	0.360	3.484	
		3	0.475	0.483	4.792	
		4	0.480	0.404	4.420	
		5	0.437	0.436	4.365	
17	Quartzite-2	1	0.425	0.406	4.158	4.134
		2	0.425	0.406	4.157	
		3	0.425	0.445	4.352	
		4	0.442	0.367	4.045	
		5	0.430	0.396	4.130	
		6	0.384	0.409	3.965	
18	Siltstone-1	1	0.114	0.103	1.086	1.150
		2	0.137	0.121	1.292	
		3	0.091	0.122	1.067	
		4	0.096	0.128	1.120	
		5	0.120	0.117	1.185	

CERCHAR abrasivity index (CAI) for saw cut rock surfaces measured at top of the stylus tip.

Sr. No.	Rock Sample	Test No.	1st Wear Flat Measurement (TOP) mm	2nd Wear Flat Measurement at 90° Rotation (TOP) mm	CAI$_{s(Top)}$ (0.1 mm)	Avg. CAI$_{s(Top)}$
19	Siltstone-2	1	0.231	0.215	2.232	2.216
		2	0.241	0.202	2.216	
		3	0.217	0.223	2.200	
		4	0.215	0.225	2.220	
		5	0.205	0.237	2.212	
20	Sandstone-1	1	0.215	0.173	1.940	1.783
		2	0.129	0.196	1.625	
		3	0.125	0.117	1.210	
		4	0.265	0.215	2.400	
		5	0.188	0.16	1.740	
21	Sandstone-2	1	0.092	0.093	0.924	0.620
		2	0.059	0.043	0.512	
		3	0.063	0.046	0.544	
		4	0.058	0.042	0.499	
		5	0.074	0.0502	0.621	
22	Sandstone-3	1	0.416	0.392	4.040	3.920
		2	0.376	0.403	3.897	
		3	0.417	0.348	3.823	
		4	0.364	0.416	3.900	
		5	0.392	0.396	3.940	
23	Sandstone-4	1	0.164	0.154	1.589	1.410
		2	0.122	0.108	1.147	
		3	0.142	0.157	1.494	
		4	0.121	0.127	1.240	
		5	0.148	0.168	1.580	
24	Sandstone-5	1	0.259	0.309	2.838	3.038
		2	0.312	0.264	2.879	
		3	0.368	0.312	3.399	
		4	0.309	0.310	3.094	
		5	0.275	0.321	2.980	
25	Sandstone-6	1	0.318	0.411	3.645	3.300
		2	0.340	0.322	3.310	
		3	0.283	0.266	2.745	
		4	0.366	0.335	3.505	
		5	0.330	0.329	3.295	
26	Sandstone-7	1	0.198	0.207	2.027	2.030
		2	0.180	0.203	1.917	
		3	0.227	0.224	2.255	
		4	0.211	0.172	1.915	
		5	0.190	0.217	2.036	
27	Sandstone-8	1	0.120	0.100	1.100	1.430
		2	0.191	0.226	2.085	
		3	0.125	0.137	1.310	
		4	0.122	0.122	1.220	
		5	0.130	0.157	1.435	

CERCHAR abrasivity index (CAI) for saw cut rock surfaces measured at top of the stylus tip.						
Sr. No.	Rock Sample	Test No.	1st Wear Flat Measurement (TOP) mm	2nd Wear Flat Measurement at 90° Rotation (TOP) mm	CAI$_{s(Top)}$ (0.1 mm)	Avg. CAI$_{s(Top)}$
28	Sandstone-9	1	0.238	0.216	2.270	
		2	0.309	0.178	2.435	
		3	0.263	0.248	2.555	2.320
		4	0.170	0.233	2.015	
		5	0.300	0.165	2.325	
29	Sandstone-10	1	0.144	0.143	1.435	
		2	0.119	0.079	0.990	
		3	0.156	0.164	1.600	1.394
		4	0.141	0.169	1.550	
		5	0.137	0.142	1.395	
30	Sandstone-11	1	0.249	0.200	2.245	
		2	0.119	0.252	1.855	
		3	0.194	0.181	1.875	1.950
		4	0.186	0.179	1.825	
		5	0.200	0.190	1.950	
31	Sandstone-12	1	0.178	0.180	1.790	
		2	0.129	0.144	1.365	
		3	0.147	0.180	1.635	1.621
		4	0.184	0.155	1.695	
		5	0.148	0.176	1.620	
32	Sandstone-13	1	0.212	0.191	2.015	
		2	0.173	0.158	1.655	
		3	0.164	0.159	1.615	1.640
		4	0.126	0.130	1.280	
		5	0.123	0.204	1.635	
33	Sandstone-14	1	0.096	0.151	1.235	
		2	0.177	0.159	1.680	
		3	0.117	0.094	1.055	1.260
		4	0.114	0.098	1.060	
		5	0.124	0.130	1.270	
34	Sandstone-15	1	0.204	0.154	1.790	
		2	0.175	0.139	1.570	
		3	0.191	0.173	1.820	1.940
		4	0.244	0.190	2.170	
		5	0.249	0.219	2.340	
35	Sandstone-16	1	0.452	0.407	4.295	
		2	0.383	0.355	3.690	
		3	0.414	0.422	4.180	3.973
		4	0.395	0.366	3.805	
		5	0.413	0.366	3.895	
36	Sandstone-17	1	0.303	0.394	3.483	
		2	0.391	0.377	3.840	
		3	0.371	0.386	3.785	3.675
		4	0.349	0.402	3.755	
		5	0.351	0.351	3.510	

CERCHAR abrasivity index (CAI) for saw cut rock surfaces measured at top of the stylus tip.

Sr. No.	Rock Sample	Test No.	1st Wear Flat Measurement (TOP) mm	2nd Wear Flat Measurement at 90° Rotation (TOP) mm	CAI$_{s(Top)}$ (0.1 mm)	Avg. CAI$_{s(Top)}$
37	Sandstone-18	1	0.239	0.392	3.153	3.192
		2	0.405	0.389	3.968	
		3	0.310	0.310	3.100	
		4	0.205	0.249	2.270	
		5	0.361	0.333	3.470	
38	Chamositic-Siderite	1	0.091	0.079	0.848	1.066
		2	0.130	0.109	1.195	
		3	0.128	0.150	1.390	
		4	0.082	0.084	0.832	
		5	0.100	0.113	1.065	
39	Dolomite-1	1	0.227	0.205	2.160	2.121
		2	0.242	0.206	2.240	
		3	0.222	0.207	2.145	
		4	0.208	0.180	1.940	
		5	0.214	0.210	2.120	
40	Dolomite-2	1	0.241	0.229	2.351	2.223
		2	0.236	0.209	2.225	
		3	0.212	0.244	2.280	
		4	0.231	0.236	2.335	
		5	0.186	0.199	1.925	
41	Dolomite-3	1	0.246	0.203	2.245	2.445
		2	0.262	0.300	2.810	
		3	0.225	0.231	2.280	
		4	0.272	0.353	3.125	
		5	0.170	0.183	1.765	
42	Dolomite-4	1	0.180	0.396	2.880	2.500
		2	0.258	0.236	2.470	
		3	0.211	0.284	2.475	
		4	0.226	0.272	2.490	
		5	0.185	0.252	2.185	
43	Limestone-1	1	0.178	0.125	1.513	1.017
		2	0.101	0.083	0.921	
		3	0.062	0.061	0.617	
		4	0.106	0.142	1.240	
		5	0.065	0.094	0.794	
44	Limestone-2	1	0.102	0.116	1.088	1.102
		2	0.122	0.107	1.145	
		3	0.102	0.113	1.073	
		4	0.108	0.114	1.110	
		5	0.109	0.110	1.094	
45	Limestone-3	1	0.119	0.125	1.220	1.478
		2	0.137	0.132	1.345	
		3	0.136	0.123	1.295	
		4	0.177	0.137	1.568	
		5	0.216	0.176	1.960	

CERCHAR abrasivity index (CAI) for saw cut rock surfaces measured at top of the stylus tip.						
Sr. No.	Rock Sample	Test No.	1st Wear Flat Measurement (TOP) mm	2nd Wear Flat Measurement at 90º Rotation (TOP) mm	CAI$_{s(Top)}$ (0.1 mm)	Avg. CAI$_{fb(Top)}$
46	Limestone-4	1	0.110	0.090	1.000	0.958
		2	0.078	0.075	0.765	
		3	0.118	0.106	1.120	
		4	0.113	0.076	0.945	
		5	0.089	0.103	0.960	
47	Limestone-5	1	0.108	0.120	1.140	1.161
		2	0.137	0.115	1.260	
		3	0.122	0.123	1.225	
		4	0.111	0.093	1.020	
		5	0.114	0.118	1.160	
48	Limestone-6	1	0.142	0.085	1.135	1.002
		2	0.124	0.089	1.065	
		3	0.113	0.116	1.145	
		4	0.075	0.077	0.760	
		5	0.086	0.095	0.905	
49	Limestone-7	1	0.031	0.030	0.305	0.306
		2	0.023	0.027	0.250	
		3	0.033	0.038	0.355	
		4	0.031	0.032	0.315	
		5	0.029	0.032	0.305	
50	Rock Gypsum	1	0.076	0.079	0.776	0.731
		2	0.082	0.079	0.806	
		3	0.052	0.060	0.562	
		4	0.067	0.079	0.732	
		5	0.074	0.082	0.780	
51	Marl	1	0.021	0.037	0.290	0.278
		2	0.045	0.025	0.350	
		3	0.021	0.018	0.195	
		4	0.016	0.050	0.330	
		5	0.023	0.022	0.225	

CERCHAR abrasivity index (CAI) for saw cut rock surfaces measured using side view of the stylus tip.

Sr. No.	Rock Sample	Test No.	1st Wear Flat Measurement (SIDE) mm	2nd Wear Flat Measurement at 90º Rotation (SIDE) mm	3rd Wear Flat Measurement at 90º Rotation (SIDE) mm	4th Wear Flat Measurement at 90º Rotation (SIDE) mm	CAI$_s$ (Side) (0.1 mm)	Avg. CAI$_s$ (Side)
1	Dolerite-1	1	0.232	0.251	0.232	0.251	2.415	
		2	0.304	0.304	0.304	0.304	3.040	
		3	0.222	0.222	0.222	0.222	2.220	2.816
		4	0.321	0.324	0.311	0.314	3.175	
		5	0.351	0.282	0.339	0.322	3.235	
2	Dolerite-2	1	0.270	0.284	0.270	0.284	2.773	
		2	0.236	0.280	0.236	0.280	2.580	
		3	0.275	0.284	0.275	0.284	2.795	2.673
		4	0.314	0.267	0.314	0.261	2.890	
		5	0.227	0.257	0.222	0.227	2.333	
3	Dolerite-3	1	0.318	0.318	0.318	0.318	3.182	
		2	0.212	0.207	0.212	0.207	2.097	
		3	0.261	0.265	0.261	0.265	2.630	2.990
		4	0.348	0.337	0.361	0.336	3.455	
		5	0.350	0.352	0.360	0.327	3.473	
		6	0.322	0.301	0.317	0.299	3.098	
4	Dolerite-4	1	0.222	0.222	0.222	0.222	2.220	
		2	0.243	0.223	0.243	0.223	2.326	
		3	0.222	0.202	0.222	0.202	2.116	2.220
		4	0.220	0.220	0.220	0.220	2.200	
		5	0.224	0.224	0.224	0.224	2.242	
5	Granite-1	1	0.392	0.371	0.392	0.371	3.816	
		2	0.342	0.342	0.342	0.342	3.423	
		3	0.346	0.352	0.346	0.352	3.493	3.577
		4	0.386	0.356	0.386	0.356	3.710	
		5	0.348	0.340	0.348	0.340	3.443	
6	Granite-2	1	0.384	0.377	0.384	0.377	3.802	
		2	0.463	0.498	0.463	0.498	4.809	
		3	0.386	0.318	0.386	0.318	3.522	4.040
		4	0.380	0.420	0.380	0.420	4.000	
		5	0.390	0.424	0.390	0.423	4.067	
7	Granite-3	1	0.403	0.403	0.403	0.403	4.030	
		2	0.314	0.317	0.329	0.334	3.235	
		3	0.358	0.383	0.360	0.375	3.690	3.634
		4	0.317	0.391	0.344	0.380	3.580	
		5	0.327	0.400	0.327	0.400	3.635	
8	Granite-4	1	0.383	0.343	0.383	0.343	3.633	
		2	0.255	0.263	0.255	0.263	2.589	
		3	0.344	0.343	0.396	0.378	3.653	3.111
		4	0.252	0.2422	0.252	0.286	2.581	
		5	0.267	0.347	0.267	0.359	3.100	
9	Granite-5	1	0.264	0.261	0.264	0.261	2.625	
		2	0.309	0.326	0.309	0.326	3.173	
		3	0.268	0.263	0.268	0.263	2.653	2.820
		4	0.254	0.329	0.272	0.328	2.958	
		5	0.244	0.293	0.247	0.292	2.690	

CERCHAR abrasivity index (CAI) for saw cut rock surfaces measured using side view of the stylus tip.								
Sr. No.	Rock Sample	Test No.	1st Wear Flat Measurement (SIDE) mm	2nd Wear Flat Measurement at 90° Rotation (SIDE) mm	3rd Wear Flat Measurement at 90° Rotation (SIDE) mm	4th Wear Flat Measurement at 90° Rotation (SIDE) mm	CAI_s (Side) (0.1 mm)	Avg. CAI_s (Side)
10	Granite-6	1	0.401	0.417	0.377	0.424	4.047	3.490
		2	0.317	0.376	0.328	0.338	3.397	
		3	0.324	0.306	0.314	0.305	3.122	
		4	0.359	0.352	0.324	0.333	3.420	
		5	0.335	0.341	0.357	0.361	3.485	
11	Migmatite	1	0.332	0.311	0.332	0.311	3.218	3.550
		2	0.363	0.415	0.363	0.415	3.894	
		3	0.332	0.374	0.332	0.374	3.530	
		4	0.341	0.344	0.342	0.344	3.427	
		5	0.349	0.387	0.349	0.388	3.682	
12	Andesite	1	0.362	0.378	0.365	0.340	3.613	3.250
		2	0.331	0.346	0.338	0.333	3.370	
		3	0.293	0.309	0.277	0.310	2.973	
		4	0.324	0.315	0.292	0.302	3.083	
		5	0.327	0.321	0.322	0.315	3.213	
13	Granitic Gneiss-1	1	0.291	0.249	0.291	0.249	2.700	2.870
		2	0.322	0.322	0.322	0.322	3.220	
		3	0.270	0.269	0.270	0.270	2.698	
		4	0.197	0.356	0.197	0.355	2.763	
		5	0.332	0.278	0.301	0.277	2.970	
14	Granitic Gneiss-2	1	0.402	0.347	0.393	0.333	3.688	4.262
		2	0.396	0.416	0.380	0.380	3.930	
		3	0.380	0.373	0.390	0.434	3.943	
		4	0.518	0.495	0.520	0.492	5.063	
		5	0.492	0.460	0.475	0.448	4.688	
15	Phyllite	1	0.120	0.113	0.122	0.114	1.173	1.189
		2	0.127	0.123	0.133	0.120	1.256	
		3	0.122	0.102	0.119	0.100	1.108	
		4	0.125	0.109	0.124	0.130	1.220	
		5	0.120	0.119	0.117	0.119	1.188	
16	Quartzite-1	1	0.436	0.436	0.436	0.436	4.358	3.930
		2	0.317	0.297	0.317	0.297	3.070	
		3	0.456	0.417	0.456	0.417	4.361	
		4	0.402	0.402	0.402	0.402	4.021	
		5	0.384	0.384	0.384	0.384	3.840	
17	Quartzite-2	1	0.304	0.324	0.304	0.324	3.140	3.394
		2	0.324	0.344	0.324	0.344	3.342	
		3	0.344	0.324	0.344	0.324	3.342	
		4	0.357	0.293	0.389	0.320	3.398	
		5	0.337	0.358	0.372	0.360	3.568	
		6	0.373	0.337	0.375	0.345	3.575	
18	Siltstone-1	1	0.091	0.083	0.091	0.083	0.872	0.990
		2	0.137	0.114	0.137	0.114	1.255	
		3	0.091	0.081	0.091	0.081	0.860	
		4	0.100	0.099	0.099	0.098	0.992	
		5	0.084	0.108	0.086	0.110	0.971	

CERCHAR abrasivity index (CAI) for saw cut rock surfaces measured using side view of the stylus tip.							
Sr. No.	Rock Sample	Test No.	1st Wear Flat Measurement (SIDE) mm	2nd Wear Flat Measurement at 90° Rotation (SIDE) mm	3rd Wear Flat Measurement at 90° Rotation (SIDE) mm	4th Wear Flat Measurement at 90° Rotation (SIDE) mm	CAIs (Side) (0.1 mm)	Avg. CAIs (Side)
19	Siltstone-2	1	0.164	0.154	0.164	0.154	1.591	1.536
		2	0.116	0.164	0.116	0.164	1.401	
		3	0.145	0.178	0.145	0.178	1.615	
		4	0.106	0.190	0.110	0.190	1.490	
		5	0.186	0.132	0.182	0.133	1.583	
20	Sandstone-1	1	0.129	0.230	0.132	0.231	1.810	1.524
		2	0.129	0.118	0.129	0.118	1.236	
		3	0.093	0.127	0.094	0.116	1.075	
		4	0.229	0.166	0.211	0.171	1.943	
		5	0.204	0.148	0.152	0.118	1.555	
21	Sandstone-2	1	0.058	0.063	0.052	0.064	0.593	0.710
		2	0.062	0.061	0.073	0.065	0.652	
		3	0.087	0.076	0.085	0.079	0.817	
		4	0.057	0.077	0.070	0.085	0.722	
		5	0.080	0.075	0.070	0.082	0.767	
22	Sandstone-3	1	0.318	0.318	0.318	0.318	3.176	3.240
		2	0.317	0.377	0.317	0.377	3.469	
		3	0.317	0.298	0.317	0.298	3.074	
		4	0.305	0.325	0.305	0.325	3.150	
		5	0.310	0.356	0.310	0.356	3.331	
23	Sandstone-4	1	0.102	0.105	0.102	0.105	1.034	1.050
		2	0.093	0.084	0.093	0.084	0.885	
		3	0.124	0.124	0.124	0.124	1.242	
		4	0.089	0.102	0.089	0.102	0.955	
		5	0.114	0.113	0.114	0.113	1.135	
24	Sandstone-5	1	0.226	0.247	0.226	0.247	2.365	2.437
		2	0.280	0.226	0.280	0.226	2.527	
		3	0.226	0.258	0.226	0.258	2.419	
		4	0.247	0.234	0.240	0.235	2.390	
		5	0.258	0.242	0.250	0.243	2.483	
25	Sandstone-6	1	0.325	0.294	0.244	0.338	3.003	2.840
		2	0.352	0.230	0.273	0.326	2.953	
		3	0.275	0.213	0.272	0.248	2.520	
		4	0.295	0.291	0.233	0.331	2.875	
		5	0.290	0.281	0.285	0.283	2.848	
26	Sandstone-7	1	0.179	0.158	0.170	0.152	1.648	1.670
		2	0.151	0.166	0.169	0.196	1.705	
		3	0.145	0.205	0.158	0.173	1.703	
		4	0.159	0.160	0.175	0.164	1.645	
		5	0.155	0.174	0.158	0.173	1.649	
27	Sandstone-8	1	0.186	0.159	0.193	0.145	1.708	1.420
		2	0.178	0.202	0.177	0.110	1.668	
		3	0.122	0.131	0.120	0.105	1.195	
		4	0.109	0.125	0.106	0.099	1.098	
		5	0.145	0.144	0.140	0.142	1.430	

CERCHAR abrasivity index (CAI) for saw cut rock surfaces measured using side view of the stylus tip.								
Sr. No.	**Rock Sample**	**Test No.**	**1st Wear Flat Measurement (SIDE) mm**	**2nd Wear Flat Measurement at 90° Rotation (SIDE) mm**	**3rd Wear Flat Measurement at 90° Rotation (SIDE) mm**	**4th Wear Flat Measurement at 90° Rotation (SIDE) mm**	**CAIs (Side) (0.1 mm)**	**Avg. CAIs (Side)**
28	Sandstone-9	1	0.244	0.209	0.176	0.200	2.073	
		2	0.216	0.223	0.208	0.268	2.288	
		3	0.241	0.272	0.225	0.264	2.505	2.380
		4	0.258	0.271	0.278	0.263	2.675	
		5	0.220	0.255	0.215	0.253	2.358	
29	Sandstone-10	1	0.129	0.126	0.134	0.120	1.273	
		2	0.098	0.110	0.087	0.120	1.038	
		3	0.177	0.132	0.165	0.199	1.683	1.403
		4	0.163	0.152	0.180	0.153	1.620	
		5	0.155	0.123	0.160	0.122	1.400	
30	Sandstone-11	1	0.144	0.157	0.167	0.137	1.513	
		2	0.121	0.113	0.145	0.106	1.213	
		3	0.181	0.188	0.180	0.173	1.805	1.480
		4	0.141	0.109	0.146	0.165	1.403	
		5	0.155	0.141	0.148	0.142	1.465	
31	Sandstone-12	1	0.186	0.189	0.196	0.182	1.883	
		2	0.151	0.129	0.145	0.164	1.473	
		3	0.136	0.155	0.137	0.156	1.460	1.589
		4	0.160	0.147	0.143	0.166	1.540	
		5	0.165	0.151	0.169	0.150	1.588	
32	Sandstone-13	1	0.162	0.137	0.122	0.160	1.453	
		2	0.174	0.158	0.170	0.152	1.635	
		3	0.146	0.141	0.118	0.121	1.315	1.400
		4	0.100	0.133	0.114	0.134	1.203	
		5	0.127	0.147	0.131	0.153	1.394	
33	Sandstone-14	1	0.124	0.115	0.131	0.124	1.235	
		2	0.146	0.143	0.166	0.157	1.530	
		3	0.133	0.110	0.162	0.124	1.323	1.300
		4	0.110	0.099	0.109	0.132	1.125	
		5	0.125	0.130	0.128	0.132	1.287	
34	Sandstone-15	1	0.122	0.150	0.133	0.156	1.403	
		2	0.119	0.118	0.150	0.144	1.328	
		3	0.201	0.143	0.186	0.153	1.708	1.600
		4	0.130	0.182	0.161	0.164	1.593	
		5	0.194	0.205	0.204	0.191	1.985	
35	Sandstone-16	1	0.385	0.410	0.390	0.406	3.978	
		2	0.329	0.326	0.338	0.346	3.348	
		3	0.382	0.376	0.377	0.402	3.843	3.664
		4	0.363	0.363	0.327	0.355	3.520	
		5	0.339	0.380	0.344	0.390	3.633	
36	Sandstone-17	1	0.302	0.278	0.313	0.286	2.948	
		2	0.294	0.303	0.259	0.283	2.849	
		3	0.306	0.315	0.281	0.307	3.023	2.881
		4	0.287	0.263	0.300	0.256	2.766	
		5	0.277	0.305	0.273	0.273	2.820	

CERCHAR abrasivity index (CAI) for saw cut rock surfaces measured using side view of the stylus tip.							
Sr. No.	Rock Sample	Test No.	1st Wear Flat Measurement (SIDE) mm	2nd Wear Flat Measurement at 90° Rotation (SIDE) mm	3rd Wear Flat Measurement at 90° Rotation (SIDE) mm	4th Wear Flat Measurement at 90° Rotation (SIDE) mm	CAI$_s$ (Side) (0.1 mm)	Avg. CAI$_s$ (Side)
37	Sandstone-18	1	0.159	0.185	0.167	0.147	1.645	2.339
		2	0.288	0.287	0.324	0.282	2.953	
		3	0.284	0.271	0.271	0.282	2.770	
		4	0.169	0.232	0.168	0.225	1.983	
		5	0.226	0.243	0.228	0.240	2.343	
38	Chamositic-Siderite	1	0.133	0.109	0.120	0.096	1.145	0.926
		2	0.079	0.085	0.077	0.077	0.795	
		3	0.110	0.103	0.108	0.089	1.025	
		4	0.078	0.065	0.082	0.070	0.738	
		5	0.090	0.097	0.089	0.095	0.927	
39	Dolomite-1	1	0.213	0.176	0.194	0.216	1.998	2.082
		2	0.150	0.209	0.191	0.228	1.945	
		3	0.220	0.224	0.241	0.202	2.218	
		4	0.218	0.208	0.230	0.211	2.168	
		5	0.190	0.209	0.220	0.213	2.080	
40	Dolomite-2	1	0.198	0.191	0.179	0.170	1.845	1.818
		2	0.203	0.186	0.191	0.145	1.813	
		3	0.182	0.186	0.179	0.195	1.855	
		4	0.197	0.230	0.234	0.179	2.100	
		5	0.138	0.144	0.153	0.155	1.475	
41	Dolomite-3	1	0.170	0.191	0.242	0.148	1.878	2.041
		2	0.280	0.192	0.234	0.205	2.278	
		3	0.200	0.199	0.201	0.187	1.968	
		4	0.248	0.281	0.256	0.263	2.620	
		5	0.169	0.124	0.165	0.127	1.462	
42	Dolomite-4	1	0.177	0.274	0.217	0.241	2.273	2.125
		2	0.227	0.198	0.240	0.193	2.145	
		3	0.220	0.192	0.190	0.264	2.165	
		4	0.205	0.222	0.206	0.223	2.140	
		5	0.200	0.150	0.215	0.196	1.903	
43	Limestone-1	1	0.062	0.052	0.062	0.052	0.571	0.571
		2	0.052	0.052	0.052	0.052	0.519	
		3	0.062	0.062	0.062	0.062	0.623	
		4	0.049	0.057	0.049	0.057	0.530	
		5	0.058	0.064	0.060	0.063	0.612	
44	Limestone-2	1	0.098	0.089	0.098	0.089	0.935	0.906
		2	0.091	0.100	0.091	0.100	0.954	
		3	0.072	0.093	0.072	0.093	0.827	
		4	0.106	0.078	0.104	0.079	0.917	
		5	0.092	0.088	0.091	0.088	0.898	
45	Limestone-3	1	0.116	0.118	0.111	0.127	1.178	1.400
		2	0.122	0.121	0.133	0.137	1.283	
		3	0.129	0.127	0.125	0.113	1.235	
		4	0.148	0.153	0.146	0.148	1.488	
		5	0.169	0.184	0.183	0.191	1.818	

CERCHAR abrasivity index (CAI) for saw cut rock surfaces measured using side view of the stylus tip.

Sr. No.	Rock Sample	Test No.	1st Wear Flat Measurement (SIDE) mm	2nd Wear Flat Measurement at 90º Rotation (SIDE) mm	3rd Wear Flat Measurement at 90º Rotation (SIDE) mm	4th Wear Flat Measurement at 90º Rotation (SIDE) mm	CAI$_s$ (Side) (0.1 mm)	Avg. CAI$_s$ (Side)
46	Limestone-4	1	0.087	0.097	0.105	0.090	0.948	
		2	0.121	0.144	0.125	0.128	1.295	
		3	0.137	0.100	0.119	0.115	1.178	1.098
		4	0.099	0.108	0.088	0.094	0.973	
		5	0.104	0.115	0.104	0.115	1.095	
47	Limestone-5	1	0.141	0.109	0.128	0.125	1.258	
		2	0.112	0.107	0.112	0.119	1.125	
		3	0.109	0.109	0.105	0.113	1.090	1.109
		4	0.101	0.092	0.108	0.084	0.963	
		5	0.111	0.110	0.112	0.110	1.108	
48	Limestone-6	1	0.110	0.101	0.098	0.082	0.978	
		2	0.104	0.080	0.109	0.116	1.023	
		3	0.099	0.104	0.093	0.096	0.980	0.863
		4	0.068	0.072	0.058	0.060	0.645	
		5	0.062	0.075	0.080	0.059	0.690	
49	Limestone-7	1	0.027	0.024	0.022	0.026	0.248	
		2	0.020	0.023	0.020	0.022	0.213	
		3	0.025	0.025	0.024	0.022	0.240	0.229
		4	0.024	0.019	0.022	0.022	0.218	
		5	0.027	0.018	0.027	0.019	0.227	
50	Rock Gypsum	1	0.044	0.028	0.044	0.028	0.363	
		2	0.028	0.040	0.028	0.040	0.339	
		3	0.059	0.040	0.059	0.040	0.498	0.435
		4	0.040	0.047	0.040	0.047	0.435	
		5	0.053	0.055	0.054	0.054	0.540	
51	Marl	1	0.020	0.021	0.019	0.025	0.213	
		2	0.019	0.023	0.025	0.019	0.215	
		3	0.013	0.015	0.017	0.017	0.155	0.194
		4	0.020	0.012	0.018	0.018	0.170	
		5	0.022	0.021	0.023	0.021	0.217	

CERCHAR abrasivity index (CAI) for freshly broken rock surfaces measured at top of the stylus tip.

Sr. No.	Rock Sample	Test No.	1st Wear Flat Measurement (TOP) mm	2nd Wear Flat Measurement at 90° Rotation (TOP) mm	$CAI_{fb(Top)}$ (0.1 mm)	Avg. $CAI_{fb(Top)}$
1	Dolerite-1	1	0.363	0.414	3.884	3.627
		2	0.383	0.425	4.039	
		3	0.323	0.269	2.960	
		4	0.302	0.309	3.056	
		5	0.388	0.299	3.435	
		6	0.481	0.397	4.39	
2	Dolerite-2	1	0.383	0.351	3.669	4.074
		2	0.404	0.311	3.573	
		3	0.302	0.358	3.299	
		4	0.563	0.505	5.340	
		5	0.453	0.445	4.490	
3	Dolerite-3	1	0.544	0.482	5.130	4.650
		2	0.383	0.354	3.684	
		3	0.517	0.404	4.603	
		4	0.487	0.440	4.635	
		5	0.543	0.495	5.190	
4	Dolerite-4	1	0.443	0.435	4.392	4.450
		2	0.424	0.380	4.018	
		3	0.484	0.508	4.958	
		4	0.415	0.416	4.155	
		5	0.439	0.489	4.640	
5	Granite-1	1	0.605	0.427	5.158	5.273
		2	0.544	0.432	4.880	
		3	0.548	0.730	6.388	
		4	0.363	0.570	4.665	
		5	0.656	0.398	5.270	
6	Granite-2	1	0.608	0.402	5.051	4.980
		2	0.443	0.427	4.352	
		3	0.512	0.530	5.210	
		4	0.545	0.516	5.305	
		5	0.516	0.481	4.985	
7	Granite-3	1	0.544	0.510	5.270	5.283
		2	0.443	0.564	5.037	
		3	0.665	0.468	5.665	
		4	0.602	0.649	6.255	
		5	0.352	0.486	4.190	
8	Granite-4	1	0.484	0.613	5.483	5.081
		2	0.524	0.567	5.455	
		3	0.476	0.495	4.855	
		4	0.578	0.558	5.680	
		5	0.341	0.445	3.930	
9	Granite-5	1	0.402	0.489	4.455	4.480
		2	0.506	0.521	5.135	
		3	0.357	0.39	3.735	
		4	0.379	0.542	4.605	
		5	0.371	0.523	4.470	

CERCHAR abrasivity index (CAI) for freshly broken rock surfaces measured at top of the stylus tip.						
Sr. No.	Rock Sample	Test No.	1st Wear Flat Measurement (TOP) mm	2nd Wear Flat Measurement at 90º Rotation (TOP) mm	CAI$_{fb(Top)}$ (0.1 mm)	Avg. CAI$_{fb(Top)}$
10	Granite-6	1	0.483	0.512	4.975	4.987
		2	0.445	0.484	4.645	
		3	0.470	0.499	4.845	
		4	0.507	0.533	5.200	
		5	0.514	0.540	5.270	
11	Migmatite	1	0.425	0.371	3.982	3.605
		2	0.507	0.340	4.234	
		3	0.284	0.236	2.602	
		4	0.362	0.163	2.623	
		5	0.519	0.398	4.585	
12	Andesite	1	0.411	0.400	4.055	5.154
		2	0.459	0.543	5.008	
		3	0.525	0.544	5.343	
		4	0.531	0.536	5.335	
		5	0.601	0.605	6.028	
13	Granitic Gneiss-1	1	0.324	0.347	3.356	3.570
		2	0.325	0.314	3.196	
		3	0.429	0.403	4.158	
		4	0.319	0.327	3.230	
		5	0.410	0.372	3.910	
14	Granitic Gneiss-2	1	0.476	0.535	5.055	5.025
		2	0.513	0.426	4.695	
		3	0.340	0.485	4.125	
		4	0.616	0.806	7.110	
		5	0.461	0.367	4.140	
15	Phyllite	1	0.196	0.194	1.950	2.677
		2	0.270	0.249	2.595	
		3	0.234	0.212	2.230	
		4	0.265	0.334	2.995	
		5	0.364	0.359	3.615	
16	Quartzite-1	1	0.576	0.595	5.853	4.703
		2	0.475	0.425	4.502	
		3	0.354	0.397	3.754	
		4	0.450	0.488	4.690	
		5	0.473	0.470	4.716	
17	Quartzite-2	1	0.506	0.426	4.662	4.594
		2	0.506	0.480	4.932	
		3	0.425	0.452	4.387	
		4	0.447	0.377	4.120	
		5	0.455	0.405	4.295	
		6	0.461	0.573	5.170	
18	Siltstone-1	1	0.151	0.167	1.588	1.440
		2	0.120	0.110	1.150	
		3	0.151	0.168	1.595	
		4	0.150	0.210	1.800	
		5	0.113	0.105	1.094	

CERCHAR abrasivity index (CAI) for freshly broken rock surfaces measured at top of the stylus tip.						
Sr. No.	Rock Sample	Test No.	1st Wear Flat Measurement (TOP) mm	2nd Wear Flat Measurement at 90º Rotation (TOP) mm	$CAI_{fb(Top)}$ (0.1 mm)	Avg. $CAI_{fb(Top)}$
19	Siltstone-2	1	0.212	0.190	2.011	2.302
		2	0.217	0.183	2.001	
		3	0.215	0.236	2.257	
		4	0.321	0.256	2.885	
		5	0.240	0.231	2.355	
20	Sandstone-1	1	0.251	0.228	2.395	2.067
		2	0.188	0.171	1.795	
		3	0.211	0.191	2.010	
		4	0.183	0.173	1.778	
		5	0.267	0.204	2.357	
21	Sandstone-2	1	0.102	0.139	1.203	1.250
		2	0.122	0.154	1.380	
		3	0.102	0.131	1.163	
		4	0.122	0.128	1.250	
		5	0.110	0.156	1.256	
22	Sandstone-3	1	0.297	0.403	3.501	3.550
		2	0.396	0.364	3.801	
		3	0.317	0.355	3.360	
		4	0.376	0.352	3.640	
		5	0.368	0.322	3.450	
23	Sandstone-4	1	0.157	0.142	1.496	1.540
		2	0.163	0.177	1.698	
		3	0.142	0.143	1.426	
		4	0.152	0.138	1.450	
		5	0.159	0.167	1.630	
24	Sandstone-5	1	0.238	0.248	2.428	2.931
		2	0.217	0.280	2.482	
		3	0.208	0.194	2.008	
		4	0.525	0.312	4.185	
		5	0.326	0.385	3.555	
25	Sandstone-6	1	0.310	0.311	3.105	3.210
		2	0.325	0.349	3.370	
		3	0.353	0.270	3.115	
		4	0.282	0.371	3.265	
		5	0.296	0.344	3.200	
26	Sandstone-7	1	0.136	0.145	1.405	1.680
		2	0.219	0.207	2.130	
		3	0.194	0.173	1.835	
		4	0.129	0.141	1.350	
		5	0.180	0.156	1.679	
27	Sandstone-8	1	0.106	0.111	1.085	1.140
		2	0.087	0.073	0.800	
		3	0.142	0.144	1.430	
		4	0.135	0.114	1.245	
		5	0.129	0.099	1.139	

CERCHAR abrasivity index (CAI) for freshly broken rock surfaces measured at top of the stylus tip.						
Sr. No.	Rock Sample	Test No.	1st Wear Flat Measurement (TOP) mm	2nd Wear Flat Measurement at 90º Rotation (TOP) mm	CAI$_{fb(Top)}$ (0.1 mm)	Avg. CAI$_{fb(Top)}$
28	Sandstone-9	1	0.216	0.244	2.300	
		2	0.180	0.244	2.120	
		3	0.277	0.321	2.990	2.690
		4	0.334	0.342	3.380	
		5	0.204	0.328	2.660	
29	Sandstone-10	1	0.152	0.147	1.495	
		2	0.170	0.177	1.735	
		3	0.187	0.108	1.475	1.570
		4	0.149	0.166	1.575	
		5	0.136	0.178	1.569	
30	Sandstone-11	1	0.167	0.225	1.960	
		2	0.178	0.192	1.850	
		3	0.242	0.191	2.165	1.930
		4	0.168	0.184	1.760	
		5	0.226	0.157	1.915	
31	Sandstone-12	1	0.185	0.107	1.460	
		2	0.144	0.162	1.530	
		3	0.141	0.108	1.245	1.281
		4	0.102	0.076	0.890	
		5	0.121	0.135	1.279	
32	Sandstone-13	1	0.250	0.223	2.365	
		2	0.230	0.190	2.100	
		3	0.197	0.158	1.775	2.160
		4	0.208	0.269	2.385	
		5	0.199	0.236	2.175	
33	Sandstone-14	1	0.140	0.125	1.325	
		2	0.115	0.137	1.260	
		3	0.112	0.099	1.055	1.230
		4	0.137	0.118	1.275	
		5	0.110	0.137	1.235	
34	Sandstone-15	1	0.146	0.123	1.345	
		2	0.193	0.173	1.830	
		3	0.207	0.145	1.760	1.700
		4	0.197	0.144	1.705	
		5	0.184	0.189	1.865	
35	Sandstone-16	1	0.603	0.758	6.805	
		2	0.537	0.634	5.855	
		3	0.595	0.702	6.485	6.355
		4	0.619	0.659	6.390	
		5	0.582	0.666	6.240	
36	Sandstone-17	1	0.326	0.548	4.370	
		2	0.291	0.292	2.915	
		3	0.430	0.491	4.605	3.820
		4	0.406	0.341	3.735	
		5	0.308	0.387	3.475	

CERCHAR abrasivity index (CAI) for freshly broken rock surfaces measured at top of the stylus tip.						
Sr. No.	Rock Sample	Test No.	1st Wear Flat Measurement (TOP) mm	2nd Wear Flat Measurement at 90º Rotation (TOP) mm	$CAI_{fb(Top)}$ (0.1 mm)	Avg. $CAI_{fb(Top)}$
37	Sandstone-18	1	0.254	0.342	2.980	
		2	0.475	0.409	4.420	
		3	0.274	0.283	2.785	3.481
		4	0.394	0.401	3.975	
		5	0.339	0.310	3.245	
38	Chamositic-Siderite	1	0.251	0.630	4.407	
		2	0.093	0.091	0.918	
		3	0.080	0.081	0.805	1.837
		4	0.135	0.109	1.219	
		5	0.170	0.197	1.835	
39	Dolomite-1	1	0.177	0.159	1.680	
		2	0.164	0.152	1.580	
		3	0.153	0.172	1.625	1.568
		4	0.153	0.124	1.385	
		5	0.173	0.141	1.570	
40	Dolomite-2	1	0.176	0.207	1.915	
		2	0.189	0.246	2.175	
		3	0.221	0.223	2.220	1.979
		4	0.173	0.187	1.800	
		5	0.166	0.191	1.785	
41	Dolomite-3	1	0.206	0.215	2.105	
		2	0.200	0.160	1.800	
		3	0.232	0.218	2.250	2.052
		4	0.204	0.227	2.155	
		5	0.187	0.203	1.950	
42	Dolomite-4	1	0.230	0.290	2.600	
		2	0.263	0.229	2.460	
		3	0.214	0.250	2.320	2.410
		4	0.215	0.249	2.320	
		5	0.217	0.253	2.350	
43	Limestone-1	1	0.143	0.167	1.551	
		2	0.122	0.129	1.253	
		3	0.114	0.115	1.145	1.260
		4	0.096	0.155	1.255	
		5	0.115	0.103	1.090	
44	Limestone-2	1	0.142	0.126	1.341	
		2	0.113	0.105	1.090	
		3	0.147	0.140	1.435	1.207
		4	0.092	0.091	0.915	
		5	0.132	0.118	1.250	
45	Limestone-3	1	0.172	0.113	1.425	
		2	0.207	0.150	1.787	
		3	0.115	0.126	1.205	1.631
		4	0.211	0.193	2.020	
		5	0.147	0.197	1.720	

CERCHAR abrasivity index (CAI) for freshly broken rock surfaces measured at top of the stylus tip.						
Sr. No.	Rock Sample	Test No.	1st Wear Flat Measurement (TOP) mm	2nd Wear Flat Measurement at 90º Rotation (TOP) mm	$CAI_{fb(Top)}$ (0.1 mm)	Avg. $CAI_{fb(Top)}$
46	Limestone-4	1	0.099	0.085	0.920	
		2	0.112	0.093	1.025	
		3	0.087	0.083	0.850	0.961
		4	0.112	0.098	1.050	
		5	0.090	0.102	0.960	
47	Limestone-5	1	0.119	0.099	1.090	
		2	0.084	0.078	0.810	
		3	0.128	0.125	1.265	1.051
		4	0.115	0.093	1.040	
		5	0.109	0.101	1.049	
48	Limestone-6	1	0.103	0.144	1.235	
		2	0.085	0.079	0.820	
		3	0.109	0.091	1.000	0.912
		4	0.124	0.065	0.945	
		5	0.056	0.056	0.560	
49	Limestone-7	1	0.025	0.044	0.345	
		2	0.027	0.041	0.340	
		3	0.032	0.047	0.395	0.335
		4	0.025	0.027	0.260	
		5	0.028	0.038	0.333	
50	Rock Gypsum	1	0.079	0.071	0.750	
		2	0.076	0.065	0.705	
		3	0.093	0.101	0.971	0.809
		4	0.064	0.092	0.780	
		5	0.098	0.070	0.839	
51	Marl	1	0.015	0.015	0.150	
		2	0.023	0.026	0.245	
		3	0.023	0.022	0.225	0.207
		4	0.021	0.027	0.240	
		5	0.012	0.023	0.175	

CERCHAR abrasivity index (CAI) for freshly broken rock surfaces measured using side view of the stylus tip.

Sr. No.	Rock Sample	Test No.	1st Wear Flat Measurement (SIDE) mm	2nd Wear Flat Measurement at 90º Rotation (SIDE) mm	3rd Wear Flat Measurement at 90º Rotation (SIDE) mm	4th Wear Flat Measurement at 90º Rotation (SIDE) mm	CAI$_{fb}$ (Side) (0.1 mm)	Avg. CAI$_{fb}$ (Side)
1	Dolerite-1	1	0.262	0.262	0.262	0.262	2.619	3.083
		2	0.302	0.282	0.302	0.282	2.922	
		3	0.355	0.274	0.349	0.274	3.130	
		4	0.377	0.371	0.349	0.368	3.663	
		5	0.222	0.362	0.268	0.380	3.080	
2	Dolerite-2	1	0.322	0.283	0.322	0.283	3.025	3.150
		2	0.282	0.262	0.282	0.262	2.720	
		3	0.181	0.242	0.181	0.242	2.116	
		4	0.413	0.474	0.407	0.461	4.388	
		5	0.308	0.379	0.346	0.368	3.503	
3	Dolerite-3	1	0.343	0.363	0.343	0.363	3.526	3.851
		2	0.343	0.302	0.343	0.302	3.226	
		3	0.343	0.383	0.343	0.383	3.627	
		4	0.403	0.413	0.410	0.394	4.049	
		5	0.437	0.536	0.568	0.390	4.828	
4	Dolerite-4	1	0.365	0.363	0.365	0.363	3.638	3.590
		2	0.383	0.322	0.383	0.322	3.526	
		3	0.363	0.363	0.363	0.363	3.627	
		4	0.355	0.330	0.338	0.352	3.436	
		5	0.356	0.353	0.383	0.398	3.725	
5	Granite-1	1	0.489	0.413	0.459	0.440	4.503	4.502
		2	0.403	0.423	0.403	0.423	4.131	
		3	0.363	0.403	0.363	0.403	3.831	
		4	0.580	0.695	0.460	0.635	5.925	
		5	0.396	0.408	0.405	0.439	4.120	
6	Granite-2	1	0.363	0.363	0.363	0.363	3.627	4.110
		2	0.342	0.303	0.342	0.303	3.223	
		3	0.546	0.520	0.438	0.439	4.856	
		4	0.429	0.504	0.440	0.522	4.738	
		5	0.418	0.402	0.418	0.404	4.105	
7	Granite-3	1	0.383	0.485	0.383	0.485	4.340	4.150
		2	0.322	0.282	0.322	0.282	3.023	
		3	0.504	0.443	0.504	0.443	4.735	
		4	0.562	0.561	0.563	0.509	5.488	
		5	0.284	0.351	0.269	0.362	3.165	
8	Granite-4	1	0.383	0.403	0.383	0.403	3.929	4.031
		2	0.403	0.424	0.403	0.424	4.133	
		3	0.406	0.414	0.421	0.436	4.193	
		4	0.433	0.498	0.352	0.549	4.580	
		5	0.357	0.317	0.341	0.330	3.363	
9	Granite-5	1	0.336	0.363	0.336	0.363	3.496	3.450
		2	0.396	0.419	0.396	0.419	4.073	
		3	0.282	0.288	0.282	0.288	2.848	
		4	0.355	0.326	0.355	0.326	3.404	
		5	0.352	0.348	0.332	0.339	3.428	

CERCHAR abrasivity index (CAI) for freshly broken rock surfaces measured using side view of the stylus tip.								
Sr. No.	Rock Sample	Test No.	1st Wear Flat Measurement (SIDE) mm	2nd Wear Flat Measurement at 90º Rotation (SIDE) mm	3rd Wear Flat Measurement at 90º Rotation (SIDE) mm	4th Wear Flat Measurement at 90º Rotation (SIDE) mm	CAI$_{fb}$ (Side) (0.1 mm)	Avg. CAI$_{fb}$ (Side)
10	Granite-6	1	0.489	0.516	0.428	0.437	4.675	4.687
		2	0.522	0.512	0.507	0.541	5.205	
		3	0.438	0.420	0.441	0.444	4.358	
		4	0.479	0.451	0.454	0.473	4.643	
		5	0.481	0.466	0.440	0.435	4.555	
11	Migmatite	1	0.385	0.304	0.385	0.304	3.445	3.210
		2	0.344	0.304	0.344	0.304	3.241	
		3	0.305	0.290	0.305	0.290	2.975	
		4	0.321	0.273	0.278	0.301	2.933	
		5	0.349	0.329	0.345	0.359	3.455	
12	Andesite	1	0.316	0.332	0.385	0.352	3.463	4.425
		2	0.559	0.412	0.498	0.432	4.753	
		3	0.474	0.426	0.492	0.438	4.573	
		4	0.478	0.370	0.472	0.433	4.383	
		5	0.474	0.519	0.455	0.534	4.955	
13	Granitic Gneiss-1	1	0.284	0.324	0.284	0.324	3.039	3.270
		2	0.263	0.324	0.263	0.324	2.937	
		3	0.385	0.385	0.385	0.385	3.848	
		4	0.304	0.315	0.303	0.316	3.095	
		5	0.345	0.341	0.344	0.342	3.430	
14	Granitic Gneiss-2	1	0.326	0.374	0.319	0.377	3.490	4.164
		2	0.402	0.403	0.354	0.362	3.803	
		3	0.343	0.327	0.352	0.310	3.330	
		4	0.741	0.536	0.714	0.589	6.450	
		5	0.399	0.321	0.448	0.331	3.748	
15	Phyllite	1	0.177	0.159	0.193	0.169	1.745	2.184
		2	0.196	0.216	0.220	0.221	2.133	
		3	0.197	0.191	0.193	0.205	1.965	
		4	0.204	0.212	0.214	0.215	2.113	
		5	0.344	0.246	0.318	0.278	2.964	
16	Quartzite-1	1	0.475	0.418	0.475	0.418	4.467	3.932
		2	0.456	0.396	0.456	0.396	4.259	
		3	0.337	0.277	0.337	0.277	3.070	
		4	0.435	0.436	0.436	0.437	4.360	
		5	0.299	0.402	0.297	0.403	3.503	
17	Quartzite-2	1	0.324	0.344	0.324	0.344	0.324	3.652
		2	0.304	0.304	0.304	0.304	0.304	
		3	0.344	0.425	0.344	0.425	0.344	
		4	0.387	0.331	0.362	0.333	3.533	
		5	0.358	0.297	0.338	0.390	3.458	
		6	0.533	0.409	0.515	0.420	4.693	
18	Siltstone-1	1	0.133	0.125	0.133	0.125	1.286	1.250
		2	0.130	0.123	0.130	0.123	1.264	
		3	0.121	0.121	0.121	0.121	1.206	
		4	0.126	0.120	0.126	0.120	1.230	
		5	0.122	0.131	0.122	0.131	1.265	

CERCHAR abrasivity index (CAI) for freshly broken rock surfaces measured using side view of the stylus tip.							
Sr. No.	Rock Sample	Test No.	1st Wear Flat Measurement (SIDE) mm	2nd Wear Flat Measurement at 90° Rotation (SIDE) mm	3rd Wear Flat Measurement at 90° Rotation (SIDE) mm	4th Wear Flat Measurement at 90° Rotation (SIDE) mm	CAI_fb (Side) (0.1 mm)	Avg. CAI_fb (Side)
19	Siltstone-2	1	0.198	0.142	0.198	0.142	1.698	1.872
		2	0.178	0.169	0.178	0.169	1.736	
		3	0.222	0.192	0.222	0.192	2.071	
		4	0.200	0.200	0.187	0.185	1.930	
		5	0.182	0.203	0.197	0.188	1.925	
20	Sandstone-1	1	0.180	0.246	0.194	0.223	2.108	1.764
		2	0.219	0.212	0.221	0.241	2.233	
		3	0.132	0.140	0.145	0.138	1.388	
		4	0.159	0.169	0.175	0.166	1.673	
		5	0.140	0.129	0.180	0.118	1.417	
21	Sandstone-2	1	0.070	0.112	0.070	0.112	0.909	0.860
		2	0.089	0.098	0.089	0.098	0.933	
		3	0.085	0.068	0.085	0.068	0.764	
		4	0.081	0.086	0.081	0.086	0.836	
		5	0.091	0.097	0.072	0.082	0.855	
22	Sandstone-3	1	0.277	0.297	0.277	0.297	2.872	2.840
		2	0.297	0.357	0.297	0.357	3.271	
		3	0.219	0.258	0.219	0.258	2.386	
		4	0.320	0.279	0.320	0.280	2.998	
		5	0.235	0.299	0.235	0.300	2.672	
23	Sandstone-4	1	0.112	0.120	0.112	0.120	1.158	1.220
		2	0.116	0.123	0.116	0.123	1.197	
		3	0.122	0.137	0.122	0.137	1.295	
		4	0.118	0.119	0.120	0.116	1.183	
		5	0.140	0.113	0.140	0.114	1.267	
24	Sandstone-5	1	0.183	0.226	0.183	0.226	2.043	2.275
		2	0.226	0.215	0.226	0.215	2.201	
		3	0.151	0.140	0.151	0.140	1.451	
		4	0.232	0.259	0.298	0.245	2.585	
		5	0.311	0.350	0.292	0.285	3.095	
25	Sandstone-6	1	0.299	0.340	0.342	0.333	3.285	3.210
		2	0.294	0.305	0.301	0.265	2.913	
		3	0.301	0.303	0.319	0.355	3.195	
		4	0.332	0.340	0.381	0.335	3.470	
		5	0.304	0.325	0.316	0.330	3.187	
26	Sandstone-7	1	0.138	0.119	0.129	0.129	1.288	1.380
		2	0.141	0.193	0.173	0.167	1.685	
		3	0.142	0.100	0.155	0.157	1.385	
		4	0.113	0.118	0.130	0.115	1.190	
		5	0.138	0.129	0.142	0.132	1.352	
27	Sandstone-8	1	0.100	0.142	0.090	0.131	1.158	1.250
		2	0.113	0.111	0.099	0.119	1.105	
		3	0.156	0.155	0.132	0.134	1.443	
		4	0.122	0.128	0.127	0.146	1.308	
		5	0.128	0.135	0.123	0.108	1.235	

CERCHAR abrasivity index (CAI) for freshly broken rock surfaces measured using side view of the stylus tip.								
Sr. No.	Rock Sample	Test No.	1st Wear Flat Measurement (SIDE) mm	2nd Wear Flat Measurement at 90º Rotation (SIDE) mm	3rd Wear Flat Measurement at 90º Rotation (SIDE) mm	4th Wear Flat Measurement at 90º Rotation (SIDE) mm	CAI$_{fb}$ (Side) (0.1 mm)	Avg. CAI$_{fb}$ (Side)
28	Sandstone-9	1	0.249	0.246	0.232	0.217	2.360	
		2	0.235	0.255	0.188	0.244	2.305	
		3	0.212	0.285	0.267	0.239	2.508	2.610
		4	0.336	0.307	0.322	0.341	3.265	
		5	0.297	0.245	0.292	0.211	2.612	
29	Sandstone-10	1	0.148	0.151	0.133	0.168	1.500	
		2	0.114	0.159	0.147	0.123	1.358	
		3	0.143	0.140	0.137	0.135	1.388	1.443
		4	0.147	0.162	0.146	0.156	1.528	
		5	0.157	0.135	0.152	0.132	1.440	
30	Sandstone-11	1	0.146	0.137	0.157	0.146	1.465	
		2	0.154	0.153	0.137	0.164	1.520	
		3	0.148	0.169	0.132	0.153	1.505	1.490
		4	0.156	0.148	0.151	0.145	1.500	
		5	0.140	0.152	0.138	0.156	1.465	
31	Sandstone-12	1	0.135	0.126	0.130	0.110	1.253	
		2	0.125	0.140	0.131	0.146	1.355	
		3	0.107	0.105	0.096	0.120	1.070	1.147
		4	0.105	0.098	0.088	0.073	0.910	
		5	0.128	0.109	0.124	0.098	1.148	
32	Sandstone-13	1	0.197	0.190	0.195	0.210	1.980	
		2	0.174	0.196	0.236	0.190	1.990	
		3	0.147	0.155	0.164	0.163	1.573	1.810
		4	0.160	0.171	0.182	0.161	1.685	
		5	0.199	0.154	0.187	0.189	1.822	
33	Sandstone-14	1	0.125	0.128	0.134	0.130	1.293	
		2	0.152	0.109	0.133	0.134	1.320	
		3	0.125	0.126	0.154	0.128	1.333	1.310
		4	0.144	0.116	0.133	0.125	1.295	
		5	0.141	0.120	0.129	0.133	1.308	
34	Sandstone-15	1	0.120	0.123	0.134	0.120	1.243	
		2	0.120	0.178	0.132	0.159	1.473	
		3	0.153	0.149	0.165	0.149	1.540	1.450
		4	0.166	0.149	0.165	0.127	1.518	
		5	0.143	0.141	0.138	0.177	1.498	
35	Sandstone-16	1	0.502	0.525	0.557	0.686	5.675	
		2	0.495	0.569	0.570	0.486	5.300	
		3	0.616	0.648	0.600	0.595	6.148	5.532
		4	0.535	0.545	0.474	0.520	5.185	
		5	0.558	0.549	0.505	0.552	5.410	
36	Sandstone-17	1	0.309	0.296	0.333	0.306	3.108	
		2	0.223	0.165	0.159	0.188	1.838	
		3	0.373	0.318	0.311	0.316	3.295	2.913
		4	0.341	0.305	0.278	0.352	3.190	
		5	0.372	0.273	0.300	0.309	3.135	

Sr. No.	Rock Sample	Test No.	1st Wear Flat Measurement (SIDE) mm	2nd Wear Flat Measurement at 90º Rotation (SIDE) mm	3rd Wear Flat Measurement at 90º Rotation (SIDE) mm	4th Wear Flat Measurement at 90º Rotation (SIDE) mm	CAI$_{fb}$ (Side) (0.1 mm)	Avg. CAI$_{fb}$ (Side)
			CERCHAR abrasivity index (CAI) for freshly broken rock surfaces measured using side view of the stylus tip.					
37	Sandstone-18	1	0.243	0.176	0.276	0.192	2.218	
		2	0.262	0.276	0.268	0.273	2.698	
		3	0.235	0.234	0.229	0.222	2.300	2.385
		4	0.198	0.191	0.220	0.180	1.973	
		5	0.277	0.273	0.266	0.279	2.738	
38	Chamositic-Siderite	1	0.174	0.152	0.165	0.179	1.675	
		2	0.092	0.087	0.085	0.060	0.810	
		3	0.077	0.090	0.086	0.064	0.793	1.018
		4	0.088	0.077	0.075	0.077	0.793	
		5	0.103	0.096	0.101	0.108	1.020	
39	Dolomite-1	1	0.197	0.176	0.158	0.172	1.758	
		2	0.147	0.119	0.169	0.184	1.548	
		3	0.159	0.191	0.181	0.125	1.640	1.608
		4	0.166	0.147	0.144	0.137	1.485	
		5	0.148	0.185	0.170	0.141	1.610	
40	Dolomite-2	1	0.193	0.156	0.169	0.149	1.668	
		2	0.225	0.201	0.182	0.192	2.000	
		3	0.213	0.150	0.190	0.208	1.903	1.787
		4	0.168	0.165	0.180	0.177	1.725	
		5	0.159	0.146	0.163	0.187	1.638	
41	Dolomite-3	1	0.180	0.195	0.156	0.182	1.783	
		2	0.174	0.208	0.151	0.195	1.820	
		3	0.196	0.229	0.192	0.217	2.084	1.895
		4	0.154	0.210	0.168	0.188	1.800	
		5	0.186	0.215	0.191	0.203	1.988	
42	Dolomite-4	1	0.221	0.285	0.211	0.254	2.428	
		2	0.178	0.248	0.217	0.246	2.223	
		3	0.199	0.194	0.210	0.190	1.983	2.149
		4	0.196	0.185	0.188	0.190	1.898	
		5	0.221	0.285	0.211	0.254	2.428	
43	Limestone-1	1	0.101	0.101	0.101	0.101	1.013	
		2	0.122	0.123	0.122	0.123	1.224	
		3	0.102	0.103	0.115	0.101	1.053	1.062
		4	0.084	0.136	0.098	0.106	1.060	
		5	0.090	0.102	0.099	0.093	0.960	
44	Limestone-2	1	0.089	0.093	0.089	0.093	0.910	
		2	0.107	0.084	0.107	0.084	0.955	
		3	0.094	0.112	0.094	0.112	1.030	0.938
		4	0.088	0.083	0.088	0.083	0.855	
		5	0.103	0.081	0.100	0.092	0.940	

CERCHAR abrasivity index (CAI) for freshly broken rock surfaces measured using side view of the stylus tip.							
Sr. No.	Rock Sample	Test No.	1st Wear Flat Measurement (SIDE) mm	2nd Wear Flat Measurement at 90º Rotation (SIDE) mm	3rd Wear Flat Measurement at 90º Rotation (SIDE) mm	4th Wear Flat Measurement at 90º Rotation (SIDE) mm	CAIfb (Side) (0.1 mm)	Avg. CAIfb (Side)
45	Limestone-3	1	0.118	0.120	0.168	0.120	1.315	1.455
		2	0.187	0.165	0.192	0.157	1.751	
		3	0.126	0.114	0.109	0.110	1.148	
		4	0.182	0.152	0.188	0.154	1.690	
		5	0.145	0.129	0.155	0.120	1.370	
46	Limestone-4	1	0.110	0.126	0.116	0.120	1.180	1.188
		2	0.130	0.159	0.148	0.143	1.450	
		3	0.095	0.102	0.119	0.110	1.065	
		4	0.087	0.091	0.119	0.125	1.055	
		5	0.120	0.111	0.130	0.115	1.190	
47	Limestone-5	1	0.114	0.103	0.096	0.107	1.050	1.130
		2	0.110	0.117	0.105	0.135	1.168	
		3	0.121	0.108	0.110	0.093	1.080	
		4	0.130	0.123	0.128	0.108	1.223	
		5	0.117	0.119	0.112	0.103	1.128	
48	Limestone-6	1	0.105	0.086	0.107	0.093	0.978	0.690
		2	0.069	0.060	0.055	0.063	0.618	
		3	0.087	0.065	0.086	0.066	0.760	
		4	0.067	0.062	0.052	0.058	0.598	
		5	0.050	0.050	0.053	0.045	0.495	
49	Limestone-7	1	0.039	0.018	0.021	0.017	0.238	0.252
		2	0.031	0.026	0.027	0.022	0.265	
		3	0.028	0.033	0.020	0.024	0.263	
		4	0.022	0.024	0.027	0.024	0.243	
		5	0.025	0.026	0.027	0.022	0.250	
50	Rock Gypsum	1	0.059	0.079	0.059	0.079	0.693	0.503
		2	0.040	0.040	0.040	0.040	0.396	
		3	0.040	0.044	0.040	0.044	0.420	
		4	0.060	0.039	0.059	0.040	0.495	
		5	0.055	0.047	0.044	0.058	0.510	
51	Marl	1	0.013	0.012	0.016	0.011	0.130	0.186
		2	0.023	0.017	0.022	0.019	0.203	
		3	0.021	0.022	0.023	0.024	0.226	
		4	0.024	0.019	0.022	0.017	0.205	
		5	0.017	0.014	0.016	0.019	0.165	

APPENDIX B.

CERCHAR ROCK ABRASIVITY TEST RESULTS FOR SATURATED ROCKS

CERCHAR abrasivity index (CAI) for saw cut saturated rock surfaces measured at top of the stylus tip.

Sr. No.	Rock Sample	Test No.	1st Wear Flat Measurement (TOP) mm	2nd Wear Flat Measurement at 90° Rotation (TOP) mm	$CAI_{ss(Top)}$ (0.1 mm)	Avg. $CAI_{ss(Top)}$
1	Siltstone-1	1	0.104	0.134	1.190	1.147
		2	0.131	0.096	1.135	
		3	0.108	0.138	1.230	
		4	0.131	0.091	1.111	
		5	0.112	0.102	1.070	
2	Siltstone-2	1	0.230	0.289	2.595	2.488
		2	0.258	0.266	2.620	
		3	0.272	0.264	2.680	
		4	0.211	0.272	2.415	
		5	0.214	0.212	2.130	
3	Sandstone-1	1	0.119	0.125	1.220	1.423
		2	0.145	0.180	1.625	
		3	0.151	0.156	1.535	
		4	0.185	0.115	1.500	
		5	0.109	0.138	1.235	
4	Sandstone-2	1	0.145	0.136	1.405	1.276
		2	0.124	0.145	1.345	
		3	0.159	0.106	1.325	
		4	0.087	0.104	0.955	
		5	0.147	0.123	1.350	
5	Sandstone-3	1	0.248	0.281	2.645	2.653
		2	0.306	0.349	3.275	
		3	0.219	0.189	2.040	
		4	0.256	0.293	2.745	
		5	0.275	0.237	2.560	
6	Sandstone-4	1	0.108	0.178	1.430	1.371
		2	0.123	0.153	1.380	
		3	0.137	0.124	1.305	
		4	0.133	0.146	1.395	
		5	0.140	0.129	1.345	
7	Sandstone-5	1	0.313	0.263	2.878	3.292
		2	0.254	0.363	3.085	
		3	0.319	0.331	3.250	
		4	0.286	0.397	3.413	
		5	0.329	0.438	3.836	
8	Sandstone-6	1	0.283	0.318	3.006	2.940
		2	0.334	0.333	3.335	
		3	0.264	0.232	2.480	
		4	0.253	0.260	2.565	
		5	0.332	0.331	3.314	
9	Sandstone-7	1	0.138	0.174	1.555	1.474
		2	0.160	0.162	1.610	
		3	0.138	0.132	1.350	
		4	0.150	0.140	1.450	
		5	0.144	0.137	1.405	

CERCHAR abrasivity index (CAI) for saw cut saturated rock surfaces measured at top of the stylus tip.						
Sr. No.	Rock Sample	Test No.	1st Wear Flat Measurement (TOP) mm	2nd Wear Flat Measurement at 90° Rotation (TOP) mm	CAI$_{ss(Top)}$ (0.1 mm)	Avg. CAI$_{ss(Top)}$
10	Sandstone-8	1	0.133	0.160	1.465	1.426
		2	0.140	0.145	1.425	
		3	0.140	0.193	1.665	
		4	0.106	0.084	0.950	
		5	0.146	0.179	1.625	
11	Sandstone-9	1	0.277	0.245	2.610	2.221
		2	0.153	0.276	2.145	
		3	0.147	0.282	2.145	
		4	0.208	0.236	2.220	
		5	0.196	0.201	1.986	
12	Sandstone-10	1	0.147	0.121	1.340	1.321
		2	0.122	0.144	1.330	
		3	0.109	0.146	1.275	
		4	0.112	0.095	1.035	
		5	0.116	0.196	1.560	
13	Sandstone-11	1	0.165	0.160	1.625	1.682
		2	0.142	0.111	1.265	
		3	0.204	0.143	1.735	
		4	0.164	0.197	1.805	
		5	0.172	0.224	1.980	
14	Sandstone-12	1	0.124	0.124	1.240	1.148
		2	0.124	0.111	1.176	
		3	0.096	0.104	1.001	
		4	0.132	0.103	1.175	
		5	0.124	0.124	1.240	
15	Sandstone-13	1	0.180	0.260	2.200	1.805
		2	0.170	0.145	1.575	
		3	0.128	0.180	1.540	
		4	0.183	0.205	1.940	
		5	0.144	0.210	1.770	
16	Sandstone-14	1	0.115	0.111	1.130	1.140
		2	0.141	0.137	1.390	
		3	0.087	0.101	0.940	
		4	0.130	0.123	1.266	
		5	0.099	0.096	0.975	
17	Sandstone-15	1	0.168	0.143	1.555	1.836
		2	0.189	0.168	1.785	
		3	0.127	0.172	1.495	
		4	0.206	0.211	2.085	
		5	0.252	0.200	2.260	
18	Sandstone-17	1	0.206	0.260	2.330	2.675
		2	0.273	0.311	2.920	
		3	0.194	0.237	2.155	
		4	0.347	0.392	3.695	
		5	0.218	0.237	2.275	

CERCHAR abrasivity index (CAI) for saw cut saturated rock surfaces measured at top of the stylus tip.					
Sr. No.	Rock Sample	Test No.	1st Wear Flat Measurement (TOP) mm	2nd Wear Flat Measurement at 90º Rotation (TOP) mm	$CAI_{ss(Top)}$ (0.1 mm)	Avg. $CAI_{ss(Top)}$
19	Sandstone-18	1	0.345	0.271	3.078	2.761
		2	0.251	0.288	2.695	
		3	0.369	0.298	3.335	
		4	0.297	0.231	2.640	
		5	0.173	0.238	2.055	
20	Chamositic-Siderite	1	0.092	0.098	0.950	1.152
		2	0.101	0.121	1.110	
		3	0.137	0.137	1.370	
		4	0.091	0.111	1.011	
		5	0.135	0.129	1.320	
21	Dolomite-1	1	0.175	0.142	1.585	2.126
		2	0.237	0.210	2.235	
		3	0.203	0.230	2.165	
		4	0.244	0.206	2.250	
		5	0.241	0.238	2.395	
22	Dolomite-2	1	0.224	0.205	2.145	1.928
		2	0.210	0.198	2.040	
		3	0.147	0.192	1.695	
		4	0.184	0.166	1.750	
		5	0.203	0.199	2.010	
23	Dolomite-3	1	0.206	0.220	2.130	2.096
		2	0.167	0.185	1.760	
		3	0.259	0.197	2.280	
		4	0.249	0.194	2.215	
		5	0.203	0.217	2.100	
24	Dolomite-4	1	0.134	0.189	1.615	2.082
		2	0.173	0.211	1.920	
		3	0.275	0.224	2.495	
		4	0.195	0.215	2.050	
		5	0.216	0.250	2.330	
25	Limestone-1	1	0.162	0.138	1.500	1.355
		2	0.123	0.124	1.234	
		3	0.140	0.126	1.330	
		4	0.150	0.130	1.400	
		5	0.124	0.138	1.311	
26	Limestone-2	1	0.095	0.096	0.955	1.316
		2	0.118	0.114	1.160	
		3	0.123	0.132	1.275	
		4	0.196	0.179	1.875	
		5	0.119	0.144	1.315	
27	Limestone-3	1	0.090	0.118	1.040	1.115
		2	0.133	0.168	1.505	
		3	0.099	0.092	0.955	
		4	0.119	0.106	1.125	
		5	0.087	0.103	0.950	

\multicolumn{7}{l}{CERCHAR abrasivity index (CAI) for saw cut saturated rock surfaces measured at top of the stylus tip.}

Sr. No.	Rock Sample	Test No.	1st Wear Flat Measurement (TOP) mm	2nd Wear Flat Measurement at 90° Rotation (TOP) mm	$CAI_{ss(Top)}$ (0.1 mm)	Avg. $CAI_{ss(Top)}$
28	Limestone-4	1	0.116	0.114	1.150	1.181
		2	0.121	0.105	1.130	
		3	0.123	0.123	1.230	
		4	0.118	0.127	1.225	
		5	0.122	0.112	1.170	
29	Limestone-5	1	0.127	0.127	1.270	1.141
		2	0.120	0.122	1.211	
		3	0.110	0.112	1.110	
		4	0.108	0.087	0.975	
		5	0.108	0.120	1.139	
30	Limestone-6	1	0.069	0.091	0.800	0.621
		2	0.051	0.053	0.520	
		3	0.039	0.054	0.465	
		4	0.066	0.071	0.685	
		5	0.063	0.064	0.635	
31	Limestone-7	1	0.014	0.025	0.195	0.244
		2	0.021	0.025	0.230	
		3	0.029	0.024	0.265	
		4	0.026	0.020	0.230	
		5	0.026	0.034	0.300	
32	Rock Gypsum	1	0.017	0.021	0.190	0.168
		2	0.017	0.019	0.178	
		3	0.014	0.016	0.151	
		4	0.014	0.018	0.160	
		5	0.014	0.018	0.161	
33	Marl	1	0.015	0.024	0.195	0.223
		2	0.017	0.028	0.225	
		3	0.019	0.024	0.213	
		4	0.017	0.030	0.235	
		5	0.023	0.027	0.249	

CERCHAR abrasivity index (CAI) for saw cut saturated rock surfaces measured using side view of the stylus tip.

Sr. No.	Rock Sample	Test No.	1st Wear Flat Measurement (SIDE) mm	2nd Wear Flat Measurement at 90º Rotation (SIDE) mm	3rd Wear Flat Measurement at 90º Rotation (SIDE) mm	4th Wear Flat Measurement at 90º Rotation (SIDE) mm	CAI_{SS} (Side) (0.1 mm)	Avg. CAI_{SS} (Side)
1	Siltstone-1	1	0.082	0.077	0.082	0.077	0.795	
		2	0.090	0.070	0.090	0.070	0.800	
		3	0.089	0.071	0.089	0.071	0.800	0.837
		4	0.089	0.072	0.089	0.078	0.820	
		5	0.096	0.094	0.103	0.095	0.970	
2	Siltstone-2	1	0.220	0.260	0.232	0.234	2.365	
		2	0.248	0.195	0.211	0.192	2.115	
		3	0.234	0.259	0.192	0.256	2.353	2.057
		4	0.174	0.174	0.209	0.211	1.920	
		5	0.149	0.135	0.155	0.175	1.535	
3	Sandstone-1	1	0.114	0.121	0.109	0.115	1.148	
		2	0.130	0.150	0.151	0.157	1.470	
		3	0.155	0.125	0.131	0.118	1.323	1.210
		4	0.144	0.093	0.142	0.115	1.235	
		5	0.094	0.072	0.107	0.077	0.875	
4	Sandstone-2	1	0.081	0.069	0.081	0.069	0.752	
		2	0.080	0.097	0.080	0.097	0.885	
		3	0.081	0.077	0.081	0.077	0.790	0.817
		4	0.085	0.074	0.082	0.069	0.775	
		5	0.097	0.089	0.089	0.078	0.883	
5	Sandstone-3	1	0.235	0.216	0.235	0.216	2.255	
		2	0.260	0.234	0.260	0.234	2.470	
		3	0.154	0.192	0.154	0.192	1.730	2.152
		4	0.247	0.224	0.247	0.224	2.355	
		5	0.180	0.210	0.180	0.210	1.950	
6	Sandstone-4	1	0.129	0.098	0.129	0.098	1.135	
		2	0.093	0.110	0.093	0.110	1.015	
		3	0.111	0.115	0.111	0.115	1.130	1.093
		4	0.097	0.115	0.097	0.115	1.060	
		5	0.109	0.116	0.109	0.116	1.125	
7	Sandstone-5	1	0.244	0.260	0.288	0.218	2.525	
		2	0.293	0.303	0.310	0.298	3.010	
		3	0.284	0.269	0.281	0.248	2.705	2.870
		4	0.255	0.281	0.244	0.335	2.788	
		5	0.324	0.320	0.308	0.377	3.323	
8	Sandstone-6	1	0.271	0.279	0.278	0.268	2.740	
		2	0.310	0.320	0.306	0.258	2.985	
		3	0.222	0.228	0.215	0.218	2.208	2.644
		4	0.273	0.276	0.273	0.277	2.747	
		5	0.241	0.267	0.241	0.267	2.540	
9	Sandstone-7	1	0.124	0.113	0.121	0.135	1.233	
		2	0.126	0.135	0.138	0.146	1.363	
		3	0.128	0.122	0.131	0.110	1.228	1.282
		4	0.153	0.138	0.143	0.135	1.423	
		5	0.116	0.115	0.111	0.123	1.163	

CERCHAR abrasivity index (CAI) for saw cut saturated rock surfaces measured using side view of the stylus tip.							
Sr. No.	Rock Sample	Test No.	1st Wear Flat Measurement (SIDE) mm	2nd Wear Flat Measurement at 90° Rotation (SIDE) mm	3rd Wear Flat Measurement at 90° Rotation (SIDE) mm	4th Wear Flat Measurement at 90° Rotation (SIDE) mm	CAI_{ss} (Side) (0.1 mm)	Avg. $CAI_{ss(Side)}$
10	Sandstone-8	1	0.120	0.123	0.118	0.097	1.145	1.117
		2	0.124	0.110	0.109	0.118	1.153	
		3	0.110	0.113	0.096	0.110	1.073	
		4	0.115	0.090	0.102	0.091	0.995	
		5	0.123	0.118	0.113	0.134	1.220	
11	Sandstone-9	1	0.212	0.232	0.249	0.220	2.283	1.893
		2	0.178	0.226	0.202	0.208	2.035	
		3	0.141	0.167	0.139	0.189	1.590	
		4	0.184	0.185	0.206	0.203	1.945	
		5	0.160	0.144	0.156	0.185	1.613	
12	Sandstone-10	1	0.112	0.121	0.105	0.125	1.158	1.044
		2	0.113	0.117	0.122	0.125	1.193	
		3	0.087	0.110	0.073	0.085	0.888	
		4	0.083	0.089	0.095	0.072	0.848	
		5	0.102	0.115	0.110	0.127	1.135	
13	Sandstone-11	1	0.149	0.144	0.135	0.147	1.438	1.312
		2	0.085	0.103	0.096	0.105	0.973	
		3	0.145	0.130	0.131	0.134	1.350	
		4	0.130	0.149	0.119	0.139	1.343	
		5	0.140	0.153	0.157	0.133	1.458	
14	Sandstone-12	1	0.109	0.124	0.126	0.115	1.185	1.033
		2	0.097	0.118	0.101	0.105	1.053	
		3	0.103	0.102	0.086	0.098	0.973	
		4	0.102	0.086	0.084	0.097	0.923	
		5	0.109	0.124	0.126	0.115	1.185	
15	Sandstone-13	1	0.169	0.158	0.163	0.164	1.635	1.442
		2	0.134	0.138	0.161	0.145	1.445	
		3	0.131	0.128	0.123	0.119	1.253	
		4	0.158	0.144	0.149	0.141	1.480	
		5	0.139	0.134	0.140	0.146	1.398	
16	Sandstone-14	1	0.098	0.074	0.079	0.101	0.880	0.984
		2	0.094	0.102	0.127	0.117	1.100	
		3	0.079	0.076	0.094	0.097	0.865	
		4	0.112	0.124	0.128	0.124	1.220	
		5	0.099	0.074	0.096	0.073	0.855	
17	Sandstone-15	1	0.121	0.124	0.139	0.138	1.305	1.611
		2	0.147	0.142	0.141	0.162	1.480	
		3	0.116	0.122	0.128	0.135	1.253	
		4	0.175	0.200	0.228	0.186	1.973	
		5	0.208	0.216	0.180	0.213	2.043	
18	Sandstone-17	1	0.157	0.186	0.173	0.195	1.778	2.054
		2	0.189	0.193	0.173	0.176	1.828	
		3	0.201	0.145	0.203	0.142	1.728	
		4	0.311	0.278	0.307	0.285	2.953	
		5	0.210	0.197	0.191	0.196	1.985	

CERCHAR abrasivity index (CAI) for saw cut saturated rock surfaces measured using side view of the stylus tip.							
Sr. No.	Rock Sample	Test No.	1st Wear Flat Measurement (SIDE) mm	2nd Wear Flat Measurement at 90º Rotation (SIDE) mm	3rd Wear Flat Measurement at 90º Rotation (SIDE) mm	4th Wear Flat Measurement at 90º Rotation (SIDE) mm	CAI_{ss} (Side) (0.1 mm)	Avg. $CAI_{ss(Side)}$
19	Sandstone-18	1	0.211	0.217	0.207	0.189	2.060	2.046
		2	0.240	0.229	0.243	0.231	2.358	
		3	0.234	0.188	0.197	0.190	2.023	
		4	0.194	0.173	0.193	0.197	1.893	
		5	0.208	0.194	0.185	0.171	1.895	
20	Chamositic-Siderite	1	0.065	0.089	0.065	0.086	0.763	1.051
		2	0.102	0.115	0.090	0.118	1.063	
		3	0.121	0.124	0.115	0.109	1.173	
		4	0.113	0.104	0.108	0.075	1.000	
		5	0.129	0.129	0.110	0.135	1.258	
21	Dolomite-1	1	0.152	0.110	0.125	0.113	1.250	1.739
		2	0.195	0.215	0.149	0.185	1.860	
		3	0.163	0.152	0.164	0.185	1.660	
		4	0.166	0.186	0.193	0.190	1.838	
		5	0.195	0.219	0.227	0.193	2.085	
22	Dolomite-2	1	0.197	0.221	0.201	0.170	1.973	1.703
		2	0.177	0.162	0.178	0.180	1.743	
		3	0.155	0.130	0.139	0.182	1.515	
		4	0.161	0.161	0.162	0.175	1.648	
		5	0.169	0.169	0.154	0.163	1.638	
23	Dolomite-3	1	0.229	0.189	0.223	0.189	2.075	1.942
		2	0.168	0.182	0.182	0.164	1.740	
		3	0.181	0.181	0.182	0.240	1.960	
		4	0.183	0.232	0.198	0.184	1.993	
		5	0.189	0.190	0.200	0.199	1.945	
24	Dolomite-4	1	0.161	0.167	0.151	0.136	1.538	1.756
		2	0.165	0.177	0.154	0.183	1.698	
		3	0.201	0.179	0.156	0.180	1.790	
		4	0.172	0.185	0.180	0.160	1.743	
		5	0.223	0.218	0.180	0.183	2.010	
25	Limestone-1	1	0.100	0.124	0.127	0.129	1.200	1.121
		2	0.092	0.090	0.116	0.119	1.043	
		3	0.133	0.107	0.101	0.107	1.120	
		4	0.097	0.110	0.117	0.113	1.092	
		5	0.118	0.112	0.118	0.112	1.150	
26	Limestone-2	1	0.090	0.109	0.123	0.121	1.108	1.190
		2	0.096	0.137	0.105	0.118	1.140	
		3	0.126	0.111	0.142	0.121	1.250	
		4	0.108	0.124	0.124	0.149	1.263	
		5	0.117	0.122	0.116	0.121	1.189	

CERCHAR abrasivity index (CAI) for saw cut saturated rock surfaces measured using side view of the stylus tip.							
Sr. No.	Rock Sample	Test No.	1st Wear Flat Measurement (SIDE) mm	2nd Wear Flat Measurement at 90º Rotation (SIDE) mm	3rd Wear Flat Measurement at 90º Rotation (SIDE) mm	4th Wear Flat Measurement at 90º Rotation (SIDE) mm	CAI_{ss} (Side) (0.1 mm)	Avg. $CAI_{ss(Side)}$
27	Limestone-3	1	0.086	0.081	0.076	0.092	0.838	0.901
		2	0.148	0.139	0.100	0.140	1.318	
		3	0.077	0.086	0.081	0.085	0.823	
		4	0.065	0.070	0.087	0.075	0.743	
		5	0.074	0.083	0.074	0.082	0.783	
28	Limestone-4	1	0.110	0.098	0.096	0.115	1.048	1.100
		2	0.107	0.100	0.126	0.118	1.128	
		3	0.109	0.096	0.095	0.094	0.985	
		4	0.118	0.120	0.126	0.130	1.233	
		5	0.115	0.105	0.116	0.106	1.105	
29	Limestone-5	1	0.112	0.097	0.109	0.121	1.098	1.006
		2	0.120	0.105	0.111	0.111	1.118	
		3	0.091	0.087	0.094	0.103	0.938	
		4	0.093	0.083	0.086	0.087	0.873	
		5	0.098	0.100	0.106	0.097	1.003	
30	Limestone-6	1	0.035	0.049	0.042	0.051	0.443	0.480
		2	0.056	0.038	0.044	0.043	0.451	
		3	0.046	0.037	0.033	0.032	0.370	
		4	0.064	0.058	0.060	0.057	0.598	
		5	0.054	0.051	0.059	0.052	0.540	
31	Limestone-7	1	0.011	0.018	0.015	0.017	0.153	0.188
		2	0.021	0.019	0.020	0.018	0.195	
		3	0.013	0.016	0.013	0.013	0.138	
		4	0.019	0.021	0.016	0.015	0.178	
		5	0.027	0.030	0.027	0.027	0.278	
32	Rock Gypsum	1	0.015	0.011	0.016	0.010	0.130	0.128
		2	0.015	0.015	0.010	0.014	0.135	
		3	0.017	0.011	0.018	0.010	0.140	
		4	0.013	0.011	0.009	0.010	0.108	
		5	0.017	0.010	0.015	0.009	0.128	
33	Marl	1	0.016	0.009	0.017	0.016	0.145	0.145
		2	0.012	0.015	0.015	0.013	0.138	
		3	0.015	0.011	0.011	0.010	0.118	
		4	0.014	0.010	0.018	0.011	0.133	
		5	0.013	0.024	0.018	0.021	0.190	

CERCHAR abrasivity index (CAI) for saturated freshly broken rock surfaces measured at top of the stylus tip.

Sr. No.	Rock Sample	Test No.	1st Wear Flat Measurement (TOP) mm	2nd Wear Flat Measurement at 90º Rotation (TOP) mm	CAI$_{sfb(Top)}$ (0.1 mm)	Avg. CAI$_{sfb(Top)}$
1	Siltstone-1	1	0.142	0.105	1.235	1.346
		2	0.146	0.161	1.535	
		3	0.105	0.117	1.110	
		4	0.148	0.153	1.505	
		5	0.129	0.140	1.345	
2	Siltstone-2	1	0.249	0.244	2.465	2.124
		2	0.214	0.229	2.215	
		3	0.169	0.179	1.740	
		4	0.214	0.206	2.100	
		5	0.206	0.214	2.100	
3	Sandstone-1	1	0.137	0.197	1.670	1.401
		2	0.135	0.146	1.405	
		3	0.116	0.110	1.130	
		4	0.154	0.116	1.352	
		5	0.132	0.158	1.448	
4	Sandstone-2	1	0.121	0.141	1.310	1.326
		2	0.160	0.152	1.560	
		3	0.102	0.135	1.183	
		4	0.145	0.132	1.385	
		5	0.093	0.146	1.195	
5	Sandstone-3	1	0.337	0.316	3.265	3.457
		2	0.316	0.491	4.035	
		3	0.364	0.316	3.400	
		4	0.300	0.326	3.130	
		5	0.305	0.386	3.455	
6	Sandstone-4	1	0.136	0.136	1.360	1.438
		2	0.174	0.102	1.379	
		3	0.177	0.138	1.575	
		4	0.151	0.146	1.487	
		5	0.135	0.143	1.389	
7	Sandstone-5	1	0.338	0.459	3.983	3.554
		2	0.365	0.312	3.385	
		3	0.303	0.340	3.215	
		4	0.331	0.411	3.710	
		5	0.335	0.361	3.478	
8	Sandstone-6	1	0.258	0.195	2.265	2.655
		2	0.223	0.221	2.220	
		3	0.358	0.338	3.480	
		4	0.243	0.247	2.450	
		5	0.298	0.274	2.860	
9	Sandstone-7	1	0.178	0.229	2.035	1.830
		2	0.203	0.166	1.845	
		3	0.161	0.153	1.571	
		4	0.205	0.175	1.900	
		5	0.178	0.182	1.800	

CERCHAR abrasivity index (CAI) for saturated freshly broken rock surfaces measured at top of the stylus tip.						
Sr. No.	Rock Sample	Test No.	1st Wear Flat Measurement (TOP) mm	2nd Wear Flat Measurement at 90° Rotation (TOP) mm	CAI_fbs(Top) (0.1 mm)	Avg. CAI_fbs(Top)
10	Sandstone-8	1	0.105	0.115	1.100	1.348
		2	0.155	0.173	1.640	
		3	0.116	0.130	1.230	
		4	0.128	0.176	1.520	
		5	0.103	0.098	1.005	
		6	0.120	0.127	1.235	
		7	0.158	0.183	1.705	
11	Sandstone-9	1	0.184	0.192	1.880	2.450
		2	0.246	0.275	2.605	
		3	0.213	0.199	2.060	
		4	0.269	0.271	2.700	
		5	0.266	0.335	3.005	
12	Sandstone-10	1	0.117	0.173	1.450	1.323
		2	0.102	0.119	1.105	
		3	0.145	0.138	1.416	
		4	0.109	0.121	1.150	
		5	0.120	0.179	1.495	
13	Sandstone-11	1	0.223	0.206	2.145	2.351
		2	0.194	0.155	1.745	
		3	0.180	0.266	2.230	
		4	0.446	0.293	3.695	
		5	0.157	0.231	1.940	
14	Sandstone-12	1	0.138	0.126	1.321	1.371
		2	0.144	0.120	1.320	
		3	0.129	0.135	1.320	
		4	0.145	0.170	1.575	
		5	0.121	0.143	1.320	
15	Sandstone-13	1	0.185	0.204	1.945	1.573
		2	0.164	0.187	1.754	
		3	0.115	0.161	1.382	
		4	0.102	0.164	1.330	
		5	0.114	0.177	1.456	
16	Sandstone-14	1	0.133	0.175	1.540	1.284
		2	0.136	0.113	1.245	
		3	0.084	0.122	1.031	
		4	0.127	0.174	1.505	
		5	0.099	0.121	1.100	
17	Sandstone-15	1	0.187	0.174	1.805	1.603
		2	0.186	0.163	1.745	
		3	0.181	0.130	1.555	
		4	0.146	0.115	1.305	
		5	0.156	0.165	1.605	

Sr. No.	Rock Sample	Test No.	1st Wear Flat Measurement (TOP) mm	2nd Wear Flat Measurement at 90° Rotation (TOP) mm	CAI$_{fbs(Top)}$ (0.1 mm)	Avg. CAI$_{fbs(Top)}$
18	Sandstone-17	1	0.304	0.280	2.920	3.280
		2	0.318	0.314	3.160	
		3	0.391	0.340	3.655	
		4	0.383	0.349	3.660	
		5	0.347	0.254	3.005	
19	Sandstone-18	1	0.375	0.278	3.265	2.685
		2	0.160	0.247	2.035	
		3	0.319	0.319	3.188	
		4	0.168	0.175	1.715	
		5	0.323	0.321	3.220	
20	Chamositic-Siderite	1	0.102	0.113	1.075	1.137
		2	0.092	0.105	0.985	
		3	0.137	0.123	1.300	
		4	0.106	0.115	1.105	
		5	0.119	0.125	1.220	
21	Dolomite-1	1	0.143	0.156	1.495	1.866
		2	0.208	0.213	2.105	
		3	0.179	0.189	1.840	
		4	0.200	0.188	1.940	
		5	0.212	0.178	1.950	
22	Dolomite-2	1	0.153	0.129	1.410	1.859
		2	0.257	0.259	2.580	
		3	0.154	0.139	1.465	
		4	0.205	0.194	1.995	
		5	0.178	0.191	1.845	
23	Dolomite-3	1	0.360	0.347	3.535	2.665
		2	0.270	0.221	2.455	
		3	0.207	0.223	2.150	
		4	0.239	0.265	2.520	
		5	0.240	0.293	2.665	
24	Dolomite-4	1	0.155	0.193	1.740	1.628
		2	0.136	0.131	1.335	
		3	0.144	0.168	1.560	
		4	0.158	0.167	1.625	
		5	0.185	0.191	1.880	
25	Limestone-1	1	0.092	0.073	0.825	0.919
		2	0.077	0.061	0.690	
		3	0.113	0.085	0.990	
		4	0.135	0.119	1.270	
		5	0.090	0.074	0.820	
26	Limestone-2	1	0.136	0.187	1.615	1.106
		2	0.078	0.073	0.755	
		3	0.096	0.092	0.940	
		4	0.103	0.090	0.965	
		5	0.120	0.131	1.255	

CERCHAR abrasivity index (CAI) for saturated freshly broken rock surfaces measured at top of the stylus tip.

CERCHAR abrasivity index (CAI) for saturated freshly broken rock surfaces measured at top of the stylus tip.						
Sr. No.	Rock Sample	Test No.	1st Wear Flat Measurement (TOP) mm	2nd Wear Flat Measurement at 90º Rotation (TOP) mm	CAI$_{fbs(Top)}$ (0.1 mm)	Avg. CAI$_{fbs(Top)}$
27	Limestone-3	1	0.162	0.117	1.395	1.153
		2	0.130	0.089	1.095	
		3	0.114	0.101	1.075	
		4	0.110	0.125	1.175	
		5	0.097	0.108	1.025	
28	Limestone-4	1	0.127	0.118	1.225	1.323
		2	0.127	0.114	1.205	
		3	0.131	0.142	1.365	
		4	0.140	0.143	1.415	
		5	0.147	0.134	1.405	
29	Limestone-5	1	0.131	0.109	1.200	1.285
		2	0.122	0.132	1.270	
		3	0.144	0.138	1.410	
		4	0.125	0.127	1.260	
		5	0.132	0.125	1.285	
30	Limestone-6	1	0.084	0.076	0.800	0.702
		2	0.080	0.074	0.770	
		3	0.061	0.079	0.700	
		4	0.067	0.071	0.690	
		5	0.046	0.064	0.548	
31	Limestone-7	1	0.051	0.048	0.495	0.277
		2	0.014	0.023	0.185	
		3	0.016	0.020	0.180	
		4	0.030	0.029	0.295	
		5	0.024	0.022	0.230	
32	Rock Gypsum	1	0.014	0.014	0.140	0.167
		2	0.019	0.022	0.205	
		3	0.016	0.014	0.150	
		4	0.016	0.015	0.155	
		5	0.019	0.018	0.185	
33	Marl	1	0.017	0.014	0.156	0.164
		2	0.017	0.018	0.175	
		3	0.017	0.020	0.185	
		4	0.016	0.018	0.170	
		5	0.013	0.014	0.135	

CERCHAR abrasivity index (CAI) for saturated freshly broken rock surfaces measured using side view of the stylus tip.

Sr. No.	Rock Sample	Test No.	1st Wear Flat Measurement (SIDE) mm	2nd Wear Flat Measurement at 90° Rotation (SIDE) mm	3rd Wear Flat Measurement at 90° Rotation (SIDE) mm	4th Wear Flat Measurement at 90° Rotation (SIDE) mm	CAI$_{fbs}$ (Side) (0.1 mm)	Avg. CAI$_{fbs}$ (Side)
1	Siltstone-1	1	0.070	0.099	0.070	0.099	0.845	1.034
		2	0.117	0.107	0.117	0.107	1.120	
		3	0.089	0.073	0.089	0.073	0.809	
		4	0.137	0.136	0.137	0.136	1.365	
		5	0.096	0.110	0.096	0.111	1.032	
2	Siltstone-2	1	0.198	0.207	0.195	0.190	1.975	1.569
		2	0.160	0.157	0.163	0.139	1.548	
		3	0.136	0.146	0.147	0.132	1.403	
		4	0.146	0.143	0.155	0.162	1.515	
		5	0.123	0.166	0.130	0.143	1.405	
3	Sandstone-1	1	0.155	0.133	0.140	0.146	1.435	1.309
		2	0.121	0.128	0.144	0.138	1.328	
		3	0.135	0.109	0.109	0.113	1.165	
		4	0.125	0.128	0.126	0.127	1.264	
		5	0.133	0.138	0.133	0.137	1.353	
4	Sandstone-2	1	0.099	0.128	0.099	0.128	1.135	0.944
		2	0.071	0.105	0.071	0.105	0.879	
		3	0.101	0.112	0.101	0.112	1.065	
		4	0.105	0.091	0.093	0.110	0.998	
		5	0.062	0.070	0.054	0.073	0.648	
5	Sandstone-3	1	0.253	0.349	0.314	0.244	2.900	2.679
		2	0.214	0.231	0.285	0.230	2.400	
		3	0.266	0.280	0.356	0.297	2.998	
		4	0.200	0.245	0.257	0.266	2.420	
		5	0.273	0.262	0.274	0.262	2.677	
6	Sandstone-4	1	0.079	0.104	0.079	0.104	0.915	1.043
		2	0.097	0.105	0.097	0.105	1.010	
		3	0.124	0.117	0.124	0.117	1.205	
		4	0.102	0.101	0.102	0.101	1.015	
		5	0.106	0.108	0.106	0.108	1.070	
7	Sandstone-5	1	0.234	0.239	0.254	0.242	2.423	2.327
		2	0.155	0.211	0.221	0.190	1.943	
		3	0.181	0.235	0.222	0.207	2.113	
		4	0.260	0.257	0.248	0.279	2.610	
		5	0.261	0.246	0.255	0.257	2.548	
8	Sandstone-6	1	0.213	0.223	0.232	0.227	2.238	2.368
		2	0.235	0.227	0.163	0.206	2.078	
		3	0.244	0.301	0.280	0.291	2.790	
		4	0.219	0.218	0.220	0.217	2.184	
		5	0.245	0.265	0.245	0.265	2.550	
9	Sandstone-7	1	0.177	0.157	0.217	0.179	1.825	1.693
		2	0.182	0.172	0.175	0.156	1.713	
		3	0.121	0.156	0.171	0.171	1.548	
		4	0.156	0.156	0.188	0.182	1.705	
		5	0.166	0.160	0.176	0.167	1.673	

CERCHAR abrasivity index (CAI) for saturated freshly broken rock surfaces measured using side view of the stylus tip.							
Sr. No.	Rock Sample	Test No.	1st Wear Flat Measurement (SIDE) mm	2nd Wear Flat Measurement at 90º Rotation (SIDE) mm	3rd Wear Flat Measurement at 90º Rotation (SIDE) mm	4th Wear Flat Measurement at 90º Rotation (SIDE) mm	CAI$_{fbs}$ (Side) (0.1 mm)	Avg. CAI$_{fbs}$ (Side)
10	Sandstone-8	1	0.106	0.100	0.115	0.102	1.058	1.194
		2	0.120	0.154	0.152	0.138	1.410	
		3	0.120	0.104	0.130	0.124	1.195	
		4	0.117	0.139	0.139	0.127	1.305	
		5	0.112	0.088	0.113	0.100	1.033	
		6	0.112	0.074	0.115	0.114	1.038	
		7	0.127	0.128	0.142	0.131	1.320	
11	Sandstone-9	1	0.156	0.154	0.171	0.127	1.520	2.165
		2	0.215	0.353	0.239	0.286	2.733	
		3	0.145	0.161	0.189	0.154	1.623	
		4	0.201	0.259	0.218	0.267	2.363	
		5	0.248	0.301	0.241	0.245	2.588	
12	Sandstone-10	1	0.105	0.154	0.138	0.122	1.298	1.260
		2	0.120	0.105	0.146	0.115	1.215	
		3	0.137	0.135	0.125	0.119	1.290	
		4	0.116	0.105	0.128	0.130	1.198	
		5	0.118	0.136	0.141	0.125	1.300	
13	Sandstone-11	1	0.196	0.185	0.170	0.196	1.868	1.806
		2	0.149	0.121	0.133	0.152	1.388	
		3	0.136	0.147	0.131	0.156	1.425	
		4	0.281	0.204	0.265	0.189	2.348	
		5	0.191	0.165	0.206	0.239	2.003	
14	Sandstone-12	1	0.113	0.107	0.130	0.132	1.205	1.243
		2	0.132	0.111	0.122	0.093	1.145	
		3	0.133	0.145	0.158	0.118	1.385	
		4	0.112	0.112	0.120	0.125	1.173	
		5	0.125	0.128	0.129	0.141	1.308	
15	Sandstone-13	1	0.121	0.149	0.140	0.183	1.483	1.325
		2	0.158	0.178	0.153	0.159	1.620	
		3	0.148	0.130	0.121	0.119	1.295	
		4	0.104	0.092	0.083	0.092	0.928	
		5	0.137	0.135	0.126	0.121	1.298	
16	Sandstone-14	1	0.118	0.091	0.098	0.111	1.045	1.046
		2	0.134	0.114	0.099	0.127	1.185	
		3	0.098	0.087	0.101	0.102	0.970	
		4	0.093	0.110	0.104	0.095	1.005	
		5	0.105	0.102	0.101	0.101	1.023	
17	Sandstone-15	1	0.159	0.136	0.160	0.139	1.485	1.373
		2	0.153	0.153	0.153	0.172	1.578	
		3	0.134	0.160	0.132	0.120	1.365	
		4	0.113	0.091	0.109	0.113	1.065	
		5	0.138	0.136	0.138	0.137	1.372	

CERCHAR abrasivity index (CAI) for saturated freshly broken rock surfaces measured using side view of the stylus tip.							
Sr. No.	Rock Sample	Test No.	1st Wear Flat Measurement (SIDE) mm	2nd Wear Flat Measurement at 90º Rotation (SIDE) mm	3rd Wear Flat Measurement at 90º Rotation (SIDE) mm	4th Wear Flat Measurement at 90º Rotation (SIDE) mm	CAI_{fbs} (Side) (0.1 mm)	Avg. CAI_{fbs} (Side)
18	Sandstone-17	1	0.187	0.199	0.196	0.199	1.953	2.156
		2	0.205	0.196	0.206	0.212	2.048	
		3	0.270	0.273	0.273	0.266	2.705	
		4	0.248	0.262	0.243	0.231	2.460	
		5	0.160	0.152	0.167	0.166	1.613	
19	Sandstone-18	1	0.201	0.213	0.214	0.229	2.143	1.559
		2	0.178	0.191	0.160	0.183	1.780	
		3	0.165	0.157	0.138	0.149	1.523	
		4	0.098	0.104	0.090	0.100	0.980	
		5	0.136	0.147	0.134	0.131	1.370	
20	Chamositic-Siderite	1	0.092	0.094	0.074	0.080	0.850	0.986
		2	0.092	0.103	0.087	0.114	0.990	
		3	0.110	0.106	0.100	0.104	1.050	
		4	0.125	0.093	0.097	0.099	1.035	
		5	0.102	0.100	0.090	0.109	1.003	
21	Dolomite-1	1	0.129	0.142	0.124	0.125	1.300	1.399
		2	0.202	0.167	0.162	0.145	1.690	
		3	0.141	0.143	0.130	0.130	1.360	
		4	0.143	0.149	0.136	0.132	1.400	
		5	0.120	0.137	0.101	0.140	1.245	
22	Dolomite-2	1	0.126	0.153	0.127	0.126	1.330	1.609
		2	0.200	0.197	0.230	0.186	2.033	
		3	0.128	0.109	0.116	0.106	1.148	
		4	0.198	0.158	0.212	0.194	1.905	
		5	0.177	0.156	0.170	0.149	1.630	
23	Dolomite-3	1	0.271	0.277	0.294	0.301	2.858	2.177
		2	0.190	0.172	0.155	0.220	1.843	
		3	0.200	0.217	0.181	0.224	2.055	
		4	0.213	0.200	0.191	0.201	2.013	
		5	0.219	0.200	0.232	0.195	2.115	
24	Dolomite-4	1	0.150	0.153	0.130	0.154	1.466	1.363
		2	0.106	0.101	0.125	0.142	1.185	
		3	0.139	0.132	0.142	0.122	1.338	
		4	0.140	0.134	0.156	0.148	1.445	
		5	0.144	0.131	0.127	0.150	1.380	
25	Limestone-1	1	0.077	0.062	0.087	0.057	0.708	0.866
		2	0.068	0.068	0.065	0.055	0.640	
		3	0.142	0.072	0.143	0.074	1.078	
		4	0.116	0.119	0.105	0.105	1.113	
		5	0.096	0.061	0.093	0.066	0.790	

CERCHAR abrasivity index (CAI) for saturated freshly broken rock surfaces measured using side view of the stylus tip.							
Sr. No.	Rock Sample	Test No.	1st Wear Flat Measurement (SIDE) mm	2nd Wear Flat Measurement at 90º Rotation (SIDE) mm	3rd Wear Flat Measurement at 90º Rotation (SIDE) mm	4th Wear Flat Measurement at 90º Rotation (SIDE) mm	CAI_{fbs} (Side) (0.1 mm)	Avg. CAI_{fbs} (Side)
26	Limestone-2	1	0.095	0.103	0.142	0.106	1.115	0.814
		2	0.043	0.054	0.060	0.034	0.478	
		3	0.074	0.072	0.073	0.076	0.738	
		4	0.055	0.076	0.064	0.062	0.643	
		5	0.109	0.101	0.107	0.121	1.095	
27	Limestone-3	1	0.142	0.114	0.109	0.127	1.230	0.990
		2	0.110	0.101	0.110	0.087	1.020	
		3	0.087	0.110	0.092	0.101	0.975	
		4	0.099	0.101	0.077	0.098	0.938	
		5	0.087	0.055	0.086	0.086	0.785	
28	Limestone-4	1	0.083	0.101	0.102	0.102	0.970	1.174
		2	0.117	0.102	0.118	0.108	1.113	
		3	0.110	0.116	0.104	0.126	1.140	
		4	0.147	0.113	0.142	0.145	1.368	
		5	0.127	0.131	0.133	0.120	1.278	
29	Limestone-5	1	0.113	0.123	0.117	0.106	1.148	1.137
		2	0.122	0.099	0.115	0.118	1.135	
		3	0.117	0.117	0.102	0.128	1.160	
		4	0.101	0.108	0.115	0.118	1.105	
		5	0.117	0.110	0.117	0.111	1.136	
30	Limestone-6	1	0.061	0.057	0.051	0.055	0.560	0.534
		2	0.044	0.064	0.048	0.061	0.543	
		3	0.053	0.048	0.048	0.046	0.488	
		4	0.053	0.065	0.062	0.056	0.590	
		5	0.061	0.045	0.047	0.042	0.488	
31	Limestone-7	1	0.043	0.042	0.038	0.040	0.408	0.211
		2	0.021	0.012	0.017	0.010	0.150	
		3	0.017	0.012	0.010	0.014	0.133	
		4	0.017	0.025	0.015	0.017	0.184	
		5	0.022	0.017	0.016	0.018	0.183	
32	Rock Gypsum	1	0.012	0.011	0.009	0.011	0.108	0.142
		2	0.018	0.013	0.023	0.019	0.183	
		3	0.011	0.016	0.011	0.015	0.133	
		4	0.010	0.015	0.014	0.015	0.135	
		5	0.015	0.014	0.015	0.016	0.150	
33	Marl	1	0.010	0.015	0.013	0.014	0.130	0.111
		2	0.011	0.007	0.009	0.011	0.095	
		3	0.015	0.013	0.013	0.013	0.135	
		4	0.010	0.012	0.009	0.014	0.113	
		5	0.007	0.007	0.008	0.011	0.083	

APPENDIX C.

LCPC ROCK ABRASIVITY TEST RESULTS

LCPC abrasivity co-efficient for dry rock samples

Sr. No.	Rock Sample	Test No.	Mass of Insert Before Test, m_o (g)	Mass of Insert After Test, m (g)	Mass of Sample Fraction (4/6.3-mm) (g)	ABR$_{(dry)}$ (g/t)	Avg. ABR$_{(dry)}$ (g/t)
1	Dolerite-1	1	45.080	44.752	500.00	656.00	616.00
		2	45.978	45.690	500.00	576.00	
2	Dolerite-2	1	45.992	45.880	501.00	223.00	235.53
		2	45.946	45.822	500.00	248.06	
3	Dolerite-3	1	46.226	46.136	500.00	180.00	186.00
		2	46.069	45.973	502.00	192.00	
4	Dolerite-4	1	46.22	45.50	500.50	1440.56	1391.28
		2	45.99	45.32	500.00	1342.00	
5	Granite-1	1	46.248	46.074	500.50	348.00	359.64
		2	46.267	46.081	500.00	371.28	
6	Granite-2	1	46.142	45.978	501.00	328.12	319.36
		2	45.029	44.874	500.00	310.60	
7	Granite-3	1	45.981	45.771	500.50	419.23	415.58
		2	46.353	46.147	500.00	411.93	
8	Granite-4	1	46.029	45.794	500.50	469.00	477.52
		2	45.301	45.058	500.00	486.04	
9	Granite-5	1	43.92	43.15	500.00	1541.00	1534.50
		2	46.39	45.63	500.00	1528.00	
10	Granite-6	1	45.13	44.54	500.00	1176.00	1273.00
		2	46.36	45.68	500.00	1370.00	
11	Migmatite	1	46.239	46.086	501.00	305.00	301.40
		2	46.279	46.130	500.00	297.80	
12	Andesite	1	46.13	45.45	500.00	1362.00	1385.00
		2	46.24	45.53	500.00	1408.00	
13	Granitic Gneiss-1	1	46.244	46.159	501.00	169.00	171.66
		2	46.206	46.119	500.00	174.32	
14	Granitic Gneiss-2	1	46.12	45.90	500.00	436.00	429.00
		2	46.25	46.04	500.00	422.00	
15	Phyllite	1	45.94	45.89	500.00	98.00	80.00
		2	46.24	46.21	500.00	62.00	
16	Quartzite-1	1	46.280	46.036	499.50	489.00	498.50
		2	46.138	45.884	500.00	508.00	
17	Quartzite-2	1	45.890	45.305	500.00	1171.00	1208.00
		2	46.341	45.719	500.00	1245.00	
18	Siltstone-1	1	46.14	46.11	500.00	62.00	63.00
		2	46.16	46.13	500.00	64.00	
19	Siltstone-2	1	46.040	45.816	500.00	448.00	476.00
		2	46.450	46.198	501.00	504.00	
20	Sandstone-1	1	46.321	46.214	500.00	215.00	218.00
		2	46.382	46.272	500.00	221.00	
21	Sandstone-2	1	46.20	46.17	500.00	62.00	102.00
		2	45.65	45.58	500.00	132.00	
		3	46.14	46.09	500.00	98.00	
		4	46.43	46.38	500.00	116.00	
22	Sandstone-3	1	46.005	45.637	500.00	736.00	744.00
		2	46.559	46.183	500.00	752.00	

LCPC abrasivity co-efficient for dry rock samples							
Sr. No.	Rock Sample	Test No.	Mass of Insert Before Test, m_o (g)	Mass of Insert After Test, m (g)	Mass of Sample Fraction (4/6.3-mm) (g)	$ABR_{(dry)}$ (g/t)	Avg. $ABR_{(dry)}$ (g/t)
23	Sandstone-4	1	46.16	46.08	500.50	143.86	159.93
		2	45.11	45.02	500.00	176.00	
24	Sandstone-5	1	46.189	46.082	500.00	215.00	228.00
		2	46.390	46.269	500.00	241.00	
25	Sandstone-6	1	46.313	46.074	500.00	478.62	474.00
		2	43.839	43.604	500.00	469.38	
26	Sandstone-7	1	45.129	45.018	500.00	223.00	226.00
		2	44.565	44.451	500.00	229.00	
27	Sandstone-8	1	44.921	44.832	500.00	178.00	186.00
		2	45.982	45.885	500.00	194.00	
28	Sandstone-9	1	46.238	46.036	500.00	405.00	406.00
		2	44.294	44.090	501.00	407.00	
29	Sandstone-10	1	46.425	46.299	500.00	252.00	260.00
		2	44.527	44.393	500.00	268.00	
30	Sandstone-11	1	46.453	46.388	500.00	130.00	134.00
		2	45.184	45.115	500.00	138.00	
31	Sandstone-12	1	46.460	46.411	500.00	98.00	91.00
		2	46.369	46.327	500.00	84.00	
32	Sandstone-13	1	46.051	45.936	500.00	231.00	232.00
		2	43.839	43.722	500.50	233.00	
33	Sandstone-14	1	46.268	46.239	500.00	58.00	57.00
		2	45.698	45.670	500.00	56.00	
34	Sandstone-15	1	46.304	46.096	500.00	416.00	424.00
		2	47.042	46.826	500.00	432.00	
35	Sandstone-16	1	47.305	46.590	500.50	1428.00	1444.56
		2	45.731	45.000	500.00	1461.12	
36	Sandstone-17	1	44.696	44.373	500.00	646.00	633.00
		2	46.290	45.980	500.00	620.00	
37	Sandstone-18	1	46.168	45.797	500.00	743.00	740.00
		2	46.032	45.664	500.00	737.00	
38	Chamositic-Siderite	1	46.193	46.191	500.00	4.20	4.00
		2	46.196	46.194	500.00	3.80	
39	Dolomite-1	1	46.461	46.159	500.00	605.00	642.00
		2	45.169	44.829	501.00	679.00	
40	Dolomite-2	1	46.002	45.852	500.00	300.00	304.00
		2	46.332	46.178	500.00	308.00	
41	Dolomite-3	1	45.734	45.564	500.00	340.00	336.00
		2	46.004	45.838	500.00	332.00	
42	Dolomite-4	1	45.902	45.796	500.00	212.00	208.00
		2	46.233	46.131	500.00	204.00	
43	Limestone-1	1	44.943	44.941	500.00	5.00	6.00
		2	45.802	45.799	500.00	7.00	
44	Limestone-2	1	46.273	46.270	500.00	6.00	7.00
		2	46.395	46.391	500.50	7.99	

LCPC abrasivity co-efficient for dry rock samples

Sr. No.	Rock Sample	Test No.	Mass of Insert Before Test, m_o (g)	Mass of Insert After Test, m (g)	Mass of Sample Fraction (4/6.3-mm) (g)	$ABR_{(dry)}$ (g/t)	$ABR_{(dry)}$ (g/t)
45	Limestone-3	1	46.306	46.302	500.00	8.00	8.00
		2	46.039	46.035	500.50	8.00	
46	Limestone-4	1	46.051	46.047	499.50	8.22	8.01
		2	47.786	47.782	500.00	7.80	
47	Limestone-5	1	46.298	46.296	499.00	4.10	4.01
		2	46.246	46.244	500.00	3.92	
48	Limestone-6	1	44.604	44.595	500.00	19.00	20.00
		2	45.989	45.978	500.00	21.00	
49	Limestone-7	1	44.665	44.661	501.00	7.56	7.98
		2	45.433	45.429	500.00	8.40	
50	Rock Gypsum	1	46.386	46.382	500.00	8.25	8.00
		2	46.483	46.479	500.00	7.75	
51	Marl	1	46.121	46.106	500.50	29.97	32.99
		2	46.057	46.039	500.00	36.00	

Results of LCPC abrasivity tests conducted at 15% (75 grams) water content

Sr. No.	Rock Sample	m_o (g)	M (g)	M (g)	$ABR_{(15\%)}$ (g/t)	$M_{1.6}$ (g)	$BR_{(15\%)}$ (%)
1	Dolerite-3	46.94	46.50	500.00	882.00	119.00	23.80
2	Dolerite-4	45.06	44.10	500.00	1934.00	77.50	15.50
3	Granite-4	46.39	46.15	500.00	478.00	230.00	46.00
4	Granite-5	46.04	45.11	500.00	1862.00	75.00	15.00
5	Granite-6	46.26	45.43	500.00	1660.00	148.00	29.60
6	Andesite	46.58	45.58	500.00	2008.00	98.00	19.60
7	Granitic Gneiss-1	46.14	45.88	500.00	516.00	274.00	54.80
8	Granitic Gneiss-2	46.17	46.09	500.00	156.00	194.00	38.80
9	Phyllite	45.08	44.93	500.00	306.00	157.00	31.40
10	Siltstone-1	46.04	45.86	500.00	372.00	134.00	26.80
11	Sandstone-2	45.35	45.33	500.00	40.00	196.50	39.3
12	Sandstone-3	46.20	45.77	500.00	848.00	174.00	34.80
13	Sandstone-4	45.82	45.80	500.00	42.00	165.00	33.00
14	Sandstone-5	45.96	45.85	500.00	214.00	197.50	39.50
15	Sandstone-12	46.26	46.25	500.00	26.00	187.50	37.50
16	Sandstone-14	46.37	46.36	500.00	10.00	184.00	36.80
17	Sandstone-15	46.98	46.51	500.00	930.00	151.00	30.20
18	Sandstone-17	46.88	46.21	500.00	1330.00	174.00	34.80
19	Limestone-3	45.97	45.96	500.00	14.00	197.00	39.40
20	Marl	46.13	46.12	500.00	8.00	100.00	20.00

m_o - mass of insert before test; m- Mass of insert after test; M- Mass of sample fraction (4/6.3-mm) in grams; $M_{1.6}$ - Mass of tested sample fraction passing 1.6 mm sieve.

Results of LCPC abrasivity tests conducted at 30% (150 grams) water content

Sr. No.	Rock Sample	m_o (g)	M (g)	M (g)	$ABR_{(30\%)}$ (g/t)	$M_{1.6}$ (g)	$BR_{(30\%)}$ (%)
1	Dolerite-3	46.28	45.74	500.00	1086.00	83.00	16.60
2	Dolerite-4	46.23	45.32	500.00	1814.00	65.50	13.10
3	Granite-4	45.82	45.42	500.00	788.00	233.50	46.7
4	Granite-5	46.12	45.24	500.00	1758.00	68.00	13.60
5	Granite-6	46.32	45.50	500.00	1642.00	99.00	19.80
6	Andesite	45.95	45.02	500.00	1856.00	81.00	16.20
7	Granitic Gneiss-1	45.89	45.59	500.00	606.00	278.00	55.60
8	Granitic Gneiss-2	48.23	47.92	500.00	620.00	275.00	55.00
9	Phyllite	46.30	46.20	500.00	200.00	232.50	46.50
10	Siltstone-1	47.13	46.96	500.00	346.00	106.00	21.20
11	Sandstone-2	46.26	46.12	500.00	270.00	433.50	86.70
12	Sandstone-3	46.12	45.63	500.00	986.00	153.00	30.60
13	Sandstone-4	46.20	46.02	500.00	358.00	356.00	71.20
14	Sandstone-5	46.09	45.90	500.00	384.00	217.00	43.40
15	Sandstone-12	46.08	45.96	500.00	252.00	404.00	80.80
16	Sandstone-14	46.15	46.08	500.00	142.00	354.00	70.80
17	Sandstone-15	46.20	45.76	500.00	886.00	115.00	23.00
18	Sandstone-17	46.16	45.61	500.00	1108.00	164.00	32.80
19	Limestone-3	45.97	45.95	500.00	24.00	120.00	24.00
20	Marl	45.01	44.96	500.00	92.00	267.00	53.40

m_o - mass of insert before test; m- Mass of insert after test; M- Mass of sample fraction (4/6.3-mm) in grams; $M_{1.6}$ - Mass of tested sample fraction passing 1.6 mm sieve.

Results of LCPC abrasivity tests conducted at 45% (225 grams) water content

Sr. No.	Rock Sample	m_o (g)	M (g)	M (g)	$ABR_{(45\%)}$ (g/t)	$M_{1.6}$ (g)	$BR_{(45\%)}$ (%)
1	Dolerite-3	46.02	45.50	500.00	1032.00	83.00	16.60
2	Dolerite-4	46.34	45.42	500.00	1836.00	61.50	12.30
3	Granite-4	46.02	45.74	500.00	560.00	195.00	39.00
4	Granite-5	46.21	45.27	500.00	1874.00	55.00	11.00
5	Granite-6	46.14	45.37	500.00	1548.00	109.00	21.80
6	Andesite	46.17	45.28	500.00	1778.00	64.00	12.80
7	Granitic Gneiss-1	46.43	46.22	500.00	420.00	215.00	43.00
8	Granitic Gneiss-2	45.87	45.66	500.00	426.00	223.00	44.60
9	Phyllite	46.51	46.47	500.00	98.00	208.50	41.70
10	Siltstone-1	46.06	45.90	500.00	322.00	95.00	19.00
11	Sandstone-2	45.63	45.57	500.00	132.00	302.00	60.40
12	Sandstone-3	46.21	45.81	498.00	791.17	136.55	27.31
13	Sandstone-4	46.05	45.97	500.00	158.00	269.00	53.80
14	Sandstone-5	46.39	46.29	500.00	206.00	185.00	37.00
15	Sandstone-12	46.37	46.31	500.00	118.00	306.00	61.20
16	Sandstone-14	46.50	46.44	500.00	132.00	366.00	73.20
17	Sandstone-15	46.32	45.92	500.00	798.00	112.50	22.50
18	Sandstone-17	46.23	45.81	500.00	854.00	142.00	28.40
19	Limestone-3	45.98	45.97	500.00	22.00	112.00	22.40
20	Marl	46.26	46.24	500.00	42.00	177.00	35.40

m_o - mass of insert before test; m- Mass of insert after test; M- Mass of sample fraction (4/6.3-mm) in grams; $M_{1.6}$ - Mass of tested sample fraction passing 1.6 mm sieve.

Results of LCPC abrasivity tests conducted at 60% (300 grams) water content

Sr. No.	Rock Sample	m_o (g)	M (g)	M (g)	$ABR_{(60\%)}$ (g/t)	$M_{1.6}$ (g)	$BR_{(60\%)}$ (%)
1	Dolerite-3	45.51	45.04	500.00	942.00	86.00	17.20
2	Dolerite-4	46.07	45.21	500.00	1714.00	63.00	12.60
3	Granite-4	46.12	45.88	500.00	484.00	192.50	38.50
4	Granite-5	46.15	45.26	500.00	1770.00	67.00	13.40
5	Granite-6	45.92	45.25	500.00	1342.00	86.00	17.20
6	Andesite	46.24	45.34	500.00	1798.00	73.00	14.60
7	Granitic Gneiss-1	45.94	45.76	500.00	356.00	209.00	41.80
8	Granitic Gneiss-2	46.18	45.98	500.00	394.00	211.00	42.20
9	Phyllite	46.30	46.26	500.00	82.00	188.00	37.70
10	Siltstone-1	46.04	45.90	500.00	266.00	105.00	21.00
11	Sandstone-2	46.23	46.17	500.00	108.00	266.50	53.30
12	Sandstone-3	46.30	45.97	500.00	666.00	138.00	27.60
13	Sandstone-4	45.95	45.90	500.00	102.00	74.00	14.80
14	Sandstone-5	46.16	46.06	500.00	200.00	191.00	38.20
15	Sandstone-12	46.14	46.10	500.00	84.00	262.00	52.40
16	Sandstone-14	46.39	46.36	500.00	56.00	314.00	62.80
17	Sandstone-15	46.96	46.63	500.00	670	100.50	20.10
18	Sandstone-17	46.17	45.76	500.00	816.00	145.00	29.00
19	Limestone-3	46.06	46.06	500.00	12.00	111.50	22.30
20	Marl	46.29	46.28	500.00	28.00	153.00	30.60

m_o - mass of insert before test; m- Mass of insert after test; M- Mass of sample fraction (4/6.3-mm) in grams; $M_{1.6}$ - Mass of tested sample fraction passing 1.6 mm sieve.

APPENDIX D.

NTNU/SINTEF ABRASIVITY TEST RESULTS

Results of Sievers' J-Value (SJ) Miniature Drill test.

Sr. No.	Rock Sample	Drill Hole Depth (mm)						Average Depth (mm)	Sievers'J Value (1/10) mm
		1	2	3	4	5	6		
1	Dolerite-3	8.25	5.25	9.25	4.25	5.25	----	6.45	64.50
2	Dolerite-4	12.00	4.00	25.00	6.00	13.00	15.50	12.58	125.83
3	Granite-6	1.60	2.30	1.90	8.70	----	----	3.63	36.25
4	Andesite	2.40	1.95	3.20	3.40	1.50	1.70	2.36	23.58
5	Granitic Gneiss-2	51.60	52.37	92.53	49.13	37.20	----	56.57	565.65
6	Quartzite-1	2.25	2.75	2.25	1.00	----	----	2.06	20.63
7	Sandstone-2	113.17	113.33	108.00	110.00	111.25	107.50	110.54	1105.41
8	Sandstone-3	76.60	76.60	83.10	65.10	53.20	49.20	67.30	673.00
9	Sandstone-14	132.30	98.65	112.05	94.75	----	----	109.44	1094.38
10	Sandstone-16	1.50	1.30	0.60	1.60	1.50	1.10	1.27	12.67

Results of Abrasion Value Steel (AVS) Test conducted on coarser [99% < 1mm and (70 ± 5) % < 0.71 mm] test fraction.

Sr. No.	Rock Sample	Test No.	Weight of Bit Before Test (g)	Weight of Bit After Test (g)	AVS (mg)	Avg. AVS (mg)
1	Dolerite-3	1	48.240	48.228	12.00	10.00
		2	47.631	47.623	8.00	
2	Dolerite-4	1	47.574	47.562	12.00	11.00
		2	47.556	47.546	10.00	
3	Granite-6	1	47.785	47.756	29.00	30.50
		2	47.714	47.682	32.00	
4	Andesite	1	57.288	57.282	6.00	5.33
		2	57.330	57.324	6.00	
		3	57.328	57.324	4.00	
5	Granitic Gneiss-2	1	57.380	57.341	39.00	36.50
		2	57.324	57.29	34.00	
6	Quartzite-1	1	57.470	57.432	38.00	40.00
		2	48.048	48.006	42.00	
7	Sandstone-2	1	57.093	57.067	26.00	26.00
		2	57.300	57.274	26.00	
8	Sandstone-3	1	57.215	57.195	20.00	20.00
		2	56.851	56.831	20.00	
9	Sandstone-14	1	57.093	57.072	21.00	21.00
		2	57.087	57.066	21.00	
10	Sandstone-16	1	57.451	57.431	20.00	20.00
		2	57.455	57.435	20.00	

Results of Abrasion Value Steel (AVS) test conducted on NTNU/SINTEF standard [99% < 1mm and (70 ± 5) % < 0.50 mm] test fraction.

Sr. No.	Rock Sample	Test No.	Weight of Bit Before Test (g)	Weight of Bit After Test (g)	AVS (mg)	Avg. AVS (mg)
1	Dolerite-3	1	47.839	47.831	8.00	8.00
		2	47.699	47.691	8.00	
2	Dolerite-4	1	48.029	48.0195	9.50	9.25
		2	47.823	47.814	9.00	
3	Granite-6	1	47.707	47.682	25.00	26.50
		2	47.819	47.791	28.00	
4	Andesite	1	57.436	57.432	4.00	4.00
		2	57.464	57.460	4.00	
5	Granitic Gneiss-2	1	57.376	57.341	35.00	33.50
		2	47.899	47.867	32.00	
6	Quartzite-1	1	47.778	47.743	35.00	37.00
		2	47.958	47.919	39.00	
7	Sandstone-2	1	57.055	57.030	25.00	25.00
		2	57.210	57.185	25.00	
8	Sandstone-3	1	47.482	47.463	19.00	19.00
		2	56.985	56.966	19.00	
9	Sandstone-14	1	56.859	56.841	18.00	18.00
		2	57.060	57.042	18.00	
10	Sandstone-16	1	47.840	47.824	16.00	17.50
		2	47.801	47.782	19.00	

Results of Abrasion Value Steel (AVS) test conducted on fine [99% < 1mm and (70 ± 5) % < 0.25 mm] test fraction.

Sr. No.	Rock Sample	Test No.	Weight of Bit Before Test (g)	Weight of Bit After Test (g)	AVS (mg)	Avg. AVS (mg)
1	Dolerite-3	1	47.851	47.846	5.00	5.50
		2	47.638	47.632	6.00	
2	Dolerite-4	1	47.706	47.697	9.00	8.50
		2	47.891	47.883	8.00	
3	Granite-6	1	47.755	47.734	21.00	24.00
		2	47.639	47.613	26.00	
		3	47.499	47.474	25.00	
4	Andesite	1	48.325	48.322	3.00	3.00
		2	57.444	57.441	3.00	
5	Granitic Gneiss-2	1	57.486	57.455	31.00	29.50
		2	47.922	47.894	28.00	
6	Quartzite-1	1	47.743	47.707	36.00	34.50
		2	47.725	47.692	33.00	
7	Sandstone-2	1	57.162	57.138	24.00	23.50
		2	47.406	47.383	23.00	
8	Sandstone-3	1	47.936	47.923	13.00	13.00
		2	47.392	47.379	13.00	
9	Sandstone-14	1	56.815	56.799	16.00	15.00
		2	47.897	47.883	14.00	
10	Sandstone-16	1	48.105	48.095	10.00	8.00
		2	47.886	47.880	6.00	

Results of Abrasion Value Steel (AVS) test conducted on finer [99% < 1mm and (70 ± 5) % < 0.15 mm] test fraction.
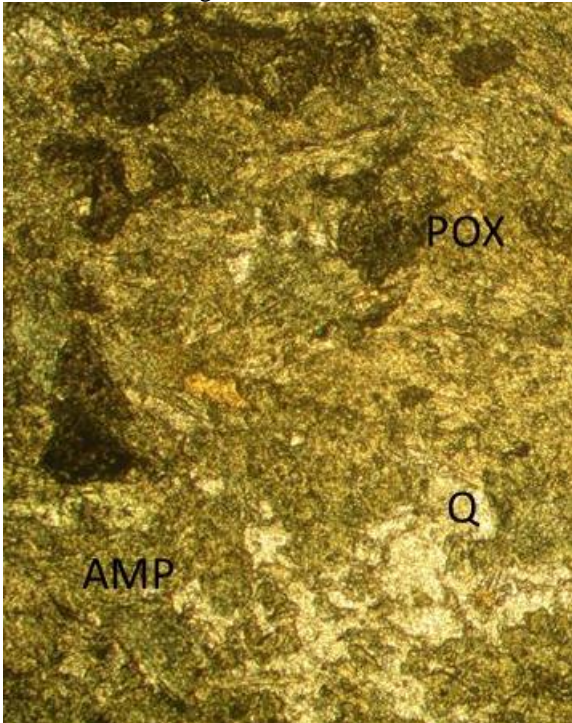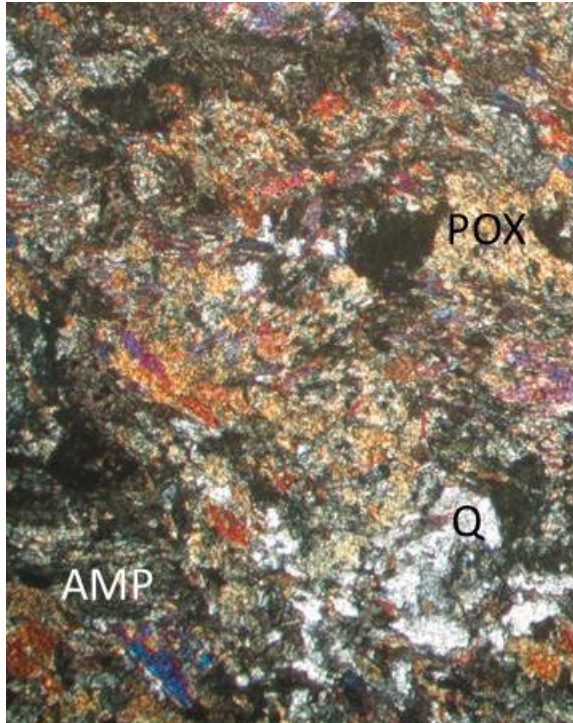
Sr. No.	Rock Sample	Test No.	Weight of Bit Before Test (g)	Weight of Bit After Test (g)	AVS (mg)	Avg. AVS (mg)
1	Dolerite-3	1	48.249	48.245	4.00	3.50
		2	47.724	47.721	3.00	
2	Dolerite-4	1	47.821	47.815	6.00	6.00
		2	47.661	47.655	6.00	
3	Granite-6	1	57.438	57.425	13.00	12.5
		2	47.725	47.713	12.00	
4	Andesite	1	57.589	57.587	2.00	1.50
		2	57.366	57.365	1.00	
5	Granitic Gneiss-2	1	57.553	57.527	26.00	26.00
		2	47.943	47.917	26.00	
6	Quartzite-1	1	47.815	47.782	33.00	32.00
		2	47.695	47.665	30.00	
		3	47.886	47.853	33.00	
7	Sandstone-2	1	47.568	47.549	19.00	21.00
		2	47.300	47.277	23.00	
8	Sandstone-3	1	47.683	47.673	10.00	9.00
		2	47.226	47.218	8.00	
9	Sandstone-14	1	47.692	47.684	8.00	8.00
		2	47.983	47.975	8.00	
10	Sandstone-16	1	48.013	48.006	7.00	7.00
		2	48.306	48.299	7.00	

Results of Abrasion Value Steel (AVS) test conducted at the disc speed of 10 RPM by using NTNU/SINTEF standard test fraction [99% < 1mm and (70 ± 5) % < 0.50 mm].
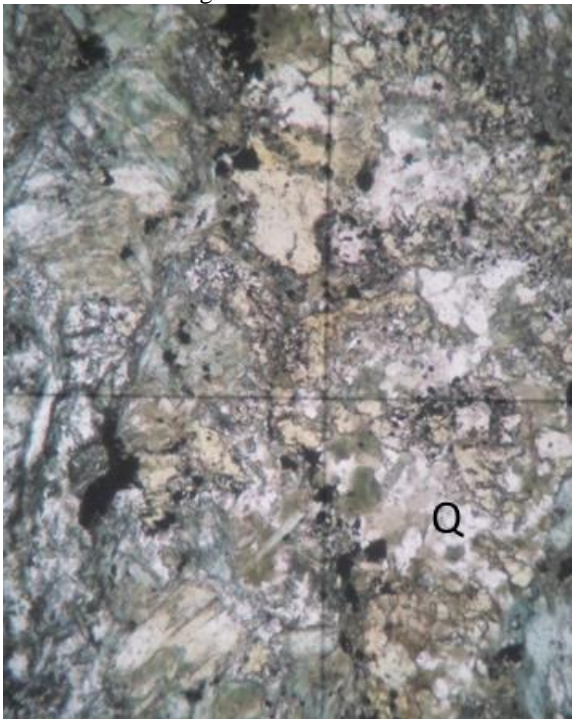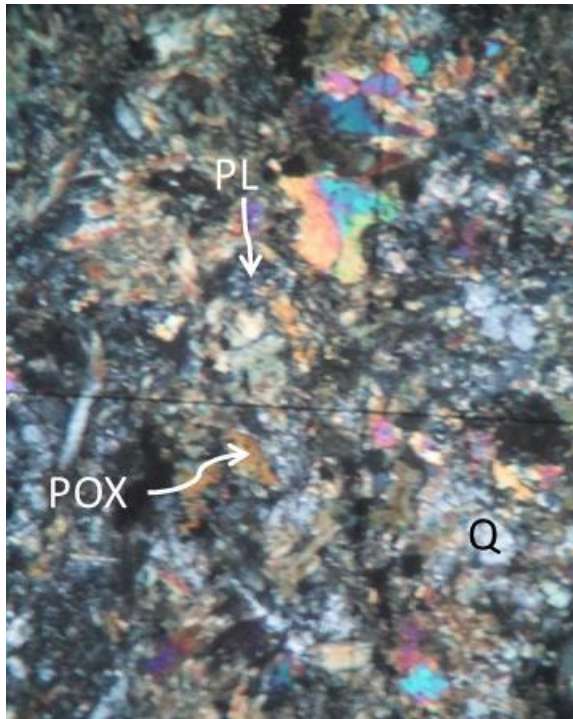
Sr. No.	Rock Sample	Test No.	Weight of Bit Before Test (g)	Weight of Bit After Test (g)	AVS (mg)	Avg. AVS (mg)
1	Dolerite-3	1	56.602	56.590	12.00	11.50
		2	47.503	47.492	11.00	
2	Dolerite-4	1	56.150	56.140	10.00	10.50
		2	56.176	56.165	11.00	
3	Granite-6	1	47.696	47.662	34.00	35.67
		2	47.461	47.426	35.00	
		3	56.690	56.652	38.00	
4	Andesite	1	56.897	56.890	7.00	6.00
		2	47.189	47.184	5.00	
5	Granitic Gneiss-2	1	56.356	56.320	36.00	35.00
		2	47.530	47.496	34.00	
6	Quartzite-1	1	56.367	56.328	39.00	38.50
		2	56.742	56.704	38.00	
7	Sandstone-2	1	47.495	47.467	28.00	29.00
		2	56.315	56.285	30.00	
8	Sandstone-3	1	56.352	56.330	22.00	21.50
		2	47.295	47.274	21.00	
9	Sandstone-14	1	56.606	56.586	20.00	19.50
		2	47.674	47.655	19.00	
10	Sandstone-16	1	56.707	56.683	24.00	24.50
		2	47.700	47.675	25.00	
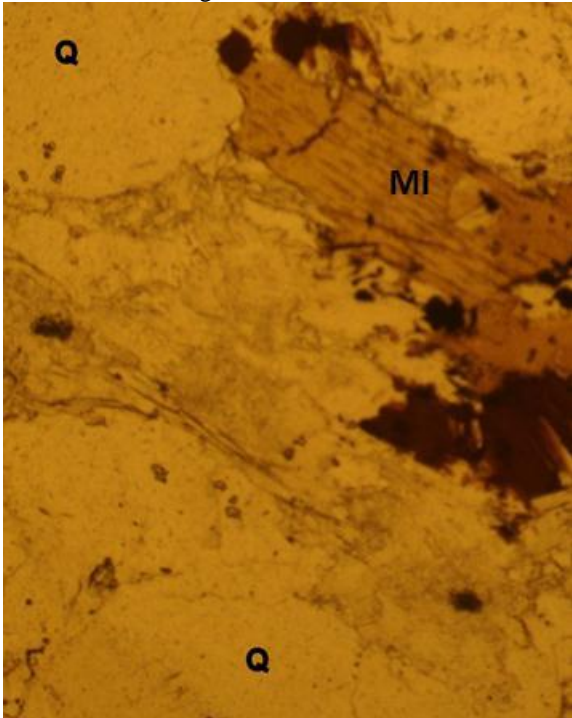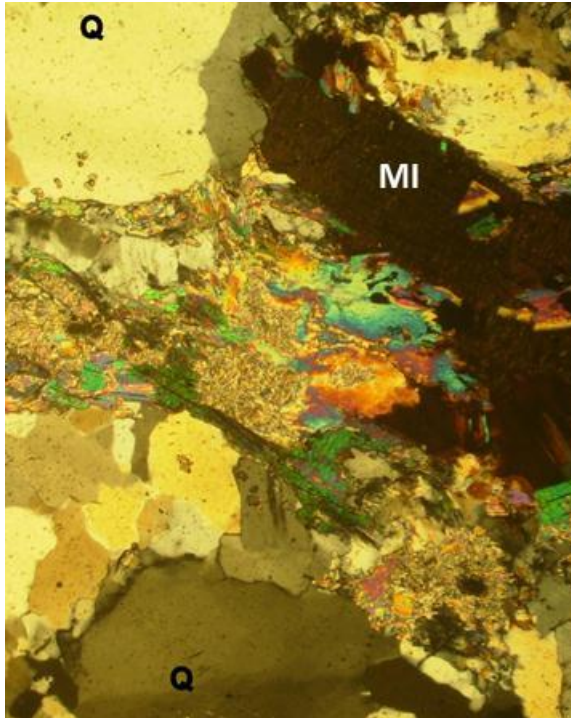
APPENDIX E.

PETROGRAPHIC DESCRIPTION
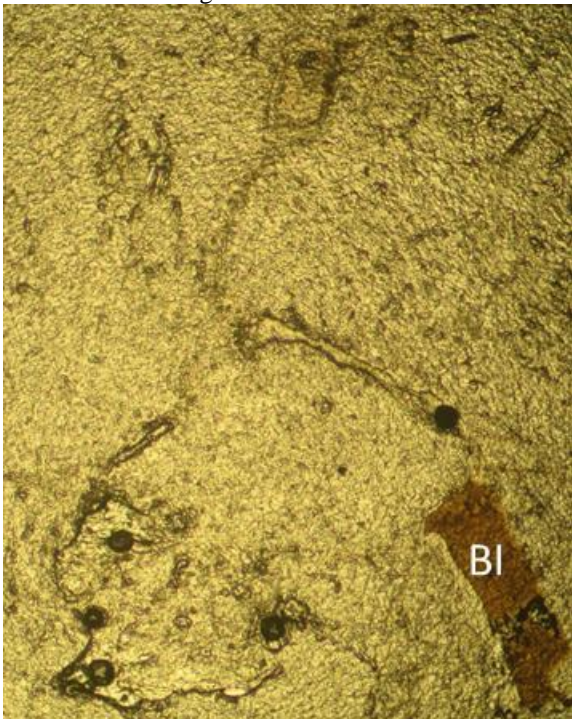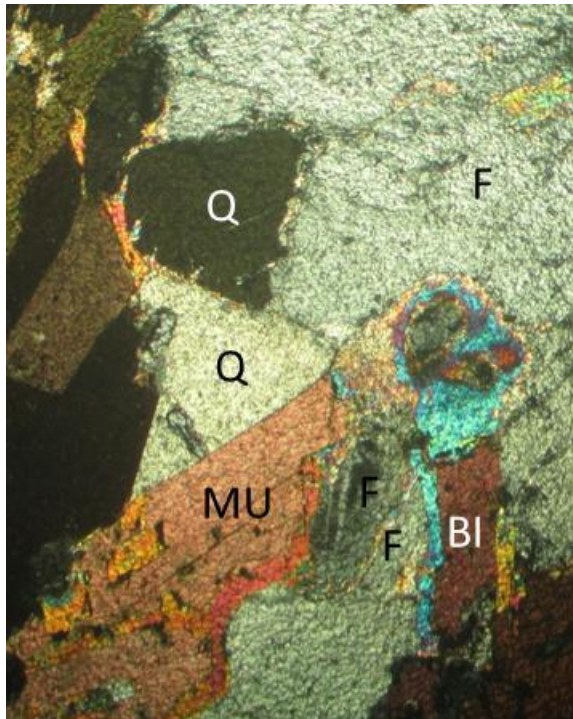
PETROGRAPHIC DESCRIPTION: Dolerite-1 (Kayan)

Name: Yasir Majeed **Date:** June, 2015. **Location:** University of Engineering and Technology (UET), Lahore, Pakistan.			**Macroscopic Description:** Green, fine grained and high in strength.	
Geological Formation: Salkhala (Metabasites)				

Mineral Description

Thin Section Number	Point Count	Mineral	Volume (%)	Mean Grain Size (mm)
1	300	Pyroxene	40.00	0.32
		Quartz	5.00	0.22
		Amphibole	13.00	0.35
		Muscovite	0.50	0.51
		Biotite	0.50	0.59
		Feldspars	40.00	0.52
		Magnetite	0.50	0.07
		Zircon	0.50	0.09
		Mean Overall Grain Size (mm)		0.33

General Remarks:

Petrographic Classification: Dolerite

<div align="center">Enlargement 4×</div>

Plane Polarized Light	Crossed Polars

* Q: Quartz; POX: Pyroxene; AMP: Amphibole
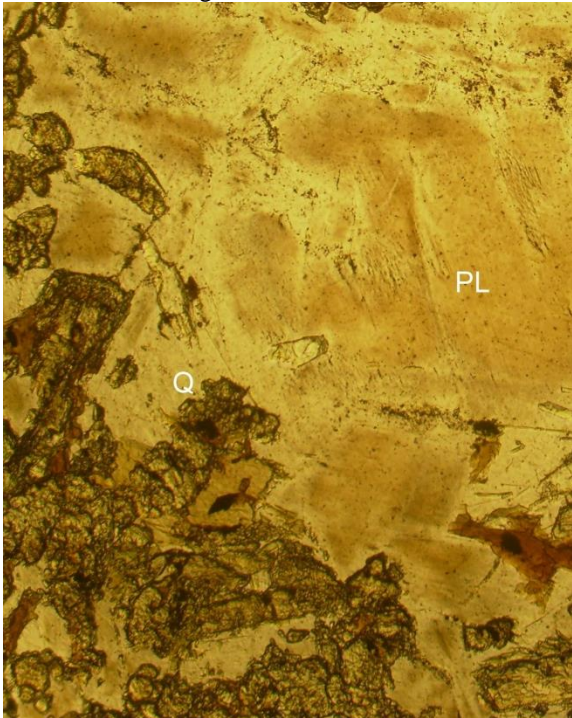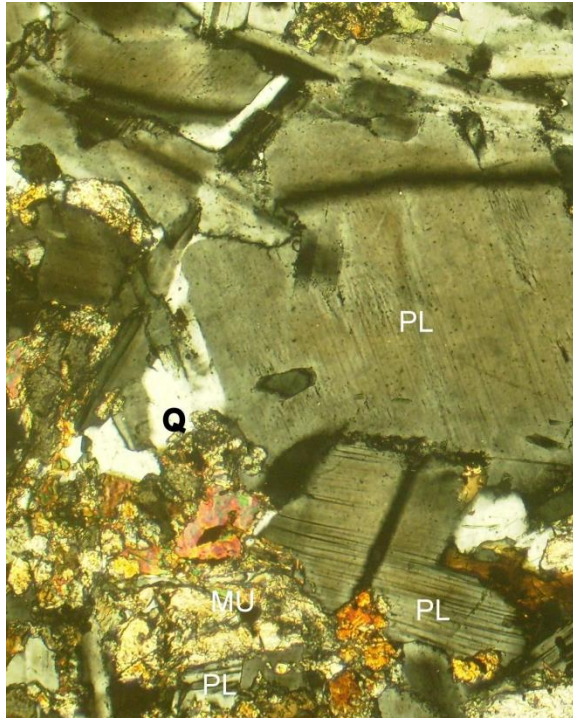
PETROGRAPHIC DESCRIPTION: Dolerite-3 (Jhugian)				
Name: Yasir Majeed **Date:** July , 2014. **Location:** University of Engineering and Technology (UET), Lahore, Pakistan.			**Macroscopic Description:** Green, fine grained and high in strength.	
Geological Formation: Salkhala (Metabasites)				
Mineral Description				
Thin Section Number	**Point Count**	**Mineral**	**Volume (%)**	**Mean Grain Size (mm)**
2	300	Pyroxene	35.00	1.74
		Plagioclase	48.00	0.60
		Quartz	7.00	0.23
		Mica	1.00	0.20
		Epidote	2.00	0.15
		Zircon	1.00	0.18
		Chlorite	3.00	0.26
		Calcite	3.00	0.60
		Mean Overall Grain Size (mm)		0.49
General Remarks:				
Petrographic Classification: Dolerite.				
Enlargement 4×				
Plane Polarized Light		Crossed Polars		
* Q: Quartz; POX: Pyroxene; PL: Plagioclase; CL: Chlorite				
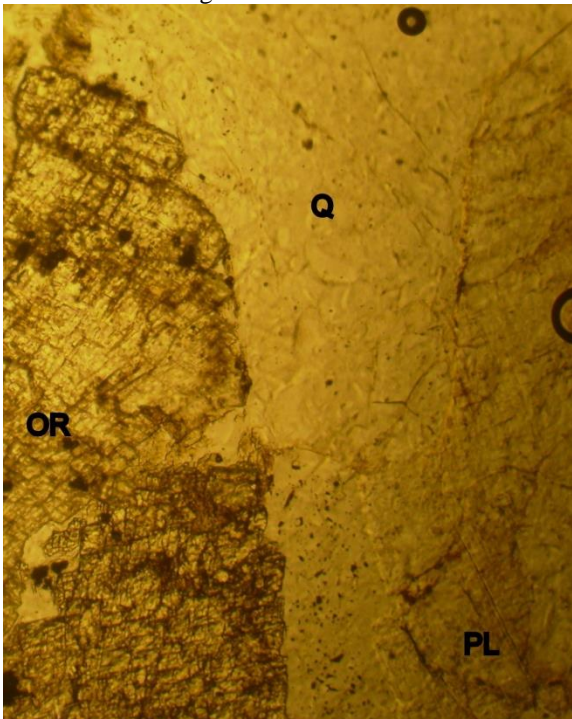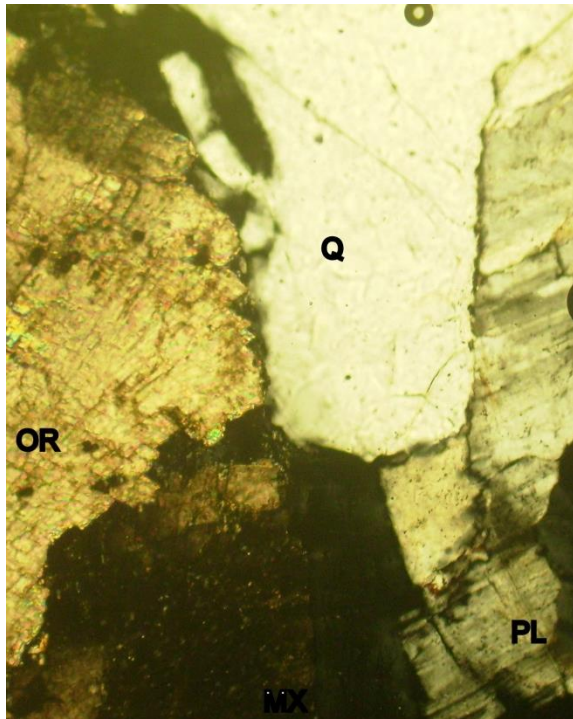
PETROGRAPHIC DESCRIPTION: Dolerite-4 (Silanwali)				
Name: Yasir Majeed **Date:** July , 2014. **Location:** University of Engineering and Technology (UET), Lahore, Pakistan. **Geological Formation:** Kirana Complex			**Macroscopic Description:** Greenish grey, fine to medium grained and high in strength.	
Mineral Description				
Thin Section Number	**Point Count**	**Mineral**	**Volume (%)**	**Mean Grain Size (mm)**
3	300	Plagioclase	58.00	0.49
		Pyroxene	12.00	0.36
		Quartz	18.00	0.36
		Muscovite	2.50	0.29
		Zircon	3.00	0.28
		Glassy Matrix	3.00	0.46
		Chlorite	3.50	0.23
		Mean Overall Grain Size (mm)		0.35
General Remarks:				
Petrographic Classification: Dolerite				
Enlargement 5×				

Plane Polarized Light

Crossed Polars

* Q: Quartz; POX: Pyroxene; PL: Plagioclase

PETROGRAPHIC DESCRIPTION: Granite-2 (Sandok)				
Name: Yasir Majeed **Date:** July , 2014. **Location:** University of Engineering and Technology (UET), Lahore, Pakistan.			**Macroscopic Description:** Greyish white, coarse grained and medium in strength.	
Geological Formation: Salkhala (Leucogranite)				
Mineral Description				
Thin Section Number	**Point Count**	**Mineral**	**Volume (%)**	**Mean Grain Size (mm)**
4	300	Quartz	74.00	1.10
		Feldspars	22.00	1.20
		Muscovite	2.50	1.38
		Biotite	1.00	1.35
		Sericite	0.50	0.69
		Mean Overall Grain Size (mm)		1.14
General Remarks: Interlocking matrix of quartz and feldspars.				
Petrographic Classification: White Granite				
Enlargement 4×				
Plane Polarized Light		Crossed Polars		
* Q: Quartz; MI: Microcline				

PETROGRAPHIC DESCRIPTION: Granite-3 (Sarsangar)

Name: Yasir Majeed **Date:** May, 2015. **Location:** University of Engineering and Technology (UET), Lahore, Pakistan.			**Macroscopic Description:** Greyish white, coarse grained and medium in strength.	
Geological Formation: Salkhala (Leucogranite)				

Mineral Description

Thin Section Number	Point Count	Mineral	Volume (%)	Mean Grain Size (mm)
5	300	Quartz	65.00	1.30
		Feldspars	24.00	1.56
		Muscovite	4.00	1.44
		Biotite	2.50	0.87
		Magnetite	0.50	0.16
		Sericite	4.00	1.34
		Mean Overall Grain Size (mm)		1.11

General Remarks: Interlocking matrix of quartz and feldspars.

Petrographic Classification: White Granite.

Enlargement 4×	
Plane Polarized Light	Crossed Polars

* Q: Quartz; MU: Muscovite
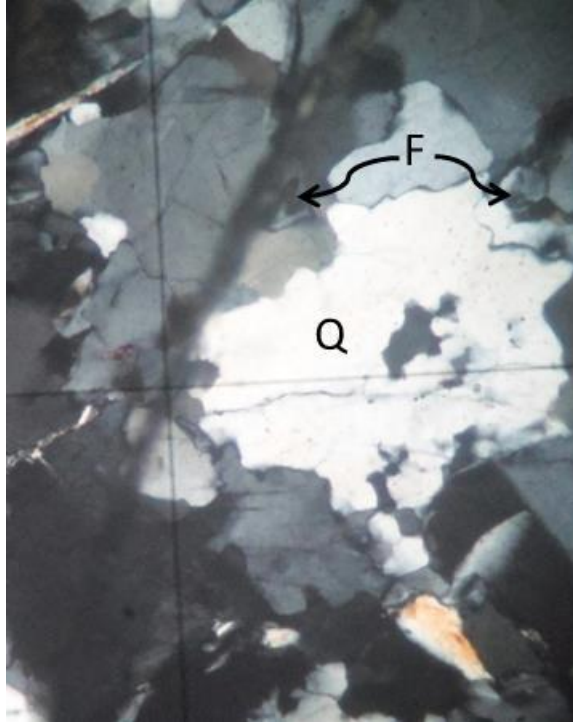
PETROGRAPHIC DESCRIPTION: Granite-4 (Keran)				
Name: Yasir Majeed **Date:** May, 2015. **Location:** University of Engineering and Technology (UET), Lahore, Pakistan.			**Macroscopic Description:** Greyish white, coarse grained and low in strength.	
Geological Formation: Salkhala (Leucogranite)				
Mineral Description				
Thin Section Number	**Point Count**	**Mineral**	**Volume (%)**	**Mean Grain Size (mm)**
6	300	Quartz	67.00	1.19
		Feldspars	24.00	2.06
		Muscovite	2.50	1.05
		Biotite	2.00	1.19
		Zircon	0.50	0.21
		Garnet	0.50	0.35
		Sericite	1.50	6.00
		Mean Overall Grain Size (mm)		1.72
General Remarks: Interlocking matrix of quartz and feldspars.				
Petrographic Classification: White Granite				
Enlargement 4×				
Plane Polarized Light		Crossed Polars		

* Q: Quartz; F: Feldspar; MU: Muscovite; BI: Biotite
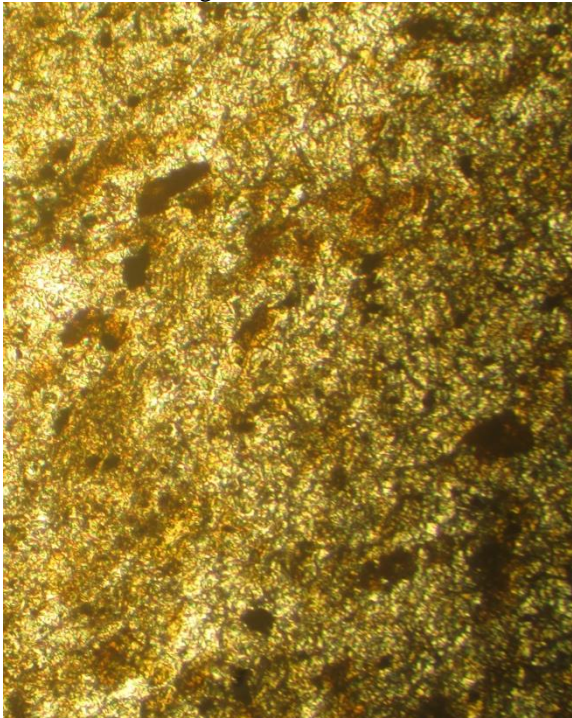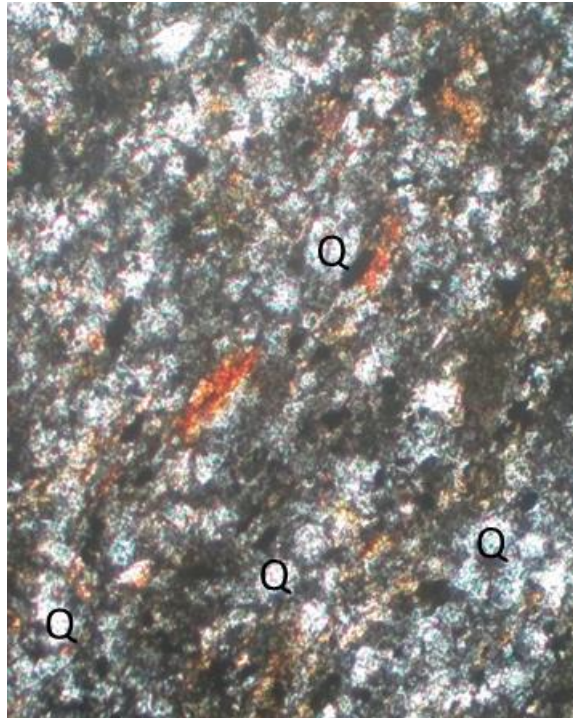
PETROGRAPHIC DESCRIPTION: Granite-5				
Name: Yasir Majeed **Date:** July , 2014. **Location:** University of Engineering and Technology (UET), Lahore, Pakistan.			**Macroscopic Description:** Greyish black, coarse grained and high in strength.	
Geological Formation: Mansehra Granite				
Mineral Description				
Thin Section Number	**Point Count**	**Mineral**	**Volume (%)**	**Mean Grain Size (mm)**
7	300	Quartz	73.00	0.39
		Feldspars	24.50	1.48
		Micas	1.50	0.84
		Magnetite	0.75	1.11
		Epidote	0.25	0.40
		Mean Overall Grain Size (mm)		0.84
General Remarks: Interlocking matrix of quartz and feldspars.				
Petrographic Classification: Granite				
Enlargement 4×				
Plane Polarized Light		Crossed Polars		

* Q: Quartz; PL: Plagioclase; MU: Muscovite;
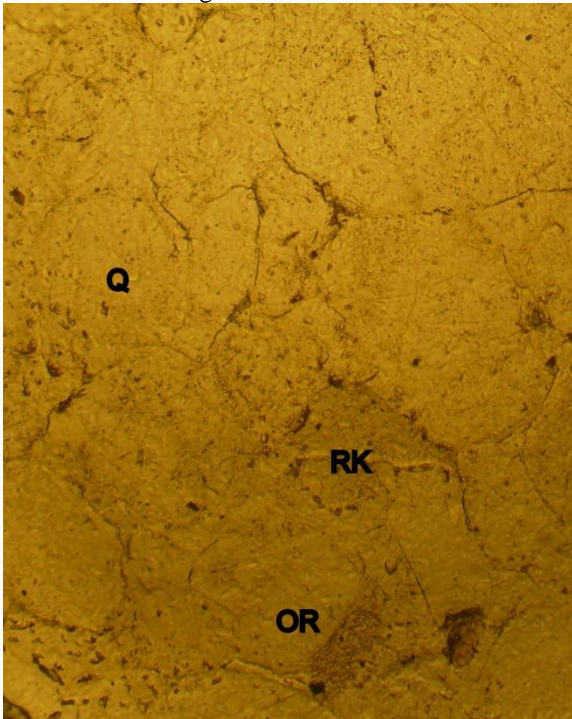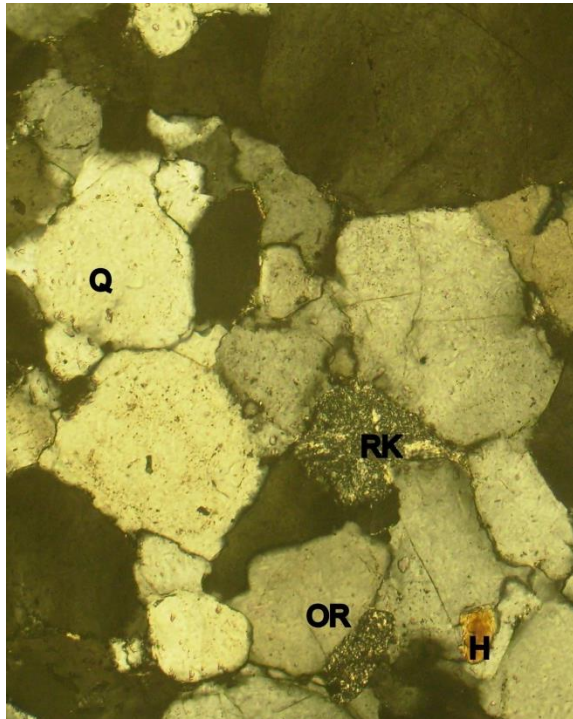
PETROGRAPHIC DESCRIPTION: Granite-6				
Name: Yasir Majeed **Date:** July , 2014. **Location:** University of Engineering and Technology (UET), Lahore, Pakistan.			**Macroscopic Description:** Pink, coarse grained and low in strength.	
Geological Formation: Tobra				
Mineral Description				
Thin Section Number	**Point Count**	**Mineral**	**Volume (%)**	**Mean Grain Size (mm)**
8	300	Quartz	24.60	2.50
		Plagioclase	7.20	2.24
		Microcline	59.80	1.29
		Hematite	1.44	0.36
		Micas	1.72	1.36
		Zircon	2.80	0.21
		Sericite	2.44	2.81
		Mean Overall Grain Size (mm)		1.54
General Remarks: Interlocking matrix of quartz and feldspars.				
Petrographic Classification: Pink Granite				
Enlargement 4×				
Plane Polarized Light		Crossed Polars		
* Q: Quartz; OR: Orthoclase; PL: Plagioclase				
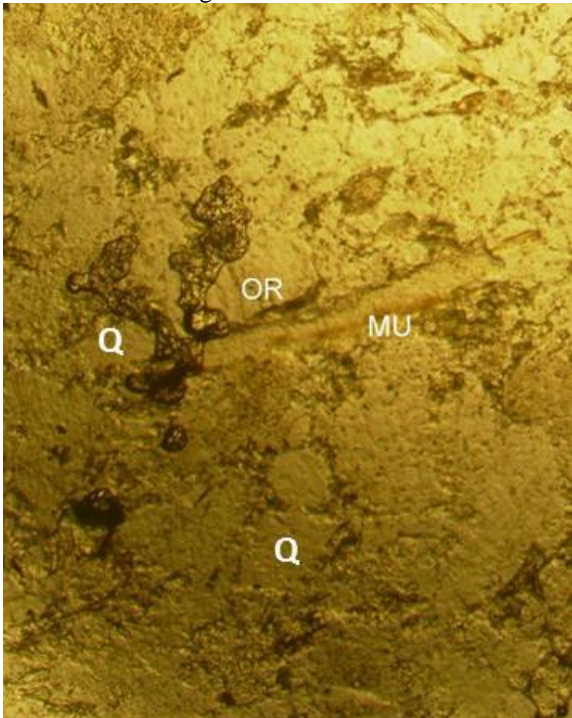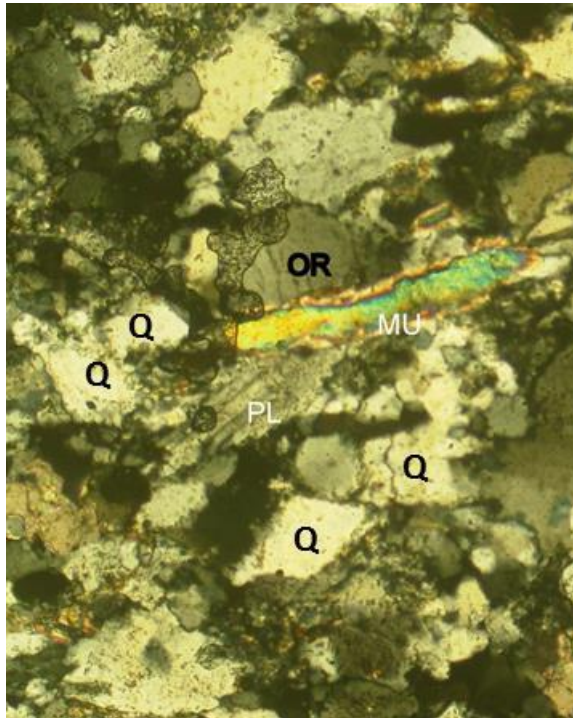
PETROGRAPHIC DESCRIPTION: Migmatite				
Name: Yasir Majeed **Date:** July , 2014. **Location:** University of Engineering and Technology (UET), Lahore, Pakistan.			**Macroscopic Description:** Greyish white, coarse grained and medium in strength.	
Geological Formation: Salkhala (Naril Group)				
Mineral Description				
Thin Section Number	**Point Count**	**Mineral**	**Volume (%)**	**Mean Grain Size (mm)**
9	300	Quartz	70.00	1.21
		Microcline	13.00	3.51
		Plagioclase	7.50	2.10
		Muscovite	3.50	0.90
		Biotite	2.50	1.12
		Zircon	0.50	0.23
		Iron Oxide	1.00	0.98
		Sericite	2.00	0.76
		Mean Overall Grain Size (mm)		1.35
General Remarks: Interlocking matrix of quartz and feldspars.				
Petrographic Classification: Migmatite.				
Enlargement 4×				
Plane Polarized Light		Crossed Polars		

* Q: Quartz; M: Microcline; OR: Orthoclase
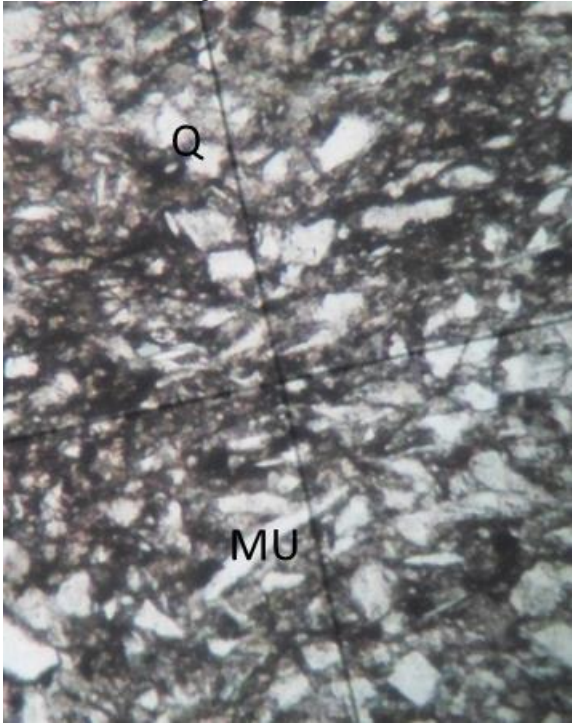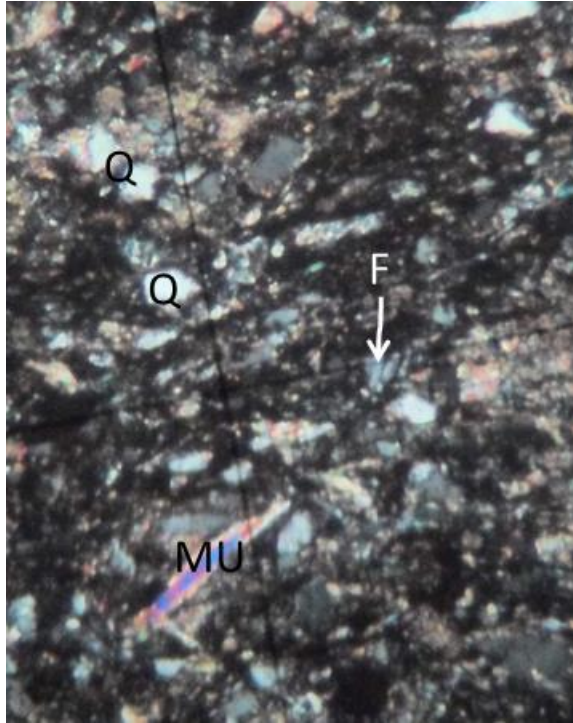
PETROGRAPHIC DESCRIPTION: Andesite

Name: Yasir Majeed	Macroscopic Description: Greyish black, coarse grained and high in strength.
Date: June, 2015.	
Location: University of Engineering and Technology (UET), Lahore, Pakistan.	
Geological Formation: Salkhala (Sharda Group)	

Mineral Description

Thin Section Number	Point Count	Mineral	Volume (%)	Mean Grain Size (mm)
10	300	Pyroxene	27.00	0.60
		Quartz	10.00	0.18
		Amphibole	15.00	1.10
		Feldspars	40.00	0.99
		Biotite	2.50	0.42
		Magnetite	0.50	0.30
		Mean Overall Grain Size (mm)		0.599

General Remarks:

Petrographic Classification: Andesite

Enlargement 4×

Plane Polarized Light	Crossed Polars

* Q: Quartz; POX: Pyroxene; PL: Plagioclase

PETROGRAPHIC DESCRIPTION: Granitic Gneiss-1

Name: Yasir Majeed **Date:** July , 2014. **Location:** University of Engineering and Technology (UET), Lahore, Pakistan.	**Macroscopic** Description: Light greyish white, coarse grained and medium strength rock sample.

Geological Formation: Salkhala (Naril Group)

Mineral Description

Thin Section Number	Point Count	Mineral	Volume (%)	Mean Grain Size (mm)
11	300	Quartz	73.00	0.57
		Potassium Feldspar	13.00	1.38
		Plagioclase	8.00	1.25
		Muscovite	3.50	0.65
		Biotite	2.00	0.80
		Zircon	0.50	0.16
		Mean Overall Grain Size (mm)		0.800

General Remarks: Interlocking matrix of quartz and feldspars.

Petrographic Classification: Ganitic Gneiss

Enlargement 5×

Plane Polarized Light | Crossed Polars

* Q: Quartz; F: Feldspar
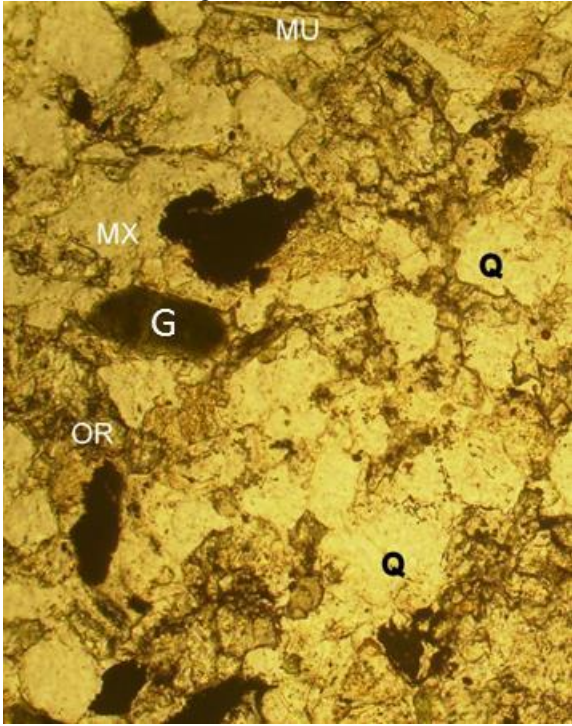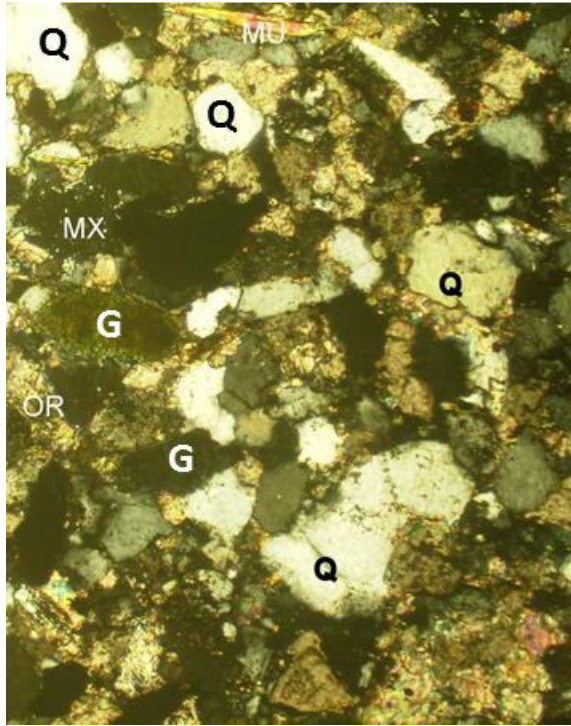
PETROGRAPHIC DESCRIPTION: Phyllite				
Name: Yasir Majeed **Date:** May, 2015. **Location:** University of Engineering and Technology (UET), Lahore, Pakistan.		**Macroscopic Description:** Medium green, coarse grained and medium strength phyllite.		
Geological Formation: Abbottabad				
Mineral Description				
Thin Section Number	**Point Count**	**Mineral**	**Volume (%)**	**Mean Grain Size (mm)**
12	300	Quartz	50.00	0.14
		Feldspars	10.00	0.13
		Muscovite	3.50	1.19
		Biotite	4.50	0.65
		Hematite	0.50	1.82
		Mean Overall Grain Size (mm)		0.784
General Remarks: Quartz is strained.				
Petrographic Classification: Phyllite				
Enlargement 4×				
Plane Polarized Light		Crossed Polars		
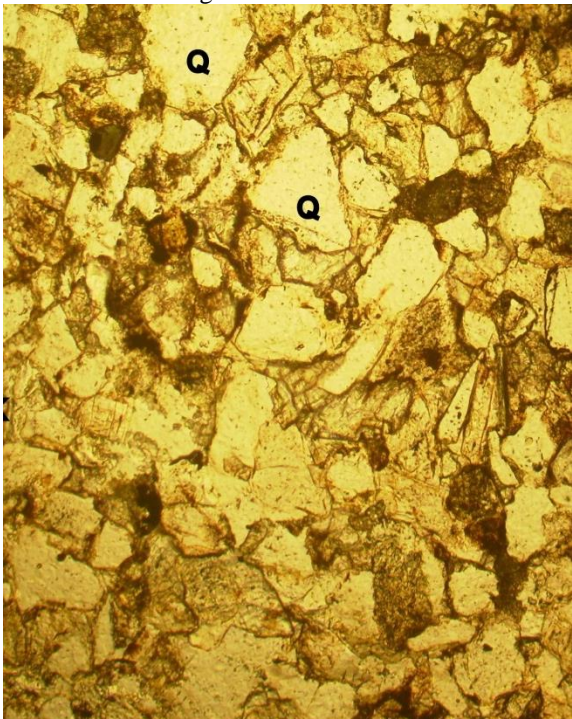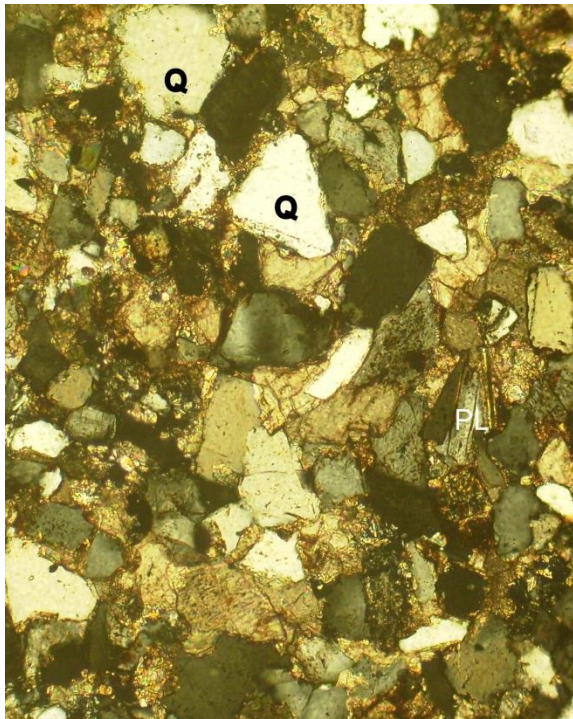
* Q: Quartz

PETROGRAPHIC DESCRIPTION: Quartzite-1	
Name: Yasir Majeed **Date:** July , 2014. **Location:** University of Engineering and Technology (UET), Lahore, Pakistan. **Geological Formation:** Abbottabad	**Macroscopic Description:** Dirty white, medium grained and moderate in strength.

Mineral Description

Thin Section Number	Point Count	Mineral	Volume (%)	Mean Grain Size (mm)
13	300	Quartz	90.60	0.737
		Feldspars	2.20	0.410
		Chert	3.00	0.435
		Tourmaline	1.30	0.326
		Zircon	0.30	0.247
		Opaques (Hematite and Magnetite)	1.20	0.172
		Clay	0.50	< 0.050
		Chlorite	0.90	0.167
		Mean Overall Grain Size (mm)		0.318

General Remarks: Interlocking matrix of quartz grains.

Petrographic Classification: Quartzite.

<div align="center">Enlargement 4×</div>

Plane Polarized Light	Crossed Polars

* Q: Quartz; OR: Orthoclase (Feldspar); RK: Rock (Chert); H: Hematite
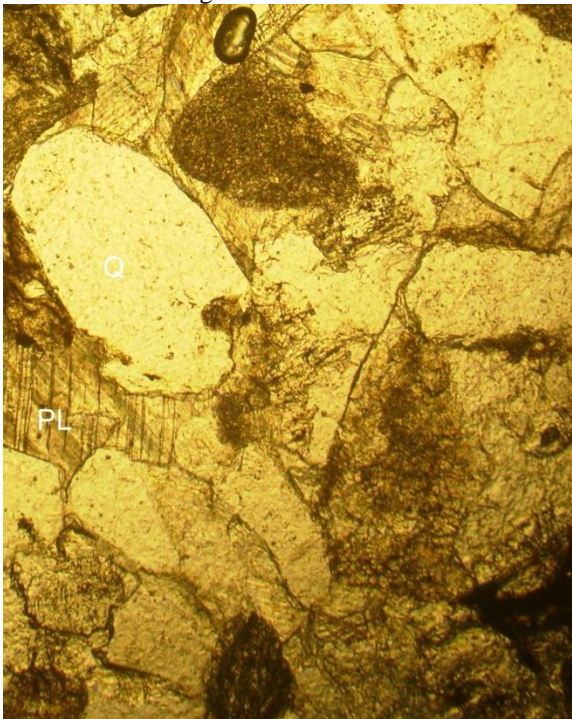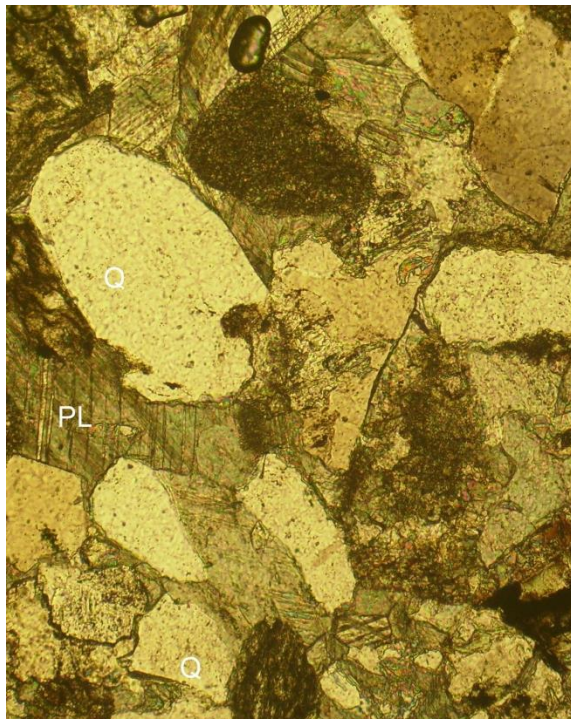
PETROGRAPHIC DESCRIPTION: Quartzite-2				
Name: Yasir Majeed **Date:** July , 2014. **Location:** University of Engineering and Technology (UET), Lahore, Pakistan.			**Macroscopic Description:** Medium to dark grey, medium grained and high in strength.	
Geological Formation: Tobra				
Mineral Description				
Thin Section Number	**Point Count**	**Mineral**	**Volume (%)**	**Mean Grain Size (mm)**
14	300	Quartz	48.50	0.538
		Feldspars	4.30	0.352
		Muscovite	5.80	0.428
		Biotite	2.40	0.157
		Tourmaline	1.10	0.264
		Zircon	0.30	0.242
		Opaques (Hematite and Magnetite)	1.70	0.257
		Micro Crystalline Quartz	22.30	0.078
		Carbonate	2.80	0.322
		Chlorite	1.30	0.397
		Mean Overall Grain Size (mm)		0.304
General Remarks: Interlocking matrix of quartz grains.				
Petrographic Classification: Quartzite				
Enlargement 4×				
Plane Polarized Light			Crossed Polars	
* Q: Quartz; OR: Orthoclase (Feldspar); PL: Plagioclase (Feldspar); MU: Muscovite				
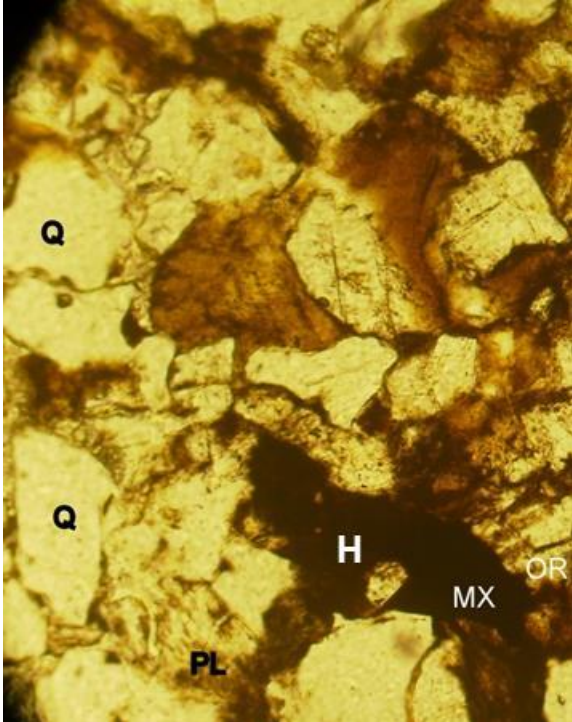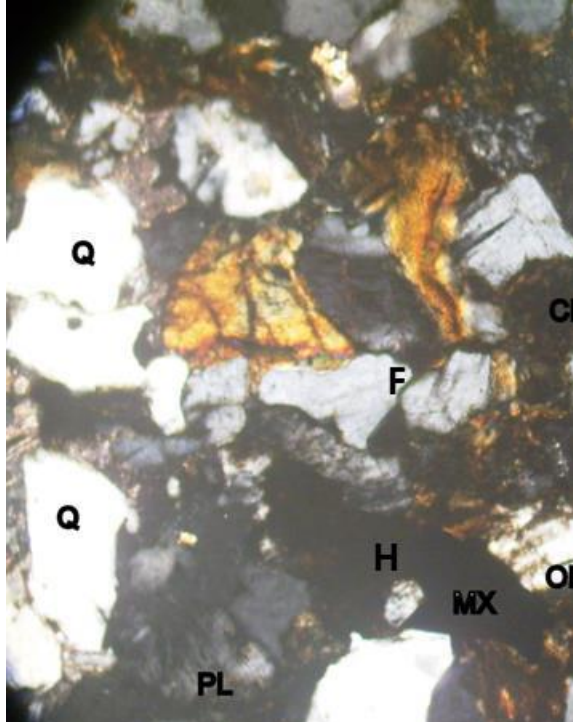
PETROGRAPHIC DESCRIPTION: Siltstone-1

Name: Yasir Majeed	Macroscopic Description: Reddish brown, fine grained and moderate strength siltstone.
Date: July , 2014.	
Location: University of Engineering and Technology (UET), Lahore, Pakistan.	
Geological Formation: Murree	

Mineral Description

Thin Section Number	Point Count	Mineral	Volume (%)	Mean Grain Size (mm)
15	300	Quartz	15.20	0.225
		Feldspars	13.00	0.537
		Micas (Muscovite and Biotite)	5.00	0.177
		Hematite	5.00	0.167
		Sericite	7.00	0.518
		Calcite	24.80	0.359
		Clay	30.00	< 0.050
		Mean Overall Grain Size (mm)		0.290

General Remarks: Calcareous rock sample.

Petrographic Classification: Siltstone.

Enlargement 6×	
Plane Polarized Light	Crossed Polars

* Q: Quartz; F: Feldspar; MU: Muscovite
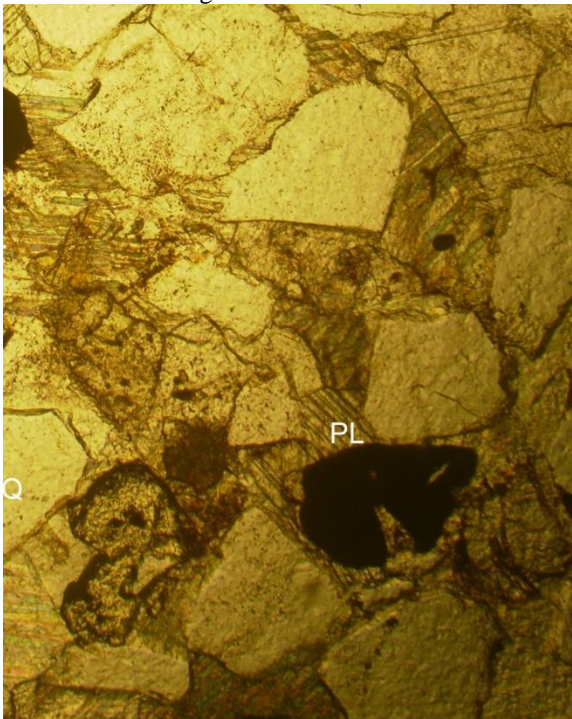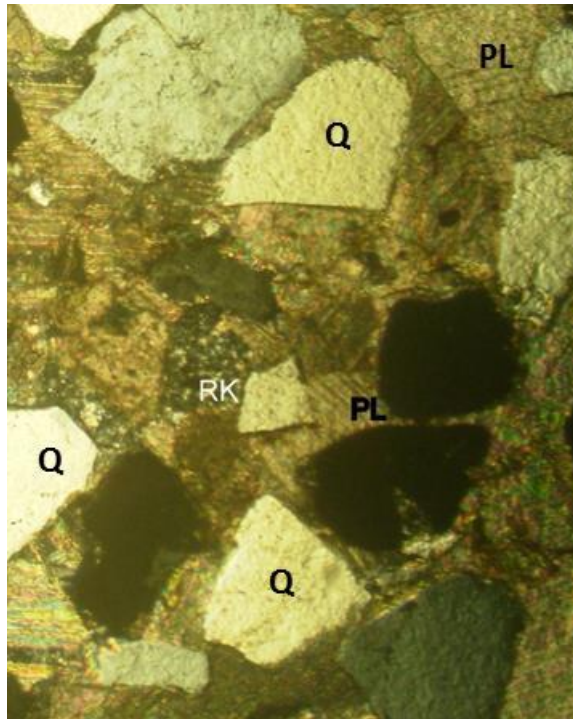
PETROGRAPHIC DESCRIPTION: Siltstone-2

Name: Yasir Majeed **Date:** June, 2015. **Location:** University of Engineering and Technology (UET), Lahore, Pakistan.	**Macroscopic Description:** Creamish, fine grained and medium in strength.
Geological Formation: Tobra	

Mineral Description

Thin Section Number	Point Count	Mineral	Volume (%)	Mean Grain Size (mm)
16	300	Dolomite	33.00	0.123
		Quartz	22.00	0.154
		Hematite	1.50	0.178
		Feldspar	35.00	0.168
		Biotite	1.00	0.596
		Muscovite	1.00	0.170
		Epidote	0.50	0.054
		Clay	6.00	< 0.004
		Mean Overall Grain Size (mm)		0.206

General Remarks: Arenaceous sandy

Petrographic Classification: Siltstone

Enlargement 5×

Plane Polarized Light

Crossed Polars

* Q: Quartz; F: Feldspar; MU: Muscovite
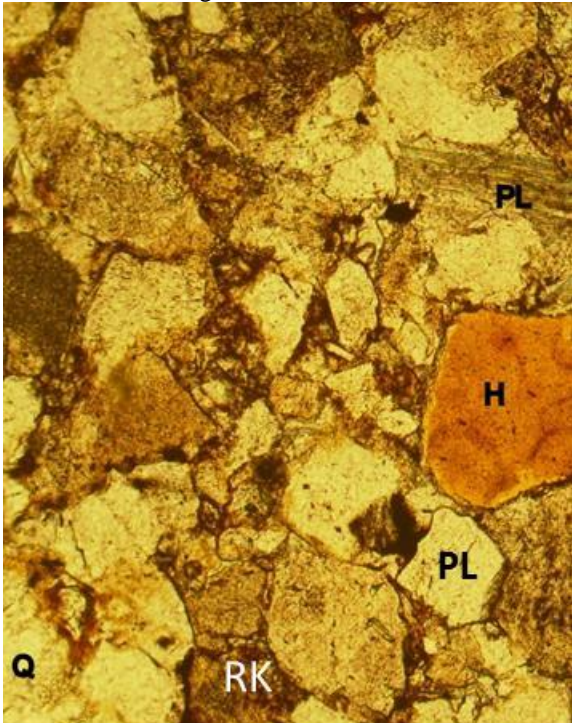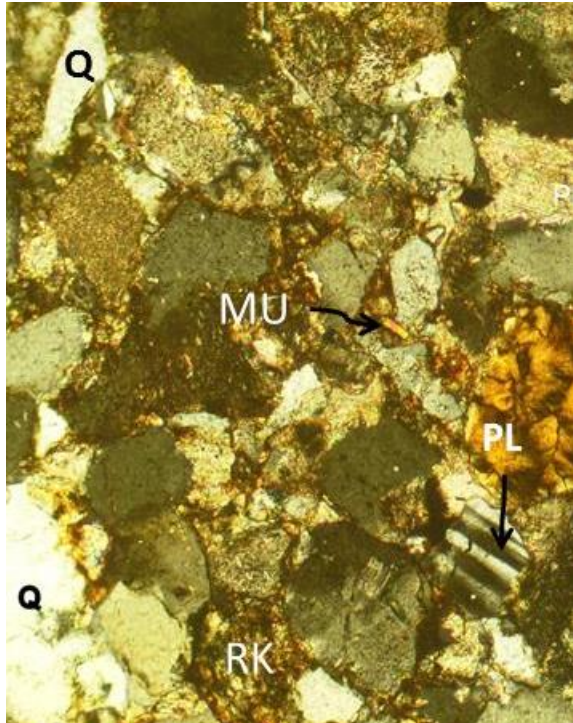
PETROGRAPHIC DESCRIPTION: Sandstone-1

Name: Yasir Majeed **Date:** July , 2014. **Location:** University of Engineering and Technology (UET), Lahore, Pakistan.	**Macroscopic Description:** Greenish grey, coarse grained and low in strength.
Geological Formation: Tobra	

Mineral Description

Thin Section Number	Point Count	Mineral	Volume (%)	Mean Grain Size (mm)
17	300	Quartz	68.00	0.413
		Feldspars	9.50	0.979
		Muscovite	2.50	0.458
		Biotite	1.50	0.446
		Epidote	0.50	0.252
		Glauconite	3.50	0.431
		Chlorite	1.50	0.382
		Carbonate Shells	2.50	2.866
		Sericite	3.50	1.011
		Glassy Matrix	7.00	< 0.050
		Mean Overall Grain Size (mm)		0.729

General Remarks: Glauconitic sandstone.

Petrographic Classification: Lithic arenite sandstone.

<table>
<tr><td colspan="2" align="center">Enlargement 4×</td></tr>
<tr><td>Plane Polarized Light</td><td>Crossed Polars</td></tr>
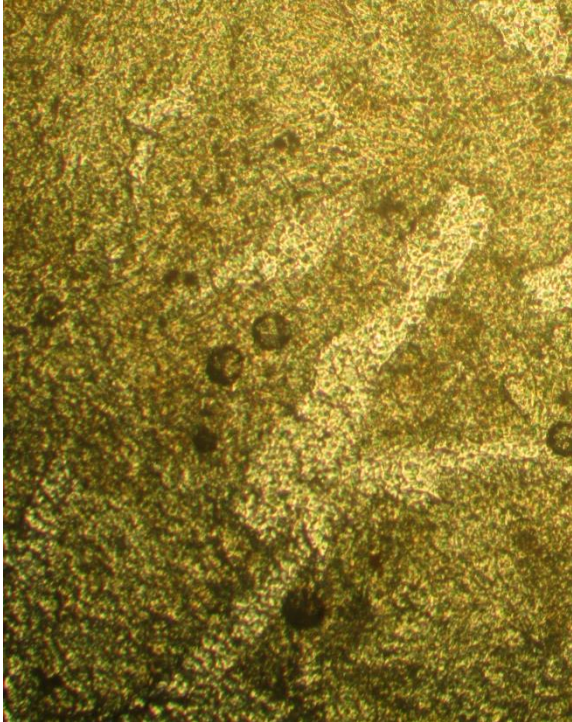<tr><td colspan="2"></td></tr>
</table>

* Q: Quartz; OR: Orthoclase (Feldspar); MU: Muscovite; G: Glauconite; MX: Matrix

PETROGRAPHIC DESCRIPTION: Sandstone-2

Name: Yasir Majeed **Date:** July , 2014. **Location:** University of Engineering and Technology (UET), Lahore, Pakistan.	**Macroscopic Description:** Brown, fine grained and low strength sandstone.
Geological Formation: Khewra	

Mineral Description

Thin Section Number	Point Count	Mineral	Volume (%)	Mean Grain Size (mm)
18	300	Quartz	67.00	0.237
		Feldspars	20.00	0.200
		Muscovite	1.50	0.268
		Chlorite	0.50	0.085
		Sericite	1.00	0.276
		Hematite	1.00	0.158
		Glassy matrix	9.00	< 0.050
		Mean Overall Grain Size (mm)		0.204

General Remarks: Arkosic sandstone.

Petrographic Classification: Feldspathic wacke sandstone.

<div align="center">Enlargement 4×</div>

Plane Polarized Light	Crossed Polars

* Q: Quartz; PL: Plagioclase (Feldspar)

PETROGRAPHIC DESCRIPTION: Sandstone-3				
Name: Yasir Majeed **Date:** July , 2014. **Location:** University of Engineering and Technology (UET), Lahore, Pakistan.		**Macroscopic Description:** Medium grey, coarse grained and high in strength.		
Geological Formation: Murree				
Mineral Description				
Thin Section Number	**Point Count**	**Mineral**	**Volume (%)**	**Mean Grain Size (mm)**
19	300	Quartz	64.00	0.588
		Feldspars	15.00	0.546
		Muscovite	4.00	0.532
		Biotite	3.00	0.889
		Hematite	3.00	0.556
		Sericite	2.00	0.480
		Chert	9.00	0.435
		Mean Overall Grain Size (mm)		0.575
General Remarks: Quartz grains are angular and contact is sutured.				
Petrographic Classification: Quartz wacke sandstone.				
Enlargement 4×				
Plane Polarized Light		Crossed Polars		

* Q: Quartz; PL: Plagioclase (Feldspar)
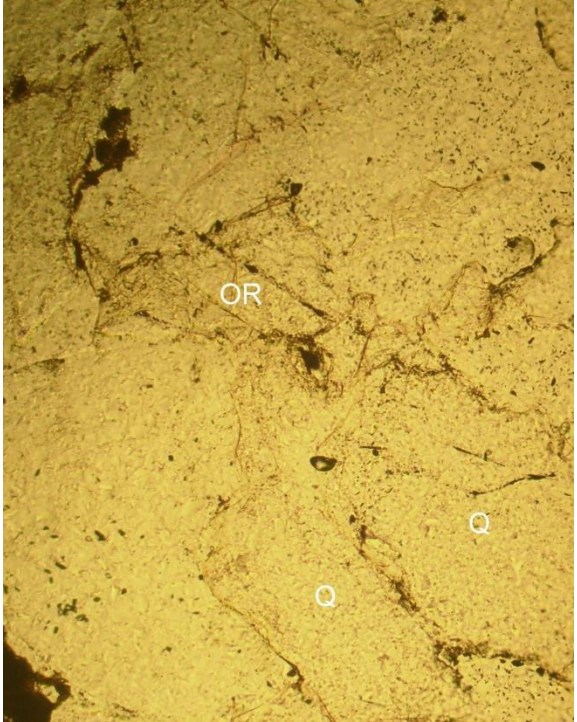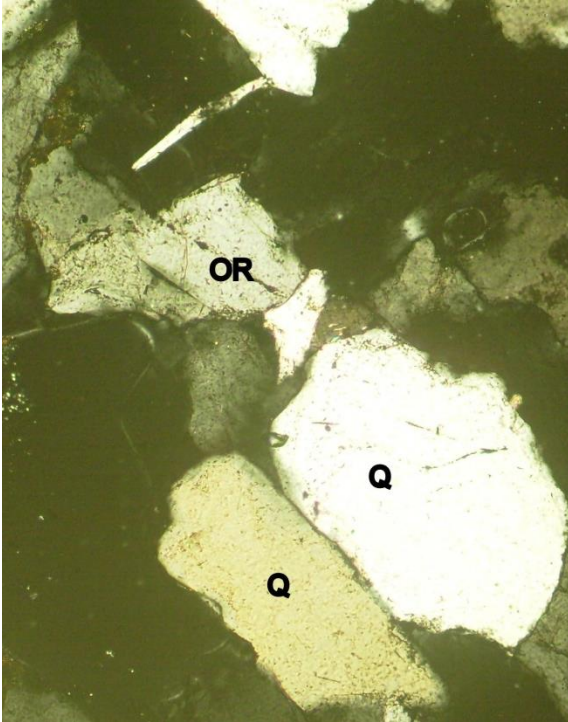
PETROGRAPHIC DESCRIPTION: Sandstone-4				
Name: Yasir Majeed **Date:** July , 2014. **Location:** University of Engineering and Technology (UET), Lahore, Pakistan.		**Macroscopic Description:** Light to dark olive green, medium grained and low in strength.		
Geological Formation: Tobra				
Mineral Description				
Thin Section Number	**Point Count**	**Mineral**	**Volume (%)**	**Mean Grain Size (mm)**
20	300	Quartz	78.00	0.392
		Feldspars	17.00	0.276
		Hematite	0.50	0.374
		Muscovite	1.50	0.384
		Biotite	2.50	0.441
		Sericite	0.50	0.466
		Mean Overall Grain Size (mm)		0.389
General Remarks:				
Petrographic Classification: Sub-arkose sandstone				
Enlargement 4×				
Plane Polarized Light		Crossed Polars		

* Q: Quartz; F: Feldspar; PL: Plagioclase (Feldspar); OR: Orthoclase (Feldspar); H: Hematite
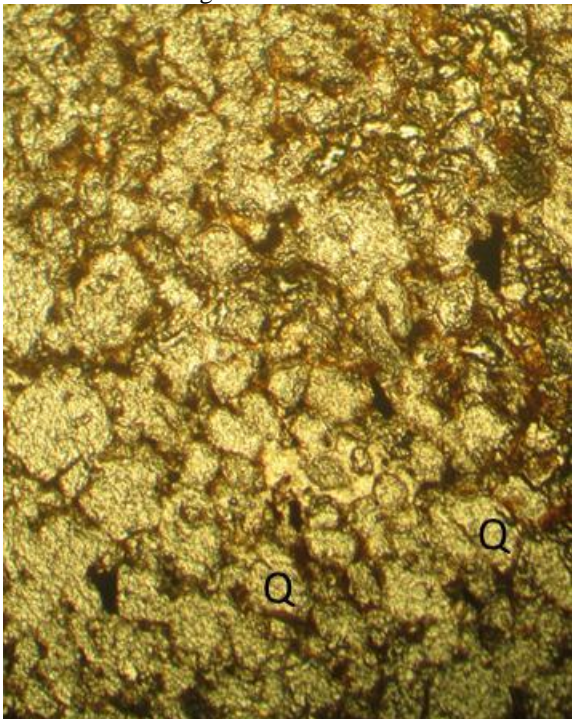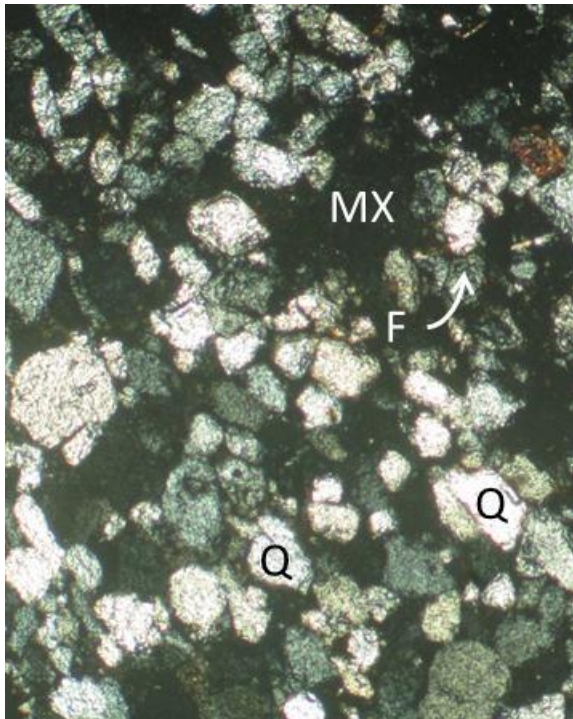
PETROGRAPHIC DESCRIPTION: Sandstone-5				
Name: Yasir Majeed **Date:** July , 2014. **Location:** University of Engineering and Technology (UET), Lahore, Pakistan.			**Macroscopic Description:** Olive green yellowish, medium to coarse grained and low in strength.	
Geological Formation: Dandot				
Mineral Description				
Thin Section Number	**Point Count**	**Mineral**	**Volume (%)**	**Mean Grain Size (mm)**
21	300	Quartz	62.30	0.513
		Chert	4.70	0.472
		Feldspars	28.00	0.479
		Muscovite	1.50	0.415
		Epidote	1.50	0.329
		Sericite	1.50	0.704
		Hematite	0.50	0.446
		Mean Overall Grain Size (mm)		0.480
General Remarks:				
Petrographic Classification: Arkosic sandstone.				
Enlargement 4×				

Plane Polarized Light	Crossed Polars

* Q: Quartz; PL: Plagioclase (Feldspar); RK: Rock (Chert)
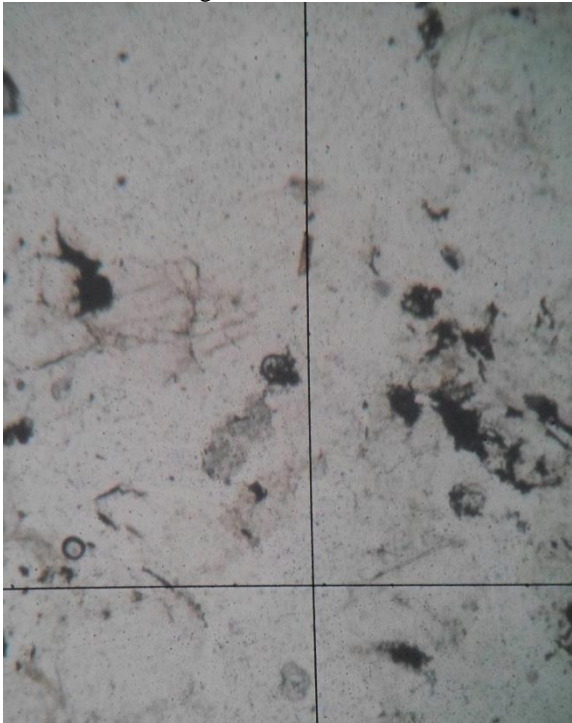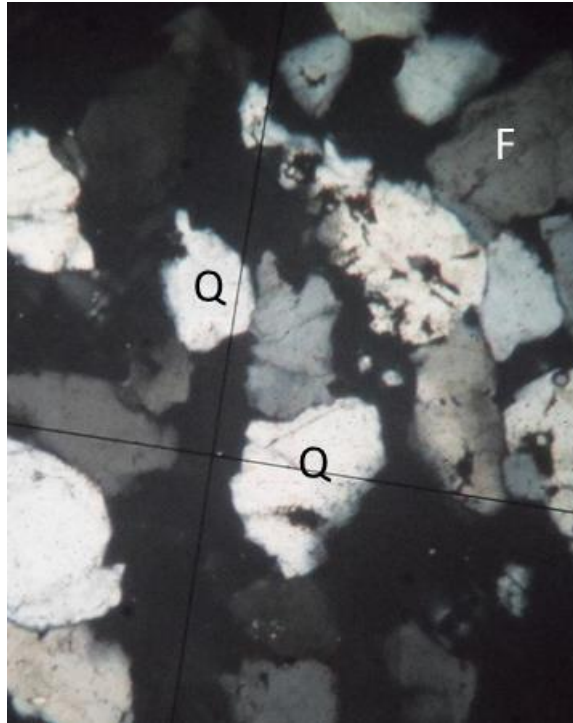
PETROGRAPHIC DESCRIPTION: Sandstone-6				
Name: Yasir Majeed **Date:** July , 2014. **Location:** University of Engineering and Technology (UET), Lahore, Pakistan.			**Macroscopic Description:** Light to medium brown, coarse grained and moderately high in strength.	
Geological Formation: Tobra				
Mineral Description				
Thin Section Number	**Point Count**	**Mineral**	**Volume (%)**	**Mean Grain Size (mm)**
22	300	Quartz	70.10	0.716
		Rock Fragments (Quartz)	22.60	2.419
		Plagioclase	1.00	0.385
		Potassium Feldspar	0.70	0.698
		Micas (Muscovite and Biotite)	1.00	0.549
		Chert	1.30	0.752
		Zircon	0.30	0.237
		Sericite	1.00	0.716
		Hematite	0.40	0.767
		Carbonate	1.10	1.565
		Chlorite	0.50	0.129
		Mean Overall Grain Size (mm)		0.812
General Remarks:				
Petrographic Classification: Lithic arenite				
Enlargement 4×				

Plane Polarized Light	Crossed Polars

* Q: Quartz; PL: Plagioclase (Feldspar); MU: Muscovite; RK: Rock Fragments; H: Hematite
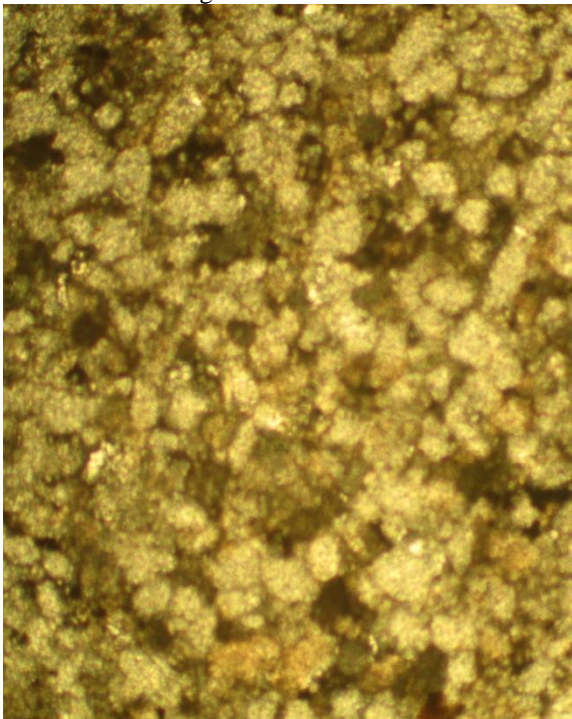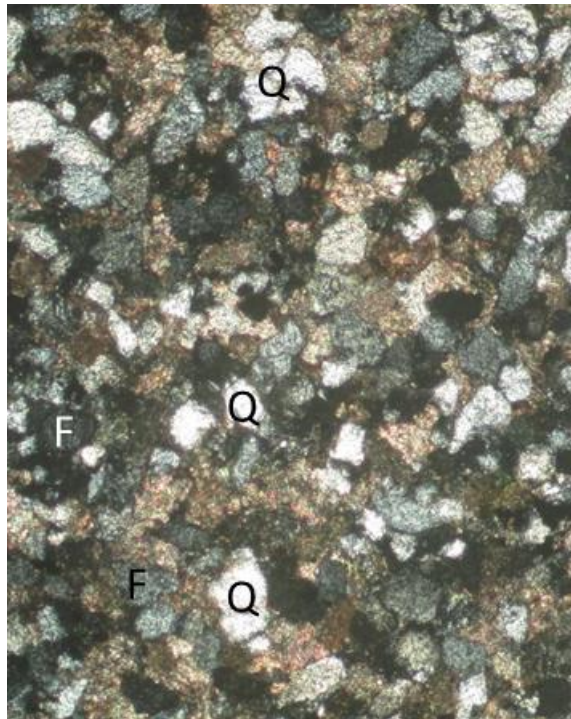
PETROGRAPHIC DESCRIPTION: Sandstone-7				
Name: Yasir Majeed **Date:** July , 2014. **Location:** University of Engineering and Technology (UET), Lahore, Pakistan.			**Macroscopic Description:** White, fine grained and medium strength rock sample.	
Geological Formation: Chhidru				
Mineral Description				
Thin Section Number	**Point Count**	**Mineral**	**Volume (%)**	**Mean Grain Size (mm)**
23	300	Quartz	67.50	0.106
		Polygrain Quartz	26.50	0.485
		Plagioclase	1.30	0.167
		K-Feldspar	0.80	0.149
		Epidote	1.30	0.109
		Chert	0.60	0.294
		Lithic Fragments	2.00	0.533
		Mean Overall Grain Size (mm)		0.263
General Remarks:				
Petrographic Classification: Quartz wacke				
Enlargement 4×				
Plane Polarized Light		Crossed Polars		

* Q: Quartz; OR: Orthoclase; PL: Plagioclase
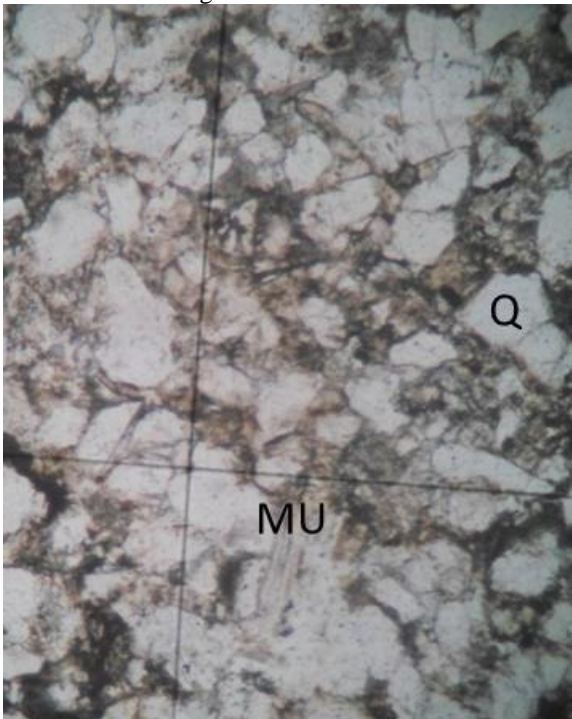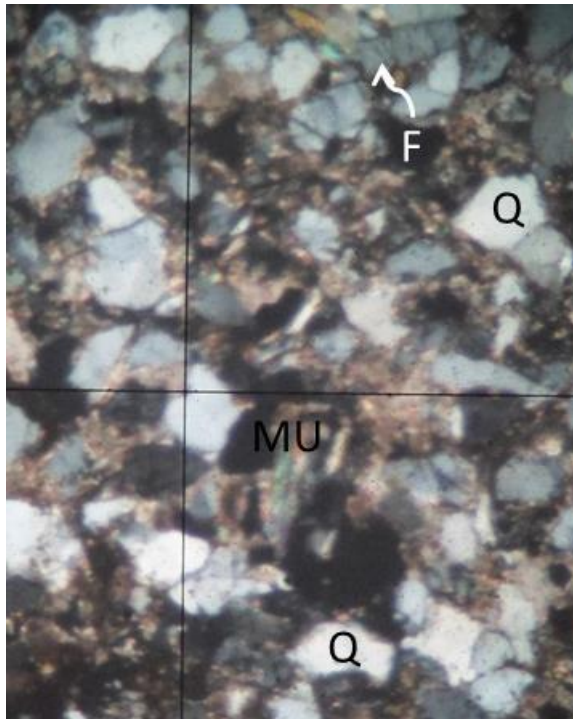
PETROGRAPHIC DESCRIPTION: Sandstone-8				
Name: Yasir Majeed **Date:** July , 2014. **Location:** University of Engineering and Technology (UET), Lahore, Pakistan.			**Macroscopic Description:** Light pink, coarse grained and low in strength.	
Geological Formation: Warchha (Speckled)				
Mineral Description				
Thin Section Number	**Point Count**	**Mineral**	**Volume (%)**	**Mean Grain Size (mm)**
24	300	Quartz	55.50	0.414
		Plagioclase	12.00	0.400
		Potassium Feldspars	7.90	0.356
		Muscovite	4.00	0.817
		Rock Fragments	6.70	0.340
		Zircon	0.50	0.195
		Sericite	4.00	0.497
		Glassy Matrix	9.40	3.500
		Mean Overall Grain Size (mm)		0.815

General Remarks:

Petrographic Classification: Feldspathic wacke.

Enlargement 4×

Plane Polarized Light

Crossed Polars

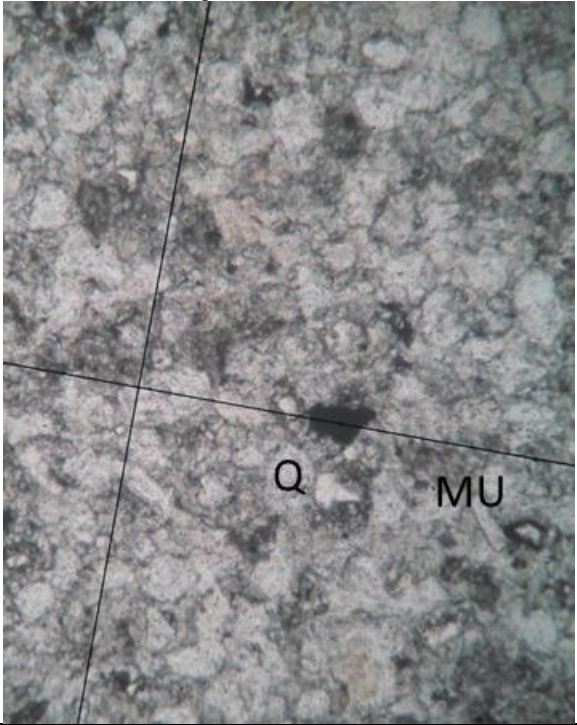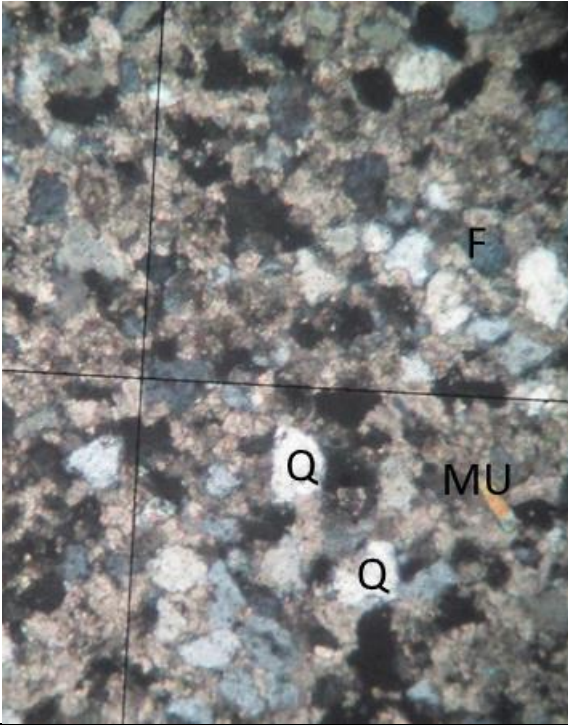* Q: Quartz; OR: Orthoclase (Feldspar); MX: Matrix
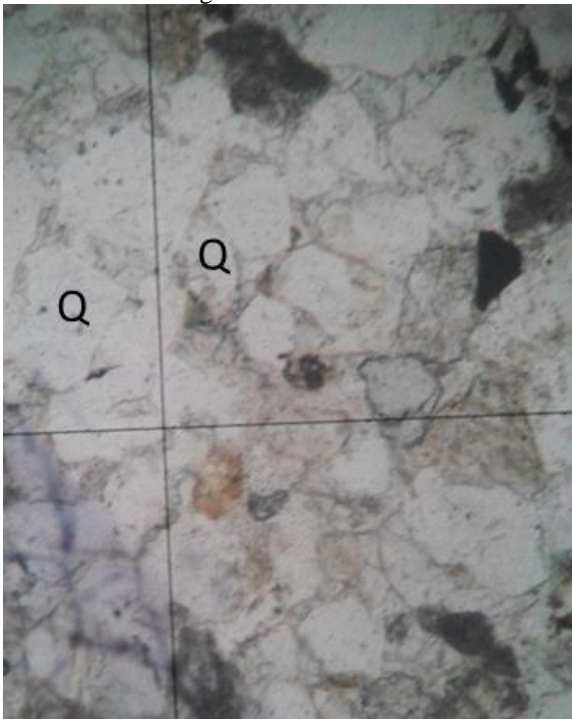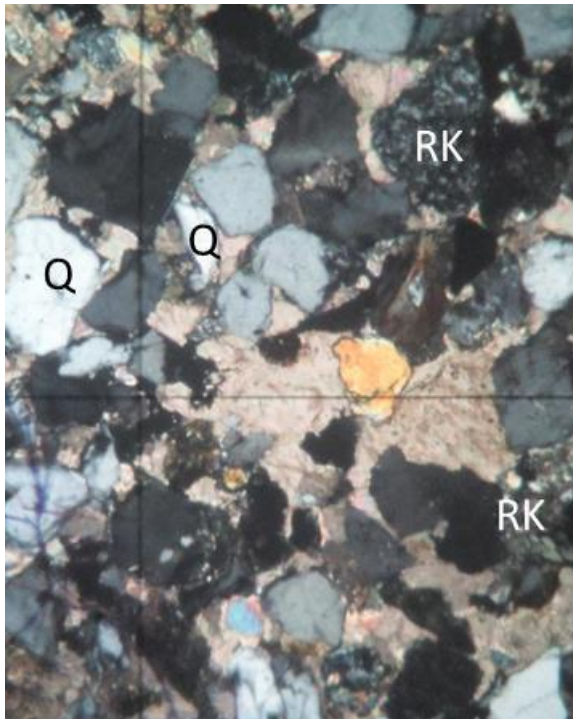
PETROGRAPHIC DESCRIPTION: Sandstone-9

Name: Yasir Majeed **Date:** July , 2014. **Location:** University of Engineering and Technology (UET), Lahore, Pakistan. **Geological Formation:** Lumshiwal	**Macroscopic Description:** Light greyish yellow, coarse grained and low in strength.

Mineral Description

Thin Section Number	Point Count	Mineral	Volume (%)	Mean Grain Size (mm)
25	300	Quartz	78.00	0.588
		Feldspars	12.00	0.447
		Glauconite	0.50	1.198
		Muscovite	0.50	0.774
		Lithic Fragments	9.00	0.361
		Quartz	78.00	0.588
		Mean Overall Grain Size (mm)		0.674

General Remarks: Sub-angular to sub-rounded and rounded in texture.

Petrographic Classification: Sub-arkose sandstone

<div align="center">Enlargement 4×</div>

Plane Polarized Light	Crossed Polars

* Q: Quartz; OR: Orthoclase (Feldspar)
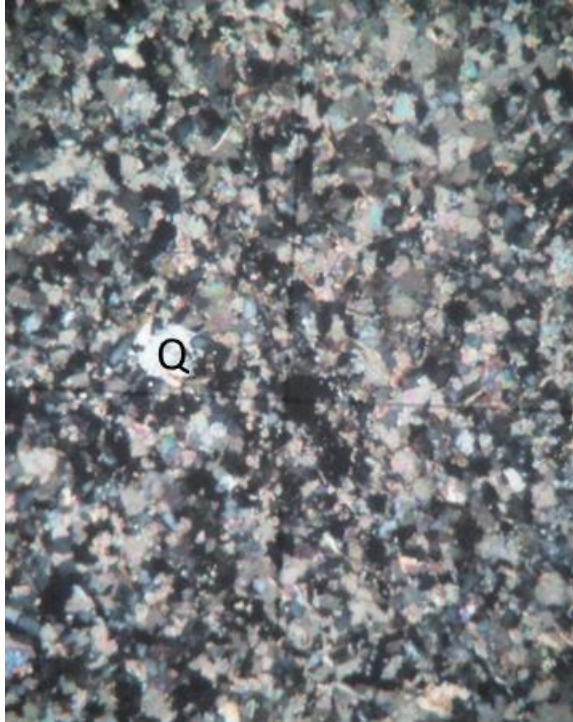
PETROGRAPHIC DESCRIPTION: Sandstone-10

Name: Yasir Majeed **Date:** May, 2015. **Location:** University of Engineering and Technology (UET), Lahore, Pakistan.	**Macroscopic Description:** Medium brownish grey, medium to coarse grained and low in strength.
Geological Formation: Hangu	

Mineral Description

Thin Section Number	Point Count	Mineral	Volume (%)	Mean Grain Size (mm)
26	300	Quartz	75.00	0.452
		Feldspars	4.50	0.307
		Muscovite	1.00	0.603
		Biotite	1.00	0.421
		Glauconite	0.50	0.202
		Limonite	1.00	0.210
		Glassy Matrix	17.00	< 0.004
		Mean Overall Grain Size (mm)		0.366

General Remarks: Sub-angular to sub-rounded in texture

Petrographic Classification: Sublithic wacke sandstone

Enlargement 4×

Plane Polarized Light	Crossed Polars

* Q: Quartz; F: Feldspar; MX: Matrix
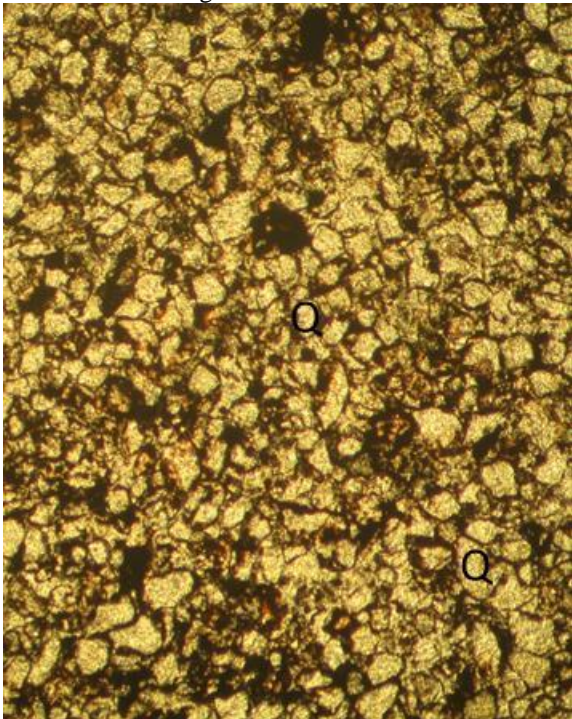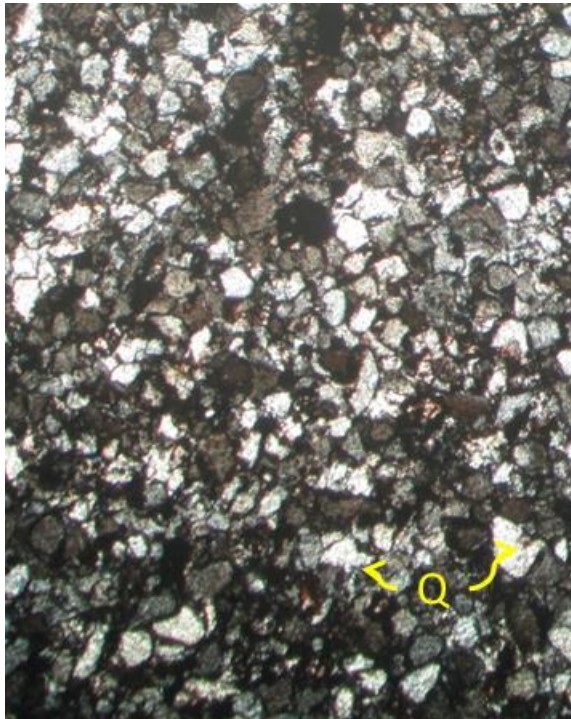
PETROGRAPHIC DESCRIPTION: Sandstone-11

Name: Yasir Majeed	Macroscopic Description: Maroon, coarse grained and low in strength.
Date: July , 2014.	
Location: University of Engineering and Technology (UET), Lahore, Pakistan.	
Geological Formation: Datta	

Mineral Description

Thin Section Number	Point Count	Mineral	Volume (%)	Mean Grain Size (mm)
27	300	Quartz	73.00	0.581
		Feldspars	16.00	0.563
		Muscovite	2.50	0.618
		Chert	1.50	0.405
		Zircon	0.50	0.091
		Sericite	3.50	1.529
		Hematite	1.00	0.333
		Glassy Matrix	2.00	<0.004
		Mean Overall Grain Size (mm)		0.589

General Remarks: Sub-arkose sandstone.

Petrographic Classification: Quartz arenite sandstone.

Enlargement 5×

Plane Polarized Light

Crossed Polars

* Q: Quartz; F: Feldspar
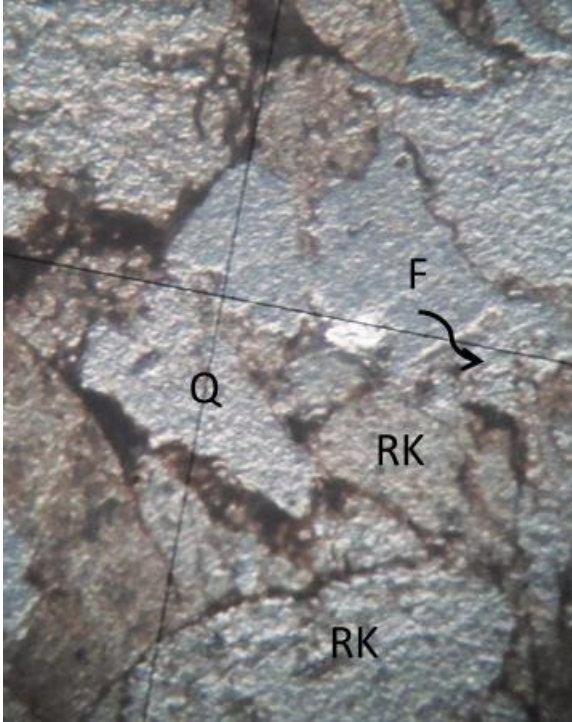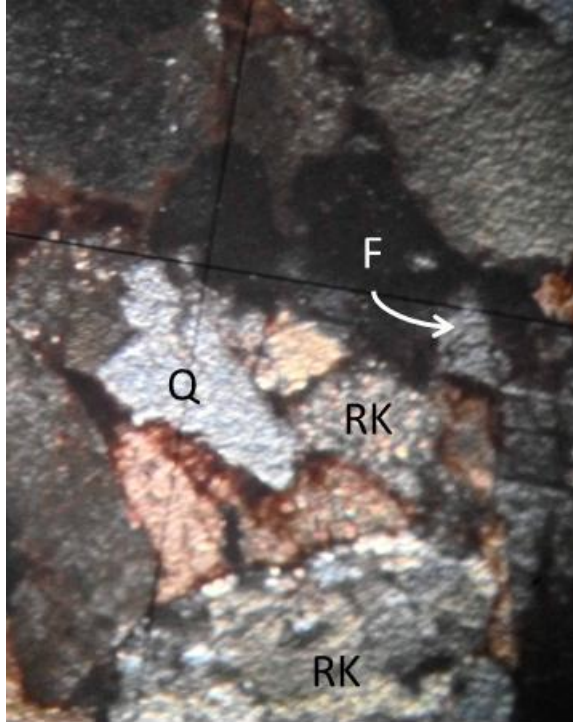
PETROGRAPHIC DESCRIPTION: Sandstone-12				
Name: Yasir Majeed **Date:** May, 2015. **Location:** University of Engineering and Technology (UET), Lahore, Pakistan.			**Macroscopic Description:** Light pink, medium to fine grained and low strength sandstone.	
Geological Formation: Warchha				
Mineral Description				
Thin Section Number	**Point Count**	**Mineral**	**Volume (%)**	**Mean Grain Size (mm)**
28	300	Quartz	55.00	0.240
		Potassium Feldspar	27.00	0.235
		Muscovite	0.50	0.256
		Biotite	0.50	1.229
		Glauconite	0.50	0.145
		Hematite	0.50	0.150
		Matrix (Clay)	16.0	<0.004
		Mean Overall Grain Size (mm)		0.376

General Remarks: The grains are well sorted with sub-angular to sub-rounded in texture.

Petrographic Classification: Arkosicwacke sandstone.

<div align="center">Enlargement 4×</div>

Plane Polarized Light

Crossed Polars

* Q: Quartz; F: Feldspar
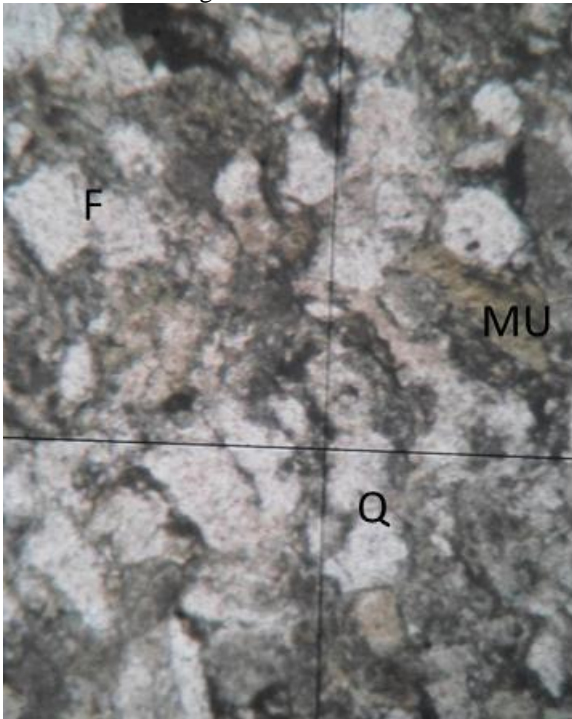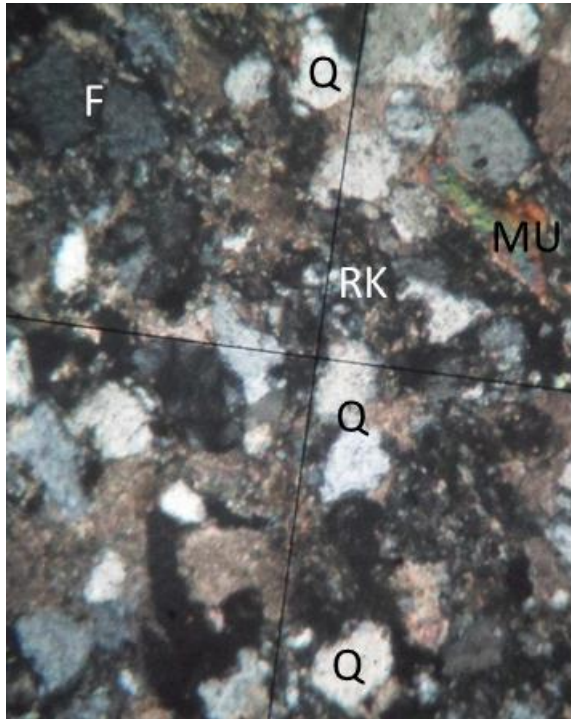
PETROGRAPHIC DESCRIPTION: Sandstone-13				
Name: Yasir Majeed **Date:** July , 2014. **Location:** University of Engineering and Technology (UET), Lahore, Pakistan.			**Macroscopic Description:** Light brownish grey, medium grained and low in strength.	
Geological Formation: Amb				
Mineral Description				
Thin Section Number	**Point Count**	**Mineral**	**Volume (%)**	**Mean Grain Size (mm)**
29	300	Quartz	77.00	0.273
		Feldspars	17.50	0.266
		Muscovite	2.50	0.616
		Biotite	1.20	0.681
		Sericite	0.50	1.933
		Hematite	0.80	0.260
		Zircon	0.50	0.152
		Mean Overall Grain Size (mm)		0.597
General Remarks:				
Petrographic Classification: Sub arkosic sandstone.				
Enlargement 5×				

Plane Polarized Light

Crossed Polars

* Q: Quartz; F: Feldspar; MU: Muscovite
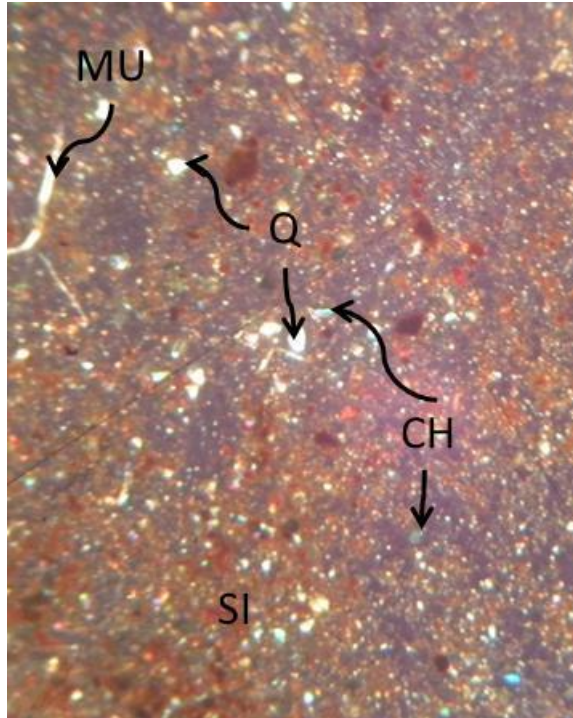
PETROGRAPHIC DESCRIPTION: Sandstone-14

Name: Yasir Majeed	**Macroscopic Description:** Light to medium grey, medium to coarse grained and low in strength.
Date: July , 2014.	
Location: University of Engineering and Technology (UET), Lahore, Pakistan.	
Geological Formation: Nagri	

Mineral Description

Thin Section Number	**Point Count**	**Mineral**	**Volume (%)**	**Mean Grain Size (mm)**
30	300	Quartz	72.50	0.431
		Rock Fragments	4.00	0.413
		Feldspars	18.00	0.376
		Muscovite	1.50	0.983
		Biotite	0.50	0.444
		Sericite	1.00	0.500
		Hematite	0.50	0.328
		Zircon	0.50	0.253
		Glassy Matrix	1.50	1.144
		Mean Overall Grain Size (mm)		0.542

General Remarks:

Petrographic Classification: Lithic arenite

Enlargement 5×

Plane Polarized Light | Crossed Polars

* Q: Quartz; RK: Rock Fragments
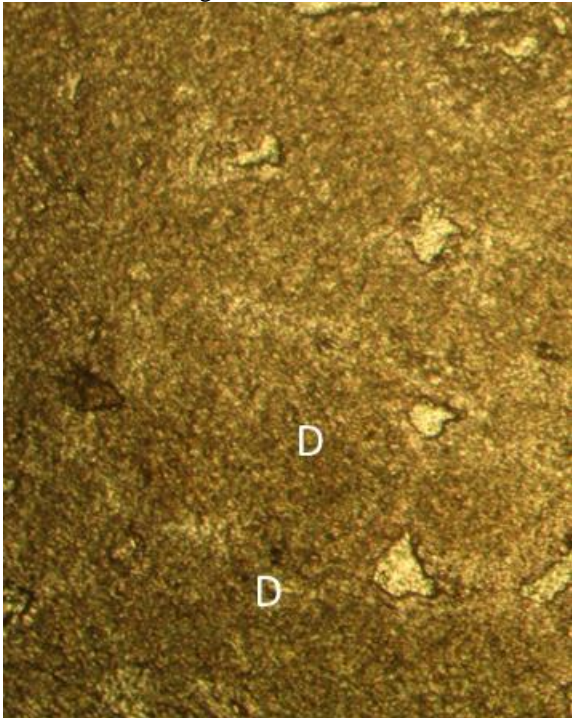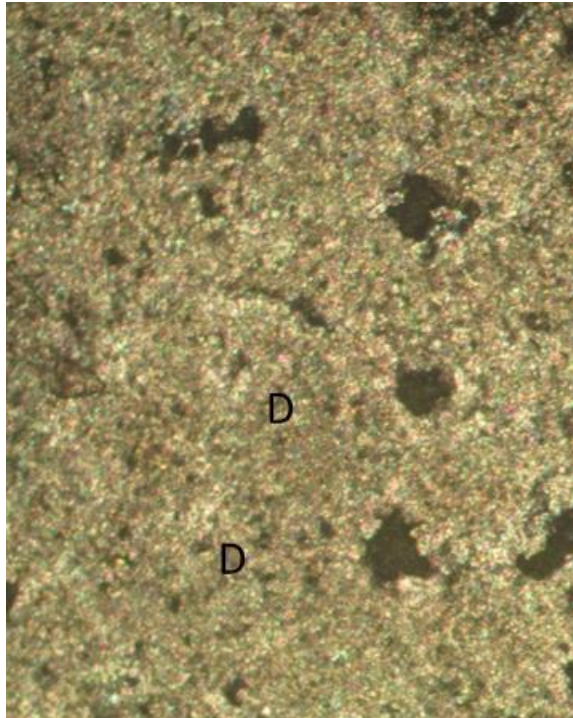
PETROGRAPHIC DESCRIPTION: Sandstone-15

Name: Yasir Majeed	Macroscopic Description: Light greenish grey, fine grained and medium strength sandstone.
Date: July , 2014.	
Location: University of Engineering and Technology (UET), Lahore, Pakistan.	
Geological Formation: Kussak	

Mineral Description

Thin Section Number	Point Count	Mineral	Volume (%)	Mean Grain Size (mm)
31	300	Quartz	78.00	0.090
		Feldspars	17.00	0.115
		Muscovite	3.50	0.289
		Biotite	0.50	0.510
		Sericite	0.50	0.206
		Hematite	0.50	0.263
		Mean Overall Grain Size (mm)		0.246

General Remarks: Micaceous sandstone.

Petrographic Classification: Sublith arenite sandstone.

<div align="center">Enlargement 5×</div>

Plane Polarized Light	Crossed Polars

* Q: Quartz
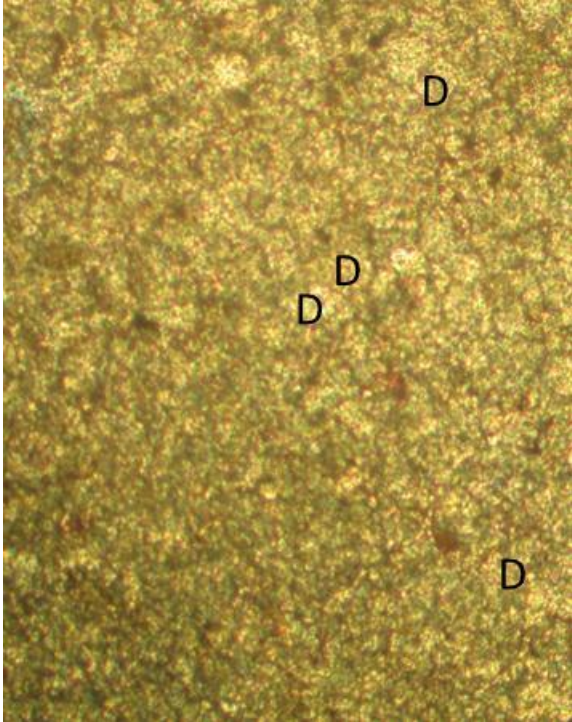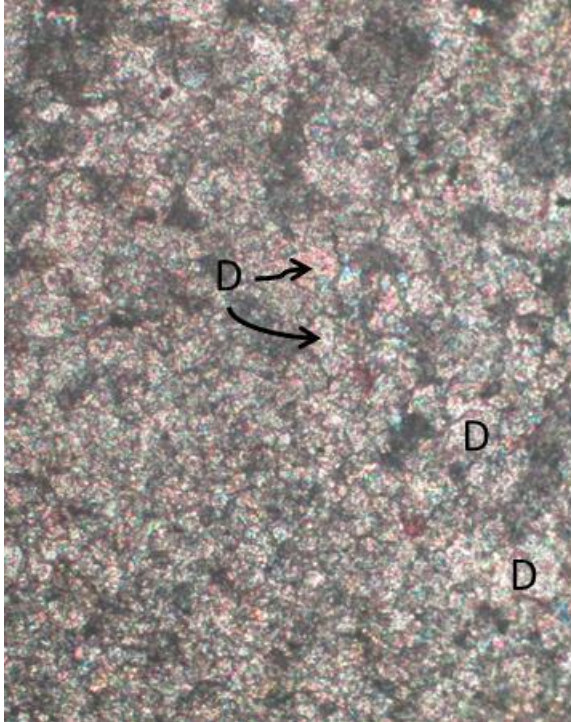
PETROGRAPHIC DESCRIPTION: Sandstone-16				
Name: Yasir Majeed **Date:** May, 2015. **Location:** University of Engineering and Technology (UET), Lahore, Pakistan.			**Macroscopic Description:** Reddish brown, fine grained, compact and high strength sandstone.	
Geological Formation: Hazira				
Mineral Description				
Thin Section Number	**Point Count**	**Mineral**	**Volume (%)**	**Mean Grain Size (mm)**
32	300	Quartz	95.00	0.272
		Feldspars	3.00	0.153
		Muscovite	0.50	0.271
		Biotite	0.50	0.434
		Limonite	0.50	0.156
		Glauconite	0.50	0.254
		Mean Overall Grain Size (mm)		0.257
General Remarks: The quartz grains are sub-angular to sub-rounded in shape, well sorted and have sutured contact.				
Petrographic Classification: Quartz arenite sandstone.				
Enlargement 4×				
Plane Polarized Light			Crossed Polars	
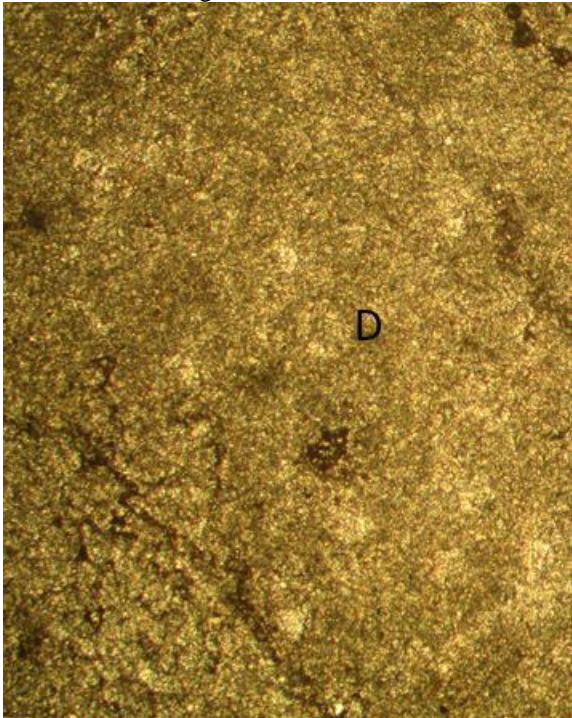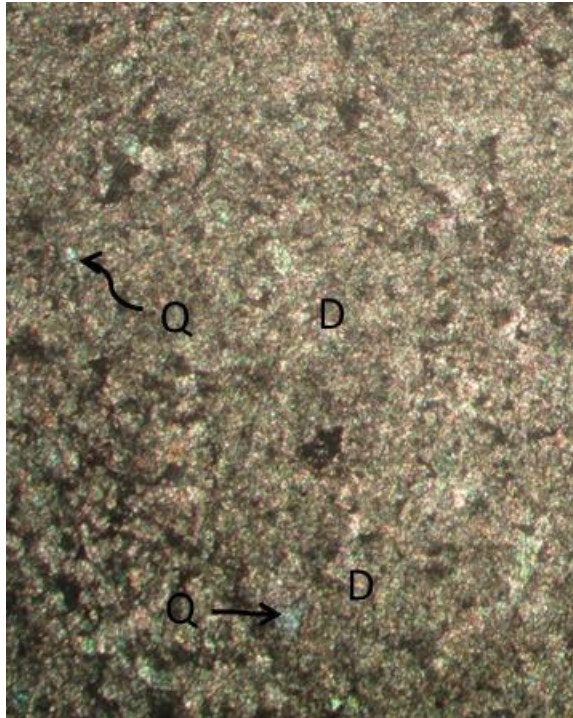
| * Q: Quartz | | | | |

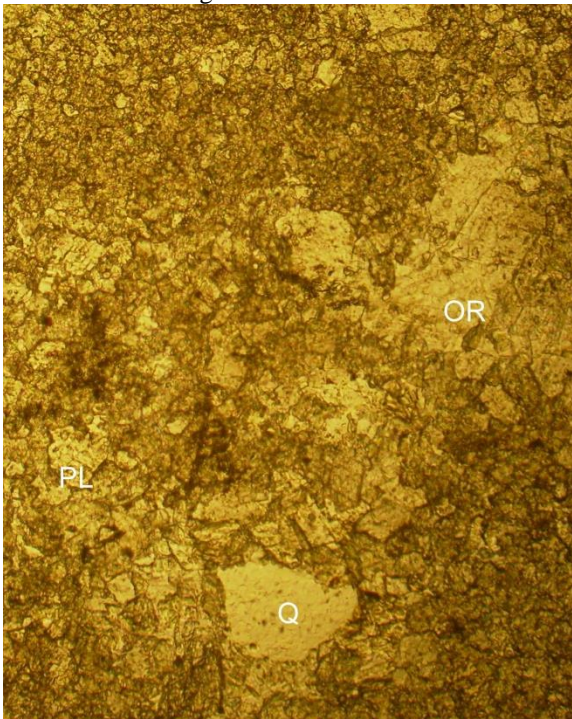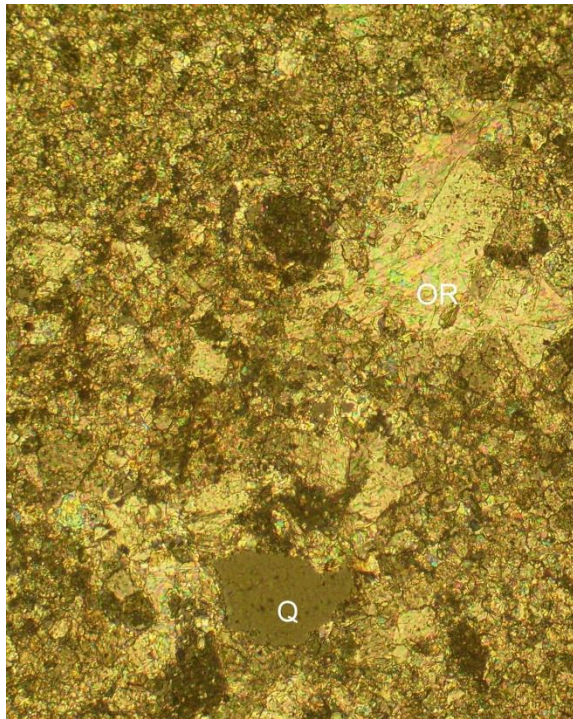| PETROGRAPHIC DESCRIPTION: Sandstone-17				
Name: Yasir Majeed **Date:** August, 2015. **Location:** University of Engineering and Technology (UET), Lahore, Pakistan.			**Macroscopic Description:** Redish brown, medium grained and moderately strong sandstone.	
Geological Formation: Warchha (Red)				
Mineral Description				
Thin Section Number	**Point Count**	**Mineral**	**Volume (%)**	**Mean Grain Size (mm)**
33	300	Quartz	56.00	0.729
		Feldspar	28.00	0.615
		Hematite	3.00	0.392
		Mica (Muscovite and Biotite)	1.00	0.259
		Clay	9.00	0.002
		Lithic Fragments	3.00	1.189
		Mean Overall Grain Size (mm)		0.531
General Remarks:				
Petrographic Classification: Lithic arenite sandstone.				
Enlargement 5×				
Plane Polarized Light		Crossed Polars		

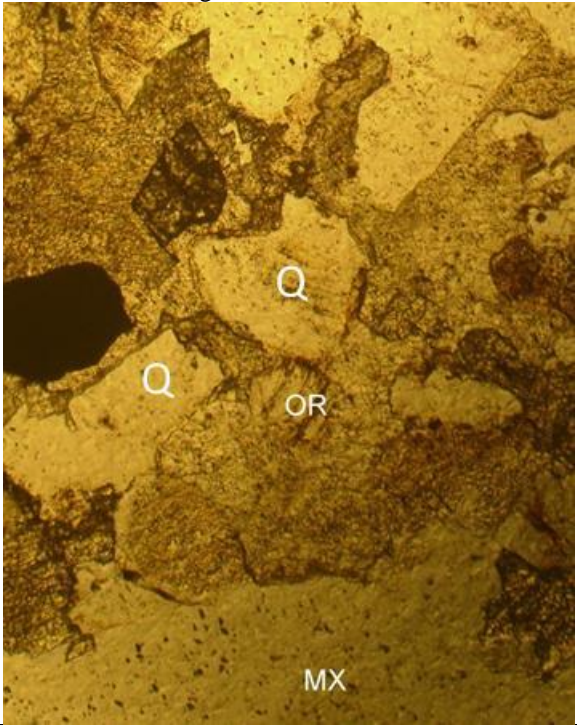* Q: Quartz; F: Feldspar; RK: Rock Fragments
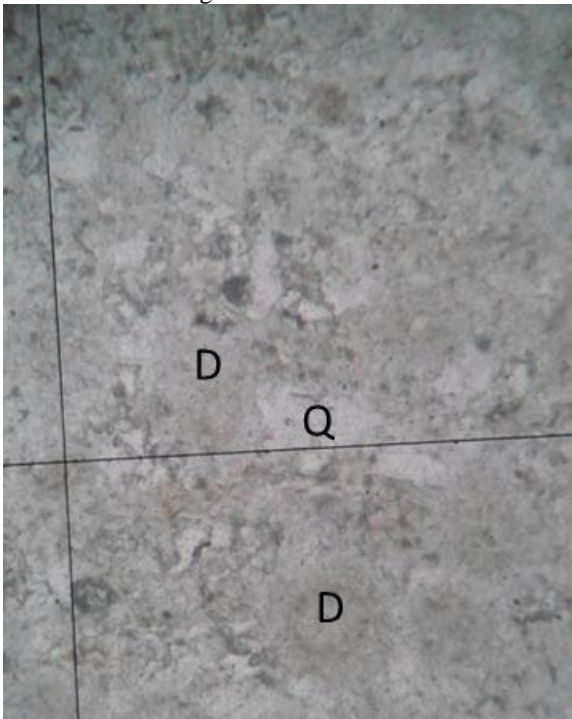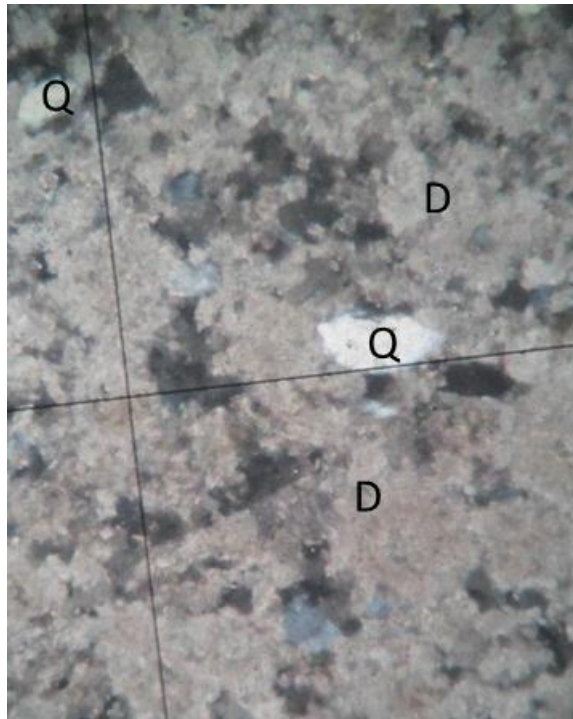
PETROGRAPHIC DESCRIPTION: Sandstone-18

Name: Yasir Majeed Date: February, 2016. Location: University of Engineering and Technology (UET), Lahore, Pakistan.	Macroscopic Description: Medium grey, fine grained and medium strength sandstone.
Geological Formation: Murree	

Mineral Description

Thin Section Number	Point Count	Mineral	Volume (%)	Mean Grain Size (mm)
34	300	Quartz	61.00	0.246
		Feldspar	20.00	0.219
		Calcite	7.00	0.279
		Muscovite	3.00	0.218
		Hematite	2.00	0.227
		Lithic Fragments	7.00	0.287
		Mean Overall Grain Size (mm)		0.246

General Remarks: The rock sample is subarkosic, compact and well cemented sandstone. However the cementing material is mostly calcite.

Petrographic Classification: Lithic arenite sandstone.

Enlargement 5×

Plane Polarized Light	Crossed Polars

* Q: Quartz; F: Feldspar; MU: Muscovite; RK: Rock Fragments
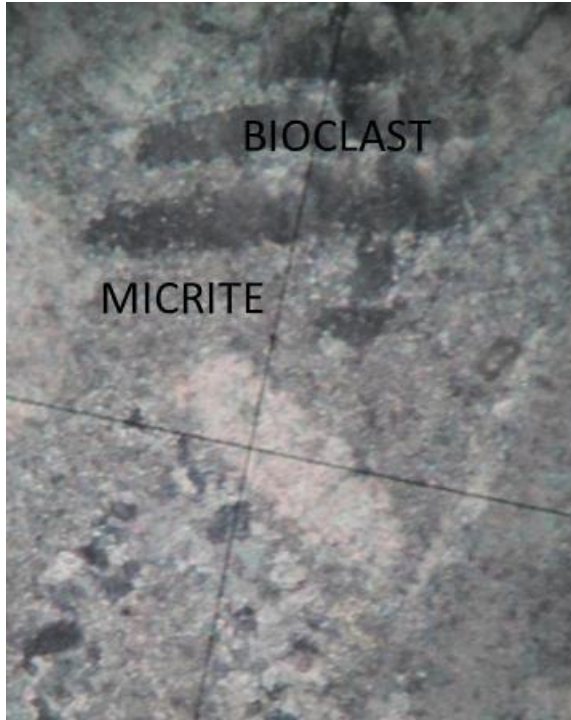
PETROGRAPHIC DESCRIPTION: Chamositic Siderite					
Name: Yasir Majeed **Date:** March, 2016. **Location:** University of Engineering and Technology (UET), Lahore, Pakistan.			**Macroscopic Description: Rusty brown and greenish, fine grained and medium in strength.**		
Geological Formation: Chichali					
Mineral Description					
Thin Section Number	**Point Count**	**Mineral**		**Volume (%)**	**Mean Grain Size (mm)**
35	300	Siderite		50.00	0.223
		Chamosite		34.00	0.311
		Quartz		13.00	0.079
		Muscovite		1.00	0.232
		Rock Matrix		2.00	0.002
		Mean Overall Grain Size (mm)			0.169
General Remarks:					
Petrographic Classification: Chamositic Siderite.					
Enlargement 4×					
Plane Polarized Light			Crossed Polars		

* Q: Quartz; MU: Muscovite; CH: Chamosite; SI: Siderite
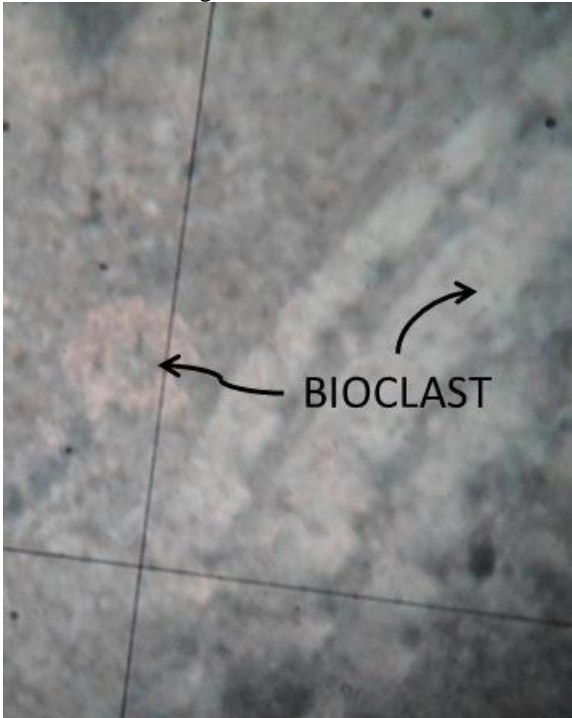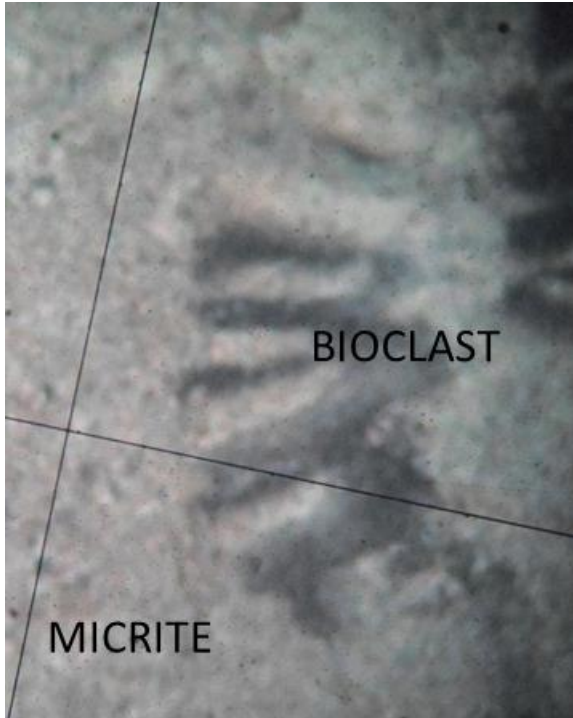
PETROGRAPHIC DESCRIPTION: Dolomite-1				
Name: Yasir Majeed **Date:** June, 2015. **Location:** University of Engineering and Technology (UET), Lahore, Pakistan.			**Macroscopic Description:** Greyish white, fine grained and low in strength.	
Geological Formation: Kingriali				
Mineral Description				
Thin Section Number	**Point Count**	**Mineral**	**Volume (%)**	**Mean Grain Size (mm)**
36	300	Dolomite	96.00	0.111
		Quartz	1.00	0.053
		Calcite	0.50	0.065
		Muscovite	1.00	0.221
		Biotite	1.50	0.415
		Mean Overall Grain Size (mm)		0.173
General Remarks:				
Petrographic Classification: Dolomite.				
Enlargement 4×				
Plane Polarized Light		Crossed Polars		
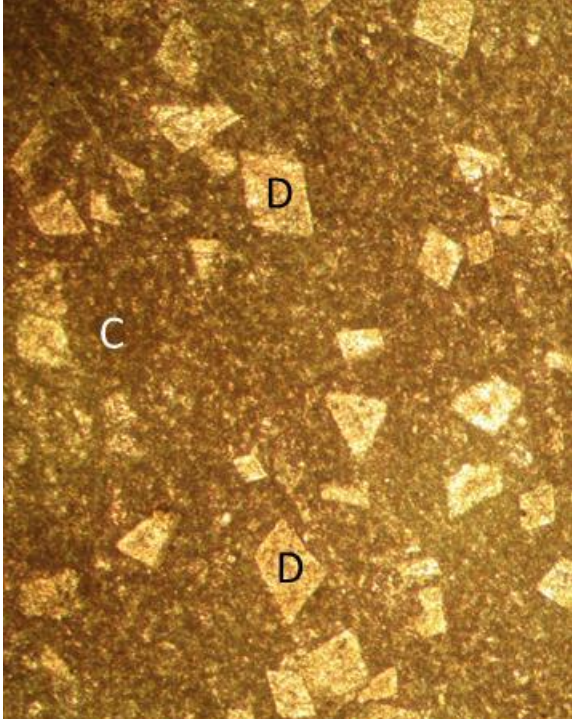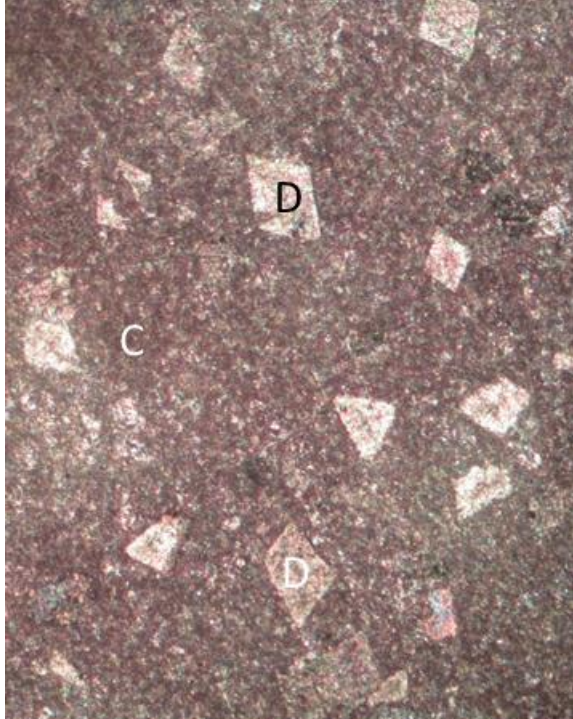
* D: Dolomite

PETROGRAPHIC DESCRIPTION: Dolomite-2				
Name: Yasir Majeed **Date:** June, 2015. **Location:** University of Engineering and Technology (UET), Lahore, Pakistan. **Geological Formation:** Jutana			**Macroscopic Description:** Medium grey, fine grained and moderately high in strength.	
Mineral Description				
Thin Section Number	**Point Count**	**Mineral**	**Volume (%)**	**Mean Grain Size (mm)**
37	300	Dolomite	94.00	0.248
		Quartz	2.00	0.047
		Hematite	0.50	0.080
		Magnetite	0.50	0.054
		Muscovite	1.50	0.297
		Biotite	1.50	0.681
		Mean Overall Grain Size (mm)		0.235

General Remarks:

Petrographic Classification: Dolomite.

Enlargement 4×

Plane Polarized Light — Crossed Polars
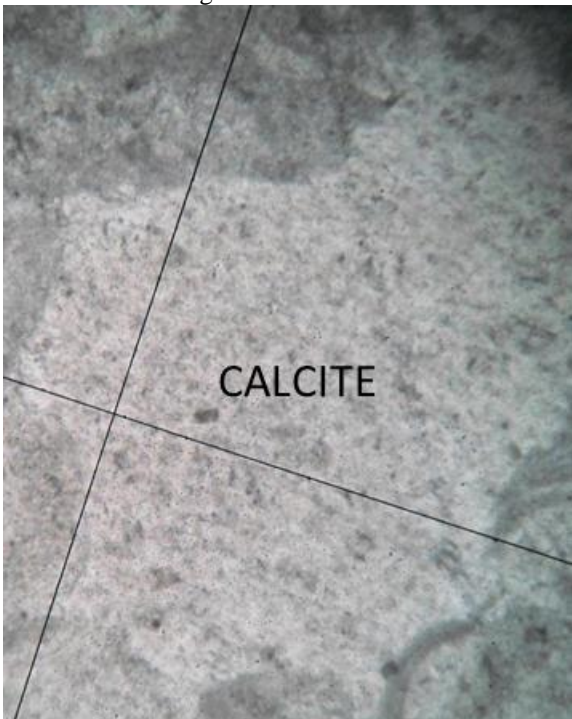
* D: Dolomite

PETROGRAPHIC DESCRIPTION: Dolomite-3					
Name: Yasir Majeed **Date:** June, 2015. **Location:** University of Engineering and Technology (UET), Lahore, Pakistan.			**Macroscopic Description:** Light pink, medium to coarse grained and medium in strength.		
Geological Formation: Abbottabad					
Mineral Description					
Thin Section Number	**Point Count**	**Mineral**		**Volume (%)**	**Mean Grain Size (mm)**
38	300	Dolomite		92.00	0.229
		Quartz		2.50	0.345
		Calcite		4.50	0.360
		Muscovite		0.50	0.394
		Biotite		0.50	0.802
		Mean Overall Grain Size (mm)			0.426
General Remarks:					
Petrographic Classification: Pink Dolomite.					
Enlargement 4×					
Plane Polarized Light			Crossed Polars		

* D: Dolomite; Q: Quartz
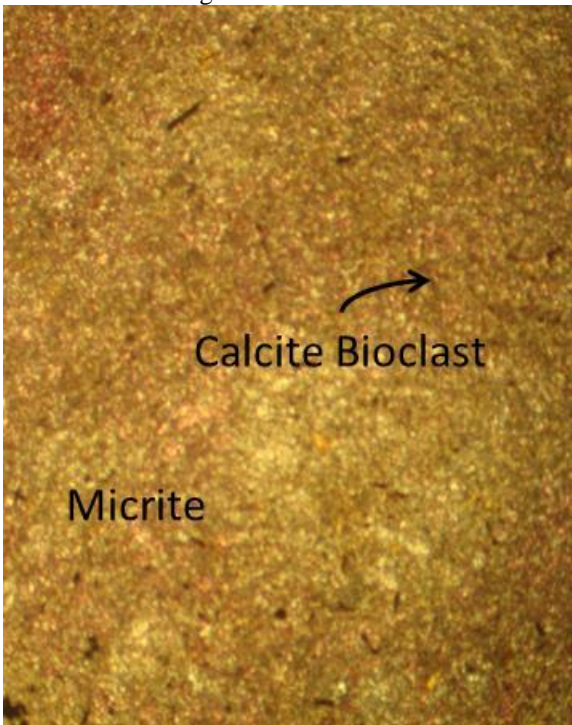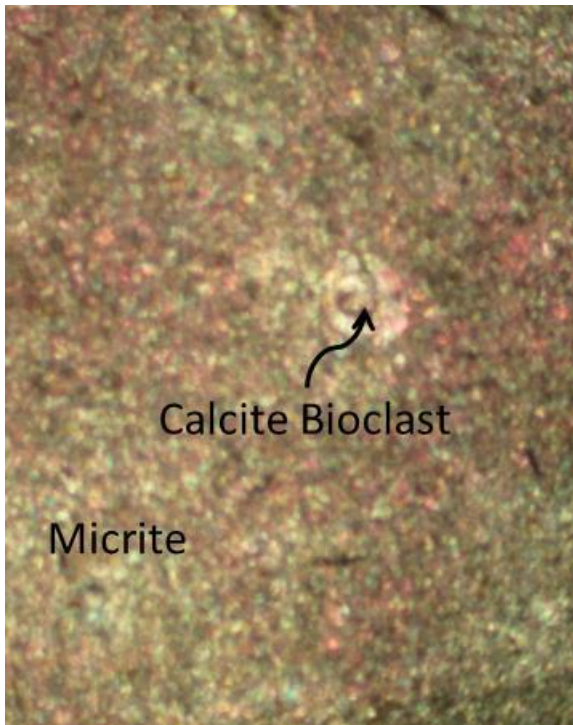
PETROGRAPHIC DESCRIPTION: Dolomite-4				
Name: Yasir Majeed **Date:** June, 2015. **Location:** University of Engineering and Technology (UET), Lahore, Pakistan.			**Macroscopic Description:** Dirty white, fine grained, moderately high in strength.	
Geological Formation: Jutana				
Mineral Description				
Thin Section Number	**Point Count**	**Mineral**	**Volume (%)**	**Mean Grain Size (mm)**
39	300	Dolomite	75.00	0.139
		Quartz	10.00	0.175
		Hematite	3.00	0.149
		Feldspar	9.00	0.158
		Biotite	0.50	0.482
		Muscovite	0.50	0.183
		Rock Matrix	2.00	< 0.004
		Mean Overall Grain Size (mm)		0.214
General Remarks:				
Petrographic Classification: Dolomite.				
Enlargement 5×				
Plane Polarized Light		Crossed Polars		

* D: Dolomite; Q: Quartz
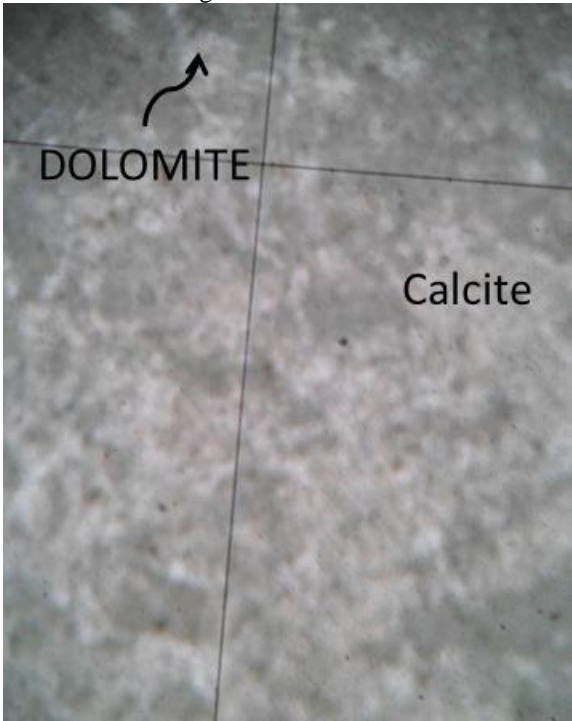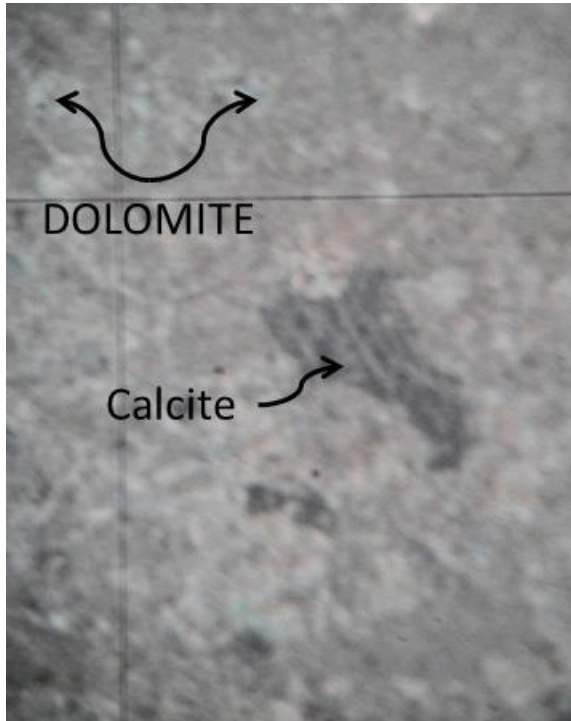
PETROGRAPHIC DESCRIPTION: Limestone-1				
Name: Yasir Majeed **Date:** February, 2016. **Location:** University of Engineering and Technology (UET), Lahore, Pakistan.		**Macroscopic Description:** Light creamish grey, medium to coarse grained and medium in strength.		
Geological Formation: Sakesar Limestone				
Mineral Description				
Thin Section Number	**Point Count**	**Mineral**	**Volume (%)**	**Mean Grain Size (mm)**
40	300	Dolomite	16.00	0.302
		Calcite Bioclasts	27.50	1.158
		Hematite	0.50	0.096
		Calcitic Micrite	55.50	0.002
		Biotite	0.50	0.867
		Mean Overall Grain Size (mm)		0.485
General Remarks: Fossileferrous dolomitic limestone.				
Petrographic Classification: Limestone.				
Enlargement 5×				
Plane Polarized Light		Crossed Polars		
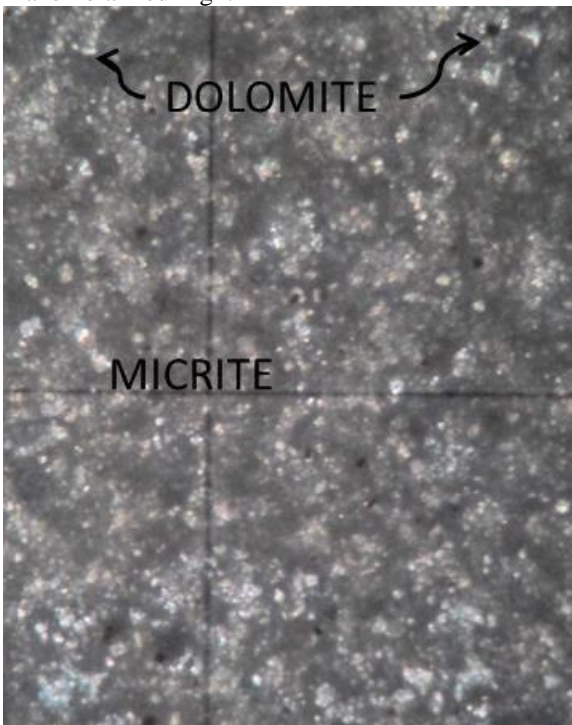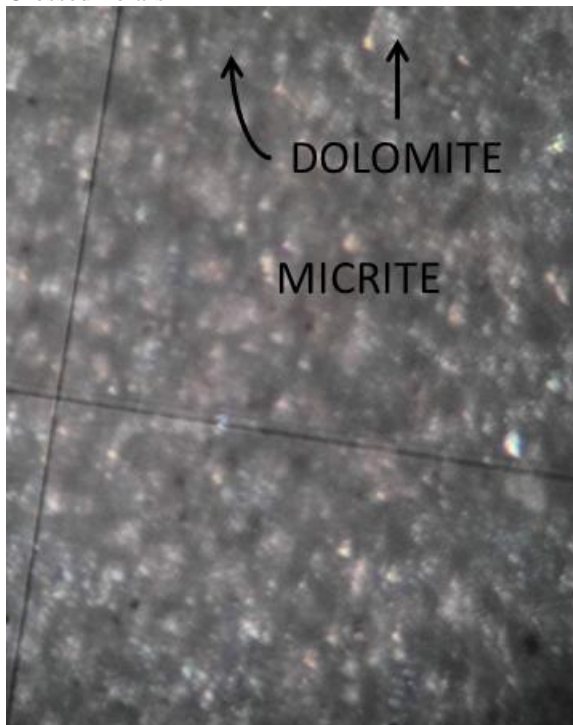
PETROGRAPHIC DESCRIPTION: Limestone-2				
Name: Yasir Majeed **Date:** June, 2015. **Location:** University of Engineering and Technology (UET), Lahore, Pakistan. **Geological Formation:** Sakesar Limestone			**Macroscopic Description:** Creamish to light grey, medium to coarse grained and moderately high in strength.	
Mineral Description				
Thin Section Number	**Point Count**	**Mineral**	**Volume (%)**	**Mean Grain Size (mm)**
41	300	Dolomite	16.00	0.302
		Calcite Bioclasts	28.00	1.158
		Hematite	0.50	0.096
		Calcitic Micrite	55.00	0.002
		Biotite	0.50	0.867
		Mean Overall Grain Size (mm)		0.485
General Remarks: Dolomitic limestone with abundant fossils.				
Petrographic Classification: Limestone.				
Enlargement 5×				
Plane Polarized Light			Crossed Polars	
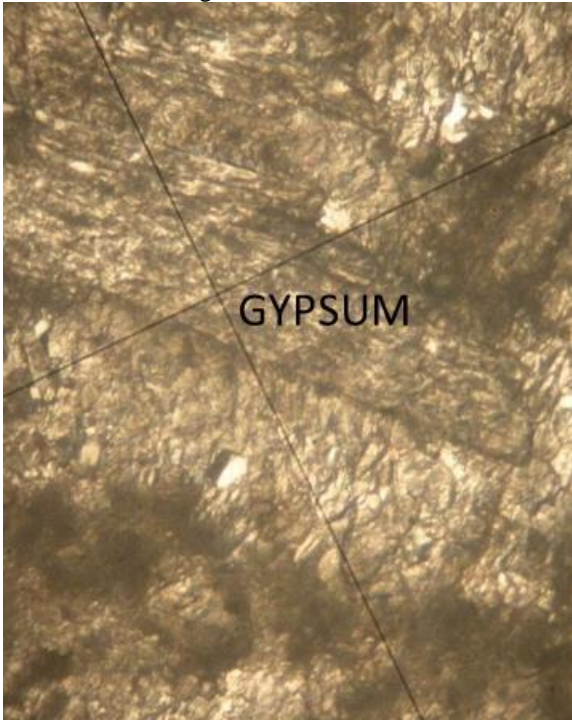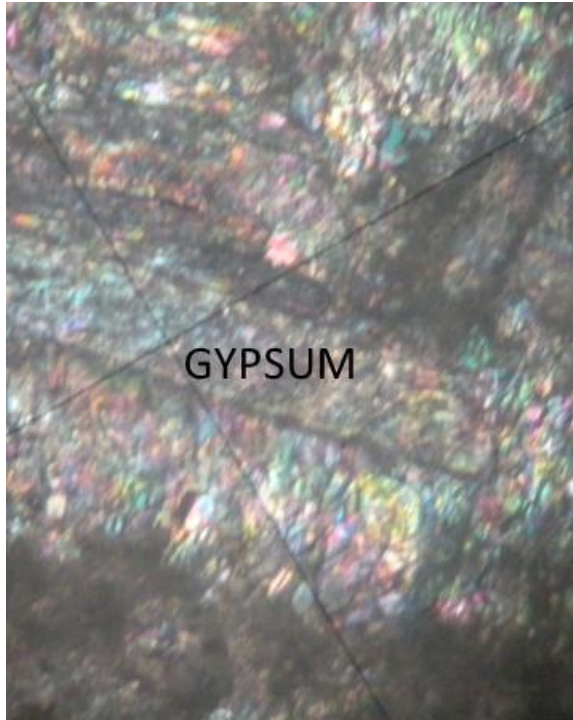
PETROGRAPHIC DESCRIPTION: Limestone-3				
Name: Yasir Majeed **Date:** June, 2015. **Location:** University of Engineering and Technology (UET), Lahore, Pakistan. **Geological Formation:** Samana Suk			**Macroscopic Description:** Medium to dark grey, coarse grained, medium strength limestone.	
Mineral Description				
Thin Section Number	**Point Count**	**Mineral**	**Volume (%)**	**Mean Grain Size (mm)**
42	300	Dolomite	36.00	0.268
		Calcite	25.00	5.686
		Magnetite	1.00	0.090
		Calcitic Micrite	38.00	0.002
		Mean Overall Grain Size (mm)		1.512
General Remarks: Dolomitic limestone.				
Petrographic Classification: Limestone.				
Enlargement 4×				
Plane Polarized Light		Crossed Polars		

* D: Dolomite; C: Calcitic Micrite
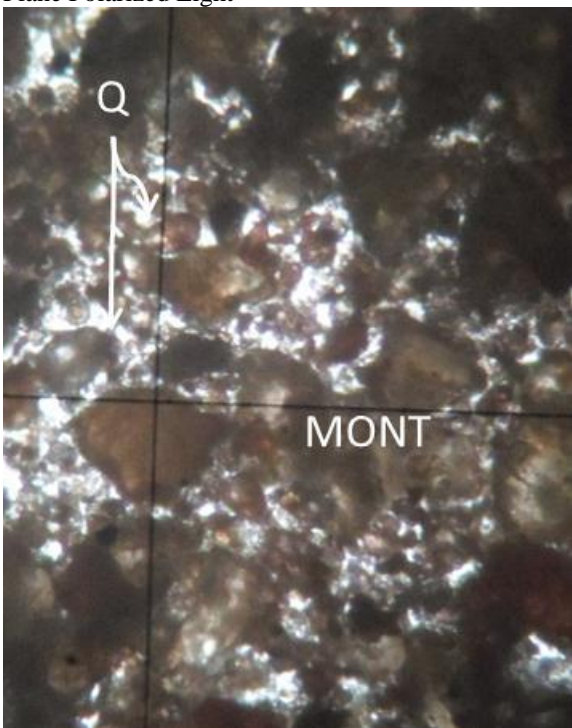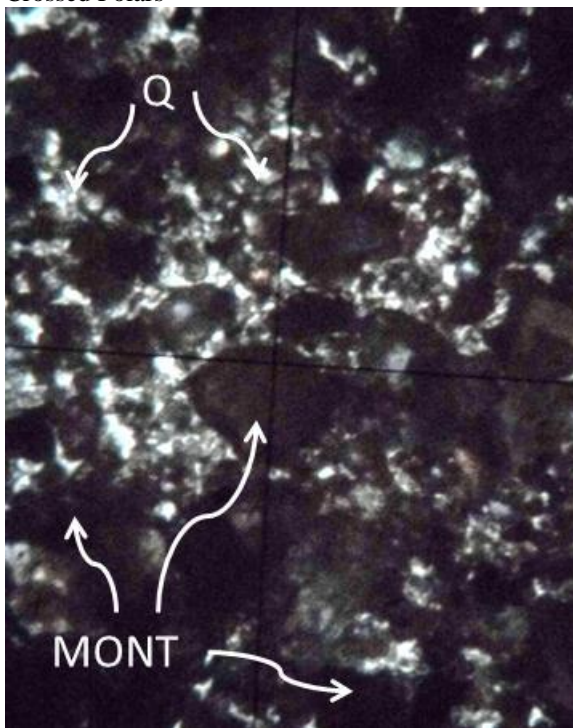
PETROGRAPHIC DESCRIPTION: Limestone-4					
Name: Yasir Majeed **Date:** June, 2015. **Location:** University of Engineering and Technology (UET), Lahore, Pakistan.			**Macroscopic Description:** Dirty white or creamish, coarse grained and low in strength.		
Geological Formation: Wargal					
Mineral Description					
Thin Section Number	**Point Count**	**Mineral**		**Volume (%)**	**Mean Grain Size (mm)**
43	300	Calcite		35.00	1.235
		Calcite Bioclasts		55.00	0.757
		Dolomite		0.50	0.810
		Calcitic Micrite		9.00	0.002
		Biotite		0.50	0.686
		Mean Overall Grain Size (mm)			0.698
General Remarks: Fossileferrous limestone.					
Petrographic Classification: Limestone.					
Enlargement 5×					
Plane Polarized Light			Crossed Polars		

CALCITE

CALCITE

PETROGRAPHIC DESCRIPTION: Limestone-5				
Name: Yasir Majeed **Date:** June, 2015. **Location:** University of Engineering and Technology (UET), Lahore, Pakistan.			**Macroscopic Description:** Medium to dark grey, coarse grained and medium in strength.	
Geological Formation: Sakesar Limestone				
Mineral Description				
Thin Section Number	**Point Count**	**Mineral**	**Volume (%)**	**Mean Grain Size (mm)**
44	300	Calcitic Micrite	91.00	0.002
		Calcite Bioclasts	7.50	0.621
		Magnetite	0.50	0.126
		Muscovite	0.50	0.637
		Biotite	0.50	0.796
		Mean Overall Grain Size (mm)		0.436
General Remarks: Fossiliferrous micrite.				
Petrographic Classification: Limestone.				
Enlargement 4×				
Plane Polarized Light		Crossed Polars		

Plane Polarized Light — Calcite Bioclast, Micrite

Crossed Polars — Calcite Bioclast, Micrite

PETROGRAPHIC DESCRIPTION: Limestone-6

Name: Yasir Majeed **Date:** March, 2016. **Location:** University of Engineering and Technology (UET), Lahore, Pakistan.	**Macroscopic Description:** Medium to dark grey, coarse grained and medium strength limestone.
Geological Formation: Samana Suk	

Mineral Description

Thin Section Number	**Point Count**	**Mineral**	**Volume (%)**	**Mean Grain Size (mm)**
45	300	Calcite	13.00	2.825
		Calcite Bioclasts	12.00	0.618
		Dolomite	35.00	0.170
		Hematite	1.00	0.143
		Calcitic Micrite	39.00	0.002
		Mean Overall Grain Size (mm)		0.751

General Remarks: Dolomitic limestone.

Petrographic Classification: Limestone.

Enlargement 5×

Plane Polarized Light

Crossed Polars

PETROGRAPHIC DESCRIPTION: Limestone-7					
Name: Yasir Majeed **Date:** March, 2016. **Location:** University of Engineering and Technology (UET), Lahore, Pakistan. **Geological Formation:** Nammal			**Macroscopic Description:** Creamish, fine grained and strength limestone.		
Mineral Description					
Thin Section Number	**Point Count**	**Mineral**		**Volume (%)**	**Mean Grain Size (mm)**
46	300	Calcite		20.00	0.287
		Dolomite		25.00	0.141
		Hematite		1.00	0.098
		Calcitic Micrite		54.00	0.002
		Mean Overall Grain Size (mm)			0.132
General Remarks: Fossiliferrous limestone.					
Petrographic Classification: Limestone.					
Enlargement 6×					

Plane Polarized Light

Crossed Polars

PETROGRAPHIC DESCRIPTION: Rock Gypsum					
Name: Yasir Majeed **Date:** March, 2016. **Location:** University of Engineering and Technology (UET), Lahore, Pakistan. **Geological Formation:** Salt Range			**Macroscopic Description:** Greyish white, medium grained and low in strength.		
Mineral Description					
Thin Section Number	**Point Count**	**Mineral**		**Volume (%)**	**Mean Grain Size (mm)**
47	300	Gypsum		99.00	0.461
		Hematite		1.00	0.267
		Mean Overall Grain Size (mm)			0.364
General Remarks: This rock sample characterizes evaporate sedimentation.					
Petrographic Classification: Rock Gypsum					
Enlargement 4×					
Plane Polarized Light			Crossed Polars		

GYPSUM

GYPSUM

PETROGRAPHIC DESCRIPTION: Marl				
Name: Yasir Majeed **Date:** March, 2016. **Location:** University of Engineering and Technology (UET), Lahore, Pakistan.			**Macroscopic Description:** Medium bright red, fine grained and very low in strength.	
Geological Formation: Salt Range				
Mineral Description				
Thin Section Number	**Point Count**	**Mineral**	**Volume (%)**	**Mean Grain Size (mm)**
48	300	Montmorillonite	74.00	0.233
		Quartz	21.00	0.101
		Dolomite	4.00	0.216
		Mica (Muscovite and Biotite)	1.00	0.145
		Mean Overall Grain Size (mm)		0.174
General Remarks:				
Petrographic Classification: Marl				
Enlargement 6×				
Plane Polarized Light		Crossed Polars		
* MONT: Montmorillonite; Q: Quartz				

APPENDIX F.

UNIAXIAL COMPRESSIVE STRENGTH (UCS) TEST RESULTS

Uniaxial Compressive Strength test results for dry rock samples.

Sr. No.	Rock Sample	Test No.	Length, l (mm)	Diameter, d (mm)	Area (mm²)	Peak Failure Force, P (N)	UCS (MPa)	Avg. UCS (MPa)
1	Dolerite-1	1	134.43	53.80	2273.58	548379.00	241.20	214.50
		2	137.75	53.85	2277.81	469899.00	206.29	
		3	135.02	53.95	2286.84	448019.40	195.91	
2	Dolerite-2	1	128.05	52.78	2188.47	457146.00	208.89	212.10
		2	132.05	53.98	2289.10	492797.45	215.28	
		3	130.00	53.85	2277.81	483191.84	212.13	
3	Dolerite-3	1	137.72	53.78	2272.17	361989.00	159.31	199.30
		2	138.42	54.10	2299.01	441253.80	191.93	
		3	134.00	54.00	2290.52	565116.60	246.72	
4	Dolerite-4	1	119.77	47.77	1792.24	106732.80	59.55	140.50
		2	130.00	47.67	1784.74	245250.00	137.41	
		3	127.83	47.72	1788.49	301167.00	168.39	
		4	126.75	47.71	1788.48	382590.00	213.92	
		5	128.80	47.72	1788.49	135378.00	75.69	
		6	127.42	47.73	1789.74	336483.00	188.01	
5	Granite-1	1	135.57	53.93	2284.87	94666.50	41.43	40.21
		2	85.37	41.28	1338.74	52189.20	38.98	
		3	113.65	41.23	1335.49	53713.69	40.22	
6	Granite-2	1	137.87	54.02	2291.93	189333.00	82.60	83.81
		2	84.62	41.26	1337.65	85150.80	63.65	
		3	126.75	53.72	2266.54	238383.00	105.17	
7	Granite-3	1	136.45	53.73	2267.95	214839.00	94.73	77.62
		2	130.07	53.57	2253.90	136359.00	60.50	
8	Granite-4	1	137.27	53.70	2265.14	88290.00	38.98	53.89
		2	130.77	53.55	2252.50	154998.00	68.81	
9	Granite-5	1	137.61	54.58	2340.27	607239.00	259.47	231.99
		2	131.63	54.58	2339.70	832869.00	355.97	
		3	120.41	54.56	2338.27	188352.00	80.55	
10	Granite-6	1	51.65	41.88	1377.93	70632.00	51.26	44.80
		2	109.80	42.00	1385.84	53170.20	38.37	
		3	108.97	42.02	1386.72	62125.14	44.79	
11	Migmatite	1	140.40	54.02	2291.93	120663.00	52.65	56.76
		2	128.80	53.78	2272.17	138321.00	60.88	
12	Andesite	1	111.59	42.11	1392.89	323730.00	232.42	231.46
		2	111.91	42.29	1404.82	345312.00	245.80	
		3	110.74	42.09	1391.57	287433.00	206.55	
		4	113.45	42.13	1393.99	366403.50	262.84	
		5	107.03	42.05	1388.70	221215.50	159.30	
		6	130.46	54.16	2304.11	649422.00	281.85	
13	Granitic Gneiss-1	1	137.43	53.40	2239.90	152055.00	67.88	69.22
		2	126.12	53.38	2238.50	157941.00	70.56	
14	Granitic Gneiss-2	1	135.89	54.51	2334.27	122134.50	52.32	54.53
		2	118.93	54.57	2339.13	170694.00	72.97	
		3	94.06	41.68	1364.59	67198.50	49.24	
		4	89.28	41.90	1379.03	80442.00	58.33	
		5	86.36	41.93	1380.79	54936.00	39.79	

Uniaxial Compressive Strength test results for dry rock samples.							
Sr. No.	Rock Sample	Test No.	Length, l (mm)	Diameter, d (mm)	Area (mm²)	Peak Failure Force, P (N)	UCS (MPa)	Avg. UCS (MPa)
15	Phyllite	1	Is = 73.50 MPa					54.33
		2	Is = 85.56 MPa					
		3	Is = 24.66 MPa					
		4	Is = 33.60 MPa					
16	Quartzite-1	1	116.58	54.58	2340.27	131944.42	56.38	56.390
		2	137.38	54.48	2331.42	151564.50	65.01	
		3	126.42	54.47	2330.56	111343.50	47.78	
17	Quartzite-2	1	87.50	41.35	1343.07	186390.00	138.78	147.03
		2	95.73	41.52	1353.91	210228.30	155.27	
18	Siltstone-1	1	134.44	54.62	2343.70	147640.50	62.99	49.30
		2	127.79	54.22	2309.22	123606.00	53.53	
		3	137.48	54.28	2314.33	72594.00	31.37	
19	Siltstone-2	1	93.61	41.81	1373.11	112324.50	81.80	57.88
		2	95.19	41.87	1377.28	77008.50	55.91	
		3	89.39	41.90	1379.03	49540.50	35.92	
20	Sandstone-1	1	89.53	41.53	1355.00	29430.00	21.72	39.80
		2	82.63	41.48	1351.74	78234.75	57.88	
21	Sandstone-2	1	110.54	41.90	1379.25	70632.00	51.21	41.55
		2	111.76	41.94	1381.45	71122.50	51.48	
		3	108.90	42.08	1391.13	77499.00	55.71	
		4	101.80	42.10	1392.23	25015.50	17.97	
		5	111.70	41.84	1374.87	43164.00	31.40	
22	Sandstone-3	1	135.50	55.64	2431.47	362970.00	149.28	127.60
		2	136.49	55.94	2457.76	324956.25	132.22	
		3	135.95	55.72	2438.46	321277.50	131.75	
		4	138.06	55.88	2453.07	259965.00	105.98	
		5	137.42	55.98	2461.86	292436.10	118.79	
23	Sandstone-4	1	136.80	54.36	2321.44	57879.00	24.93	26.73
		2	104.04	41.73	1367.86	39730.50	29.05	
		3	101.23	41.70	1365.68	35806.50	26.22	
24	Sandstone-5	1	53.33	41.67	1364.15	81226.80	54.85	44.00
		2	67.38	41.47	1350.87	49246.20	35.22	
		3	83.57	41.89	1378.37	68670.00	49.82	
		4	74.14	54.50	2333.42	90252.00	36.11	
25	Sandstone-6	1	96.60	41.72	1366.99	150877.80	106.79	109.73
		2	91.30	41.37	1344.15	156763.80	112.60	
		3	127.35	53.78	2272.17	249484.71	109.80	
26	Sandstone-7	1	130.17	53.80	2273.58	135378.00	59.54	61.51
		2	100.38	41.40	1346.32	88486.20	63.50	
		3	128.70	54.26	2312.34	142185.79	61.49	
27	Sandstone-8	1	136.67	53.48	2246.90	37278.00	16.59	11.04
		2	100.03	41.13	1329.03	10087.33	7.59	
		3	135.18	54.42	2326.29	20797.20	8.94	
28	Sandstone-9	1	133.20	53.37	2237.10	64549.80	28.85	29.04
		2	96.23	40.83	1309.71	39730.50	29.24	
		3	131.51	54.52	2334.56	70828.20	30.34	

Uniaxial Compressive Strength test results for dry rock samples.								
Sr. No.	Rock Sample	Test No.	Length, l (mm)	Diameter, d (mm)	Area (mm²)	Peak Failure Force, P (N)	UCS (MPa)	Avg. UCS (MPa)
29	Sandstone-10	1	137.02	53.23	2224.52	26068.00	11.72	16.69
		2	96.55	40.15	1265.44	28518.00	21.66	
30	Sandstone-11	1	135.67	53.73	2267.95	30411.00	13.41	21.19
		2	100.40	41.32	1340.90	40221.00	28.97	
		3	146.63	53.48	2246.90	49050.00	21.83	
31	Sandstone-12	1	135.60	53.42	2241.30	66217.50	29.54	27.08
		2	96.15	41.40	1346.32	34335.00	25.50	
		3	138.32	54.49	2332.28	61140.73	26.22	
32	Sandstone-13	1	139.67	53.77	2270.77	103887.90	45.75	46.40
		2	101.17	41.45	1349.57	65727.00	47.07	
		3	124.35	53.60	2256.71	104666.21	46.38	
33	Sandstone-14	1	131.20	53.60	2256.71	37278.00	16.52	17.07
		2	99.92	40.90	1313.99	24034.50	18.29	
		3	134.43	54.10	2298.73	37699.14	16.40	
34	Sandstone-15	1	111.68	42.04	1388.26	43654.50	31.45	69.04
		2	87.10	42.01	1386.06	70141.50	50.60	
		3	111.60	41.97	1383.42	26977.50	19.50	
		4	134.54	54.45	2328.85	309015.00	132.69	
		5	135.19	54.45	2329.14	258493.50	110.98	
35	Sandstone-16	1	103.79	54.29	2314.90	188352.00	81.37	129.00
		2	118.92	54.06	2295.33	409077.00	178.22	
		3	107.32	53.94	2285.15	290376.00	127.07	
36	Sandstone-17	1	137.34	54.32	2317.46	108400.50	46.78	56.76
		2	122.89	54.10	2298.73	109872.00	47.80	
		3	119.29	54.26	2312.91	175108.50	75.71	
37	Sandstone-18	1	112.74	43.85	1510.38	119682.00	79.24	82.77
		2	108.02	46.02	1663.80	120172.50	72.23	
		3	103.40	45.85	1651.06	159903.00	96.85	
38	Chamositic-Siderite	1	96.02	41.42	1346.54	74970.00	53.82	51.72
		2	94.80	41.22	1333.57	68502.00	49.61	
39	Dolomite-1	1	97.60	41.47	1350.66	100846.80	74.67	61.84
		2	93.10	41.72	1366.99	72790.20	53.25	
		3	118.33	53.65	2260.92	130251.72	57.61	
40	Dolomite-2	1	133.49	54.07	2296.46	365422.50	159.12	144.42
		2	135.17	54.13	2301.84	275170.50	119.54	
		3	130.08	54.17	2304.68	261436.50	113.44	
		4	137.11	54.10	2299.29	426735.00	185.59	
41	Dolomite-3	1	92.61	41.84	1375.30	111834.00	81.32	99.93
		2	118.70	41.82	1373.77	221215.50	161.03	
		3	140.96	54.42	2326.00	133612.20	57.44	
42	Dolomite-4	1	137.30	54.00	2290.24	335992.50	146.71	132.70
		2	137.34	54.13	2301.56	146169.00	63.51	
		3	139.56	54.09	2298.16	356103.00	154.95	
		4	135.15	54.12	2300.43	321768.00	139.87	
		5	140.72	53.98	2289.10	362773.80	158.48	

Uniaxial Compressive Strength test results for dry rock samples.							
Sr. No.	Rock Sample	Test No.	Length, l (mm)	Diameter, d (mm)	Area (mm²)	Peak Failure Force, P (N)	UCS (MPa)	Avg. UCS (MPa)
43	Limestone-1	1	106.10	41.90	1379.03	32863.50	23.83	65.26
		2	109.00	41.60	1359.35	155488.50	114.38	
		3	106.85	41.70	1365.90	40221.00	29.45	
		4	104.30	41.50	1352.83	175108.50	129.44	
		5	106.00	41.90	1379.03	67689.00	49.08	
		6	106.10	41.90	1379.03	102024.00	73.98	
		7	107.00	41.70	1365.90	50031.00	36.63	
44	Limestone-2	1	137.00	54.00	2290.52	279585.00	122.06	95.78
		2	138.00	54.00	2290.52	93195.00	40.69	
		3	136.70	54.00	2290.52	253098.00	110.50	
		4	136.40	54.00	2290.52	252117.00	110.07	
		5	138.10	54.00	2290.52	253098.00	110.50	
		6	136.70	54.00	2290.52	297243.00	129.77	
		7	138.10	54.00	2290.52	224649.00	98.08	
		8	140.00	54.00	2290.52	102024.00	44.54	
45	Limestone-3	1	137.12	54.46	2329.71	206010.00	88.43	80.70
		2	140.37	54.48	2331.68	115758.00	49.65	
		3	141.52	54.47	2330.31	329616.00	141.45	
		4	138.65	54.52	2334.56	172656.00	73.96	
		5	137.83	54.47	2330.31	111834.00	47.99	
		6	138.75	54.25	2311.78	190314.00	82.32	
46	Limestone-4	1	135.73	53.75	2269.36	96334.20	42.45	66.45
		2	96.48	41.40	1346.32	126058.50	90.47	
47	Limestone-5	1	94.20	41.85	1354.14	142100.00	100.10	92.75
		2	94.62	41.53	1340.05	119560.00	85.39	
48	Limestone-6	1	137.50	54.20	2307.52	102024.00	44.21	69.89
		2	138.80	54.20	2307.52	347274.00	150.50	
		3	138.50	54.30	2316.04	161865.00	69.89	
		4	139.10	54.40	2324.58	52974.00	22.79	
		5	138.10	54.40	2324.58	239364.00	102.97	
		6	139.80	54.20	2307.52	151074.00	65.47	
		7	140.80	54.20	2307.52	102024.00	44.21	
		8	143.39	54.30	2316.32	99081.00	42.78	
		9	109.98	54.29	2314.90	181485.00	78.40	
		10	102.61	41.75	1369.39	111834.00	81.67	
		11	110.65	41.77	1370.27	52483.50	38.30	
		12	103.52	41.79	1371.80	133906.50	97.61	
49	Limestone-7	1	96.31	54.16	2304.11	38749.50	16.82	20.08
		2	94.13	54.25	2311.49	65236.50	28.22	
		3	98.92	41.56	1356.52	20601.00	15.19	
50	Rock Gypsum	1	99.08	41.84	1374.87	12507.75	9.10	13.53
		2	103.69	41.58	1358.27	25015.50	18.42	
		3	108.41	41.49	1351.96	17658.00	13.06	

Uniaxial Compressive Strength test results for dry rock samples.							
Sr. No.	Rock Sample	Test No.	Length, l (mm)	Diameter, d (mm)	Area (mm^2)	Peak Failure Force, P (N)	UCS (MPa)	Avg. UCS (MPa)
51	Marl	1	126.32	54.07	2296.18	10791.00	4.70	5.35
		2	129.55	53.81	2274.71	11772.00	5.18	
		3	129.78	53.99	2289.67	14616.90	6.38	
		4	123.70	53.99	2289.67	11772.00	5.14	

Uniaxial Compressive Strength test results for fully saturated rock samples.

Sr. No.	Rock Sample	Test No.	Length, l (mm)	Diameter, d (mm)	Area (mm^2)	Peak Failure Force, P (N)	UCS$_{(Sat)}$ (MPa)	Avg. UCS$_{(Sat)}$ (MPa)
1	Siltstone-1	1	110.63	54.15	2303.26	22072.50	9.58	17.30
		2	130.45	53.70	2265.14	54445.50	24.04	
		3	110.43	41.18	1332.26	21091.50	15.83	
		4	124.43	54.20	2307.52	45616.50	19.77	
2	Siltstone-2	1	93.57	41.63	1361.53	53955.00	39.63	56.07
		2	90.28	41.77	1370.27	105751.80	77.18	
		3	130.87	53.77	2270.77	116739.00	51.41	
3	Sandstone-1	1	76.85	41.37	1344.15	35414.10	26.35	19.10
		2	96.17	41.57	1357.18	16088.40	11.85	
4	Sandstone-2	1	127.20	54.42	2326.00	86131.80	37.03	26.20
		2	130.47	53.70	2265.14	57290.40	25.29	
		3	134.92	54.00	2290.52	37278.00	16.27	
5	Sandstone-3	1	118.22	53.87	2279.22	199143.00	87.37	85.33
		2	105.08	55.98	2461.86	205029.00	83.28	
6	Sandstone-4	1	129.55	53.63	2259.52	30901.50	13.68	13.57
		2	136.13	53.65	2260.92	21582.00	9.55	
		3	132.32	53.45	2244.10	39240.00	17.49	
7	Sandstone-5	1	58.38	41.58	1358.27	29920.50	20.70	40.27
		2	49.32	41.68	1364.81	50227.20	33.31	
		3	91.28	41.77	1370.27	90252.00	65.86	
		4	60.85	41.87	1376.84	59997.96	41.22	
8	Sandstone-6	1	104.42	54.12	2300.43	169713.00	73.77	66.30
		2	109.23	42.00	1385.62	87309.00	61.06	
		3	98.75	41.78	1371.36	90742.50	64.06	
9	Sandstone-7	1	132.20	53.77	2270.77	136947.60	60.31	58.03
		2	141.83	54.15	2303.26	128412.90	55.75	
10	Sandstone-8	1	124.52	53.92	2283.45	11772.00	5.16	17.55
		2	117.20	53.97	2287.69	69160.50	30.23	
		3	112.33	54.40	2324.58	40122.90	17.26	
11	Sandstone-9	1	135.57	54.15	2303.26	24525.00	10.65	14.15
		2	115.60	54.38	2323.15	48559.50	20.90	
		3	134.23	54.13	2301.84	25113.60	10.91	

Uniaxial Compressive Strength test results for fully saturated rock samples.								
Sr. No.	Rock Sample	Test No.	Length, l (mm)	Diameter, d (mm)	Area (mm²)	Peak Failure Force, P (N)	UCS(Sat) (MPa)	Avg. UCS(Sat) (MPa)
12	Sandstone-10	1	116.37	53.32	2232.91	49050.00	21.97	13.04
		2	116.17	40.63	1296.91	14715.00	10.93	
		3	95.02	40.53	1290.54	8338.50	6.22	
13	Sandstone-11	1	111.27	41.63	1361.53	25015.50	17.78	19.74
		2	106.60	41.43	1348.48	34335.00	24.62	
		3	113.93	54.50	2333.13	39240.00	16.82	
14	Sandstone-12	1	123.35	53.33	2234.31	54936.00	24.59	23.60
		2	112.62	53.70	2265.14	62784.00	27.72	
		3	115.68	53.50	2248.30	41594.40	18.50	
15	Sandstone-13	1	105.05	54.43	2327.43	85347.00	36.67	30.65
		2	126.77	53.92	2283.45	51012.00	22.34	
		3	134.48	53.97	2287.69	75340.80	32.93	
16	Sandstone-14	1	126.87	53.60	2256.71	11379.60	5.04	4.84
		2	128.05	54.07	2296.18	11477.70	5.00	
		3	134.73	53.77	2270.77	10202.40	4.49	
17	Sandstone-15	1	114.95	53.65	2260.92	35316.00	15.62	43.73
		2	110.55	41.70	1365.90	62784.00	45.97	
		3	145.45	53.60	2256.71	148131.00	65.64	
		4	110.72	53.78	2272.17	108400.50	47.71	
18	Sandstone-17	1	134.47	54.25	2311.78	87309.00	37.70	60.90
		2	137.43	54.13	2301.84	154017.00	66.91	
		3	108.32	41.72	1366.99	114286.50	78.10	
19	Sandstone-18	1	112.75	45.50	1626.18	113796.00	69.98	61.97
		2	121.50	45.28	1610.73	112324.50	69.74	
		3	116.80	45.95	1658.51	76616.10	46.20	
20	Chamositic-Siderite	1	66.13	53.92	2283.45	144207.00	57.63	38.79
		2	77.18	41.67	1363.72	42183.00	30.56	
		3	74.37	41.72	1366.99	39240.00	28.18	
21	Dolomite-1	1	61.80	54.35	2320.31	68179.50	26.35	33.50
		2	83.23	53.98	2289.10	37474.20	15.66	
		3	129.17	41.38	1345.23	81423.00	58.50	
22	Dolomite-2	1	121.30	53.75	2269.36	73575.00	32.42	67.75
		2	128.15	53.82	2274.99	90742.50	39.89	
		3	124.10	54.20	2307.52	302148.00	130.94	
23	Dolomite-3	1	133.65	54.13	2301.84	133906.50	58.17	55.52
		2	121.55	41.68	1364.81	87112.80	63.83	
		3	100.20	41.68	1364.81	60822.00	44.56	
24	Dolomite-4	1	120.50	53.62	2258.11	97217.10	43.05	57.94
		2	115.77	53.50	2248.30	168732.00	75.05	
		3	106.77	41.68	1364.81	76027.50	55.71	
25	Limestone-1	1	100.78	41.68	1364.81	60822.00	44.56	60.85
		2	107.77	41.47	1350.66	129492.00	95.87	
		3	105.68	41.65	1362.62	57388.50	42.12	

Uniaxial Compressive Strength test results for fully saturated rock samples.								
Sr. No.	Rock Sample	Test No.	Length, l (mm)	Diameter, d (mm)	Area (mm^2)	Peak Failure Force, P (N)	UCS$_{(Sat)}$ (MPa)	Avg. UCS$_{(Sat)}$ (MPa)
26	Limestone-2	1	133.68	53.87	2279.22	168732.00	74.03	48.74
		2	133.23	53.92	2283.45	86818.50	38.02	
		3	127.23	53.90	2282.04	77989.50	34.18	
27	Limestone-3	1	134.80	53.80	2273.58	55917.00	24.59	29.64
		2	134.50	54.22	2308.94	49050.00	21.24	
		3	130.75	53.85	2277.81	98100.00	43.07	
28	Limestone-4	1	124.63	53.98	2289.10	85347.00	37.28	37.21
		2	130.98	53.92	2283.45	86328.00	37.81	
		3	131.90	53.93	2284.87	83483.10	36.54	
29	Limestone-5	1	129.85	42.00	1385.62	126058.50	87.21	80.79
		2	69.87	54.25	2311.78	186390.00	74.37	
30	Limestone-6	1	135.05	53.92	2283.45	105457.50	46.18	32.25
		2	133.65	53.92	2283.45	34335.00	15.04	
		3	130.25	53.92	2283.45	58860.00	25.78	
		4	133.92	54.27	2313.20	97119.00	41.98	
31	Limestone-7	1	119.23	53.68	2263.73	55917.00	24.70	32.13
		2	80.25	41.62	1360.44	23053.50	16.95	
		3	82.97	41.50	1352.83	74065.50	54.75	
32	Rock Gypsum	1	108.10	41.43	1348.48	7063.20	5.24	8.48
		2	106.60	41.55	1356.09	5984.10	4.41	
		3	95.15	41.73	1368.08	21582.00	15.78	
33	Marl	1	136.23	53.87	2279.22	2943.00	1.29	2.10
		2	132.25	53.42	2241.30	3139.20	1.40	
		3	151.45	52.68	2180.18	7866.64	3.61	

APPENDIX G.

BRAZILIAN TENSILE STRENGTH (BTS) TEST RESULTS

Brazilian Tensile Strength test results for dry rock samples.

Sr. No.	Rock Sample	Test No.	Thickness, t (mm)	Diameter, d (mm)	Peak Failure Force, P (N)	BTS = $\frac{2 \times P}{\pi \times d \times t}$ (MPa)	Avg. BTS (MPa)
1	Dolerite-1	1	27.20	53.67	11772.00	5.13	6.76
		2	27.73	53.95	19718.10	8.39	
2	Dolerite-2	1	29.07	52.65	19620.00	8.16	8.16
		2	28.07	53.77	19374.75	8.17	
3	Dolerite-3	1	28.75	53.83	22563.00	9.28	9.82
		2	26.95	53.72	23544.00	10.35	
4	Dolerite-4	1	29.56	47.63	27860.40	12.60	13.73
		2	32.96	47.73	34629.30	14.01	
		3	30.16	47.71	34825.50	15.40	
		4	35.27	47.78	34138.80	12.89	
5	Granite-1	1	29.18	53.58	3924.00	1.60	1.60
		2	27.18	53.60	3237.30	1.41	
		3	28.55	53.72	4316.40	1.79	
6	Granite-2	1	29.32	52.93	5886.00	2.41	3.37
		2	26.90	53.75	9810.00	4.32	
7	Granite-3	1	27.53	53.70	7161.30	3.08	3.69
		2	25.15	53.63	9123.30	4.31	
		3	27.92	53.27	8583.75	3.67	
8	Granite-4	1	27.12	53.60	5101.20	2.23	2.23
		2	24.13	53.60	2452.50	1.21	
		3	29.00	53.75	7985.34	3.26	
9	Granite-5	1	27.61	54.62	36198.90	15.28	18.65
		2	27.44	54.50	43850.70	18.66	
		3	27.56	54.49	53562.60	22.70	
		4	27.62	54.61	36395.10	15.36	
		5	22.77	54.63	41496.30	21.24	
10	Granite-6	1	28.77	54.37	5591.70	2.28	2.30
		2	32.25	54.17	6376.50	2.32	
11	Migmatite	1	29.93	53.83	4905.00	1.94	2.27
		2	24.02	53.92	5297.40	2.60	
12	Andesite	1	27.97	54.25	36297.00	15.23	14.07
		2	30.72	54.30	38455.20	14.68	
		3	28.07	54.30	29430.00	12.29	
13	Granitic Gneiss-1	1	30.87	53.67	5395.50	2.07	4.07
		2	23.72	53.65	10006.20	5.01	
		3	28.22	53.58	12164.40	5.12	
14	Granitic Gneiss-2	1	29.11	54.50	6740.06	2.70	3.19
		2	29.58	54.53	6938.32	2.74	
		3	30.92	54.52	9449.35	3.57	
		4	29.04	54.50	9317.18	3.75	
15	Phyllite	1	19.61	54.44	4110.39	2.45	4.10
		2	21.05	54.48	10329.93	5.73	
16	Quartzite-1	1	30.81	54.42	11085.30	4.21	4.35
		2	30.58	54.41	11772.00	4.50	
		3	30.21	54.40	11183.40	4.33	

Brazilian Tensile Strength test results for dry rock samples.							
Sr. No.	Rock Sample	Test No.	Thickness, t (mm)	Diameter, d (mm)	Peak Failure Force, P (N)	BTS = $\frac{2 \times P}{\pi \times d \times t}$ (MPa)	Avg. BTS (MPa)
17	Quartzite-2	1	25.23	53.87	27860.40	13.05	14.58
		2	24.03	53.83	32765.40	16.12	
18	Siltstone-1	1	28.32	54.22	13949.82	5.78	7.36
		2	29.77	54.53	22170.60	8.69	
		3	32.30	54.33	21385.80	7.76	
		4	30.55	54.18	8829.00	3.40	
		5	32.57	54.18	30999.60	11.18	
19	Siltstone-2	1	26.61	54.21	27173.70	11.99	9.02
		2	26.90	54.15	11232.45	4.91	
		3	26.79	54.21	23151.60	10.15	
20	Sandstone-1	1	27.03	53.62	4512.60	1.98	1.85
		2	25.62	53.63	3139.20	1.45	
		3	24.30	53.67	5395.50	2.63	
		4	23.92	53.63	2648.70	1.31	
21	Sandstone-2	1	26.70	54.23	1765.80	0.78	0.48
		2	27.90	54.32	1667.70	0.70	
		3	23.43	54.27	392.40	0.20	
		4	30.00	54.00	1520.55	0.60	
		5	28.73	54.35	294.30	0.12	
22	Sandstone-3	1	28.27	55.72	15156.45	6.13	6.38
		2	33.00	55.69	15892.20	5.50	
		3	29.39	55.94	21532.95	8.34	
		4	34.03	55.71	16578.90	5.57	
23	Sandstone-4	1	28.15	54.44	4163.00	1.73	1.45
		2	28.28	54.43	3171.81	1.31	
		3	27.47	54.29	3303.97	1.41	
		4	27.78	54.34	3171.81	1.34	
24	Sandstone-5	1	26.13	54.45	5738.85	2.57	2.84
		2	23.77	54.44	3384.45	1.67	
		3	31.25	54.55	11477.70	4.29	
25	Sandstone-6	1	25.45	53.70	10398.60	4.84	6.03
		2	29.93	53.82	18266.22	7.22	
26	Sandstone-7	1	27.63	53.80	14813.10	6.34	7.32
		2	28.27	53.80	19816.20	8.29	
		3	26.73	54.28	16677.00	7.32	
27	Sandstone-8	1	26.15	53.68	2516.27	1.14	1.31
		2	27.47	53.95	3443.31	1.48	
		3	29.82	53.68	3286.35	1.31	
28	Sandstone-9	1	26.55	53.78	4635.23	2.07	1.87
		2	26.15	53.83	3708.18	1.68	
29	Sandstone-10	1	27.62	53.48	1986.53	0.86	0.72
		2	24.53	53.60	1509.76	0.73	
		3	25.37	53.30	1258.13	0.59	
30	Sandstone-11	1	26.32	53.83	5032.53	2.26	2.05
		2	28.63	53.95	4502.79	1.86	
31	Sandstone-12	1	25.88	53.97	2516.27	1.15	1.61
		2	24.93	53.62	4370.36	2.08	
		3	24.68	53.72	3335.40	1.60	

Brazilian Tensile Strength test results for dry rock samples.							
Sr. No.	Rock Sample	Test No.	Thickness, t (mm)	Diameter, d (mm)	Peak Failure Force, P (N)	BTS = $\frac{2 \times P}{\pi \times d \times t}$ (MPa)	Avg. BTS (MPa)
32	Sandstone-13	1	26.93	53.41	4237.92	1.88	1.60
		2	25.00	53.50	2781.14	1.32	
33	Sandstone-14	1	24.67	53.60	1787.87	0.86	0.86
		2	25.57	53.40	1854.09	0.86	
34	Sandstone-15	1	27.15	54.17	10643.85	4.61	6.10
		2	27.40	54.10	15499.80	6.66	
		3	27.53	54.07	13390.65	5.73	
		4	29.80	54.07	15843.15	6.26	
		5	28.80	54.03	17756.10	7.26	
35	Sandstone-16	1	29.73	54.10	63470.70	25.12	22.67
		2	28.57	54.25	49834.80	20.47	
		3	29.80	54.20	65727.00	25.90	
		4	28.95	54.20	56211.30	22.80	
		5	31.10	54.10	50325.30	19.04	
36	Sandstone-17	1	28.26	54.27	8829.00	3.66	4.20
		2	27.28	54.27	8338.50	3.59	
		3	25.78	54.33	11772.00	5.35	
37	Sandstone-18	1	24.38	45.22	13930.20	8.04	6.01
		2	25.89	43.96	9319.50	5.21	
		3	26.62	44.86	8927.10	4.76	
38	Chamositic-Siderite	1	28.98	53.60	20404.80	8.36	8.08
		2	28.67	53.80	18933.30	7.81	
39	Dolomite-1	1	28.55	53.93	16304.22	6.74	6.54
		2	28.00	53.85	15009.30	6.34	
		3	27.88	53.73	15401.70	6.54	
40	Dolomite-2	1	30.17	54.15	27566.10	10.74	11.96
		2	29.52	54.20	27860.40	11.09	
		3	29.52	54.12	30509.10	12.16	
		4	29.58	54.15	18148.50	7.21	
		5	28.92	54.10	42379.20	17.24	
41	Dolomite-3	1	29.12	54.60	29626.20	11.86	12.53
		2	28.12	54.65	32078.70	13.29	
		3	29.40	54.50	31195.80	12.39	
		4	28.27	54.50	34727.40	14.35	
		5	28.78	54.58	26536.05	10.75	
42	Dolomite-4	1	29.45	54.25	19423.80	7.74	6.65
		2	26.78	54.18	12753.00	5.59	
		3	26.72	54.02	10006.20	4.41	
		4	29.38	54.13	19080.45	7.64	
		5	27.22	54.13	18246.60	7.88	

Brazilian Tensile Strength test results for dry rock samples.							
Sr. No.	Rock Sample	Test No.	Thickness, t (mm)	Diameter, d (mm)	Peak Failure Force, P (N)	$BTS = \frac{2 \times P}{\pi \times d \times t}$ (MPa)	Avg. BTS (MPa)
43	Limestone-1	1	27.20	53.85	8829.00	3.84	5.01
		2	27.55	53.90	17069.40	7.32	
		3	27.05	54.00	6867.00	2.99	
		4	26.90	53.85	10791.00	4.74	
		5	25.90	53.95	18246.60	8.31	
		6	26.10	53.90	6180.30	2.80	
		7	26.87	54.00	13243.50	5.81	
		8	26.05	53.95	15892.20	7.20	
		9	27.55	53.80	4414.50	1.90	
		10	27.13	54.00	11919.15	5.18	
44	Limestone-2	1	26.07	53.80	16971.30	7.70	4.60
		2	26.82	53.55	5101.20	2.26	
		3	26.00	54.00	14420.70	6.54	
		4	27.30	53.70	13145.40	5.71	
		5	27.87	53.60	3139.20	1.34	
		6	26.97	53.75	2452.50	1.08	
		7	27.20	53.80	13439.70	5.85	
		8	25.77	53.80	16971.30	7.79	
		9	26.52	53.40	9810.00	4.41	
		10	25.27	53.55	7161.30	3.37	
45	Limestone-3	1	28.00	54.40	11772.00	4.92	5.62
		2	31.00	54.20	9810.00	3.72	
		3	30.00	54.25	20601.00	8.06	
		4	29.00	54.20	11772.00	4.77	
		5	28.00	54.25	14715.00	6.17	
		6	26.00	54.30	16677.00	7.52	
		7	30.00	54.25	15696.00	6.14	
		8	28.00	54.40	11772.00	4.92	
		9	26.00	54.20	9810.00	4.43	
		10	27.00	54.25	12753.00	5.54	
46	Limestone-4	1	29.72	53.70	9810.00	3.91	5.39
		2	29.23	53.85	16971.30	6.86	
		3	28.88	53.72	13145.40	5.39	
47	Limestone-5	1	26.03	54.00	15127.02	6.85	7.89
		2	27.70	53.93	20993.40	8.94	
48	Limestone-6	1	27.00	54.15	5886.00	2.56	3.31
		2	32.00	54.20	3924.00	1.44	
		3	29.00	54.05	5886.00	2.39	
		4	32.00	54.15	9810.00	3.60	
		5	29.00	54.00	8829.00	3.59	
		6	29.00	54.20	13734.00	5.56	
		7	31.00	54.15	7848.00	2.98	
		8	28.00	54.05	10791.00	4.54	
		9	26.00	54.10	7848.00	3.55	
		10	28.00	54.20	6867.00	2.88	

Brazilian Tensile Strength test results for dry rock samples.

Sr. No.	Rock Sample	Test No.	Thickness, t (mm)	Diameter, d (mm)	Peak Failure Force, P (N)	$BTS = \frac{2 \times P}{\pi \times d \times t}$ (MPa)	Avg. BTS (MPa)
49	Limestone-7	1	29.64	54.13	18148.50	7.20	7.83
		2	28.94	53.92	18344.70	7.48	
		3	24.12	54.05	18050.40	8.81	
50	Rock Gypsum	1	22.56	54.18	2246.70	1.17	1.33
		2	29.60	54.00	2472.12	0.98	
		3	29.00	54.31	4096.92	1.66	
		4	23.76	54.12	3066.08	1.52	
51	Marl	1	26.72	54.00	2013.01	0.89	0.78
		2	26.74	54.02	1059.48	0.47	
		3	25.83	54.01	529.74	0.24	
		4	29.39	54.00	2476.53	0.99	
		5	25.77	54.15	2873.84	1.31	

Brazilian Tensile Strength test results for fully saturated rock samples.

Sr. No.	Rock Sample	Test No.	Thickness, t (mm)	Diameter, d (mm)	Peak Failure Force, P (N)	$BTS_{(Sat)} = \frac{2 \times P}{\pi \times d \times t}$ (MPa)	Avg. $BTS_{(Sat)}$ (MPa)
1	Siltstone-1	1	30.18	54.20	2452.50	0.95	2.05
		2	27.25	53.87	5395.50	2.34	
		3	26.27	54.25	6376.50	2.85	
2	Siltstone-2	1	26.27	53.87	16677.00	7.50	6.77
		2	27.87	53.75	11772.00	5.00	
		3	25.68	54.22	17069.40	7.80	
3	Sandstone-1	1	27.07	53.63	434.78	0.19	2.11
		2	28.38	53.57	7151.49	2.99	
		3	24.95	54.02	6356.88	3.00	
		4	26.27	54.03	5032.53	2.26	
4	Sandstone-2	1	24.87	54.17	162.36	0.08	0.11
		2	27.35	54.20	349.63	0.15	
5	Sandstone-3	1	26.18	55.03	1373.40	0.61	2.46
		2	25.63	54.97	882.90	0.40	
		3	27.50	55.02	7946.10	3.34	
		4	31.65	55.83	15205.50	5.48	
6	Sandstone-4	1	26.50	53.57	2511.36	1.13	0.91
		2	26.82	53.50	1721.66	0.76	
		3	28.18	53.68	1986.53	0.84	
7	Sandstone-5	1	27.83	54.52	4330.62	1.82	2.74
		2	25.47	54.12	4767.66	2.20	
		3	27.85	54.27	9998.84	4.21	
8	Sandstone-6	1	28.18	53.95	490.50	0.21	1.20
		2	28.08	53.87	3433.50	1.44	
		3	25.52	54.03	3796.47	1.75	
		4	24.42	53.98	2913.57	1.41	
9	Sandstone-7	1	28.37	53.82	9397.98	3.92	2.56
		2	27.20	53.82	4815.83	2.09	
		3	26.38	54.25	3727.80	1.66	

Brazilian Tensile Strength test results for fully saturated rock samples.
Sr. No.	**Rock Sample**	**Test No.**	**Thickness, t (mm)**	**Diameter, d (mm)**	**Peak Failure Force, P (N)**	$\mathbf{BTS_{(Sat)}} = \frac{2 \times P}{\pi \times d \times t}$ **(MPa)**	**Avg. BTS$_{(Sat)}$ (MPa)**
10	Sandstone-8	1	24.42	54.00	1787.86	0.86	0.98
		2	26.83	54.00	1827.59	0.80	
		3	22.85	54.42	2383.83	1.22	
		4	25.75	54.42	2251.40	1.02	
11	Sandstone-9	1	25.68	54.05	3509.53	1.61	1.78
		2	25.42	54.05	3628.71	1.68	
		3	24.82	54.43	4370.36	2.06	
12	Sandstone-10	1	23.62	53.33	2638.89	1.33	1.00
		2	24.53	53.73	1981.62	0.96	
		3	23.40	53.28	1844.28	0.94	
		4	24.62	53.37	1579.41	0.77	
13	Sandstone-11	1	25.02	53.48	2516.27	1.20	1.96
		2	27.88	53.83	5694.71	2.41	
		3	24.78	53.90	4767.66	2.27	
14	Sandstone-12	1	25.08	53.42	3085.74	1.47	1.41
		2	26.38	53.00	3430.06	1.56	
		3	25.48	53.38	2781.14	1.30	
		4	22.98	53.68	2516.27	1.30	
15	Sandstone-13	1	24.57	53.97	3337.35	1.60	1.75
		2	26.02	54.00	4304.14	1.95	
		3	27.62	54.42	4022.10	1.70	
16	Sandstone-14	1	24.17	53.20	1986.53	0.98	0.88
		2	24.02	53.57	1642.18	0.81	
		3	25.70	54.08	1840.85	0.84	
17	Sandstone-15	1	27.82	53.63	8338.50	3.56	3.91
		2	26.90	53.88	9711.90	4.27	
		3	29.37	53.88	9711.90	3.91	
18	Sandstone-17	1	26.10	54.20	490.50	0.22	1.37
		2	27.97	54.12	4414.50	1.86	
		3	24.73	54.12	1471.50	0.70	
		4	29.73	54.35	6867.00	2.70	
19	Sandstone-18	1	26.43	45.22	7455.60	3.97	3.94
		2	27.23	45.35	10006.20	5.16	
		3	25.55	44.05	4905.00	2.77	
		4	24.75	45.88	6867.00	3.85	
20	Chamositic-Siderite	1	28.43	53.80	7357.50	3.06	4.15
		2	23.82	54.20	9319.50	4.60	
		3	24.15	54.07	9810.00	4.78	
21	Dolomite-1	1	27.78	53.55	3629.70	1.55	3.86
		2	26.22	53.95	8534.70	3.84	
		3	26.52	53.93	13905.68	6.19	
22	Dolomite-2	1	25.33	53.85	18639.00	8.70	8.22
		2	25.90	53.83	16382.70	7.48	
		3	26.12	54.08	18835.20	8.49	

Brazilian Tensile Strength test results for fully saturated rock samples.							
Sr. No.	Rock Sample	Test No.	Thickness, t (mm)	Diameter, d (mm)	Peak Failure Force, P (N)	$BTS_{(Sat)} = \frac{2 \times P}{\pi \times d \times t}$ (MPa)	Avg. BTS$_{(Sat)}$ (MPa)
23	Dolomite-3	1	25.50	54.07	4905.00	2.26	4.66
		2	24.90	53.80	23544.00	11.19	
		3	25.88	53.87	1177.20	0.54	
24	Dolomite-4	1	24.93	53.47	5886.00	2.81	3.83
		2	26.45	53.52	10791.00	4.85	
25	Limestone-1	1	25.58	53.45	294.30	0.14	1.22
		2	25.37	53.80	2452.50	1.14	
		3	24.32	53.68	3335.40	1.63	
		4	26.63	53.72	4414.50	1.96	
26	Limestone-2	1	23.53	53.88	3237.30	1.63	2.64
		2	25.38	53.85	9123.30	4.25	
		3	24.53	53.95	6474.60	3.11	
		4	25.70	53.95	3433.50	1.58	
27	Limestone-3	1	24.37	53.87	12262.50	5.95	5.42
		2	26.45	53.93	12360.60	5.52	
		3	22.85	53.75	9810.00	5.08	
		4	25.50	53.73	6033.15	2.80	
		5	26.68	53.80	17461.80	7.74	
28	Limestone-4	1	27.70	53.90	5493.60	2.34	3.11
		2	27.75	53.90	8829.00	3.76	
		3	23.62	53.87	6474.60	3.24	
29	Limestone-5	1	26.62	54.23	10791.00	4.76	5.13
		2	28.60	54.18	13832.10	5.68	
		3	27.83	54.25	11772.00	4.96	
30	Limestone-6	1	24.93	53.88	6867.00	3.25	2.77
		2	25.38	53.80	3433.50	1.60	
		3	24.33	53.90	5984.10	2.90	
		4	25.05	53.93	7063.20	3.33	
31	Limestone-7	1	28.92	53.65	490.50	0.20	0.76
		2	30.87	53.52	3433.50	1.32	
32	Rock Gypsum	1	28.28	54.25	1602.46	0.66	1.36
		2	27.53	54.20	3178.44	1.36	
		3	27.02	54.23	4131.97	1.80	
		4	30.67	54.23	4237.92	1.62	
33	Marl	1	26.55	53.83	238.38	0.11	0.33
		2	23.67	53.47	1589.22	0.80	
		3	24.28	53.67	185.41	0.09	

APPENDIX H.

TEST RESULTS OF SCHIMAZEK'S F-VALUE AND RAI

Schimazek's F-Value and RAI Calculations for Dry Rock Samples

Rock Sample: Dolerite-1						
Minerals	**Quantity (%)**	**Grain Size (mm)**	**Rosiwal Hardness**	**Quartz Equivalent (%)**	**Schemazek's F-value (N/mm)**	**RAI**
Pyroxene	40.00	0.32	35	14.00		
Quartz	5.00	0.22	100	5.00		
Amphibole	13.00	0.35	18	2.34		
Muscovite	0.50	0.51	4	0.02		
Biotite	0.50	0.59	4	0.02	0.94	80.19
Feldspars	40.00	0.52	35	14.00		
Magnetite	0.50	0.07	34	0.17		
Zircon	0.50	0.09	367	1.84		
Total Quartz Equivalent Content				37.39		
Rock BTS (Air Dried) = 6.76 MPa			Rock UCS (Air Dried) = 214.50 MPa			

Rock Sample: Dolerite-3						
Minerals	**Quantity (%)**	**Grain Size (mm)**	**Rosiwal Hardness**	**Quartz Equivalent (%)**	**Schemazek's F-value (N/mm)**	**RAI**
Pyroxene	35.00	1.74	35	12.25		
Plagioclase	48.00	0.60	35	16.80		
Quartz	7.00	0.23	4	0.04		
Mica	1.00	0.20	100	7.00		
Epidote	2.00	0.15	54	1.08	3.33	81.63
Zircon	1.00	0.18	367	3.67		
Chlorite	3.00	0.26	0.9	0.03		
Calcite	3.00	0.60	3	0.09		
Total Quartz Equivalent Content				40.96		
Rock BTS (Air Dried) = 9.82 MPa			Rock UCS (Air Dried) = 199.30 MPa			

Rock Sample: Dolerite-4						
Minerals	**Quantity (%)**	**Grain Size (mm)**	**Rosiwal Hardness**	**Quartz Equivalent (%)**	**Schemazek's F-value (N/mm)**	**RAI**
Plagioclase	58.00	0.49	35	20.30		
Pyroxene	12.00	0.36	35	4.20		
Quartz	18.00	0.36	100	18.00		
Muscovite	2.50	0.29	4	0.10		
Zircon	3.00	0.28	367	11.01	2.89	75.54
Glassy Matrix	3.00	0.46	4	0.12		
Chlorite	3.50	0.23	0.9	0.03		
Total Quartz Equivalent Content				53.76		
Rock BTS (Air Dried) = 13.73 MPa			Rock UCS (Air Dried) = 140.50 MPa			

Rock Sample: Granite-2

Minerals	Quantity (%)	Grain Size (mm)	Rosiwal Hardness	Quartz Equivalent (%)	Schemazek's F-value (N/mm)	RAI
Quartz	74.00	1.10	100	74.00		
Feldspars	22.00	1.20	35	7.70		
Muscovite	2.50	1.38	4	0.10	3.07	68.61
Biotite	1.00	1.35	4	0.04		
Sericite	0.50	0.69	4	0.02		
Total Quartz Equivalent Content				81.86		
Rock BTS (Air Dried) = 3.37 MPa			Rock UCS (Air Dried) = 83.81 MPa			

Rock Sample: Granite-3

Minerals	Quantity (%)	Grain Size (mm)	Rosiwal Hardness	Quartz Equivalent (%)	Schemazek's F-value (N/mm)	RAI
Quartz	65.00	1.30	100	65.00		
Feldspars	24.00	1.56	35	8.40		
Muscovite	4.00	1.44	4	0.16		
Biotite	2.50	0.87	4	0.10	3.62	57.35
Magnetite	0.50	0.16	34	0.17		
Sericite	4.00	1.34	1.5	0.06		
Total Quartz Equivalent Content				73.89		
Rock BTS (Air Dried) = 3.69 MPa			Rock UCS (Air Dried) = 77.61 MPa			

Rock Sample: Granite-4

Minerals	Quantity (%)	Grain Size (mm)	Rosiwal Hardness	Quartz Equivalent (%)	Schemazek's F-value (N/mm)	RAI
Quartz	67.00	1.19	100	67.00		
Feldspars	24.00	2.06	35	8.40		
Muscovite	2.50	1.05	4	0.10		
Biotite	2.00	1.19	4	0.08	2.19	42.28
Zircon	0.50	0.21	367	1.84		
Garnet	0.50	0.35	203	1.02		
Sericite	1.50	6.00	1.5	0.02		
Total Quartz Equivalent Content				78.45		
Rock BTS (Air Dried) = 2.23 MPa			Rock UCS (Air Dried) = 53.90 MPa			

Rock Sample: Granite-5						
Minerals	Quantity (%)	Grain Size (mm)	Rosiwal Hardness	Quartz Equivalent (%)	Schemazek's F-value (N/mm)	RAI
Quartz	73.00	0.39	100	73.00		
Feldspars	24.50	1.48	35	8.58		
Micas	1.50	0.84	4	0.06	7.70	190.38
Magnetite	0.75	1.11	34	0.26		
Epidote	0.25	0.40	69	0.17		
Total Quartz Equivalent Content				82.06		
Rock BTS (Air Dried) = 18.65 MPa			Rock UCS (Air Dried) = 231.99 MPa			

Rock Sample: Granite-6						
Minerals	Quantity (%)	Grain Size (mm)	Rosiwal Hardness	Quartz Equivalent (%)	Schemazek's F-value (N/mm)	RAI
Quartz	24.60	2.50	100	24.60		
Plagioclase	7.20	2.24	35	2.52		
Microcline	59.80	1.29	35	20.93		
Hematite	1.44	0.36	25	0.36	2.22	26.37
Micas	1.72	1.36	4	0.07		
Zircon	2.80	0.21	367	10.28		
Sericite	2.44	2.81	4	0.10		
Total Quartz Equivalent Content				58.85		
Rock BTS (Air Dried) = 2.30 MPa			Rock UCS (Air Dried) = 44.80 MPa			

Rock Sample: Migmatite						
Minerals	Quantity (%)	Grain Size (mm)	Rosiwal Hardness	Quartz Equivalent (%)	Schemazek's F-value (N/mm)	RAI
Quartz	70.00	1.21	100	70.00		
Microcline	13.00	3.51	35	4.55		
Plagioclase	7.50	2.10	35	2.63		
Muscovite	3.50	0.90	4	0.14		
Biotite	2.50	1.12	4	0.10	2.44	45.17
Zircon	0.50	0.23	367	1.84		
Hematite	1.00	0.98	25	0.25		
Sericite	2.00	0.76	4	0.08		
Total Quartz Equivalent Content				79.58		
Rock BTS (Air Dried) = 2.27 MPa			Rock UCS (Air Dried) = 56.76 MPa			

357

Rock Sample: Andesite

Minerals	Quantity (%)	Grain Size (mm)	Rosiwal Hardness	Quartz Equivalent (%)	Schemazek's F-value (N/mm)	RAI
Pyroxene	27.00	0.60	35	9.45		
Quartz	10.00	0.18	100	10.00		
Amphibole	15.00	1.10	18	2.70		
Feldspars	40.00	0.99	35	14.00	3.44	84.30
Biotite	2.50	0.42	4	0.10		
Magnetite	0.50	0.30	34	0.17		
Total Quartz Equivalent Content				36.42		
Rock BTS (Air Dried) = 14.07 MPa			Rock UCS (Air Dried) = 231.46 MPa			

Rock Sample: Granitic Gneiss-1

Minerals	Quantity (%)	Grain Size (mm)	Rosiwal Hardness	Quartz Equivalent (%)	Schemazek's F-value (N/mm)	RAI
Quartz	73	0.565	100	73.00		
Potassium - Feldspars	13	1.375	35	4.55		
Plagioclase	8	1.247	35	2.80		
Muscovite	3.5	0.654	4	0.14	2.10	57.04
Biotite	2	0.798	4	0.08		
Zircon	0.5	0.162	367	1.84		
Total Quartz Equivalent Content				82.41		
Rock BTS (Air Dried) = 4.07 MPa			Rock UCS (Air Dried) = 69.22 MPa			

Rock Sample: Phyllite

Minerals	Quantity (%)	Grain Size (mm)	Rosiwal Hardness	Quartz Equivalent (%)	Schemazek's F-value (N/mm)	RAI
Quartz	50.00	0.14	100	50.00		
Feldspars	10.00	0.13	35	3.50		
Muscovite	3.50	1.19	4	0.14	0.32	29.31
Biotite	4.50	0.65	4	0.18		
Hematite	0.50	1.82	25	0.13		
Total Quartz Equivalent Content				53.95		
Rock BTS (Air Dried) = 4.10 MPa			Rock UCS (Air Dried) = 54.33 MPa			

Rock Sample: Quartzite-1

Minerals	Quantity (%)	Grain Size (mm)	Rosiwal Hardness	Quartz Equivalent (%)	Schemazek's F-value (N/mm)	RAI
Quartz	90.60	0.737	100	90.60		
Feldspars	2.20	0.410	35	0.77		
Chert	3.00	0.435	100	3.00		
Tourmaline	1.30	0.326	102	1.33		
Zircon	0.30	0.247	367	1.10	3.01	54.57
Opaques (Hematite and Magnetite)	1.20	0.172	34	0.41		
Clay	0.50	< 0.050	4	0.02		
Chlorite	0.90	0.167	0.9	0.01		
Total Quartz Equivalent Content				96.78		
Rock BTS (Air Dried) = 4.35 MPa			Rock UCS (Air Dried) = 56.39 MPa			

Rock Sample: Quartzite-2

Minerals	Quantity (%)	Grain Size (mm)	Rosiwal Hardness	Quartz Equivalent (%)	Schemazek's F-value (N/mm)	RAI
Quartz	48.50	0.538	100	48.50		
Feldspars	4.30	0.352	35	1.51		
Muscovite	5.80	0.428	4	0.23		
Biotite	2.40	0.157	4	0.10		
Tourmaline	1.10	0.264	102	1.12		
Zircon	0.30	0.242	367	1.10	4.26	110.82
Opaques (Hematite and Magnetite)	1.70	0.257	25	0.43		
Micro Crystalline Quartz	22.30	0.078	100	22.30		
Carbonate	2.80	0.322	3	0.08		
Chlorite	1.30	0.397	0.9	0.01		
Total Quartz Equivalent Content				75.38		
Rock BTS (Air Dried) = 14.58 MPa			Rock UCS (Air Dried) = 147.03 MPa			

Rock Sample: Siltstone-1

Minerals	Quantity (%)	Grain Size (mm)	Rosiwal Hardness	Quartz Equivalent (%)	Schemazek's F-value (N/mm)	RAI
Quartz	15.20	0.225	100	15.20		
Feldspars	13.00	0.537	35	4.55		
Micas (Muscovite and Biotite)	5.00	0.177	4	0.20		
Hematite	5.00	0.167	25	1.25		
Sericite	7.00	0.518	4	0.28	0.48	11.55
Calcite	24.80	0.359	3	0.74		
Clay	30.00	< 0.050	4	1.20		
Total Quartz Equivalent Content				23.42		
Rock BTS (Air Dried) = 7.36 MPa			Rock UCS (Air Dried) = 49.30 MPa			

Rock Sample: Siltstone-2

Minerals	Quantity (%)	Grain Size (mm)	Rosiwal Hardness	Quartz Equivalent (%)	Schemazek's F-value (N/mm)	RAI
Dolomite	33.00	0.123	5.1	1.683		
Quartz	22.00	0.154	100	22.000		
Hematite	1.50	0.178	25	0.375		
Feldspar	35.00	0.168	33.9	11.865		
Biotite	1.00	0.596	1.5	0.015	0.52	21.02
Muscovite	1.00	0.170	1.5	0.015		
Epidote	0.50	0.054	54	0.270		
Clay	6.00	< 0.050	1.5	0.090		
Total Quartz Equivalent Content				36.310		
Rock BTS (Air Dried) = 9.02 MPa			Rock UCS (Air Dried) = 57.88 MPa			

Rock Sample: Sandstone-1

Minerals	Quantity (%)	Grain Size (mm)	Rosiwal Hardness	Quartz Equivalent (%)	Schemazek's F-value (N/mm)	RAI
Quartz	68.00	0.413	100	68.00		
Feldspars	9.50	0.979	35	3.33		
Muscovite	2.50	0.458	4	0.10		
Biotite	1.50	0.446	4	0.06		
Epidote	0.50	0.252	54	0.27		
Glauconite	3.50	0.431	0.3	0.01	0.59	28.77
Chlorite	1.50	0.382	0.9	0.01		
Carbonate Shells	2.50	2.866	3	0.08		
Sericite	3.50	1.011	4	0.14		
Glassy Matrix	7.00	< 0.050	4	0.28		
Total Quartz Equivalent Content				72.270		
Rock BTS (Air Dried) = 1.85 MPa			Rock UCS (Air Dried) = 39.80 MPa			

Rock Sample: Sandstone-2

Minerals	Quantity (%)	Grain Size (mm)	Rosiwal Hardness	Quartz Equivalent (%)	Schemazek's F-value (N/mm)	RAI
Quartz	67.00	0.237	100	67.00		
Feldspars	20.00	0.200	47.5	9.50		
Muscovite	1.50	0.268	6.1	0.09		
Chlorite	0.50	0.085	0.9	0.00	0.09	32.20
Sericite	1.00	0.276	6.1	0.06		
Hematite	1.00	0.158	25	0.25		
Glassy matrix	9.00	< 0.050	6.1	0.55		
Total Quartz Equivalent Content				77.50		
Rock BTS (Air Dried) = 0.48 MPa			Rock UCS (Air Dried) = 41.55 MPa			

Rock Sample: Sandstone-3

Minerals	Quantity (%)	Grain Size (mm)	Rosiwal Hardness	Quartz Equivalent (%)	Schemazek's F-value (N/mm)	RAI
Quartz	64.00	0.588	100	64.00		
Feldspars	15.00	0.546	35	5.25		
Muscovite	4.00	0.532	4	0.16		
Biotite	3.00	0.889	4	0.12	2.87	101.26
Hematite	3.00	0.556	25	0.75		
Sericite	2.00	0.480	4	0.08		
Chert	9.00	0.435	100	9.00		
Total Quartz Equivalent Content				79.36		
Rock BTS (Air Dried) = 6.38 MPa			Rock UCS (Air Dried) = 127.60 MPa			

Rock Sample: Sandstone-4

Minerals	Quantity (%)	Grain Size (mm)	Rosiwal Hardness	Quartz Equivalent (%)	Schemazek's F-value (N/mm)	RAI
Quartz	78.00	0.392	100	78.00		
Feldspars	17.00	0.276	35	5.95		
Hematite	0.50	0.374	25	0.13		
Muscovite	1.50	0.384	4	0.06	0.47	22.52
Biotite	2.50	0.441	4	0.10		
Sericite	0.50	0.466	4	0.02		
Total Quartz Equivalent Content				84.26		
Rock BTS (Air Dried) = 1.45 MPa			Rock UCS (Air Dried) = 26.73 MPa			

Rock Sample: Sandstone-5

Minerals	Quantity (%)	Grain Size (mm)	Rosiwal Hardness	Quartz Equivalent (%)	Schemazek's F-value (N/mm)	RAI
Quartz	62.30	0.513	100	62.30		
Chert	4.70	0.472	74	3.48		
Feldspars	28.00	0.479	35	9.80		
Muscovite	1.50	0.415	4	0.06	1.10	33.72
Epidote	1.50	0.329	54	0.81		
Sericite	1.50	0.704	4	0.06		
Hematite	0.50	0.446	25	0.13		
Total Quartz Equivalent Content				76.63		
Rock BTS (Air Dried) = 2.84 MPa			Rock UCS (Air Dried) = 44.00 MPa			

Rock Sample: Sandstone-6

Minerals	Quantity (%)	Grain Size (mm)	Rosiwal Hardness	Quartz Equivalent (%)	Schemazek's F-value (N/mm)	RAI
Quartz	70.10	0.716	100	70.10		
Rock Fragments (Quartz)	22.60	2.419	74	16.72		
Plagioclase	1.00	0.385	35	0.35		
Potassium Feldspar	0.70	0.698	35	0.25		
Micas (Muscovite and Biotite)	1.00	0.549	4	0.04		
Chert	1.30	0.752	74	0.96	5.55	98.43
Zircon	0.30	0.237	367	1.10		
Sericite	1.00	0.716	4	0.04		
Hematite	0.40	0.767	25	0.10		
Carbonate	1.10	1.565	3	0.03		
Chlorite	0.50	0.129	0.9	0.005		
Total Quartz Equivalent Content				89.70		
Rock BTS (Air Dried) = 6.03 MPa			Rock UCS (Air Dried) = 109.73 MPa			

Rock Sample: Sandstone-7

Minerals	Quantity (%)	Grain Size (mm)	Rosiwal Hardness	Quartz Equivalent (%)	Schemazek's F-value (N/mm)	RAI
Quartz	67.50	0.106	100	67.50		
Polygrain Quartz	26.50	0.485	74	19.61		
Plagioclase	1.30	0.167	35	0.46		
K-Feldspar	0.80	0.149	35	0.28	1.27	55.17
Epidote	1.30	0.109	54	0.70		
Chert	0.60	0.294	74	0.44		
Lithic Fragments	2.00	0.533	35	0.70		
Total Quartz Equivalent Content				89.69		
Rock BTS (Air Dried) = 7.32 MPa			Rock UCS (Air Dried) = 61.51 MPa			

Rock Sample: Sandstone-8

Minerals	Quantity (%)	Grain Size (mm)	Rosiwal Hardness	Quartz Equivalent (%)	Schemazek's F-value (N/mm)	RAI
Quartz	55.50	0.414	100	55.50		
Plagioclase	12.00	0.400	35	4.20		
Potassium Feldspars	7.90	0.356	35	2.77		
Muscovite	4.00	0.817	4	0.16		
Rock Fragments	6.70	0.340	64.33	4.31	0.38	7.65
Zircon	0.50	0.195	367	1.84		
Sericite	4.00	0.497	4	0.16		
Glassy Matrix	9.40	3.500	4	0.38		
Total Quartz Equivalent Content				69.31		
Rock BTS (Air Dried) = 1.31 MPa			Rock UCS (Air Dried) = 11.04 MPa			

Rock Sample: Sandstone-9						
Minerals	**Quantity (%)**	**Grain Size (mm)**	**Rosiwal Hardness**	**Quartz Equivalent (%)**	**Schemazek's F-value (N/mm)**	**RAI**
Quartz	78.00	0.588	100	78.00		
Feldspars	12.00	0.447	35	4.20		
Glauconite	0.50	1.198	0.6	0.00	0.91	24.53
Muscovite	0.50	0.774	4	0.02		
Lithic Fragments	9.00	0.361	25	2.25		
Total Quartz Equivalent Content				84.47		
Rock BTS (Air Dried) = 1.87 MPa			Rock UCS (Air Dried) = 29.04 MPa			

Rock Sample: Sandstone-10						
Minerals	**Quantity (%)**	**Grain Size (mm)**	**Rosiwal Hardness**	**Quartz Equivalent (%)**	**Schemazek's F-value (N/mm)**	**RAI**
Quartz	75.00	0.452	100	75.00		
Feldspars	4.50	0.307	35	1.58		
Muscovite	1.00	0.603	4	0.04		
Biotite	1.00	0.421	4	0.04	0.24	12.84
Glauconite	0.50	0.202	0.3	0.00		
Limonite	1.00	0.210	25	0.25		
Glassy Matrix	17.00	0.002	1.5	0.26		
Total Quartz Equivalent Content				76.91		
Rock BTS (Air Dried) = 0.70 MPa			Rock UCS (Air Dried) = 16.69 MPa			

Rock Sample: Sandstone-11						
Minerals	**Quantity (%)**	**Grain Size (mm)**	**Rosiwal Hardness**	**Quartz Equivalent (%)**	**Schemazek's F-value (N/mm)**	**RAI**
Quartz	73.00	0.581	100	73.00		
Feldspars	16.00	0.563	35	5.60		
Muscovite	2.50	0.618	4	0.10		
Chert	1.50	0.405	100	1.50		
Zircon	0.50	0.091	367	1.84	0.96	17.46
Sericite	3.50	1.529	4	0.14		
Hematite	1.00	0.333	25	0.25		
Glassy Matrix	2.00	0.002	1.5	0.03		
Total Quartz Equivalent Content				82.43		
Rock BTS (Air Dried) = 2.05 MPa			Rock UCS (Air Dried) = 21.18 MPa			

Rock Sample: Sandstone-12						
Minerals	Quantity (%)	Grain Size (mm)	Rosiwal Hardness	Quartz Equivalent (%)	Schemazek's F-value (N/mm)	RAI
Quartz	55.00	0.240	100	55.00		
Potassium Feldspar	27.00	0.235	35	9.45		
Muscovite	0.50	0.256	4	0.02		
Biotite	0.50	1.229	4	0.02	0.25	17.50
Glauconite	0.50	0.145	0.3	0.002		
Hematite	0.50	0.150	25	0.13		
Matrix (Clay)	16.0	<0.004	1.5	0.24		
Total Quartz Equivalent Content				64.62		
Rock BTS (Air Dried) = 1.61 MPa			Rock UCS (Air Dried) = 27.09 MPa			

Rock Sample: Sandstone-13						
Minerals	Quantity (%)	Grain Size (mm)	Rosiwal Hardness	Quartz Equivalent (%)	Schemazek's F-value (N/mm)	RAI
Quartz	77.00	0.273	100	77.00		
Feldspars	17.50	0.266	35	6.13		
Muscovite	2.50	0.616	4	0.10		
Biotite	1.20	0.681	4	0.05	0.37	39.59
Sericite	0.50	1.933	4	0.02		
Hematite	0.80	0.260	25	0.20		
Zircon	0.50	0.152	367	1.84		
Total Quartz Equivalent Content				85.33		
Rock BTS (Air Dried) = 1.60 MPa			Rock UCS (Air Dried) = 46.40 MPa			

Rock Sample: Sandstone-14						
Minerals	Quantity (%)	Grain Size (mm)	Rosiwal Hardness	Quartz Equivalent (%)	Schemazek's F-value (N/mm)	RAI
Quartz	72.50	0.431	100	72.50		
Rock Fragments	4.00	0.413	74	2.96		
Feldspars	18.00	0.376	35	6.30		
Muscovite	1.50	0.983	4	0.06		
Biotite	0.50	0.444	4	0.02	0.31	14.32
Sericite	1.00	0.500	4	0.04		
Hematite	0.50	0.328	25	0.13		
Zircon	0.50	0.253	367	1.84		
Glassy Matrix	1.50	1.144	4	0.06		
Total Quartz Equivalent Content				83.90		
Rock BTS (Air Dried) = 0.86 MPa			Rock UCS (Air Dried) = 17.07 MPa			

Rock Sample: Sandstone-15

Minerals	Quantity (%)	Grain Size (mm)	Rosiwal Hardness	Quartz Equivalent (%)	Schemazek's F-value (N/mm)	RAI
Quartz	78.00	0.090	100	78.00		
Feldspars	17.00	0.115	35	5.95		
Muscovite	3.50	0.289	4	0.14		
Biotite	0.50	0.510	4	0.02	0.48	58.17
Sericite	0.50	0.206	4	0.02		
Hematite	0.50	0.263	25	0.13		
Total Quartz Equivalent Content				84.26		
Rock BTS (Air Dried) = 6.10 MPa			Rock UCS (Air Dried) = 69.04 MPa			

Rock Sample: Sandstone-16

Minerals	Quantity (%)	Grain Size (mm)	Rosiwal Hardness	Quartz Equivalent (%)	Schemazek's F-value (N/mm)	RAI
Quartz	95.00	0.272	100	95.00		
Feldspars	3.00	0.153	35	1.05		
Muscovite	0.50	0.271	4	0.02		
Biotite	0.50	0.434	4	0.02	5.91	124.88
Limonite	0.50	0.156	25	0.13		
Glauconite	0.50	0.254	0.3	0.002		
Total Quartz Equivalent Content				96.22		
Rock BTS (Air Dried) = 22.67 MPa			Rock UCS (Air Dried) = 129.79 MPa			

Rock Sample: Sandstone-17

Minerals	Quantity (%)	Grain Size (mm)	Rosiwal Hardness	Quartz Equivalent (%)	Schemazek's F-value (N/mm)	RAI
Quartz	56.00	0.729	100	56.00		
Feldspar	28.00	0.615	35	9.80		
Hematite	3.00	0.392	25	0.75		
Mica (Muscovite and Biotite)	1.00	0.259	4	0.04	2.04	38.65
Clay	9.00	0.002	4	0.36		
Lithic Fragments	3.00	1.189	38	1.14		
Total Quartz Equivalent Content				68.09		
Rock BTS (Air Dried) = 4.20 MPa			Rock UCS (Air Dried) = 56.76 MPa			

Rock Sample: Sandstone-18

Minerals	Quantity (%)	Grain Size (mm)	Rosiwal Hardness	Quartz Equivalent (%)	Schemazek's F-value (N/mm)	RAI
Quartz	61.00	0.246	100	61.00		
Feldspar	20.00	0.219	35	7.00		
Calcite	7.00	0.279	2	0.14		
Muscovite	3.00	0.218	4	0.12	1.05	59.12
Hematite	2.00	0.227	25	0.50		
Lithic Fragments	7.00	0.287	38	2.66		
Total Quartz Equivalent Content				71.42		
Rock BTS (Air Dried) = 6.01 MPa			Rock UCS (Air Dried) = 82.77 MPa			

Rock Sample: Chamositic Siderite

Minerals	Quantity (%)	Grain Size (mm)	Rosiwal Hardness	Quartz Equivalent (%)	Schemazek's F-value (N/mm)	RAI
Siderite	50.00	0.223	3.84	1.92		
Chamosite	34.00	0.311	1.68	0.57		
Quartz	13.00	0.079	100	13.00	0.13	8.07
Muscovite	1.00	0.232	4	0.04		
Rock Matrix	2.00	0.002	4	0.08		
Total Quartz Equivalent Content				15.61		
Rock BTS (Air Dried) = 8.08 MPa			Rock UCS (Air Dried) = 51.72 MPa			

Rock Sample: Dolomite-1

Minerals	Quantity (%)	Grain Size (mm)	Rosiwal Hardness	Quartz Equivalent (%)	Schemazek's F-value (N/mm)	RAI
Dolomite	96.00	0.111	5.1	4.90		
Quartz	1.00	0.053	100	1.00		
Calcite	0.50	0.065	2	0.01	0.04	3.71
Muscovite	1.00	0.221	4	0.04		
Biotite	1.50	0.415	4	0.06		
Total Quartz Equivalent Content				6.01		
Rock BTS (Air Dried) = 6.54 MPa			Rock UCS (Air Dried) = 61.84 MPa			

Rock Sample: Dolomite-2

Minerals	Quantity (%)	Grain Size (mm)	Rosiwal Hardness	Quartz Equivalent (%)	Schemazek's F-value (N/mm)	RAI
Dolomite	94.00	0.248	5.1	4.70		
Quartz	2.00	0.047	100	2.00		
Hematite	0.50	0.080	25	0.13		
Magnetite	0.50	0.054	34	0.17	0.16	10.17
Muscovite	1.50	0.297	1.5	0.02		
Biotite	1.50	0.681	1.5	0.02		
Total Quartz Equivalent Content				7.04		
Rock BTS (Air Dried) = 11.96 MPa			Rock UCS (Air Dried) = 144.43 MPa			

Rock Sample: Dolomite-3

Minerals	Quantity (%)	Grain Size (mm)	Rosiwal Hardness	Quartz Equivalent (%)	Schemazek's F-value (N/mm)	RAI
Dolomite	92.00	0.229	5.1	4.69		
Quartz	2.50	0.345	100	2.50		
Calcite	4.50	0.360	2	0.09	0.25	7.32
Muscovite	0.50	0.394	4	0.02		
Biotite	0.50	0.802	4	0.02		
Total Quartz Equivalent Content				7.32		
Rock BTS (Air Dried) = 12.53 MPa			Rock UCS (Air Dried) = 99.93 MPa			

Rock Sample: Dolomite-4

Minerals	Quantity (%)	Grain Size (mm)	Rosiwal Hardness	Quartz Equivalent (%)	Schemazek's F-value (N/mm)	RAI
Dolomite	75.00	0.139	5.1	3.83		
Quartz	10.00	0.175	100	10.00		
Hematite	3.00	0.149	25	0.75		
Feldspar	9.00	0.158	35	3.15	0.19	23.58
Biotite	0.50	0.482	4	0.02		
Muscovite	0.50	0.183	4	0.02		
Rock Matrix	2.00	0.002	1.5	0.03		
Total Quartz Equivalent Content				17.77		
Rock BTS (Air Dried) = 6.65 MPa			Rock UCS (Air Dried) = 132.70 MPa			

Rock Sample: Limestone-1

Minerals	Quantity (%)	Grain Size (mm)	Rosiwal Hardness	Quartz Equivalent (%)	Schemazek's F-value (N/mm)	RAI
Dolomite	16.00	0.302	5.1	0.82		
Calcite Bioclasts	27.50	1.158	2	0.55		
Hematite	0.50	0.096	25	0.13	0.05	1.71
Calcitic Micrite	55.50	0.002	2	1.11		
Biotite	0.50	0.867	4	0.02		
Total Quartz Equivalent Content				2.62		
Rock BTS (Air Dried) = 5.01 MPa			Rock UCS (Air Dried) = 65.26 MPa			

Rock Sample: Limestone-2

Minerals	Quantity (%)	Grain Size (mm)	Rosiwal Hardness	Quartz Equivalent (%)	Schemazek's F-value (N/mm)	RAI
Dolomite	16.00	0.302	5.1	0.82		
Calcite Bioclasts	28.00	1.158	1.91	0.53		
Hematite	0.50	0.096	25	0.13	0.04	2.49
Calcitic Micrite	55.00	0.002	2	1.10		
Biotite	0.50	0.867	4	0.02		
Total Quartz Equivalent Content				2.60		
Rock BTS (Air Dried) = 4.60 MPa			Rock UCS (Air Dried) = 95.78 MPa			

Rock Sample: Limestone-3

Minerals	Quantity (%)	Grain Size (mm)	Rosiwal Hardness	Quartz Equivalent (%)	Schemazek's F-value (N/mm)	RAI
Dolomite	36.00	0.268	5.1	1.84		
Calcite	25.00	5.686	2	0.50		
Magnetite	1.00	0.090	34	0.34	0.19	2.77
Calcitic Micrite	38.00	0.002	2	0.76		
Total Quartz Equivalent Content				3.44		
Rock BTS (Air Dried) = 5.62 MPa			Rock UCS (Air Dried) = 80.70 MPa			

Rock Sample: Limestone-4

Minerals	Quantity (%)	Grain Size (mm)	Rosiwal Hardness	Quartz Equivalent (%)	Schemazek's F-value (N/mm)	RAI
Calcite	35.00	1.235	2	0.70		
Calcite Bioclasts	55.00	0.757	2	1.10		
Dolomite	0.50	0.810	5.1	0.03	0.09	1.35
Calcitic Micrite	9.00	0.002	2	0.18		
Biotite	0.50	0.686	4	0.02		
Total Quartz Equivalent Content				2.03		
Rock BTS (Air Dried) = 5.39 MPa			Rock UCS (Air Dried) = 66.45 MPa			

Rock Sample: Limestone-5

Minerals	Quantity (%)	Grain Size (mm)	Rosiwal Hardness	Quartz Equivalent (%)	Schemazek's F-value (N/mm)	RAI
Calcitic Micrite	91.00	0.002	2	1.82		
Calcite Bioclasts	7.50	0.621	2.5	0.19		
Magnetite	0.50	0.126	34	0.17	0.01	2.06
Muscovite	0.50	0.637	4	0.02		
Biotite	0.50	0.796	4	0.02		
Total Quartz Equivalent Content				2.22		
Rock BTS (Air Dried) = 7.89 MPa			Rock UCS (Air Dried) = 92.75 MPa			

Rock Sample: Limestone-6

Minerals	Quantity (%)	Grain Size (mm)	Rosiwal Hardness	Quartz Equivalent (%)	Schemazek's F-value (N/mm)	RAI
Calcite	13.00	2.825	2	0.26		
Calcite Bioclasts	12.00	0.618	2	0.24		
Dolomite	35.00	0.170	5.1	1.79	0.04	2.32
Hematite	1.00	0.143	25	0.25		
Calcitic Micrite	39.00	0.002	2	0.78		
Total Quartz Equivalent Content				3.32		
Rock BTS (Air Dried) = 3.31 MPa			Rock UCS (Air Dried) = 69.89 MPa			

Rock Sample: Limestone-7						
Minerals	Quantity (%)	Grain Size (mm)	Rosiwal Hardness	Quartz Equivalent (%)	Schemazek's F-value (N/mm)	RAI
Calcite	20.00	0.287	2	0.40		
Dolomite	25.00	0.141	5.1	1.28		
Hematite	1.00	0.098	25	0.25	0.03	0.60
Calcitic Micrite	54.00	0.002	2	1.08		
Total Quartz Equivalent Content				3.01		
Rock BTS (Air Dried) = 7.83 MPa			Rock UCS (Air Dried) = 20.08 MPa			

Rock Sample: Rock Gypsum						
Minerals	Quantity (%)	Grain Size (mm)	Rosiwal Hardness	Quartz Equivalent (%)	Schemazek's F-value (N/mm)	RAI
Gypsum	99.00	0.461	0.3	0.30		
Hematite	1.00	0.267	25	0.25	0.00271	0.07
Total Quartz Equivalent Content				0.55		
Rock BTS (Air Dried) = 1.33 MPa			Rock UCS (Air Dried) = 13.53 MPa			

Rock Sample: Marl						
Minerals	Quantity (%)	Grain Size (mm)	Rosiwal Hardness	Quartz Equivalent (%)	Schemazek's F-value (N/mm)	RAI
Montmorillonite	74.00	0.233	4	2.96		
Quartz	21.00	0.101	100	21.00		
Dolomite	4.00	0.216	5.1	0.20	0.02	1.29
Mica (Muscovite and Biotite)	1.00	0.145	4	0.04		
Total Quartz Equivalent Content				24.20		
Rock BTS (Air Dried) = 0.78 MPa			Rock UCS (Air Dried) = 5.35 MPa			

Schimazek's F-Value and RAI Calculations for Saturated Rock Samples

Rock Sample: Siltstone-1						
Minerals	Quantity (%)	Grain Size (mm)	Rosiwal Hardness	Quartz Equivalent (%)	Schemazek's F-value$_{(Sat)}$ (N/mm)	RAI$_{(Sat)}$
Quartz	15.20	0.225	100	15.20		
Feldspars	13.00	0.537	35	4.55		
Micas (Muscovite and Biotite)	5.00	0.177	4	0.20		
Hematite	5.00	0.167	25	1.25	0.13	4.05
Sericite	7.00	0.518	4	0.28		
Calcite	24.80	0.359	3	0.74		
Clay	30.00	< 0.050	4	1.20		
Total Quartz Equivalent Content				23.42		
Rock BTS (Saturated) = 2.05 MPa			Rock UCS (Saturated) = 17.30 MPa			

Rock Sample: Siltstone-2

Minerals	Quantity (%)	Grain Size (mm)	Rosiwal Hardness	Quartz Equivalent (%)	Schemazek's F-value$_{(Sat)}$ (N/mm)	RAI$_{(Sat)}$
Dolomite	33.00	0.123	5.1	1.683		
Quartz	22.00	0.154	100	22.000		
Hematite	1.50	0.178	25	0.375		
Feldspar	35.00	0.168	33.9	11.865		
Biotite	1.00	0.596	1.5	0.015	0.39	20.36
Muscovite	1.00	0.170	1.5	0.015		
Epidote	0.50	0.054	54	0.270		
Clay	6.00	< 0.050	1.5	0.090		
Total Quartz Equivalent Content				36.31		
Rock BTS (Saturated) = 6.77 MPa			Rock UCS (Saturated) = 56.07 MPa			

Rock Sample: Sandstone-1

Minerals	Quantity (%)	Grain Size (mm)	Rosiwal Hardness	Quartz Equivalent (%)	Schemazek's F-value$_{(Sat)}$ (N/mm)	RAI$_{(Sat)}$
Quartz	68.00	0.413	100	68.00		
Feldspars	9.50	0.979	35	3.33		
Muscovite	2.50	0.458	4	0.10		
Biotite	1.50	0.446	4	0.06		
Epidote	0.50	0.252	54	0.27		
Glauconite	3.50	0.431	0.3	0.01	0.67	13.80
Chlorite	1.50	0.382	0.9	0.01		
Carbonate Shells	2.50	2.866	3	0.08		
Sericite	3.50	1.011	4	0.14		
Glassy Matrix	7.00	< 0.050	4	0.28		
Total Quartz Equivalent Content				72.27		
Rock BTS (Saturated) = 2.11 MPa			Rock UCS (Saturated) = 19.10 MPa			

Rock Sample: Sandstone-2

Minerals	Quantity (%)	Grain Size (mm)	Rosiwal Hardness	Quartz Equivalent (%)	Schemazek's F-value$_{(Sat)}$ (N/mm)	RAI$_{(Sat)}$
Quartz	67.00	0.237	100	67.00		
Feldspars	20.00	0.200	47.5	9.50		
Muscovite	1.50	0.268	6.1	0.09		
Chlorite	0.50	0.085	0.9	0.00		
Sericite	1.00	0.276	6.1	0.06	0.02	20.31
Hematite	1.00	0.158	25	0.25		
Glassy matrix	9.00	< 0.050	6.1	0.55		
Total Quartz Equivalent Content				77.50		
Rock BTS (Saturated) = 0.11 MPa			Rock UCS (Saturated) = 26.20 MPa			

Rock Sample: Sandstone-3

Minerals	Quantity (%)	Grain Size (mm)	Rosiwal Hardness	Quartz Equivalent (%)	Schemazek's F-value(Sat) (N/mm)	RAI(Sat)
Quartz	64.00	0.588	100	64.00		
Feldspars	15.00	0.546	35	5.25		
Muscovite	4.00	0.532	4	0.16		
Biotite	3.00	0.889	4	0.12	1.11	67.72
Hematite	3.00	0.556	25	0.75		
Sericite	2.00	0.480	4	0.08		
Chert	9.00	0.435	100	9.00		
Total Quartz Equivalent Content				79.36		
Rock BTS (Saturated) = 2.46 MPa			Rock UCS (Saturated) = 85.33 MPa			

Rock Sample: Sandstone-4

Minerals	Quantity (%)	Grain Size (mm)	Rosiwal Hardness	Quartz Equivalent (%)	Schemazek's F-value(Sat) (N/mm)	RAI(Sat)
Quartz	78.00	0.392	100	78.00		
Feldspars	17.00	0.276	35	5.95		
Hematite	0.50	0.374	25	0.13		
Muscovite	1.50	0.384	4	0.06	0.29	11.43
Biotite	2.50	0.441	4	0.10		
Sericite	0.50	0.466	4	0.02		
Total Quartz Equivalent Content				84.26		
Rock BTS (Saturated) = 0.91 MPa			Rock UCS (Saturated) = 13.57 MPa			

Rock Sample: Sandstone-5

Minerals	Quantity (%)	Grain Size (mm)	Rosiwal Hardness	Quartz Equivalent (%)	Schemazek's F-value(Sat) (N/mm)	RAI(Sat)
Quartz	62.30	0.513	100	62.30		
Chert	4.70	0.472	74	3.48		
Feldspars	28.00	0.479	35	9.80		
Muscovite	1.50	0.415	4	0.06	1.06	30.86
Epidote	1.50	0.329	54	0.81		
Sericite	1.50	0.704	4	0.06		
Hematite	0.50	0.446	25	0.13		
Total Quartz Equivalent Content				76.63		
Rock BTS (Saturated) = 2.74 MPa			Rock UCS (Saturated) = 40.27 MPa			

Rock Sample: Sandstone-6

Minerals	Quantity (%)	Grain Size (mm)	Rosiwal Hardness	Quartz Equivalent (%)	Schemazek's F-value(Sat) (N/mm)	RAI(Sat)
Quartz	70.10	0.716	100	70.10		
Rock Fragments (Quartz)	22.60	2.419	74	16.72		
Plagioclase	1.00	0.385	35	0.35		
Potassium Feldspar	0.70	0.698	35	0.25		
Micas (Muscovite and Biotite)	1.00	0.549	4	0.04		
Chert	1.30	0.752	74	0.96	1.11	59.47
Zircon	0.30	0.237	367	1.10		
Sericite	1.00	0.716	4	0.04		
Hematite	0.40	0.767	25	0.10		
Carbonate	1.10	1.565	3	0.03		
Chlorite	0.50	0.129	0.9	0.005		
Total Quartz Equivalent Content				89.70		
Rock BTS (Saturated) = 1.20 MPa			Rock UCS (Saturated) = 66.30 MPa			

Rock Sample: Sandstone-7

Minerals	Quantity (%)	Grain Size (mm)	Rosiwal Hardness	Quartz Equivalent (%)	Schemazek's F-value(Sat) (N/mm)	RAI(Sat)
Quartz	67.50	0.106	100	67.50		
Polygrain Quartz	26.50	0.485	74	19.61		
Plagioclase	1.30	0.167	35	0.46		
K-Feldspar	0.80	0.149	35	0.28	0.44	52.05
Epidote	1.30	0.109	54	0.70		
Chert	0.60	0.294	74	0.44		
Lithic Fragments	2.00	0.533	35	0.70		
Total Quartz Equivalent Content				89.69		
Rock BTS (Saturated) = 2.56 MPa			Rock UCS (Saturated) = 58.03 MPa			

Rock Sample: Sandstone-8

Minerals	Quantity (%)	Grain Size (mm)	Rosiwal Hardness	Quartz Equivalent (%)	Schemazek's F-value(Sat) (N/mm)	RAI(Sat)
Quartz	55.50	0.414	100	55.50		
Plagioclase	12.00	0.400	35	4.20		
Potassium Feldspars	7.90	0.356	35	2.77		
Muscovite	4.00	0.817	4	0.16		
Rock Fragments	6.70	0.340	64.33	4.31	0.28	12.16
Zircon	0.50	0.195	367	1.84		
Sericite	4.00	0.497	4	0.16		
Glassy Matrix	9.40	3.500	4	0.38		
Total Quartz Equivalent Content				69.31		
Rock BTS (Saturated) = 0.98 MPa			Rock UCS (Saturated) = 17.55 MPa			

Rock Sample: Sandstone-9

Minerals	Quantity (%)	Grain Size (mm)	Rosiwal Hardness	Quartz Equivalent (%)	Schemazek's F-value$_{(Sat)}$ (N/mm)	RAI$_{(Sat)}$
Quartz	78.00	0.588	100	78.00		
Feldspars	12.00	0.447	35	4.20		
Glauconite	0.50	1.198	0.6	0.00	0.87	11.96
Muscovite	0.50	0.774	4	0.02		
Lithic Fragments	9.00	0.361	25	2.25		
Total Quartz Equivalent Content				84.47		
Rock BTS (Saturated) = 1.78 MPa			Rock UCS (Saturated) = 14.15 MPa			

Rock Sample: Sandstone-10

Minerals	Quantity (%)	Grain Size (mm)	Rosiwal Hardness	Quartz Equivalent (%)	Schemazek's F-value$_{(Sat)}$ (N/mm)	RAI$_{(Sat)}$
Quartz	75.00	0.452	100	75.00		
Feldspars	4.50	0.307	35	1.58		
Muscovite	1.00	0.603	4	0.04		
Biotite	1.00	0.421	4	0.04	0.34	10.03
Glauconite	0.50	0.202	0.3	0.00		
Limonite	1.00	0.210	25	0.25		
Glassy Matrix	17.00	0.002	1.5	0.26		
Total Quartz Equivalent Content				76.91		
Rock BTS (Saturated) = 1.00 MPa			Rock UCS (Saturated) = 13.04 MPa			

Rock Sample: Sandstone-11

Minerals	Quantity (%)	Grain Size (mm)	Rosiwal Hardness	Quartz Equivalent (%)	Schemazek's F-value$_{(Sat)}$ (N/mm)	RAI$_{(Sat)}$
Quartz	73.00	0.581	100	73.00		
Feldspars	16.00	0.563	35	5.60		
Muscovite	2.50	0.618	4	0.10		
Chert	1.50	0.405	100	1.50		
Zircon	0.50	0.091	367	1.84	0.92	16.66
Sericite	3.50	1.529	4	0.14		
Hematite	1.00	0.333	25	0.25		
Glassy Matrix	2.00	0.002	1.5	0.03		
Total Quartz Equivalent Content				82.43		
Rock BTS (Saturated) = 1.96 MPa			Rock UCS (Saturated) = 19.74 MPa			

Rock Sample: Sandstone-12

Minerals	Quantity (%)	Grain Size (mm)	Rosiwal Hardness	Quartz Equivalent (%)	Schemazek's F-value(Sat) (N/mm)	RAI(Sat)
Quartz	55.00	0.240	100	55.00		
Potassium Feldspar	27.00	0.235	35	9.45		
Muscovite	0.50	0.256	4	0.02		
Biotite	0.50	1.229	4	0.02	0.22	15.25
Glauconite	0.50	0.145	0.3	0.002		
Hematite	0.50	0.150	25	0.13		
Matrix (Clay)	16.0	<0.004	1.5	0.24		
Total Quartz Equivalent Content				64.62		
Rock BTS (Saturated) = 1.41 MPa			Rock UCS (Saturated) = 23.60 MPa			

Rock Sample: Sandstone-13

Minerals	Quantity (%)	Grain Size (mm)	Rosiwal Hardness	Quartz Equivalent (%)	Schemazek's F-value(Sat) (N/mm)	RAI(Sat)
Quartz	77.00	0.273	100	77.00		
Feldspars	17.50	0.266	35	6.13		
Muscovite	2.50	0.616	4	0.10		
Biotite	1.20	0.681	4	0.05	0.40	26.15
Sericite	0.50	1.933	4	0.02		
Hematite	0.80	0.260	25	0.20		
Zircon	0.50	0.152	367	1.84		
Total Quartz Equivalent Content				85.33		
Rock BTS (Saturated) = 1.75 MPa			Rock UCS (Saturated) = 30.65 MPa			

Rock Sample: Sandstone-14

Minerals	Quantity (%)	Grain Size (mm)	Rosiwal Hardness	Quartz Equivalent (%)	Schemazek's F-value(Sat) (N/mm)	RAI(Sat)
Quartz	72.50	0.431	100	72.50		
Rock Fragments	4.00	0.413	74	2.96		
Feldspars	18.00	0.376	35	6.30		
Muscovite	1.50	0.983	4	0.06		
Biotite	0.50	0.444	4	0.02	0.31	4.07
Sericite	1.00	0.500	4	0.04		
Hematite	0.50	0.328	25	0.13		
Zircon	0.50	0.253	367	1.84		
Glassy Matrix	1.50	1.144	4	0.06		
Total Quartz Equivalent Content				83.90		
Rock BTS (Saturated) = 0.88 MPa			Rock UCS (Saturated) = 4.84 MPa			

Rock Sample: Sandstone-15

Minerals	Quantity (%)	Grain Size (mm)	Rosiwal Hardness	Quartz Equivalent (%)	Schemazek's F-value$_{(Sat)}$ (N/mm)	RAI$_{(Sat)}$
Quartz	78.00	0.090	100	78.00		
Feldspars	17.00	0.115	35	5.95		
Muscovite	3.50	0.289	4	0.14		
Biotite	0.50	0.510	4	0.02	0.31	36.85
Sericite	0.50	0.206	4	0.02		
Hematite	0.50	0.263	25	0.13		
Total Quartz Equivalent Content				84.26		
Rock BTS (Saturated) = 3.91 MPa			Rock UCS (Saturated) = 43.73 MPa			

Rock Sample: Sandstone-17

Minerals	Quantity (%)	Grain Size (mm)	Rosiwal Hardness	Quartz Equivalent (%)	Schemazek's F-value$_{(Sat)}$ (N/mm)	RAI$_{(Sat)}$
Quartz	56.00	0.729	100	56.00		
Feldspar	28.00	0.615	35	9.80		
Hematite	3.00	0.392	25	0.75		
Mica (Muscovite and Biotite)	1.00	0.259	4	0.04	0.67	41.47
Clay	9.00	0.002	4	0.36		
Lithic Fragments	3.00	1.189	38	1.14		
Total Quartz Equivalent Content				68.09		
Rock BTS (Saturated) = 1.37 MPa			Rock UCS (Saturated) = 60.90 MPa			

Rock Sample: Sandstone-18

Minerals	Quantity (%)	Grain Size (mm)	Rosiwal Hardness	Quartz Equivalent (%)	Schemazek's F-value$_{(Sat)}$ (N/mm)	RAI$_{(Sat)}$
Quartz	61.00	0.246	100	61.00		
Feldspar	20.00	0.219	35	7.00		
Calcite	7.00	0.279	2	0.14		
Muscovite	3.00	0.218	4	0.12	0.69	44.26
Hematite	2.00	0.227	25	0.50		
Lithic Fragments	7.00	0.287	38	2.66		
Total Quartz Equivalent Content				71.42		
Rock BTS (Saturated) = 3.94 MPa			Rock UCS (Saturated) = 61.97 MPa			

Rock Sample: Chamositic Siderite

Minerals	Quantity (%)	Grain Size (mm)	Rosiwal Hardness	Quartz Equivalent (%)	Schemazek's F-value$_{(Sat)}$ (N/mm)	RAI$_{(Sat)}$
Siderite	50.00	0.223	3.84	1.92		
Chamosite	34.00	0.311	1.68	0.57		
Quartz	13.00	0.079	100	13.00	0.07	6.06
Muscovite	1.00	0.232	4	0.04		
Rock Matrix	2.00	0.002	4	0.08		
Total Quartz Equivalent Content				15.61		
Rock BTS (Saturated) = 4.15 MPa			Rock UCS (Saturated) = 38.79 MPa			

Rock Sample: Dolomite-1

Minerals	Quantity (%)	Grain Size (mm)	Rosiwal Hardness	Quartz Equivalent (%)	Schemazek's F-value$_{(Sat)}$ (N/mm)	RAI$_{(Sat)}$
Dolomite	96.00	0.111	5.1	4.90		
Quartz	1.00	0.053	100	1.00		
Calcite	0.50	0.065	2	0.01	0.02	2.01
Muscovite	1.00	0.221	4	0.04		
Biotite	1.50	0.415	4	0.06		
Total Quartz Equivalent Content				6.01		
Rock BTS (Saturated)= 3.86 MPa			Rock UCS (Saturated) = 33.50 MPa			

Rock Sample: Dolomite-2

Minerals	Quantity (%)	Grain Size (mm)	Rosiwal Hardness	Quartz Equivalent (%)	Schemazek's F-value$_{(Sat)}$ (N/mm)	RAI$_{(Sat)}$
Dolomite	94.00	0.248	5.1	4.70		
Quartz	2.00	0.047	100	2.00		
Hematite	0.50	0.080	25	0.13		
Magnetite	0.50	0.054	34	0.17	0.11	4.77
Muscovite	1.50	0.297	1.5	0.02		
Biotite	1.50	0.681	1.5	0.02		
Total Quartz Equivalent Content				7.04		
Rock BTS (Saturated) = 8.22 MPa			Rock UCS (Saturated) = 67.75 MPa			

Rock Sample: Dolomite-3

Minerals	Quantity (%)	Grain Size (mm)	Rosiwal Hardness	Quartz Equivalent (%)	Schemazek's F-value$_{(Sat)}$ (N/mm)	RAI$_{(Sat)}$
Dolomite	92.00	0.229	5.1	4.69		
Quartz	2.50	0.345	100	2.50		
Calcite	4.50	0.360	2	0.09	0.09	4.07
Muscovite	0.50	0.394	4	0.02		
Biotite	0.50	0.802	4	0.02		
Total Quartz Equivalent Content				7.32		
Rock BTS (Saturated) = 4.66 MPa			Rock UCS (Saturated) = 55.52 MPa			

Rock Sample: Dolomite-4

Minerals	Quantity (%)	Grain Size (mm)	Rosiwal Hardness	Quartz Equivalent (%)	Schemazek's F-value$_{(Sat)}$ (N/mm)	RAI$_{(Sat)}$
Dolomite	75.00	0.139	5.1	3.83		
Quartz	10.00	0.175	100	10.00		
Hematite	3.00	0.149	25	0.75		
Feldspar	9.00	0.158	35	3.15	0.11	10.29
Biotite	0.50	0.482	4	0.02		
Muscovite	0.50	0.183	4	0.02		
Rock Matrix	2.00	0.002	1.5	0.03		
Total Quartz Equivalent Content				17.77		
Rock BTS (Saturated) = 3.83 MPa			Rock UCS (Saturated) = 57.94 MPa			

Rock Sample: Limestone-1

Minerals	Quantity (%)	Grain Size (mm)	Rosiwal Hardness	Quartz Equivalent (%)	Schemazek's F-value$_{(Sat)}$ (N/mm)	RAI$_{(Sat)}$
Dolomite	16.00	0.302	5.1	0.82		
Calcite Bioclasts	27.50	1.158	2	0.55		
Hematite	0.50	0.096	25	0.13	0.01	1.59
Calcitic Micrite	55.50	0.002	2	1.11		
Biotite	0.50	0.867	4	0.02		
Total Quartz Equivalent Content				2.62		
Rock BTS (Saturated) = 1.22 MPa			Rock UCS (Saturated)= 60.85 MPa			

Rock Sample: Limestone-2						
Minerals	Quantity (%)	Grain Size (mm)	Rosiwal Hardness	Quartz Equivalent (%)	Schemazek's F-value$_{(Sat)}$ (N/mm)	RAI$_{(Sat)}$
Dolomite	16.00	0.302	5.1	0.82		
Calcite Bioclasts	28.00	1.158	1.91	0.53		
Hematite	0.50	0.096	25	0.13	0.02	1.27
Calcitic Micrite	55.00	0.002	2	1.10		
Biotite	0.50	0.867	4	0.02		
Total Quartz Equivalent Content				2.60		
Rock BTS (Saturated) = 2.64 MPa			Rock UCS (Saturated)= 48.74 MPa			

Rock Sample: Limestone-3						
Minerals	Quantity (%)	Grain Size (mm)	Rosiwal Hardness	Quartz Equivalent (%)	Schemazek's F-value$_{(Sat)}$ (N/mm)	RAI$_{(Sat)}$
Dolomite	36.00	0.268	5.1	1.84		
Calcite	25.00	5.686	2	0.50		
Magnetite	1.00	0.090	34	0.34	0.18	1.02
Calcitic Micrite	38.00	0.002	2	0.76		
Total Quartz Equivalent Content				3.44		
Rock BTS (Saturated) = 5.42 MPa			Rock UCS (Saturated) = 29.64 MPa			

Rock Sample: Limestone-4						
Minerals	Quantity (%)	Grain Size (mm)	Rosiwal Hardness	Quartz Equivalent (%)	Schemazek's F-value$_{(Sat)}$ (N/mm)	RAI$_{(Sat)}$
Calcite	35.00	1.235	2	0.70		
Calcite Bioclasts	55.00	0.757	2	1.10		
Dolomite	0.50	0.810	5.1	0.03	0.05	0.75
Calcitic Micrite	9.00	0.002	2	0.18		
Biotite	0.50	0.686	4	0.02		
Total Quartz Equivalent Content				2.03		
Rock BTS (Saturated) = 3.11 MPa			Rock UCS (Saturated) = 37.21 MPa			

Rock Sample: Limestone-5						
Minerals	Quantity (%)	Grain Size (mm)	Rosiwal Hardness	Quartz Equivalent (%)	Schemazek's F-value$_{(Sat)}$ (N/mm)	RAI$_{(Sat)}$
Calcitic Micrite	91.00	0.002	2	1.82		
Calcite Bioclasts	7.50	0.621	2.5	0.19		
Magnetite	0.50	0.126	34	0.17	0.008	1.79
Muscovite	0.50	0.637	4	0.02		
Biotite	0.50	0.796	4	0.02		
Total Quartz Equivalent Content				2.22		
Rock BTS (Saturated) = 5.13 MPa			Rock UCS (Saturated) = 80.79 MPa			

Rock Sample: Limestone-6

Minerals	Quantity (%)	Grain Size (mm)	Rosiwal Hardness	Quartz Equivalent (%)	Schemazek's F-value$_{(Sat)}$ (N/mm)	RAI$_{(Sat)}$
Calcite	13.00	2.825	2	0.26		
Calcite Bioclasts	12.00	0.618	2	0.24		
Dolomite	35.00	0.170	5.1	1.79	0.03	1.07
Hematite	1.00	0.143	25	0.25		
Calcitic Micrite	39.00	0.002	2	0.78		
Total Quartz Equivalent Content				3.32		
Rock BTS (Saturated) = 2.77 MPa			Rock UCS (Saturated) = 32.25 MPa			

Rock Sample: Limestone-7

Minerals	Quantity (%)	Grain Size (mm)	Rosiwal Hardness	Quartz Equivalent (%)	Schemazek's F-value$_{(Sat)}$ (N/mm)	RAI$_{(Sat)}$
Calcite	20.00	0.287	2	0.40		
Dolomite	25.00	0.141	5.1	1.28		
Hematite	1.00	0.098	25	0.25	0.002	0.96
Calcitic Micrite	54.00	0.002	2	1.08		
Total Quartz Equivalent Content				3.01		
Rock BTS (Saturated) = 0.76 MPa			Rock UCS (Saturated) = 32.13 MPa			

Rock Sample: Rock Gypsum

Minerals	Quantity (%)	Grain Size (mm)	Rosiwal Hardness	Quartz Equivalent (%)	Schemazek's F-value$_{(Sat)}$ (N/mm)	RAI$_{(Sat)}$
Gypsum	99.00	0.461	0.3	0.30		
Hematite	1.00	0.267	25	0.25	0.00276	0.05
Total Quartz Equivalent Content				0.55		
Rock BTS (Saturated) = 1.36 MPa			Rock UCS (Saturated) = 8.48 MPa			

Rock Sample: Marl

Minerals	Quantity (%)	Grain Size (mm)	Rosiwal Hardness	Quartz Equivalent (%)	Schemazek's F-value$_{(Sat)}$ (N/mm)	RAI$_{(Sat)}$
Montmorillonite	74.00	0.233	4	2.96		
Quartz	21.00	0.101	100	21.00		
Dolomite	4.00	0.216	5.1	0.20	0.009	0.51
Mica (Muscovite and Biotite)	1.00	0.145	4	0.04		
Total Quartz Equivalent Content				24.20		
Rock BTS (Saturated) = 0.33 MPa			Rock UCS (Saturated) = 2.10 MPa			

BIBLIOGRAPHY

Abu Bakar MZ (2006) A critical review of rock abrasivity measurement methods. M.Sc. Dissertation, University of Leeds.

Abu Bakar MZ (2012) Saturation effects on mechanical excavatability of Roubidoux sandstone under selected rock cutting tools. Ph.D. Dissertation, Missouri University of Science and Technology.

Abu Bakar MZ, Gertsch LS (2011) Saturation effects on disc cutting of sandstone. American Rock Mechanics Association, 45th US Rock Mechanics/Geomechanics Symposium, San Francisco, CA. 254: 1-9.

Abu Bakar MZ, Gertsch LS (2012) Radial pick cutting performance in dry and saturated sandstone. Society for Mining, Metallurgy and Exploration 332: 396-405.

Abu Bakar MZ, Gertsch LS (2013) Evaluation of saturation effects on drag pick cutting of a brittle sandstone from full scale linear cutting tests. Tunnelling and Underground Space Technology 34: 124-134.

Abu Bakar MZ, Iqbal MM, Majeed Y, Zahoor MK, Fowell RJ (2014) Reduced propeller speed effects on LCPC rock abrasivity test. Pakistan Journal of Science 66(1): 25-28.

Abu Bakar MZ, Majeed Y, Rostami J (2016) Effects of rock water content on CERCHAR abrasivity index. Wear 368-369: 132-145, DOI: 10.1016/j.wear.2016.09.007.

Adebayo B, Akande JM (2015) Analysis of button bit wear and performance of Down-The-Hole hammer drill. Ghana Mining Journal 15(2): 36-41.

AFNOR (1990) Granulats – Essai d'abrasivite'et de broyabilité. Association Francaise de Normalisation (NF P 18-579) Paris.

AFNOR (2000) Determination du pouvoir abrasive d'une roche-Partie 1: Essai de rayure avec une pointe (NF P 94-430-1) Paris.

A.F.T.E.S. (1982) Proposals concerning the measurement and testing to be performed in connection with a mechanical cutting: characterization of rocks on samples. Working Group N-4, Mechanized Excavation.

Al-Ameen SI, Waller MD (1992b) Petrographic analysis for assessing the abrasiveness of coal measures rocks. Dep. Min. Resource Eng. Mag. 44: 29-34.

Al-Ameen SI, Waller MD (1993b) The prediction of abrasive wear in mining equipment.

AL-Ameen SI, Waller MD (1994) The influence of rock strength and abrasive mineral content on the Cerchar Abrasivity Index. Engineering Geology 36: 293-301.

Alavi Gharahbagh E, Rostami J, Palomino AM (2011) New soil abrasion testing method for soft ground tunneling applications. Tunnelling and Underground Space Technology 26: 604-613.

Alber M (2008a) Stress dependency of the Cerchar abrasivity index (CAI) and its effects on wear of selected rock cutting tools. Tunnelling and Underground Space Technology 23: 351-359.

Alber M (2008b) An integrated approach to penetration, advance rates and disc cutter wear for hard rock TBM drives. Geomechanics and Tunneling 1(1): 29-37.

Alber M, Yarali O, Dahl F, Bruland A, Kasling H, Michalakopoulos TN, Cardu M, Hagan P, Aydm H, Ozarslan A (2014) ISRM suggested method for determining the abrasivity of rock by the CERCHAR abrasivity test. Rock Mechanics Rock Engineering 47: 261-266.

Altinoluk S (1981) Investigations into the effects of tungsten carbide composition and geometry on the durability of rock excavation tools. Ph.D. Thesis, University of Newcastle upon Tyne.

Alvarez GM, Babuska R (1999) Fuzzy model for the prediction of unconfined compressive strength of rock samples. International Journal of Rock Mechanics and Mining Sciences 36: 339-349.

ASTM-D4543 (2008) Standard practices for preparing rock core as cylindrical test specimens and verifying conformance to dimensional and shape tolerances. American Society for Testing and Materials.

ASTM-D7625-10 (2012) Standard test method for laboratory determination of abrasiveness of rock using the CERCHAR method. American Society for Testing and Materials.

Atkinson T, Cassapi VB, Singh RN (1986a) Assessment of abrasive wear resistance potential in rock excavation machinery. International Journal of Mining and Geological Engineering 3: 151-163.

Atkinson T, Denby B, Cassapi VB (1986b) Problems associated with rock material properties in surface mining equipment selection. Transactions Institute of Mining and Metallurgy Section-A: Mineral Industry 95: A80-A86.

Bailey SG, Perrott CM (1974) Wear processes exhibited by WC-Co rotary cutters in mining. Wear 29: 117-128.

Bamford WE (1984) Tests for assessing the drillability, cuttability and rippabililty of rocks are being internationally standardized. Australian Geomechanics Society-Excavation Characteristics Seminar.

Barzegari G, Uromeihy A, Zhao J (2015) Parametric study of soil abrasivity for predicting wear issue in TBM tunneling projects. Tunnelling and Underground Space Technology 48: 43-57.

Becker H, Lemmes F (1984) Rock-physical examinations in roadway drivage. Tunnel 2/84: 71-76.

Beckhaus K (2010) Die abrasivität von gesteinen und ihre baubetriebliche auswirkung auf die bohrpfahlherstellung. Bauaktuell 1No.1.

Bell FG (1987) The physical and mechanical properties of the Fell sandstones, Northumberland, England. Engineering Geology 12:1-29.

Bilgin N, Copur H, Balci C (2014) Mechanical excavation in mining and civil industries. CRC Press, Taylor and Francis Group.

Bisschop F (1991) The analysis of a laboratory cutting and abrasion test to be applied in rock cutting dredging. Classified Internal Report, Memoirs of the Centre for Engineering Geology in the Netherlands, Delft University of Technology 81: 105.

Blombery RI, Perrot CM, Robinson PM (1974) Abrasive wear of tungsten carbide-Cobalt composites. I. wear mechanisms. Materials Science and Engineering 13: 93-100.

Brainard WA, Buckley DH (1975) Dynamic SEM wear studies of tungsten carbide cermets. ASLE Transactions 19(4): 309-318.

Brace WF, Martin RJ (1968) A test of the law of effective stress for crystalline rocks of low porosity. International Journal of Rock Mechanics and Mining Sciences, 5: 415-426.

Broch E (1979) Changes in rock strength caused by water. In Proceedings of 4th Congress of International Society for Rock Mechanics, Montreux, Switzerland 1: 71–75.

Brown ET (1981) Rock characterization, testing and monitoring. ISRM Suggested Methods, Pergamon Press, Oxford pp. 221.

Bruland A (1998) Drillability test methods. Project Report 13A-98, p. 18.

Bruland A (2000) Hard rock tunnel boring. PhD. Dissertation, Vol. 3, Advance rate and cutter wear, Norwegian University of Sciences and Technology of Trondheim (NTNU), Report No. 1B-98.

Bruland A (2016) Personal Communication.

Büchi E, Mathier JF, Wyss Ch. (1995) Rock abrasivity − a significant cost factor for mechanical tunneling in loose and hard rock. Tunnel 5/95: 38-44.

Calkins JA, Matin ASA (1968) The geology and mineral resources of the Garhi Habibullah quadrangle and Kakul area, Hazara District, West Pakistan. U.S. Geol. Survey, Project Report (IR) Pk-38 pp.55.

CERCHAR (1986) Centre d'Etudes et des Recherches des Charbonages de France. The CERCHAR abrasiveness index, Verneuil.

Colback PSB, Wiid BL (1965) The influence of moisture content on the compressive strength of rocks. In Proceedings of the 3rd Rock Mechanics Symposium, Toronto, Canada pp. 65-83.

Chaudary MN, Ahmad SA, Mateen A (1999) Some postulates on the tectono-magmatism, tectono-stratigraphy and economic potential of Kirana Malani-Basin, Indo Pakistan. Pakistan Journal of Hydrocarbon, Res. Islamabad, Pakistan 11: 52-68.

Czichos H, Habig KH (2010) Tribologie-Handbuch. Wiesbaden; Viehweg+Teubner Verlag.

Dahl F (2003) Draft of DRI, BWI, CLI standard. Available at http://www.drillability.com.

Dahl F, Grøv E, Breivik E (2007) Development of a new direct test method for estimating cutter life based on the Sievers' J miniature drill test. Tunnelling and Underground Space Technology 22 (1): 106–116.

Dahl F, Bruland A, Jakobsen PD, Nilsen B, Grøv E (2012) Classification of properties influencing the drillability of rocks, based on the NTNU/SINTEF test method. Tunnelling and Underground Space Technology 28: 150-158.

Deketh HJR (1991) Determination of optimum conditions for the modified pin-on-disc test. Memoirs of the Centre for Engineering Geology in the Netherlands 85: 27.

Deketh HJR (1995) Wear of rock cutting tools (Laboratory experiments on the abrasivity of rock). A.A. Balkema.

Deketh HJR, Grima MA, Hergarden IM, Giezen, Verhoef PNW (1998) Towards the prediction of rock excavation machine performance. Bulletin of Engineering Geology and the Environment 57: 3-15.

Deliormanli AH (2012) Cerchar abrasivity index (CAI) and its relation to strength and abrasion test methods for marble stones. Construction and Building Materials, 30: 16-21.

Denis A, Durville JL, Massieu E, Thorin R (1986) Problemes poses par un calcaire tres poreux dans I'etude de la stabilite d'une carrier souterraine. Proceedings of the 5th Congress of the International Association of Engineering Geology, Buenos Aires 549-557.

DIN 50 320 (1979) Wear. Definitions, system analysis of wear occurrences. Classification of the wear field. Deutsches Institut fur Normung e.V., Berlin: pp. 8.

Dipova N (2012) Investigation of the relationships between abrasiveness and strength properties of weak limestone along a tunnel route. Journal of Geological Engineering, 36: 23-34.

Dobereiner L (1984) Engineering geology of weak sandstones. PhD. Thesis, Imperial College London.

Doeg HH (1960) Cemented hard metals- their basis with particular reference to the tungsten carbide cobalt system. Journal of South African Institute of Mining and Metallurgy 60: 663.

Drucker P (2011) Validity of the LCPC abrasivity coefficient through the example of a recent Danube gravel. Geomechanics and Tunneling 4(6): 681-691.

Drucker P (2013) Über die Abrasivität von Lockergestein und den Werkzeugverschleiß im Spezialtiefbau. Dissertation TU Wien.

Düllmann J, Alber M, Plinninger RJ (2014) Determining soil abrasiveness by use of index tests versus using intrinsic soil parameters. Geomechanics and Tunneling 7(1): 87-97.

Dyke CG (1984) The pre-peak deformation characteristics of sandstone at varying moisture contents. M.Sc. Thesis, Imperial College London.

Dyke CG, Dobereiner L (1991) Evaluating the strength and deformability of sandstones. Quarterly Journal of Engineering Geology 24:123-134.

Er S, Tugrul A (2016) Estimation of Cerchar abrasivity index of granitic rocks in Turkey by geological properties using regression analysis. Bulletin of Engineering Geology and the Environment DOI: 10.1007/s10064-016-0853-y.

Erguler ZA, Ulusay R (2009) Water induced variations in mechanical properties of clay bearing rocks. International Journal of Rock Mechanics and Mining Science 46: 355-370.

Espallargas N, Jakobsen PD, Langmaack L, Macias FJ (2014) Influence of corrosion on the abrasion of cutter steel used in TBM tunneling. Rock Mechanics and Rock Engineering, DOI 10.1007/s00603-014-0552-6.

Ewendt G (1989) Erfassung der Gesteinsabrasivität und Prognose des Werkzeugverschleißes beim maschinellen Tunnelvortrieb mit Diskenmeißeln, Bochumer geol. u. geot. Arbeiten 33. Bochum.

Farrokh E, Rostami J, Askilsrud OG (2013) A discussion on TBM cutter change time and cutter life. SME Annual Meeting, Denver, CO Preprint 13-105: 1-4.

Ferreira R, Monteiro LCC, Peres JE, Prado Jr. FA de A (1981) Analise de alguns fatores que infleum na Resistencia a compressao do arenito Bauru. 3rd Brazilian Congress of Engineering Geology (ABGE), Itapema 3:89-102.

Festl J (2006) The LCPC test – A possibility to determine soil abrasivity? Bachelor thesis, Technische Universität München.

Ford LM, Friedman M (1983) Optimization of rock-cutting tools used in coal mining. In Proceedings of the 24th U.S. Symposium on Rock Mechanics, Texas pp. 725-732.

Fowell RJ (1970) A simple method for assessing the machineability of rocks. Tunnels and Tunnelling 2(4): 251-253.

Fowell RJ, Johnson ST (1991) Cuttability assessment applied to drag tool tunneling machines. Proceedings of 7th International Congress on Rock Mechanics pp. 985-990.

Fowell RJ, Abu Bakar MZ (2007) A review of the Cerchar and LCPC rock abrasivity measurement methods. In Proceeding of the 11th Congress of the International Society for Rock Mechanics 155-160.

Gehring K (1995) Prognosis of advance rates and wear for underground mechanized excavations. Felbau 13: 439-448.

Geological Map of Pakistan (1993) Geological Survey of Pakistan. Printed by Graphic Publishers, Karachi Scale 1:1000,000.

Gharahbagh EA, Rostami J, Ghasemi AR, Tonon F (2011) Review of rock abrasion testing. In Proceeding of the 45th US Rock Mechanics/Geomechanics Symposium 11-141.

Gharahbagh EA, Rostami J, Talebi K (2014) Experimental study of the effect of conditioning on abrasive wear and torque requirement of full face tunneling machines. Tunnelling and Underground Space Technology 41: 127-136.

Ghasemi A (2010) Study of CERCHAR abrasivity index and potential modifications for more consistent measurement of rock abrasion. M.sc. Dissertation, Pennsylvania State University, USA.

Ghazanfar M, Baig MS, Chaudhry MN (1983) Geology of Tithwal Kel area Neelum valley, and Jammu and Kashmir. Kashmir Jour. Geol. 1: 1-10.

Gokceoglu C (2002) A fuzzy triangular chart to predict the uniaxial compressive strength of Ankara agglomerates from their petrographic composition. Engineering Geology 66:39-51.

Gokceoglu C, Zorlu K (2004) A fuzzy model to predict the uniaxial compressive strength and the modulus of elasticity of a problematic rock. Engineering Applications of Artificial Intelligence 17:61-72.

Golden J, Rowe GW (1960) Wear of the hard and soft phases in Cobalt-bonded tungsten carbide. British Journal of Applied Physics 11: 517-520.

Golovanevskiy VA, Bearman RA (2008) Gouging abrasion test for rock abrasiveness testing. International Journal of Mineral Processing, Elsevier, Amsterdam 85: 111–120.

Gonzalez C, Arroyo M, Gens A (2014) Abrasivity measures on geotechnical materials of the Barcelona area. In Proceedings of Rock Engineering and Rock Mechanics: Structures in and on Rock Masses, Taylor and Francis Group, London 978-1-138-00149-7.

Gonzalez C, Arroyo M, Gens A (2015) Wear and abrasivity: observations from EPB drives in mixed soft - rock sections. Geomechanics and Tunnelling 8(3): 258-264.

Gunsallus KL, Kulhawy FH (1984) A comparative evaluation of rock strength measures. International Journal of Rock Mechanics, Mining Science and Geomechanical Abstracts 21:233-248.

Gwildis UG, Sass I, Rostami J, Gilbert, MB (2010) Soil abrasion effects on TBM tunneling. In: ITA AITES World Tunnel Congress, Vancouver, British Columbia, Canada.

Hair JF, Black WC, Babin BJ, Anderson RE (2009) Multivariate data analysis. 7th Edition, Prentice Hall, Newyork.

Hamzaban MT, Memarian H, Rostami J (2014a) Continuous monitoring of pin tip wear and penetration into rock surface using a new Cerchar abrasivity testing device. Rock Mechanics Rock Engineering 47:689-701 (DOI 10.1007/s00603-013-0397-4).

Hamzaban MT, Memarian H, Rostami J, Ghasemi-Monfared H (2014b) Study of rock-pin interaction in Cerchar abrasivity test. International Journal of Rock Mechanics and Mining Sciences 72: 100-108.

Hashemnejad A, Ghafoori M, Azali ST (2015) Utilizing water, mineralogy and sedimentary properties to predict LCPC abrasivity coefficient. Bulletin of Engineering Geology and the Environment DOI: 10.1007/s10064-015-0799-9.

Hassani FP, Whittaker BN, Scoble MJ (1979) Strength characteristics of rocks associated with open cast coal mining in the UK. Proceedings of the 20th U.S. Symposium on Rock Mechanics, Austin 347-356.

Hawkins AB, McConnell BJ (1992) Sensitivity of sandstone strength and deformability to changes in moisture content. Quarterly Journal of Engineering Geology, 25: 115-130.

Heinrich R (1995) Untersuchungen zur Abrasivität von Böden als verschleißbestimmender Kennwert. Dissertation, Technische Universität Bergakademie Freiberg.

Hood MC, Roxborough FF (1992) Rock breakage: mechanical. In: SME mining engineering handbook. Society for Mining, Metallurgy and Exploration, Inc., Littleton, pp. 680-721.

Ho YK, So STC, Lau TMF, Kwok RCM (2015) Abrasiveness of common rocks in Hong Kong. Rock Mechanics and Rock Engineering DOI: 10.1007/s00603-015-0873-0.

Howarth DF (1987) The effect of pre-existing microcavities on mechanical rock performance in sedimentary and crystalline rocks. International Journal of Rock Mechanics, Mining Science and Geomechanical Abstracts 24:223-233.

Hui Y, Xueliang J, Na L (2014) Experimental study on mechanical property of peridotite under water-rock interaction. EJGE 19:1179-1188.

Iphar M, Goktan RM (2003) The effect of liquids on mechanical strength and abrasiveness of rocks. Eng. And Arch. Fac. Osmangazi University 17(1): 1-15.

ISRM (1978a) Suggested methods for determining tensile strength of rock materials. International Journal of Rocks Mechanics and Mining Sciences and Geomechanics 15: 99-103.

ISRM (1978b) Suggested methods for determining sound velocity. International Journal of Rocks Mechanics and Mining Sciences and Geomechanics 15: 53-58.

ISRM (1979a) Suggested methods for determining the uniaxial compressive strength and deformability of rock materials. International Journal of Rocks Mechanics and Mining Sciences and Geomechanics 16: 135-140.

ISRM (1979b) Suggested methods for determining water content, porosity, density, absorption and related properties and swelling and slake-durability index properties. International Journal of Rocks Mechanics and Mining Sciences and Geomechanics 16: 141-156.

Jaeger W (1988) An investigation into the abrasive capacity of rock. Memoirs of the Centre of Engineering Geology in the Netherlands 52: 99.

Jakobsen P, Lohne J (2013) Challenges of methods and approaches for estimating soil abrasivity in crushed rock TBM tunneling. Wear 308: 166-173.

Jakobsen PD, Bruland A, Dahl F (2013) Review and assessment of the NTNU/SINTEF soil abrasion test (SAT^{TM}) for determination of abrasiveness of soil and soft ground. Tunnelling and Underground Space Technology 37: 107-114.

Jakobsen PD, Langmaack L, Dahl F, Breivik T (2013) Development of the soft ground abrasion tester (SGAT) to predict TBM tool wear, torque and thrust. Tunnelling and Underground Space Technology 38: 398-408.

Janach W, Merminod A (1982) Rock abrasivity test with a modified Schmidt hammer. International Journal of Rock Mechanics, Mining Sciences and Geomechanics Abst. 19: 43-45.

Jhonson ST, Fowell RJ (1986) Compressive strength is not enough (Assessing pick wear for drag tool-equiped machines). In Proceedings of the 27th US Symposium Rock Mechanics, Tuscaloosa, Ala., USA 840-845.

Kahraman S, Alber M, Fener M, Gunaydin O (2010) The usability of Cerchar abrasivity index for the prediction of UCS and E of Misis Fault Breccia: Regression and artificial neural analysis. Expert Systems with Applications 37: 8750-8756.

Kahraman E, Kahraman S (2015) The performance prediction of Roadheaders from easy testing methods. Bulletin of Engineering Geology and the Environment DOI: 10.1007/s10064-015-0801-2.

Kahraman S, Fener M, Käsling H, Thuro K (2016) The influences of textural parameters of grains on the LCPC abrasivity of coarse-grained igneous rocks. Tunnelling and Underground Space Technology 58: 216-223.

Karakus M, Kumral M, Kilic O (2005) Predicting elastic properties of intact rocks from index tests using multiple regression modeling. International Journal of Rocks Mechanics and Mining Sciences and geomechanics 42: 323-330.

Kasling H, Thuro K (2010) Determining abrasivity of rock and soil in the laboratory. In 11th IAEG Congress. Auckland. New Zealand, p 235 1973-1980.

Kennedy P (2008) A guide to econometrics. 6th Edition Oxford: Willey Blackwell.

Kenny P, Wright AC (1974) Mechanism of wear of cemented carbide tips on rock cutting tools. Wear 30: 377-383.

Khandelwal M, Ranjith PG (2010) Correlating index properties of rocks with P-wave measurements. Journal of Applied Geophysics 71:1-5.

Kitaowa M, Endo G, Hoshino K (1977) Influence of moisture on the mechanical properties of soft rock. Proceedings of the 5th National Symposium on Rock Mechanics, Japan.

Ko TY, Kim TK, Son Y, Jeon S (2016) Effect of geomechanical properties on Cerchar Abrasivity Index (CAI) and its implication to TBM tunneling. Tunnelling and Underground Space Technology 57: 99-111.

Köhler M, Maidl U, Martak L (2011) Abrasiveness and tool wear in shield tunneling in soil. Geomechanics and Tunneling 4(1): 36-53.

Koshima A, Frota RGQ, Lorano MH, Hoshisk JCB de F (1983) Comportamento e propriedades geomechanicas do arenito Bauru. Simposio Geotecnico Sobre Bacio Alto Parana, ABGE-ABMS-CBMR, Sanpaulo, 2b 173-189.

Krapivin MG, Manakov VM, Michajlov VG (1967) Untersuchungen der temperature und ihers einflusses auf den verschleiß der schneidwerkzeuge von vortriebsmachinen beim schneiden in sandstein. Izvest VUZ, Gorn 10: 84-89.

Kumaraswamy S, Mozumdar BK (1987) Bucket wheel excavator performances at Neyveli Lignite Mine. Mining Science and Technology 4: 213-223.

Küpferle J, Röttger A, Alber M, Theisen W (2015) Assessment of the LCPC abrasiveness test from the view of material science. Geomechanics and Tunneling 8(3): 211-220.

Küpferle J, Röttger A, Theisen W, Alber M (2016) The RUB Tunnelling Device - a newly developed test method to analyze and determine the wear of excavation tools in soils. Tunnelling and Underground Space Technology 59: 1-6.

Labas M, Krepelka F, Ivanicova L (2012) Assessment of abrasiveness for research of rock cutting. Acta Montanistica Slovaca 1: 65-73.

Lagerquist M (1975) A study of the thermal fatigue crack propagation in WC-Co cemented carbide. Powder Metallurgy 18(35): 71-88.

Larsen-Basse J (1973) Wear of hard metals in rock drilling: a survey of the literature. Powder Metallurgy 16(31): 1-32.

Larsen-Basse J, Perrott CM, Robinson PM (1974) Abrasive wear of tungsten carbide-Cobalt composites. I. rotary drilling tests. Materials Science and Engineering 13: 83-91.

Lemmerhofer C (2010) Schleifsteine aus Niederösterreich: Petrologie und Technische Eigenschaften. Masterarbeit, Universität Wien.

Lyman R, Longnecker M (2010) An introduction to statistical methods and data analysis. 6th Edition, Brooks/Cole Cengage Learning, Canada

Macias FJ, Dahl F, Bruland A (2015) New rock abrasivity test method for tool life assessments on hard tunnel boring: the rolling indentation abrasion test (RIAT). Rock Mechanics and Rock Engineering DOI: 10.1007/s00603-015-0854-3.

Maidl B, Schmid L, Ritz W, Herrenknecht M (2001) Tunnelbohrmaschinen im artgestein. Ernst & Sohn p. 350.

Majeed Y, Abu Bakar MZ (2015) Statistical evaluation of CERCHAR Abrasivity Index (CAI) measurement methods and dependence on petrographic and mechanical properties of selected rocks of Pakistan. Bulletin of Engineering Geology and the Environment DOI: 10.1007/s10064-015-0799-5.

Malik RH, Schouppe M, Fontan D, Verkaeren J, Martinotti G, Ahmed KS, Qureshi S (1996). Geology of the Neelum valley, district Muzaffarabad, Azad Kashmir, Pakistan. Geol. Bull. Univ. Peshawar 29: 91-111.

Mammen J, Saydam S, Hagan PA (2009) Study on the effect of moisture content on rock cutting performance. In Proceedings of the Coal Operators Conference, University of Wollongong & the Australian Institute of Mining and Metallurgy, Aziz, N (ed) pp. 340-347.

Matern NV, Hjelmer A (1943) Försök med pågrus (''Tests with Chippings''), Medelande nr. 65, Statens väginstitut, Stockholm, 65 pp. (English summary, pp. 56–60).

McFeat-Smith I, Fowell RJ (1977) Correlation of rock properties and the cutting performance of tunneling machines. In Proceedings of Conference on Rock Engineering, Newcastle upon Tyne 581-602.

Michalakopoulos TN, Anagnostou VG, Bassanou ME, Panagiotou GN (2006) The influence of steel styli hardness on the Cerchar abrasiveness index value. International Journal of Rock Mechanics and Mining Sciences 43: 321-327.

Mirmehrabi H, Ghafoori M, Lashkaripour G (2015) Impact of some geological parameters on soil abrasiveness. Bulletin of Engineering Geology and the Environment DOI: 10.1007/s10064-015-0837-3.

Mosleh M, Gharahbagh EA, Rostami J (2013) Effects of relative hardness and moisture on tool wear in soil excavation operations. Wear 302:1555-1559.

Muftuoglu YV (1983) A study of factors affecting diggability in British surface coal mines. PhD. Dissertation, University of Nottingham.

Nilsen B, Dahl F, Raleigh P, Holzhäuser J (2006a) Abrasivity of soils in TBM tunneling. Tunnels and Tunnelling International pp. 36-38.

Nilsen B, Dahl F, Raleigh P, Holzhäuser J (2006b) Abrasivity testing for rock and soils. Tunnels and Tunnelling International pp. 47-49.

Nilsen B, Dahl F, Raleigh P, Holzhäuser J (2006c) SAT: NTNU's new soil abrasion test. Tunnels and Tunnelling International pp. 43-45.

Nilsen B, Dahl F, Holzhäuser J, Raleigh P (2007) New test methodology for estimating the abrasiveness of soils for TBM tunneling. In Proceedings of the RETC, pp. 104-116.

Nizamoglu S (1978) Contrubution a L'etude du Fonctionnement des Tunneliers "Plein Section" et Analysc de L'usure de Leurs Outils de Coupe. These Pour Obtenir le Grade de Docteur Ing. Ecole des Mines de Nancy, pp. 139.

O'Reilly MP, Tough SG, Pirrie ND, Hignett HJ, Roxborough FF (1979) Tunnelling trials in chalk. In: Proceedings of the Institution of Civil Engineers, London, UK, Ed. J.S. Davis, Part 2, 67: 255-283.

Paschen D (1980) Petrographic and geomechanical characterization of Ruhr area carboniferous rocks for the determination of their wear behavior. PhD dissertation, Technische Unversitat Claustahl 202.

Pells PJN (2004) Substance and mass properties for the design of engineering structures in the Hawkesbury sandstone. Aust Geomech 39:1-21.

Perera MSA, Ranjith PG, Peter M (2011) Effects of saturation medium and pressure on strength parameters of Latrobe Valley brown coal: Carbon dioxide, water and nitrogen saturations. Energy 36: 6941-6947.

Perez S, Karakus M, Sepulveda E (2015) A preliminary study on the role of acoustic emission on inferring Cerchar abrasivity index of rocks using artificial neural network. Wear 344-345:1-8.

Phillips HR, Roxborough FF (1981) The influence of tool material on the wear rate of rock cutting picks. In: Proceedings of the 34th Annual Conference of Australian Institute of Metals, Brisbane pp. 52-56.

Plinninger RJ (2002) Klassifizierung und Prognose von Werkzeugverschleiß bei konventionellen Gebirgslösungsverfahren im Festgestein. Münchner Geologische Hefte, Reihe B – Angewandte Geologie, 17: 147.

Plinninger RJ, Spaun G, Thuro K (2002) Prediction and classification of tool wear in drill and blast tunneling. In proceedings of the 9th IAEG Congress- Engineering Geology for Developing Countries pp. 2226-2236.

Plinninger RJ, Kasling H, Thuro K, Spaun G (2003) Testing conditions and geomechanical properties influencing the CERCHAR abrasiveness index (CAI) value. International Journal of Rock Mechanics and Mining Sciences 40: 259-263.

Plinninger RJ, Kasling H, Thuro K (2004) Wear prediction in hard rock excavation using the CERCHAR Abrasiveness Index (CAI). Proceeding of the EUROCK and 53rd Geomechanics Colloquium, Schubert 599-604.

Plinninger RJ (2008) Abrasiveness assessment for hard rock drilling. Geomechanics and Tunneling 1: 38-46.

Plinninger RJ, Restner U (2008) Abrasiveness testing, quo vadis?- a commented overview of abrasiveness testing methods. Geomechanics and Tunneling 1: 61-70.

Plinninger RJ (2010) Hardrock abrasivity investigation using the Rock Abrasivity Index (RAI). Williams et al. (eds), Taylor and Francis Group, London pp. 3445-3452.

Plinninger RJ (2015) Personal Communication.

Poulsen BA, Shen B, Williams DJ, Huddlestone-Holmes C, Erarslan N, Qin J (2014) Strength reduction on saturation of coal and coal measures rocks with implications for coal pillar strength. International Journal of Rock Mechanics and Mining Sciences, 71: 41-52.

Priest SD, Selvakumar S (1982) The failure characteristics of selected British rocks. A Report to the Transport and Research Laboratory, Department of Environment and Transport, Imperial College, London.

Rehbinder P, Lichtman V (1957) Effect of surface active media on strains and rupture in solids. Proceedings 2nd International Congress on Surface Activity 563-582.

Rogers S, Robert B (1991) Wear mechanisms associated with rock excavation using attack picks. Mining Science and Technology 12: 317-323.

Rosiwal A (1896) New research findings on the hardness of minerals and rocks. Verhandlungen der Königl. Geol. Reichsanstalt, Wien 17 and 18: 475-491.

Rosiwal A (1916) New findings on the hardness determination of minerals and rocks – an absolute measure for the hardness of brittle materials. Verhandlungen der Königl. Geol. Reichsanstalt, Wien 5 and 6: 117-147.

Rostami J, Ozdemir L, Bruland A, Dahl F (2005) Review of issues related to Cerchar abrasivity testing and their implications on Geotechnical investigations and cutter cost estimates. In Proceedings of the RETC. pp. 738-751.

Rostami J, Gharahbagh EA, Palomino AM, Mosleh M (2012) Development of soil abrasivity testing for soft ground tunneling using shield machines. Tunnelling and Underground Space Technology 28:245-256.

Rostami J, Ghasemi AR, Gharahbagh EA, Dogruoz C, Dahl F (2013) Study of dominant factors affecting Cerchar Abrasivity Index. Rock Mechanics Rock Engineering DOI 10.1007/s00603-013-0487-3.

Roxborough FF, Rispin A (1973) The mechanical cutting characteristics of the lower chalk. Tunnels and Tunnelling 4: 5-67.

Roxborough FF, Philips HW (1974) Experimental studies on the excavation on the rock using picks. In proceedings of the 3rd Congress of International Society of Rock Mechanics, Advances in Rockmechanics, Volume II, Part B.

Roxborough FF (1987) The role of some basic rock properties in assessing cuttability. Proceedings Seminar "Tunnels – Wholly Engineered Structures". IE Australia.

Samaranayake VA (2009) Statistical data analysis. STAT-353 course, Missouri University of Science and Technology, Rolla, MO, USA.

Schimazek J, Knatz H (1970) The influence of rock composition on cutting velocity and chisel wear of tunneling machines. Glückauf 106, 274–278.

Schimazek J, Knatz H (1976) The assessment of cuttability of rocks by drag and roller bits. Ertzmetall 29: 113-119.

Schumacher L (2004) Auslegung und Einsatzbedingungen von Tunnelvortriebsmaschinen im Hartgestein. Felsbau, 22, Essen (Glückauf) 3: 21-28.

Selmer-Olsen R, Lien R (1960) Bergartens borbarhet og sprengbarhet. Teknisk Ukeblad nr. 34, Oslo, pp. 3–11.

Selmer-Olsen R, Blindheim OT (1970) On the drillability of rock by percussive drilling. In Proceedings of 2nd Congress of ISRM, Belgrade.

Shah SMI (2009) Stratigraphy of Pakistan. MEMOIRS of the Geological Survey of Pakistan, Quetta. 22: 1-355.

Singh RN, Hassani FP, Elkington PJ (1983) The application of strength and deformation index testing to the stability assessment of coal measures excavation. Proceeding of the 24th US Symposium of Rock Mechanics 599-609.

Sommer K, Heinz RSJ (2010) Verschleiß metallischerWerkstoffe. Wiesbaden: Vieweg + Teubner Verlag.

Soni DK (2015) Effect of saturation and deformation rate on split tensile strength for various sedimentary rocks. International conference Data Mining, Civil and Mechanical Engineering, Bali, Indonesia 53-55.

Stanford J, Hagan P (2009) An assessment of the impact of stylus metallurgy on Cerchar abrasiveness index. In Proceedings of the Coal Operators Conference, 348-355.

Stjernberg KG, Fischer U, Hugoson NI (1975) Wear mechanisms due to different rock drilling conditions. Powder Metallurgy 18(35): 89-106.

Stolarski TA (2000) Tribology in machine design. Butterworth Heinemann, Oxford.

Suana M, Peters T (1982) The cerchar abrasivity index and its relation to rock mineralogy and petrography. Rock Mechanics 15:1-7.

Szlavin J (1974) Relationship between some physical properties of rock determined by laboratory tests. International Journal of Rock Mechanics Science and Geochemistry 2: 57-66.

Tarigh Azali S, Moammeri H (2012) EPB-TBM tunnelling in abrasive ground, Esfahan Metro Line 1. WTC ITA-AITES 2012 World Tunnel Congress, Thailand.

Tarkoy PJ (1973) A study of rock properties and tunnel boring machine advance rates in two mica schist formations. In Proceedings of the 15th Symposium of Rock Mechanics, Custer State Park, South Dakota, pp.415-447.

Teichert C (1967) Nature of Permian glacial record, Salt Range and Khisor Range, West Pakistan. Neues Jahrb, Geol. Palaeont., Abh. 129(2): 167-184.

Thuro K (1997) Prediction of drillability in hard rock tunneling by drilling and blasting. In Proceedings of the World Tunnel Congress-Tunnels for People 1: 103-108.

Thuro K, Plinninger RJ (2003) Hard rock tunnel boring, cutting, drilling and blasting: rock parameters for excavatability. In proceedings of the 10th ISRM International Congress on Rock Mechanics, Johannesburg, South Africa pp. 1227-1234.

Thuro K, Singer J, Käsling H, Bauer M (2006) Soil abrasivity assessment using the LCPC testing device. Felsbau 24: 37-45.

Thuro K, Singer J, Käsling H, Bauer M (2007) Determining abrasivity with the LCPC test. In Proceedings of the 1st Canada-U.S. Rock Mechanics Symposium, Vancouver B.C.

Thuro K, Käsling H (2009) Classification of the abrasiveness of soil and rock. Geomechanics and Tunneling 2(2): 179-188.

Tiryaki B, Dikmen AC (2006) Effects of rock properties on specific cutting energy in linear cutting of sandstones by picks. Rock Mechanics and Rock Engineering 39(2) 89-120.

Uetz H (1986) Abrasion and erosion. Carl Hauser Verlag, München, pp. 829.

US Army Corps of Engineers (1995) http://gsl.erdc.usace.army.mil/SL/MTC/handbook/RT/RTH/116-95.pdf, accessed July 9, 2012.

Van Eeckhout EM (1976) The mechanisms of strength reduction due to moisture in coal mine shales. International Journal of Rock Mechanics and Mining Sciences and Geomechanics, 13: 61-67.

Vasarhelyi B (2003) Some observations regarding the strength and deformability of sandstones in dry and saturated conditions. Bulletin of Engineering Geology and the Environment 62: 245-249.

Verhoef PNW, Vanden Bold HJ, Vermeer ThWM (1990) Influence of microscopic structure on the abrasivity of rock as determined by the pin-on-disc test. Proceedings 6th International Congress IAEG, Amsterdam 495-504.

Verhoef PNW (1997) Wear of rock cutting tools (Implications for the site investigation of rock dredging projects). A.A. Balkema.

Vutukuri VS (1974) The effect of liquids on the tensile strength of limestone. International Journal of Rock Mechanics and Mining Sciences and Geomechanics, 11: 27-29.

Wadia DN (1931) The syntaxis of the north-west Himalayas: Its rocks, tectonics and orogeny. Ibid., Recs. 65(2): 189-220.

Wadia DN (1934) The Cambrian-Trias sequences of north-western Kashmir, parts of Muzaffarabad and Baramula district. Rec. Geol. Sum. India 66(2): 12-234.

Wellinger K, Uetz H (1955) Gleitverschleiß, Spülverschleiß, Strahlverschleiß unter der Wirkung von körnigen Stoffen. VDIForschungsheft 449, Ausgabe B Band 21. Düsseldorf.

West G (1981) A Review of Rock Abrasiveness Testing for Tunnelling. In Proc. International Symposium on Weak Rock, Tokyo, 21-24 September, PP 585-594.

West G (1986) A relation between abrasiveness and quartz content for some Coal Measures sediments. International Journal of Mining and Geological Engineering, 4: 73-78.

West G (1989) Rock abrasiveness testing for tunneling. International Journal of Rock Mechanics, Mining Sciences and Geomechanics, Abstr., 26: 151-160.

Wiid BL (1970) The influence of moisture content on the pre-rupture fracturing of two rock types. Proceedings of the 2nd Congress of the International Society of Rock Mechanics, Belgrade 3:239-245.

Yarali O, Yasar E, Bacak G, Ranjith PG (2008) A study of rock abrasivity and tool wear in coal measures rocks. International Journal of Coal Geology 74: 53-66.

Yilmaz NG, Yurdakul M, Goktan RM (2007) Prediction of radial bit cutting force in high-strength rocks using multiple linear regression analysis. Internation Journal of Rock Mechanics and Mining Sciences 44: 962-970.

Yilmaz I (2010) Influence of water content on the strength and deformability of gypsum. International Journal of Rock Mechanics and Mining Science 47: 342-347.

Zare S, Bruland A (2013) Applications of NTNU/SINTEF drillability indices in hard rock tunneling. Rock Mechanics and Rock Engineering 46: 179-187.

Zum Gahr KH (1987) Microstructure and wear of metals. Elsevier, Amsterdam PP 560.

VITA

After completeing the higher secondary school education, Yasir Majeed joined the Mining Engineering Department at the University of Engineering and Technology (UET) Lahore. He earned his B.Sc. in Mining Engineering in July, 1999. After graduating from the UET, he served at M/s. Geo Mineral Associates as Assistant Mining engineer. In 2004, he joined Directorate General of Mines and Minerals (DGM&M) Punjab as Assistant Director Mines and Minerals. He remained involved in the grant of Mining concessions of major minerals both for small scale and large scale mining. Meanwhile, he also enrolled himself in the M.Sc. Mining Engineering program at UET, Lahore as a part time candidate. After leaving the DGM&M Punjab, he joined the faculty of Mining Engineering in May, 2007, as Lecturer. He obtained his M.Sc. in Mining Engineering in September, 2007. After serving the department as Lecturer he was promoted as Assistant Profressor in year 2011. He also started pursuing his PhD. in Mining Engineering at UET, Lahore in year 2011 and remained involved in this research area under the kind supervision of Dr. Muhammad Zubair Abu Bakar.

PUBLICATIONS